VIETNAM GENERAL CONFEDERATION OF LABOUR
TON DUC THANG UNIVERSITY
FACULTY OF ELECTRICAL & ELECTRONICS ENGINEERING

TRAN THANH PHONG

PUBLISHED ARTICLES

HO CHI MINH CITY, YEAR 2024

DANH MỤC CÁC BÀI BÁO CÔNG BỐ

1. Huynh, Van Van, **Phong Thanh Tran*,** Bui Le Ngoc Minh, Anh Tuan Tran, Dao Huy Tuan, Tam Minh Nguyen, and Phan-Tu Vu. "New second-order sliding mode control design for load frequency control of a power system." Energies 13, no. 24 (2020): 6509.
2. Huynh, Van Van, **Phong Thanh Tran*,** Tien Minh Nguyen, Van-Duc Phan, and Viet-Thanh Pham. "Advanced Sliding Mode Observer Design for Load Frequency Control of Multiarea Multisource Power Systems." International Transactions on Electrical Energy Systems 2022.
3. Van Van Huynh, **Phong Thanh Tran*,** and Chau Si Thien Dong, Bach Dinh Hoang, "Sliding Surface Design for Sliding Mode Load Frequency Control of Multi Area Multi Source Power System", IEEE Transactions on Industrial Informatics, 2024.
4. **Phong Thanh Tran,** Van Van Huynh and Chau Si Thien Dong, Bach Dinh Hoang, "Automatic Generation Control based Sliding Mode Observer Design for Multi-Area Multi-Source Power Systems", the 7th International Conference on Advanced Engineering – Theory and Applications, 2022.
5. **Phong Thanh Tran,** Van Van Huynh, Chau Thien Si Dong, and Bach Hoang Dinh. "Sliding Mode-Based Load Frequency Control of a Power System with Multi-Source Power Generation." In 2023 International Conference on System Science and Engineering (ICSSE), pp. 142-147. IEEE, 2023.
6. Tran, Anh-Tuan, Bui Le Ngoc Minh, **Phong Thanh Tran,** Van Van Huynh, Van-Duc Phan, Viet-Thanh Pham, and Tam Minh Nguyen. "Adaptive integral second order sliding mode control design for load frequency control of large-scale power system with communication delays." Complexity 2021.
7. Van Huynh, Van, **Phong Thanh Tran,** Tuan Anh Tran, Dao Huy Tuan, and Van-Duc Phan. "Extended state observer-based load frequency controller for three area interconnected power system." TELKOMNIKA (Telecommunication Computing Electronics and Control) 19, no. 3 (2021): 1001-1009.
8. Huynh, Van Van, Bui Le Ngoc Minh, Emmanuel Nduka Amaefule, Anh-Tuan Tran, and **Phong Thanh Tran.** "Highly robust observer sliding mode-based frequency control for multi area power systems with renewable power plants." Electronics 10,

no. 3 (2021): 274.

9. Tran, Anh-Tuan, Bui Le Ngoc Minh, Van Van Huynh, **Phong Thanh Tran,** Emmanuel Nduka Amaefule, Van-Duc Phan, and Tam Minh Nguyen. "Load frequency regulator in interconnected power system using second order sliding mode control combined with state estimator." Energies 14, no. 4 (2021): 863.
10. Huynh, Van Van, Bui Le Ngoc Minh, Emmanuel Nduka Amaefule, Anh-Tuan Tran, **Phong Thanh Tran,** Van-Duc Phan, Viet-Thanh Pham, and Tam Minh Nguyen. "Load Frequency Control for Multi-Area Power Plants with Integrated Wind Resources." Applied Sciences 11, no. 7 (2021): 3051.
11. Tran Anh-Tuan, **Phong Thanh Tran,** and Van Van Huynh. "Load Frequency Control for Power System using Generalized Extended State Observer." Journal of Advanced Engineering and Computation 5, no. 1 (2021): 1-18.

energies

MDPI

Article

New Second-Order Sliding Mode Control Design for Load Frequency Control of a Power System

Van Van Huynh [1], Phong Thanh Tran [1,*], Bui Le Ngoc Minh [2], Anh Tuan Tran [1], Dao Huy Tuan [1], Tam Minh Nguyen [2] and Phan-Tu Vu [3]

1 Faculty of Electrical & Electronics Engineering, Ton Duc Thang University, Ho Chi Minh City 700000, Vietnam; huynhvanvan@tdtu.edu.vn (V.V.H.); trananhtuan.st@tdtu.edu.vn (A.T.T.); daohuytuan@tdtu.edu.vn (D.H.T)

2 Faculty of Electrical and Electronics Engineering, Ho Chi Minh City University of Technology and Education, Ho Chi Minh City 700000, Vietnam; 1726002@student.hcmute.edu.vn (B.L.N.M.); tamnm@hcmute.edu.vn (T.M.N.)

3 Department of Power Systems of Ho Chi Minh City University of Technology, Vietnam National University, Ho Chi Minh City 700000, Vietnam; vptu@vnuhcm.edu.vn

* Correspondence: tranthanhphong.st@tdtu.edu.vn; Tel.: +84-936967379

Received: 19 September 2020; Accepted: 3 December 2020; Published: 9 December 2020

Abstract: The implementation of the sliding mode control (SMC) for load frequency control of power networks becomes difficult due to the chattering phenomenon of high-frequency switching. This chattering problem in SMC is extremely dangerous for actuators used in power systems. In this paper, a continuous control strategy by combining a second-order mode and integral siding surface is proposed as a possible solution to this problem. The proposed second-order integral sliding mode control (SOISMC) law not only rejects chattering phenomenon in control input, but also guarantees the robustness of the multi-area power network, which has an effect on parametric uncertainties such as the load variations and the matched or mismatched parameter uncertainties. Moreover, the reporting of the simulation indicates that the proposed controller upholds the quality requirement by controlling with operating conditions in the larger range, rejects disturbance, reduces the transient response of frequency, eliminates the overshoot problem, and can better address load uncertainties compared to several previous control methods. The simulation results also show that the proposed SOISMC can be used for practical multi-area power network to lessen high parameter uncertainties and load disturbances.

Keywords: load frequency control; multi-area power system; second order sliding mode control

1. Introduction

In general terms, a power network includes a connection of electrical components that can be divided into a generator that supply the power, the transmission system that inducts the power to the load from the centers of electricity generation, and the distribution system that supply the power to neighboring industries, hospitals, homes and the other kinds of load [1,2]. Therefore, different load changes continuously and progressively occur with the demand of reactive and active power by the neighboring industries, homes etc. In practical power networks, the frequency deviation is caused by increasing real power demand and the voltage as well is impacted by variation of reactive power. To continue meeting the real power demands, the load frequency needs to be controlled. The principal standard of the load frequency control (LFC) is to keep the frequency of power system and voltage uniform at its nominal value during and when there is load change. In A conventional power system, governor droop speed control and auxiliary back-up control are used to regulate frequency (i.e., frequency controllers) while automatic voltage regulates (AVR) for the voltage supply by many power companies. Since the inception of interconnected multi-area power networks, they have become more economical and reliable. The big challenges with the proposed control design, especially for LFC in tie multi-area power network, are a great deal of problems such as unpredicted external disturbances, parameters of uncertainties and even the nonlinear model of uncertainties in power systems. However, the targets of LFC are to keep at minimum the transient response deviations in each area frequency and interchange of tie-line power and to guarantee their steady state errors to be zero. LFC normalizes the frequency of power system, enables to maintain system dynamics, and provides certain conditions to ensure quality assurance of the power supply [3–5].

In literature, there are many control schemes such as proportion integration derivative (PID) control, internal model control scheme, model predictive model control, fuzzy logic method, artificial intelligence control, SMC and so on that have been discussed. The topics have been introduced in [6–30]. In a prescribed power network environment, the above mentioned-LFC approaches with matched and mismatched uncertainties elements are used in a power system. The proposed PID-type controllers apply to present several control models in [6–9]. In [6,7], the linear algebraic equations have been used in these methods to find controller parameters. Based on the direct synthesis scheme and chaotic algorithm method were given in frequency domain to finalize and optimize the method of PID controller for interconnected power network. The extended controller of PID method by using the low pass filter was a strategy of tuning its way in [8]. The differential evolutionary scheme using a parallel two-degree freedom of the PID controller for LFC of the power network was incorporated into a power system in [9]. Nevertheless, most traditional PID controller methods with fixed gain were designed under normal operating conditions of power systems. In addition, these proposed approaches were always used in tuning or selecting modes, such as the fundamental method of trial and error without analytical methods for determining and optimizing the parameters of interconnected multi-area power networks. Therefore, it is very difficult to find out the best proposed control schemes to finalize the good performance in larger range of the practical operating conditions. Beside PID control techniques mentioned above, the model predictive control or fuzzy logic control or intelligent control is one of the best options. To reduce the regulation burden of the control area without regulation capacity, the proposed cooperative based on differential games was designed for supplying the power via tie-line between two areas of the power systems [10]. In [11], the scheme of LFC for power systems was suggested and developed based on the direct adaptive fuzzy logic method. The suggestion of model predictive controller for LFC was investigated and developed in [12]. In deregulated environments [13], a model predictive controller for LFC for the power system introduced a Kalman filter for state estimation with a linear active disturbance rejection scheme method to evaluate and quickly repay the disturbances. The simple scheme to LFC control design for power networks with parametric uncertainties and load disturbances was represented in [14]. In [15], this paper was presented by an internal adaptive LFC controller based on internal model control structure used the least square method and applied for both cases of static controller gain and adaptive controller gain. In [16], a novel fuzzy controller with a filtered derivative exploit and fractional order integrator was suggested and developed to resolve an automatic generation control problem in an interconnected multi-area power network. The study of intelligent control for LFC was used in an extended classifier system with constant-valued inputs to modify traditional frequency model [17]. The above methods contained the important results to resolve and build LFC problem in power systems. Unfortunately, some limitations of these controller methods are too complicated and of high order and requirement for on-line parameters identification implies for power system.

Among these presented control approaches, the SMC is attractive and powerful due to its ability to quickly converge, is useful to implement in power systems and is robust to external disturbances, system parameter variations and insensitivity with model errors of system. The SMC approach mainly include two steps: the selection of the sliding mode surface, and the design of the sliding mode controller. SMC has been used to solve the LFC problems of power networks with load disturbances and parameter uncertainties [18–30]. It is also perhaps insensitive to changes in the plant parameters and as well as improving system performance of transient control. In [18] was presented by another direction of a distributed sliding mode control approach for optimal LFC to control and regulate the system frequency and minimize the costs of power generation in power networks. The adaptive SMC problem of nonlinear Markovian jump systems was proposed in [19] to investigate and build in assuring the stochastic stability of power network. The design of a sliding-mode perturbation observer-based SMC was introduced and designed to enhance the stability of interconnected multi-area power networks in [20]. The proposed approach for LFC was presented and developed by a nonlinear SMC with matched and mismatched uncertainties, and it was applied to test in three control area power systems [21]. The non-linear SMC for LFC approach in [22,23] is robust and powerful in its ability to upgrade the performance of dynamic system. In [24,25], a method design is applied for power systems of LFC based on SOISMC theory and disturbance uncertainties observer to improve the stability of power system. The generalized extended state observer based on first-order SMC control was developed for a multi-area power network where parameter uncertainties were not considered [31].

In [32], the full order SMC was proposed to design an LFC scheme for a two-area power system, which is achieved when all the parameters of power system are at nominal values. The parameter uncertainties were not highlighted in an adaptive SMC method [33]. The LFC problems in power networks can be solved by the above approaches using SMC technique. However, the sliding mode load frequency controller given in [18–25] and [31–33] suffer from a major limitation known as the chattering phenomenon because of the discontinuous control signal used in the SMC. Such chattering has many negative effects in LFC in control areas of a power system since it may damage the control actuator and excite the undesirable unmodeled dynamics, which probably leads to a degradation and/or instability in system performance.

In this article, a continuous SMC strategy based on a SOISMC approach is introduced and developed for LFC of an interconnected multi-area power network. The major contributions of this research are the following:

- The second-order sliding mode controller based on integral sliding surface is offered to ensure the shortening of the frequency's transient response to avoid the overshoot.
- The performance of the power system is improved in the sense of reducing the chattering in comparison with the same SMC technique without using continuous controller. Therefore, the limitation of the first-order sliding mode control approach given in [26,33] has been solved.
- A new LMI technique is derived to guarantee the stability of whole system via Lyapunov theory.
- The simulation results show and clearly prove the usefulness, the effectiveness and the robustness of the proposed second order SMC approach against the various disturbances such as matched, mismatched uncertainties and load variations. In comparison, the performance of the proposed SOISMC is better than the previous control by using differential games method given in [10].

The remain parts of this paper are presented in the following. A mathematical model of a multi-area interconnected power network is indicated in Section 2. The following proposed new second-order sliding mode load frequency control design is shown in Section 3. The discussion and simulation results are implied to evaluate the new second-order sliding mode control approach in Section 4. Lastly, the conclusion is discussed in Section 5.

2. Mathematical Model of an Interconnected Multi-Area Power Network

In this section, we first consider introducing a mathematical model or the dynamic model of the power network, and then analyzing the problem formulation of power systems. In studies, we realize that a multi-area power network is not only complicated but also nonlinear in a dynamic system with the parametric uncertainties and load variations. During the normal operation of power networks, the slow changes of load and resource appear in power system. That is a reason why we can linearize the dynamic model of power system around the point of normal system operation [26–30].

The proposed control law of LFC is designed for interconnected multi-area power network, which is presented in Figure 1 [26–30]:

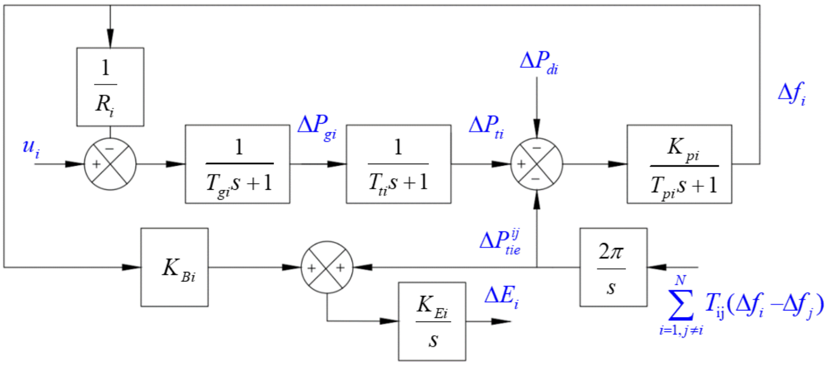

Figure 1. The simple block chart of the *i*th area of a multi-area power network.

The frequency dynamic behavior of *i*th area details in this section can be used in the following differential equation:

$$\Delta \dot{f}_i(t) = -\frac{1}{T_{pi}}\Delta f_i(t) + \frac{K_{pi}}{T_{pi}}\Delta P_{ti}(t) - \frac{K_{pi}}{T_{pi}}\Delta P_{di}(t) - \frac{K_{pi}}{T_{pi}}\Delta P_{tie}^{ij}(t) \tag{1}$$

$$\Delta \dot{P}_{ti}(t) = -\frac{1}{T_{ti}}\Delta P_{ti}(t) + \frac{1}{T_{ti}}\Delta P_{gi}(t) \tag{2}$$

$$\Delta \dot{P}_{gi}(t) = -\frac{1}{R_i T_{gi}}\Delta f_i(t) - \frac{1}{T_{gi}}\Delta P_{g_i}(t) + \frac{1}{T_{gi}}u_i(t) \tag{3}$$

$$\Delta \dot{E}_i = K_{Bi}K_{Ei}\Delta f_i + K_{Ei}\Delta P_{tie}^{ij} \tag{4}$$

$$\Delta \dot{P}_{tie}^{ij} = \sum_{\substack{j=1 \\ j\neq i}}^{N} 2\pi T_{ij}[\Delta f_i(t) - \Delta f_j(t)] \tag{5}$$

where i = 1 to N and N is defined the number of control areas, $\Delta f_i(t)$ and $\Delta f_j(t)$ are incremental changes in frequency of each control area, $\Delta P_{ti}(t)$ is incremental change in governor output command, $\Delta P_{gi}(t)$ is incremental change in governor valve position of each area, $\Delta P_{tie}^{ij}(t)$ is total tie line power change between control *i*th area and all other control areas, $\Delta P_{di}(t)$ is incremental change in local load of each area, $\frac{1}{K_{pi}} = D_i$ is equivalent system damping coefficient of control area, $\frac{T_{pi}}{K_{pi}} = M_i$ is equivalent inertia constant of control area, T_{ij} is tie-line power coefficient between *i*th area and *j*th area. T_{gi} is time constants of governor, T_{ti} is steam turbine time constant, T_{pi} is power system time constant, respectively. K_{pi}, R_i, K_{Ei}, K_{Bi} are power system gain, droop coefficient of individual area, speed regulation coefficient and frequency bias factor. Therefore, the state space modeling of *i*th area of the matrix form showing in the dynamic equations from (1) to (5) is given by (6):

$$\dot{x}_i(t) = A_i x_i(t) + B_i u_i(t) + \sum_{\substack{j=1 \\ j\neq i}}^{N} H_{ij}x_j(t) + F_i\Delta P_{di}(t) \tag{6}$$

where,

$$x_i(t) = \begin{bmatrix} \Delta f_i(t) & \Delta P_{ti}(t) & \Delta P_{gi}(t) & \Delta E_i(t) & \Delta P_{tie}^{ij}(t) \end{bmatrix}^T$$

$$A_i = \begin{bmatrix} -\frac{1}{T_{pi}} & \frac{K_{pi}}{T_{pi}} & 0 & 0 & -\frac{K_{pi}}{T_{pi}} \\ 0 & -\frac{1}{T_{ti}} & \frac{1}{T_{ti}} & 0 & 0 \\ -\frac{1}{R_i T_{pi}} & 0 & -\frac{1}{T_{gi}} & 0 & 0 \\ K_{Bi}K_{Ei} & 0 & 0 & 0 & K_{Ei} \\ \sum\limits_{\substack{j=1 \\ j\neq i}}^{N} 2\pi T_{ij} & 0 & 0 & 0 & 0 \end{bmatrix}, H_{ij} = \begin{bmatrix} 0 & 0 & 0 & 0 & 0 \\ 0 & 0 & 0 & 0 & 0 \\ 0 & 0 & 0 & 0 & 0 \\ 0 & 0 & 0 & 0 & 0 \\ \sum\limits_{\substack{j=1 \\ j\neq i}}^{N} 2\pi T_{ij} & 0 & 0 & 0 & 0 \end{bmatrix}$$

$$B_i = \begin{bmatrix} 0 & 0 & \frac{1}{T_{gi}} & 0 & 0 \end{bmatrix}^T, F_i = \begin{bmatrix} -\frac{K_{pi}}{T_{pi}} & 0 & 0 & 0 & 0 \end{bmatrix}^T$$

and $x_i(t) \in R^{n_i}$ is the state vector, $x_j(t) \in R^{n_j}$ is the neighboring state vector of $x_i(t)$, $u_i(t) \in R^{m_i}$ is the control vector, $A_i \in R^{n_i \times n_i}$, $B_i \in R^{n_i \times m_i}$, $F_i \in R^{n_i \times k_i}$ are matrices of the nominal parameters, n_i is the number of state variables of ith area, m_i is the number of control input variables of ith area.

In a practical power network, the operation point varies constantly and is induced by load disturbance and fluctuating resources. Considering the uncertainties and parameter variations, the power system model can also be described as

$$\begin{aligned} \dot{x}_i(t) = {} & [A_i + \Theta_i(x_i, t)]x_i(t) + B_i[u_i(t) + \xi_i(x_i, t)] \\ & + \sum_{\substack{j=1 \\ j\neq i}}^{N} [H_{ij} + \Xi_{ij}(x_j, t)]x_j(t) + F_i \Delta P_{di}(t) \end{aligned} \tag{7}$$

where $\Theta_i(x_i, t)$ is time varying parameter uncertainties in the state matrix, $\Xi_{ij}(x_j, t)$ is time varying parameter uncertainties in the interconnected matrix and $\xi_i(x_i, t)$ is the disturbance input. Furthermore, we can call the aggregated uncertainties and the number of areas is 1 to N:

$$L_i(x_i, t) = \Theta_i(x_i, t)x_i(t) + B_i \xi_i(x_i, t) + \sum_{\substack{j=1 \\ j\neq i}}^{N} \Xi_{ij}(x_j, t)x_j(t) + F_i \Delta P_{di}(t) \tag{8}$$

So, the dynamic model (6) can also be presented by:

$$\dot{x}_i(t) = A_i x_i(t) + B_i u_i(t) + \sum_{\substack{j=1 \\ j\neq i}}^{N} H_{ij} x_j(t) + L_i(x_i, t) \tag{9}$$

where the aggregated disturbance $L_i(x_i, t)$ represents the uncertainties with the matched part and mismatched part.

Assumption 1. *It is assumed that aggregateddisturbance $L_i(x_i, t)$ and the differential of $L_i(x_i, t)$ arebounded,i.e., there exist known scalars γ_i and $\overline{\gamma}_i$ such that $\|L_i(x_i, t)\| \leq \gamma_i$ and $\|\dot{L}_i(x_i, t)\| \leq \overline{\gamma}_i$, where $\|.\|$ is the matrix norm.*

In order to prove the stability, we recall the lemma as below:

Lemma 1. **[34].** *Let* $\mathbf{X}$ *and* $\mathbf{Y}$ *are actual matrices with appropriate dimension then, for any scalar$\mu > 0$, the sequent matrix inequality obtains*

$$\mathbf{X}^{\mathbf{T}}\mathbf{Y} + \mathbf{Y}^{\mathbf{T}}\mathbf{X} \leq \mu \mathbf{X}^{\mathbf{T}}\mathbf{X} + \mu^{-1}\mathbf{Y}^{\mathbf{T}}\mathbf{Y}. \tag{10}$$

3. A New Second Order Sliding Mode Load Frequency Control Design

In this section, a new SOISMC method is suggested and developed for power networks with parametric uncertainties and disturbances. To solve this problem, we work step-by-step to design and implement the new proposed controller approach. Firstly, the integral sliding surface is represented for the multi-area power system to assure that whole power networks are asymptotically stable. Secondly, the second-order SMC law design based on Lyapunov stability theorem is introduced to prove that the system states reach the sliding manifold, and the system states stay on the sliding manifold thereafter under external disturbances and internal parameter uncertainties.

3.1. Stability Analysis of the Multi-Area Power Network in Sliding Mode Dynamics

In detail, we first begin to propose and build an integral sliding surface for an interconnected multi-area power network (9)

$$\sigma_i[x_i(t)] = G_i x_i(t) - \int_0^t G_i(A_i - B_i K_i)x_i(\tau)d\tau \tag{11}$$

where G_i is constant matrix and K_i is the design matrix, matrix G_i is chosen to guarantee that matrix $G_i\,B_i$ is nonsingular. The design matrix $K_i \in R^{m_i \times n_i}$ is selected to satisfy the inequality condition of the power system.

$$\mathrm{Re}[\lambda_{\max}(A_i - B_i K_i)] < 0 \tag{12}$$

If we recognize and differentiate $\sigma_i[x_i(t)]$ with respect to time combined with (9), then

$$\dot{\sigma}_i[x_i(t)] = G_i[A_i x_i(t) + B_i u_i(t) + \sum_{\substack{j=1 \\ j\neq i}}^{N} H_{ij}x_j(t) + L_i(x_i,t) - G_i(A_i - B_i K_i)x_i(t)] \tag{13}$$

So, the setting $\sigma_i[x_i(t)] = \dot{\sigma}_i[x_i(t)] = 0$, the equivalent control is rewritten by

$$u_i^{eq}(t) = -(G_i B_i)^{-1}[G_i A_i x_i(t) + \sum_{\substack{j=1 \\ j\neq i}}^{N} G_i H_{ij}x_j(t) + G_i L_i(x_i,t) - G_i(A_i - B_i K_i)x_i(t)] \tag{14}$$

Substituting $u_i(t)$ with $u_i^{eq}(t)$ into the power systems (9) yields the sliding motion.

$$\dot{x}_i(t) = (A_i - B_i K_i)x_i(t) + [I_i - B_i(G_i B_i)^{-1}G_i]L_i(x_i,t) + \sum_{\substack{j=1 \\ j\neq i}}^{N} [I_i - B_i(G_i B_i)^{-1}G_i]H_{ij}x_j(t) \tag{15}$$

The following theorem makes a condition that the second-order sliding mode dynamic Equation (13) is asymptotically stable.

Theorem 1. *The sliding motion (15) is asymptotically stable if and only if there includes symmetric positive definite matrix* P_i *,* $i = 1, 2, \ldots, N$ *, and positive scalars* $\hat{\varepsilon}_i$ *and* α_j *such that the following LMIs obtains*

$$\begin{bmatrix} (A_i - B_iK_i)^T P_i + P_i(A_i - B_iK_i) + \sum\limits_{\substack{j=1 \\ j\neq i}}^{N} \alpha_j^{-1} H_{ji}^T H_{ji} & P_i[I_i - B_i(G_iB_i)^{-1}G_i] \\ [I_i - B_i(G_iB_i)^{-1}G_i]^T P_i & -\hat{\varepsilon}_i^{-1} \end{bmatrix} < 0 \tag{16}$$

Proof 1. To study and analyze stability of the sliding motion (15), we choose the Lyapunov function as follows:

$$V = \sum_{i}^{N} x_i^T(t) P_i x_i(t) \tag{17}$$

where $P_i > 0$ satisfies (17) Then, taking the time derivative of (17) and using Equation (15), we have

$$\begin{aligned} \dot{V} &= \sum_{i=1}^{N} \dot{x}_i^T(t) P_i x_i(t) + x_i^T(t) P_i \dot{x}_i(t) \\ &= \sum_{i=1}^{N} \{x_i^T(t)[(A_i - B_iK_i)^T P_i + P_i(A_i - B_iK_i)]x_i(t) + \sum_{\substack{j=1 \\ j\neq i}}^{N} x_j^T(t) H_{ij}^T [I_i - B_i(G_iB_i)^{-1}G_i]^T P_i x_i(t) \\ &+ \sum_{\substack{j=1 \\ j\neq i}}^{N} x_i^T(t) P_i [I_i - B_i(G_iB_i)^{-1}G_i] H_{ij} x_j(t) + x_i^T(t) P_i [I_i - B_i(G_iB_i)^{-1}G_i] L_i(x_i, t) \\ &+ L_i^T(x_i, t)[I_i - B_i(G_iB_i)^{-1}G_i] T P_i x_i(t)\} \end{aligned} \tag{18}$$

Applying Lemma 1 to Equation (18), we have:

$$\begin{aligned} \dot{V} \leq &\sum_{i=1}^{N} \{x_i^T(t)[(A_i - B_iK_i)^T P_i + P_i(A_i - B_iK_i)]x_i(t) \sum_{\substack{j=1 \\ j\neq i}}^{N} x_i^T(t) \alpha_i^{-1} H_{iJ}^T H_{ij} x_j \\ &+ \sum_{\substack{j=1 \\ j\neq i}}^{N} x_i^T(t) \alpha_i P_i [I_i - B_i(G_iB_i)^{-1}G_i][I_i - B_i(G_iB_i)^{-1}G_i]^T P_i x_i(t) \\ &+ x_i^T(t) \beta_i P_i [I_i - B_i(G_iB_i)^{-1}G_i][I_i - B_i(G_iB_i)^{-1}G_i]^T P_i x_i(t) + \beta_i^{-1} L_i^T(x_i, t) L_i(x_i, t)\} \end{aligned} \tag{19}$$

Since $\sum\limits_{i=1}^{N} \sum\limits_{\substack{j=1 \\ j\neq i}}^{N} x_j^T(t) \alpha_i^{-1} H_{ij}^T H_{ij} x_j(t) = \sum\limits_{i=1}^{N} \sum\limits_{\substack{j=1 \\ j\neq i}}^{N} x_i^T(t) \alpha_j^{-1} H_{ji}^T H_{ji} x_i(t)$ we achieve that:

$$\begin{aligned} \dot{V} \leq &\sum_{i=1}^{N} \Big\{ x_i^T(t)[(A_i - B_iK_i)^T P_i + P_i(A_i - B_iK_i) + \hat{\varepsilon}_i P_i [I_i - B_i(G_iB_i)^{-1}G_i][I_i - B_i(G_iB_i)^{-1}G_i]^T P_i \\ &+ \sum_{\substack{j=1 \\ j\neq i}}^{N} \alpha_j^{-1} H_{ji}^T H_{ji}] x_i(t) + \sum_{i=1}^{N} \mu_i \end{aligned} \tag{20}$$

where $\hat{\varepsilon}_i = \alpha_i(N-1) + \beta_i$ and $\mu_i = \beta_i^{-1}\gamma_i^2$. In addition, by the Schur complement of [35], LMIs (20) is equivalent to this inequality:

$$(A_i - B_iK_i)^T P_i + P_i(A_i - B_iK_i) + \varepsilon_i P_i[I_i - B_i(G_iB_i)^{-1}G_i][I_i - B_i(G_iB_i)^{-1}G_i]^T P_i + \sum_{\substack{j=1 \\ j\neq i}}^{N} \alpha_j^{-1} H_{ji}^T H_{ji} = -\Omega_i < 0 \quad (21)$$

According to Equations (20) and (21), we obtain

$$\dot{V} \le \sum_{i=1}^{N} [-\lambda_{\min}(\Omega_i)\|x_i(t)\|^2 + \mu_i] \quad (22)$$

where the constant value μ_i and the eigenvalue $\lambda_{\min}(\Omega_i) > 0$. Therefore, $\dot{V} < 0$ is achieved with $\|x_i(t)\| > \sqrt{\frac{\mu_i}{\lambda_{\min}(\Omega_i)}}$. Hence, the sliding motion of system (15) is asymptotically stable. □

3.2. Load Frequency Controller Design

In the previous step, we introduce and prove that power networks with an integral sliding surface (ISS) work to be asymptotically stable and smooth in the sliding mode under assured conditions. In the next step, a new SOISMC scheme is presented for the multi-area interconnected power network to eliminate chattering and oscillating in the ISS. The main purpose of proposed control scheme is to effect on the second order derivative of the sliding variables $\sigma_i[x_i(t)]$. By using the discontinuous control signal $\dot{u}_i(t)$, it is simple to make $\sigma_i[x_i(t)]$ and $\dot{\sigma}_i[x_i(t)]$ converge to zero. So, the input control signal $u_i(t)$ of power systems can be obtained by integrating the discontinuous signal $\dot{u}_i(t)$ to make continuous signal $u_i(t)$. Therefore, the second-order SMC approach removes some undesired frequency oscillations in the control signal of power system.

We define and establish the sliding manifold $S_i[x_i(t)]$ as

$$S_i[x_i(t)] = \dot{\sigma}_i[x_i(t)] + \delta_i\sigma_i[x_i(t)] \quad (23)$$

and

$$\dot{S}_i[x_i(t)] = \ddot{\sigma}_i[x_i(t)] + \delta_i\dot{\sigma}_i[x_i(t)] \quad (24)$$

where $\delta_i > 0$ is a positive constant. According to Equation (9), the Equation (24) can be rewritten as

$$\begin{aligned} \dot{S}_i[x_i(t)] = G_i[A_i\dot{x}_i(t) + B_i\dot{u}_i(t) + \sum_{\substack{j=1 \\ j\neq i}}^{N} H_{ij}\dot{x}_j(t) + \dot{L}_i(x_i,t)] \\ -G_i(A_i - B_iK_i)\dot{x}_i(t) + \delta_i\dot{\sigma}_i[x_i(t)] \end{aligned} \quad (25)$$

Based on the definition of sliding surface and sliding manifold, the continuous decentralized second-order sliding mode LFC for power networks be given as follows:

$$\dot{u}_i(t) = -(G_iB_i)^{-1}[\|G_i\|\|B_i\|\|K_i\|\|\dot{x}_i(t)\| + \sum_{\substack{j=1 \\ j\neq i}}^{N} \|G_j\|\|H_{ji}\|\|\dot{x}_i(t)\| + \delta_i\|\dot{\sigma}_i[x_i(t)]\| + \|G_i\|\overline{\gamma}_i + \overline{\varepsilon}]\frac{S_i[x_i(t)]}{\|S_i[x_i(t)]\|} \quad (26)$$

Then we have the following main results.

Theorem 2. *Consider the closed loop of the power systems* (15) *with the continuous sliding mode controller* (26). *Then, every solution trajectory is directed towards the sliding manifold* $S_i[x_i(t)] = 0$ *and once the trajectory hits the sliding manifold* $S_i[x_i(t)] = 0$ *it remains on the sliding manifold thereafter.*

Proof 2. The Lyapunov function is introduced as below

$$\overline{V}(t) = \sum_{i=1}^{N} \left\| S_i[x_i(t)] \right\| \tag{27}$$

So, taking the derivative of $\overline{V}(t)$ that we have:

$$\begin{aligned}\dot{\overline{V}} &= \sum_{i=1}^{N} \frac{S_i^T[x_i(t)]}{\|S_i[x_i(t)]\|} \dot{S}_i[x_i(t)] \\ &= \sum_{i=1}^{N} \frac{S_i^T[x_i(t)]}{\|S_i[x_i(t)]\|} \{G_i[A_i \dot{x}_i(t) + B_i \dot{u}_i(t) + \sum_{\substack{j=1 \\ j \neq i}}^{N} H_{ij} \dot{x}_j(t) + \dot{L}_i(x_i,t)] \\ &\quad - G_i(A_i - B_i K_i) \dot{x}_i(t) + \delta_i \dot{\sigma}_i[x_i(t)]\}\end{aligned} \tag{28}$$

According to Equation (24) and property $\|AB\| \le \|A\|\|B\|$, it generates

$$\begin{aligned}\dot{\overline{V}} &= \sum_{i=1}^{N} \{G_i B_i K_i \dot{x}_i(t) + \delta_i \dot{\sigma}_i[x_i(t)] + \sum_{\substack{j=1 \\ j \neq i}}^{N} G_i H_{ij} \dot{x}_j(t) + G_i \dot{L}_i(x_i,t)\} + \sum_{i=1}^{N} \frac{S_i^T[x_i(t)]}{\|S_i[x_i(t)]\|} G_i B_i \dot{u}_i(t) \\ &\le \sum_{i=1}^{N} \{\|G_i\|\|B_i\|\|K_i\| \left\| \dot{x}_i(t) \right\| + \delta_i \left\| \dot{\sigma}_i[x_i(t)] \right\| + \sum_{\substack{j=1 \\ j \neq i}}^{N} \|G_i\| \left\| H_{ij} \right\| \left\| \dot{x}_j(t) \right\| + \|G_i\| \left\| \dot{L}_i(x_i,t) \right\| \} \\ &\quad + \sum_{i=1}^{N} \frac{S_i^T[x_i(t)]}{\|S_i[x_i(t)]\|} G_i B_i \dot{u}_i(t)\end{aligned} \tag{29}$$

Using Assumption 1 we achieve:

$$\begin{aligned}\dot{\overline{V}} &\le \sum_{i=1}^{N} \{\|G_i\|\|B_i\|\|K_i\| \left\| \dot{x}_i(t) \right\| + \delta_i \left\| \dot{\sigma}_i[x_i(t)] \right\| + \|G_i\| \overline{\gamma}_i + \sum_{\substack{j=1 \\ j \neq i}}^{N} \left\| G_j \right\| \left\| H_{ji} \right\| \left\| \dot{x}_i(t) \right\| \} \\ &\quad + \sum_{i=1}^{N} \frac{S_i^T[x_i(t)]}{\|S_i[x_i(t)]\|} G_i B_i \dot{u}_i(t)\end{aligned} \tag{30}$$

Using the control law (24) yields:

$$\dot{\overline{V}} \le -\sum_{i=1}^{N} \overline{\varepsilon}_i \tag{31}$$

The above inequality implies that the state trajectories of the multi-area power system (8) reach the sliding manifold $S_i[x_i(t)] = 0$ and stay on it thereafter. □

4. Simulation Results

To analysis and evaluate the new SOISMC approach for LFC in the two-area power network, the system parameters were obtained in [10,26,33]. The reporting of simulation 1, simulation 2 and simulation 3 are discussed with their different conditions in operation as follows:

4.1. Simulation 1

A typical two-area conventional power network is considered. The proposed controller is tested and analyzed in the system to explain the robustness and effectiveness as suggested for second order integral sliding mode controller. The parameters of both control areas in power systems were given in [10] as shown in Table 1.

Table 1. The parameters of both control areas in power systems.

Parameter	T_{pi}[s]	K_{pi}[Hz/p.u.MW]	T_{ti}[s]	T_{gi}[s]	R_i[Hz/p.u.MW]	T_{12} [Hz/p.u.MW/rad]
Value for both areas	20 s	12	0.3	0.08	2.4	0.2545

Case 1. At first, we assume that the system parameters are at nominal values. The load disturbances acting on the system are $\Delta P_{d1} = 0.01$ p.u. at $t_1 = 5$ s in area 1 and $\Delta P_{d2} = 0.03$ p.u. at $t_2 = 3$ s in area 2 of power system. The frequency deviation of both area 1Δf_1 and area 2 Δf_2, tie-line power deviation ΔP_{tie1}, ΔP_{tie2} and the control input of area 1 u_1 and area 2 u_2 are shown in Figures 2–4. Additionally, the settling time for the frequency deviation to converge to zero is about 3 s, which shows rapid response time to clear the disturbance as compared to 20–25 s response time given in [10]. It is easy to say that the proposed SOISMC creates a good dynamic response. Above all, the second-order law is used by the proposed controller to reduce overshoot and oscillation as well as the re-equipment of the system responses. The simulation results of Figures 2–4 demonstrate the superiority of removing the chattering problem in finite frequency and verifying the usefulness of the proposed second-order integral sliding mode control law.

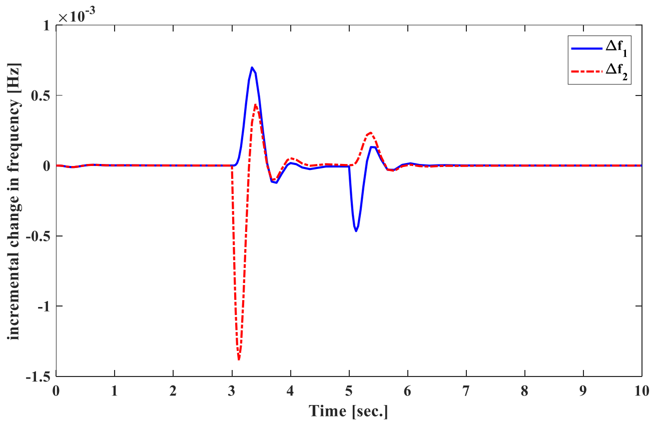

Figure 2. Frequency deviations [Hz] of the control areas 1 and 2 with matched disturbances.

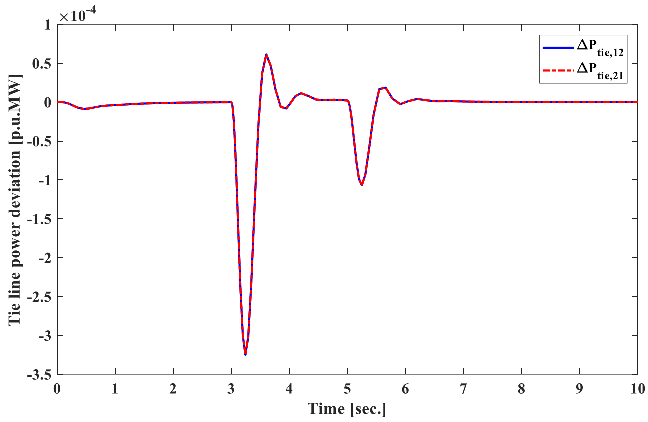

Figure 3. Tie line power deviation [p.u.MW] with matched disturbances.

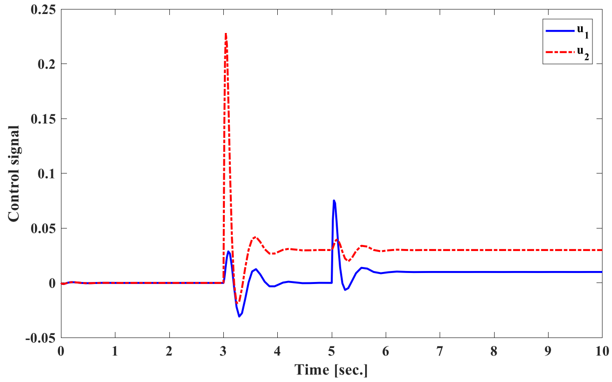

Figure 4. Control input [p.u.] of two control areas with matched disturbances.

Remark 1. *The new proposed controller shows robustness and fast response against load disturbance better than previous approaches as seen in* [10]. *In detail, the load disturbance is clear, and the system is restored back to steady state at short settling time with smaller overshoots.*

Case 2. To apply and carry out the proposed SOISMC scheme to the model of the power system in Figure 1, we consider the parameters of mismatched uncertainties in this case and the random load variations are used to test the suggested controller. To further validate the robustness of the proposed controller, random load disturbances show in Figure 5 and parameter nominal values with ±20% deviation are introduced to the system. The results of Figure 6 show the proposed controller response to deviations in frequency of the first and second areas, respectively, while Figure 7 presents the tie-line power flow signal. Figure 8 displays the control signals in both areas.

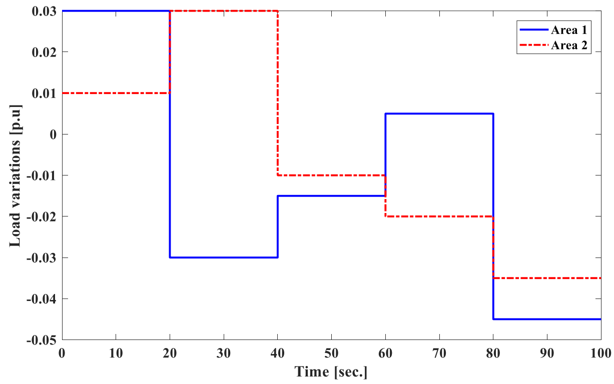

Figure 5. Variation load [p.u.] of areas 1 and 2 of the power system.

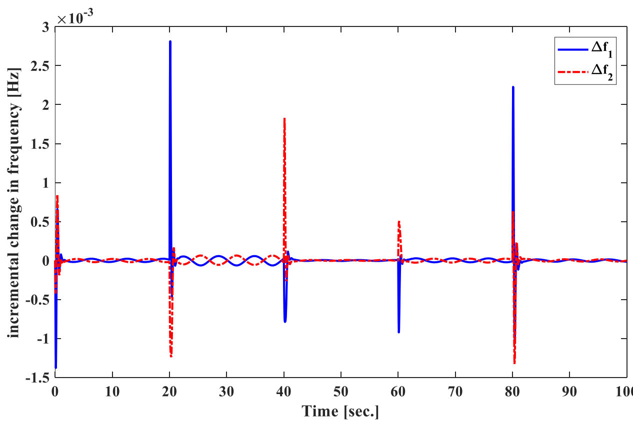

Figure 6. Frequency deviations [Hz] of the control areas 1 and 2 with matched disturbances.

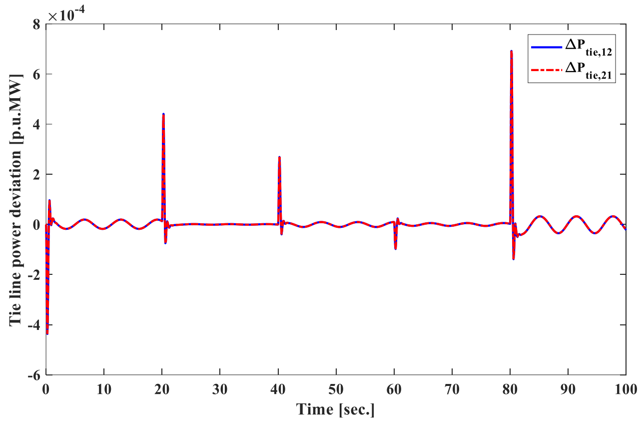

Figure 7. Tie line power deviation [p.u.MW] with matched disturbances.

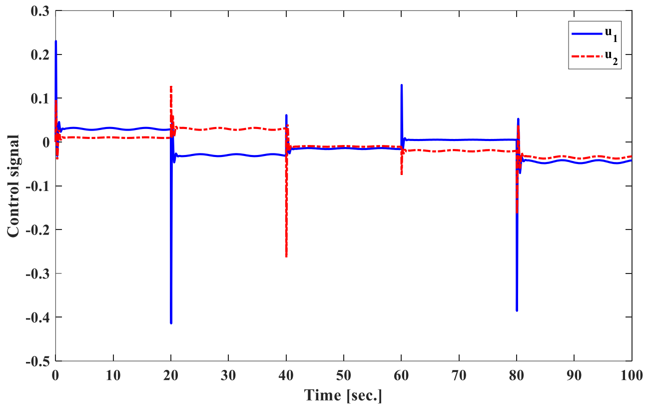

Figure 8. Control input [p.u.] of two control areas with matched disturbances.

4.2. Simulation 2

In this part, three cases are examined. The power system parameters of the two-area power network were given in [26] as shown Table 2.

Table 2. Parameters of load frequency control scheme.

Parameter	T_{pi}[s]	K_{pi} [Hz/p.u.MW]	T_{ti}[s]	T_{gi} [s]	[Hz/p.u.MW]	T_{12}[Hz/p.u.MW/rad]
Value for both areas	20	120	0.3	0.08	2.4	0.5450

Case 1. To proceed, we again assume the system operate under nominal parameters. Load disturbances perturbing on the system are $\Delta P_{d1} = 0.01$ p.u at $t_1 = 1$ s in area 1 and $\Delta P_{d2} = 0.02$ p.u. at $t_2 = 1$ s in area 2 of power network. Figure 9 displays the signal of frequency deviation of control area 1 and 2, at the time $t = 1$ s, the step load disturbances in both areas is significantly increased, then the proposed controller receives the error signal of frequency from sensor and controls the frequency deviation to converge zero about 3 s. The tie-line power flow signal of each area is also represented in Figure 10. Control signals of both areas are shown in Figure 11 without chattering and small control energy. So, a new scheme called SOISMC law has been showed in the simulation results from Figures 9–11 to indicate that the power system carries a good transient response to decrease and avoid the chattering problem. It is easy to conclude that the errors of frequency, errors of tie-line power and, even errors of control area can reach to zero at short time compared with previous control approach given in [26].

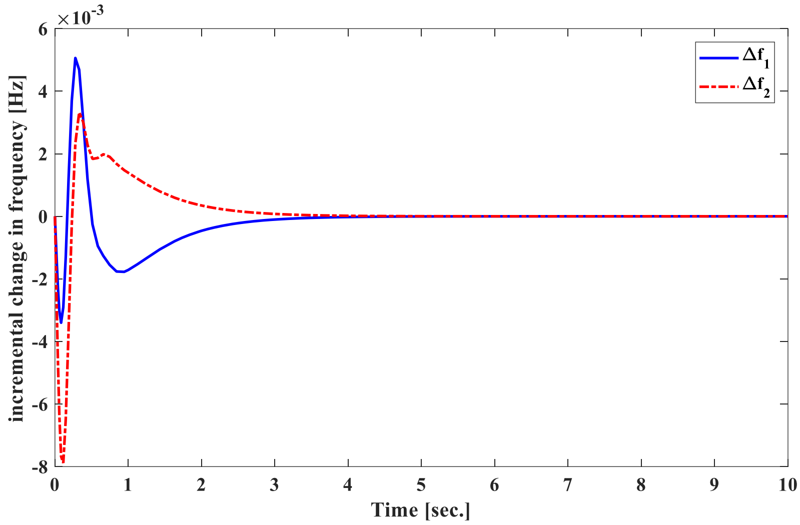

Figure 9. Frequency deviation [Hz] of control areas 1 and 2 with matched disturbances.

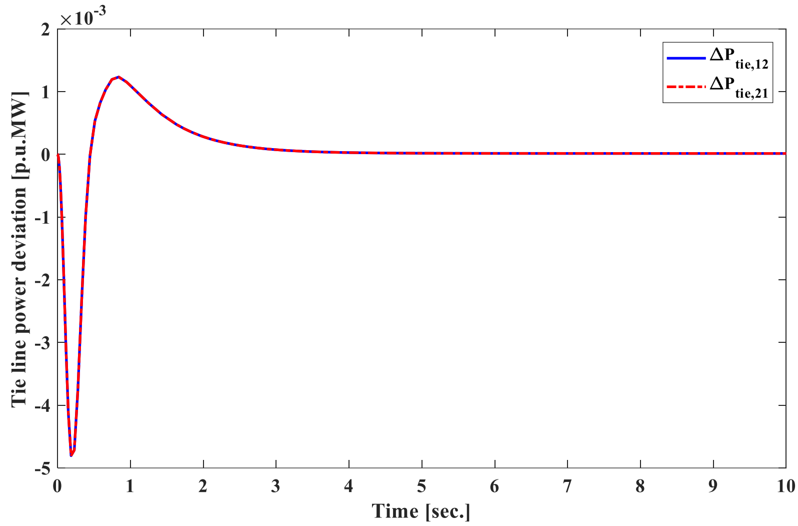

Figure 10. Tie-line power deviation [p.u.MW] of control areas 1 and 2 with matched disturbances.

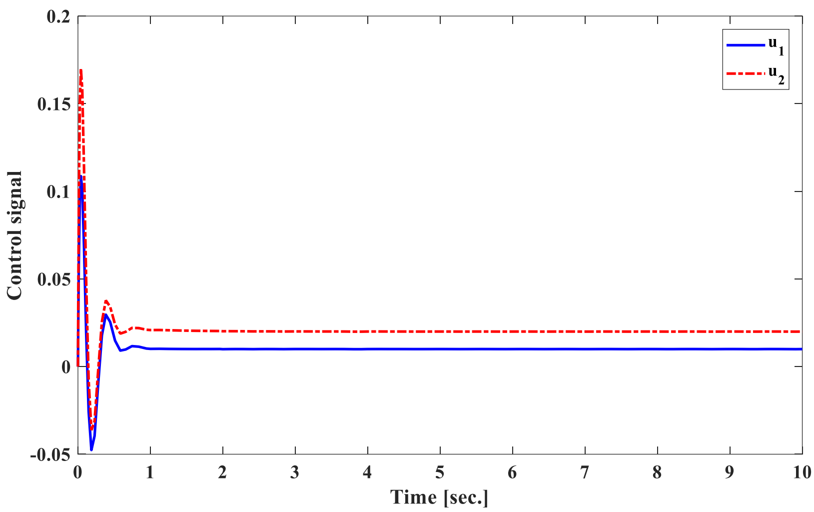

Figure 11. Control input [p.u.] of two control areas with matched disturbances.

Case 2. In the previous cases, an interconnected multi-area power network works excellently under the parameters of matched and mismatched uncertainties. To analyze and investigate in different condition, ±20% deviation of the nominal parameters is again assume and load disturbance $\Delta P_{d1} = 0.02$ p.u at $t_1 = 1$ s in area 1 and the load disturbance $\Delta P_{d2} = 0.03$ p.u at $t_2 = 1$ s in area 2 to implement and examine the powerful system response of the designed SOISMC approach.

In the second case, the system responses in the frequencies of generator and the changes of tie-line power to the load demand are considered to apply for the new approach. The results are shown in Figure 12 for frequency deviation, Figure 13 for tie-line power deviation, and Figure 14 for control input signal. Figure 12 presents the frequency deviate of generators to point out that the proposed second order approach helps the power system reach to ordinary value about 5–6 s after load disturbances happen in the system. The scheduled value of tie-line power deviation is indicated in Figure 13. The comparative results between the suggested SOISMC approach and the previous method given in [26] show that the proposed method in Table 3 achieves a good transient response, such as smaller transient deviation and shorter settling time in terms of load disturbances.

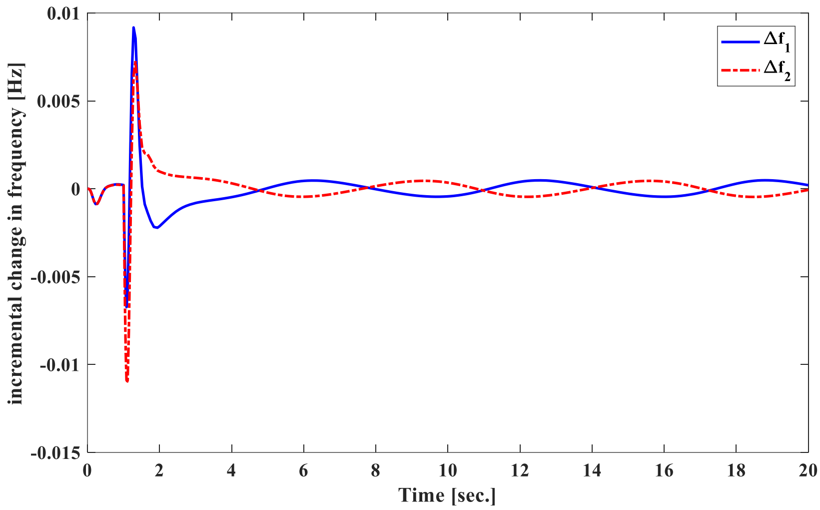

Figure 12. Frequency [Hz] of control area 1 and area 2 under mismatched disturbances.

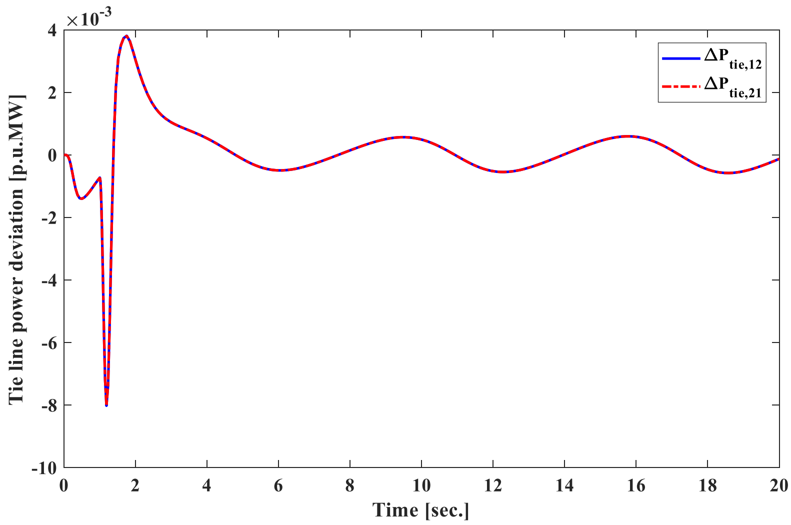

Figure 13. Tie-line power [p.u.MW] of control areas 1 and area 2 under mismatched disturbances.

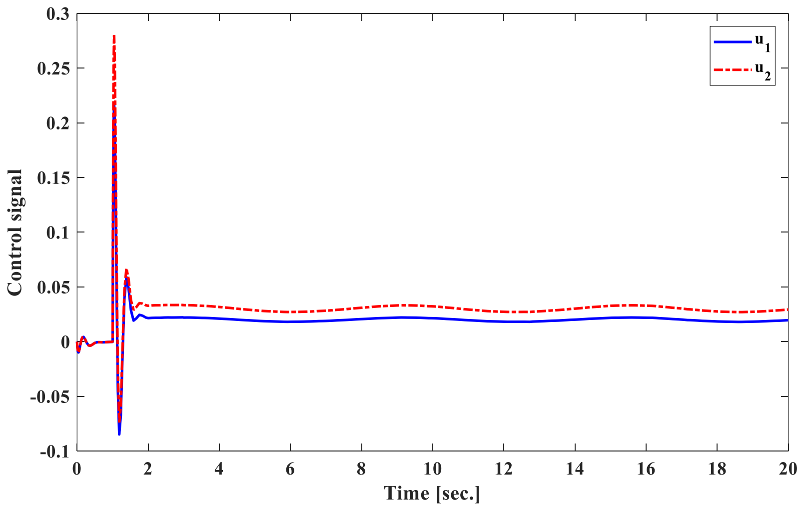

Figure 14. Control input [p.u.] of two control areas under mismatched disturbances.

Table 3. Setting time T_s and Maximum over shoot calculation of SOISMC and different SMC method.

Kinds of Controller	The Proposed SOISMC Approach		Different Sliding Mode Control Scheme For LFC	
Parameters	T_s[s]	**Max.O.S** [Hz]	T_s[s]	**Max.O.S** [Hz]
Δf_1	5	0.0090	105	0.0200
Δf_2	6	0.0070	110	0.0150

In the detailed analysis, it is simple to see in Figures 12 and 13 that the suggested control approach not only executes faster disturbance estimation but also makes a faster convergence rate and smaller oscillatory system response in chattering alleviation effect in comparison with the previous scheme in [26]. In both control areas, the incremental change in actual tie line power flow from control area-1 to 2 and control input effort are necessary to make the frequency droop down fast using proposed controller are shown in Figures 13 and 14. The incremental change in actual tie-line flow indicates inappreciable oscillatory transient response. Particularly, the proposed SOISMC controller enhances the characteristic of system damping. It was realized that the chattering effects are totally removed to deal to fact that the proposed second switching law is the principle of the effectiveness of the transient response. Thus, the proposed control approach performs well compared to [26] in the presence of the changed load disturbances.

Remark 2. *This chattering problem in SMC is exceedingly damaging for actuators used in power systems. The proposed controller gives the correct signal and utilizes energy to compensate for frequency damping for main control consisting of governor. So that, the droop speed control of the governor will correctly actuate the valve to provide needed steam to the turbine to increase mechanical inertia power to match the load change or demand. Therefore, the setting time and overshoot are better in comparison with the proposed approach given in* [26].

Remark 3. *In this proposed approach, it is one of the most achievable objectives to finalize the mismatched disturbances and get shorter settling time and smaller transient deviation and lesser oscillation in terms of load disturbances for power system by the application of the second order control law. Therefore, some limitations of other control strategies in paper* [26] *have been resolved, such as reducing chattering effect and improving transient response.*

Case 3. In the last case, we use and study load variations and the mismatched parameter uncertainties in the two-areas power system. We apply the random load to power networks under the same condition of case 2.

To prove the advantage of the proposed SOISMC approach, a random load variation is given in Figure 15 applied for two-area power networks. The simulation report displays from Figures 16–18 of the frequency deviations, tie-line power and control input signal to clearly present the performances of waveform for the different situations in the case of load variations and the mismatched parameter uncertainties. Therefore, that is a practical evidence of the suggested control scheme is powerful to limit and reduce the chattering phenomenon of power system. The other words, the suggested controller upgrades the characteristics of damping system. Consequently, the suggested controllers reach the nominal frequency and are reduced to zero in the exchange deviation of tie-line power with a good dynamic response of minimizing overshoots and shortening settling time comparing with the previous scheme in [26].

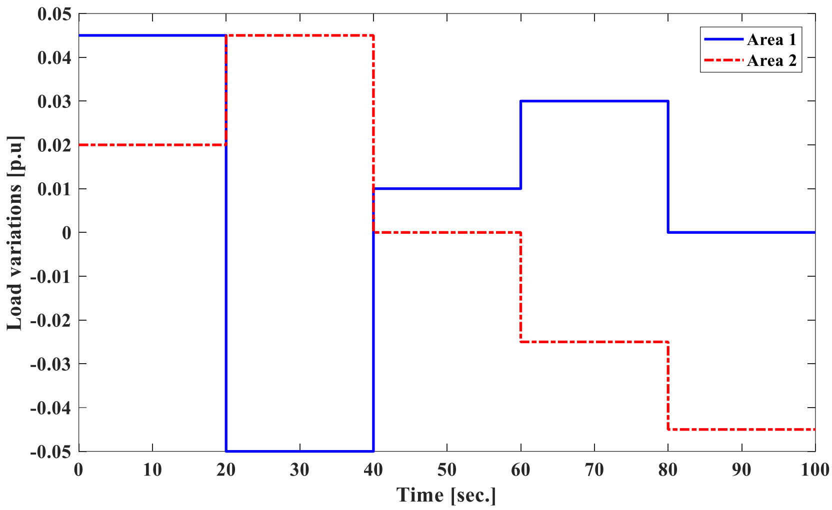

Figure 15. Variation load [p.u.] of areas 1 and 2 of the power system.

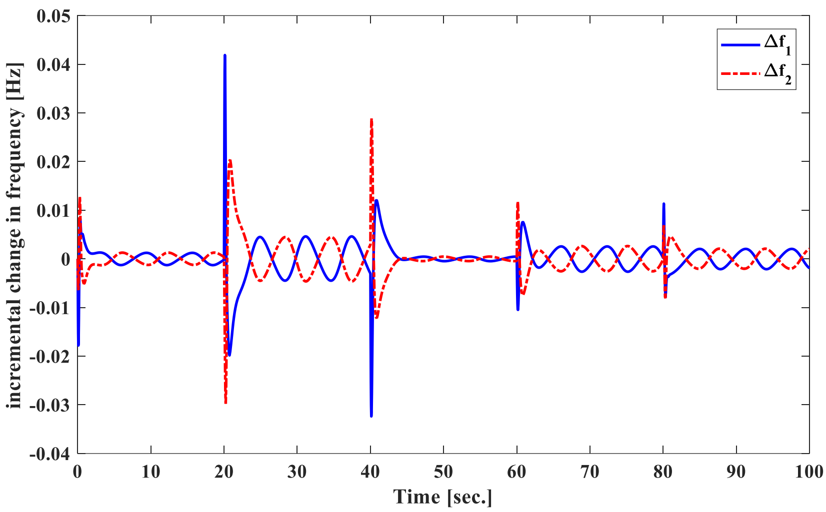

Figure 16. Frequency [Hz] of both control under load variations and the mismatched parameter uncertainties.

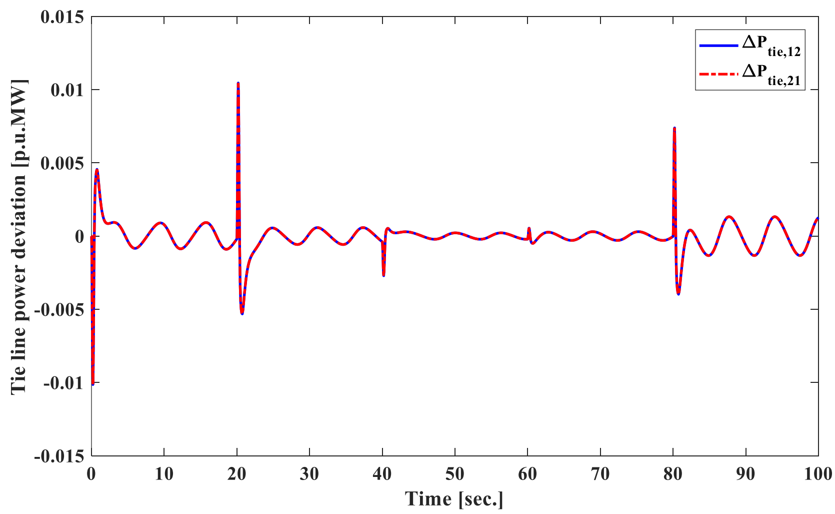

Figure 17. Tie-line power [p.u.MW] under load variations and the mismatched parameter uncertainties.

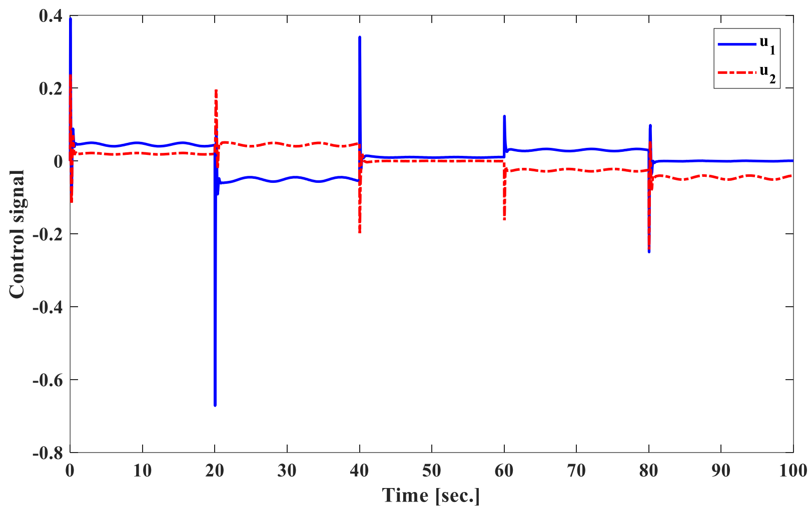

Figure 18. Control input [p.u.] under load variations and the mismatched parameter uncertainties.

Remark 4. By *reporting of two simulation results above, the new second order variable structure control approach achieves affective response performance under various conditions such as the matched or mismatched uncertainties and load variations appearing in power networks. The suggested control scheme is applied and developed to remove and eliminate load disturbance in power system, restore the nominal point of system performance, and subtract the influence of load disturbances. This SOISMC is proved that have a good strategy to avoid chattering problem in SMC and achieve nominal system performance recovery.*

4.3. Simulation 3

In this simulation, the aim is to compare with [33] to determine the validation of the proposed SOISMC. Therefore, the parameter of the system is obtained therein. A step load disturbance is set as 0.01 p.u. at t = 0 s in the first power control area follow by a step load disturbance is set as 0.01 p.u. at t = 0 s in the second area and the uncertain parameters in the two-area benchmark system are assumed to vary within 15% of their nominal values. The performance of proposed SOISMC is investigated to compare with a novel adaptive sliding mode control method give in [33]. From the simulation report, Figures 19–22 confirm the validity of the proposed approach in terms of external disturbances and parameter changes. The increased load demand is 1% of the nominal values used in power system, the frequency deviates as shown by the under/overshoot in Figures 19 and 20 and restores the resisting nominal value in about 4.5 s.

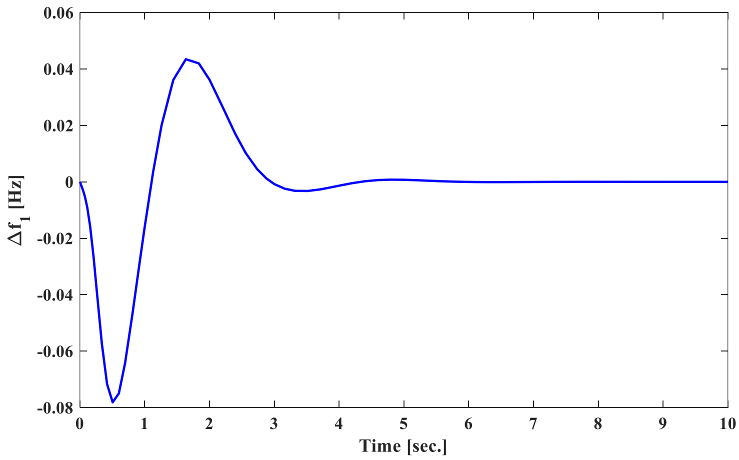

Figure 19. Frequency [Hz] of control area 1 under matched disturbances.

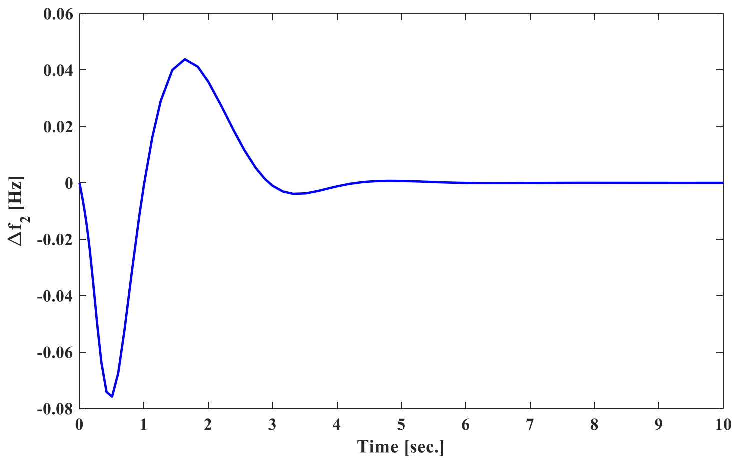

Figure 20. Frequency [Hz] of control area 1 under matched disturbances.

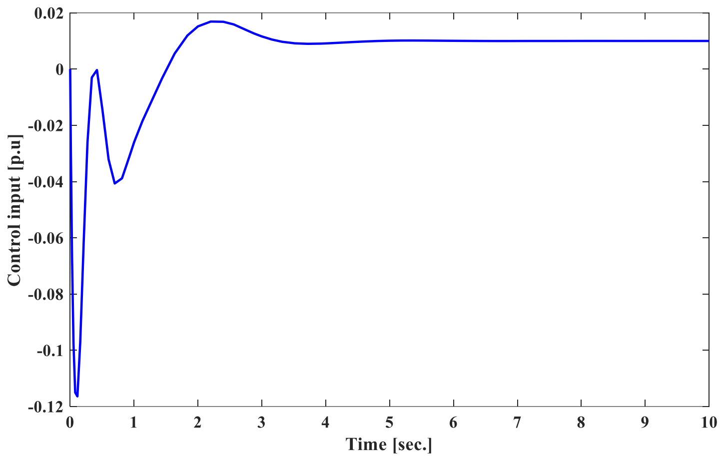

Figure 21. Control input [p.u.] of the first control area under matched disturbances.

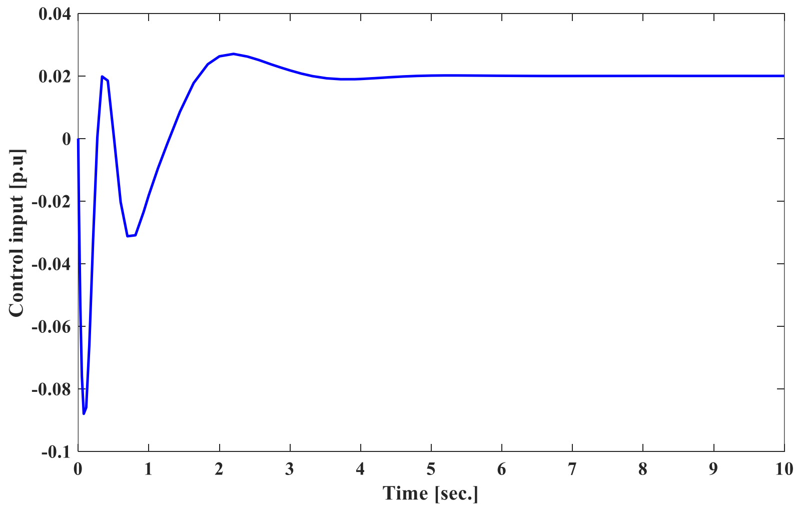

Figure 22. Control input [p.u.] of the second control area under matched disturbances.

Remark 5. *In actuality, the parameter uncertainties always exist due to wearing out of components or variation of operating points. In the simulation 3, we study the LFC problem of the power network with load changes and parameter uncertainties, with the help of the proposed SOISMC, the frequencies of all areas return to the normal value in about 4.5 s after load disturbances occur. Therefore, the superiority of the proposed SOISMC in terms of chattering, overshoot and response time in comparison with the proposed adaptive sliding mode control method is also verified.*

5. Conclusions

In conclusion, a new SOISMC scheme is introduced and proposed to build the controller to resolve and balance the active power of an interconnected multi-area power system. The suggested approach not only assured the stability of power networks but also considerably decreased the chattering problem in the power systems. An integral sliding surface-based second-order SMC is presented to ensure shortens the transient response of frequency, reduce the high overshoot and work out the priority problem of active power balance. The performance of an interconnected multi-area power system is proved in the solution of removing the chattering problem in comparison with the previous control method. Once again, to the best of our knowledge, the proposed SMC based on the FLC scheme shows excellent benefits, such as the advantages of robustness and usefulness of SMC and chattering elimination of FLC in real applications. Simulation results indicate that the powerful proposed control method removes the chattering phenomenon of the frequency occurring in this system without reducing the robustness of power system. By reducing the chattering in the control input, the proposed controller provides the correct signal to control mechanical inertia power to match the load change or demand, which is used fully for application in practical power networks to address high parameter uncertainties and load disturbances.

Author Contributions: Conceptualization V.V.H., P.T.T.; Methodology P.T.T., A.T.T., D.H.T.; Software A.T.T., D.H.T.; Validation V.V.H., P.T.T; Writing—original draft preparation P.T.T.; Writing—review and editing V.V.H.; Supervision B.L.N.M., T.M.N., P.-T.V. All authors have read and agreed to the published version of the manuscript.

Funding: This research is funded by Foundation for Science and Technology Development of Ton Duc Thang University (FOSTECT), website: http://fostect.tdtu.edu.vn, under Grant FOSTECT.2017.BR.05.

Conflicts of Interest: The authors declare no conflict of interest.

References

1. Vijay, V.; James, C.; Paul, A.; Fouad, A. *Power system control and stability*; Wiley-IEEE Press: Hoboken, NJ, USA, 2019.
2. Devendra, K. *Techniques and Its Applications in Electrical Engineering*; Springer: Berlin/Heidelberg, Germany, 2008.
3. Fu, C.; Tan, W. Decentralized load frequency control for power systems with communication delays via active disturbance rejection. *IET Gener. Transm. Distrib.* **2018**, *12*, 1751–8687.
4. Zhang, Y.; Yang, T. Decentralized switching control strategy for load frequency control in multi-area power systems with time delay and packet lose. *IEEE Access* **2020**, *8*, 15838–15850. [CrossRef]
5. Guha, D.; Roy, P.K.; Banerjee, S. Load frequency control of interconnected power system using grey wolf optimization. *Swarm Evol. Comput.* **2016**, *27*, 97–115. [CrossRef]
6. Anwar, M.N.; Pan, S. A new PID load frequency controller design method in frequency domain through direct synthesis approach. *Electr. Power Energy Syst.* **2015**, *67*, 560–569. [CrossRef]
7. Farahani, M.; Ganjefar, S.; Alizadeh, M. PID controller adjustment using chaotic optimization algorithm for multi-area load frequency control. *IET Control. Theory Appl.* **2012**, *6*, 1984–1992. [CrossRef]
8. Sonkar, P.; Rahi, O.P. Tuning of modified PID load frequency controller for interconnected system with wind power plant via IMC tuning method. In Proceedings of the 4th IEEE Uttar Pradesh Section International Conference on Electrical, Computer and Electronics, Mathura, India, 26–28 October 2017.
9. Sahu, R.K.; Panda, S.; Rout, U.K. DE optimized parallel 2-DOF PID controller for load frequency control of power system with governor dead-band nonlinearity. *Electr. Power Energy Syst.* **2013**, *49*, 19–33. [CrossRef]
10. Chen, H.; Ye, R.; Wang, X.; Lu, R. Cooperative control of power system load and frequency by using differential games. *IEEE Trans. Control Syst. Technol.* **2015**, *23*, 882–897. [CrossRef]
11. Yousef, H.A.; AL-Kharusi, K.; Albadi, M.H.; Hosseinzadeh, N. Load frequency control of a multi-area power system: An adaptive fuzzy logic approach. *IEEE Trans. Power Syst.* **2014**, *29*, 1822–1830. [CrossRef]
12. Zeng, G.Q.; Xie, X.Q.; Chen, M.R. An adaptive model predictive load frequency control method for multi-area interconnected power systems with photovoltaic generations. *Electr. Power Energy Syst.* **2017**, *10*, 1840. [CrossRef]
13. Hao, Y.; Tan, W.; Li, D. Decentralized active disturbance rejection Control for LFC in deregulated environments. In Proceedings of the 33rd Chinese Control Conference, Nanjing, China, 28–30 July 2014.
14. Saxena, S.; Hote, Y.V. Load frequency control in power systems via internal model control scheme and model-order reduction. *IEEE Trans. Power Syst.* **2013**, *28*, 2749–2757. [CrossRef]
15. Rehiara, A.B.; Yorino, N.; Sasaki, Y.; Zoka, Y. An adaptive load frequency control based on least square method. *Adv. Model. Control Wind Hydrog.* **2020**, *49*, 220.
16. Gheisarnejad, M.; Khooban, M.H. Design an optimal fuzzy fractional proportional integral derivative controller with derivative filter for load frequency control in power systems. *Trans. Inst. Meas. Control* **2019**, *1*, 1–19. [CrossRef]
17. Daneshfar, F. Intelligent load-frequency control in a deregulated environment: Continuous-valued input, extended classifier system approach. *IET Gener. Transm. Distrib.* **2013**, *7*, 551–559. [CrossRef]
18. Trip, S.; Cucuzzella, C.; De Persis, A.; Schaft, A.; Ferrara, A. Passivity-based design of sliding modes for optimal load frequency control. *IEEE Trans. Control Syst. Technol.* **2019**, *27*, 1893–1906. [CrossRef]
19. Li, H.Y.; Shi, P.; Yao, D.Y.; Wu, L.G. Observer-based adaptive sliding mode control of nonlinear markovian jump systems. *Automatica* **2016**, *64*, 133–142. [CrossRef]
20. Yang, B.; Yu, T.; Shu, H.; Yao, W.; Jiang, L. Sliding-mode perturbation observer-based sliding-mode control design for stability enhancement of multi-machine power systems. *Trans. Inst. Meas. Control* **2018**, *41*, 1418–1434. [CrossRef]
21. Prasad, S.; Purwar, S.; Kishor, N. Non-linear sliding mode load frequency control in multi-area power system. *Control Eng. Pract.* **2017**, *61*, 81–92. [CrossRef]
22. Mi, Y.; Fu, Y.; Wang, C.; Wang, P. Decentralized sliding mode load frequency control for multi-area power systems. *IEEE Trans. Power Syst.* **2013**, *28*, 4301–4309. [CrossRef]
23. Sheetla, P.; Shubhi, P.; Nand, K. H-infinity based non-linear sliding mode controller for frequency regulation in interconnected power systems with constant and time-varying delays, IET Generation. *Transm. Distrib.* **2016**, *10*, 2771–2784.
24. Xu, Y. A robust load frequency control scheme for power systems based on second order sliding mode and extended disturbance observer. *IEEE Trans. Ind. Inform.* **2018**, *14*, 3076–3086.

25. Zheng, Y.; Liu, J.; Liu, X.; Fang, D.; Wu, L. Adaptive second order sliding mode control design for a class of nonlinear systems with unknown input. *Math. Probl. Eng.* **2015**, *5*, 1–7. [CrossRef]
26. Jianping, G. Load frequency control of a two area-power system with non-reheat turbines by SMC approach. *J. Energy Power Eng.* **2015**, *9*, 566–573. [CrossRef]
27. Mi, Y.; Fu, Y.; Li, D.; Wang, C.; Loh, P.C.; Wang, P. The sliding mode load frequency control for hybrid power system based on disturbance observer. *Int. J. Electr. Power Energy Syst.* **2016**, *74*, 446–452. [CrossRef]
28. Dianwei, Q.; Shiwen, T.; Xiangjie, L. Load frequency control for micro hydro power plants by sliding mode and model order reduction. *Automatika* **2017**, *56*, 318–330.
29. Dianwei, Q.; Shiwen, T.; Hong, L.; Xiangjie, L. Load frequency control by neural-network-based integral sliding mode for nonlinear power systems with wind turbines. *Neurocomputing* **2016**, *173*, 875–885.
30. Le, N.M.B.; Van, V.H.; Nguyen, T.M.; Tsai, Y.W. Decentralized adaptive double integral sliding mode controller for multi-area power systems. *Math. Probl. Eng.* **2018**, *2018*, 1–11.
31. Prasad, S.; Purwar, S.; Kishor, N. Load frequency regulation using observer based non-linear sliding mode control. *Int. J. Electr. Power Energy Syst.* **2019**, *104*, 178–193. [CrossRef]
32. Jianping, G. Application of full order sliding mode control based on different areas power system with load frequency control. *ISA Trans.* **2019**, *92*, 23–24.
33. Guo, J. Application of a novel adaptive sliding mode control method to the load frequency control. *Eur. J. Control* **2020**, *12*, 3050–3071. [CrossRef]
34. Khargonekar, P.P.; Petersen, I.R.; Zhou, K. Robust stabilization of uncertain linear systems: Quadratic stabilizability and H^{∞} control theory. *IEEE Trans. Autom. Control* **1990**, *35*, 356–361. [CrossRef]
35. Boyd, S.; Ghaoui, E.L.; Feron, E.; Balakrishna, V. *Linear Matrix Inequalities in System and Control Theory*; SIAM: Philadelphia, PN, USA, 1994.

Hindawi
International Transactions on Electrical Energy Systems
Volume 2022, Article ID 6587194, 21 pages
https://doi.org/10.1155/2022/6587194

WILEY | Hindawi

Research Article

Advanced Sliding Mode Observer Design for Load Frequency Control of Multiarea Multisource Power Systems

Van Van Huynh,[1] **Phong Thanh Tran**,[1] **Tien Minh Nguyen**,[1] **Van-Duc Phan**,[2] **and Viet-Thanh Pham**[1]

[1] *Modeling Evolutionary Algorithms Simulation and Artificial Intelligence, Faculty of Electrical & Electronics Engineering, Ton Duc Thang University, Ho Chi Minh City, Vietnam*
[2] *Faculty of Automobile Technology, Van Lang University, Ho Chi Minh City, Vietnam*

Correspondence should be addressed to Phong Thanh Tran; tranthanhphong.st@tdtu.edu.vn

Received 21 December 2021; Accepted 16 February 2022; Published 16 March 2022

Academic Editor: Faroque Azam

Recently, to balance the increased electricity demands and total generated power, the multiarea power system (MAPS) has been introduced with multipower sources such as gas, nuclear, hydro, and thermal, which will impact the load frequency control (LFC). Therefore, the LFC of the two-area gas-hydro-thermal power system (TAGHTPS) is introduced by applying the single-phase sliding mode control-based state observer (SPSMCBSO). In this scheme, the TAGHTPS is the first model that considers the uncertainties of the parameters in the state and the interconnected matrix. Second, the state observer is employed to estimate the state variables for the feedback control. Third, the SPSMCBSO is developed to modify the basic sliding mode control to improve the performance of TAGHTPS in terms of overshoot and settling time. In addition, the SPSMCBSO is established to rely fully on the state observer so that the difficulty in the state variable measurement is solved. Fourth, the TAGHTPS stability analysis is performed using a new linear matrix inequality (LMI) scheme—Lyapunov stability theory. Lastly, the simulation results are shown and compared to recently established classical control methods to validate the SPSMCBSO choice of application for the LFC of the multiarea multisource power system (MAMSPS).

1. Introduction

The main aim of power system (PS) control is always to balance the total net generated power and the electrical load. This can be viewed when the frequency is kept at the permissible level. However, if the industry's load-dependent frequency increases, it will impact the PS frequency and cause changes between total net power and load demand. Matching total generation power with load is accomplished with load frequency control (LFC) [1]. Over the years, researchers have applied classical control methods to the LFC of PS. To achieve the classical scheme, the PS is modeled and represented in the transfer function. In review, the model allows only for the maximum of two inputs, which are frequency error and load disturbance, to be monitored. Furthermore, classical control schemes such as proportional-integral (PI) and proportional-integral-differential (PID) methods use control gains to adjust the parameters associated with the PS LFC after measuring the frequency error and load disturbance. The PI and PID schemes have been widely used for the industrial LFC of perturbed PS. As the electricity demand increases day by day, the PS begins to grow in size, shape, and complexity, which leads to the LFC of PS becoming more complicated. In reality, large PSs such as multiarea power system (MAPS), which includes many generating sets in each area, are characterized with long frequency transient time delay, area control error (ACE), parameter uncertainties, subsystem parameter deviation, random load disturbance, nonlinearity problem, tie-line power flow control problem, etc. These characteristics have an impact on the LFC of the MAPS. Therefore, the MAPS modeling requires these characteristics to be considered. However, many existing PS models for the LFC are not suitable to handle the above characteristics because it only allows for two inputs to be monitored. Recently, control engineers have solved the above problem by representing the PS model in state-space form, which allows for multi-inputs using the modern control. Meanwhile, some methods such as intelligent control (i.e., fuzzy logic), optimal control (i.e., particle swarm optimization (PSO)), adaptive technique, and observer scheme combined with classical PI and PID have been developed to study the LFC of MAPS. In [2], the fuzzy logic technique was applied to select the PI algorithm for the LFC of two PS areas following the frequency change. Based on load demand, the proposed control scheme using the PI parameters was updated online using fuzzy logic rules. Indirect adaptive fuzzy logic control combined with classical PI has been applied to track unknown parameters for the MAPS LFC, and the results have been shown to be superior compared with the classical control method [3]. In the case where some parameters of the MAPS are difficult to access, the observer scheme was employed. The Luenberger observer was the first to be used in which the PS is reconstructed to estimate the system state variables for the LFC of the original MAPS [4]. Observer PI was developed to study the LFC of the single area PS and was compared with the basic Luenberger observer to validate its superiority [4]. In practice, the LFC is required to be highly robust against large disturbances. Hence, variable structure control (VSC) was developed for the LFC of MAPS. The sliding mode control (SMC) scheme is the most popular of the VSC. Their designs follow the selection of the sliding surface and the construction of the switching law and control law that implies that variables must be brought to the surface and remain therein in the finite reaching time [5–9]. The SMC is very important because of its robustness and resistance to large disturbances. The SMC has already been studied for the LFC of MAPS [10–20]. Over time, several methods have been combined with the MAPS SMC to handle the LFC problem of MAPS. A novel adaptive technique based on SMC was utilized for MAPS LFC under step load disturbance [21]. On the other hand, the SMC via the observer has been applied for the LFC of MAPS where some state variables of the system were difficult to access, and the SMC was designed to fully depend on the observer [21]. The SMC-based integral output feedback control was developed for the MAPS LFC against certain disturbances [22]. The single-phase SMC was designed to modify the basic SMC so that variable trajectories get to the surface without reaching time and remain there for all time, making it highly robust for the LFC of MAPS. Recently, single-phase SMC via observer was newly established for the LFC of MAPS under the influence of a step load and a random load disturbance [23]. This method is further used for the LFC of New England 39-bus system under random load disturbance [23]. In [19], the controller parameter is determined using grey wolf optimization and particle swarm optimization approaches to get an ideal outcome in a sliding mode controller for frequency management in an interconnected power system. Because of the discontinuous control component in [20], the traditional integral SMC suffers the flaw of chattering. However, the above conventional SMC methods were applied for the LFC of MAPS consisting of thermal plants or hydro alone in each area without considering the mismatched disturbance and load variation. In reality, MAPS consists of the combination of many generators in each area, such as nuclear, hydro, gas, and thermal, which can be referred to as multiarea multisource power system (MAMSPS). In studies, only a few works have been done to study the LFC of the MSMAPS. A concept and implementation of a structured generation-based PID control using the bacterial foraging algorithm (BFA) had been utilized for the LFC of the two-area gas-hydro-thermal power system (TAGHTPS) after the step load change [24]. For automatic generation control, a novel teaching learning-based optimization (TLBO) algorithm with 2-degree-of-freedom of proportional-integral-derivative (2-DOF PID) controller has also been developed for LFC to improve the dynamic of TAGHTPS under load disturbance [25]. In addition, proportional-integral-derivative (PID) structured regulators of the optimized generation control (OGC) strategy for interconnected two control zones of diverse-source power systems are designed using a new artificial intelligence (AI) technique known as the Jaya algorithm [26]. These works were done only to study the LFC of the TAGHTPS under load disturbances, and the TAGHTPS is modeled without considering the impact of parameter and interconnection uncertainties in the system state matrix.

Aside from that, the SMC has been utilized in conjunction with a state estimator to observe the MAPS disturbance to enhance the system's performance by eliminating chattering [27–31]. In [30], a reduced-order disturbance observer based on SMC is used in a hybrid power system to decrease frequency deviation. Based on system conditions and expected disturbance, an adaptive super-twisting SMC is constructed. In [31], the nonlinear disturbance observer evaluates the mismatch between electrical power and mechanical power, which is subsequently used in the controller design to adjust for the disturbance. The disturbance observer is utilized in conjunction with the suggested fractional order three-degree-of-freedom tilt integral derivative controller in [32] to effectively predict the wind velocity's uncertain profile and enrich the control law.

These controllers were created utilizing a reduced observer controller or a nonlinear disturbance observer to notice load changes and maintain nominal frequency if all system state variables are measured. However, if some MAPS state variables are not measurable or impossible to measure, this cannot be guaranteed for the actual implementation of these above controllers. As a result, the design of an LFC based on a novel SMC where the state observer is entirely integrated into the sliding surface and an SPSMCBSO is employed to overcome the concerns above is motivated. Furthermore, the selection of switching strategies and sliding surfaces is critical. The switching strategy is used to shift the system states and keep them converged at a certain sliding surface. As a result, a novel single-phase sliding surface is built. The single-phase switching surface ensures robustness at the reaching stage without reaching time.

In summary, we model the TAGHTS taking into account the impact of parameter and interconnection uncertainties on the state matrix and proposed the SPSMCBSO to study the LFC of the TAGHTPS under load disturbance, deviation of subsystem parameters, and impact of parameter uncertainties, which is simple and less stressful to implement.

Meanwhile, this is the first time that the SPSMCBSO is used for the LFC of TAGHTPS, which is validated compared with the recently established above classical methods. In this work, the major contributions are stated as follows:

(i) The SPSMCBSO was designed to rely entirely on the state observer, making it particularly effective for the MAMSPS LFC, where some variables are difficult to obtain.

(ii) The novel controller is established to modify the basic SMC such that the order of the PS making it highly robust against disturbance is different than that of the basic SMC, which depends on the reaching time.

(iii) The Lyapunov stability theory-based novel linear matrix inequality (LMI) approach is used to theoretically show whole-system stabilization.

(iv) In comparison with recent LFC approaches [24–26, 30–32], the novel SMC through single-phase sliding surface does not require reaching time, ensuring greater system performance in terms of settling time and overshoot under the matched or mismatched disturbance and load variation.

2. Mathematical Model of the Interconnected Multiarea Multisource Power Network

In this section, the block chart of PS is presented. Dynamic models of power systems are generally nonlinear. The MAPS consists of many generating sets such as nuclear, gas, hydro, and gas plant in each area. This can be viewed as the MAMS. However, the nuclear plant is known as a base load system and does not apply to the LFC of MAPS [24–26]. The gas plant can adapt to the demand for random loads, enabling it to fit the LFC system. Therefore, in this section, we consider TAGHTPS in each area, as shown in Figure 1. Area control error (ACE) is computed as the power error from the linear combination of the power error of the link network and the system frequency errors.

Taking into account the impact of the interconnection matrix and load disturbance, the PS model is constructed in the differential equation as follows:

$$\Delta\dot{f}_i = -\frac{\Delta f_i}{T_{PS_i}} + \frac{\Delta P_{pt_i} K_{PS_i}\alpha_{i1}}{T_{PS_i}} + \frac{\Delta P_{Gh_i} K_{PS_i}\alpha_{i2}}{T_{PS_i}} + \frac{\Delta P_{Gg_i} K_{PS_i}\alpha_{i3}}{T_{PS_i}} - \frac{K_{PS_i} a_{ij}}{T_{PS_i}}\Delta P_{tie_{ij}} - \frac{K_{PS_i}}{T_{PS_i}}\Delta P_{D_i}, \tag{1}$$

$$\Delta\dot{P}_{pt_i} = \frac{\Delta P_{Gt_i}}{T_{T_i}} - \frac{\Delta P_{pt_i}}{T_{T_i}}, \tag{2}$$

$$\Delta\dot{P}_{Gt_i} = -\frac{\Delta P_{Gt_i}}{T_{R_i}} + \frac{\Delta X_{Et_i}}{T_{R_i}} - \frac{\Delta X_{Et_i} K_{R_i}}{T_{SG_i}} - \frac{\Delta f_i K_{R_i}}{T_{SG_i} R_{i1}} + \frac{\Delta ACE_i K_{R_i}}{T_{SG_i}} + \frac{U_{i1} K_{R_i}}{T_{SG_i}}, \tag{3}$$

$$\Delta\dot{X}_{Et_i} = -\frac{\Delta X_{Et_i}}{T_{SG_i}} - \frac{\Delta f_i}{T_{SG_i} R_{i1}} + \frac{\Delta ACE_i}{T_{SG_i}} + \frac{U_{i1}}{T_{SG_i}}, \tag{4}$$

$$\Delta\dot{P}_{Gh_i} = \frac{2\Delta P_{Rh_i}}{T_{W_i}} - \frac{2\Delta P_{Gh_i}}{T_{W_i}} - \frac{2\Delta X_{Eh_i}}{T_{RH_i}} + \frac{2\Delta P_{Rh_i}}{T_{RH_i}} + \frac{2\Delta X_{Eh_i} T_{RS_i}}{T_{RH_i} T_{GH_i}} + \frac{2\Delta f_i T_{RS_i}}{R_{i2} T_{RH_i} T_{GH_i}} - \frac{2\Delta ACE_i T_{RS_i}}{T_{RH_i} T_{GH_i}} - \frac{2U_{i2} T_{RS_i}}{T_{RH_i} T_{GH_i}}, \tag{5}$$

$$\Delta\dot{P}_{Rh_i} = \frac{\Delta X_{Eh_i}}{T_{RH_i}} - \frac{\Delta P_{Rh_i}}{T_{RH_i}} - \frac{\Delta X_{Eh_i} T_{RS_i}}{T_{RH_i} T_{GH_i}} - \frac{\Delta f_i T_{RS_i}}{R_{i2} T_{RH_i} T_{GH_i}} + \frac{\Delta ACE_i T_{RS_i}}{T_{RH_i} T_{GH_i}} + \frac{U_{i2} T_{RS_i}}{T_{RH_i} T_{GH_i}}, \tag{6}$$

$$\Delta\dot{X}_{Eh_i} = -\frac{\Delta X_{Eh_i}}{T_{GH_i}} - \frac{\Delta f_i}{T_{GH_i} R_{i2}} + \frac{\Delta ACE_i}{T_{GH_i}} + \frac{U_{i2}}{T_{GH_i}}, \tag{7}$$

$$\Delta\dot{P}_{Gg_i} = -\frac{\Delta P_{Gg_i}}{T_{CD_i}} + \frac{\Delta P_{Rg_i}}{T_{CD_i}}, \tag{8}$$

$$\Delta\dot{P}_{Rg_i} = -\frac{\Delta P_{Rg_i}}{T_{F_i}} + \frac{\Delta X_{Vg_i}}{T_{F_i}} + \frac{\Delta X_{Vg_i} T_{CR_i}}{Y_{G_i} T_{F_i}} - \frac{\Delta X_{Eg_i} T_{CR_i}}{Y_{G_i} T_{F_i}} + \frac{\Delta X_{Eg_i} c_{g_i} X_{G_i} T_{CR_i}}{b_{g_i} Y_{G_i} T_{F_i}} + \frac{\Delta f_i X_{G_i} T_{CR_i}}{R_{i3} b_{g_i} Y_{G_i} T_{F_i}} - \frac{\Delta ACE_i X_{G_i} T_{CR_i}}{b_{g_i} Y_{G_i} T_{F_i}} - \frac{U_{i3} X_{G_i} T_{CR_i}}{b_{g_i} Y_{G_i} T_{F_i}}, \tag{9}$$

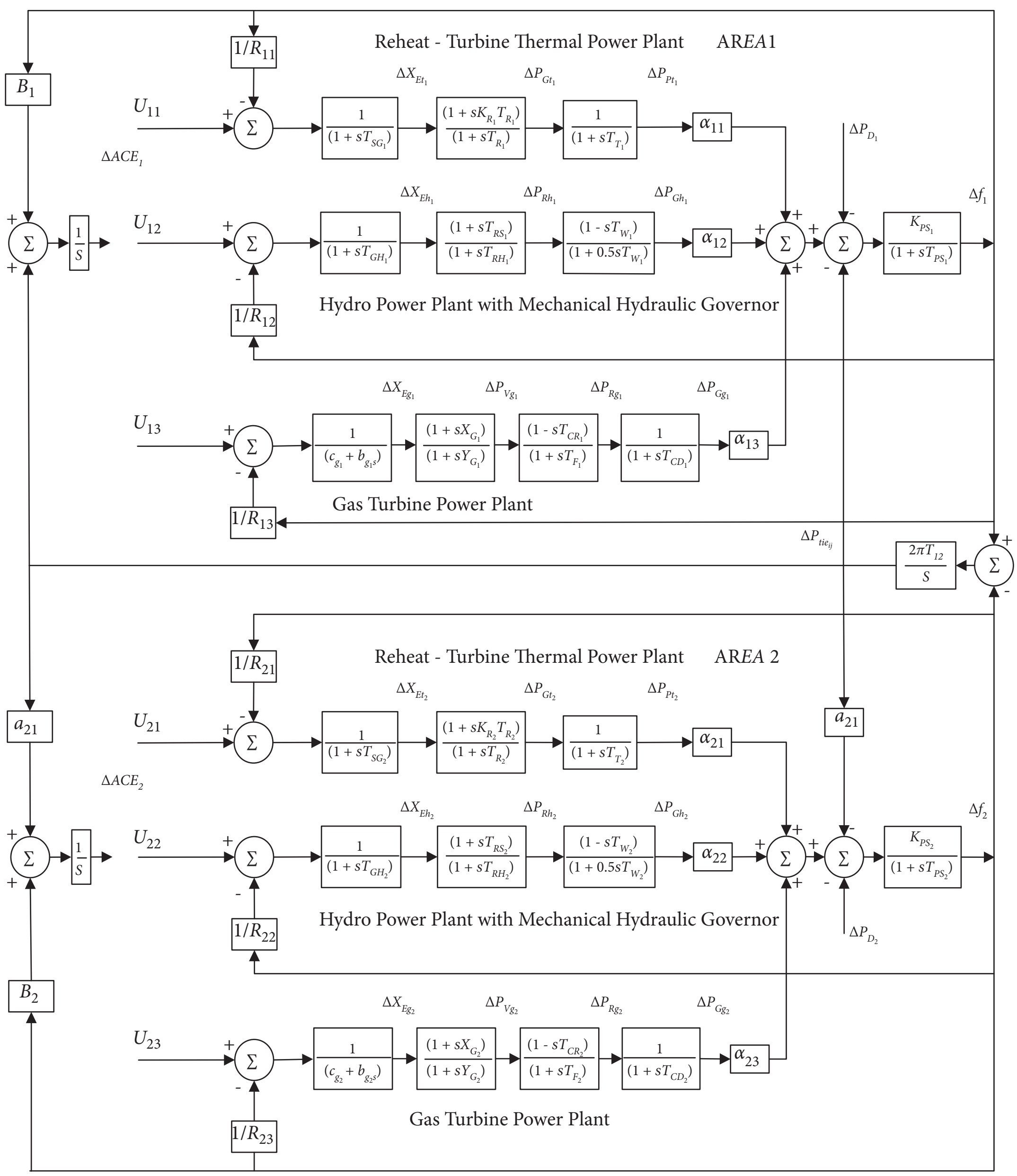

Figure 1: LFC block diagram of a TAMSPS.

$$\Delta \dot{P}_{Vg_i} = -\frac{\Delta P_{Vg_i}}{Y_{G_i}} + \frac{\Delta X_{Eg_i}}{Y_{G_i}} - \frac{\Delta X_{Eg_i} c_{g_i} X_{G_i}}{b_{g_i} Y_{G_i}} - \frac{\Delta f_i X_{G_i}}{R_{i3} b_{g_i} Y_{G_i}} + \frac{\Delta ACE_i X_{G_i}}{b_{g_i} Y_{G_i}} + \frac{U_{i3} X_{G_i}}{b_{g_i} Y_{G_i}}, \quad (10)$$

$$\Delta \dot{X}_{Eg_i} = -\frac{\Delta X_{Eg_i} c_{g_i}}{b_{g_i}} - \frac{\Delta f_i}{b_{g_i} R_{i3}} + \frac{\Delta ACE_i}{b_{g_i}} + \frac{U_{i3}}{b_{g_i}}, \quad (11)$$

$$\Delta A\dot{C}E_i = B_i \Delta f_i + a_{ij} \Delta P_{tie_{ij}}, \quad (12)$$

$$\Delta \dot{P}_{tie_{ij}} = \sum_{\substack{j=1 \\ j \neq i}}^{L} 2\pi T_{ij} \left(\Delta f_i - \Delta f_j\right), \quad (13)$$

where ΔP_{pt_i} is the change in thermal turbine speed changer position (p.u.MW), ΔP_{Gh_i} is change in hydro-turbine speed changer position (p.u.MW), ΔP_{Gg_i} is change in gas turbine speed changer position (p.u.MW), ΔP_{D_i} is total incremental charge in the local load of the control area (p.u.MW), Δf_i andΔf_j are incremental change in frequency of each control area (Hz), and $\Delta P_{tie_{ij}}$ is incremental change in actual tie-line power flow from control areas 1 to 2 (p.u.MW), and ΔACE_i is the area control error. By using the dynamic equations from (1)–(13) the ith area of the PS state-space model is given in (14) as follows:

$$\dot{x}_i(t) = A_i x_i(t) + B_i u_i(t) + \sum_{\substack{j=1\\ j\neq i}}^{L} H_{ij} + \Delta H_{ij} x_j(t) + F_i \Delta P_{di}(t), \tag{14}$$

and the above equation is the state-space form of the TAGHTPS. Here, $x_i(t) = \left[\Delta f_i\, \Delta P_{pt_i}\, \Delta P_{Gt_i}\, \Delta X_{Et_i}\, \Delta P_{Gh_i}\, \Delta P_{Rh_i}\, \Delta X_{Eh_i} \Delta P_{Gg_i}\, \Delta P_{Rg_i}\, \Delta P_{Vg_i} \Delta X_{Eg_i} \Delta ACE_i \Delta P_{tie_{ij}}\right]^T$ is the state vector, $x_j(t)$ is the interconnected system state vector of $x_i(t)$, $u_i(t)$ is the control vector, and $\Delta P_{di}(t)$ is the disturbance. A_i, B_i, H_{ij}, andF_i are the system matrices given as follows:

$$A_i = \begin{bmatrix} A_{i1} & A_{i2} \\ A_{i3} & A_{i4} \end{bmatrix},$$

$$A_{i1} = \begin{bmatrix}
-\frac{1}{T_{PS_i}} & \frac{K_{PS_i}\alpha_{i1}}{T_{PS_i}} & 0 & 0 & \frac{K_{PS_i}\alpha_{i2}}{T_{PS_i}} & 0 & 0 \\
0 & -\frac{1}{T_{T_i}} & \frac{1}{T_{T_i}} & 0 & 0 & 0 & 0 \\
-\frac{K_{R_i}}{T_{SG_i}R_{i1}} & 0 & -\frac{1}{T_{R_i}} & \frac{1}{T_{R_i}} - \frac{K_{R_i}}{T_{SG_i}} & 0 & 0 & 0 \\
-\frac{1}{T_{SG_i}R_{i1}} & 0 & 0 & -\frac{1}{T_{SG_i}} & 0 & 0 & 0 \\
\frac{2T_{RS_i}}{R_{i2}T_{RH_i}T_{GH_i}} & 0 & 0 & 0 & -\frac{2}{T_{W_i}} & \frac{2}{T_{W_i}} + \frac{2}{T_{RH_i}} & \frac{2T_{RS_i}}{T_{RH_i}T_{GH_i}} - \frac{2}{T_{RH_i}} \\
-\frac{T_{RS_i}}{R_{i2}T_{RH_i}T_{GH_i}} & 0 & 0 & 0 & 0 & -\frac{1}{T_{RH_i}} & \frac{1}{T_{RH_i}} - \frac{T_{RS_i}}{T_{RH_i}T_{GH_i}} \\
-\frac{1}{T_{GH_i}R_{i2}} & 0 & 0 & 0 & 0 & 0 & \frac{1}{T_{GH_i}}
\end{bmatrix},$$

$$A_{i2} = \begin{bmatrix} \dfrac{K_{PS_i}\alpha_{i3}}{T_{PS_i}} & 0 & 0 & 0 & 0 & -\dfrac{K_{PS_i}a_{ij}}{T_{PS_i}} \\ 0 & 0 & 0 & 0 & 0 & 0 \\ 0 & 0 & 0 & 0 & 0 & 0 \\ 0 & 0 & 0 & 0 & 0 & 0 \\ 0 & 0 & 0 & 0 & 0 & 0 \\ 0 & 0 & 0 & 0 & 0 & 0 \\ 0 & 0 & 0 & 0 & 0 & 0 \end{bmatrix},$$

$$A_{i3} = \begin{bmatrix} 0 & 0 & 0 & 0 & 0 & 0 & 0 \\ \dfrac{X_{G_i}T_{CR_i}}{R_{i3}b_{g_i}Y_{G_i}T_{F_i}} & 0 & 0 & 0 & 0 & 0 & 0 \\ -\dfrac{X_{G_i}}{R_{i3}b_{g_i}Y_{G_i}} & 0 & 0 & 0 & 0 & 0 & 0 \\ -\dfrac{1}{R_{i3}b_{g_i}} & 0 & 0 & 0 & 0 & 0 & 0 \\ B_i & 0 & 0 & 0 & 0 & 0 & 0 \\ \sum\limits_{\substack{j=1 \\ j\neq i}}^{L} -2\pi T_{\mathrm{ij}} & 0 & 0 & 0 & 0 & 0 & 0 \end{bmatrix},$$

$$A_{i4} = \begin{bmatrix} -\dfrac{1}{T_{CD_i}} & \dfrac{1}{T_{CD_i}} & 0 & 0 & 0 & 0 \\ 0 & -\dfrac{1}{T_{F_i}} & \dfrac{1}{T_{F_i}} + \dfrac{T_{CR_i}}{Y_{G_i}T_{F_i}} & \dfrac{c_{g_i}X_{G_i}T_{CR_i}}{b_{g_i}Y_{G_i}T_{F_i}} - \dfrac{T_{CR_i}}{Y_{G_i}T_{F_i}} & 0 & 0 \\ 0 & 0 & -\dfrac{1}{Y_{G_i}} & \dfrac{1}{Y_{G_i}} - \dfrac{c_{g_i}X_{G_i}}{b_{g_i}Y_{G_i}} & 0 & 0 \\ 0 & 0 & 0 & -\dfrac{c_{g_i}}{b_{G_i}} & 0 & 0 \\ 0 & 0 & 0 & 0 & 0 & a_{ij} \\ 0 & 0 & 0 & 0 & 0 & 0 \end{bmatrix},$$

$$B_i = \begin{bmatrix} 0 & 0 & \frac{K_{R_i}}{T_{SG_i}} & \frac{1}{T_{SG_i}} & 0 & 0 & 0 & 0 & 0 & 0 & 0 & 0 & 0 \\ 0 & 0 & 0 & 0 & -\frac{2T_{RS_i}}{T_{RH_i}T_{GH_i}} & \frac{T_{RS_i}}{T_{RH_i}T_{GH_i}} & \frac{1}{T_{GH_i}} & 0 & 0 & 0 & 0 & 0 & 0 \\ 0 & 0 & 0 & 0 & 0 & 0 & 0 & 0 & -\frac{X_{G_i}T_{CR_i}}{b_{g_i}Y_{G_i}T_{F_i}} & \frac{X_{G_i}}{b_{g_i}Y_{G_i}} & \frac{1}{b_{g_i}} & 0 & 0 \end{bmatrix}^T,$$

$$F_i = \begin{bmatrix} -\frac{K_{PS_i}}{T_{PS_i}} & 0 & 0 & 0 & 0 & 0 & 0 & 0 & 0 & 0 & 0 & 0 & 0 \end{bmatrix}^T,$$

$$H_{ij} = \begin{bmatrix} 0 & 0 & 0 & 0 & 0 & 0 & 0 & 0 & 0 & 0 & 0 & 0 & 0 \\ 0 & 0 & 0 & 0 & 0 & 0 & 0 & 0 & 0 & 0 & 0 & 0 & 0 \\ 0 & 0 & 0 & 0 & 0 & 0 & 0 & 0 & 0 & 0 & 0 & 0 & 0 \\ 0 & 0 & 0 & 0 & 0 & 0 & 0 & 0 & 0 & 0 & 0 & 0 & 0 \\ 0 & 0 & 0 & 0 & 0 & 0 & 0 & 0 & 0 & 0 & 0 & 0 & 0 \\ 0 & 0 & 0 & 0 & 0 & 0 & 0 & 0 & 0 & 0 & 0 & 0 & 0 \\ 0 & 0 & 0 & 0 & 0 & 0 & 0 & 0 & 0 & 0 & 0 & 0 & 0 \\ 0 & 0 & 0 & 0 & 0 & 0 & 0 & 0 & 0 & 0 & 0 & 0 & 0 \\ 0 & 0 & 0 & 0 & 0 & 0 & 0 & 0 & 0 & 0 & 0 & 0 & 0 \\ 0 & 0 & 0 & 0 & 0 & 0 & 0 & 0 & 0 & 0 & 0 & 0 & 0 \\ 0 & 0 & 0 & 0 & 0 & 0 & 0 & 0 & 0 & 0 & 0 & 0 & 0 \\ 0 & 0 & 0 & 0 & 0 & 0 & 0 & 0 & 0 & 0 & 0 & 0 & 0 \\ -2\pi T_{ij} & 0 & 0 & 0 & 0 & 0 & 0 & 0 & 0 & 0 & 0 & 0 & 0 \end{bmatrix}. \tag{15}$$

In practical interconnected MAMSPS, changes in operating points constantly influence the fluctuating sources of load. This factor can be considered as parameter uncertainties. Introducing this factor, system (14) can be rewritten as follows:

$$\begin{aligned} \dot{x}_i(t) = {} & [A_i + \Sigma_i(x_i,t)]x_i(t) + B_i[u_i(t) + \psi_i(x_i,t)] \\ & + \sum\nolimits_{\substack{j=1 \\ j\neq i}}^{L} [H_{ij} + \Xi_{ij}(x_j,t)]x_j(t) + F_i \Delta P_{di}(t), \end{aligned} \tag{16}$$

where $\Sigma_i(x_i,t)$ and $\Xi_{ij}(x_j,t)$ are time-varying parameter uncertainties and$B_i\psi_i(x_i,t)$ is the input disturbance. In other words, the aggregate uncertainty is therefore given as follows:

$$\begin{aligned} \Phi_i(x_i,t) = {} & \Sigma_i(x_i,t)x_i(t) + B_i\psi_i(x_i,t) \\ & + \sum_{\substack{j=1 \\ j\neq i}}^{L} \Xi_{ij}x_j(t) + F_i\Delta P_{di}(t). \end{aligned} \tag{17}$$

Therefore, the new dynamic model can be expressed as follows:

$$\begin{aligned} \dot{x}_i(t) &= A_i x_i(t) + B_i u_i(t) + \sum_{\substack{j=1 \\ j\neq i}}^{L} H_{ij}x_j(t) + \Phi_i(x_i,t) \\ y_i &= C_i x_i, \end{aligned} \tag{18}$$

where $\Phi_i(x_i,t)$ is the aggregated disturbance that represents the uncertainties of the matched and mismatched parameters. If we consider the state-space model (17), the designing of the controller $u_i(t)$ is very important and it is based on the choice of the control engineers. Several techniques have been designed for $u_i(t)$ as seen in the literature. Meanwhile, to design the novel $u_i(t)$, we first make the following assumptions and recall the lemmas as follows.

Assumption 1. The system matrix (A_i, B_i) is controllable and (A_i, C_i) is observable.

Assumption 2. It is assumed that the load disturbance $\Phi_i(x_i,t)$ is bounded, such that $\|\Phi_i(x_i,t)\| \leq \gamma_i$, where γ_i is the known scalar and $\|.\|$ is the matrix norm.

Lemma 1. *[22, 33]: if X and Y are real matrix of suitable dimension, then, for any scalar $\mu > 0$, the following matrix inequality holds:*

$$\mathbf{X}^{\mathbf{T}}\mathbf{Y} + \mathbf{Y}^{\mathbf{T}}\mathbf{X} \leq \mu\mathbf{X}^{\mathbf{T}}\mathbf{X} + \mu^{-1}\mathbf{Y}^{\mathbf{T}}\mathbf{Y}. \tag{19}$$

Lemma 2. *[22, 33]: for a given inequality:*

$$\begin{bmatrix} Q(x) & S(x) \\ S(x)^T & R(x) \end{bmatrix} < 0, \tag{20}$$

where $Q(x) = Q(x)^T$ and $R(x) = R(x)^T$ such that $S(x)$ depends on the affinity on x; therefore, $R(x) < 0$ and $Q(x) - S(x)R(x)^{-1}S(x)^T < 0$.

3. Design of the Power System State Estimator

Few works have applied observer techniques to solve the LFC of PS where some state variables are uneasy to solve. The state observer was invented to estimate the state variables of the system and reject disturbance by reconstructing the original PS model. The advantage is that the reconstructed PS model is nearly the same as the original PS model. The LFC of MAMSPS where some state variables are difficult to access can benefit from the observer scheme. For this reason, we apply the observer method to reconstruct the model of the original TAGHTPS (18) as follows:

$$\begin{aligned} \dot{\hat{x}}_i(t) &= A_i\hat{x}_i(t) + B_iu_i(t) + \sum_{\substack{j=1 \\ j\neq i}}^{L} H_{ij}\hat{x}_j(t) + \Gamma_i(y_i - \hat{y}_i) \\ \hat{y}_i &= C_i\hat{x}_i, \end{aligned} \tag{21}$$

where Γ_i is the observer gain, $\hat{x}_i(t)$ is the estimation of $x_i(t)$, y_i is the output vector, and $\hat{y}_i$ is the state observer output, respectively. It can be calculated using the pole placement method. Next, we examine the state error dynamic where the state error is given as follows:

$$\tilde{x}_i(t) = x_i(t) - \hat{x}_i(t). \tag{22}$$

Taking the derivative of the error $\tilde{x}_i$, we have the following:

$$\dot{\tilde{x}}_i = (A_i - \Gamma_iC_i)\tilde{x}_i + \sum_{\substack{j=1 \\ j\neq i}}^{L} H_{ij}\tilde{x}_j + \Phi_i(x_i,t). \tag{23}$$

The state error tends to zero depending on the eigenvalue of $(A_i - \Gamma_iC_i)$.

Remark 1. In this scheme, it is called a full-order state observer when the state observer observes all state variables of the system, regardless of whether some state variables are valuable for direct measurement. The mathematical model of the observer is basically the same as that of the plant, except that we include an additional term that includes the estimation error to compensate for inaccuracies in matrices A_i and B_i and the lack of the initial error.

4. Integral Single-Phase Sliding Surface Design

In practice, the LFC scheme is required to be highly robust against certain disturbances to achieve MAMSPS stability. Over the years, the SMC has been applied to attenuate various disturbances for the LFC of MAPS [12, 16–19]. The SMC design follows the selection of a sliding surface (SS) and the construction of a switching law and an equivalent control law [5–15]. The reachability of system state variable trajectories to the SS using the basic SMC depends on a finite reach time. However, the PS with a long transient time might cause a drawback to the basic SMC. With this information, we propose that the SPSMCBSO and the sliding surface without reaching phase (SSWRP) are given as follows:

$$\eta_i[\hat{x}_i(t)] = \mathrm{M}_i\hat{x}_i(t) - \int_0^t \mathrm{M}_i(A_i - B_i\Lambda_i)\hat{x}_i(t)\mathrm{d}\tau - \mathrm{M}_i\hat{x}_i(0)e^{-\delta_it}, \tag{24}$$

where the matrix M_i is selected to promise that the matrix M_iB_i is nonsingular. The design matrix $\Lambda_i \in R^{m_i\times n_i}$ is chosen satisfying the nonlinearity condition.

$$\mathrm{Re}[\lambda_{\max}(A_i - B_i\Lambda_i)] < 0. \tag{25}$$

If we take derivative of $\eta_i[\hat{x}_i(t)]$ with respect to time, we have the following:

$$\begin{aligned} \dot{\eta}_i[\hat{x}_i(t)] = &\left[\mathrm{M}_iA_i\hat{x}_i(t) + \mathrm{M}_iB_iu_i(t) + \sum_{\substack{j=1 \\ j\neq i}}^{L} \mathrm{M}_iH_{ij}\hat{x}_j(t) + \mathrm{M}_i\Gamma_i(y_i - \hat{y}_i)\right] \\ &- \mathrm{M}_i(A_i - B_i\Lambda_i)\hat{x}_i(t) + \delta_i\mathrm{M}_i\hat{x}_i(0)e^{-\delta_it}. \end{aligned} \tag{26}$$

As $\dot{\eta}_i(t) = \eta_i(t) = 0$, then we can derive the equivalent control as follows:

$$\begin{aligned} u_i^{eq}(t) &= -(\mathrm{M}_i B_i)^{-1}\left[\mathrm{M}_i A_i \hat{x}_i(t) + \sum_{\substack{j=1\\ j\neq i}}^{L} \mathrm{M}_i H_{ij}\hat{x}_j(t) + \mathrm{M}_i\Gamma_i(y_i - \hat{y}_i) - \mathrm{M}_i(A_i - B_i\Lambda_i)\hat{x}_i(t) + \delta_i \mathrm{M}_i\hat{x}_i(0)e^{-\delta_i t}\right] \\ &= -(\mathrm{M}_i B_i)^{-1}\left[\mathrm{M}_i B_i\Lambda_i\hat{x}_i(t) + \mathrm{M}_i\Gamma_i(y_i - \hat{y}_i) + \delta_i\mathrm{M}_i\hat{x}_i(0)e^{-\delta_i t} + \sum_{\substack{j=1\\ j\neq i}}^{L} \mathrm{M}_i H_{ij}\hat{x}_j(t)\right]. \end{aligned} \tag{27}$$

By closing the loop system, we substitute (27) into (18):

$$\begin{aligned} \dot{x}_i(t) &= (A_i - B_i\Lambda_i)x_i(t) + \left(B_i\Lambda_i - B_i(\mathrm{M}_iB_i)^{-1}\mathrm{M}_i\Gamma_iC_i\right)\tilde{x}_i(t) + \sum_{\substack{j=1\\ j\neq i}}^{L}\left[H_{ij} - B_i(\mathrm{M}_iB_i)^{-1}\mathrm{M}_iH_{ij}\right]x_j(t) \\ &+ \sum_{\substack{j=1\\ j\neq i}}^{L} B_i(\mathrm{M}_iB_i)^{-1}\mathrm{M}_iH_{ij}\tilde{x}_j(t) + \Phi_i(x_i,t) - \delta_iB_i(\mathrm{M}_iB_i)^{-1}\mathrm{M}_i\hat{x}_i(0)e^{-\delta_i t}. \end{aligned} \tag{28}$$

To observe the MAMSPS (18), we combine (23) and (28) in the following equation:

$$\begin{bmatrix} \dot{x}_i \\ \dot{\tilde{x}}_i \end{bmatrix} = \begin{bmatrix} A_i - B_i\Lambda_i & \Theta_i \\ 0 & A_i - \Gamma_iC_i \end{bmatrix}\begin{bmatrix} x_i \\ \tilde{x}_i \end{bmatrix} + \sum_{\substack{j=1\\ j\neq i}}^{L}\begin{bmatrix} H_{ij} - \Upsilon_iH_{ij} & \Upsilon_iH_{ij} \\ 0 & H_{ij} \end{bmatrix}\begin{bmatrix} x_j \\ \tilde{x}_j \end{bmatrix} + \begin{bmatrix} \Phi_i(x_i,t) \\ \Phi_i(x_i,t) \end{bmatrix} + \begin{bmatrix} \mathrm{N}_ie^{-\delta_i t} \\ 0 \end{bmatrix}, \tag{29}$$

where $\Theta_i = B_i\Lambda_i - B_i(\mathrm{M}_iB_i)^{-1}\mathrm{M}_i\Gamma_iC_i$, $\mathrm{N}_i = -\delta_iB_i(\mathrm{M}_iB_i)^{-1}\mathrm{M}_i\hat{x}_i(0)$, and $\Upsilon_i = B_i(\mathrm{M}_iB_i)^{-1}\mathrm{M}_i$.

Equation (29) is the dynamic system of the MAMSPS. Hence, we analyze the stability of (29) via the new LMI given in (30), which is accompanied by the theorem as stated.

Theorem 1. *Equation (29) is asymptotic stable if the symmetric positive definite matrices Π_i and $\overline{\Pi}_i$, where $i = 1, 2, \ldots, L$, and the positive scalars λ_i, $\underset{\rho}{i}$, and $\underset{\widehat{\gamma}}{i}$ are assumed so that the below new LMI holds:*

$$\begin{bmatrix} \mathrm{X}_i & \Pi_i\Theta_i & \Pi_i & \Pi_iN_i & 0 \\ \Theta_i^T\Pi_i & \overline{\mathrm{X}}_i & 0 & 0 & \overline{\Pi}_i \\ \Pi_i & 0 & -\lambda_i^{-1} & 0 & 0 \\ N_i^T\Pi_i & 0 & 0 & -\widehat{\gamma}_i^{-1} & 0 \\ 0 & \overline{\Pi}_i & 0 & 0 & -\rho_i^{-1} \end{bmatrix} < 0, \tag{30}$$

where $\mathrm{X}_i = \Pi_i(A_i - B_i\Lambda_i) + (A_i - B_i\Lambda_i)^T\Pi_i + \sum_{j=1_{j\neq i}}^{L}[\overline{\lambda}_j(H_{ji} - \Upsilon_jH_{ji})^T(H_{ji} - \Upsilon_jH_{ji})]$ *and* $\overline{\mathrm{X}}_i = \overline{\Pi}_i(A_i - \Gamma_iC_i) + (A_i - \Gamma_iC_i)^T\overline{\Pi}_i + \sum_{j=1_{j\neq i}}^{L}[\widetilde{\lambda}_j^{-1}H_{ji}^TH_{ji}] + \sum_{j=1_{j\neq i}}^{L}[\widehat{\lambda}_j(\Upsilon_jH_{ji})^T\Upsilon_jH_{ji}]$.

Proof. of Theorem 1: Lyapunov's function [6, 34] is selected as follows:

$$V = \sum_{i=1}^{L}\begin{bmatrix} x_i \\ \tilde{x}_i \end{bmatrix}^T\begin{bmatrix} \Pi_i & 0 \\ 0 & \overline{\Pi}_i \end{bmatrix}\begin{bmatrix} x_i \\ \tilde{x}_i \end{bmatrix}, \tag{31}$$

where $\Pi_i > 0$ and $\overline{\Pi}_i > 0$ satisfy (30) for $i = 1, 2, \ldots, L$. Then, taking the derivative of time, we have the following:

$$\begin{aligned}
\dot{V} &= \sum_{i=1}^{L}\begin{bmatrix}\dot{x}_i\\ \dot{\tilde{x}}_i\end{bmatrix}^T\begin{bmatrix}\Pi_i & 0\\ 0 & \overline{\Pi}_i\end{bmatrix}\begin{bmatrix}x_i\\ \tilde{x}_i\end{bmatrix}+\sum_{i=1}^{L}\begin{bmatrix}x_i\\ \tilde{x}_i\end{bmatrix}^T\begin{bmatrix}\Pi_i & 0\\ 0 & \overline{\Pi}_i\end{bmatrix}\begin{bmatrix}\dot{x}_i\\ \dot{\tilde{x}}_i\end{bmatrix}\\
&= \sum_{i=1}^{L}\left\{\begin{bmatrix}x_i\\ \tilde{x}_i\end{bmatrix}^T\begin{bmatrix}\Pi_i\left(A_i-B_i\Lambda_i\right)+\left(A_i-B_i\Lambda_i\right)^T\Pi_i & \Pi_i\Theta_i\\ \Theta_i^T\Pi_i & \overline{\Pi}_i\left(A_i-\Gamma_i C\right)_i+\left(A_i-\Gamma_i C_i\right)^T\overline{\Pi}_i\end{bmatrix}\begin{bmatrix}x_i\\ \tilde{x}_i\end{bmatrix}\right\}\\
&+\sum_{i=1}^{L}\left[x_i^T\Pi_i \mathrm{N}_i e^{-\delta_i t}+\left(e^{-\delta_i t}\right)^T N_i^T\Pi_i x_i\right]\\
&+\sum_{i=1}^{L}\sum_{\substack{j=1\\ j\neq i}}^{L}\left[x_j^T\left(H_{ij}-\Upsilon_i H_{ij}\right)^T\Pi_i x_i+x_i^T\Pi_i\left(H_{ij}-\Upsilon_i H_{ij}\right)x_j\right]\\
&+\sum_{i=1}^{L}\sum_{\substack{j=1\\ j\neq i}}^{L}\left[\tilde{x}_j^T\left(\Upsilon_i H_{ij}\right)^T\Pi_i x_i+x_i^T\Pi_i\Upsilon_i H_{ij}\tilde{x}_j\right]\\
&+\sum_{i=1}^{L}\sum_{\substack{j=1\\ j\neq i}}^{L}\left(\tilde{x}_i^T\overline{\Pi}_i H_{ij}\tilde{x}_j+\tilde{x}_j^T H_{ij}^T\overline{\Pi}_i\tilde{x}_i\right)\\
&+\sum_{i=1}^{L}\left[\tilde{x}_i^T\overline{\Pi}_i\Phi_i+x_i^T\Pi_i\Phi_i+\Phi_i^T\Pi_i x_i+\Phi_i^T\overline{\Pi}_i\tilde{x}_i\right].
\end{aligned}\tag{32}$$

Introducing Lemma 1 into equation (32), we get the following:

$$\begin{aligned}
\dot{V} \leq &\sum_{i=1}^{L}\left\{\begin{bmatrix}x_i\\ \tilde{x}_i\end{bmatrix}^T\begin{bmatrix}\Pi_i\left(A_i-B_i\Lambda_i\right)+\left(A_i-B_i\Lambda_i\right)^T\Pi_i & \Pi_i\Theta_i\\ \Theta_i^T\Pi_i & \overline{\Pi}_i\left(A_i-\Gamma_i C_i\right)+\left(A_i-\Gamma_i C_i\right)^T\overline{\Pi}_i\end{bmatrix}\begin{bmatrix}x_i\\ \tilde{x}_i\end{bmatrix}\right\}\\
&+\sum_{i=1}^{L}\sum_{\substack{j=1\\ j\neq i}}^{L}\left[\overline{\lambda}_i x_j^T\left(H_{ij}-\Upsilon_i H_{ij}\right)^T\left(H_{ij}-\Upsilon_i H_{ij}\right)x_j\right]\\
&+\sum_{i=1}^{L}\sum_{\substack{j=1\\ j\neq i}}^{L}\left[\overline{\lambda}_i^{-1}x_i^T\Pi_i\Pi_i x_i+\widehat{\lambda}_i\tilde{x}_j^T\left(\Upsilon_i H_{ij}\right)^T\Upsilon_i H_{ij}\tilde{x}_j\right]\\
&+\sum_{i=1}^{L}\sum_{\substack{j=1\\ j\neq i}}^{L}\left(\widehat{\lambda}_i^{-1}x_i^T\Pi_i\Pi_i x_i+\tilde{\lambda}_i\tilde{x}_i^T\overline{\Pi}_i\overline{\Pi}_i\tilde{x}_i+\tilde{\lambda}_i^{-1}\tilde{x}_j^T H_{ij}^T H_{ij}\tilde{x}_j\right)\\
&+\sum_{i=1}^{L}\left[\overline{\gamma}_i\tilde{x}_i^T\overline{\Pi}_i\overline{\Pi}_i\tilde{x}_i+\overline{\gamma}_i^{-1}\Phi_i^T\Phi_i+\tilde{\gamma}_i x_i^T\Pi_i\Pi_i x_i+\tilde{\gamma}_i^{-1}\Phi_i^T\Phi_i\right]\\
&+\sum_{i=1}^{L}\left[\widehat{\gamma}_i^{-1}x_i^T\Pi_i \mathrm{N}_i N_i^T\Pi_i x_i+\widehat{\gamma}_i\left(e^{-\delta_i t}\right)^T e^{-\delta_i t}\right].
\end{aligned}\tag{33}$$

Since

$$\sum_{i=1}^{L}\sum_{\substack{j=1\\ j\neq i}}^{L}\overline{\lambda}_i x_j^T\left(H_{ij}-\Upsilon_i H_{ij}\right)^T\left(H_{ij}-\Upsilon_i H_{ij}\right)x_j=\sum_{i=1}^{L}\sum_{\substack{j=1\\ j\neq i}}^{L}\overline{\lambda}_j x_i^T\left(H_{ji}-\Upsilon_j H_{ji}\right)^T\left(H_{ji}-\Upsilon_j H_{ji}\right)x_i\sum_{i=1}^{L}\sum_{\substack{j=1\\ j\neq i}}^{L}\widehat{\lambda}_i\widetilde{x}_j^T\left(\Upsilon_i H_{ij}\right)^T\Upsilon_i H_{ij}\widetilde{x}_j$$
$$=\sum_{i=1}^{L}\sum_{\substack{j=1\\ j\neq i}}^{L}\widehat{\lambda}_j\widetilde{x}_i^T\left(\Upsilon_i H_{ij}\right)^T\Upsilon_j H_{ji}\widetilde{x}_i, \tag{34}$$

$$\sum_{i=1}^{L}\sum_{\substack{j=1\\ j\neq i}}^{L}\widetilde{\lambda}_i^{-1}\widetilde{x}_j^T H_{ij}^T H_{ij}\widetilde{x}_j=\sum_{i=1}^{L}\sum_{\substack{j=1\\ j\neq i}}^{L}\widetilde{\lambda}_j^{-1}\widetilde{x}_i^T H_{ji}^T H_{ji}\widetilde{x}_i, \tag{35}$$

we

$$\begin{aligned}\dot{V}\leq&\sum_{i=1}^{L}\left\{\begin{bmatrix}x_i\\ \widetilde{x}_i\end{bmatrix}^T\begin{bmatrix}\Pi_i\left(A_i-B_i\Lambda_i\right)+\left(A_i-B_i\Lambda_i\right)^T\Pi_i & \Pi_i\Theta_i\\ \Theta_i^T\Pi_i & \overline{\Pi}_i\left(A_i-\Gamma_i C_i\right)+\left(A_i-\Gamma_i C_i\right)^T\overline{\Pi}_i\end{bmatrix}\begin{bmatrix}x_i\\ \widetilde{x}_i\end{bmatrix}\right\}\\
&+\sum_{i=1}^{L}\sum_{\substack{j=1\\ j\neq i}}^{L}\left[\overline{\lambda}_j x_i^T\left(H_{ji}-\Upsilon_j H_{ji}\right)^T\left(H_{ji}-\Upsilon_j H_{ji}\right)x_i\right]\\
&+\sum_{i=1}^{L}\sum_{\substack{j=1\\ j\neq i}}^{L}\left[\overline{\lambda}_i^{-1}x_i^T\Pi_i\Pi_i x_i+\widehat{\lambda}_j\widetilde{x}_i^T\left(\Upsilon_j H_{ji}\right)^T\Upsilon_j H_{ji}\widetilde{x}_i\right]\\
&+\sum_{i=1}^{L}\sum_{\substack{j=1\\ j\neq i}}^{L}\left(\widehat{\lambda}_i^{-1}x_i^T\Pi_i\Pi_i x_i+\widetilde{\lambda}_i\widetilde{x}_i^T\overline{\Pi}_{ii}\overline{\Pi}_{ii}\widetilde{x}_i+\widetilde{\lambda}_j^{-1}\widetilde{x}_i^T H_{ji}^T H_{ji}\widetilde{x}_i\right)\\
&+\sum_{i=1}^{L}\left[\overline{\gamma}_i\widetilde{x}_i^T\overline{\Pi}_i\overline{\Pi}_i\widetilde{x}_i+\widetilde{\gamma}_i x_i^T\Pi_i\Pi_i x_i+\overline{\gamma}_i^{-1}\Phi_i^T\Phi_i+\widetilde{\gamma}_i^{-1}\Phi_i^T\Phi_i\right]\\
&+\sum_{i=1}^{L}\left[\widehat{\gamma}_i^{-1}x_i^T\Pi_i\mathrm{N}_i N_i^T\Pi_i x_i+\widehat{\gamma}_i\left(e^{-\delta_i t}\right)^T e^{-\delta_i t}\right]\\
\leq&\sum_{i=1}^{L}\left\{\begin{bmatrix}x_i\\ \widetilde{x}_i\end{bmatrix}^T\begin{bmatrix}\Omega_i & \Pi_i\Theta_i\\ \Theta_i^T\Pi_i & \overline{\Omega}_i\end{bmatrix}\begin{bmatrix}x_i\\ \widetilde{x}_i\end{bmatrix}\right\}\\
&+\sum_{i=1}^{L}\left[\left(\overline{\gamma}_i^{-1}+\widetilde{\gamma}_i^{-1}\right)\gamma_i^2\right]+\sum_{i=1}^{L}\left[\widehat{\gamma}_i\left(e^{-\delta_i t}\right)^T e^{-\delta_i t}\right].\end{aligned} \tag{36}$$

where $\lambda_i=(N-1)(\overline{\lambda}_i^{-1}+\widehat{\lambda}_i^{-1})+\widetilde{\gamma}_i$ and $\rho_i=\widetilde{\lambda}_i(N-1)+\overline{\gamma}_i$, $\Omega_i=\Pi_i(A_i-B_i\Lambda_i)+(A_i-B_i\Lambda_i)^T\Pi_i+\widehat{\gamma}_i^{-1}\Pi_i\mathrm{N}_i N_i^T\Pi_i$ $+\lambda_i\Pi_i\Pi_i+\sum_{j=1_{j\neq i}}^{L}[\overline{\lambda}_j(H_{ji}-\Upsilon_j H_{ji})^T(H_{ji}-\Upsilon_j H_{ji})]$ and $\overline{\Omega}_i=\overline{\Pi}_i(A_i-\Gamma_i C_i)+(A_i-\Gamma_i C_i)^T\overline{\Pi}_i+\rho_i\overline{\Pi}_i\overline{\Pi}_i+\sum_{j=1_{j\neq i}}^{L}[\widetilde{\lambda}_j^{-1}H_{ji}^T H_{ji}]+\sum_{j=1_{j\neq i}}^{L}[\widehat{\lambda}_j(\Upsilon_j H_{ji})^T\Upsilon_j H_{ji}]$.

Furthermore, by the Schur complement of [33], the LMI is similar to the following:

$$\Psi_i=\begin{bmatrix}\Omega_i & \Pi_i\Theta_i\\ \Theta_i^T\Pi_i & \overline{\Omega}_i\end{bmatrix}<0. \tag{37}$$

Combining (36) and (37), we get the following:

$$\dot{V} \le \sum_{i=1}^{L}\left(-\rho_{\min}(\Psi_i)\left\|\begin{bmatrix} x_i \\ \tilde{x}_i \end{bmatrix}\right\|^2 + \zeta_i + \hat{\gamma}_i e^{-2\delta_i t}\right), \tag{38}$$

where $\zeta_i = \sum_{i=1}^{L}[(\overline{\gamma}_i^{-1} + \tilde{\gamma}_i^{-1})\gamma_i^2]$ is the constant value and the eigenvalue $\rho_{\min}(\Psi_i) > 0$. The term $\frac{i}{\gamma}e^{-2\delta_i t}$ will be approaching zero when the time is approaching infinite. Hence, $\dot{V} < 0$ is derived with $\left\|\begin{bmatrix} x_i \\ \tilde{x}_i \end{bmatrix}\right\| > \sqrt{(\zeta_i/\rho_{\min}(\Psi_i))}$, which shows that the system is asymptotic stable. □

5. Total Output Feedback Sliding Mode Controller Design

In this segment, we design the decentralized single-phase SMC scheme (DSPSMCS) for the LFC of the MAMSPS (18) as follows:

$$\begin{aligned} u_i(t) = {} & -(\mathrm{M}_i B_i)^{-1}\left[\|\mathrm{M}_i\|\|B_i\|\|\Lambda_i\|\|\hat{x}_i(t)\|\right] \\ & + \delta_i\|\mathrm{M}_i\|\|\hat{x}_i(0)\|e^{-\delta_i t} + \|\mathrm{M}_i\|\|\Gamma_i\|\|(y_i - \hat{y}_i)\| \\ & + \sum_{\substack{j=1 \\ j\ne i}}^{L}\left\|\mathrm{M}_j\right\|\left\|H_{ji}\right\|\|\hat{x}_i(t)\| + \theta_i\Big]\frac{\eta_i[\hat{x}(t)]}{\|\eta_i[\hat{x}_i(t)]\|}, \\ & i = 1, 2, \ldots, L, \end{aligned} \tag{39}$$

where θ_i is the positive scalar and $u_i(t)$ is the decentralized single-phase SMC scheme. In this subsection, the system state variable reachability proof is also derived with the Lyapunov function accompanying the theorem postulated below.

Theorem 2. *The SSWRP and the controller are given by equations (24) and (39), respectively. Then, the variable state trajectories of system (19) reach the single-phase sliding surface and lie on it for all time.*

Remark 2. The concept of a single-phase SMC is centered on the robustness of motion throughout the state space. The dimension of the state space is equal to the order of the motion equation in sliding mode. As a result, the resilience of complex interconnected power systems may be guaranteed throughout the system's full response, beginning with the initial time instance.

Proof. of Theorem 2: The Lyapunov function [6, 34] is given as follows:

$$V_1 = \sum_{i=1}^{L}\left(\|\eta_i[\hat{x}_i(t)]\|\right). \tag{40}$$

Using the time derivative of V_1, we obtain the following:

$$\dot{V}_1 = \sum_{i=1}^{L}\left(\frac{\eta_i^T[\hat{x}_i(t)]}{\|\eta_i[\hat{x}_i(t)]\|}\dot{\eta}_i[\hat{x}_i(t)]\right). \tag{41}$$

Substituting equation (26) into equation (41), we have the following:

$$\begin{aligned} \dot{V}_1 = {} & \sum_{i=1}^{L}\frac{\eta_i^T[\hat{x}_i(t)]}{\|\eta_i[\hat{x}_i(t)]\|}\begin{bmatrix} \mathrm{M}_i A_i\hat{x}_i(t) - \mathrm{M}_i(A_i - B_i\Lambda_i)\hat{x}_i(t) \\ +\delta_i\mathrm{M}_i\hat{x}_i(0)e^{-\delta_i t} + \mathrm{M}_i\Gamma_i(y_i - \hat{y}_i) \end{bmatrix} \\ & + \sum_{i=1}^{L}\frac{\eta_i^T[\hat{x}_i(t)]}{\|\eta_i[\hat{x}_i(t)]\|}\mathrm{M}_i B_i u_i(t) \\ & + \sum_{i=1}^{L}\sum_{\substack{j=1 \\ j\ne i}}^{L}\left[\frac{\eta_i^T[\hat{x}_i(t)]}{\|\eta_i[\hat{x}_i(t)]\|}\mathrm{M}_i H_{ij}\hat{x}_j(t)\right]. \end{aligned} \tag{42}$$

According to equation (42), property $\|AB\| \le \|A\|\|B\|$ and $\sum_{i=1}^{L}\sum_{j=1_{j\ne i}}^{L}[\|\mathrm{M}_i\|\|H_{ij}\|\|\hat{x}_j(t)\|] = \sum_{i=1}^{L}\sum_{j=1}^{L}[\|\mathrm{M}_j\|\|H_{ji}\|\|\hat{x}_i(t)\|]$, and it generates:

$$\begin{aligned} \dot{V}_1 = {} & \sum_{i=1}^{L}\left[\|\mathrm{M}_i\|\|B_i\|\|\Lambda_i\|\|\hat{x}_i(t)\| + \delta_i\|\mathrm{M}_i\|\|\hat{x}_i(0)\|e^{-\delta_i t}\right] + \sum_{i=1}^{L}\left[\|\mathrm{M}_i\|\|\Gamma_i\|\|(y_i - \hat{y}_i)\|\right] \\ & + \sum_{i=1}^{L}\sum_{\substack{j=1 \\ j\ne i}}^{L}\left[\left\|\mathrm{M}_j\right\|\left\|H_{ji}\right\|\|\hat{x}_i(t)\|\right] + \sum_{i=1}^{L}\frac{\eta_i^T[\hat{x}_i(t)]}{\|\eta_i[\hat{x}_i(t)]\|}\mathrm{M}_i B_i u_i(t). \end{aligned} \tag{43}$$

By substituting $u_i(t)$ into equation (43), we achieve the following:

$$\dot{V}_1 \le -\sum_{i=1}^{L}\theta_i < 0. \tag{44}$$

The derivative of Lyapunov's function (40) is less than zero. Therefore, the reachability proof is achieved.

Following that, Figure 2 depicts the flowchart of the proposed observer single-phase sliding mode control technique. □

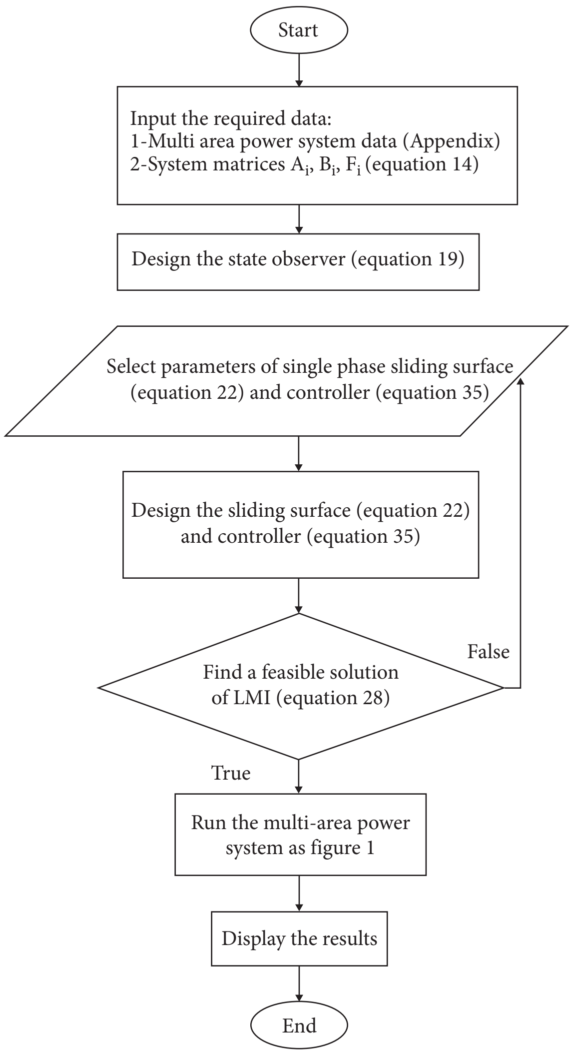

Figure 2: Flowchart of the proposed observer single-phase sliding mode-based load frequency control.

Remark 3. Paper [6, 34] *shows the LFC's stability in a power system while employing the LMI approach. In the LMI equations, however, the aforementioned method requires the discovery of four positive matrices. As a result, the suggested method only needs to locate two positive matrices in LMI equations, making finding a feasible solution easier.*

6. Simulation Results and Discussions

In this session, to test the efficiency and robustness of the proposed control strategy, the various cases in four simulations are implemented to prove the performance.

In this session, to test the efficiency and robustness of the proposed control strategy, various cases in three simulations are implemented to prove the performance of the suggested single-phase sliding mode control-based state observer (SPSMCBSO) for the LFC of the two areas gas-hydro-thermal power system (TAGHTPS) under step load disturbance, random load disturbance, and parameter uncertainties. The simulation results of the investigation are compared with recent results of the control method in [24–26, 30–32] as follows.

6.1. Simulation 1. The classical control methods are commonly used for the LFC of MAMSPS under step load disturbance. The recent application of bacterial foraging algorithm (BFA) for the design and implementation of generation-based PID structured automatic generation control algorithm was developed to investigate the LFC of TAGHTPS [24]. In this case, we test the proposed controller of PS under 1% to 2% increase in step load change with the nominal parameters kept in the same manner [24]. The frequency deviation in both areas is displayed in Figure 3 to Figure 4, and the tie-line power deviation (TLPD) is shown in Figure 5. The TAGHTPS performance with settling time and overshoot is compared rightly with that seen in [24]. It can be seen that both controllers produced smaller frequency overshoot in other words keeping the operating frequency with the permissible level ±0.001 Hz, but 8s settling time with the novel approach is comparatively lower than the settling time in [24, 30–32].

Remark 4. With this comparison [24, 30–32]*, the novel proposed SPSMCBSO controller for the LFC of MAMSPS is more robust and responsive to load disturbances than the earlier technique. The load disturbance is clearly visible, and the system is quickly restored to steady state with smaller overshoots.*

6.2. Simulation 2

Case 1. Again, the TAGHTPS with a recently developed teaching learning-based optimization (TLBO) algorithm with 2-degree-of-freedom of proportional-integral-derivative (2-DOF PID) controller was simulated with 0.01 p.u.MW load disturbance in each area and nominal parameters are given as demonstrated in [25]. To analyze the performance of PS, we propose SPSMCBSO and then simulate the TAGHTPS response with the proposed approach in the same manner as in [25]. The frequency variation in both areas is given in Figure 6. The TLPD is presented in Figure 7 accordingly. Both frequency overshoots in every area seem to be better, but the 7 s settling time with the novel approach is very low compared with 13 s settling time seen in [25]. Table 1 compares the two controllers in detail. This means that the proposed system is a superior option for the MAMSPS LFC since it is easier to execute and less stressful.

Case 2. As industrial activities continue to increase, the electricity demands from neighboring industries, hospitals, homes, and other kinds of load also increase. On the other hand, the MAMSPSs are required to meet the demands with frequency kept at the permissible level. Therefore, we assume the electricity demands as a random load disturbance applied to each area of the TAGHTPS as shown in Figure 8. The subsystem parameters are assumed to be nominal as in case 1 of this simulation.

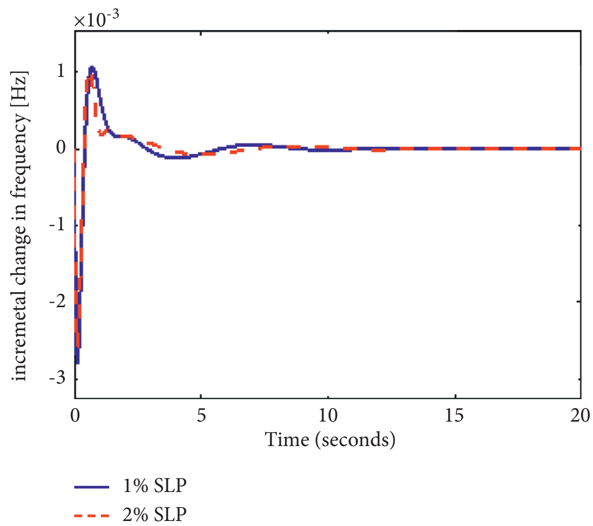

FIGURE 3: Frequency deviation (Hz) with 1% to 2% step load in area 1.

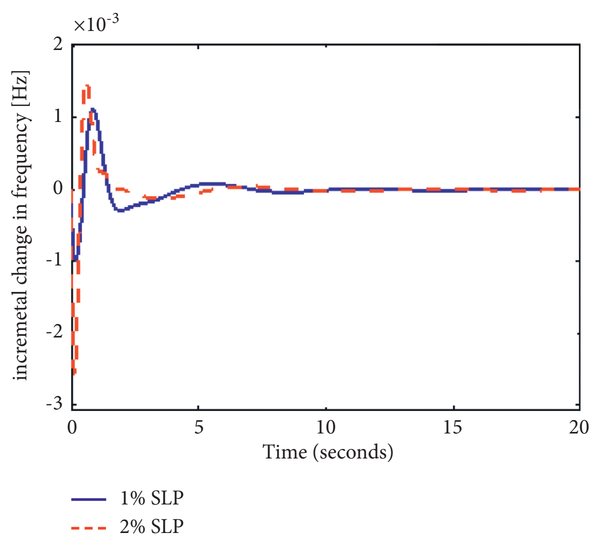

FIGURE 4: Frequency deviation (Hz) with 1% to 2% step load in area 2.

The frequency oscillation in both areas is shown in Figure 9 to Figure 10, while TLPD is displayed in Figure 11. The frequency response in Figures 9 and 10 has improved under random load changes. Again, the frequency is kept at tolerable level during operation, therefore validating the proposed SPSMCBSO for the LFC of MAMSPS.

Remark 5. TAGHTPS was simulated with only step load disturbance from demands of customers as seen in [25]. However, in reality, demands from load change daily, so this demand is assumed to be a random load change, which is subjected to the PS. Under the random load condition of the TAGHTPS, the proposed SPSMCBSO proves to be very useful for the stability of the power system, making it better for the LFC of MAMSPS.

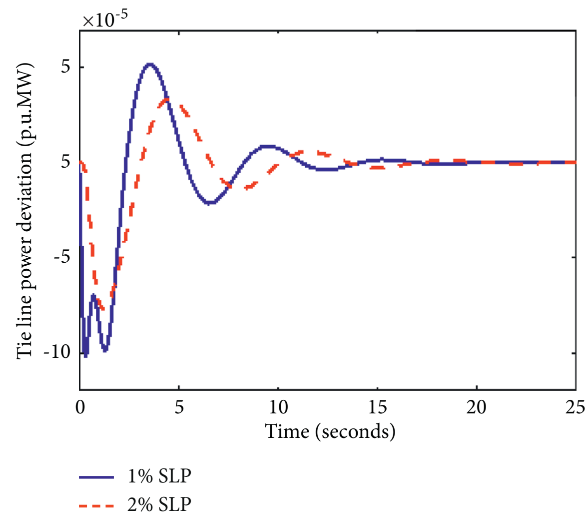

FIGURE 5: Tie-line power variation (p.u.MW).

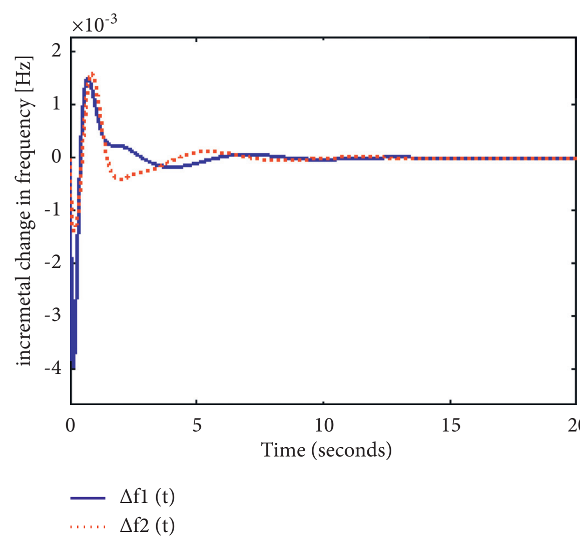

FIGURE 6: Frequency deviation (Hz) with 1% step load in area 1 and area 2.

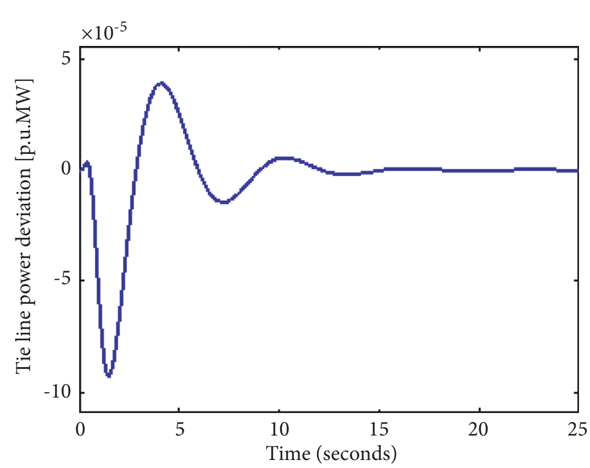

FIGURE 7: Tie-line power variation (p.u.MW).

Table 1: Setting time T_s(s) and maximum overshoot MOS(Hz) comparison.

Controller	The proposed method		The recent method in [25]	
Parameter	$T_s[s]$	MOS (Hz)	$T_s[s]$	MOS (Hz)
Δf_1	7	0.004	13	0.019
Δf_2	7	0.0012	13	0.017

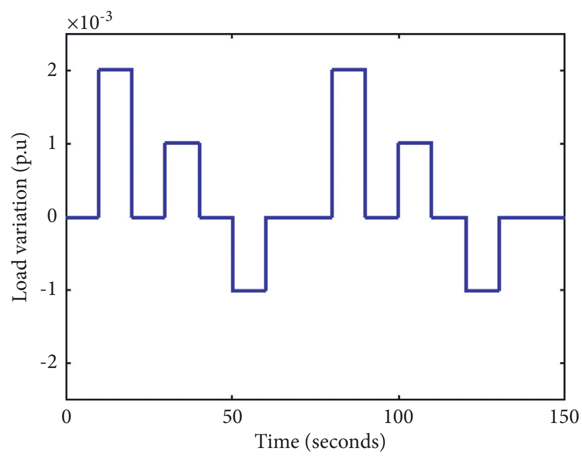

Figure 8: Random load variation.

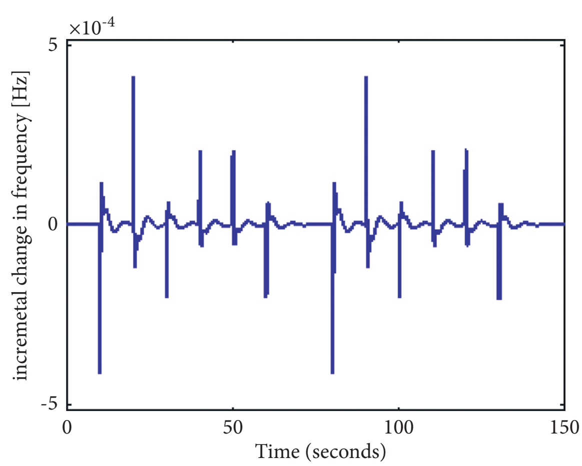

Figure 9: Frequency variation (Hz) in area 1.

6.3. Simulation 3

Case 3. The TAGHTPS response was simulated again using the Jaya method to develop PID structured regulators for the optimized generation control (OGC) strategy, using a step load disturbance of 1% and the subsystem parameter from [26]. The above applied the metaheuristic algorithm to optimize the control parameter search for PS. However, implementing this strategy for the LFC of MAMSPS might be challenging as well. In review, the metaheuristic approach is quite complex and time-consuming too. In other words, we again proposed the SPSMCBSO, which is simpler to implement. In this case, we simulate the TAGHTPS response with the proposed approach under a similar condition to the one observed in [26]. The frequency variation in area 1 is shown in Figure 12, while in area 2, the frequency deviation is shown in Figure 13. The TLPD is given in Figure 14, respectively. Both controllers are seen with better overshoot, but 5 s settling time with the proposed approach again is comparatively lower than the 8 s settling time with the controller in [26]. Table 2 shows a detailed comparison of both controllers. This further implies that the proposed scheme is a better choice for the MAMSPS LFC, which is very simple and less stressful to implement.

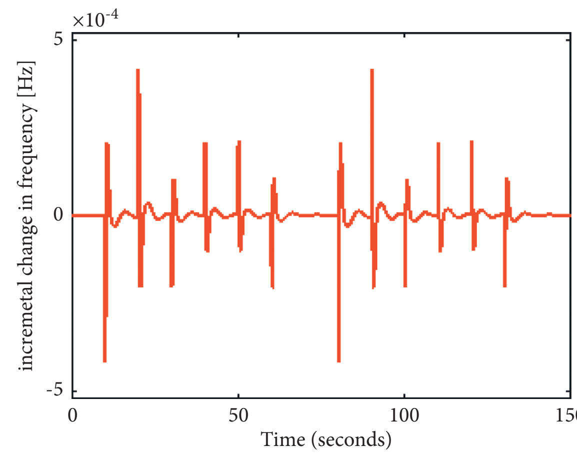

Figure 10: Frequency variation (Hz) in area 2.

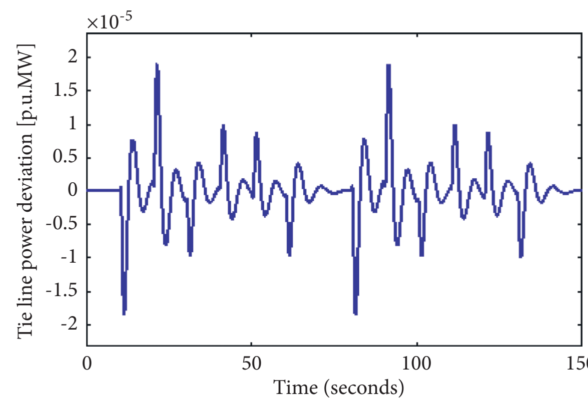

Figure 11: Change in tie-line power (p.u.MW).

Case 4. As industrial activity grows, so does the need for power from surrounding enterprises, hospitals, households, and other types of loads, MAMSPS, on the other hand, must meet the needs with a frequency that is within acceptable limits. As a result, as illustrated in Figure 15, we treat electrical needs as a random load disturbance applied to each section of the TAGHTPS.

Figures 16 and 17 depict the frequency oscillation in both locations, whereas Figure 18 depicts the TLPD. Under random load variations, the frequency response in Figures 16 and 17 has improved. The frequency is maintained at a reasonable level during operation, validating the proposed SPSMCBSO for the MAMSPS LFC.

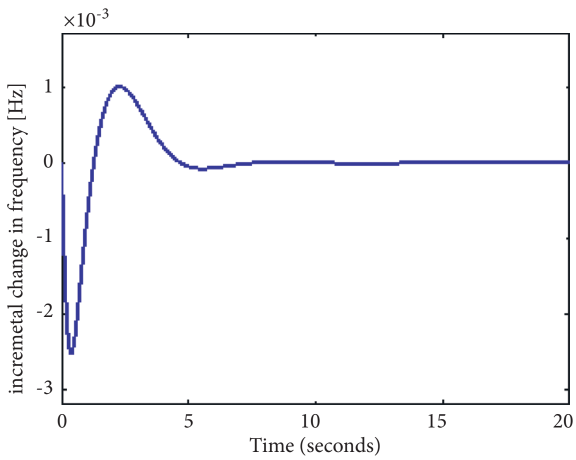

Figure 12: Frequency variation (Hz) in area 1.

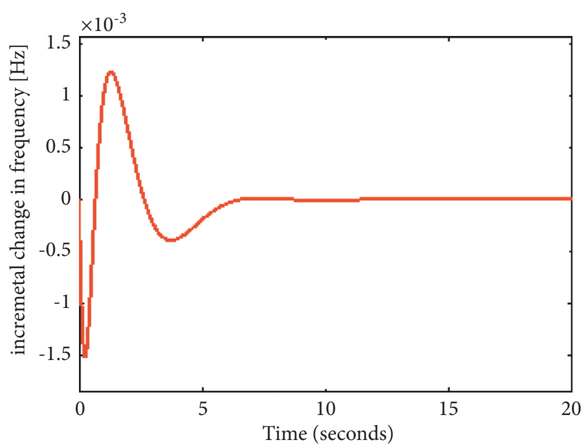

Figure 13: Frequency variation (Hz) in area 2.

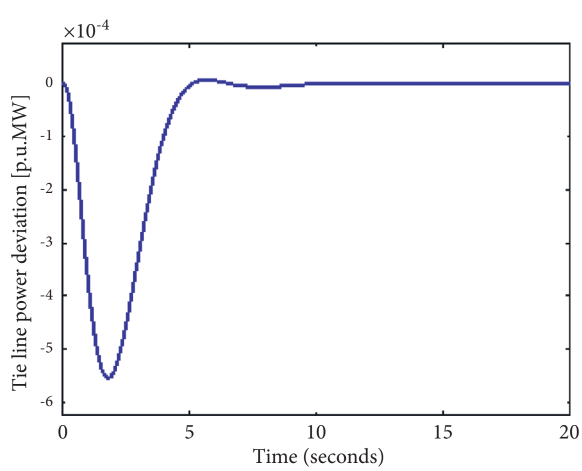

Figure 14: Change in tie-line power (p.u.MW).

Case 5. To be more realistic in achieving a better LFC of MAMSPS, it is required for the controller to be robust against certain disturbances such as random load change, parameter uncertainties, and subsystem parameter deviation. Therefore,

Table 2: Setting time T_s(s) and maximum overshoot MOS(Hz) comparison.

Controller	The proposed method		The recent method in [26]	
Parameter	$T_s[s]$	MOS (Hz)	$T_s[s]$	MOS (Hz)
Δf_1	5	0.0025	8	0.007
Δf_2	6.25	0.0015	8	0.003

in this case, we simulate the TAGHTPS response under random load disturbance as shown in Figure 19 and ±20 deviation in subsystem parameters. We also assume mismatched uncertainties in the system state matrix as a result of the change in valve positions of the TAGHTPS represented in the cosine function given as follows.

We have $\Delta A_1 = \Delta A_2 = [\,\Delta A_{11} \;\; \Delta A_{12}\,]$, where:

$$\Delta A_{11} = \begin{bmatrix} 0 & 0 & 0 & 0 & 0 & 0 & 0 \\ 0 & 0 & 0 & 0 & 0 & 0 & 0 \\ 4\cos(t) & 0 & 0 & 0 & 0 & 0 & 0 \\ 0.46\cos(t) & 0 & 0 & \cos(t) & 0 & 0 & 0 \\ \cos(t) & 0 & 0 & 0 & 0 & \cos(t) & 0 \\ \cos(t) & 0 & 0 & 0 & 0 & 0 & 0 \\ 0 & 0 & 0 & 0 & 0 & 0 & 0 \\ 0 & 0 & 0 & 0 & 0 & 0 & 0 \\ \cos(t) & 0 & 0 & 0 & 0 & 0 & 0 \\ \cos(t) & 0 & 0 & 0 & 0 & 0 & 0 \\ 0 & 0 & 0 & 0 & 0 & 1.6\cos(t) & 0 \\ 0 & 0 & 0 & 0 & 0 & 0 & 0 \\ 0 & 0 & 0 & 0 & 0 & 0 & 0 \end{bmatrix}$$

t

$$\Delta A_{12} = \begin{bmatrix} 0 & 0 & 0 & 0 & 0 & 0 \\ 0 & 0 & 0 & 0 & 0 & 0 \\ 0 & 0 & 0 & 0 & 0 & 0 \\ 0 & 0 & 0 & 0 & 0 & 0 \\ 0 & 0 & 0 & 0 & 0 & 0 \\ 0 & 0 & 0 & 0 & 0 & 0 \\ 0 & 0 & 0 & 0 & 0 & 6\cos(t) \\ 0 & 0 & 0 & 0 & 0 & 0 \\ 0 & 0 & 0 & \cos(t) & 0 & 0 \\ 0 & 0 & 0.2\cos(t) & \cos(t) & 0 & 0 \\ 0 & 0 & 0 & 0 & 0 & 0 \\ 0 & 0 & 0 & 0 & 0 & 0 \\ 0 & 0 & 0 & 0 & 0 & 0 \end{bmatrix} \quad (45)$$

The frequency fluctuation in both areas is given in Figure 20, while TLPD is in Figure 21. The proposed SPSMCBSO maintained higher robustness by rejecting the various disturbances and keeping the frequency at the operating permissible point with the TLPD properly managed as well.

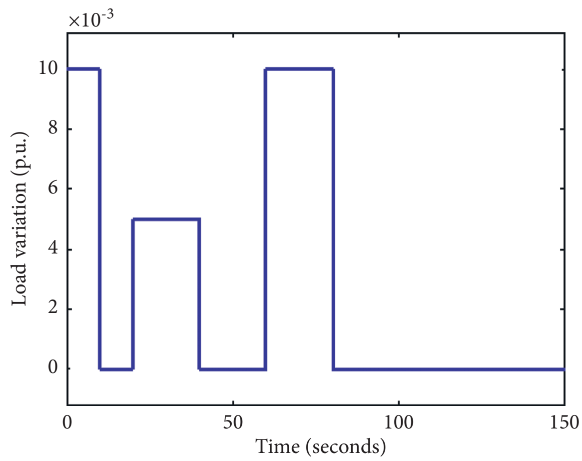

Figure 15: Random load variation.

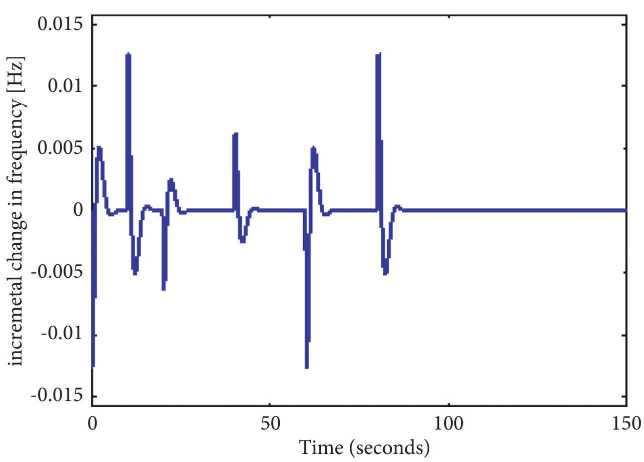

Figure 16: Frequency variation (Hz) in area 1.

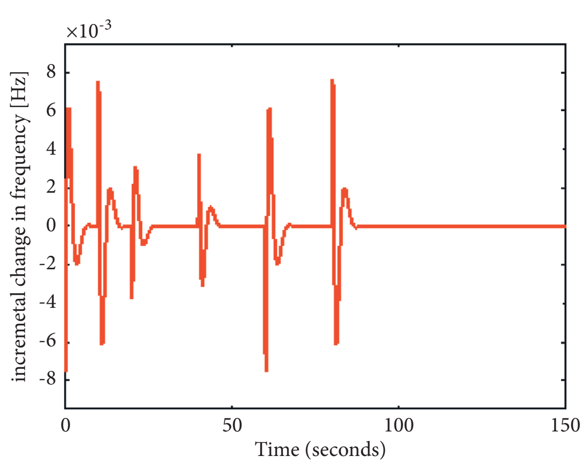

Figure 17: Frequency variation (Hz) in area 2.

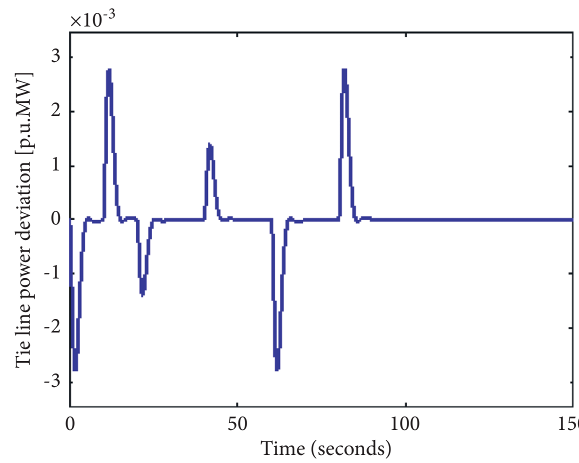

Figure 18: Change in tie-line power (p.u.MW).

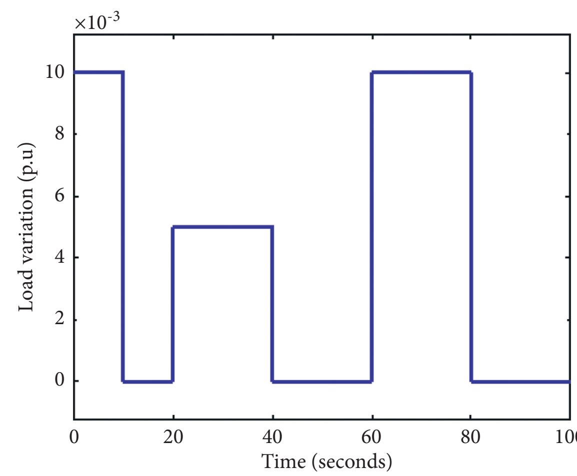

Figure 19: Variation in random load.

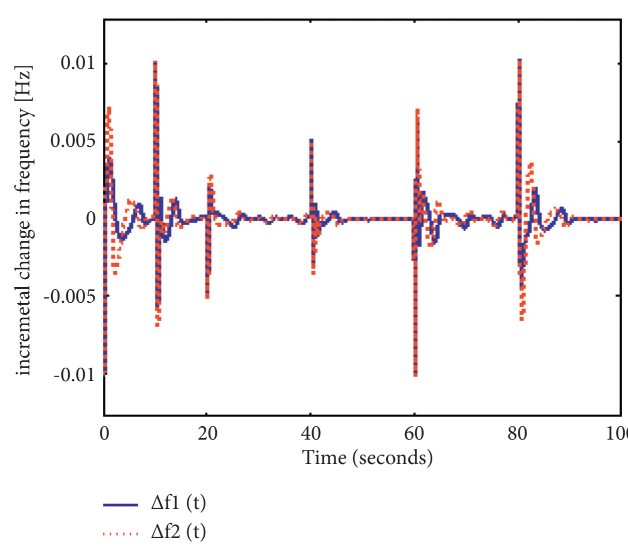

Figure 20: Frequency deviations (Hz) in area 1 and area 2.

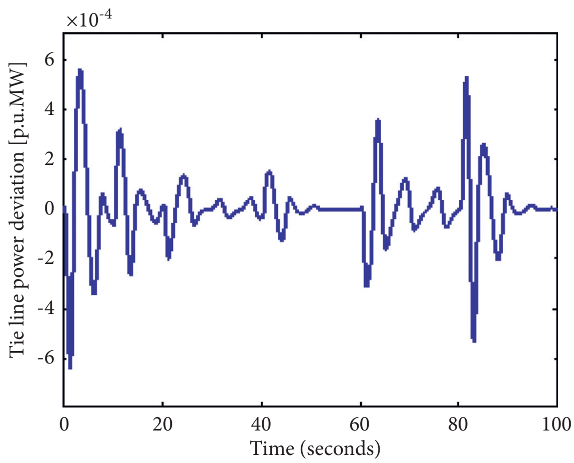

Figure 21: Changes in tie-line power (p.u.MW).

Remark 6. The TAGHTPS response has been simulated against the step load disturbance and random load changes to compare the optimal controller given in [26]. *The results were seen better; however, the LFC schemes are required to be robust against wide range of disturbances. Therefore, the proposed single-phase sliding mode control-based state observer (SPSMCBSO) scheme is simulated under parameter uncertainties, subsystem parameter deviations, random load disturbance, and step load change and it proves to be robust by rejecting these disturbances and maintaining the TAGHTPS stability.*

6.4. Simulation 4. To investigate the computational efficacy of SPSMCBSO scheme, the study is extended to a complex and realistic system, namely four-area multisource power system. Area 1, area 2, area 3, and area 4 consist of thermal-hydro-gas plant in each control area. The transfer function model of test system is available in Figure 1 with $i = 4$. The comparative transient responses of test simulation 4 after 1% step load disturbance are depicted in Figures 22 and 23. The optimal controller parameters obtained by the proposed approach are presented from the frequency vitiation of four areas in Figure 22. The fluctuations in tie-line power are clearly shown in Figure 23.

In detail, the typical transient specifications in terms of peak undershoot and settling time of system oscillations are noted to manage and keep the frequency at the operating permissible point with the changes in the tie-line properly managed and the proposed control scheme.

Remark 7. A SPSMCBSO controller is designed for load frequency control of four-area interconnected power systems. The proposed single-phase surface and the designed decentralized SMC can reduce the overshoot and improve the response speed and can also limit the deviation of frequency to zero. Therefore, the designed controller is robust and effective to control the matching and mismatched parameter uncertainties of interconnected multiarea systems.

Remark 8. From simulation 1 to simulation 4, a sensitivity analysis is undertaken to evaluate the benefit of the proposed SPSMCBSO scheme-based LFC. The settling times and

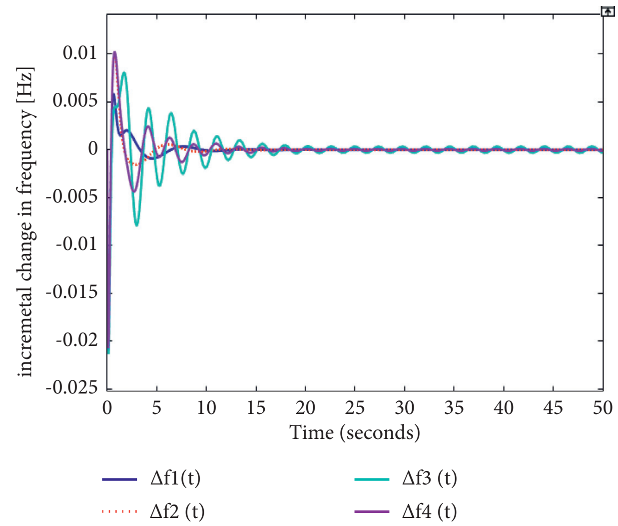

Figure 22: Frequency variation (Hz) in area 1, area 2, area 3, and area 4.

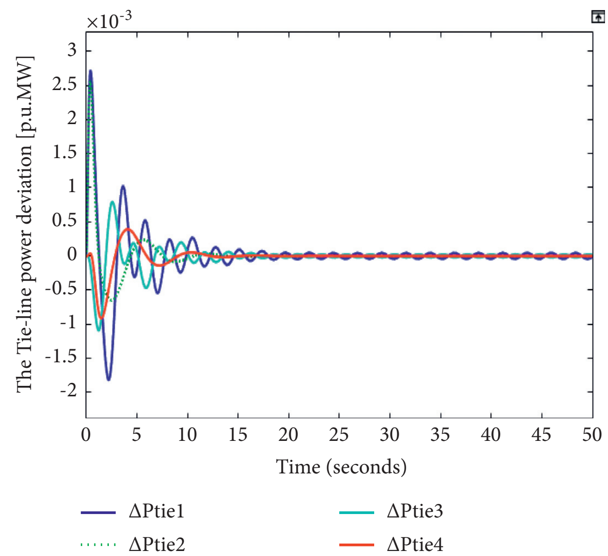

Figure 23: Changes in tie-line power (p.u.MW).

minimum under/overshoot value under normal and varied conditions for the concerned power system are offered in each case. It is clearly viewed that performance values are changing within the acceptable limits and almost equal to the respective values obtained at the nominal condition. Hence, it may be concluded that the proposed controller gains are insensitive to the matched and mismatched disturbance and the parameter variations and perform satisfactorily under the wide change in the loading condition and system parameters compared with [24–26, 30–32].

7. Conclusions

In this study, for the first time, the single-phase sliding mode control-based state observer (SPSMCBSO) is developed for the load frequency control (LFC) of the multiarea multisource power system (MAMSPS). To test the feasibility of the constructed SPSMCBSO, the two-area gas-hydro-thermal power system (TAGHTPS) model is chosen. Furthermore, the uncertainty of the state and interconnected parameters is considered for the TAGHTPS model. The proof of the stability of TAGHTPS is established by a new linear matrix inequality via the Lyapunov theory. The superiority of the SPSMCBSO is concentrated in the comparison of the simulation results with the results of some recent methods. It is evident that the performance improvement of the TAGHTPS with the proposed SPSMCBSO is better than that of the recently mentioned methods. Furthermore, the SPSMCBSO further demonstrated robustness and is not affected by subsystem parameter deviation, random load disturbance, and parameter uncertainty in state and interconnected matrix. Therefore, the proposed SPSMCBSO is very useful for the LFC of MAMSPS.

Appendix

A. Norminal Parameters of Power System

Nominal System Data A [24, 26]. $T_{SG} = 0.08\,s$, $K_R = 0.3$ $T_R = 10$, $T_T = 0.3\,s$, $T_{GH} = 41.6\,s$, $T_{RS} = 5\,s$, $T_{RH} = 0.513\,s$, $T_W = 0.3\,s$, $C_g = 1$, $b_g = 1$,
$X_G = 0.6\ s$, $Y_G = 1$, $T_{CR} = 0.01\ s$, $T_F = 0.23\ s$, $T_{CD} = 0.2\ s, K_p = 120\,T_p = 20\ s, T_{12} = 0.0433\ pu\mathrm{MW/rad}$.

Nominal System Data B [25]. $T_{SG} = 0.08\ s$, $K_R = 0.3$ $T_R = 10$, $T_T = 0.3\ s$, $T_{GH} = 28.75\ s$, $T_{RS} = 5\ s$, $T_{RH} = 0.2\ s$, $T_W = 1\ s\ C_g = 1$, $b_g = 1$, $X_G = 0.6\ s$, $Y_G = 1$, $T_{CR} = 0.01\ s$, $T_F = 0.23\ s$, $T_{CD} = 0.2\ s$, $K_p = 68.9566\ \mathrm{Hz/pu}$, $T_p = 11.49\ s$, $T_{12} = 0.0433\ \mathrm{puMW/rad}$.

B. LMI's Positive Matrices

By solving LMI (28), it is easy to verify that conditions in Theorem 1 are satisfied with positive matrices:

$$\Pi_1 = \begin{bmatrix}
0.0138 & 0.0041 & 0.0021 & -0.0006 & 0.0033 & -0.0051 & 0.0020 & 0.0114 & 0.0026 & 0.0037 & -0.0021 & 0.0869 & -0.0208 \\
0.0041 & 0.0021 & -0.0056 & 0.0017 & 0.0012 & 0.0006 & 0.0003 & 0.0041 & 0.0012 & -0.0002 & 0.0002 & 0.0226 & -0.0044 \\
0.0021 & -0.0056 & 0.1624 & -0.0486 & -0.0052 & 0.2168 & -0.0394 & 0.0006 & -0.0034 & 0.0270 & -0.0164 & 0.0740 & -0.0416 \\
-0.0006 & 0.0017 & -0.0486 & 0.0146 & 0.0016 & -0.0648 & 0.0118 & -0.0002 & 0.0010 & -0.0081 & 0.0049 & -0.0220 & 0.0124 \\
0.0033 & 0.0012 & -0.0052 & 0.0016 & 0.0013 & -0.0139 & 0.0028 & 0.0028 & 0.0007 & 0.0006 & -0.0004 & 0.0222 & -0.0049 \\
-0.0051 & 0.0006 & 0.2168 & -0.0648 & -0.0139 & 1.3665 & -0.2417 & -0.0036 & -0.0031 & 0.0179 & -0.0112 & -0.0024 & 0.0013 \\
0.0020 & 0.0003 & -0.0394 & 0.0118 & 0.0028 & -0.2417 & 0.0429 & 0.0015 & 0.0007 & -0.0029 & 0.0018 & 0.0077 & -0.0018 \\
0.0114 & 0.0041 & 0.0006 & -0.0002 & 0.0028 & -0.0036 & 0.0015 & 0.0136 & 0.0042 & -0.0087 & 0.0054 & 0.0696 & -0.0171 \\
0.0026 & 0.0012 & -0.0034 & 0.0010 & 0.0007 & -0.0031 & 0.0007 & 0.0042 & 0.0037 & -0.0176 & 0.0107 & 0.0135 & -0.0024 \\
0.0037 & -0.0002 & 0.0270 & -0.0081 & 0.0006 & 0.0179 & -0.0029 & -0.0087 & -0.0176 & 0.1240 & -0.0749 & 0.0382 & -0.0163 \\
-0.0021 & 0.0002 & -0.0164 & 0.0049 & -0.0004 & -0.0112 & 0.0018 & 0.0054 & 0.0107 & -0.0749 & 0.0452 & -0.0224 & 0.0097 \\
0.0869 & 0.0226 & 0.0740 & -0.0220 & 0.0222 & -0.0024 & 0.0077 & 0.0696 & 0.0135 & 0.0382 & -0.0224 & 0.7435 & -0.2275 \\
-0.0208 & -0.0044 & -0.0416 & 0.0124 & -0.0049 & 0.0013 & -0.0018 & -0.0171 & -0.0024 & -0.0163 & 0.0097 & -0.2275 & 0.1241
\end{bmatrix}, \tag{B.1}$$

$$\overline{\Pi}_1 = \begin{bmatrix}
64.7884 & -0.1475 & -1.6068 & -0.0044 & -0.9755 & -0.9224 & 0.0080 & -0.4101 & -0.0057 & -0.0057 & 0.0011 & -0.1122 & 0.3507 \\
-0.1475 & 0.1135 & -0.0062 & 0.0049 & -0.0039 & -0.0036 & -0.0037 & -0.0484 & -0.0026 & 0.0010 & 0.0042 & 0.0251 & 0.0103 \\
-1.6068 & -0.0062 & 15.3860 & 0.0557 & -13.6827 & -11.9157 & 0.0116 & -0.0158 & 0.0007 & 0.0006 & 0.0004 & 0.0174 & -0.0102 \\
-0.0044 & 0.0049 & 0.0557 & 0.8313 & -0.0498 & -0.0437 & -0.0066 & 0.0073 & 0.0001 & 0.0003 & 0.0002 & -0.0037 & -0.0014 \\
-0.9755 & -0.0039 & -13.6827 & -0.0498 & 28.2715 & -7.5486 & -0.0539 & -0.0099 & 0.0004 & 0.0003 & 0.0002 & 0.0107 & -0.0057 \\
-0.4101 & -0.0036 & -11.9157 & -0.0437 & -7.5486 & 30.3862 & 0.0361 & -0.0091 & 0.0003 & 0.0004 & 0.0002 & 0.0101 & -0.0057 \\
-0.4101 & -0.0037 & 0.0116 & -0.0066 & -0.0539 & 0.0361 & 0.2837 & -0.0044 & -0.0027 & 0.0035 & 0.0005 & 0.0021 & 0.0007 \\
-0.4101 & -0.0484 & -0.0158 & 0.0073 & -0.0099 & -0.0091 & -0.0044 & 0.1362 & -0.1001 & 0.0001 & 0.0064 & -0.0685 & -0.0226 \\
-0.0057 & -0.0026 & 0.0007 & 0.0001 & 0.0004 & 0.0003 & -0.0027 & -0.1001 & 0.2433 & -0.1489 & -0.0024 & 0.0514 & 0.0179 \\
-0.0062 & 0.0010 & 0.0006 & 0.0003 & 0.0003 & 0.0004 & 0.0035 & 0.0001 & -0.1489 & 0.1762 & 0.0408 & -0.0003 & 0.0002 \\
0.0011 & 0.0251 & 0.0004 & 0.0002 & 0.0002 & 0.0002 & 0.0005 & 0.0064 & 0.0514 & 0.0408 & 1.3812 & -0.0033 & -0.0011 \\
-0.1122 & 0.0251 & 0.0174 & -0.0037 & 0.0107 & 0.0101 & 0.0021 & -0.0685 & 0.0514 & -0.0003 & -0.0033 & 24.8397 & -0.7063 \\
0.3507 & 0.0103 & -0.0102 & -0.0014 & -0.0057 & -0.0057 & 0.0007 & -0.0226 & 0.0179 & 0.0002 & -0.0011 & -0.7063 & 39.6651
\end{bmatrix}, \tag{B.2}$$

$$\Pi_2 = \begin{bmatrix} 0.0076 & 0.0023 & 0.0039 & -0.0012 & 0.0017 & -0.0022 & 0.0009 & 0.0064 & 0.0016 & 0.0015 & -0.0008 & 0.0494 & 0.0124 \\ 0.0023 & 0.0011 & -0.0010 & 0.0003 & 0.0006 & 0.0003 & 0.0001 & 0.0022 & 0.0007 & -0.0001 & 0.0001 & 0.0133 & 0.0030 \\ 0.0039 & -0.0010 & 0.0634 & -0.0190 & -0.0013 & 0.1258 & -0.0223 & 0.0024 & -0.0014 & 0.0159 & -0.0096 & 0.0473 & 0.0191 \\ -0.0012 & 0.0003 & -0.0190 & 0.0057 & 0.0004 & -0.0376 & 0.0067 & -0.0007 & 0.0004 & -0.0048 & 0.0029 & -0.0141 & -0.0057 \\ 0.0017 & 0.0006 & -0.0013 & 0.0004 & 0.0006 & -0.0077 & 0.0015 & 0.0014 & 0.0004 & 0.0002 & -0.0001 & 0.0122 & 0.0030 \\ -0.0022 & 0.0003 & 0.1258 & -0.0376 & -0.0077 & 0.7498 & -0.1326 & -0.0028 & -0.0021 & 0.0134 & -0.0083 & 0.0044 & 0.0017 \\ 0.0009 & 0.0001 & -0.0223 & 0.0067 & 0.0015 & -0.1326 & 0.0235 & 0.0009 & 0.0005 & -0.0023 & 0.0014 & 0.0032 & 0.0007 \\ 0.0064 & 0.0022 & 0.0024 & -0.0007 & 0.0014 & -0.0028 & 0.0009 & 0.0069 & 0.0022 & -0.0039 & 0.0024 & 0.0406 & 0.0102 \\ 0.0016 & 0.0007 & -0.0014 & 0.0004 & 0.0004 & -0.0021 & 0.0005 & 0.0022 & 0.0018 & 0.0590 & 0.0050 & 0.0082 & 0.0016 \\ 0.0015 & -0.0001 & 0.0159 & -0.0048 & 0.0002 & 0.0134 & -0.0023 & -0.0039 & -0.0083 & 0.0590 & -0.0356 & 0.0203 & 0.0089 \\ -0.0008 & 0.0001 & -0.0096 & 0.0029 & -0.0001 & -0.0083 & 0.0014 & 0.0024 & 0.0050 & -0.0356 & 0.0215 & -0.0119 & -0.0053 \\ 0.0494 & 0.0133 & 0.0473 & -0.0141 & 0.0122 & 0.0044 & 0.0032 & 0.0406 & 0.0082 & 0.0203 & -0.0119 & 0.4141 & 0.1260 \\ 0.0124 & 0.0030 & 0.0191 & -0.0057 & 0.0030 & 0.0017 & 0.0007 & 0.0102 & 0.0016 & 0.0089 & -0.0053 & 0.1260 & 0.0645 \end{bmatrix}, \tag{B.3}$$

$$\overline{\Pi}_2 = \begin{bmatrix} 26.4556 & -0.0849 & -0.5551 & -0.0020 & -0.3222 & -0.3368 & -0.0013 & -0.2382 & -0.0044 & -0.0045 & -0.0004 & -0.0282 & -0.2007 \\ -0.0849 & 0.0768 & -0.0034 & 0.0033 & -0.0023 & -0.0021 & -0.0021 & -0.0329 & -0.0025 & 0.0004 & 0.0028 & 0.0113 & -0.0192 \\ -0.5551 & -0.0034 & 3.8551 & 0.0140 & -3.4083 & -2.9718 & 0.0027 & -0.0089 & 0.0004 & 0.0003 & 0.0002 & 0.0058 & 0.0003 \\ -0.0020 & 0.0033 & 0.0140 & 0.5542 & -0.0123 & -0.0114 & -0.0042 & 0.0048 & 0.0002 & 0.0002 & 0.0001 & -0.0017 & 0.0026 \\ -0.3222 & -0.0023 & -3.4083 & -0.0123 & 7.0583 & -1.8762 & -0.0134 & -0.0058 & 0.0002 & 0.0002 & 0.0001 & 0.0036 & -0.0002 \\ -0.3368 & -0.0021 & -2.9718 & -0.0114 & -1.8762 & 7.5944 & 0.0072 & -0.0051 & 0.0001 & 0.0002 & 0.0001 & 0.0031 & -0.0000 \\ -0.0013 & -0.0021 & 0.0027 & -0.0042 & -0.0134 & 0.0072 & 0.1911 & -0.0026 & -0.0022 & 0.0022 & 0.0002 & 0.0010 & -0.0013 \\ -0.2382 & -0.0329 & -0.0089 & 0.0048 & -0.0058 & -0.0051 & -0.0026 & 0.0887 & -0.0668 & 0.0003 & 0.0043 & -0.0295 & 0.0467 \\ -0.0044 & -0.0025 & 0.0004 & 0.0002 & 0.0002 & 0.0001 & -0.0022 & -0.0668 & 0.1626 & -0.0989 & -0.0216 & 0.0228 & -0.0363 \\ -0.0045 & 0.0004 & 0.0003 & 0.0002 & 0.0002 & 0.0002 & 0.0022 & 0.0003 & -0.0989 & 0.1171 & 0.0273 & -0.0000 & 0.0002 \\ -0.0004 & 0.0028 & 0.0002 & 0.0001 & 0.0001 & 0.0001 & 0.0002 & 0.0043 & -0.0216 & 0.0273 & 0.9202 & -0.0015 & 0.0023 \\ -0.0282 & 0.0113 & 0.0058 & -0.0017 & 0.0036 & 0.0031 & 0.0010 & -0.0295 & 0.0228 & -0.0000 & -0.0015 & 8.2364 & 3.0052 \\ -0.2007 & -0.0192 & 0.0003 & 0.0026 & -0.0002 & -0.0000 & -0.0013 & 0.0467 & -0.0363 & 0.0002 & 0.0023 & 3.0052 & 11.7695 \end{bmatrix}, \tag{B.4}$$

and the scalars $\lambda_1 = 10, \rho_1 = 10, \widehat{\gamma}_1 = 20, \lambda_2 = 20, \rho_2 = 20$, and $\widehat{\gamma}_2 = 30$.

Nomenclature

ACE: Area control error
DSPSMCS: Decentralized single-phase sliding mode control scheme
DE: Differential evolution
MAPS: Multiarea power system
MAMSPS: Multiarea multisource power system
LMI: Linear matrix inequality
LFC: Load frequency control
TAGHTPS: Two-area gas-hydro-thermal power system
SPSMCBSO: Single-phase sliding mode control-based state observer
PS: Power system
PI: Proportional-integral
PID: Proportional-integral-differential
PSO: Particle swarm optimization
VSC: Variable structure control
SMC: Sliding mode control
OHS: Harmonic search
FOTID: Fractional order tilt integral derivative
PFA: Pathfinder algorithm
RFB: Redox flow battery
TLPD: Tie-line power deviation.

Data Availability

The data used to support the findings of this study are available from the corresponding author upon request.

Conflicts of Interest

The authors declare that they have no conflicts of interest.

References

[1] V. Vijay, C. James, A. Paul, and A. Fouad, *Power System Control and Stability*, Wiley-IEEE Press, Hoboken, NJ, USA, 2019.

[2] T. Hussein and A. Shamekh, "Design of pi fuzzy logic gain scheduling load frequency control in two-area power systems," *Design*, vol. 3, no. 2, 2019.

[3] H. Yousef, "Adaptive fuzzy logic load frequency control of multi-area power system," *International Journal of Electrical Power & Energy Systems*, vol. 68, pp. 384–395, 2015.

[4] A. A. Hussein, S. S. Salih, and Y. G. Ghasm, "Implementation of proportional-integral-observer techniques for load frequency control of power system," *Procedia Computer Science*, vol. 109, pp. 754–762, 2017.

[5] Y. Mi, Y. Fu, D. Li, C. Wang, P. C. Loh, and P. Wang, "The sliding mode load frequency control for hybrid power system based on disturbance observer," *International Journal of Electrical Power & Energy Systems*, vol. 74, pp. 446–452, Jan. 2016.

[6] K. Liao and Y. Xu, "A robust load frequency control scheme for power systems based on second-order sliding mode and extended disturbance observer," *IEEE Transactions on Industrial Informatics*, vol. 14, no. 7, pp. 3076–3086, July 2018.

[7] M. C. Tang and Y. He, "Improved sliding mode design for load frequency control of power system integrated an adaptive learning strategy," *IEEE Transactions on Industrial Electronics*, vol. 64, no. 8, pp. 6742–6751, 2017.

[8] B. Le Ngoc Minh, V. V. Huynh, T. M. Nguyen, and Y. W. Tsai, "Decentralized adaptive double integral sliding mode controller for multi-area power systems," *Mathematical Problems in Engineering*, vol. 2018, Article ID 2672436, 11 pages, 2018.

[9] D. Qian, S. Tong, and X. Liu, "Load frequency control for micro hydro power plants by sliding mode and model order reduction," *Automatika*, vol. 56, no. 3, pp. 318–330, 2015.

[10] S. Prasad, S. Purwar, and N. Kishor, "Non-linear sliding mode load frequency control in multi-area power system," *Control Engineering Practice*, vol. 61, pp. 81–92, 2017.

[11] H. Bevrani, *Robust Power System Frequency Control, Power Electronics and Power Systems*, Springer, Berlin, Germany, 2014.

[12] A. E. Onyeka, Y. Xing-Gang, Z. Mao, B. Jiang, and Q. Zhang, "Robust decentralized load frequency control for interconnected time delay power systems using sliding mode techniques," *IET Control Theory & Applications*, vol. 14, no. 3, pp. 470–480, 2019.

[13] S. Trip, M. Cucuzzella, C. De Persis, A. van der Schaft, and A. Ferrara, "Passivity-based design of sliding modes for optimal load frequency control," *IEEE Transactions on Control Systems Technology*, vol. 27, no. 5, pp. 1893–1906, 2019.

[14] J. Guo, "Load frequency control of a two-area power system with non-reheat turbines by the SMC approach," *Journal of Energy and Power Engineering*, vol. 9, pp. 566–573, 2015.

[15] X. Su, X. Liu, and Y.-D. Song, "Event-Triggered sliding-mode control for multi-area power systems," *IEEE Transactions on Industrial Electronics*, vol. 64, no. 8, pp. 6732–6741, 2017.

[16] S. Prasad, S. Purwar, and N. Kishor, "Non-linear sliding mode load frequency control in multi-area power system," *Control Engineering Practice*, vol. 61, pp. 81–92 2017.

[17] J. Guo, "Application of full order sliding mode control based on different areas power system with load frequency control," *ISA Transactions*, vol. 92, pp. 23–34, 2019.

[18] Lv. Xinxin, X. Sun, Y. Cao, and V. Dinavahi, "Event-triggered load frequency control for multi-area power systems based on Markov model: a global sliding mode control approach," *IET Generation, Transmission & Distribution*, vol. 14, pp. 4878–4887, 2020.

[19] A. Kumar, N. M. Anwar, and S. Kumar, "Sliding mode controller design for frequency regulation in an interconnected power system," *Protection and Control of Modern Power Systems*, vol. 6, pp. 1–12, 2021.

[20] S. Abhayadev, "Smooth integral sliding mode control for the load frequency control in a two area interconnected power system," in *Proceedings of the International Conference on IoT Based Control Networks & Intelligent Systems, ICICNIS 2021*, Chennai, Tamil Nadu, December 2020.

[21] S. Prasad, S. Purwar, and N. Kishor, "Load frequency regulation using observer based non-linear sliding mode control," *International Journal of Electrical Power & Energy Systems*, vol. 104, pp. 178–193, 2019.

[22] A.-T. Tran, B. L. N. Minh, V. V. Huynh et al., "Load frequency regulator in interconnected power system using second-order sliding mode control combined with state estimator," *Energies*, vol. 14, no. 4, pp. 863, 2021.

[23] H. VV, B. N. L. Minh, E. N. Amaefule, A. T. Tran, and T. P. Tran, "Highly robust observer sliding mode-based frequency control for multi-area power systems with renewable power plants," *Electronics*, vol. 10, p. 274.

[24] N. Hakimuddin, I. Nasiruddin, and T. S. Hota, "Generation-based automatic generation control with multisource power system using bacterial foraging algorithm," *Engineering Reports*, vol. 2, pp. 77–85, 2020.

[25] R. K. Sahu, R. Panda, U. K. Rout, and D. K. Sahoo, "Teaching learning based optimization algorithm for automatic generation control of power system using 2-DOF PID controller," *International Journal of Electrical Power & Energy Systems*, vol. 77, pp. 287–301, 2016.

[26] G. Nidhi, K. Narendra, and B. Chitti, "JAYA optimized generation control strategy for interconnected diverse source power system with varying participation," *Energy Sources, Part A: Recovery, Utilization, and Environmental Effects*, vol. 1, pp. 1–17, 2019.

[27] S. Qiao, L. Xinghua, and X. Gaoxi, "Observer-based sliding mode load frequency control of power systems under deception attack"," *Complexity*, vol. 12, p. 115, 2021.

[28] Z. Wang, Y. Liu, Z. Yang, and W. Yang, "Load frequency control of multi-region interconnected power systems with wind power and electric vehicles based on sliding mode control," *Energies*, vol. 14, no. 8, p. 2288, 2021.

[29] M. Wei, S. Lin, Y. Zhao, H. Wang, and Q. Liu, "An adaptive sliding mode control based on disturbance observer for LFC," *Frontiers in Energy Research*, vol. 11, p. 555, 2021.

[30] A. Dev, S. Anand, and M. K. Sarkar, "Nonlinear disturbance observer based adaptive super twisting sliding mode load frequency control for nonlinear interconnected power network," *Asian Journal of Control*, vol. 23, no. 5, pp. 2484–2494, 2021.

[31] V. Patel, D. Guha, and S. Purwar, "Frequency regulation of hybrid power system using reduced order disturbance observer-based integral sliding mode controller," in *Proceedings of the 2020 21st National Power Systems Conference*, pp. 1–6, IEEE, Gandhinagar, India, December 2020.

[32] D. Guha, P. K. Roy, and S. Banerjee, "Disturbance observer aided optimized fractional-order three-degree-of-freedom tilt-integral-derivative controller for load frequency control of power systems," *IET Generation*, Transmission & Distribution, vol. 14, p. 5867, 2021.

[33] J. H. Park, *Recent Advances in Control Problems of Dynamical Systems and Networks*, Springer International Publishing, Berlin, Germany, 2021.

[34] S. Manikandan and P. Kokil, "Stability analysis of load frequency control system with constant communication delays," *IFAC-PapersOnLine*, vol. 53, no. 1, pp. 338–343, 2020.

Sliding Surface Design for Sliding Mode Load Frequency Control of Multi Area Multi Source Power System

Van Van Huynh, Phong Thanh Tran, Chau Thien Si Dong, Bach Dinh Hoang, *Member, IEEE*, and Okyay Kaynak, *Life Fellow, IEEE*

***Abstract*—A new load frequency control (LFC) technique for a multi-area steam-hydropower system (MASHPS) with parameter uncertainty is proposed in this research. A second-order SMC via double integrated sliding surface is meant to improve MASHPS frequency regulation, tie-line power management, and dependability. This strategy not only increases asymptotic stability and dependability of MASHPS, but it also reduces the chattering problem that is inherent in first order sliding mode control (SMC). Furthermore, the new linear matrix inequality (LMI) based on Lyapunov stability is used to analyse the entire MASHPS stabilization. For the LFC research, the efficient achievement of the proposed technique is investigated in a two-area steam-hydropower system (TASHPS). Under parameter uncertainties and various assumed load disturbances (LDs) from households, commercial buildings, and industries, the proposed second-order SMC via double integral sliding surface (SOSDISS) proves to be highly robust and improves the MASHPS response in terms of frequency regulation, tie-line power management, and system reliability when compared to other existing proposed methods with less uncertainty consideration. Overall, the results indicate that the novel approach is feasible for MASHPS LFC and power system reliability.**

***Index Terms*—Integral sliding surface, load frequency control, power system, sliding mode control.**

NOMENCLATURE

IMAPS: Interconnected multi area power system; TASHPS: Two-area steam-hydropower system; PS: Power system; PI: Proportional-integral; PID: Proportional-integral-differential; SMC: Sliding mode control; LFC: Load frequency control; LMI: Linear matrix inequality; SOSDISS: Second-order SMC via double integral sliding; MASHPS: Multi-area steam-hydropower system; MAPS: Multi area power system; GWO: Grey wolf optimization; LDs: Load disturbances; SM: Sliding manifold.

Manuscript received Dec 20, 2022; revised Oct 8, 2023; accepted Jan 17, 2024.

Van Van Huynh, Phong Thanh Tran, Chau Thien Si Dong, Bach Dinh Hoang are with the Modeling Evolutionary Algorithms Simulation and Artificial Intelligence, Faculty of Electrical and Electronics Engineering, Ton Duc Thang University, Ho Chi Minh City, Viet Nam (e-mail: huynhvanvan@tdtu.edu.vn; Corresponding author e-mail: tranthanhphong.st@tdtu.edu.vn).

Okyay Kaynak is with the Turkish Academy of Sciences and Bogaziçi University Turkey (e-mail: okyay.kaynak@boun.edu.tr).

I. INTRODUCTION

STEAM and hydropower plants are the most widely used power systems because of their high-power output efficiencies and constant supply of steam/hydro to their turbines. The interconnection of steam and hydro in each area of a multiarea power system (MAPS) can reduce the cost of the power supply. Power companies can easily buy bulk power from neighboring power plants to feed their consumers rather than generate power from their old power sets [1]. However, the major concerns are based on the reliability of MAPS. Due to the imbalance state, tie-line power exchange and off-nominal frequency will occur, which may have negative consequences [2]. As a result, regulating the tie-line power exchange and PS frequency at the prescribed value are critical to achieving MAPS dependability, and these are the two primary goals of load frequency control (LFC). Furthermore, synchronizing these generators in a multiarea steam-hydropower system (MASHPS) is difficult and can result in parameter uncertainty due to their varied dynamic characteristics. This may have an effect on the MAPS's LFC and MASHPS's reliability. In an extensive review, a new LFC study of MASHPS was created with uncertainty of the parameters. It should be noted that many LFC techniques for MAPS have been addressed in [3]. The proportional-integral-differential (PID) approach has been the most widely utilized in industry. Many research authors have applied PID scheme based LFC to stabilize interconnected multi area power system (IMAPS) against step LDs given in [4-5]. In [6-7], PID techniques have been enhanced for the LFC application of IMAPS with mismatched and random load disturbance. These above PID schemes were designed with a specific control gain to stabilize the IMAPS at some specific operating points. However, deviation from the operating point will degrade the above PID control approaches in their applications. Optimizing the parameters of a two-area interconnected dynamic PS PID controller using a population-based hybrid particle swarm optimization-gravitational search approach (PSO-GSA) in [8] and optimizing with a new grasshopper optimization algorithm and a stacked fuzzy proportional derivative - proportional integral controller (PD-PI) in [9]. The drawback of the fuzzy logic approach is the difficulty in formulating the rules of the fuzzy set.

Hence, variable structure control (VSC) was created in practice. The most widely used VSC is the sliding mode control (SMC) system. Their schemes imply that the variables have been brought to the surface and maintained there in the limited reach time by choosing the sliding surface and constructing the switching law, among other rules [10-11]. In summary, sliding mode control (SMC)-based strategies were used to solve the PID-Fuzzy, and optimization algorithm issues. The SMC has already been used for IMAPS LFC against load disruptions, as discussed in [12-25]. In studies, the SMC is known to be insensitive to large disturbances. SMC method is simply selecting the fundamental design of a switching and equivalent control law using a sliding surface [12-15]. The SMC scheme can handle linear and nonlinear problems of a system, and it is beneficial for multivariable systems. The SMC was used to study LFC of MAPS with nonlinearities [16]. A unique adaptive SMC approach for LFC has been developed and implemented in [17]. Once again, disturbance observer-based SMC was developed as given in [18-19]. The state observer via SMC was again used for the LFC of IMAPS where the variables for state were hard to measure [20]. However, the above SMC based schemes were first order with inherent chattering phenomenon. This phenomenon causes low control accuracies because of un-modelled dynamics and the discontinuous signal present in the first-order SMC and produces undesirable MAPS dynamics. Elimination of the chattering was the use of the second order SMC for the LFC of IMAPS discussed in [21-22]. More SMC-based methods for chattering free control were also developed in [23-24]. The methods mentioned above in literature were developed to study the LFC of a steam or hydropower system alone in each area of the IMAPS with less consideration of uncertainties. Therefore, we study a new one of a two area steam hydropower system (TASHPS). The principle of a double-integral sliding mode controller (DISMC) is used in a standalone solar energy system. A pair of integrals SMC provides strong control actions in the face of system parameter uncertainties and eliminates steady-state error by applying a double integral of the tracking voltage term for error on its sliding surface. Nevertheless, increased chattering and slower transient reaction remain a challenge with DISMC. Choosing a sliding surface for the first order has a significant impact on the performance of a SMC in [27]. Therefore, the new LFC is approached with a proposed second-order SMC via double integral sliding surface. The following are the research's significant contributions for the new double integral sliding surface is designed for the MASHPS's sliding mode LFC as follows:

- The suggested second-order SMC via double integral sliding surface (SOSDISS) proves to be highly robust and improves the MASHPS response in terms of frequency regulation, tie-line power management, and system reliability of the MASHPS.

- The stability of the MASHPS is guaranteed under the new construction of sliding mode dynamic theory and Lyapunov stability theory.

- In comparison to the recent SMC approach, the power system performance has improved in terms of reduced chattering.

- The performance of the recommended control method is dependable and efficient, as evidenced by its fast frequency responses and insensitivity to parameter changes, load disturbance, load variation, delay time, and the nonlinear effects of GDB and GRC on the power network.

II. DYNAMIC MODEL OF MULTI-AREA STEAM-HYDROPOWER SYSTEM NEW

To improve the stability and reliability of a multi-area steam-hydropower system (MASHPS), an LFC is needed. The LFC of the i^{th} area multisource PS, which includes a reheated thermal power plant (PP) and a hydroelectric PP and is presented in Fig. 1. Both PS components are modelled and represented in their transfer functions together with the closed-loop LFC.

The PS is modeled in the structure of state-space by the first representing the system dynamics as follows.

$$\begin{aligned}\Delta\dot{f}_i &= -\frac{1}{T_{pi}}\Delta f_i + \frac{K_{pi}}{T_{pi}}\Delta P_{mi} + \frac{K_{pi}}{T_{pi}}\Delta P'_{mi} - \frac{K_{pi}}{T_{pi}}\Delta P_{Di} \\ &\quad - \frac{b_{ij}K_{pi}}{2\pi T_{pi}}\sum_{i=1, i\neq j}^{N} T_{ij}\left\{\Delta\delta_i(t) - \Delta\delta_j(t)\right\}\end{aligned} \tag{1}$$

$$\begin{aligned}\Delta\dot{P}_{mi} &= \frac{2T_{Ri2}}{T_{i2}T_{i1}R_{i2}}\Delta f_i - \frac{2}{T_{\mathrm{Wi}}}\Delta P_{mi} + \left(\frac{2}{T_{\mathrm{Wi}}} + \frac{2}{T_{i2}}\right)\Delta P_{vi} \\ &\quad + \left(\frac{2T_{Ri2}}{T_{i2}T_{i1}} - \frac{2}{T_{i2}}\right)\Delta P_{gi} - \frac{2T_{Ri2}}{T_{i2}T_{i1}}\Delta E_i - \frac{2T_{Ri2}}{T_{i2}T_{i1}}u_{i2}\end{aligned} \tag{2}$$

$$\begin{aligned}\Delta\dot{P}_{Vi} &= -\frac{T_{Ri2}}{T_{i2}T_{i1}R_{i2}}\Delta f_i - \frac{1}{T_{i2}}\Delta P_{vi} + \left(\frac{1}{T_{i2}} - \frac{T_{Ri2}}{T_{i2}T_{i1}}\right)\Delta P_{gi} \\ &\quad + \frac{T_{Ri2}}{T_{i2}T_{i1}}\Delta E_i + \frac{T_{Ri2}}{T_{i2}T_{i1}}u_{i2}\end{aligned} \tag{3}$$

$$\Delta\dot{P}_{gi} = -\frac{1}{T_{i1}R_{i2}}\Delta f_i - \frac{1}{T_{i1}}\Delta P_{gi} + \frac{1}{T_{i1}}\Delta E_i + \frac{1}{T_{i1}}u_{i2} \tag{4}$$

$$\begin{aligned}\Delta\dot{E}_i(t) &= K_{Ei}K_{Bi}\Delta f_i(t) \\ &\quad + K_{Ei}\frac{1}{2\pi}b_{ij}\sum_{i=1, i\neq j}^{N} T_{ij}\left\{\Delta\delta_i(t) - \Delta\delta_j(t)\right\}\end{aligned} \tag{5}$$

$$\Delta\dot{\delta}_i(t) = 2\pi\Delta f_i(t) \tag{6}$$

$$\begin{aligned}\Delta\dot{P}'_{mi} &= -\frac{1}{T_{Ri1}}\Delta P'_{mi} + \left(\frac{1}{T_{Ri1}} - \frac{K_{Ri1}}{T_{Ri1}}\right)\Delta P''_{vi} \\ &\quad + \frac{K_{Ri1}}{T_{Ri1}}\Delta P_{vi}\end{aligned} \tag{7}$$

$$\Delta\dot{P}''_{vi} = -\frac{1}{T_{t1}}\Delta P''_{vi} + \frac{1}{T_{t1}}\Delta P'_{vi} \tag{8}$$

$$\Delta\dot{P}'_{vi} = -\frac{1}{T_{gi}R_{i1}}\Delta f_i - \frac{1}{T_{gi}}\Delta P_{vi} + \frac{1}{T_{gi}}\Delta E_i + \frac{1}{T_{gi}}u_{i1} \tag{9}$$

Therefore, we can represent the above dynamics in the configuration of state-space below.

$$\dot{x}_i(t) = A_i x_i(t) + B_i u_i(t) + \sum_{\substack{i=1 \\ j\neq i}}^{N} H_{ij} x_j + F_i \Delta P_{Di}(t) \tag{10}$$

where $x_i(t) = \left[\Delta f_i(t)\ \ \Delta P_{mi}(t)\ \Delta P_{vi}(t)\ \Delta P_{gi}(t)\ \ \Delta E_i(t)\right.$
$\left.\Delta\delta_i(t)\ \Delta P'_{mi}(t)\ \Delta P''_{vi}(t)\Delta P'_{vi}(t)\right]^T$

and $x_i(t) \in R^{n_i}$ is the vector of state, $u_i(t) \in R^{m_i}$ is the input control vector, $x_j(t) \in R^{n_j}$ is the neighboring state vector of $x_i(t)$, n_i is the area's total various variables for state of i^{th} area, m_i is the area's total number of controls the input variables of the i$^{\text{th}}$ area. $A_i \in R^{n_i \times n_i}$, $B_i \in R^{n_i \times m_i}$, $F_i \in R^{n_i \times k_i}$ and H_{ij} are the nominal parameter system matrices.

In practical power network, uncertainties can be experienced either in the difference of rotor angle change of each generator which impact on the system inertia time constant of the PS or the change of valve position of the steam/hydro during load variations or the control signal's chattering phenomena provides information about disturbance experienced by first order SMC.

These are considered and represented in the system matrices and the control input, as shown.

$$\begin{aligned}\dot{x}_i(t) &= [A_i + \bar{\Theta}_i(x_i,t)]x_i(t) + B_i[u_i(t) + \xi_i(x_i,t)] \\ &+ \sum_{\substack{j=1 \\ j\neq i}}^{N}[H_{ij} + \Xi_{ij}(x_j,t)]x_j(t) + F_i\Delta P_{Di}(t)\end{aligned} \tag{11}$$

$$\begin{aligned}\bar{L}_i(x_i,t) &= \bar{\Theta}_i(x_i,t)x_i(t) + B_i\xi_i(x_i,t) \\ &+ \sum_{\substack{j=1 \\ j\neq i}}^{N}\Xi_{ij}(x_j,t)x_j(t) + F_i\Delta P_{Di}(t)\end{aligned} \tag{12}$$

So, the state-space form of (12) can then be revised to

$$\dot{x}_i(t) = A_i x_i(t) + B_i u_i(t) + \sum_{\substack{j=1 \\ j\neq i}}^{N} H_{ij} x_j(t) + \bar{L}_i(x_i,t) \tag{13}$$

where $\bar{L}_i(x_i,t)$ shows the aggregate uncertainties which consists of the mismatched and matched parts. An assumption is made and formulated coupled with a given Lemma in order to handle the aggregate uncertainties for the LFC of MASHPS (13) as follows.

Assumption 1: The assumption is aggregated disturbance $\bar{L}_i(x_i,t)$, therefore, the differential of $\dot{\bar{L}}_i(x_i,t)$ are bounded such that $\left\|\bar{L}_i(x_i,t)\right\| \le \gamma_i$ and $\left\|\dot{\bar{L}}_i(x_i,t)\right\| \le \bar{\gamma}_i$. Where γ_i and $\bar{\gamma}_i$ are the positive scalars and $\|.\|$ is the matrix norm.

Lemma 1 [27]: Let $\bar{\mathbf{X}}$ and $\bar{\mathbf{Y}}$ are realistic, appropriate-dimension matrices, then, for any scalar $\mu > 0$, following matrix inequality is obtained.

$$\bar{\mathbf{X}}^{\mathbf{T}}\bar{\mathbf{Y}} + \bar{\mathbf{Y}}^{\mathbf{T}}\bar{\mathbf{X}} \le \mu\bar{\mathbf{X}}^{\mathbf{T}}\bar{\mathbf{X}} + \mu^{-1}\bar{\mathbf{Y}}^{\mathbf{T}}\bar{\mathbf{Y}}. \tag{14}$$

Remark 1: The multi-area interconnection's current SMC scheme for LFC. The establishment of power systems is predicated on the assumption that the standard would be followed. In [13], [18-24] the majority of the aggregated uncertainty is confined by a positive constant.

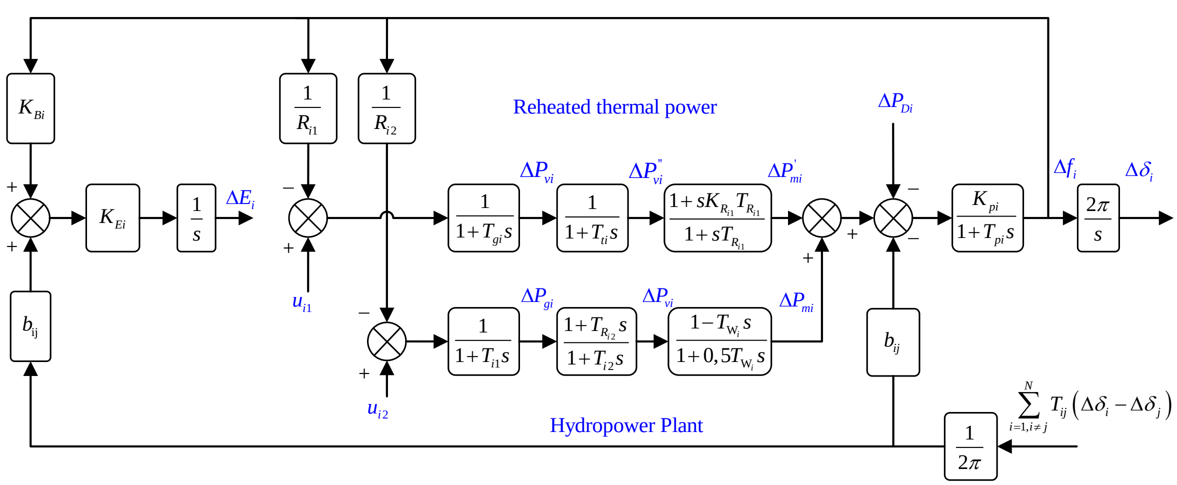

Fig. 1. Schematic diagram of a 1-zone-2 sources included thermal power plants using heat recovery turbines & hydropower plant.

where $\bar{\Theta}_i(x_i,t)$ is the time varying parameter uncertainty in the state matrix, $\Xi_{ij}(x_j,t)$ is the interconnected matrix's time-varying parameter uncertainty and $\xi_i(x_i,t)$ is the disturbance input. If we simply uncertainties in equation (11), we can get that:

To put it another way, $\left\|\bar{L}_i(x_i,t)\right\| \le \gamma_i$ and $\left\|\dot{\bar{L}}_i(x_i,t)\right\| \le \bar{\gamma}_i$ where γ_i and $\bar{\gamma}_i$ are the positive constants. This is a very restricted condition.

III. New Double Integral Sliding Surface Design

SMC based strategies were employed for the LFC of

IMAPS under a wide range of LDs given in [12-15]. The stability of the PS is determined by the sliding surface of the SMC [20-21]. Therefore, a new double integral sliding surface has been designed as given.

$$\bar{\sigma}_i[x_i(t)] = P_i x_i(t) - \int_0^t P_i(A_i - B_i\Lambda_i)x_i(\tau)d\tau - \int_0^t\int_0^t P_i(A_i - B_i\Lambda_i)x_i(\tau)d\tau d\tau \quad (15)$$

where P_i is the constant matrix and Λ_i is a design of matrix, matrix P_i is chosen in order to ensure that matrix $P_i B_i$ is nonsingular. The design of matrix $\Lambda_i \in R^{m_i \times n_i}$ is chosen to satisfy the power system's inequality criterion (9).

$$\mathrm{Re}[\lambda_{\max}(A_i - B_i\Lambda_i)] < 0 \quad (16)$$

To determine the equivalent control, we differentiate $\bar{\sigma}_i[x_i(t)]$ in terms of timing as follows:

$$\dot{\bar{\sigma}}_i[x_i(t)] = P_i[A_i x_i(t) + B_i u_i(t) + \sum_{\substack{j=1\\ j\neq i}}^{N} H_{ij}x_j(t) + \bar{L}_i(x_i,t)] - P_i(A_i - B_i\Lambda_i)x_i(t) - \int_0^t P_i(A_i - B_i\Lambda_i)x_i(\tau)d\tau \quad (17)$$

So, by equating $\bar{\sigma}_i[x_i(t)] = \dot{\bar{\sigma}}_i[x_i(t)] = 0.$ After that, the equivalent control is expressed by

$$u_i^{eq}(t) = -(P_iB_i)^{-1}[P_iA_ix_i(t) + \sum_{\substack{j=1\\ j\neq i}}^{N} P_iH_{ij}x_j(t) + P_i\bar{L}_i(x_i,t) - P_i(A_i - B_i\Lambda_i)x_i(t) - \int_0^t P_i(A_i - B_i\Lambda_i)x_i(\tau)d\tau] \quad (18)$$

To close the loop system, we substitute $u_i^{eq}(t)$ into the equation (13) to yield the PS in the sliding motion with the following.

$$\dot{x}_i(t) = (A_i - B_i\Lambda_i)x_i(t) + [I_i - B_i(P_iB_i)^{-1}P_i]\bar{L}_i(t) + \sum_{\substack{j=1\\ j\neq i}}^{N}[I_i - B_i(P_iB_i)^{-1}P_i]H_{ij}x_j(t) + \int_0^t B_i(P_iB_i)^{-1}P_i(A_i - B_i\Lambda_i)x_i(\tau)d\tau \quad (19)$$

Supporting that

$$\bar{z}_i(t) = \int_0^t x_i(\tau)d\tau;\ \tilde{z}_i(t) = x_i(t) \quad (20)$$

We have

$$\dot{\bar{z}}_i(t) = x_i(t) = \tilde{z}_i(t); \quad (21)$$

and

$$\dot{\tilde{z}}_i(t) = (A_i - B_i\Lambda_i)\tilde{z}_i(t) + [I_i - B_i(P_iB_i)^{-1}P_i]\bar{L}_i(t) + \sum_{\substack{j=1\\ j\neq i}}^{N}[I_i - B_i(P_iB_i)^{-1}P_i]H_{ij}\tilde{z}_j(t) + B_i(P_iB_i)^{-1}P_i(A_i - B_i\Lambda_i)\bar{z}_i(t) \quad (22)$$

The equation provided can be reformulated as follows:

$$\dot{\hat{z}}_i(t) = \begin{bmatrix} 0 & I \\ B_i(P_iB_i)^{-1}P_i(A_i - B_i\Lambda_i) & (A_i - B_i\Lambda_i) \end{bmatrix}\hat{z}_i(t) + \begin{bmatrix} 0 \\ [I_i - B_i(P_iB_i)^{-1}P_i] \end{bmatrix}L_i(t) + \sum_{\substack{j=1\\ j\neq i}}^{N}\begin{bmatrix} 0 & 0 \\ 0 & [I_i - B_i(P_iB_i)^{-1}P_i]H_{ij} \end{bmatrix}\begin{bmatrix} \bar{z}_j(t) \\ \tilde{z}_j(t) \end{bmatrix} \quad (23)$$

and

$$\dot{\hat{z}}_i(t) = \bar{A}_i\hat{z}_i(t) + \bar{F}_i\bar{L}_i(t) + \sum_{\substack{j=1\\ j\neq i}}^{N}\bar{H}_{ij}\hat{z}_j(t) \quad (24)$$

where $\hat{z}_i(t) = \begin{bmatrix} \bar{z}_i(t) \\ \tilde{z}_i(t) \end{bmatrix}$, $\bar{F}_i = \begin{bmatrix} 0 \\ [I_i - B_i(P_iB_i)^{-1}P_i] \end{bmatrix}$, $\bar{A}_i = \begin{bmatrix} 0 & I \\ B_i(P_iB_i)^{-1}P_i(A_i - B_i\Lambda_i) & (A_i - B_i\Lambda_i) \end{bmatrix}$, and $\bar{H}_{ij} = \begin{bmatrix} 0 & 0 \\ 0 & [I_i - B_i(P_iB_i)^{-1}P_i]H_{ij} \end{bmatrix}$.

The above power system (24) is stable, which depends on the eigenvalue of the system matrices and the careful selection of the constant matrix gain P_i and design matrix gain Λ_i of the proposed equivalent control input. Furthermore, we analyze the stability of the PS using Lyapunov theory through LMI. To do this, we state the theorem as follows.

Theorem 1: The sliding motion (24) achieves asymptotic stability when and only when symmetric positive definite matrices are present M_i, $i = 1, 2, \ldots, N$, and positive scalars $\hat{\varepsilon}_i$, ε_i, δ_j and β_i and the following LMIs are obtained.

$$\begin{bmatrix} \bar{A}_i^T\mathrm{M}_i + \mathrm{M}_i\bar{A}_i + \sum_{\substack{j=1\\ j\neq i}}^{N}\delta_j^{-1}\bar{H}_{ji}^T\bar{H}_{ji} & \mathrm{M}_i & \mathrm{M}_i\bar{F}_i \\ \mathrm{M}_i & -\hat{\varepsilon}_i^{-1} & 0 \\ \bar{F}_i^T\mathrm{M}_i & 0 & -\beta_i \end{bmatrix} < 0 \quad (25)$$

Proof 1: To analyze the stability of (19), we apply Lyapunov stability theory so that the Lyapunov function is obtained as

$$V = \sum_{i=1}^{N}\hat{z}_i^T(t)\mathrm{M}_i\hat{z}_i(t) \quad (26)$$

where $\mathrm{M}_i > 0$ satisfies (25). Then, a time derivative of (26) and substitute equation (19), to have

$$\dot{V} = \sum_{i=1}^{N}\dot{\hat{z}}_i^T(t)\mathrm{M}_i\hat{z}_i(t) + \hat{z}_i^T(t)\mathrm{M}_i\dot{\hat{z}}_i(t) = \sum_{i=1}^{N}\{\hat{z}_i^T(t)[\bar{A}_i^T\mathrm{M}_i + \mathrm{M}_i\bar{A}_i]\hat{z}_i(t) + \sum_{\substack{j=1\\ j\neq i}}^{N}\hat{z}_j^T(t)\bar{H}_{ij}^T\mathrm{M}_i\hat{z}_i(t) + \sum_{\substack{j=1\\ j\neq i}}^{N}\hat{z}_i^T(t)\mathrm{M}_i\bar{H}_{ij}\hat{z}_j(t) + \hat{z}_i^T(t)\mathrm{M}_i\bar{F}_i\bar{L}_i(t) + \bar{L}_i^T(t)\bar{F}_i^T\mathrm{M}_i\hat{z}_i(t)\} \quad (27)$$

Using Lemma 1 to solve equation (27), we have

$$\begin{aligned}\dot V \le \sum_{i=1}^{N}\{&\hat z_i^T(t)[\bar A_i^T \mathrm{M}_i + \mathrm{M}_i\bar A_i]\hat z_i(t) + \sum_{\substack{j=1\\ j\ne i}}^{N}\hat z_j^T(t)\delta_i^{-1}\bar H_{ij}^T\bar H_{ij}\hat z_j(t)\\ &+\sum_{\substack{j=1\\ j\ne i}}^{N}\hat z_i^T(t)\delta_i \mathrm{M}_i \mathrm{M}_i \hat z_i(t) + \hat z_i^T(t)\beta_i^{-1}\mathrm{M}_i\bar F_i\bar F_i^T \mathrm{M}_i\hat z_i(t)\\ &+\beta_i \bar L_i(x_i,t)\bar L_i^T(x_i,t)\}\end{aligned} \tag{28}$$

since

$$\sum_{i=1}^{N}\sum_{\substack{j=1\\ j\ne i}}^{N}\hat z_j^T(t)\delta_i^{-1}\bar H_{ij}^T\bar H_{ij}\hat z_j(t) = \sum_{i=1}^{N}\sum_{\substack{j=1\\ j\ne i}}^{N}\hat z_i^T(t)\delta_j^{-1}\bar H_{ji}^T\bar H_{ji}\hat z_i(t)$$

We achieve that.

$$\begin{aligned}\dot V \le \sum_{i=1}^{N}\{&\hat z_i^T(t)[\bar A_i^T \mathrm{M}_i + \mathrm{M}_i\bar A_i + \hat\varepsilon_i \mathrm{M}_i \mathrm{M}_i\\ &+\beta_i^{-1}\mathrm{M}_i\bar F_i\bar F_i^T \mathrm{M}_i + \sum_{\substack{j=1\\ j\ne i}}^{N}\delta_j^{-1}\bar H_{ji}^T\bar H_{ji}]\hat z_i(t) + \sum_{i=1}^{N}\varphi_i\end{aligned} \tag{29}$$

where $\hat\varepsilon_i = \delta_i(N-1)$ and $\varphi_i = \beta_i\gamma_i^2$.

Furthermore, the Schur complement, the LMIs (25) is the same as this inequality.

$$\begin{aligned}\Psi_i = {}&\bar A_i^T \mathrm{M}_i + \mathrm{M}_i\bar A_i + \sum_{\substack{j=1\\ j\ne i}}^{N}\delta_j^{-1}\bar H_{ji}^T\bar H_{ji}\\ &+\hat\varepsilon_i \mathrm{M}_i \mathrm{M}_i + \beta_i^{-1}\mathrm{M}_i\bar F_i\bar F_i^T \mathrm{M}_i < 0\end{aligned} \tag{30}$$

According to the equations (29) and (30), we obtain

$$\dot V \le \sum_{i=1}^{N}[-\lambda_{\min}(\Psi_i)\|\hat z_i(t)\|^2 + \varphi_i] \tag{31}$$

where φ_i is the constant value and the eigenvalue $\lambda_{\min}(\Psi_i) > 0$.

So, $\dot V < 0$ is made possible by $\|\hat z_i(t)\| > \sqrt{\dfrac{\varphi_i}{\lambda_{\min}(\Psi_i)}}$. As a result, the system's (19) sliding motion is asymptotically stable.

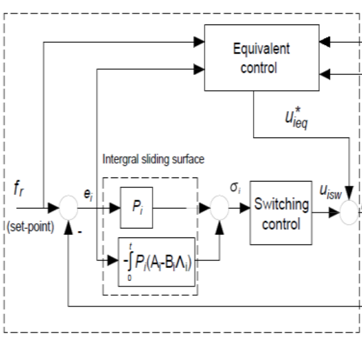

Fig. 2. Simple diagram of traditional integral sliding surface.

Remark 2: The block diagrams of the aforesaid control techniques are presented in Fig. 2 and Fig. 3 to highlight the differences and improvements of the control methods, which include classic integral SMC. The SMC using the traditional integral sliding surface results with the PI switching surface in [13], [18-24]. First, a LFC for multi-area linked PS is created using a second-order double integral SMC approach that overcomes the aforementioned constraint. Second, a double integral sliding surface-based second order sliding mode controller (SOSDISS) is presented to make improvement the closed-loop system's transient performance. However, in LFC techniques, the bound of the aggregated uncertainty of the MAPS is typically unknown in advance. As a result, determining the appropriate control system parameter to keep the system state within the boundary layer is difficult. Furthermore, the above approaches have some limitations, this includes scenarios, hence, in steady state, disturbances are not clipped from the output points and controller gains are not set excessively high to mitigate disturbances arising from unknown boundaries, parameter uncertainties, or load variations. The SOSDISS prevents the system from fluctuating and may also reset the system to its set point.

Remark 3. Under matched uncertainties, SMC based on first-order double integral surfaces can be utilized to investigate the LFC of a PS in [27]. However, in a real power network, parametric uncertainties do not always meet the matching condition. Consequently, there exist notable constraints when constructing the first order sliding mode control (SMC) to address uncertainties, ensuring nominal frequency convergence and system stability; however, system trajectories may not reach the origin point. As a result, the utilization of the second-order double sliding surface approach is introduced to guide the system trajectory towards a similar point and enhance transient performance.

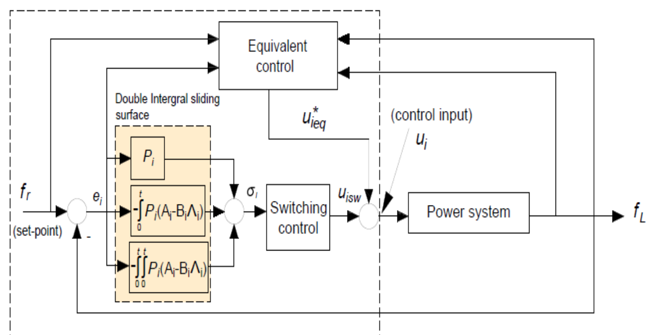

Fig. 3. Simple diagram of the double integral sliding surface.

IV. Decentralized Continuous Control Law

In this segment, the suggested decentralized second-order SMC law is suggested for LFC of the PS (19). The construction is done by simply making $\bar\sigma_i[x_i(t)]$ and $\dot{\bar\sigma}_i[x_i(t)]$ equal to zero (i.e., known as the sliding manifold) so that PS stability is improved.

In other words, the sliding manifold is defined and established $\Theta_i(t)$ as

$$\Theta_i(t) = \dot{\bar\sigma}_i[x_i(t)] + \gamma_i\bar\sigma_i[x_i(t)] \tag{32}$$

and

$$\dot\Theta_i(t) = \ddot{\bar\sigma}_i[x_i(t)] + \gamma_i\dot{\bar\sigma}_i[x_i(t)] \tag{33}$$

where $\gamma_i > 0$ is a positive constant. As stated by the formula (13), the equation (33) must be transformed into

$$\dot{\Theta}_i(t) = P_i[A_i\dot{x}_i(t) + B_i\dot{u}_i(t) + \sum_{\substack{j=1\\j\neq i}}^{N} H_{ij}\dot{x}_j(t) + \dot{L}_i(x_i,t)] \tag{34}$$
$$-P_i(A_i - B_i\Lambda_i)\dot{x}_i(t) - P_i(A_i - B_i\Lambda_i)x_i(t) + \gamma_i\dot{\bar{\sigma}}_i[x_i(t)]$$

If the sliding manifold is made equal to zero, then the proposed decentralized SMC is given as

$$\dot{u}_i(t) = -(P_iB_i)^{-1}\{\|P_i\|\|A_i\|\|\dot{x}_i(t)\| + \sum_{\substack{j=1\\j\neq i}}^{N}\|P_j\|\|H_{ji}\|\|\dot{x}_i(t)\|$$
$$+\|P_i\|\|(B_i\Lambda_i - A_i)\|\|\dot{x}_i(t)\| + \|P_i\|\|(B_i\Lambda_i - A_i)\|\|x_i(t)\| \tag{35}$$
$$+\gamma_i\|\dot{\bar{\sigma}}_i[x_i(t)]\| + \|P_i\|\bar{\gamma}_i + \upsilon_i\}\frac{\Theta_i^T(t)}{\|\Theta_i(t)\|}$$

To satisfy the above proposed control input (35), the system variables trajectories must be forcefully driven to the sliding manifold (SM) and remain therein at finite reaching time to ensure the PS's asymptotic stability (19) asymptotic stability. Therefore, we again examine the system's stability by the given theorem.

Theorem 2: Consider the PS's closed loop (19) with the controller for continuous sliding mode (35). Following that, each solution trajectory is pointed at the SM $\Theta_i(t) = 0$ and once the trajectory hits the SM $\Theta_i(t) = 0$ it remains on the SM thereafter.

Proof 2: As shown below, the Lyapunov's function is introduced.

$$\bar{V}(t) = \sum_{i=1}^{N}\|\Theta_i(t)\| \tag{36}$$

Hence, using a derivation of $\bar{V}(t)$ then we get

$$\dot{\bar{V}} = \sum_{i=1}^{N}\frac{\Theta_i^T(t)}{\|\Theta_i(t)\|}\dot{\Theta}_i(t)$$
$$= \sum_{i=1}^{N}\frac{\Theta_i^T(t)}{\|\Theta_i(t)\|}\{P_i[A_i\dot{x}_i(t) + B_i\dot{u}_i(t) + \sum_{\substack{j=1\\j\neq i}}^{N}H_{ij}\dot{x}_j(t)$$
$$+\dot{L}_i(x_i,t)] - P_i(A_i - B_i\Lambda_i)\dot{x}_i(t) - P_i(A_i - B_i\Lambda_i)x_i(t)$$
$$+\gamma_i\dot{\sigma}_i[x_i(t)]\} \tag{37}$$
$$= \sum_{i=1}^{N}\frac{\Theta_i^T(t)}{\|\Theta_i(t)\|}\{P_iA_i\dot{x}_i(t) + P_iB_i\dot{u}_i(t) + \sum_{\substack{j=1\\j\neq i}}^{N}P_iH_{ij}\dot{x}_j(t)$$
$$+P_i\dot{L}_i(x_i,t) + P_i(B_i\Lambda_i - A_i)\dot{x}_i(t) + P_i(B_i\Lambda_i - A_i)x_i(t)$$
$$+\gamma_i\dot{\bar{\sigma}}_i[x_i(t)]\}$$

In light of the formula (37) as well as property $\|AB\| \le \|A\|\|B\|$, it produces

$$\dot{\bar{V}} \le \sum_{i=1}^{N}\{\|P_i\|\|A_i\|\|\dot{x}_i(t)\| + \sum_{\substack{j=1\\j\neq i}}^{N}\|P_i\|\|H_{ij}\|\|\dot{x}_j(t)\|$$
$$+\|P_i\|\|(B_i\Lambda_i - A_i)\|\|\dot{x}_i(t)\| + \|P_i\|\|(B_i\Lambda_i - A_i)\|\|x_i(t)\| \tag{38}$$
$$+\gamma_i\|\dot{\bar{\sigma}}_i[x_i(t)]\| + \|P_i\|\|\dot{L}_i(x_i,t)\|\} + \sum_{i=1}^{N}\frac{\Theta_i^T(t)}{\|\Theta_i(t)\|}P_iB_i\dot{u}_i(t)$$

The term $\sum_{i=1}^{N}\sum_{\substack{j=1\\j\neq i}}^{N}\|P_i\|\|H_{ij}\|\|\dot{x}_j(t)\| = \sum_{i=1}^{N}\sum_{\substack{j=1\\j\neq i}}^{N}\|P_j\|\|H_{ji}\|\|\dot{x}_i(t)\|$

and Assumption 1 we get

$$\dot{\bar{V}} \le \sum_{i=1}^{N}\{\|P_i\|\|A_i\|\|\dot{x}_i(t)\| + \sum_{\substack{j=1\\j\neq i}}^{N}\|P_j\|\|H_{ji}\|\|\dot{x}_i(t)\|$$
$$+\|P_i\|\|(B_i\Lambda_i - A_i)\|\|\dot{x}_i(t)\| + \|P_i\|\|(B_i\Lambda_i - A_i)\|\|x_i(t)\| \tag{39}$$
$$+\gamma_i\|\dot{\bar{\sigma}}_i[x_i(t)]\| + \|P_i\|\bar{\gamma}_i\} + \sum_{i=1}^{N}\frac{\Theta_i^T(t)}{\|\Theta_i(t)\|}P_iB_i\dot{u}_i(t)$$

When the control law (35) is applied, the following results are obtained:

$$\dot{\bar{V}} \le -\sum_{i=1}^{N}\upsilon_i \tag{40}$$

The Lyapunov function derivative (40) is less than or equal to zero, which implies that the state variable of dynamic system trajectories are forcefully driven to the SM $\Theta_i(t) = 0$ to make the PS (19) to be asymptotically stable.

V. Case Studies

In this part, the suggested second-order SMC via double integral sliding surface is put into practice for the LFC of a two-area steam-hydropower system (TASHPS) respectively. The LDs and aggregate uncertainties are included in the PS model for simulation. The objectives of the suggested approach for the LFC of TASHPS are to improve the stability of the PS, ensure the reliability of the power network and maintain the frequency at a tolerable point ±0.5 Hz [17]. The suggested control strategy's performance is efficient and trustworthy, as evidenced by its fast frequency responses and insensitivity to parameter changes, load disturbance, load variation, delay time, considering the nonlinear impacts of the GDB and GRC on the power network. The proposed controller performance is validated when the simulation results are compared with recent methods, which are briefly discussed in three different simulations as follows.

Simulation 1:

Case 1: The LFC of TASHSP stability has been achieved by using different meta-heuristic optimization algorithms in order to improve the fuzzy PID control parameters. A recent study was the application of grey wolf optimization (GWO) in [25]. The proposed SMC is tested in a TASHPS with choosing the same step load disturbance and system parameters as in [25]. Figs. 4 and 5 give the control area 1 and 2 frequency variations. The TASHPS tie-line power is represented in Fig. 6. From the analysis of both results, both frequencies undershoot did not exceed the tolerable point of -0.5Hz. Therefore, implies the proposed SMC is superior to the GWO based fuzzy PID method in regard to control performance and Table 1 shows detail summary of both controller's comparisons.

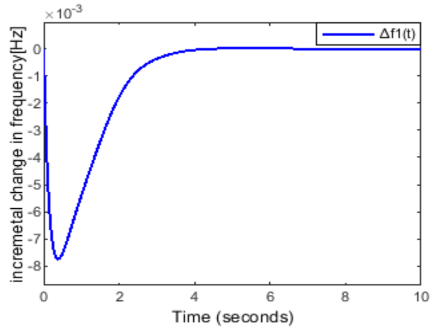

Fig. 4. Frequency of control area 1 with matched disturbances, in hertz (Hz).

TABLE I

Comparing the Maximum Overshoot MOS [Hz] and Setting Time T_s[s] .

Controller	The suggested Scheme		Different Scheme Give in [25]	
System Parameter	$T_s[s]$	MOS [Hz]	$T_s[s]$	MOS [Hz]
Δf_1	4	0.0078	6	0.15
Δf_2	3.8	0.009	10	0.025

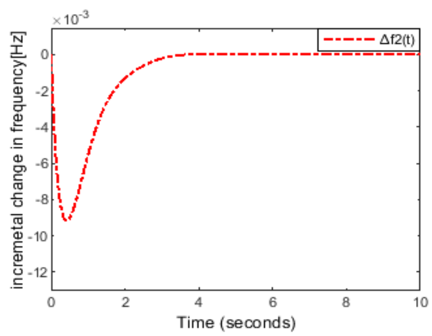

Fig. 5. Frequency of control area 2 with matched disturbances, in hertz (Hz).

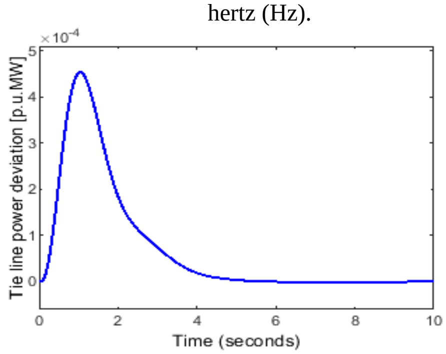

Fig. 6. With matched disturbances, tie line power variation (p.u.MW).

Remark 4: Notably, as can be seen in [25], the new controller is more resilient to load disturbances and responds more quickly. The load disturbances (LDs) are clearly visible in the details, and a steady state is restored quickly in the system with fewer overshoots.

In this context, a significant challenge in the analysis of a control PS is the identification of all closed-loop poles, with a specific focus on those that are closest to the imaginary axis or constitute the dominant pair of closed-loop poles.

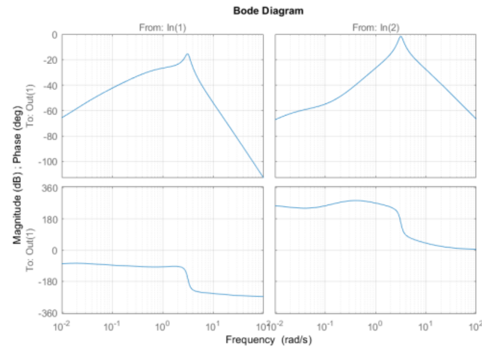

Fig. 7. The closed loop system in terms of frequency domain specifications (gain margin and phase margin).

It's important to highlight a notable advantage of the Bode diagram approach, which lies in its ability to easily assess the effects of changes in gain. The Bode diagram in Fig. 7 provides a straightforward means of determining phase and gain margins in dynamic systems. To elaborate, for the input, the gain margin is 1.3133, and the phase margin is 38.1454, while for the output, the gain margin is 1.0661, and the phase margin is infinite.

Remark 5: The phase and gain margins within a control system act as indicators of how closely the polar plot approaches a critical point. Consequently, these margins can be used as criteria for evaluating the effectiveness of the suggested control approach. It is crucial to consider both the phase and gain margins when assessing relative stability. In the context of a minimum-phase system, it is essential for both the phase and gain margins to be positive values to guarantee the stability of the system. Sufficient phase and gain margins serve as safeguards against variations in PS components and are usually defined with specific positive values in mind.

Case 2: Given this, we consider a change in the load demand from commercial business buildings in a metropolitan city. The commercial buildings load demand from control areas 1 and 2 of the TASHPS is given in [25].

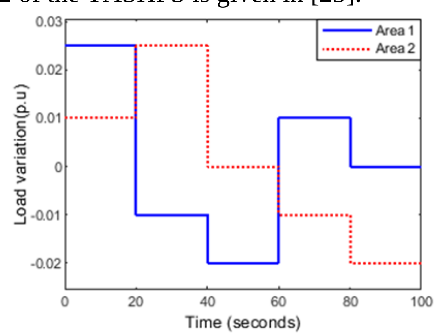

Fig. 8. Daily load curve of commercial business buildings

The demand curve is plotted and shown in Fig. 8. As the demands change, as seen from the load curve, the dynamics responses of the TASHPS change. Fig. 9 shows the frequency variation of both control area 1 and control area 2 whereas Fig. 10 illustrates the TASHPS tie-line power variation. From the Figs, the TASHPS dynamics is improved with regard to far little under/overshoot and settling time, which did not exceed the tolerable point given in [25]. This further makes the proposed method capable of a handling LFC of large power system in order to keep the power system stable and reliable.

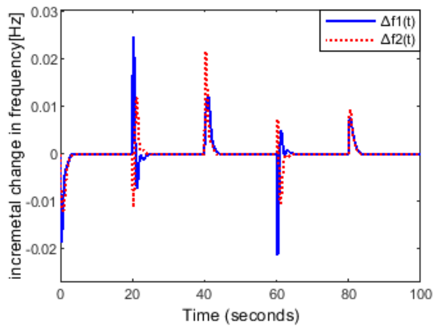

Fig. 9. First and second control areas frequency variation.

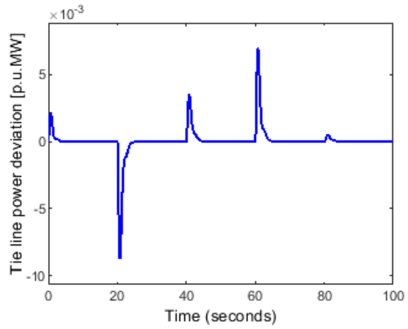

Fig. 10. TASHPS tie line power variation.

Remark 6: The SMC chattering problem is extremely damaging to the actuators utilized in PS. The suggested control scheme generates the appropriate signal and uses energy to counteract frequency damping within the primary control loop, governed by a speed controller. Consequently, the droop speed control of the governor accurately prompts the valve to supply the necessary steam to the turbine, thereby improving mechanical inertia power alignment with load variations or demands. As a result, the system exhibits fast settling time and minimal overshoot.

Case 3: Finally, we consider a more realistic problem in this case. The parameter uncertainties resulting from the different dynamic behaviours of the TASHPS which can impact the inertia time constant of the field gen sets are taken into account. This can also affect the field rotating mass of the power system, causing an imbalance between total net power generated to varying load demands. The uncertainties with mismatch condition are represented in the state matrix of the power system as defined below with cosine functions given in [26]. Also, the variation in the demands of industrial activities is considered due to frequency-sensitive loads. This industrial frequency sensitive load demand from area 1 and area 2 is conceptualized with practical knowledge and written in [25] and the load curve is shown as well in Fig. 11, respectively. The proposed method parameter matrix gain is used in the same way as in the above cases discussed. We have the parameter uncertainties $\Delta A_1 = \Delta A_2 = \begin{bmatrix} \Delta A_{11} & \Delta A_{12} \end{bmatrix}$ where:

$$\Delta A_{11} = \begin{bmatrix} 0 & 0 & 2.6\cos(t) & 0 \\ 0 & \cos(t) & 0 & 0 \\ 0 & 0 & 0 & 0 \\ 0 & 0 & 0 & 0.24\cos(t) \\ \cos(t) & 0 & 0 & 0 \\ 0 & 0 & 0 & 0.14\cos(t) \\ 2.6\cos(t) & 0 & 0 & 0 \\ 0 & 0 & 0 & 0 \\ 0 & 0 & 0 & 0 \end{bmatrix},$$

$$\Delta A_{12} = \begin{bmatrix} 0 & 0 & 0 & 0 & 0 \\ 0 & 0 & 0 & 0 & 0 \\ 0 & 0.26\cos(t) & 0 & 0 & 0 \\ 0 & 0 & 0 & 0 & 0 \\ 0 & 0 & 0 & 0 & 0 \\ 0 & 0 & 0 & 0 & 0 \\ 0 & 0 & 0 & 0 & 0 \\ 0 & 0 & 1.26\cos(t) & 0 & 0 \\ 4.6\cos(t) & 0 & 0 & 0 & 0 \end{bmatrix}$$

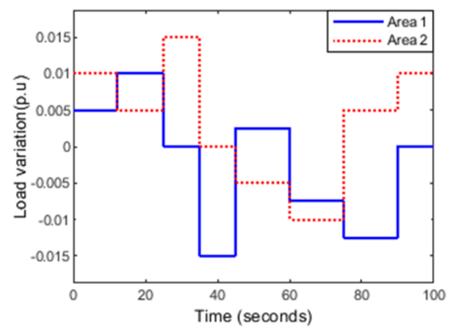

Fig. 11. Load curve due to industrial activity-based frequency sensitive loads.

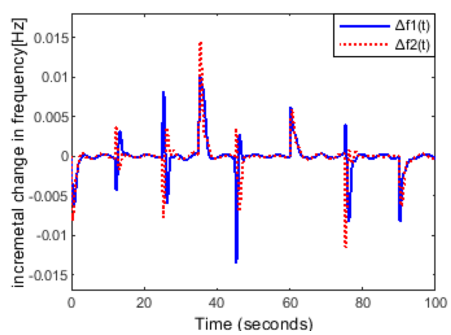

Fig. 12. Area 1 and area 2 frequency deviation under mismatched conditions.

The frequency oscillation in control area 1 and control area 2 is shown in Fig. 12 while the tie-line power is presented in Fig. 13. Fig. 12 demonstrates how the frequency variation did not exceed the tolerable level ±0.5Hz. The TASHPS tie-line power is properly managed within the schedule value as also seen in Fig. 13. So, with the proposed method better control performance for the LFC of the TASHPS when compared with other methods, this implies that it is very good for large power frequency regulation.

Remark 7: Using a double integral sliding surface based second order SMC, one of the most attainable goals in this proposed strategy is to finalise the mismatching disturbance and obtain a shorter settling time, lower transient deviation, and reduced variation for the PS in terms of LDs. As a result, various drawbacks of previous control systems discussed in journal paper [25] have been addressed, such as minimizing chattering and enhancing transient responsiveness.

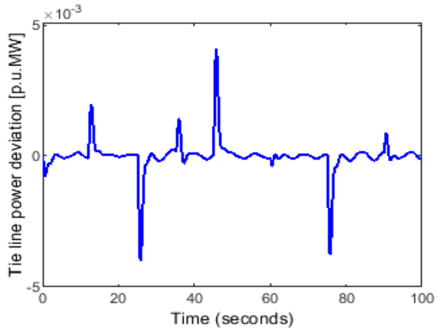

Fig. 13. TASHPS tie line power deviation under mismatched conditions.

Simulation 2: Case 1: In this scenario, a larger and more realistic PS, the New England 10-generator 39-bus PS, is used to further evaluate the performance of the suggested LFC scheme. The New England test system consists of 10 generators, 39 buses, 09 loads, 34 lines for transmission, and twelve transformers. Fig. 14 depicts a single-line schematic of the test PS. The generator settings utilized in this work are taken from [24]. All electrical generators include a speed governor. In three control sections, the three generators (G3, G7, and G9) Please provide a list of the parameters for the IEEE 39-bus New England test system in the appendix.

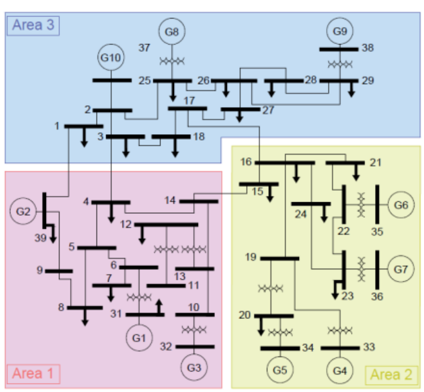

Fig.14. The block diagram of the New England 39 bus system

In this instance, it is presumed that the LFC duty is carried out by a single generator in each region, which are G1 in region 1, G7 in Area 2, and G9 in Area 3. So, the load demands in a real PS fluctuate, we used a random load fluctuation at each location, as seen in Fig.15. Fig. 16 depicts the frequency fluctuation of areas 1, 2, and 3, respectively, while Fig. 17 depicts the tie line power variation. Despite this, the system's state variables had not been monitored, the frequency fluctuation and the tie-line power flow rapidly decreased to zero. As a result, in a huge power network where system state variables are hard to evaluate, this strategy is preferable for keeping frequency and tie-line power within a safe range. The simulation findings validate the higher dynamic performance and resilience of the suggested LFC scheme.

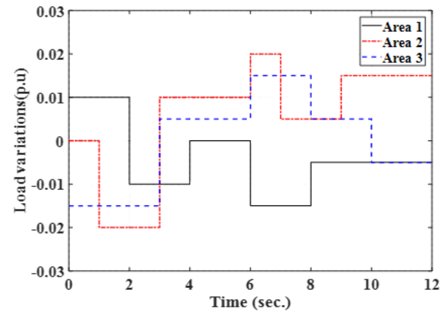

Fig.15. Random load variation

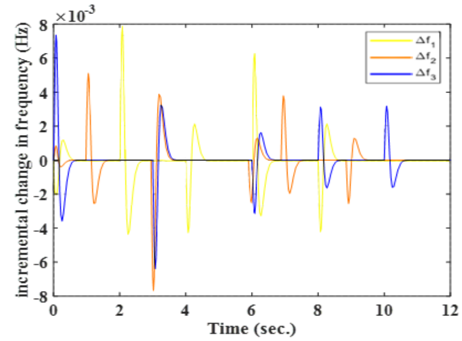

Fig.16. The dynamic responses of the frequency deviation

Remark 8. In summary, the recommended approach of utilizing a double-integral sliding surface-based second order sliding mode technique exhibited improved control performance by effectively ensuring that tie-line power and frequency remain within the desired range for power systems where quantifying system state variables is challenging. The suggested approach is incredibly powerful, not only reducing chattering but also ensuring the MAPS's resilience.

Case 2: In particular, the generation rate constraint (GRC) is generally studied by enhancing the governor-turbine system model with a limiter and a hysteresis pattern. It is essential to discuss realistic constraints and prevailing conditions such as the physical constraint of the GRC.

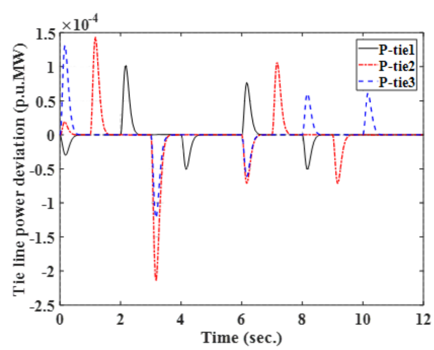

Fig. 17. The dynamic responses of the tie-line power

Due to its non-linearity, the GRC has a detrimental impact on PS performance. The GRC represents a realistic restriction on the ratio of deviation in producing power due to physical constraints. Governor dead band (GDB) is a technique for power network frequency regulation in the presence of disruptions. GDB has a distinct contour as the overall magnitude of a continuous speed shift with no consequent modification in the valve position. The use of grey wolf optimization (GWO) in [25] was a recent study. However, as observed in [24], the effects of GDB and GRC are not included in the power plant to assess the effective responsiveness of the proposed controller of power networks. In this scenario, we examine the dynamic models utilized in MAPS to represent physical limitations of GRC and GDB. The proposed SMC is tested in a MAPS with the same step load disturbance and system parameters as in [25]. A nonlinear turbine model with GRC implemented in the TASHSP and a nonlinear governor model with GDB are shown in Figure 18.

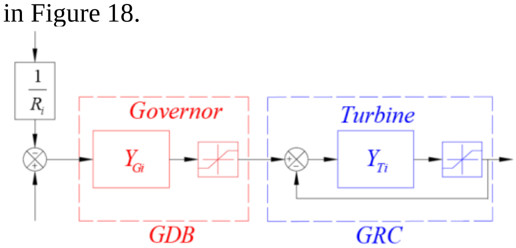

Fig.18. Nonlinear turbine model with the GRC and Nonlinear governor model with dead band in [24].

Figs. 19 and 20 show the tie-line power and frequency deviations. As can be seen, with the suggested SOSDISS controllers, transient oscillations are determined for a longer time and with a bigger amplitude than in case 1 in simulation 1. In contrast to [25] and Simulation 1 with Case 1, the suggested control approach was found to be adequate. In the transient performance of the suggested SOSDISS controller, the % overshoot and the settling time are greatly reduced under the GDB and GRC effects.

Remark 9: The feedback signal of the linked power network is greatly influenced by GRC and GDB. The simulation outcomes are contrasted with Simulation 1 with Case 1 of considering or without taking the impacts of nonlinearity into account of GDB and GRC in [25] to illustrate the durability of the proposed GESO. In contrast to previous studies, the suggested SOSDISS controller clearly reveals that transient performance has changed with needed circumstances such as the setup time and under/overshoot under the GDB and GRC. As a result, the planned SOSDISS's tiny frequency fluctuations have less impact on plant reserve capacity and the electricity market.

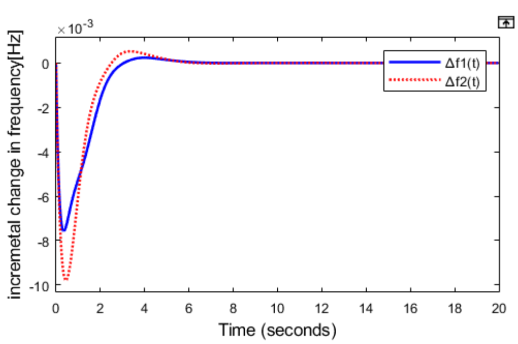

Fig. 19. The frequency responses of two areas with GRC and GRB.

Case 3: Because the same parameter uncertainty of the three regions MAPS is employed in Case 1 of Simulation 1, the nominal operating point is employed to evaluate the value and resilience of the proposed controller to LDs. Figs 21 and 22 show the fast decrease of the tie-line power and variance in frequency.

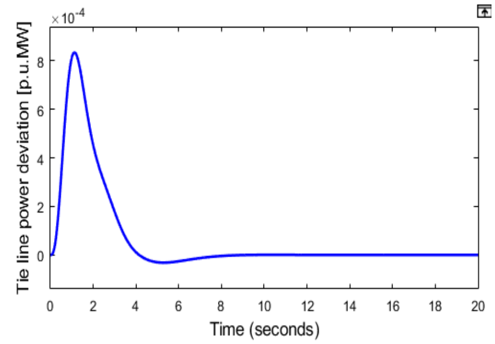

Fig. 20. Changes that respond of the tie-line power with GRC and GRB

As a result, the suggested SOSDISS controller is applied for three-area multisource multi-area PS. It also shows that the SOSDISS can stabilize the system in conjunction with the large system. When the simulation results are compared, the suggested double sliding switching surface and the planned SOSDISS can eliminate overshot, improve reaction speed, and restrict frequency variation to zero. As a result, the developed controller is resilient and effective in controlling MAPS's parameter uncertainties.

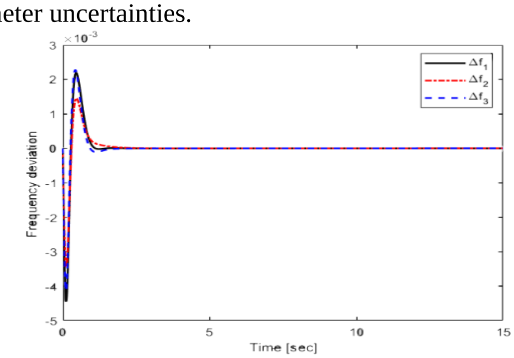

Fig. 21. The dynamic responses of frequency change in three areas

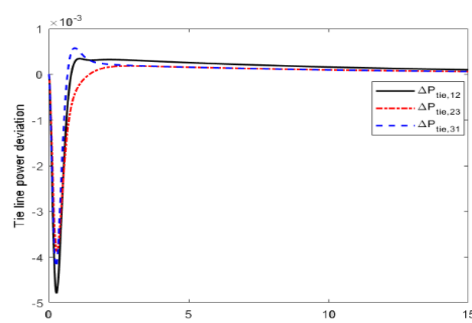

Fig. 22. The wiring tie-line's dynamic responses

Simulation 3: The presented LFC based on the suggested SOSDISS is utilized in comparison to the other LFC technique under the identical conditions in [25]. The suggested LFC based on SOSDISS has been investigated in [25] and [28] with various step load disruption effects on the MAPS under nominal parameter settings. The three-area restructured power system in Fig. 23 has a transmission time delay. The load disturbances in this instance are $\Delta P_{d1} = 0.02$, $\Delta P_{d2} = 0.015$, and $\Delta P_{d3} = 0.01$ (p.u) at $t_1 = 0$ in three areas of the MASHPS. The frequency deviation of $\Delta f_1, \Delta f_2, \Delta f_3$ for the MASHPS with delay time as $\tau_i = 5s$ ($i = 1,2,3$) are displayed in Fig. 24 to Fig. 25 are the three areas' PS tie line power variation and frequency change.

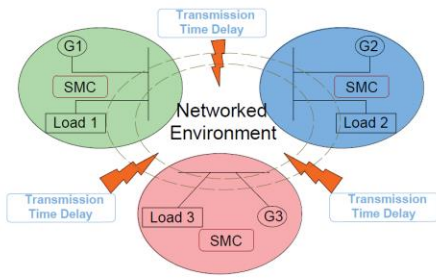

Fig. 23. A three-area restructured power system with transmission time delay.

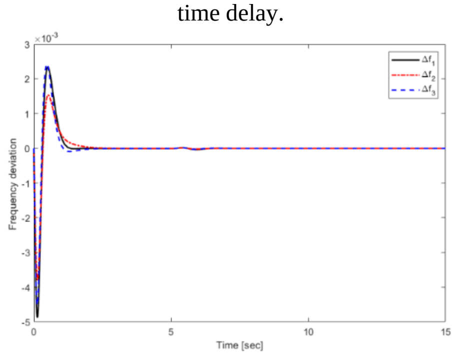

Fig.24. Frequency deviation with time delay at $\tau = 5s$

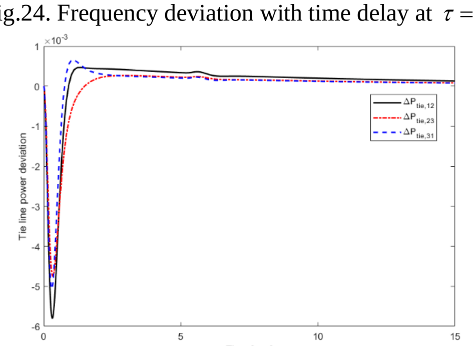

Fig.25. Tie-line deviation with time delay at $\tau = 5s$

To clarify within this research, the transient responses generated by the proposed LFC system using SOSDISS are comparable in terms of settling time and minimal overshoot magnitude.

Remark 10. The findings of the testing simulation are assigned in this section on Figs 23 to 25. The report of conclusions may result in a beneficial comparison, particularly if time delay interchange is taken into consideration for the extended power networks. As a result, the recommended SOSDISS reaches a well-balanced condition with a frequency fluctuation of zero within 1 second.

VI. Conclusion

In conclusion, a LFC study has been achieved for a TASHPS under load disturbance and parameter uncertainties. The load disturbance and uncertainties are considered and a new power system model is derived. The proposed LFC method is developed with a second-order SMC via double integral sliding surface (SOSDISS). On the other hand, a decentralised second double integral SMC is given with carefully selected matrices gains to improve the power system asymptotic stability and also reduces chattering inherent in first-order SMC. The novel linear matrix inequality based on Lyapunov theory, in which the derivative of the Lyapunov function is smaller than zero, is used to examine the asymptotic stability of the PS. To test the suggested second-order SMC performance, simulations are run on the TASHSP. Even when parameter uncertainties and random load demands from households, commercial buildings, and industries are taken into account, the suggested SOSDISS appears to be capable of handling the PS's LFC, making it suitable for MASHPS frequency regulation and PS reliability. Furthermore, both asymptotic stability and control performance are addressed throughout the controller optimization process. There are no assumptions about the distributions of the dynamics/bandwidth of the communication network with packet loss of networked control systems. In the future, we will focus on new SMC for various disturbances while considering dynamics/bandwidth of the communication network considering the impact of packet loss.

VII. Appendix

Nominal parameters for multi-area multi-source power system of IEEE 39-bus New-England of the three generators are the same at G3, G7, and G9:

$T_{gi} = 0.08\ s$, $T_{ti} = 0.3s$, $K_{Ri1} = 0.5$, $T_{Ri1} = 10\ s$, $T_{pi} = 20\ s$

$K_{pi} = 100\,Hz/puMW$, $T_{i1} = 48.7\ s$, $T_{Ri2} = 5s$, $T_{i2} = 0.513s$,

$K_{Ei} = 1$, $b_{ij} = -1$, $T_{ij} = 0.0433\ pu\text{MW/rad}$, $R_{i1} = 2.4Hz/puMW$,

$R_{i2} = 2.4Hz/puMW$

References

[1] H. Bevrani, "Robust Power System Frequency Control", in *Power Electronics and Power Systems*, Springer, 2014.
[2] M. Vijay, C. James, A. Paul, A. Fouad, "Power system control and stability" in *Wiley-IEEE Press*, Hoboken, New Jersey, USA, 2019.
[3] H. Bevrani, H. Golpîra, A. R. Messina, N. Hatziargyriou, F. Milano, "Power system frequency control: An updated review of current solutions and new challenges," *Electric Power Systems Research*, vol. 194, May. 2021.
[4] S. Saxena, Y.V. Hote, "Decentralized PID load frequency control for perturbed multi-area power systems," *International Journal of Electrical Power & Energy Systems*, vol. 81, pp. 405-415, Oct. 2016.
[5] J. Sharma, Y.V. Hote, R. Prasad, "Robust PID load frequency controller design with specific gain and phase margin for multi-area power systems," *IFAC - Papers OnLine*, vol. 51, pp. 627-632, 2018.
[6] D. Guha, P.K. Roy, S. Banerjee, "Quasi-oppositional JAYA optimized 2-degree-of-freedom PID controller for load-frequency control of interconnected power systems," *International Journal of Modelling and Simulation*, vol 42, pp. 63–85, Oct. 2022.
[7] K. Jagatheesan, B. Anand, S. Samanta, N. Dey, A.S. Ashour, and V.E. Balas, "Particle swarm optimisation-based parameters optimisation of

PID controller for load frequency control of multi-area reheat thermal power systems," *International Journal of Advanced Intelligence Paradigms*, vol. 9, pp. 464-489, 2017.

[8] V. Veerasamy, W. Abdul, I. Noor, R. Rajeswari, A. Vinayagam, M.L.Othman, H. Hizam, Satheeshkumar, and Jeevitha, "Automatic load frequency control of a multiarea dynamic interconnected power system using a hybrid PSO-GSA-Tuned PID controller," *Sustainability*, vol. 11, pp. 1-20, 2019.

[9] D. Tripathy, N.B. Choudhury, B.K. Sahu, "A novel cascaded fuzzy PD-PI controller for load frequency study of solar-thermal/wind generator-based interconnected power system using grasshopper optimization algorithm," *The International Journal of Electrical Engineering & Education*, Jun. 2020.

[10] X. Yu and O. Kaynak, "Sliding Mode Control Made Smarter: A Computational Intelligence Perspective," *IEEE Systems, Man & Cybernetics Magazine*, vol 3 (2), pp. 31-34, Apr. 2017.

[11] S. Yin, J. Qiu, H. Gao and O. Kaynak, "Descriptor reduced-order sliding mode observers design for switched systems with sensor and actuator faults," *Automatica*, vol 76, pp. 282–292, Feb. 2017.

[12] X. Su, X. Liu,Y. Song, "Event-Triggered sliding-mode control for multi-area power systems," *IEEE Transactions on Industrial Electronics*, vol. 64, pp. 6732 – 6741, Aug. 2017.

[13] Y. Mi, Y.C. Fu, Wang, P. Wang, "Decentralized sliding mode load frequency control for multi-area power systems," *IEEE Transactions on Power Systems*, vol. 28, pp. 4301-4309, Nov. 2013.

[14] A.E. Onyeka, Y. Xing-Gang, Z. Mao, B. Jiang, Q. Zhang, "Robust decentralized load frequency control for interconnected time delay power systems using sliding mode techniques," *IET Control Theory & Applications*, vol.14, pp. 470-480, Feb. 2020.

[15] J. Guo, "Application of full order sliding mode control based on different areas power system with load frequency control," *ISA transactions*, vol. 92, pp. 23-34, Sep. 2019.

[16] S. Trip, M. Cucuzzella, C. De Persis, A. Van der Schaft, A. Ferrara, "Passivity-based design of sliding modes for optimal load frequency control," *IEEE Transactions on Control Systems Technology*, vol. 27, pp. 1893-1906, Sep. 2019.

[17] J. Guo, "Application of a novel adaptive sliding mode control method to the load frequency control," *European Journal of Control*, vol. 57, pp. 172-178, Jan. 2021.

[18] Y. Mi, Y. Fu, D. Li, C. Wang, P.C. Loh, P. Wang, "The sliding mode load frequency control for hybrid power system based on disturbance observer," *International Journal of Electrical Power & Energy Systems*, vol. 74, pp. 446-452, Jan. 2016.

[19] A. Dev, M.K. Sarkar, "Robust higher order observer-based nonlinear super twisting load frequency control for multi-area power systems via sliding mode," *International Journal of Control, Automation and Systems*, vol. 17, pp. 1814-1825, Jul. 2019.

[20] V.V. Huynh, B.L.N. Minh, E.N Amaefule, A.T. Tran, P.T Tran, "Highly robust observer sliding mode-based frequency control for multi area power systems with renewable power plants," *Electronics*, vol. 10, pp. 274, 2021.

[21] V.V. Huynh, P.T. Tran, B.L.N. Minh, Tran, A.T. Tran, T.M. Nguyen, P.T. Vu, "New second-order sliding mode control design for load frequency control of a power system," *Energies*, vol. 13, pp. 24, 2020.

[22] A. Dev, M.K. Sarkar, "Load frequency control in multi-area interconnected power systems using second order sliding mode," *Novel Advancements in Electrical Power Planning and Performance*, vol. 10, pp. 300-336, 2020.

[23] K.V. Kumar, T.A. Kumar, V. Ganesh, "Chattering free sliding mode controller for load frequency control of multi-area power system in deregulated environment," *The IEEE 7th power India international conference (PIICON)*, pp. 1-6, Oct. 2017.

[24] K. Liao, Y.A. Xu, "Robust load frequency control scheme for power systems based on second order sliding mode and extended disturbance observer," *IEEE Transactions on Industrial Informatics*, vol. 14, pp. 3076-3086, Jul. 2018.

[25] J. Srilekha, C.N. Kalyan, G. Stanley, K. Suneetha, M.M. Thakreem, "Load frequency control of two area hydro-thermal system considering GRC and GDB non-linearity's with intelligent controller," *International Journal of Recent Technology and Engineering (IJRTE)*, vol. 8, pp. 4697-4705, Jan. 2020.

[26] V.V. Huynh, B.L.N Minh, B.L.N, E.N. Amaefule, A.T. Tran, P.T. Tran, V.D. Phan, V.T. Pham, T.M. Nguyen, "Load Frequency Control for Multi-Area Power Plants with Integrated Wind Resources," *Applied Sciences*, vol. 11, pp. 7, 2021.

[27] R. Pradhan, B. Subudhi, "Double integral sliding mode MPPT control of a photovoltaic system," *IEEE transactions on control systems technology*, vol. 24, pp.285-292, Jan. 2016.

[28] Y. Mi, X. Hao, Y. Liu, Y. Fu, C. Wang, P. Wang and P.C. Loh, "Sliding mode load frequency control for multi-area time-delay power system with wind power integration," *IET Generation, Transmission & Distribution, Transmission & Distribution*, vol. 11, no. 18, pp. 4644–4653, Aug. 2017.

Van Van Huynh received his Ph.D. degree in Mechanical and Automation Engineering from Da-Yeh University, Taiwan in 2015. He is currently a Lecturer in the Faculty of Electrical and Electronics Engineering, Ton Duc Thang University, Ho Chi Minh City, Vietnam. His current research interests are in sliding mode control, variable structure control, and power system control.

Phong Tran Thanh received the B.Eng. degree in physics and electronics with a major in automation and control at Ho Chi Minh University of Science, Ho Chi Minh, Vietnam, in 2010, and the M.Eng. degree in electrical engineering with a major in automation and control at International University, Ho Chi Minh National University, in 2015. His current research activities include load frequency control for power system, sliding mode control, dynamic system.

Chau Si-Thien Dong was born in Ho Chi Minh City, Vietnam. She received her M.Sc. in Automatic Control from Ho Chi Minh City University of Technology in 2003 and Ph.D. degree from VSB – Technical University of Ostrava in 2017. She is now a lecturer in the Faculty of Electrical and Electronics Engineering of Ton Duc Thang University, Ho Chi Minh City, Vietnam.

Bach H. Dinh (Member, IEEE) received his Ph.D. degree in Electrical Engineering from Heriot-Watt University, Edinburgh, United Kingdom in 2009. He is currently the head of Electrical Engineering Department at Ton Duc Thang University Vietnam. His research interests are intelligent and optimal control, computer vision, robotics, power electronics, SCADA and industrial communication networks. He is a member of the IEEE Industrial Electronics Society.

Okyay Kaynak (Life Fellow, IEEE) received the B.Sc. (First Class Hons.) and Ph.D. degrees in electronic and electrical engineering from the University of Birmingham, Birmingham, U.K., in 1969 and 1972, respectively. From 1972 to 1979, he held various positions within the industry. In 1979, he joined the Department of Electrical and Electronics Engineering, Bogaziçi University, Istanbul, Turkey, where he is currently a Professor Emeritus, holding the UNESCO Chair on Mechatronics. He has held long-term (near to or more than a year) Visiting Professor/Scholar positions at various institutions in Japan, Germany, U.S., Singapore, and China. His current research interests include the fields of intelligent control and CPS. He has authored three books and edited five and authored or coauthored more than 450 papers that have appeared in various journals, books, and conference proceedings.

Dr. Kaynak is active in international organizations, has served on many committees of IEEE and was the president of IEEE Industrial Electronics Society during 2002-2003. He was elevated to IEEE fellow status in 2003. In2016, he received the Chinese Government Friendship Award and Humboldt Research Prize. Most recently, in 2020, he received the International Research Prize of the Turkish Academy of Sciences. He is a member of this Academy.

Automatic Generation Control based Sliding Mode Observer Design for Multi-Area Multi-Source Power Systems

Phong Thanh Tran[1], Van Van Huynh[1], Chau Si Thien Dong[1] and Bach Dinh Hoang[1]

[1] Modeling Evolutionary Algorithms Simulation and Artificial Intelligence, Faculty of Electrical & Electronics Engineering, Ton Duc Thang University, Ho Chi Minh City, Vietnam
tranthanhphong.st@tdtu.edu.vn;huynhvanvan@tdtu.edu.vn

Abstract. Today, a multi-area power system (MAPS) has been implemented with a variety of power sources, including gas, hydro, thermal and nuclear, which will have an influence on load frequency regulation. Therefore, using the single-phase sliding mode control-based state observer (SPSMCBSO), load frequency control (LFC) of a deregulated two-area gas-hydro-thermal power system (TAGHTPS) is developed. Second, feedback control state variables are estimated using the state observer. Third, to enhance TAGHTPS performance in term of settling time and overshoot, the SPSMCBSO is designed to adjust the fundamental sliding mode control. Additionally, the SPSMCBSO is set up to totally depend on the state observer to resolve the issue with the state variable measurement. Finally, to verify the SPSMCBSO scheme, The results of the MATLAB/SIMULINK simulation are displayed and contrasted with newly established conventional control approaches.

Keywords: sliding mode control, state observer, power system.

1 Introduction

In power network, the basic characteristics that determine an electrical system's power quality are its frequency and voltage. Automatic generation control (AGC) is a crucial issue, especially in the case of an interconnected power system (PS), for the efficient running of the PS and for providing consumers with high-quality electricity. The primary purpose of AGC, also known as load frequency control (LFC), is to maintain the balance between generation and load demand while fluctuating consumer load needs and disturbances[1-2]. Therefore, LFC is a crucial application of control system engineering in the power system. Throughout the years, researchers have utilized conventional control techniques to develop methods for the LFC of PS [3]. Control engineers have found a solution to the issue by expressing the PS model shown in state space. Adaptive methodology, robust control, observer scheme, intelligent control (e.g., fuzzy logic, etc.) as well as traditional PID and PI have been created to analyze the LFC of MAPS [3-7]. The LFC must be extremely resilient against significant disruptions in order to be used in practice. The LFC of MAPS was therefore given the variable structure control (VSC) treatment. The most well-liked VSC is sliding mode control (SMC).

Because of its resilience and rejection of significant perturbations for the LFC of MAPS, the SMC is crucial [8-12]. The LFC problem of MAPS has been addressed throughout time by combining a number of techniques with SMC. The LFC of MAPS was given new adaptive treatment under step load disturbance [13]. The SMC through observer, on the other hand, was used for the LFC of MAPS where some state variables were impossible to obtain, and the SMC was designed to be completely dependent on the observer[14]. However, the aforementioned SMC approaches were used for the LFC of MAPS, which consists of thermal plants or hydro alone in each region. According to research, the MAPS includes combination of multiple generators in each region such as nuclear plant , hydro plant, gas plant, thermal plant, and so on, which is referred to as a multi-area multi-source power system (MAMSPS) in the industry [15-16], [18]. In [15], a generation-based PID structured automated generation control (AGC) design and implementation in a 2-area multisource PS with hydro plant, thermal plant, and gas power plants accommodated in each area. To optimize the dynamic of TAGHTPS under load disturbance, the novel teaching learning-based optimization (TLBO) technique with 2-degree freedom of proportional-integral-derivative (2-DOF PID) controller is presented for AGC [16]. These studies solely looked at the LFC of the TAGHTPS during load disturbances, and the system state matrix of the TAGHTPS was modeled without taking into account the effects of interconnection and parameter uncertainties.

The aim of this research is to ensure the system's robustness under the matched disturbance and load variation. By utilizing the SPSMCBSO technique, which is specifically effective LFC for the MAMSPS , if obtaining certain variables is challenging, the proposed controller is set up to alter the fundamental SMC in a way that the order of the PS, which makes it very resilient against disturbance, differs from the fundamental SMC's, which relies on reaching time.

2 Mathematical Model of Interconnected Multi Area Multi Source Power Network

The TAGHTPS in each of the areas shown in Fig. 1 are discussed in this section. The dynamic behavior of TAGHTPS varies in the presence of disturbance, resulting in frequency deviation that can be evaluated using the LFC of the MAMSPS [15–16], [18] such as nuclear plant, gas plant, hydro plant, gas plants, etc. in each area are linked. The TAGHTPS model in Fig. 1 is built in the state space form as follows, taking into account the disturbance such as the influence of the parameter uncertainty, subsystem parameter variation, and load disturbance:

$$\Delta\dot{f}_i = -\frac{\Delta f_i}{T_{PS_i}} + \frac{\Delta P_{pt_i} K_{PS_i}\alpha_{11}}{T_{PS_i}} + \frac{\Delta P_{Gh_i} K_{PS_i}\alpha_{21}}{T_{PS_i}} + \frac{\Delta P_{Gg_i} K_{PS_i}\alpha_{31}}{T_{PS_i}} + \frac{K_{PS_i}}{T_{PS_i}}\Delta f_i - \frac{K_{PS_i}}{T_{PS_i}}\Delta P_{D_i} \tag{1}$$

$$\Delta\dot{P}_{pt_i} = \frac{\Delta P_{Gt_i}}{T_{T_i}} + \frac{\Delta P_{pt_i}}{T_{T_i}} \tag{2}$$

$$\Delta\dot{P}_{Gt_i} = -\frac{\Delta P_{Gt_i}}{T_{R_i}} + \frac{\Delta X_{Et_i}}{T_{R_i}} - \frac{\Delta X_{Et_i} K_{R_i}}{T_{SG_i}} - \frac{\Delta f_i K_{R_i}}{T_{SG_i} R_i} + \frac{\Delta ACE_i K_{R_i}}{T_{SG_i}} \tag{3}$$

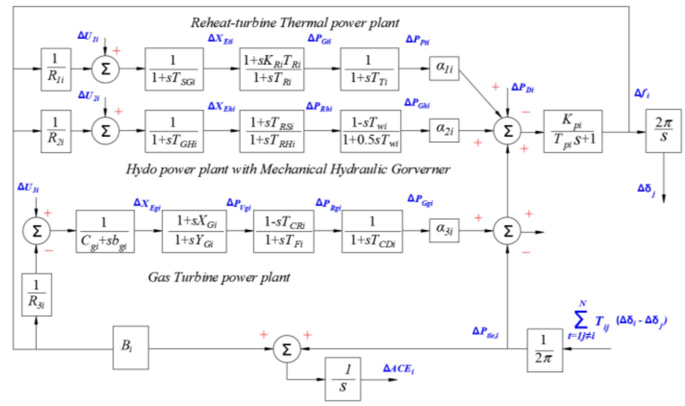

Fig. 1. The simple LFC block diagram of a TAGHTPS.

$$\Delta\dot{X}_{Et_i} = -\frac{\Delta X_{Et_i}}{T_{SG_i}} - \frac{\Delta f_i}{T_{SG_i}R_i} + \frac{\Delta ACE_i}{T_{SG_i}} \tag{4}$$

$$\Delta\dot{P}_{Gh_i} = \frac{2\Delta P_{Rh_i}}{T_{W_i}} - \frac{2\Delta P_{Gh_i}}{T_{W_i}} - \frac{2\Delta X_{Eh_i}}{T_{RH_i}} + \frac{2\Delta P_{Rh_i}}{T_{RH_i}} + \frac{2\Delta X_{Eh_i}T_{RS_i}}{T_{RH_i}T_{GH_i}} + \frac{2\Delta f_i T_{RS_i}}{R_i T_{RH_i}T_{GH_i}} - \frac{2\Delta ACE_i T_{RS_i}}{T_{RH_i}T_{GH_i}} \tag{5}$$

$$\Delta\dot{P}_{Rh_i} = \frac{\Delta X_{Eh_i}}{T_{RH_i}} - \frac{\Delta P_{Rh_i}}{T_{RH_i}} - \frac{\Delta X_{Eh_i}T_{RS_i}}{T_{RH_i}T_{GH_i}} - \frac{\Delta f_i T_{RS_i}}{R_i T_{RH_i}T_{GH_i}} + \frac{\Delta ACE_i T_{RS_i}}{T_{RH_i}T_{GH_i}} \tag{6}$$

$$\Delta\dot{X}_{Eh_i} = -\frac{\Delta X_{Eh_i}}{T_{GH_i}} - \frac{\Delta f_i}{T_{GH_i}R_i} + \frac{\Delta ACE_i}{T_{GH_i}} \tag{7}$$

$$\Delta\dot{P}_{Gg_i} = -\frac{\Delta P_{Gg_i}}{T_{CD_i}} + \frac{\Delta P_{Rg_i}}{T_{CD_i}} \tag{8}$$

$$\Delta\dot{P}_{Rg_i} = -\frac{\Delta P_{Rg_i}}{T_{F_i}} + \frac{\Delta X_{Vg_i}}{T_{F_i}} + \frac{\Delta X_{Vg_i}T_{CR_i}}{Y_{G_i}T_{F_i}} - \frac{\Delta X_{Eg_i}T_{CR_i}}{Y_{G_i}T_{F_i}} + \frac{\Delta X_{Eg_i}c_{g_i}X_{G_i}T_{CR_i}}{b_{g_i}Y_{G_i}T_{F_i}} + \frac{\Delta f_i X_{G_i}T_{CR_i}}{R_i b_{g_i}Y_{G_i}T_{F_i}} - \frac{\Delta ACE_i X_{G_i}T_{CR_i}}{b_{g_i}Y_{G_i}T_{F_i}} \tag{9}$$

$$\Delta\dot{X}_{Vg_i} = -\frac{\Delta X_{Vg_i}}{Y_{G_i}} + \frac{\Delta X_{Eg_i}}{Y_{G_i}} - \frac{\Delta X_{Eg_i}c_{g_i}X_{G_i}}{b_{g_i}Y_{G_i}} - \frac{\Delta f_i X_{G_i}}{R_i b_{g_i}Y_{G_i}} + \frac{\Delta ACE_i X_{G_i}}{b_{g_i}Y_{G_i}} \tag{10}$$

$$\Delta\dot{X}_{Eg_i} = -\frac{\Delta X_{Eg_i}c_{g_i}}{b_{g_i}} - \frac{\Delta f_i}{b_{g_i}R_i} + \frac{\Delta ACE_i}{b_{g_i}} \tag{11}$$

$$\Delta A\dot{C}E_i = B_i\Delta f_i + \Delta P_{tie_{ij}} \tag{12}$$

$$\Delta\dot{P}_{tie_{ij}} = \sum_{\substack{j=1 \\ j\neq i}}^{L} 2\pi T_{ij}(\Delta f_i - \Delta f_j) \tag{13}$$

By defining the above PS parameters in [15-16], and [18] the i^{th} area of the MAMSPS in the state space form by using the dynamics from (1)-(13) is given by (14) .

$$\dot{x}_i(t) = A_i x_i(t) + B_i u_i(t) + \sum_{\substack{j=1 \\ j \neq i}}^{L} H_{ij} + F_i \Delta P_{di}(t) \tag{14}$$

where the equation(14) is the TAGHTPS in state space.

$$x_i(t) = \begin{bmatrix} \Delta f_i & \Delta P_{pt_i} & \Delta P_{Gt_i} & \Delta X_{Et_i} & \Delta P_{Gh_i} & \Delta P_{Rh_i} & \Delta X_{Eh_i} \\ \Delta P_{Gg_i} & \Delta P_{Rg_i} & \Delta P_{Vg_i} & \Delta X_{Eg_i} & \Delta ACE_i & \Delta P_{tie_{ij}} \end{bmatrix}^T$$

is the system state, $x_j(t)$ is the status of a networked system of $x_i(t)$, $u_i(t)$ is the control input, and $\Delta P_{di}(t)$ is the disturbance vector. From (1) to (13), it is simple to take the system matrices A_i, B_i, H_{ij} and F_i .

The operating point modifications in a realistic, linked MAMSPS have a continual and ongoing impact on the varying sources of the load. This element must be thought of as parameter uncertainty. Therefore, system (14) can be rewritten by

$$\dot{x}_i(t) = A_i x_i(t) + B_i[u_i(t) + \psi_i(x_i,t)] + \sum_{\substack{j=1 \\ j \neq i}}^{L} [H_{ij} + \Xi_{ij}(x_j,t)] x_j(t) + F_i \Delta P_{di}(t) \tag{15}$$

where $\Sigma_i(x_i,t)$ and $\Xi_{ij}(x_j,t)$ are the state and interconnected parameter uncertainties and $B_i\psi_i(x_i,t)$ is a bounded disturbance. The aggregate uncertainty is given.

$$\Phi_i(x_i,t) = B_i\psi_i(x_i,t) + \sum_{\substack{j=1 \\ j \neq i}}^{L} \Xi_{ij} x_j(t) + F_i \Delta P_{di}(t) \tag{16}$$

So, using the new dynamic model as an example(17)

$$\begin{aligned} \dot{x}_i(t) &= A_i x_i(t) + B_i u_i(t) + \sum_{\substack{j=1 \\ j \neq i}}^{L} H_{ij} x_j(t) + \Phi_i(x_i,t) \\ \hat{y}_i &= C_i \hat{x}_i \end{aligned} \tag{17}$$

where $\Phi_i(x_i,t)$ is the aggregated disturbance that represents the matched parameter uncertainties. To create the novel $u_i(t)$, we start by assuming the following.

Assumption 1: If the full rank of (A_i, B_i) is controllable then the full rank of (A_i, C_i) is observable.

Assumption 2: The load disturbance is considered to be $\Phi_i(x_i,t)$ is bounded, so that $\|\Phi_i(x_i,t)\| \le \gamma_i$. Where γ_i is a known scalar and $\|.\|$ is the matrix norm.

3 Design of the State Estimator for the Power System

The fact that the original PS model and the rebuilt PS model are almost identical is an advantage. In the LFC of the MAMSPS, in which a few state variables are challenging to obtain, the observer technique can be advantageous. To rebuild a model of the original TAGHTPS, we used the observer approach (17) as bellow:

$$\dot{\hat{x}}_i(t) = A_i\hat{x}_i(t) + B_i u_i(t) + \sum_{\substack{j=1\\ j\neq i}}^{L} H_{ij}\hat{x}_j(t) + \Gamma_i\left(y_i - \hat{y}_i\right)$$
$$\hat{y}_i = C_i\hat{x}_i \tag{18}$$

where Γ_i is the gain of the observer. is the state estimation of $x_i(t)$, y_i is the state, $\hat{y}_i$ is the output of the observer output, respectively. The pole-placement method can be used to compute it. The dynamic of the state error is then examined, with the state error specified as: $\tilde{x}_i(t) = x_i(t) - \hat{x}_i(t)$

Using the error's derivative $\tilde{x}_i$ we have

$$\dot{\tilde{x}}_i = (A_i - \Gamma_i C_i)\tilde{x}_i + \sum_{\substack{j=1\\ j\neq i}}^{L} H_{ij}\tilde{x}_j + \Phi_i(x_i, t) \tag{19}$$

With relation to the eigenvalue of $(A_i - \Gamma_i C_i)$, the state error approaches to zero.

4 Design of an Integral Single Phase Sliding Surface

To achieve MAMSPS stability, the LFC system must be very resilient to specific disturbances. Over time, SMC has been used to reduce several disturbances for MAPS [7-12]. The fundamental SMC determines the reachability of system state variable trajectories to the sliding surface sliding surface (SS). A long transitory period, on the other hand, might be a disadvantage of the basic SMC. We present the SPSMCBSO using this information, and the new sliding surface is provided as.

$$\eta_i[\hat{x}_i(t)] = \mathrm{M}_i\hat{x}_i(t) - \int_0^t \mathrm{M}_i(A_i - B_i\Lambda_i)\hat{x}_i(t)d\tau - \mathrm{M}_i\hat{x}_i(0)e^{-\delta_i t} \tag{20}$$

where M_i is the constant matrix and Λ_i is the matrix of design. Matrix M_i is chosen in order to ensure that the matrix $\mathrm{M}_i B_i$ is nonsingular. The design matrix $\Lambda_i \in R^{m_i \times n_i}$ is chosen satisfying the non-linearity condition as $\mathrm{Re}[\lambda_{\max}(A_i - B_i\Lambda_i)] < 0$

If we take the time derivative of $\eta_i[\hat{x}_i(t)]$, we have

$$\dot{\eta}_i\left[\hat{x}_i(t)\right] = [\mathrm{M}_i A_i\hat{x}_i(t) + \mathrm{M}_i B_i u_i(t) + \sum_{\substack{j=1\\ j\neq i}}^{L} \mathrm{M}_i H_{ij}\hat{x}_j(t) + \mathrm{M}_i\Gamma_i\left(y_i - \hat{y}_i\right)]$$
$$-\mathrm{M}_i(A_i - B_i\Lambda_i)\hat{x}_i(t) + \delta_i\mathrm{M}_i\hat{x}_i(0)e^{-\delta_i t} \tag{21}$$

as $\dot{\eta}_i(t) = \eta_i(t) = 0$, then the equivalent control is obtained as

$$u_i^{eq}(t) = -(\mathrm{M}_i B_i)^{-1}[\mathrm{M}_i B_i\Lambda_i\hat{x}_i(t) + \mathrm{M}_i\Gamma_i\left(y_i - \hat{y}_i\right) + \delta_i\mathrm{M}_i\hat{x}_i(0)e^{-\delta_i t} + \sum_{\substack{j=1\\ j\neq i}}^{L} \mathrm{M}_i H_{ij}\hat{x}_j(t)] \tag{22}$$

we substitute (22) into (24) which gives us by closing the system's loop.

$$\dot{x}_i(t) = (A_i - B_i\Lambda_i)x_i(t) + (B_i\Lambda_i - B_i(\mathrm{M}_iB_i)^{-1}\mathrm{M}_i\Gamma_iC_i)\tilde{x}_i(t) + \sum_{\substack{j=1\\j\neq i}}^{L}[H_{ij} - B_i(\mathrm{M}_iB_i)^{-1}\mathrm{M}_iH_{ij}]x_j(t) + \sum_{\substack{j=1\\j\neq i}}^{L}B_i(\mathrm{M}_iB_i)^{-1}\mathrm{M}_iH_{ij}\tilde{x}_j(t) + \Phi_i(x_i,t) - \delta_iB_i(\mathrm{M}_iB_i)^{-1}\mathrm{M}_i\hat{x}_i(0)e^{-\delta_it} \tag{23}$$

Observing the MAMSPS (23), we combine (19) and (23) as shown in the following.

$$\begin{bmatrix}\dot{x}_i\\ \dot{\tilde{x}}_i\end{bmatrix} = \begin{bmatrix}A_i - B_i\Lambda_i & \Theta_i\\ 0 & A_i - \Gamma_iC_i\end{bmatrix}\begin{bmatrix}x_i\\ \tilde{x}_i\end{bmatrix} + \sum_{\substack{j=1\\j\neq i}}^{L}\begin{bmatrix}H_{ij} - \Upsilon_iH_{ij} & \Upsilon_iH_{ij}\\ 0 & H_{ij}\end{bmatrix}\begin{bmatrix}x_j\\ \tilde{x}_j\end{bmatrix} + \begin{bmatrix}\Phi_i(x_i,t)\\ \Phi_i(x_i,t)\end{bmatrix} + \begin{bmatrix}\mathrm{N}_ie^{-\delta_it}\\ 0\end{bmatrix} \tag{24}$$

where $\Theta_i = B_i\Lambda_i - B_i(\mathrm{M}_iB_i)^{-1}\mathrm{M}_i\Gamma_iC_i$, $\mathrm{N}_i = -\delta_iB_i(\mathrm{M}_iB_i)^{-1}\mathrm{M}_i\hat{x}_i(0)$ and $\Upsilon_i = B_i(\mathrm{M}_iB_i)^{-1}\mathrm{M}_i$. The equation (24) is the dynamics system of the MAMSPS.

5 Design of total feedback output sliding mode controller design

The single-phase SMC-based state observer (14) suggested for the MAMSPS LFC is designed in this section as given:

$$u_i(t) = -(\mathrm{M}_iB_i)^{-1}[\|\mathrm{M}_i\|\|B_i\|\|\Lambda_i\|\|\hat{x}_i(t)\| + \delta_i\|\mathrm{M}_i\|\|\hat{x}_i(0)\|e^{-\delta_it} + \|\mathrm{M}_i\|\|\Gamma_i\|\|(y_i - \hat{y}_i)\| + \sum_{\substack{j=1\\j\neq i}}^{L}\|\mathrm{M}_j\|\|H_{ji}\|\|\hat{x}_i(t)\| + \theta_i]\frac{\eta_i^T[\hat{x}_i(t)]}{\|\eta_i[\hat{x}_i(t)]\|},\quad i = 1,2,\dots,L \tag{25}$$

where δ_i is the positive constant and $u_i(t)$ is the decentralized SPSMCBSO.

Theorem: Equation (24) is asymptotic stable if variable trajectories of the MAMSPS (18) reach the single phase sliding surface and lie on it for all time.

Proof of Theorem: Lyapunov function given

$$V_1 = \sum_{i=1}^{L}(\|\eta_i[\hat{x}_i(t)]\|) \tag{26}$$

with the time derivative of V_1 to get the following equation:

$$\dot{V}_1 = \sum_{i=1}^{L}(\frac{\eta_i^T[\hat{x}_i(t)]}{\|\eta_i[\hat{x}_i(t)]\|}\dot{\eta}_i^T[\hat{x}_i(t)]). \tag{27}$$

Substitute $\hat{x}_i(t)$ in equation (27), we get

$$\dot{V}_1 = \sum_{i=1}^{L}\frac{\eta_i^T[\hat{x}_i(t)]}{\|\eta_i[\hat{x}_i(t)]\|}[\mathrm{M}_iA_i\hat{x}_i(t) - \mathrm{M}_i(A_i - B_i\Lambda_i)\hat{x}_i(t) + \delta_i\mathrm{M}_i\hat{x}_i(0)e^{-\delta_it} + \mathrm{M}_i\Gamma_i(y_i - \hat{y}_i)] + \sum_{i=1}^{L}\frac{\eta_i^T[\hat{x}_i(t)]}{\|\eta_i[\hat{x}_i(t)]\|}\mathrm{M}_iB_iu_i(t) + \sum_{i=1}^{L}\sum_{\substack{j=1\\j\neq i}}^{L}[\frac{\eta_i^T[\hat{x}_i(t)]}{\|\eta_i[\hat{x}_i(t)]\|}\mathrm{M}_iH_{ij}\hat{x}_j(t)] \tag{28}$$

With equation (28), the property $\|AB\| \le \|A\|\|B\|$ and $\sum_{i=1}^{L}\sum_{\substack{j=1\\ j\ne i}}^{L}[\|M_i\|\|H_{ij}\|\|\hat{x}_j(t)\|] = \sum_{i=1}^{L}\sum_{\substack{j=1\\ j\ne i}}^{L}[\|M_j\|\|H_{ji}\|\|\hat{x}_i(t)\|]$, we will generate

$$\dot{V}_1 = \sum_{i=1}^{L}[\|M_i\|\|B_i\|\|\Lambda_i\|\|\hat{x}_i(t)\| + \delta_i\|M_i\|\|\hat{x}_i(0)\|e^{-\delta_i t} + \|M_i\|\|\Gamma_i\|\|(y_i - \hat{y}_i)\|]$$
$$+\sum_{i=1}^{L}\sum_{\substack{j=1\\ j\ne i}}^{L}[\|M_j\|\|H_{ji}\|\|\hat{x}_i(t)\|] + \sum_{i=1}^{L}\frac{\eta_i^T[\hat{x}_i(t)]}{\|\eta_i[\hat{x}_i(t)]\|}M_i B_i u_i(t) \tag{29}$$

by substituting $u_i(t)$ in equation (29), we achieve

$$\dot{V}_1 \le -\sum_{i=1}^{L}\theta_i < 0. \tag{30}$$

The time derivative of the Lyapunov function (30) is less than zero since its value becomes a non-positive scalar. As a result, the reachability proof is obtained.

6 Simulation results and discussions

The suggested SPSMCSO for the LFC of the TAGHTPS is examined in this section deviation from step load disturbance, random load disturbance in PS parameters [18–19]. The investigation's conclusions are compared to those of traditional control approaches in the section below.

6.1 Simulation 1

Under step load disturbance, for the LFC of MAMSPS, classical control techniques are typically applied. The recent designs and implementations of PID-structured AGC using the bacterial foraging algorithm (BFA) and the Jaya approach was used to create PID structural regulators for the Optimized Generation Control (OGC) scheme are developed to explore into TAGHTPS's LFC with a step load disturbance at time t = 0 s and the nominal parameter used is shown in [15], [18]. The proposed SPSMCBSO functionality depends on the gain of the observer L.

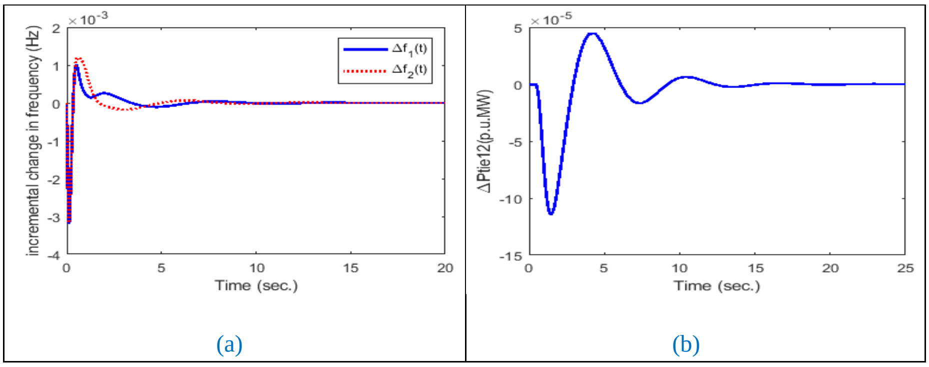

Fig. 2. (a) Deviation in frequency [Hz] with 1% step load in areas 1 and area 2 and (b) Tie line power variation [p.u.MW].

Fig. 2 (a) depicts the frequency variation in both areas, and Fig. 2 (b) depicts the tie-line power deviation. TAGHTPS performance with overshoot and settling time is correctly compared to that seen in [15]. Both controllers generated less overshoot, that is, they kept the operating frequency within the permitted limit of 0.02 Hz [17], although the 8 s settle time with the innovative technique is less than the 15 s settling time in [15] and the 9 s setting time in [18].

Remark 1: In the first simulation, the proposed SPSMCBSO offers fast stability of the TAGHTPS under step load disturbances, which improves the response of the PS better than the one in [15], [18].

6.2 Simulation 2

Case 1: Once more, the TAGHTPS was simulated using a recently designed teaching learning-based optimization (TLBO) technique with a 2-degree freedom of proportional-integral-derivative (2-DOF PID) control and minimal parameters as shown in [16]. To analyze PS performance, following our suggestion, we have to simulate for the TAGHTPS response using the suggested technique, as described in [16]. Fig. 3 (c) depicts the frequency variation in both areas . The TLPD is depicted in Fig. 3 (d). Both frequency overshoots appear to be improved in every region, however the 7 s settling time with the innovative technique is relatively short compared to the 13 s settling time found in [16]. This suggests that the suggested controller is a more suitable option for the MAMSPS LFC.

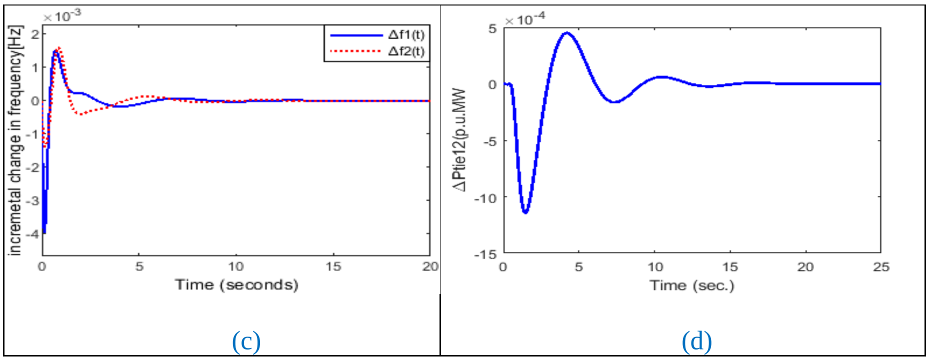

Fig. 3. (c) Frequency variation [Hz] in areas 1 and 2 and (d) Tie line power deviation [p.u.MW]

Case 2: Demand rises in tandem with the expansion of industrial operations. MAMSPS, on the other hand, are needed to satisfy the needs while keeping the frequency within acceptable range limits. As a result, we consider the power demands to be a random load disturbance delivered to each location of the TAGHTPS, as seen in Fig. 4.

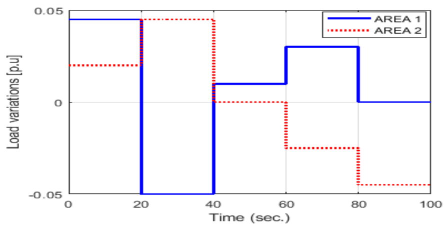

Fig. 4. Random load variation

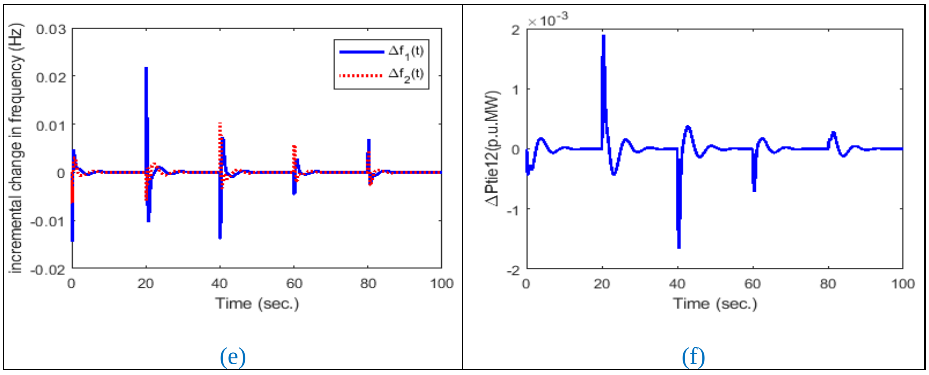

Fig. 5. (e) Frequency variation in areas 1 and 2 and (f) Changes in tie line power [p.u.MW]

The frequency oscillation is shown in Fig. 5 (e) both areas while the tie-line power fluctuation is displayed in Fig. 5 (f). The frequency response in Fig. 5 (e) is better seen under random load (RL) change. So, the system frequency is maintained tolerable.

Remark 2: As shown in [16], TAGHTPS was simulated with simply a step load disturbance. However, because load demands fluctuate on a regular basis, this demand is thought to be a RL change that is subjected to the PS. There under TAGHTPS's RL conditions, the suggested SPSMCBSO is highly advantageous for system stability, making it better for MAMSPS's LFC.

7 Simulation results and discussions

This study develops the single-phase sliding mode control-based state observer for the LFC of the multi-area multi-source power system. The two-area thermal hydro-gas power system model is selected to assess the viability of the built SPSMCBSO. The TAGHTPS model also takes state and connected parameter uncertainty into account. When the simulation results are contrasted with those of some contemporary approaches, the SPSMCBSO is clearly superior to compare the recent approaches. The SPSMCBSO further proved stability and was unaffected by subsystem parameter deviation or random load disturbance. As a result, the suggested SPSMCBSO is really beneficial for MAMSPS's LFC.

Acknowledgement

Phong Thanh Tran was funded by the Master, PhD Scholarship Programme of Vingroup Innovation Foundation (VINIF), code VINIF.2022.TS093.

References

1. Vijay, V., James, C., Paul, A., Fouad, A., Power system control and stability. 3rd edn. Wiley-IEEE Press: Hoboken, NJ, USA (2019).
2. Bevrani, H., Robust power system frequency control. 2nd edn. Power electronics and power systems, Springer, New York, NY, USA(2014).
3. Obaid, Z.A., Cipcigan, L.M., Abrahim, L., Muhssin, M.T.: Frequency control of future power systems: reviewing and evaluating challenges and new control methods, Journal of modern power systems and clean energy 7 (2), 9-25 (2019).
4. Hussein, T. ,Shamekh, A.: Design of pi fuzzy logic gain scheduling load frequency control in two-area power systems, Design 3 (2), 26 (2019).

5. Liao, K., Xu, Y.: A robust load frequency control scheme for power systems based on second order sliding mode and extended disturbance observer, IEEE Transactions on Industrial Informatics 14 (7), 3076-3086 (2018).
6. Tang, M.C., He, Y.: Improved sliding mode design for load frequency control of power system integrated an adaptive learning strategy, IEEE Transactions on Industrial Electronics 64 (8), 6742–6751 (2017).
7. Le Ngoc Minh, B., Huynh, V. V., Nguyen, T. M., Tsai, Y. W.: Decentralized adaptive double integral sliding mode controller for multiarea power systems, Mathematical Problems in Engineering, 8 (2), 11 -22 (2018).
8. Onyeka, A. E., Xing-Gang, Y., Mao, Z., Jiang, B. and Zhang, Q.: Robust decentralized load frequency control for interconnected time delay power systems using sliding mode techniques, IET Control Theory and Applications, 14 (3), 470–480, (2019).
9. Trip, S., Cucuzzella, M., Persis, C.D., Schaft, A.V.D. and Ferrara: Passivity-based design of sliding modes for optimal load frequency control, IEEE Transactions on control systems technology, 27 (5), 1893-1906 (2019).
10. Guo, J.: Application of full-order sliding mode control based on different areas power system with load frequency control, ISA transactions. 92 (1), 23-34 (2019).
11. Xinxin,Lv., Sun, X., Cao, Y., Dinavahi, V.: Event-triggered load frequency control for multi-area power systems based on Markov model: a global sliding mode control approach. IET Generation, Transmission & Distribution, 14 (3), 4878-4887 (2020).
12. Kumar, A., Anwar, N.M. and Kumar, S.: Sliding-mode controller design for frequency regulation in an interconnected power system, Protection and Control of Modern Power Systems, 6(1), 1-12 (2021).
13. Guo, J.: Application of a novel adaptive sliding mode control method to load frequency control. European Journal of Control, 57(1), 172-178 (2020).
14. Huynh, V.V., Minh, B.N.L, Amaefule, E.N., Tran, A.T., Tran,T.P.: Highly robust observer sliding mode-based frequency control for multi-area power systems with renewable power plants, Electronics,10, 274-295, (2021).
15. Hakimuddin, N., Nasiruddin, I., Hota, T.S.: Generation-based automatic generation control with multisource power system using bacterial foraging algorithm, Engineering Reports, 2, 77-85 (2020).
16. Sahu, Kumar, R., Sidhartha, P., Rout, Kumar, U., Sahoo, Kumar, D.: Teaching learning-based optimization algorithm for automatic generation control of power system using 2-DOF PID controller, International Journal of Electrical Power & Energy Systems 77(3), 287–301 (2016).
17. Park, J. H., Recent advances in control problems of dynamical systems and networks, Springer International Publishing, 1st edn. USA (2021).
18. Nidhi, G., Narendra, K., Chitti, B.: JAYA optimized generation control strategy for interconnected diverse source power system with varying participation, Energy Sources, Part A: Recovery, Utilization, and Environmental Effects 1 (2),1–17 (2019).

Appendix:

Notation. Throughout this work, the notation is quite typical X^T represents the matrix's transposition X . I_{nxm} and 0_{nxm} are applied to indicate the $n \times m$ identity matrix and the $n \times m$ zero matrix, respectively. The subscripts n and $n \times m$ are left out when the dimension is unnecessary or may be inferred from the context. $\|x\|$ stands for the Euclidean norm of vector x and $\|A\|$ denotes as compared to the matrix's induced norm A . Using the phrase $A > 0$ means that A is symmetric positive definite. A_n presents the n-dimensional Euclidean space. Sometimes function is sacrificed for simplicity $x_i(t)$ is symbolized by x_i .

VOLUME: 5 | ISSUE: 1 | 2021 | June

Load Frequency Control for Power System using Generalized Extended State Observer

Anh-Tuan TRAN[1], *Phong Thanh TRAN*[1], *Van Van HUYNH*[1,*]

[1]Faculty of Electrical & Electronics Engineering, Ton Duc Thang University, Ho Chi Minh City, Viet Nam

*Corresponding Author: Van Van HUYNH (Email: huynhvanvan@tdtu.edu.vn)
(Received: 25-Oct-2020; accepted: 13-Jan-2021; published: 31-Mar-2021)
DOI: http://dx.doi.org/10.25073/jaec.202151.307

Abstract. *This study investigates load frequency control based generalized extended state observer (GESO) for interconnected power system subject to multi-kind of the power plant. First, the mathematical model of the interconnected power system is proposed based on the dynamic model of thermal power plant with reheat turbine and hydro power plant. Second, the GESO is designed to estimate the system states and disturbances. In addition, the problem of unmeasurable of system states in the interconnected power network due to lack of sensor has been solved by using the proposed load frequency control based GESO. The numerical experiments are carried out by using MATLAB/ SIMULINK simulation. The simulation results point out that the proposed control approach has capacity to handle the uncertainties and disturbances in the interconnected power system with better transient performances in comparison with the existing control approach. The relevant dynamic models have already been used for the simulation of the physical constraints of governor dead band (GDB) and generation rate constraint (GRC) effect in the power plants. It is evident that the robustness of the suggested controller in terms of stability and effectiveness of the system.*

Keywords

Interconnected power system, load frequency control, generalized extended state observer.

1. Introduction

In large power systems, load frequency control (LFC) is one of the essential operation problems in electrical power under load and resource variation. Consequently, any changes in frequency not only impact truthfully on the operation of power networks and power system reliability but also lead to an uncertain condition for interconnected power networks. The primary goals of a power network LFC are to keep and maintain the frequency deviation and tie line power exchanges with neighbor control areas at the planned value according to a schedule [1–6].

In a power system, it is not easy to regulate the frequency in power exchange/interchange through tie-lines. Many academic researchers represented the LFC approach of typical power system utilizing different control methods in both traditional and developed techniques that have been applied to resolve the LFC problems of interconnected power networks [7–22].

To resolve problems of frequency deviation occurred by various matched or mismatched uncertainties, adaptive control is one of modern control schemes for complex power system included in various load and power control areas [7–10]. LFC control approach for interconnected power networks is introduced to establish in the direct-indirect adaptive fuzzy control strategy [7] which extends and builds up the parameter algorithms and the appropriate adaptive control law. An adaptive model predictive LFC approach in [8] for multi-area power network is used with photovoltaic generation by regrading some nonlinear features. An adaptive LFC controller is suggested [9] by making use of the least square strategy with an internal model control design in structure. In [10], the hypothesis of the suggested adaptive way is constructed by the on-line tuning method of the gain of an integral controller which is applied in the electrosearch optimization. However, the adaptive control schemes above were presented to be complex in control algorithms to deal with the variations of power network parameters subjected to the LFC approaches.

The conventional PID controllers of constant parameters and fixed system structure were investigated to solve the LFC problem for normal operating condition [11–13]. However, the characteristic of power networks is nonlinear system. Therefore, some traditional PID control methods may not have ability to improve the better performance for other operating conditions and to make the best of optimizing the PID parameters and to develop stability performance in power network with the parameter uncertainties and load disturbances.

In the different way of doing the research, sliding mode control (SMC) is not only another way to resolve LFC difficult problems but also a nonlinear control approach to be well known for improving the system performance. In detail, the SMC approach is very sensitive to validate of plant parameters as well as improve effectively in system transient performance. In recent times, there are many the SMC frequency approaches implemented to work out the problems of power networks with parameter uncertainties or load variations [14–17]. The LFC controller is suggested and developed for the interconnected power system to upgrade the system performance using the decentralized SMC [14]. However, the matched and unmatched uncertainties in power networks are not always suitable and satisfied in all of conditions. A novel adaptive SMC approach [15] is designed to the LFC in terms of the parametric derivation the external disturbances. However, there are some existing limitations such as the computation of dynamic model and control design is complex, the state cannot be observed, the response performance and waveform need to improve. In [16], the proposed SMC is applied in the basic control method with the adaptive dynamic programming approach is utilized to improve the extra control signal and to modify the frequency scheme. However, parameter uncertainties due to variable operation point was not considered and the transient performance were not very good as compared previous research. [17] is distributed sliding mode control scheme for optimal LFC to adopt a nonlinear model of a multi-area power system, including dynamic of voltage and dynamics of second order turbine-governor. However, the suggested strategy is complicated and difficult for practical implementation. The parameter uncertainties of power generation were not discussed.

From above control researches such as adaptive control, PID control and SMC control, the results are achieved under assumption that all state variables of power system can to be measurable and willingly available for system feedback. In practical application, not all state variables are measurable for system feedbacks, and then we must compute and estimate the state variables that cannot measure in the system. The proposed approach of estimating state variables is often used in observation [18–22], [26-29]. These schemes can modify and improve the unknown upper bounds of matched and mismatch uncertainties. It not only obtains the system state trajectories accomplishment but also satisfies in parameters of the system state errors. The achievement of results is correlated to LFC's of power networks in various control techniques [18-22], [26-29]. However, there are still some limitations of the above approaches such as the disturbances are not truncated from the output points in steady state and the gains of controller are not set to be really high to reduce disturbances of unknown boundaries and even, the parameter uncertainties or load variations of power system are not considered in some proposed controllers. The GESO scheme based on the non-linear SMC controller are combined to investigate the frequency variation problem and to estimate the disturbance in interconnected power network [30]. However, the performance of power system is not always satisfied under required conditions in the settling time, transient frequency variations considering GDB and GRC effect. In detail, GRC is normally considered by adding a limiter and a hysteresis pattern to the governor-turbine system model. It is essential to take into consideration the practical constraints and natural conditions such as physical constraint of generation rate constraint (GRC). The GRC has negative affect on the power network performance due to its nonlinearity nature. The GRC denotes practical constraint on the ratio of the variation in the generating power due to physical drawbacks. Governor dead band (GDB) is principle for power network frequency control in the presence of disturbances. GDB has a definite outline as the total magnitude of a continued speed change that there is no resulting variation in valve position. An observer-based control scheme is offered for LFC scheme against cyberattack uncertainties [31]. However, to test the effective response of the proposed controller of power networks, the GDB and GRC effect are not considered in the power plant.

The process of being mentally stimulated to do the control approaches is to eliminate and improve perturbations by feedback control instead of feedforward compensation control which uses the disturbance estimations to cancel out the affections in real time manner. The suggested control approach is one way of approaches for estimating and compensating the system disturbances. This scheme proves the powerful and robustness to again matched uncertainties. The contributions of the proposed GESO in this paper are as follows:

- GESO is designed to estimate the unmeasurable system state variables and the load uncertainties in the complex power system. The proposed scheme of making power system is not only secure or stable but also useful to solve the satisfactory performance with uncertainties.

- The generalized extended observer approach improves the system dynamic response to fast response in setting time and to reduce over or undershoots in power network with the dynamic model of thermal power plant with reheat turbine and hydro power plant.

- The simulation result with various cases indicates the effectively and robustness of generalized extended controller by considering parametric uncertainties in power networks.

- The report of simulation results is used to compare with the cases of considering and without considering the GDB and GRC nonlinearity effects on power network.

The paper is outlined as follows: section II shows the mathematical model of power network. The generalized extended state observer for multi-area power systems is designed in section III. Section IV represents stability analysis of power system and control scheme design of power system, the following session by simulation results in section V.

2. Mathematical model of power system

The dynamic models of power systems are generally nonlinear. The block chart of power system is presented in Fig. 1, Fig. 2 and Fig. 3. The power system includes two types of the plant as thermal power plant with reheat turbine and hydro power plant with mechanical hydraulic governor connected through tie-line power.

2.1. The thermal power plant with reheat turbine model

A thermal power plant is an electric power station to convert heat energy to electric power. Reheat turbine is a part of thermal power plants in power network in Fig. 2.

The frequency dynamic behavior of area i^{th} details in this section which can use in the fol-

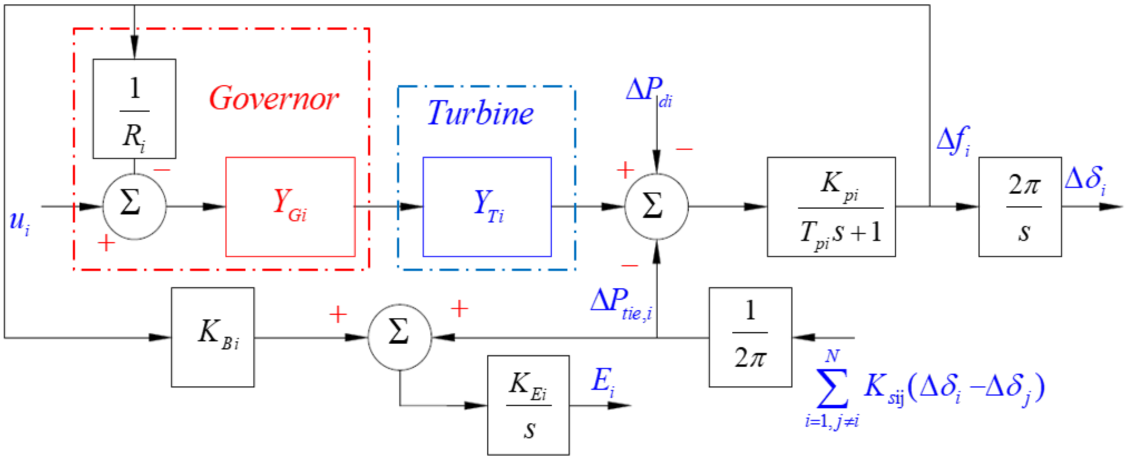

Fig. 1: The block chart of complex power network.

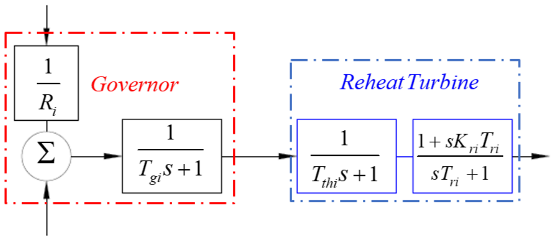

Fig. 2: The block chart of i^{th} area with reheat turbine.

lowing differential equations:

$$\Delta\dot{f}_i(t) = -\frac{1}{T_{pi}}\Delta f_i(t) + \frac{K_{Pi}}{T_{pi}}\Delta P_{mi}(t) - \frac{K_{Pi}}{2\pi T_{Pi}}\sum_{i=1,j\neq i}^{N} K_{sij}[\Delta\delta_i(t) - \Delta\delta_j(t)] - \frac{K_{Pi}}{T_{pi}}\Delta P_{di}(t) \quad (1)$$

$$\Delta\dot{P}_{mi}(t) = (\frac{1}{T_{ri}} - \frac{K_{ri}}{T_{thi}})\Delta P_{thi}(t) + \frac{K_{ri}}{T_{thi}}\Delta P_{vi}(t) - \frac{1}{T_{ri}}\Delta P_{mi}(t) \quad (2)$$

$$\Delta\dot{P}_{thi}(t) = \frac{1}{T_{thi}}\Delta P_{vi}(t) - \frac{1}{T_{thi}}\Delta P_{thi}(t) \quad (3)$$

$$\Delta\dot{P}_{vi}(t) = -\frac{1}{T_{gi}R_i}\Delta f_i(t) - \frac{1}{T_{gi}}\Delta P_{vi}(t) + \frac{1}{T_{gi}}u_i(t) \quad (4)$$

$$\Delta\dot{E}_i(t) = K_{Bi}K_{Ei}\Delta f_i(t) + \frac{K_{Ei}}{2\pi}K_{sij}[\Delta\delta_i(t) - \Delta\delta_j(t)] \quad (5)$$

$$\Delta\dot{\delta}_i(t) = 2\pi\,\Delta f_i(t) \quad (6)$$

The variables of interconnected power system are the frequency deviation, power output, governor valve position, integral control and rotor angle variation as following as bellow:

$$x_i(t) = \begin{bmatrix} \Delta f_i(t) \\ \Delta P_{mi}(t) \\ \Delta P_{thi}(t) \\ \Delta P_{vi}(t) \\ \Delta E_i(t) \\ \Delta\delta_i(t) \end{bmatrix}$$

where $i = 1, 2, .., N$ and N is the area numbers.

The interconnected power network with thermal power plant described by Fig. 1 and Fig. 2, which can be written and expressed in state-space representation below:

$$\dot{x}_i(t) = A_i x_i(t) + B_i u_i(t) + \sum_{i=1,i\neq j}^{N} H_{ij}x_j + \Gamma_i\Omega_i(t)$$
$$y_i(t) = C_i x_i(t) \quad (7)$$

The definition of following matrices is as given in the following:

$$A_i = \begin{bmatrix} -\frac{1}{T_{pi}} & \frac{K_{Pi}}{T_{pi}} & 0 & 0 & 0 & -\frac{K_{Pi}}{2\pi T_{Pi}}K_{ij} \\ 0 & -\frac{1}{T_{ri}} & (\frac{1}{T_{ri}} - \frac{K_{ri}}{T_{thi}}) & \frac{K_{ri}}{T_{thi}} & 0 & 0 \\ 0 & -\frac{1}{T_{thi}} & \frac{1}{T_{thi}} & 0 & 0 & 0 \\ -\frac{1}{T_{gi}R_i} & 0 & 0 & -\frac{1}{T_{gi}} & 0 & 0 \\ K_{Bi} & 0 & 0 & 0 & 0 & \frac{K_{Ei}}{2\pi}K_{sij} \\ 2\pi & 0 & 0 & 0 & 0 & 0 \end{bmatrix}$$

$$H_{ij} = \begin{bmatrix} 0 & 0 & 0 & 0 & 0 & -\frac{K_{Pi}}{2\pi T_{Pi}}K_{ij} \\ 0 & 0 & 0 & 0 & 0 & 0 \\ 0 & 0 & 0 & 0 & 0 & 0 \\ 0 & 0 & 0 & 0 & 0 & 0 \\ 0 & 0 & 0 & 0 & 0 & \frac{K_{Ei}}{2\pi}K_{sij} \\ 0 & 0 & 0 & 0 & 0 & 0 \end{bmatrix}$$

$$B_i = \begin{bmatrix} 0 & 0 & 0 & \frac{1}{T_{gi}} & 0 & 0 \end{bmatrix}^T$$

$$\Gamma_i = \begin{bmatrix} -\frac{K_{Pi}}{T_{pi}} & 0 & 0 & 0 & 0 & 0 \end{bmatrix}^T$$

where $x_i(t) \in R^{n_i}$ is state vector of the i^{th} area, $x_j(t) \in R^{n_i}$ is state vector of the j^{th} area, $u_i(t) \in R^{m_i}$ is the control vector, $\Omega_i(t) \in R^{m}$is the vector of the load disturbance, $y_i(t)$ is the output signal of the i^{th} area, A_i is the variable matrix of the power system of the i^{th} area, $B_i$is the output matrix of the i^{th} area, H_{ij} is the power flow between two-area, C_i is the output matrix of the i^{th} area, Γ_i is the disturbance matrix of the i^{th} area, $\Delta\dot{f}_i(t)$ is the frequency deviation of the i^{th} area, $\Delta P_{mi}(t)$ is the mechanics power variation of the turbine of the i^{th} area and $\Delta\dot{\delta}_i(t)$ is the rotor angle deviation of the i^{th} area.

2.2. The hydro power plant with hydro turbine

The hydroelectric power plant is the most common type of power system in Fig. 3. The function of a hydraulic turbine is to convert the energy of the flowing water into mechanical energy and this mechanical energy is converted from hydro-electric generator to electricity.

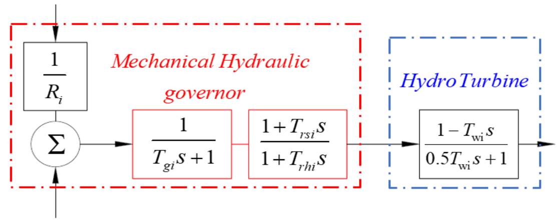

Fig. 3: The block chart of i^{th} area with hydro turbine.

$$\begin{aligned} \Delta\dot{f}_i(t) = &-\frac{1}{T_{pi}}\Delta f_i(t) + \frac{K_{pi}}{T_{pi}}\Delta P_{mi}(t) \\ &- \frac{K_{pi}}{T_{pi}}\Delta P_{di}(t) \\ &- \frac{K_{Pi}}{2\pi T_{Pi}}K_{sij}[\Delta\delta_i(t) - \Delta\delta_j(t)] \end{aligned} \tag{8}$$

$$\begin{aligned} \Delta P_{mi}(t) = &\frac{2T_{rsi}}{T_{rhi}T_{gi}R_i}\Delta f_i(t) \\ &+ (\frac{2}{T_{wi}} + \frac{2}{T_{rhi}})\Delta P_{vi}(t) \\ &- \frac{2}{T_{wi}}\Delta P_{mi}(t) - \frac{2}{T_{wi}}\Delta P_{mi}(t) \\ &+ (\frac{2T_{rsi}}{T_{rhi}T_{gi}} - \frac{2}{T_{rhi}})\Delta P_{gi}(t) \\ &- \frac{2T_{rsi}}{T_{rhi}T_{gi}}u_i(t) \end{aligned} \tag{9}$$

$$\begin{aligned} \Delta P_{vi}(t) = &\frac{-T_{rsi}}{T_{rhi}T_{gi}R_i}\Delta f_i(t) + \frac{-1}{T_{rhi}}\Delta P_{vi}(t) \\ &+ (\frac{1}{T_{rhi}} - \frac{T_{rsi}}{T_{rhi}T_{gi}})\Delta P_{gi}(t) \\ &+ \frac{T_{rsi}}{T_{rhi}T_{gi}}u_i(t) \end{aligned} \tag{10}$$

$$\Delta\dot{P}_{gi}(t) = -\frac{1}{T_{gi}R_i}\Delta f_i(t) - \frac{1}{T_{gi}}\Delta P_{gi}(t) + \frac{1}{T_{gi}}u_i(t) \qquad (11)$$

$$\Delta\dot{\delta}_i(t) = 2\pi\,\Delta f_i(t) \qquad (12)$$

The variables of interconnected power system are the frequency deviation, power output, governor valve position, integral control and rotor angle variation as following as bellow:

$$x_i(t) = \begin{bmatrix} \Delta f_i(t) \\ \Delta P_{mi}(t) \\ \Delta P_{vi}(t) \\ \Delta P_{gi}(t) \\ \Delta E_i(t) \\ \Delta\delta_i(t) \end{bmatrix}$$

where $i = 1, 2, .., N$ and N is the area numbers.

The interconnected power system with hydro power plant described by Fig. 1 and Fig. 3, which can be written and expressed in state-space representation below:

$$\begin{aligned} \dot{x}_i(t) &= A_i x_i(t) + B_i u_i(t) \\ &+ \sum_{i=1, i\neq j}^{N} H_{ij}x_j + \Gamma_i\Omega_i(t) \\ y_i(t) &= C_i x_i(t) \end{aligned} \qquad (13)$$

The definition of following matrices is as given in:

$$B_i = \begin{bmatrix} 0 & -\frac{2T_{rsi}}{T_{rhi}T_{gi}} & \frac{T_{rsi}}{T_{rhi}T_{gi}} & \frac{1}{T_{gi}} & 0 & 0 \end{bmatrix}^T$$

$$\Gamma_i = \begin{bmatrix} -\frac{K_{Pi}}{T_{pi}} & 0 & 0 & 0 & 0 & 0 \end{bmatrix}^T$$

$$H_{ij} = \begin{bmatrix} 0 & 0 & 0 & 0 & 0 & -\frac{K_{Pi}}{2\pi T_{Pi}}K_{sij} \\ 0 & 0 & 0 & 0 & 0 & 0 \\ 0 & 0 & 0 & 0 & 0 & 0 \\ 0 & 0 & 0 & 0 & 0 & 0 \\ 0 & 0 & 0 & 0 & 0 & \frac{K_{Ei}}{2\pi}K_{sij} \\ 0 & 0 & 0 & 0 & 0 & 0 \end{bmatrix}$$

3. Generalized extended state observer design

In practical application, not all state variables are measurable for system feedbacks, and then we must compute and estimate the state variables that cannot measure for the parametric uncertainties in power system. Therefore, states observer performs the function by estimating the state variables of the systems typically the output and control variable. State observers can be designed and applied only when the observability of required condition is satisfied. The GESO is recommended for using in this system because it is more sensitive with changes in parameters of load disturbance variations. To estimate state variables in the power system included both variables and load disturbances, GESO is defined as following bellow:

$$[x_i]_{n_i+1}(t) = \Omega_i(t) \qquad (14)$$

and

$$\gamma_i(t) = \frac{\Omega_i(t)}{dt} \qquad (15)$$

Then, the system in equation can be presented below:

$$\begin{aligned} \dot{\bar{x}}_i(t) &= \bar{A}_i\bar{x}_i(t) + \bar{B}_i u_i(t) \\ &+ \sum_{i=1, i\neq j}^{N} \bar{H}_{ij}x_j + F_i\gamma_i(t) \\ \bar{y}_i(t) &= \bar{C}_i\bar{x}_i(t) \end{aligned} \qquad (16)$$

where

$$\bar{x}_i(t) = \begin{bmatrix} [x_i]_{n_i\times 1} \\ [(x_i)_{n_i+1}]_{n\_i\times 1} \end{bmatrix}_{(n_i+n_i)\times 1}$$

$$A_i = \begin{bmatrix} -\frac{1}{T_{pi}} & \frac{K_{pi}}{T_{pi}} & 0 & 0 & 0 & -\frac{K_{Pi}}{2\pi T_{Pi}}K_{sij} \\ \frac{2T_{rsi}}{T_{rhi}T_{gi}R_i} & -\frac{2}{T_{wi}} & (\frac{2}{T_{wi}} + \frac{2}{T_{rhi}}) & (\frac{2T_{rsi}}{T_{rhi}T_{gi}} - \frac{2}{T_{rhi}}) & 0 & 0 \\ \frac{-T_{rsi}}{T_{rhi}T_{gi}R_i} & 0 & \frac{-1}{T_{rhi}} & (\frac{1}{T_{rhi}} - \frac{T_{rsi}}{T_{rhi}T_{gi}}) & 0 & 0 \\ -\frac{1}{T_{gi}R_i} & 0 & 0 & -\frac{1}{T_{gi}} & 0 & 0 \\ K_{Bi} & 0 & 0 & 0 & 0 & \frac{K_{Ei}}{2\pi}K_{sij} \\ 2\pi & 0 & 0 & 0 & 0 & 0 \end{bmatrix}$$

$$\bar{A}_i = \begin{bmatrix} [A_i]_{n_i \times n_i} & I_{n_i \times n_i} \\ 0_{n_i \times n_i} & 0_{n_i \times n_i} \end{bmatrix}_{(n_i+n_i)\times(n_i+n_i)}$$

$$\bar{H}_{ij} = \begin{bmatrix} [H_{ij}]_{n_i \times n_i} & 0_{n_i \times n_i} \\ 0_{n_i \times n_i} & 0_{n_i \times n_i} \end{bmatrix}_{(n_i+n_i)\times(n_i+n_i)}$$

$$\bar{B}_i = \begin{bmatrix} [B_i]_{n_i \times p_i} \\ 0_{n_i \times p_i} \end{bmatrix}_{(n_i+n_i)\times p_i}$$

$$F_i = \begin{bmatrix} 0_{n_i \times r_i} \\ I_{n_i \times r_i} \end{bmatrix}_{(n_i+n_i)\times r_i}$$

$$\bar{C}_i = \begin{bmatrix} [C_i]_{m_i \times n_i} \\ 0_{m_i \times n_i} \end{bmatrix}_{m_i\times(n_i+n_i)}$$

Assumption 1: (A_i, B_i) is controllable and $(\bar{A}_i, \bar{C}_i)$ is observable.

With regards to the state observers discussed, we will apply the notation $\hat{\bar{x}}_i$ to indicate the vector observer state. The vector $\hat{\bar{x}}_i$ of the observed state is used and applied in the state feedback to initiate the desired and required control vector.

If we call the state $\bar{x}_i$ is approximated to state$\hat{\bar{x}}_i$,the dynamical model in (17):

$$\begin{aligned} \dot{\hat{\bar{x}}}_i(t) &= \bar{A}_i\hat{\bar{x}}_i(t) + \bar{B}_iu_i(t) \\ &\quad + \sum_{i=1,i\neq j}^{N} \bar{H}_{ij}\hat{\bar{x}}_j + L_i(\bar{y}_i(t) - \hat{\bar{y}}_i(t)) \\ \dot{\hat{\bar{y}}}_i(t) &= \bar{C}_i\hat{\bar{x}}_i(t) \end{aligned} \tag{17}$$

where, $\dot{\hat{\bar{y}}}_i(t)$ is the estimator state of the output variables and matrix L_i is the observer gain, which can be designed through to place any desired eigenvalues in the left half s-plane of $(\bar{A}_i - L_i\bar{C}_i)$.

The control input is chosen as following as (18):

$$u_i(t) = K_{xi}x_i(t) + K_{di}\hat{\Omega}_i(t) \tag{18}$$

or

$$u_i(t) = K_{xi}\hat{x}_i(t) + K\_{di}\hat{\Omega}_i(t) \tag{19}$$

where $\hat{\Omega}_i(t) = [\hat{x}_i]_{n_i+1}$

From Eqs. (18) and (19), we can rewrite:

$$u_i(t) = K_i\hat{\bar{x}}_i(t) = [K_{xi} \quad K_{di}]\hat{\bar{x}}_i(t) \tag{20}$$

where, K_{xi} is the feedback control gain to be chosen so that the eigenvalues of $(A_i - B_iK_{xi})$lie in specific locations in the left-half s-plane and the lumped uncertainty compensation gain$K_{di}$is designed:

$$\begin{aligned} &K_{di} \\ &= [C_i(A_i - B_iK_{xi})^{-1}B_i]^{-1}C_i(A_i - B_iK_{xi})^{-1}\Gamma_i \end{aligned} \tag{21}$$

To solve the disturbance compensation gain: The disturbance compensation gain in (21) is no longer available since $C_i(A_i - B_iK_{xi})^{-1}B_i$ is probably non-invertible or even not a square matrix. In a case in point, it can be proved that an alternative but more typical condition.

$$\begin{aligned} &[C_i(A_i - B_iK_{xi})^{-1}B_i]^{-1}K_{di} \\ &= C_i(A_i - B_iK_{xi})^{-1}\Gamma_i \end{aligned} \tag{22}$$

It must be gratified to assure the viability of the proposed control scheme. The gain K_{di} can be resolved from (22) if the following rank condition holds:

$$\begin{aligned} &rank[C_i(A_i - B_iK_{xi})^{-1}B_i]^{-1} \\ &= rank[C_i(A_i - B_iK_{xi})^{-1}B_i]^{-1}, \\ &\qquad [C_i(A_i - B_iK_{xi})^{-1}\Gamma_i] \end{aligned} \tag{23}$$

The simple configuration of the suggested GESO is presented in Fig. 4. It shows the uncertainties which can be designed and eliminated from the output channel in steady state by this control law.

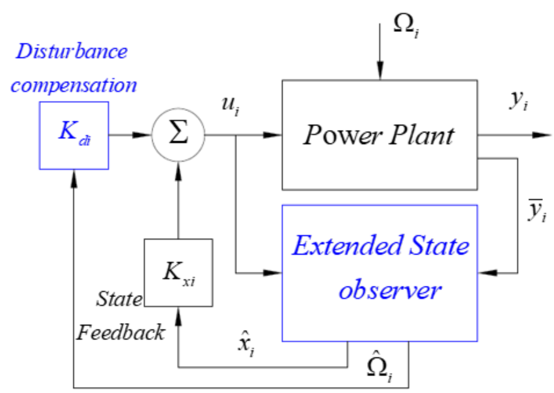

Fig. 4: The configuration of the proposed GESO [23-25], [30-31].

4. Stability of power system

The stability analysis of the multi-area power system as represented in Fig. 1 is performed in this part. The suggested control approach goals at the fundamental boundedness of all the power system signals.

Assumption 2: The lumped disturbances have to the satisfaction of the following conditions.

They get constant value in steady state of system, i.e.; $\lim_{t\to\infty}\Omega_i(t) = \zeta_i$ and $\lim_{t\to\infty}\gamma_i(t) = \lim_{t\to\infty}\dot{\Omega}_i(t) = 0$.

The state and disturbance estimation errors are defined as:

$$e_{xi}(t) = \hat{x}_i(t) - x_i(t) \tag{24}$$

and

$$e_{di}(t) = \hat{\Omega}_i(t) - \Omega_i(t) \tag{25}$$

where: $\hat{\Omega}_i(t) = [\hat{x}_i]_{n_i+1}$ is presented the estimation of the system uncertainties.

Combine (16) and the estimation error of state observers $e_i(t) = \bar{x}_i(t) - \hat{\bar{x}}_i(t)$ can be revised by:

$$\begin{aligned}\dot{e}_i(t) &= \bar{A}_i e_i(t) - L_i(\bar{y}_i(t) - \hat{\bar{y}}_i(t)) + F_i\gamma_i(t) \\ &= (\bar{A}_i - L_i\bar{C}_i)e_i(t) + F_i\gamma_i(t)\end{aligned} \tag{26}$$

Denote $F_i\gamma_i(t)$ by $u_i(t)$ and use final-value theorem, we can be obtained:

$$\begin{aligned}&\lim_{t\to\infty} e_i(t) \\ &= \lim_{t\to\infty} s(sI - (\bar{A}_i - L_i\bar{C}_i))^{-1}U_i(s) \\ &= \lim_{t\to\infty} (sI - (\bar{A}_i - L_i\bar{C}_i))^{-1} \lim_{s\to\infty} sU_i(s) \\ &= \lim_{s\to\infty} (sI - (\bar{A}_i - L_i\bar{C}_i))^{-1} \lim_{t\to\infty} u_i(t)\end{aligned} \tag{27}$$

Since $\lim_{s\to\infty}(sI - (\bar{A}_i - L_i\bar{C}_i))^{-1}$ is bounded and $\lim_{t\to\infty} u_i(t) = 0$

So, the estimation error of state observers is: $e_i(t) = \bar{x}_i(t) - \hat{\bar{x}}_i(t)$ is asymptotically stable.

Remark 1: By applying the control design to the estimation of the lumped uncertainty and the parameters of system states if the system states are not measurable. So, the proposed control law will be designed as in [23-25].

Remark 2: It is recognized that the lumped uncertainty cannot be reduced completely and totally from the state equation no matter what controller was designed. In this strategy, one of the most recent achievable aims is simply to truncate the disturbances at the output point in steady state by applying of the proposed control law. Therefore, the limitations by other control approaches in the previous papers [18-22] have been resolved.

5. Simulations and results

To test the efficiency and robustness of the proposed control strategy, the various cases in two simulations are implemented to prove the performance of GESO controller in estimating of states and avoiding the effect of matched uncertainties with external disturbance. It also reduces effect of the governor dead band (GDB) and generation rate constraint (GRC) in the power plants. These parameters of power network are presented in Table 1. The simulation results are utilized to compare with previous proposed control scheme in [5–6], [15] using MATLAB/SIMULINK.

Tab. 1: The parameters of interconnected multi-area power system [5–6], [15].

No.	Parameters	Value
1	T_{gi}	0.08
2	T_{thi}	0.3
3	K_{ri}	0.5
4	T_{ri}	10
5	T_{rsi}	5
6	T_{rhi}	28.75
7	T_{Wi}	0.3
8	R_i	2.4
9	T_{pi}	20
10	K_{pi}	120
11	K_{bi}	0.425
12	a_{ij}	-1
13	$2\pi K_{sij}$	0.215

We can issue the estimating value to find the real value. The observer gain is designed depend on the pole ρ with the eigenvalue $\bar{A}_i - L_i\bar{C}_i$ of lied in the desired locations in the left-half s-plane.

Simulation 1:

Case 1. In this case, we apply proposed controller for interconnected power network with only thermal power plant in both stations in Fig. 1 and Fig. 2.

To combine between system matrix of thermal power plant and parameter values in Table 1, the matrix values of the power network are calculated as:

$$A_1 = \begin{bmatrix} -0.05 & 6 & 0 & 0 & 0 & -0.0327 \\ 0 & -0.1 & -15667 & 1,6667 & 0 & 0 \\ 0 & -3.3333 & 3.3333 & 0 & 0 & 0 \\ -5.2083 & 0 & 0 & -12.5 & 0 & 0 \\ 0.425 & 0 & 0 & 0 & 0 & 0.0054 \\ 6.2832 & 0 & 0 & 0 & 0 & 0 \end{bmatrix}$$

$$B_1 = \begin{bmatrix} 0 & 0 & 0 & 12.5 & 0 & 0 \end{bmatrix}^T$$

$$\Gamma_1 = \begin{bmatrix} -6 & 0 & 0 & 0 & 0 & 0 \end{bmatrix}^T$$

Feedback control gain in this case can be designed as:

$$K_{x1} = \begin{bmatrix} -0.0417 & 0.0003 & -0.0781 & 0 & -6.0115 & 0.3879 \end{bmatrix} \times 10^6$$

$$K_{d1} = [-210.4250]$$

And the tie line power between both control areas is chosen as:

$$H_{12} = \begin{bmatrix} 0 & 0 & 0 & 0 & 0 & 0.0327 \\ 0 & 0 & 0 & 0 & 0 & 0 \\ 0 & 0 & 0 & 0 & 0 & 0 \\ 0 & 0 & 0 & 0 & 0 & -0.0054 \\ 0 & 0 & 0 & 0 & 0 & 0 \\ 0 & 0 & 0 & 0 & 0 & 0 \end{bmatrix}$$

where:

$A_1 = A_2$, $B_1 = B_2$, $\Gamma_1 = \Gamma_2$, $K_{x1} = K_{x2}$ and $K_{d2} = K_{d2}$

We simulate and illustrate the response of the two-area power system with nominal parameters in Table 1 and the extended observer is tested by applying the load disturbance of $\Delta P_{d1} = 0.01$ (p.u, MW) at $t = 1$ s and at $\Delta P_{d2} = 0.015$ (p.u, MW) $t = 1$ s. The simulation results of the two-area multi-area power network for case 1 that the proposed GESO are presented in Fig. 5 to Fig. 8. It is simply to observe in Fig. 5 that the frequency variation converges to zero in about 2 s. Fig. 6 and Fig. 8 indicate the mechanical power deviation and control signal deviation of two control areas. Fig. 7 presents that the tie-line power deviations reach to zero with the designed controller. In comparison between the results achieved by using proposed control method with previous research in [5–6], [15], the results of using the proposed controller are to reduce the setting time and overshoots of both in power networks. So, it is proved that the proposed controller is powerful and effective.

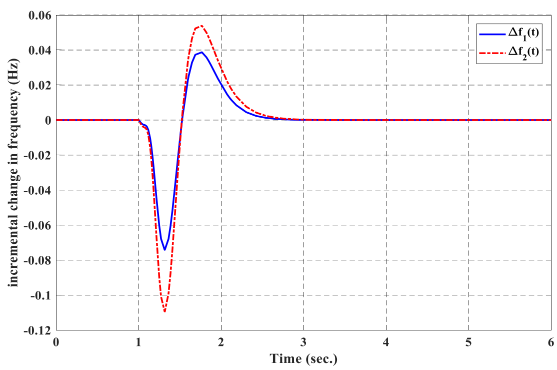

Fig. 5: Frequency deviation of two control areas.

Case 2. In the second case, the performance of proposed GESO scheme is in the presence of nonlinear term such as matched uncertainties to constate the model of the system in Fig. 1 and Fig. 3.

To combine between system matrix of hydro power plant and parameter values in Table 1, the matrix values of the power system are calculated as:

$$A_1 = \begin{bmatrix} -0.05 & 6 & 0 & 0 & 0 & -0.0327 \\ 0.4831 & -6.6667 & 6.7362 & 1.0899 & 0 & 0 \\ -0.1697 & 0 & -0.0348 & -3.2986 & 0 & 0 \\ -1.3889 & 0 & 0 & -3.3333 & 0 & 0 \\ 0.4250 & 0 & 0 & 0 & 0 & 0.0054 \\ 6.2832 & 0 & 0 & 0 & 0 & 0 \end{bmatrix}$$

$$B_1 = \begin{bmatrix} 0 & -1.1594 & 0.5797 & 3.3333 & 0 & 0 \end{bmatrix}^T$$

$$\Gamma_1 = \begin{bmatrix} -6 & 0 & 0 & 0 & 0 & 0 \end{bmatrix}^T$$

Feedback control gain in this case can be designed as:

$$K_{x1} = \begin{bmatrix} -0.0084 & -0.0012 & 0.0043 & -0.0011 & -6.8195 & 0.4481 \end{bmatrix} \times 10^6$$

$$K_{d1} = [-210.4250]$$

And the tie-line power between both control areas are chosen as:

$$H_{12} = \begin{bmatrix} 0 & 0 & 0 & 0 & 0 & 0.0327 \\ 0 & 0 & 0 & 0 & 0 & 0 \\ 0 & 0 & 0 & 0 & 0 & 0 \\ 0 & 0 & 0 & 0 & 0 & -0.0054 \\ 0 & 0 & 0 & 0 & 0 & 0 \\ 0 & 0 & 0 & 0 & 0 & 0 \end{bmatrix}$$

where:

$A_1 = A_2$, $B_1 = B_2$,$\Gamma_1 = \Gamma_2$, $K_{x1} = K_{x2}$ and $K_{d2} = K_{d2}$.

We change the hydro power plant with hydraulic governor instead of thermal power plant and the step load disturbances are kept the same with first case. The deviations in frequency of first and second power area are shown in Fig. 9. Fig. 10 shows mechanical power deviation of two control areas. Fig. 11 and Fig. 12 display in order the tie-line power deviation and control signal deviation. In each control area, the closed loop responses applying the GESO controller are simply to observe from Fig. 9 to Fig. 12 that the response performance is better in terms of settling time about 1s and under/overshoots, in comparison to the recent others proposed in [5–6], [15].

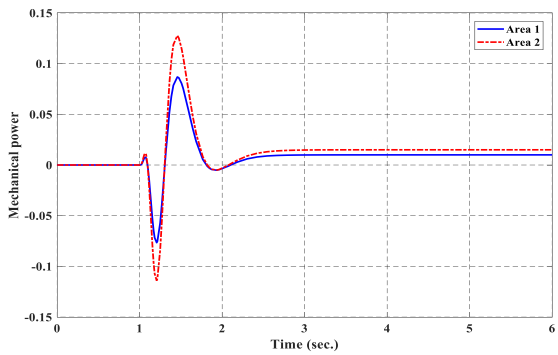

Fig. 6: Mechanical power deviation.

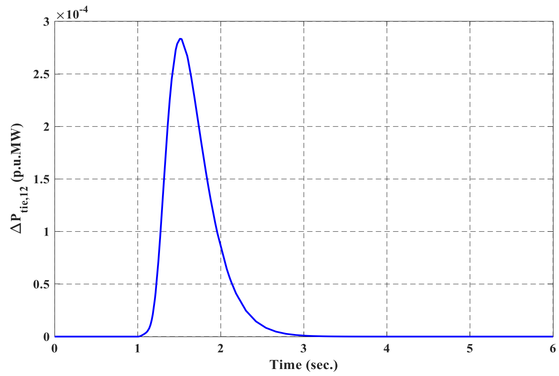

Fig. 7: The tie-line power deviation.

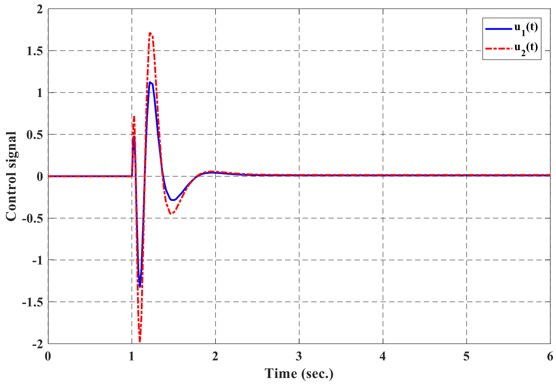

Fig. 8: Control signal deviation of two control areas.

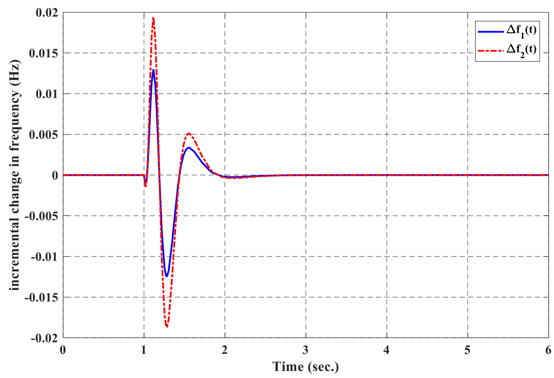

Fig. 9: Frequency deviation of two control areas.

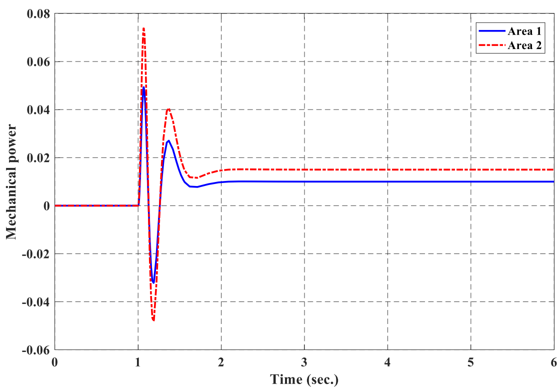

Fig. 10: Mechanical power deviation.

Remark 3: From the reporting of simulation in case 1 and case 2, the proposed approach is one of main objectives to finalize the matched disturbances and achieve shorter setting time and smaller transient deviation in terms of load disturbances for interconnected power system by

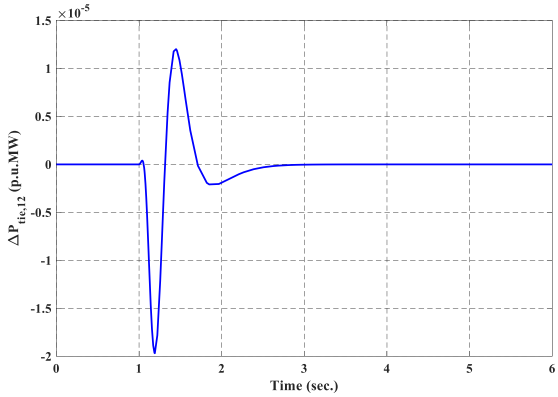

Fig. 11: The tie-line power deviation.

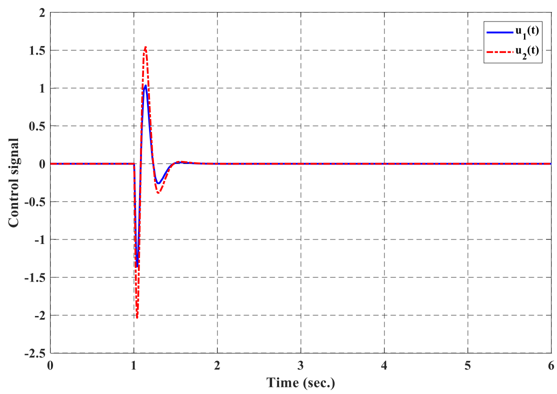

Fig. 12: Control signal deviation.

applying of the proposed GESO law. So, some limitations of other schemes in recent papers [5–6] and [15] have been resolved.

Case 3. Now, the suggested GESO control approach is used to examine by comparing with traditional LFC [5–6], [15] at random load variations. In this specific case, we consider the power system which includes two kinds of the plant as thermal power plant with reheat turbine and hydro power plant with mechanical hydraulic governor. The parameter values of the complex power system are calculated given as:

In the first area:

$$A_1 = \begin{bmatrix} -0.05 & 6 & 0 & 0 & 0 & -0.0327 \\ 0 & -0.1 & -15667 & 1,6667 & 0 & 0 \\ 0 & -3.3333 & 3.3333 & 0 & 0 & 0 \\ -5.2083 & 0 & 0 & -12.5 & 0 & 0 \\ 0.425 & 0 & 0 & 0 & 0 & 0.0054 \\ 6.2832 & 0 & 0 & 0 & 0 & 0 \end{bmatrix}$$

$$B_1 = \begin{bmatrix} 0 & 0 & 0 & 12.5 & 0 & 0 \end{bmatrix}^T$$

$$\Gamma_1 = \begin{bmatrix} -6 & 0 & 0 & 0 & 0 & 0 \end{bmatrix}^T$$

The feedback control gain can be designed:

$$K_{x1} = \begin{bmatrix} -0.0417 & 0.0003 & -0.0781 & 0 & -6.0115 & 0.3879 \end{bmatrix} \times 10^6$$

$$K_{d1} = [-210.4250]$$

And the second area:

$$A_2 = \begin{bmatrix} -0.05 & 6 & 0 & 0 & 0 & -0.0327 \\ 0.4831 & -6.6667 & 6.7362 & 1.0899 & 0 & 0 \\ -0.1697 & 0 & -0.0348 & -3.2986 & 0 & 0 \\ -1.3889 & 0 & 0 & -3.3333 & 0 & 0 \\ 0.4250 & 0 & 0 & 0 & 0 & 0.0054 \\ 6.2832 & 0 & 0 & 0 & 0 & 0 \end{bmatrix}$$

$$B_2 = \begin{bmatrix} 0 & -1.1594 & 0.5797 & 3.3333 & 0 & 0 \end{bmatrix}^T$$

$$\Gamma_2 = \begin{bmatrix} -6 & 0 & 0 & 0 & 0 & 0 \end{bmatrix}^T$$

The feedback control gain can be designed:

$$K_{x2} = \begin{bmatrix} -0.0084 & -0.0012 & 0.0043 & -0.0011 & -6.8195 & 0.4481 \end{bmatrix} \times 10^6$$

$$K_{d2} = [-210.4250]$$

And the tie-line power between two-area are chosen as:

$$H_{12} = \begin{bmatrix} 0 & 0 & 0 & 0 & 0 & 0.0327 \\ 0 & 0 & 0 & 0 & 0 & 0 \\ 0 & 0 & 0 & 0 & 0 & 0 \\ 0 & 0 & 0 & 0 & 0 & -0.0054 \\ 0 & 0 & 0 & 0 & 0 & 0 \\ 0 & 0 & 0 & 0 & 0 & 0 \end{bmatrix}$$

The actual random load disturbances are implemented and applied in both control areas of power system as presented in Fig. 13 to Fig. 17. In flowing detail, Fig. 13 shows the load variations of two control areas. The deviation in frequency of both areas is shown in Fig. 14. Fig. 15, Fig. 16 and Fig. 17 plot the frequency deviation, mechanical power deviation and control signal deviation of two control areas. The generalized extended observer controller is still designed to compute and estimate system variables. In comparison between the deviations in frequency from [5–6], [15] and the simulation results of the proposed GESO controller, the significant improvement is to reduce the magnitude of oscillation as well as minimize under or overshoots and settling time in the response performance.

Remark 4: To observe of 3 cases of simulation results above, the proposed GESO ap-

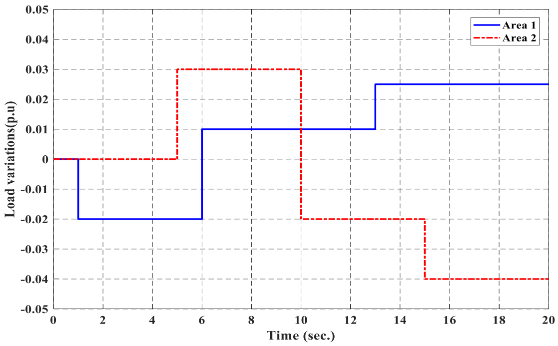

Fig. 13: Load variations of two control areas.

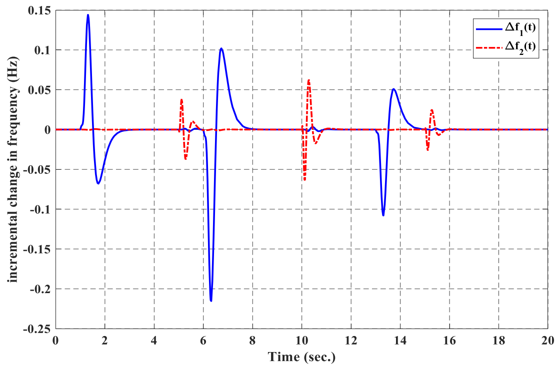

Fig. 14: Frequency deviation of two control areas.

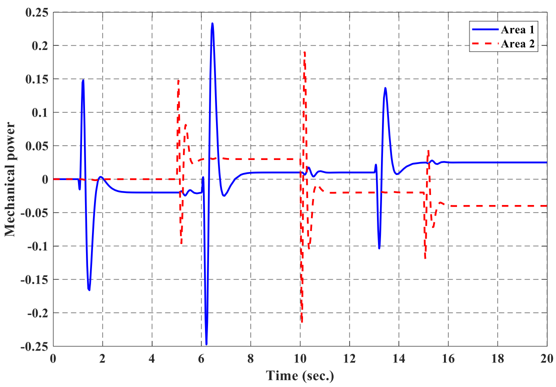

Fig. 15: Mechanical power deviation.

proach achieves affectively the response performance under conditions such as the matched uncertainties and random load variations appearing in complex power networks. The suggested control scheme is applied and developed to eliminate load disturbances and to restore the nominal point of system performance, and to reduce the influence of external disturbances.

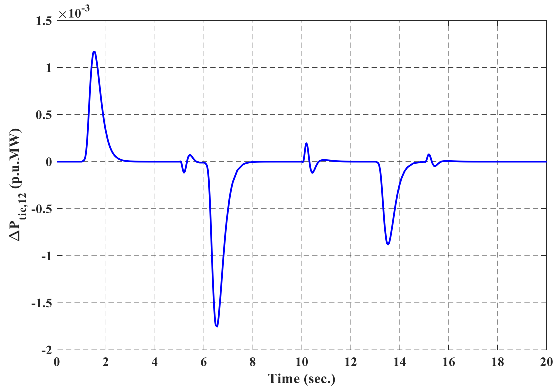

Fig. 16: The tie-line power deviation.

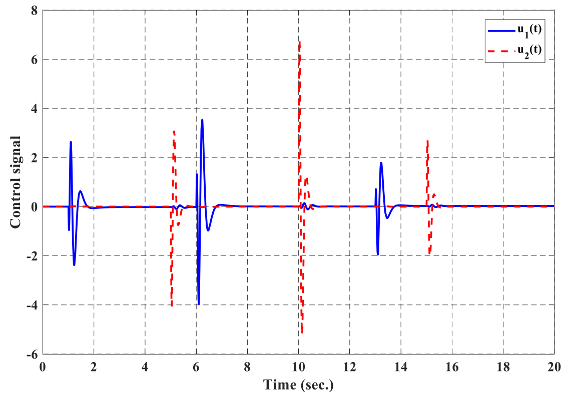

Fig. 17: Control signal deviation of two control areas.

Case 4. In this part, the frequency variation, tie-line power and control input signal are presented from Fig. 18 to Fig. 20 at different step load disturbances $\Delta P_{d1} = 0.1$ (p.u.MW) at $t = 0$ s in the first-area, $\Delta P_{d2} = 0.05$ (p.u.MW) at $t = 0$ s in the second-area. The non-reheat turbine is applied to both areas and system parameters are used the same with the one given in [28].

Delve into data analysis, the goal of any load frequency controllers is to return frequency value to the safe point. It is to be clear that we observe in Fig. 18 and Fig. 19, the proposed GESO controller obtains the normal range in frequency about 1 s at both areas and decreases tie-line power variation to zero about 3 s, respectively. The proposed GESO controller also reduces and minimizes overshoot and settling time as compared with recent studies in [5-6], [15] and with observer controller in [28].

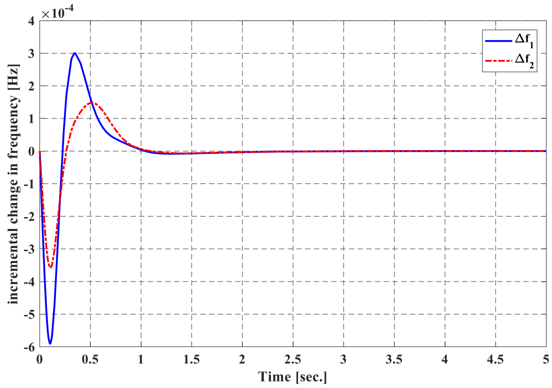

Fig. 18: Frequency deviation of two control areas.

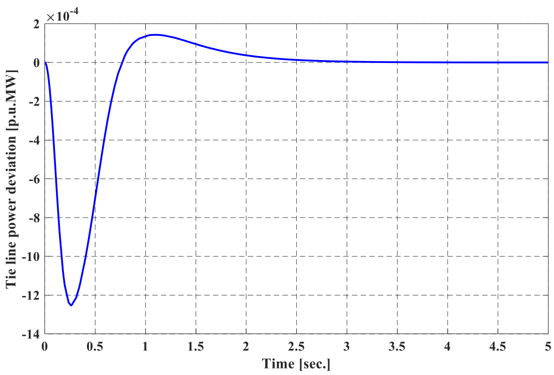

Fig. 19: The tie-line power variation.

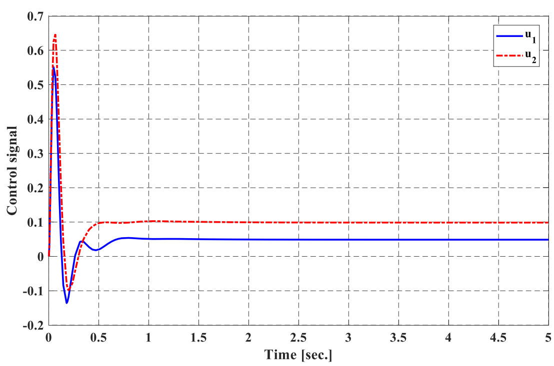

Fig. 20: Control signal.

Remark 5. It is to be noted that the suggested GESO approach has ability to estimate and compensate exactly under the matched uncertainty. In particular, the proposed control scheme makes better the system damping characteristic.

Simulation 2. In the last case, we consider the dynamic models utilized for simulation of physical constraints of GDB and GRC in the thermal power plant with reheat turbine and the hydro power plant with mechanical hydraulic governor in Fig. 21.

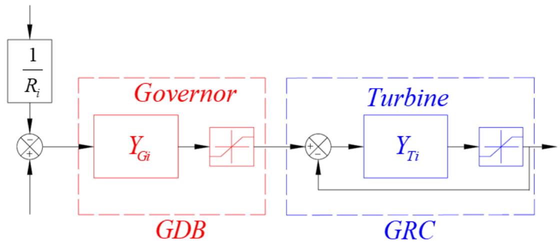

Fig. 21: Nonlinear model with GDB and GRC [32].

We test the proposed controller with the step load disturbance of $\Delta P_{d1} = 0.01$ (p.u MW) at $t = 1$ s and $\Delta P_{d2} = 0.03$ (p.u MW) at $t = 1$ s. Fig. 22, Fig. 23 and Fig. 24 represent the frequency variation, tie-line power variation and mechanical power variation in each control area. The control signal of both control area illustrates in Fig. 25. As it is clear, with the proposed GESO controllers, the transient oscillations are determined a longer time with larger amplitude than in the cases of without considering the GRC and GDB in case 1, case 2, case 3 in simulation 1. The proposed control strategy has also discovered satisfactory even in presence of GRC, GDB and step load disturbances in comparison with [30]. The overshoot percentage and settling time are synchronously significantly decreased in the transient performance of the suggested GESO controller.

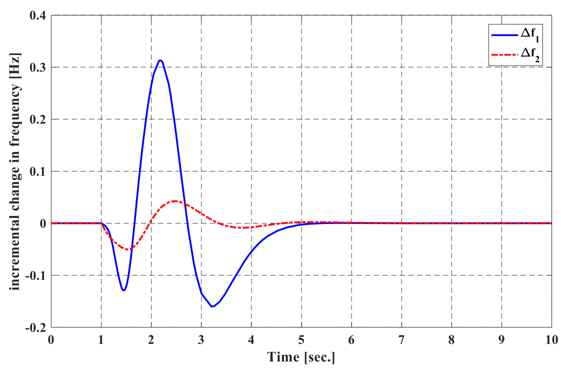

Fig. 22: Frequency variation of two control areas.

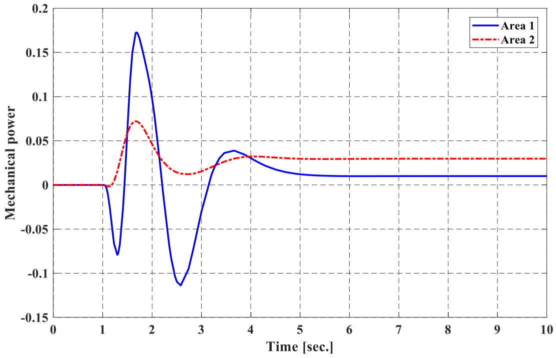

Fig. 23: Mechanical power deviation.

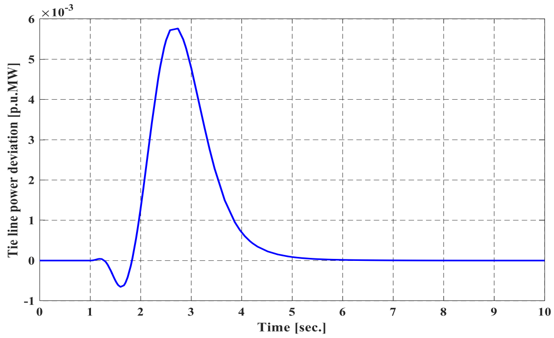

Fig. 24: The tie-line power deviation.

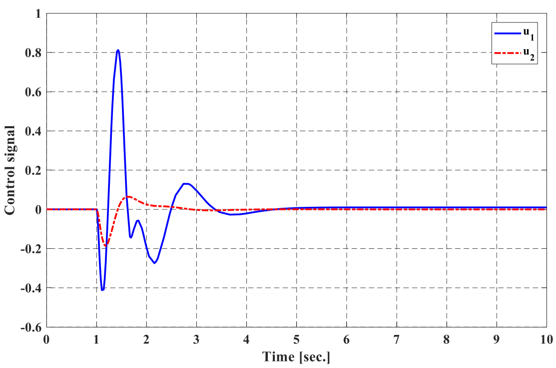

Fig. 25: Control signal.

Remark 6: The GRC and GDB impact significantly to feedback signal of the interconnected power network. To show the robustness of the proposed GESO, the simulation results are used to compare with the case of considering in [30] or without considering the GDB and GRC nonlinearity effects in [31]. The proposed controller clearly indicates that transient performance has adapted with required condition such as the setting time and under/overshoot in comparison with previous research. Thus, the small deviations in frequency with the proposed GESO have less effect on the plant reserve capacity and power market.

6. Conclusions

To solve the problem of unmeasurable of system states in interconnected power system due to lack of sensor, the load frequency control based generalized extended state observer is proposed in this paper. The generalized extended state observer is used to estimate the unmeasurable of system states and load disturbances. The proposed scheme of making the interconnected power system is not only secure and stable but also useful to solve the satisfactory performance with system parameter uncertainties. The simulation results point out that the LFC based GESO approach improves the system dynamic response to fast response in setting time and to reduce over or undershoots in power network with the dynamic model of thermal power plant with reheat turbine and hydro power plant. Moreover, the report of simulation results is used to compare with the cases of considering and without considering the GDB and GRC nonlinearity effects on power network. It is evident that the robustness of the suggested controller in terms of stability and effectiveness of system.

Acknowledgements

This research was funded by Science and Technology Development of Ton Duc Thang University (FOSTECT), website: http://fostect.tdtu.edu.vn, under Grant FOSTECT.2017.BR.05

References

[1] Chaturvedi, D.K. (2008). Techniques and its Applications in Electrical Engineering Springer.

[2] Vittal, V., Mc Calley, J.D., Anderson, P.M., & Fouad, A.A. (2019). Wiley 3rd Edition, Power System Control and Stability.

[3] Fu, C., & Tan, W. (2018). Decentralized Load Frequency Control for Power Systems with Communication Delays via Active Disturbance Rejection. *IET Generation, Transmission & Distribution, 12*(6), 1751-8687.

[4] Bernard, M.Z., Mohamed, T.H., Qudaih, Y.S., & Mitani, Y. (2014). Decentralized load frequency control in an interconnected power system using Coefficient Diagram Method. *International Journal of Electrical Power & Energy Systems, 63*(5), 65–172.

[5] Parmar, K.P.S., Majhi, S., & Kothari, D.P. (2012). Load frequency control of a realistic power system with multi-source power generation. *International Journal of Electrical Power & Energy Systems, 42*(1), 426–433.

[6] Parmar, K.P.S., Majhi, S., & Kothari, D.P. (2014). LFC of an interconnected power system with multi-source power generation in deregulated power environment. *International Journal of Electrical Power & Energy Systems, 57*(2), 277–286.

[7] Yousef, H.A., AL-Kharusi, K., Albadi, M.H., & Hosseinzadeh, N. (2014). Load Frequency Control of a Multi-Area Power System. *An Adaptive Fuzzy Logic Approach, IEEE Transactions on Power Systems, 29*(4), 1822-1830.

[8] Zeng, G.-Q., Xie, X.-Q., & Chen, M.-R., (2017). An Adaptive Model Predictive Load Frequency Control Method for Multi-Area Interconnected Power Systems with Photovoltaic Generations. *Electrical Power and Energy System, 10*(11), 1840.

[9] Rehiara, B.A., Yorino, N., Sasaki, Y., & Zoka, Y. (2020). An Adaptive Load Frequency Control Based on Least Square Method. *Advances in Modelling and Control of Wind and Hydrogenators, 49*(3), 220.

[10] Dahab, Y.A., Abubakr, H., & Mohamed, T.H. (2020). Adaptive Load Frequency Control of Power Systems using Electro-Search Optimization Supported by the Balloon Effect. *IEEE Access*, 7408–7422.

[11] Anwar, M.N.& Pan, S., (2015). A New PID Load Frequency Controller Design Method in Frequency Domain Through Direct Synthesis Approach. *Electric Power and Energy Systems, 67*(4), 560-569.

[12] Kouba, N., Menaa, M., Hasni, M., et al. (2015). Load frequency control in multiarea power system based on fuzzy logic-PID controller. *IEEE Int. Conf. on Smart Energy Grid Engineering SEGE, Oshawa, Canada, 15*(1), 1–6.

[13] Farahani, M., Ganjefar, S., Alizadeh, M. (2012). PID controller adjustment using chaotic optimization algorithm for multi-area load frequency control. *IET Control Theory Appl., 6*(2), 1984–1992.

[14] Yang, M., Yang, F., Chengshan, W., & Peng, W. (2013). Decentralized Sliding Mode Load Frequency Control for Multi-Area Power Systems. *IEEE Transactions on Power System, 28*(4), 4301-4309.

[15] Guo, J. (2020). Application of A Novel Adaptive Sliding Mode Control Method to the Load Frequency Control. *European Journal of Control, 5*(2), 3580-3601.

[16] Mu, C., Tang, Y., & He, H., (2017). Improved Sliding Mode Design for Load Frequency Control of Power System Integrated an Adaptive Learning Strategy. *IEEE Transactions on Industrial Electronics, 64*(8), 6742–6751.

[17] Trip, S., Cucuzzella, M., De Persis, C., van der Schaft, A., & Ferrara, A. (2019). Passivity-Based Design of Sliding Modes for Optimal Load Frequency Control. *IEEE Transactions on Control Systems Technology, 27*(5), 1893-1906.

[18] Li, H.Y., Shi, P., Yao, D.Y., & Wu, L.G. (2016). Observer-Based Adaptive Sliding Mode Control of Nonlinear Markovian

Jump Systems. *Automatica, 64*(1), 133-142.

[19] Khayati, K., (2015). Multivariable Adaptive Sliding-Mode Observer-Based Control for Mechanical Systems. *Canadian Journal of Electrical and Computer Engineering, 38*(3), 253-265.

[20] Wang, B., Shi, P., Karimi, H.R., & Lim, C.C. (2013). Observer-Based Sliding Mode Control for Stabilization of a Dynamic System with Delayed Output Feedback. *Mathematical Problems in Engineering, 3*(1), 1-6.

[21] Yang, B., Yu, T., Shu, H., Yao, W., & Jiang, L. (2018). Sliding-Mode Perturbation Observer-Based Sliding-Mode Control Design for Stability Enhancement of Multi-Machine Power Systems. *Transactions of the Institute of Measurement and Control, 41*(5), 1418-1434.

[22] Mi, Y., Fu, Y., Li, D., Wang, C., Loh, P.C., & Wang, P. (2016). The Sliding Mode Load Frequency Control For Hybrid Power System Based on Disturbance Observer. *International Journal of Electrical Power & Energy Systems, 74* (1), 446-452.

[23] Pawar, S.N., Chile, R.H., & Patre, B.M. (2017). Design of Generalized Extended State Observer based Control for Nonlinear Systems with Matched and Mismatched Uncertainties. *Indian Control Conference (ICC)*, 4-6.

[24] Yao, J., Jiao, Z., & Ma, D. (2014). Adaptive Robust Control of DC Motors with Extended State Observer. *IEEE Transactions on Industrial Electronics, 61*(7), 3630–3637.

[25] Wang, S., Ren, X., Na, J., & Zeng, T. (2017) Extended-State-Observer-Based Funnel Control for Nonlinear Servomechanisms with Prescribed Tracking Performance. *IEEE Transactions on Automation Science and Engineering, 14*(1), 98–108.

[26] Hossain, M., & Peng, C. (2020). Load Frequency Control for multiarea power systems under DoS attacks. *Information Sciences, 243*(1), 437-453.

[27] Haes, A., Hamedani, H., Mohamad, G., Hatziargyriou, E., & Nikos, D. (2019). A Decentralized Functional Observer based Optimal LFC Considering Unknown Inputs, Uncertainties and Cyber-Attacks. *IEEE Transactions on Power Systems, 34*(6), 4408–4417.

[28] Chen, C., Zhang, K., Yuan, K., & Wang, W. (2017). Extended Partial States Observer Based Load Frequency Control Scheme Design for Multi-area Power System Considering Wind Energy Integration. *IFAC-Papers On-Line, 50*(1), 4388–4393.

[29] Rinaldi, G., Cucuzzella, M., & Ferrara, A. (2017). Third order sliding mode observer-based approach for distributed optimal load frequency control. *IEEE Control Systems Letters, 1*(2), 215–220.

[30] Prasad, S., Purwar, S., & Kishor, N. (2019). Load frequency regulation using observer based non-linear sliding mode control. *International Journal of Electrical Power & Energy Systems, 108*(1), 178–193.

[31] Prasad, S. (2020). Counteractive control against cyber-attack uncertainties on frequency regulation in the power system: IET Cyber-Physical Systems. *Theory & Applications Research, 5*(4), 394–408.

[32] Bevrani, H. (2014). Robust Power System Frequency Control, Power Electronics and Power Systems, Springer.

About Authors

Anh-Tuan TRAN received B.Eng. degree in electrical engineering, Ton Duc Thang University (TDTU), Ho Chi Minh City, Vietnam. Currently, he is M.Eng. student in Electrical Engineering, TDTU, HCMC, Vietnam. His research topics included load frequency control and automatic voltage regulator to power systems with sliding mode control and optimal control.

Phong Thanh TRAN received the B.Eng. degree in physics and electronics with a major in automation and control at Ho Chi Minh University of Science, Ho Chi Minh, Vietnam, in 2010, and the M.Eng. degree in electrical engineering with a major in automation and control at International University, Ho Chi Minh National University, in 2015. His current research activities include power systems, siding mode control, dynamic system and load frequency control.

Van Van HUYNH has completed the Ph.D degree in automation and control from Da-Yeh University, Taiwan. He is currently a Lecturer in the Faculty of Electrical and Electronics Engineering, Ton Duc Thang University, Ho Chi Minh City, Vietnam. He has published totally 10 journal papers and more than 11 international conference papers. His current research interests are in sliding mode control, variable structure control, and power system control.

2023 INTERNATIONAL CONFERENCE ON SYSTEM SCIENCE AND ENGINEERING

July 27-28, 2023 - Ho Chi Minh City, Vietnam

HYBRID EVENT

ICSSE2023: 2023 International Conference on System Science and Engineering

Sliding Mode-Based Load Frequency Control of a Power System with Multi-Source Power Generation

(Author: Phong Thanh Tran, Van Van Huynh, Chau Thien Si Dong and Bach Hoang Dinh)

Presenter: Tran Thanh Phong - TDT University, Viet Nam

The online session **BS12: Image Processing and Control Engineering** on July 28, 2023.

Email: tranthanhphong.st@tdtu.edu.vn;huynhvanvan@tdtu.edu.vn

Ho Chi Minh, July 2023

I. Introduction about power system

II. Mathematical model of Power System

III. A case study using Second Order Sliding Mode Control Approach

IV. Simulation Results

V. Conclusions

I. Introduction about power system

The stability of an interconnected power system is its ability to return to normal or stable operation after having been subjected to some form of disturbance. Stability considerations have been recognized as an essential part of power system planning for a long time. With interconnected systems continually growing in size and extending over vast geographical regions, it is becoming increasingly more difficult to maintain synchronism between various parts of a power system.

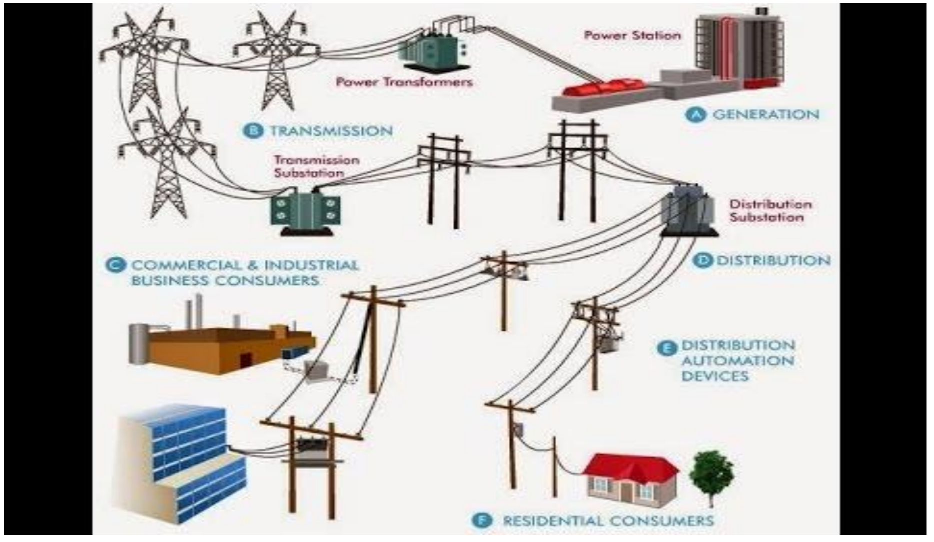

Fig. 1 - The basics of power systems

Load Frequency Control

LFC is responsible to restore system frequency. The LFC, as a major function of Automatic generation control (AGC), has been one of the important control problems in electric power system design and operation. Maintaining frequency and power interchanges with neighboring control areas at the scheduled values are the two main primary objectives of a power system LFC. These objectives are met by measuring **a control error signal, called the *area control error* (ACE),** which represents the real power imbalance **between generation and load.**

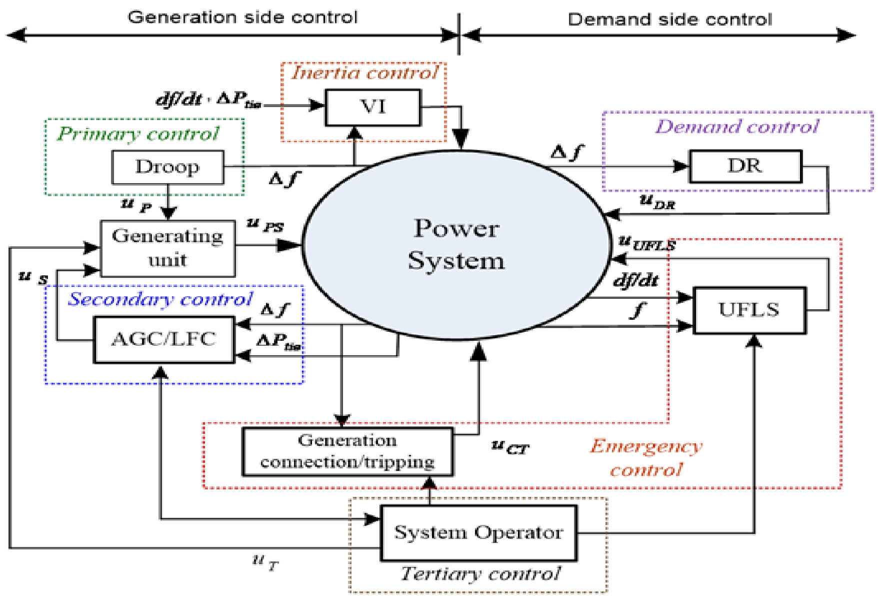

Fig.2 - Frequency control loops of power systems

Objective of this Study

- ❖ To study about the proposed sliding mode control schemes: The second order sliding mode design for load frequency control of multi-area multi-source power systems.
- ❖ To restore and maintain the normal frequency and the desired power output in the interconnected power system.
- ❖ To control the change in tie line power between control areas.
- ❖ To compare with the other control scheme in previous research.

Method to apply and use in this study

Main steps to build the advanced sliding mode control design:

- The build the differential equation or state space for interconnected multi-area multi-source power system.
- To choose the proposed second order sliding mode control with integral sliding surface and find out the dynamic system of power system.
- To design the load frequency controller with u input signal.
- To prove the stability of power system by using the Lyapunov Function.

II. Mathematical model of Power System

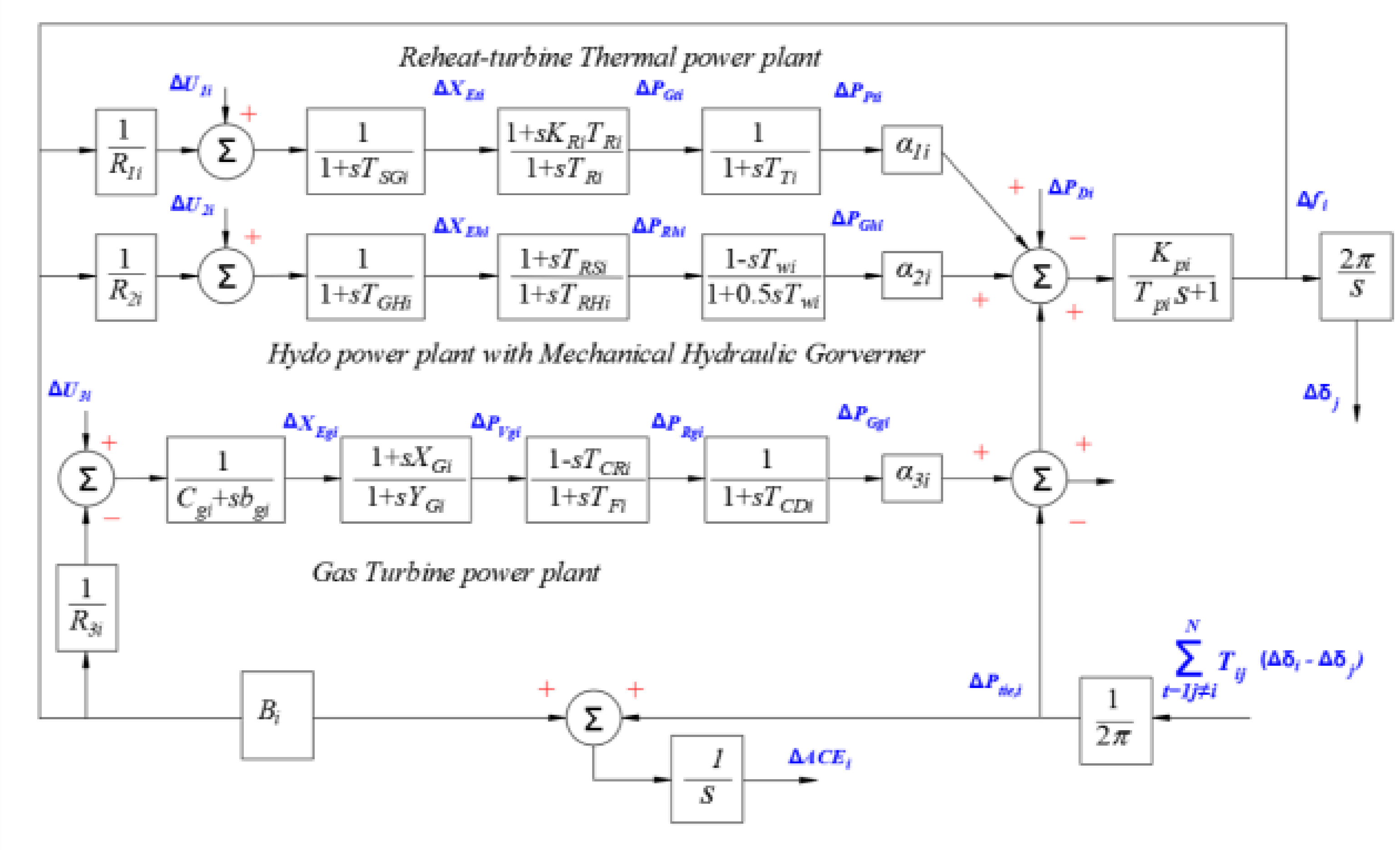

Fig. 3 - The basic block diagram of the *ith* area of a MMIPS.

Taking into account, the impact of the interconnection matrix and load disturbance, the PS model is constructed in the differential equation as follows.

$$\Delta\dot{f}_i = -\frac{\Delta f_i}{T_{PS_i}} + \frac{\Delta P_{pt_i} K_{PS_i}\alpha_{i1}}{T_{PS_i}} + \frac{\Delta P_{Gh_i} K_{PS_i}\alpha_{i2}}{T_{PS_i}} + \frac{\Delta P_{Gg_i} K_{PS_i}\alpha_{i3}}{T_{PS_i}} - \frac{K_{PS_i} a_{ij}}{T_{PS_i}}\Delta P_{tie_{ij}} - \frac{K_{PS_i}}{T_{PS_i}}\Delta P_{D_i} \qquad (1)$$

$$\Delta\dot{P}_{pt_i} = \frac{\Delta P_{Gt_i}}{T_{T_i}} - \frac{\Delta P_{pt_i}}{T_{T_i}} \qquad (2)$$

$$\Delta\dot{P}_{Gt_i} = -\frac{\Delta P_{Gt_i}}{T_{R_i}} + \frac{\Delta X_{Et_i}}{T_{R_i}} - \frac{\Delta X_{Et_i} K_{R_i}}{T_{SG_i}} - \frac{\Delta f_i K_{R_i}}{T_{SG_i} R_{i1}} + \frac{\Delta ACE_i K_{R_i}}{T_{SG_i}} + \frac{U_{i1} K_{R_i}}{T_{SG_i}} \qquad (3)$$

$$\Delta\dot{X}_{Et_i} = -\frac{\Delta X_{Et_i}}{T_{SG_i}} - \frac{\Delta f_i}{T_{SG_i} R_{i1}} + \frac{\Delta ACE_i}{T_{SG_i}} + \frac{U_{i1}}{T_{SG_i}} \qquad (4)$$

$$\Delta\dot{P}_{Gh_i} = \frac{2\Delta P_{Rh_i}}{T_{W_i}} - \frac{2\Delta P_{Gh_i}}{T_{W_i}} - \frac{2\Delta X_{Eh_i}}{T_{RH_i}} + \frac{2\Delta P_{Rh_i}}{T_{RH_i}} + \frac{2\Delta X_{Eh_i} T_{RS_i}}{T_{RH_i} T_{GH_i}} + \frac{2\Delta f_i T_{RS_i}}{R_{i2} T_{RH_i} T_{GH_i}} - \frac{2\Delta ACE_i T_{RS_i}}{T_{RH_i} T_{GH_i}} - \frac{2U_{i2} T_{RS_i}}{T_{RH_i} T_{GH_i}} \qquad (5)$$

$$\Delta\dot{P}_{Rh_i} = \frac{\Delta X_{Eh_i}}{T_{RH_i}} - \frac{\Delta P_{Rh_i}}{T_{RH_i}} - \frac{\Delta X_{Eh_i} T_{RS_i}}{T_{RH_i} T_{GH_i}} - \frac{\Delta f_i T_{RS_i}}{R_{i2} T_{RH_i} T_{GH_i}} + \frac{\Delta ACE_i T_{RS_i}}{T_{RH_i} T_{GH_i}} + \frac{U_{i2} T_{RS_i}}{T_{RH_i} T_{GH_i}} \qquad (6)$$

$$\Delta\dot{X}_{Eh_i} = -\frac{\Delta X_{Eh_i}}{T_{GH_i}} - \frac{\Delta f_i}{T_{GH_i} R_{i2}} + \frac{\Delta ACE_i}{T_{GH_i}} + \frac{U_{i2}}{T_{GH_i}} \qquad (7)$$

$$\Delta\dot{P}_{Gg_i} = -\frac{\Delta P_{Gg_i}}{T_{CD_i}} + \frac{\Delta P_{Rg_i}}{T_{CD_i}} \qquad (8)$$

$$\Delta\dot{P}_{Rg_i} = -\frac{\Delta P_{Rg_i}}{T_{F_i}} + \frac{\Delta X_{Vg_i}}{T_{F_i}} + \frac{\Delta X_{Vg_i} T_{CR_i}}{Y_{G_i} T_{F_i}} - \frac{\Delta X_{Eg_i} T_{CR_i}}{Y_{G_i} T_{F_i}} + \frac{\Delta X_{Eg_i} c_{g_i} X_{G_i} T_{CR_i}}{b_{g_i} Y_{G_i} T_{F_i}} + \frac{\Delta f_i X_{G_i} T_{CR_i}}{R_{i3} b_{g_i} Y_{G_i} T_{F_i}} - \frac{\Delta ACE_i X_{G_i} T_{CR_i}}{b_{g_i} Y_{G_i} T_{F_i}} - \frac{U_{i3} X_{G_i} T_{CR_i}}{b_{g_i} Y_{G_i} T_{F_i}} \qquad (9)$$

$$\Delta\dot{P}_{Vg_i} = -\frac{\Delta P_{Vg_i}}{Y_{G_i}} + \frac{\Delta X_{Eg_i}}{Y_{G_i}} - \frac{\Delta X_{Eg_i} c_{g_i} X_{G_i}}{b_{g_i} Y_{G_i}} - \frac{\Delta f_i X_{G_i}}{R_{i3} b_{g_i} Y_{G_i}} + \frac{\Delta ACE_i X_{G_i}}{b_{g_i} Y_{G_i}} + \frac{U_{i3} X_{G_i}}{b_{g_i} Y_{G_i}} \qquad (10)$$

$$\Delta\dot{X}_{Eg_i} = -\frac{\Delta X_{Eg_i} c_{g_i}}{b_{g_i}} - \frac{\Delta f_i}{b_{g_i} R_{i3}} + \frac{\Delta ACE_i}{b_{g_i}} + \frac{U_{i3}}{b_{g_i}} \qquad (11)$$

$$\Delta A\dot{C}E_i = B_i \Delta f_i + a_{ij} \Delta P_{tie_{ij}} \qquad (12)$$

$$\Delta\dot{P}_{tie_{ij}} = \sum_{\substack{j=1 \\ j\neq i}}^{L} 2\pi T_{ij} (\Delta f_i - \Delta f_j) \qquad (13)$$

By defining the above PS parameters, the *i-th* area of the PS state space model is given by using the dynamics equation from (1) to (13) is given by (14) .

$$\dot{x}_i(t) = A_i x_i(t) + B_i u_i(t) + \sum_{\substack{j=1 \\ j \neq i}}^{L} H_{ij} x_j(t) + F_i \Delta P_{di}(t) \qquad (14)$$

Where,

$$x_i(t) = \begin{bmatrix} \Delta f_i & \Delta P_{pt_i} & \Delta P_{Gt_i} & \Delta X_{Et_i} & \Delta P_{Gh_i} & \Delta P_{Rh_i} & \Delta X_{Eh_i} & \Delta P_{Gg_i} & \Delta P_{Rg_i} & \Delta P_{Vg_i} & \Delta X_{Eg_i} & \Delta ACE_i & \Delta P_{tie_{ij}} \end{bmatrix}^T$$

is the state vector

the aggregated disturbance $\rho_i(x_i,t)$ represents the uncertainties.

In practical interconnected MAMSPS, changes in operating points constantly influence the fluctuating sources of load. This factor can be considered as parameter uncertainties. Introducing this factor, the system (14) can be rewritten by

$$\dot{x}_i(t) = A_i x_i(t) + B_i[u_i(t) + \xi_i(x_i,t)] + \sum_{\substack{j=1 \\ j\neq i}}^{N} [H_{ij} + \Sigma_{ij}(x_j,t)] x_j(t) + F_i \Delta P_{di}(t) \quad (15)$$

where $B_i\xi_i(x_i,t)$ is disturbance input, $\Sigma_{ij}(x_j,t)$ are the interconnected parameter uncertainties

In other words, the aggregate uncertainty is therefore given as

$$\rho_i(x_i,t) = B_i\xi_i(x_i,t) + \sum_{\substack{j=1 \\ j\neq i}}^{N} \Sigma_{ij}(x_j,t) x_j(t) + F_i \Delta P_{di}(t) \quad (16)$$

Therefore, the new dynamic model can be expressed as

$$\dot{x}_i(t) = A_i x_i(t) + B_i u_i(t) + \sum_{\substack{j=1 \\ j\neq i}}^{N} H_{ij} x_j(t) + \rho_i(x_i,t) \quad (17)$$

$$y_i = C_i x_i$$

where, $\rho_i(x_i,t)$ is the aggregated disturbance that represents the uncertainties of the matched and mismatched parameters

III. A case study using Second Order Sliding Mode Control Approach

The main steps to do the second order sliding mode design for load frequency control of multi-area multi-source power systems

In the preceding stage, we introduced and demonstrated how power networks with integral sliding surfaces (ISSs) function to be asymptotically stable and smooth in the sliding mode under certain circumstances. The multi-area linked power network will receive a new (SOSMC) scheme in the following stage to stop chattering and oscillation in the ISS. As a result, certain undesirable frequency oscillations in the power system's control signal are removed using the second order SMC technique. The second order sliding mode control with integral surface is developed for the load frequency control (LFC) of the multi-area multi-source power system (MAMSPS). To test the feasibility of the constructed (SOSMC), the two-area thermal hydro-gas power system (TAGHTPS) model is chosen. Furthermore, the uncertainty of the state and interconnected parameters is considered for the TAGHTPS model

Step 1. Mathematical model of an interconnected multi-area multi-source power network

$$\dot{x}_i(t) = A_i x_i(t) + B_i u_i(t) + \sum_{\substack{j=1 \\ j \neq i}}^{N} H_{ij} x_j(t) + \rho_i(x_i, t)$$

THE MAIN STEP TO DO THE PROPOSED ADVANCE SLIDING MODE CONYROL:

Advanced sliding mode design for load frequency control of multi-area multi-source power systems

Step 2.The integral sliding surface of sliding mode control

$$\Omega_i[x_i(t)] = \Gamma_i x_i(t) - \int_0^t \Gamma_i (A_i - B_i K_i) x_i(\tau) d\tau$$

where Γ_i is constant matrix and K_i is the design matrix, matrix Γ_i is chosen to guarantee that matrix $\Gamma_i B_i$ is non-singular. The design matrix $K_i \in R^{m_i \times n_i}$ is selected to satisfy the inequality condition of the PS

We first begin to propose and build an integral sliding surface for an interconnected multi-area power network

Step 3. To find the sliding motion dynamic system of power network

$$\dot{x}_i(t) = (A_i - B_i K_i) x_i(t) + [I_i - B_i(\Gamma_i B_i)^{-1}\Gamma_i]\rho_i(x_i, t)$$
$$+ \sum_{\substack{j=1 \\ j\neq i}}^{N} [I_i - B_i(\Gamma_i B_i)^{-1}\Gamma_i] H_{ij} x_j(t)$$

The following theorem makes a condition that the second-order sliding mode dynamic equation is asymptotically stable. We prove the stability of system by using the Lyapunov function via LMIs technique.

Step 4. Load frequency controller design

Based on the definition of sliding surface and sliding manifold, the continuous decentralized second order sliding mode LFC for power networks be given as follows

$$\dot{u}_i(t) = -(\Gamma_i B_i)^{-1}[\|\Gamma_i\|\|B_i\|\|K_i\|\|\dot{x}_i(t)\| + \sum_{\substack{j=1 \\ j\neq i}}^{N}\|\Gamma_i\|\|H_{ji}\|\|\dot{x}_i(t)\|$$

$$+\delta_i\left\|\dot{\Omega}_i[x_i(t)]\right\| + \|\Gamma_i\|\bar{\gamma}_i + \bar{\varepsilon}]\frac{\chi_i[x_i(t)]}{\|\chi_i[x_i(t)]\|}$$

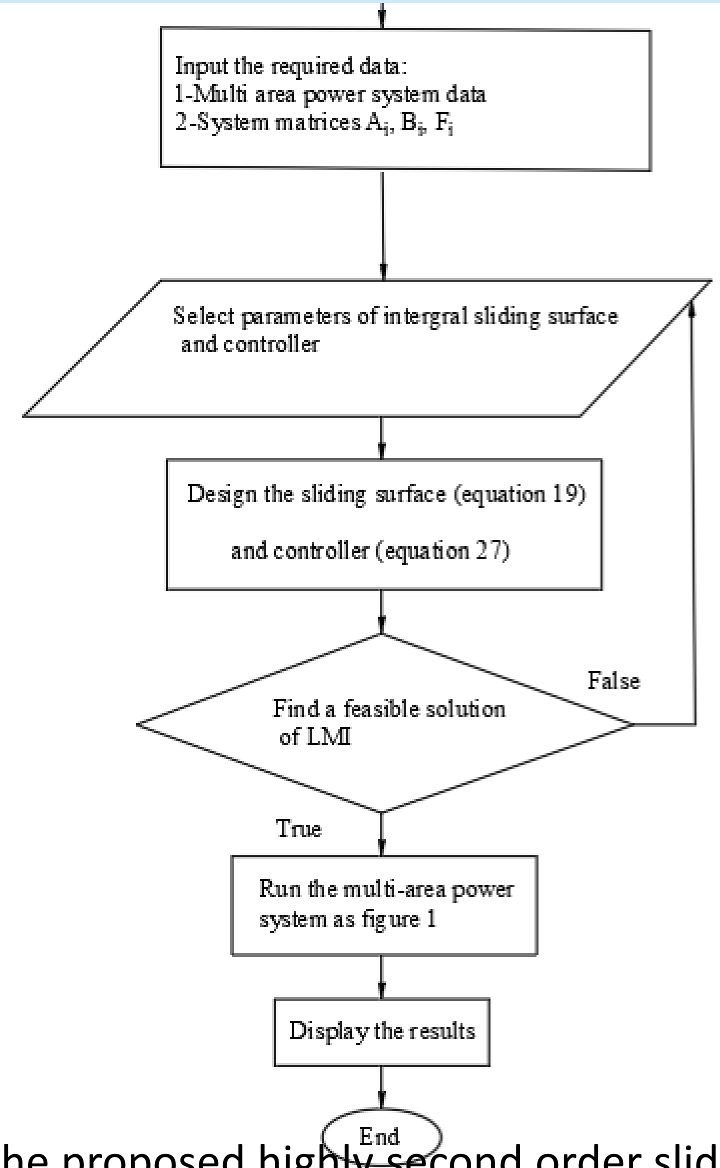

Figure 3. The flowchart of the proposed highly second order sliding mode control

IV. Simulation Results

1. Case 1

In the beginning, we presume that the system's parameters are at their nominal values. Load disturbances perturbing on the system are $\Delta P_{d1} = 0.01$ p.u at $t_1 = 1$ s in area 1 and $\Delta P_{d2} = 0.02$ p.u. at $t_2 = 1$ s in area 2 of PS. Fig. 4 through Fig. 5 depict the frequency deviation and tie-line power deviation. In addition, the frequency variation takes roughly 3 s to setting time and converge to zero, which indicates a quicker response time to the disturbance than response time stated in [15-16].

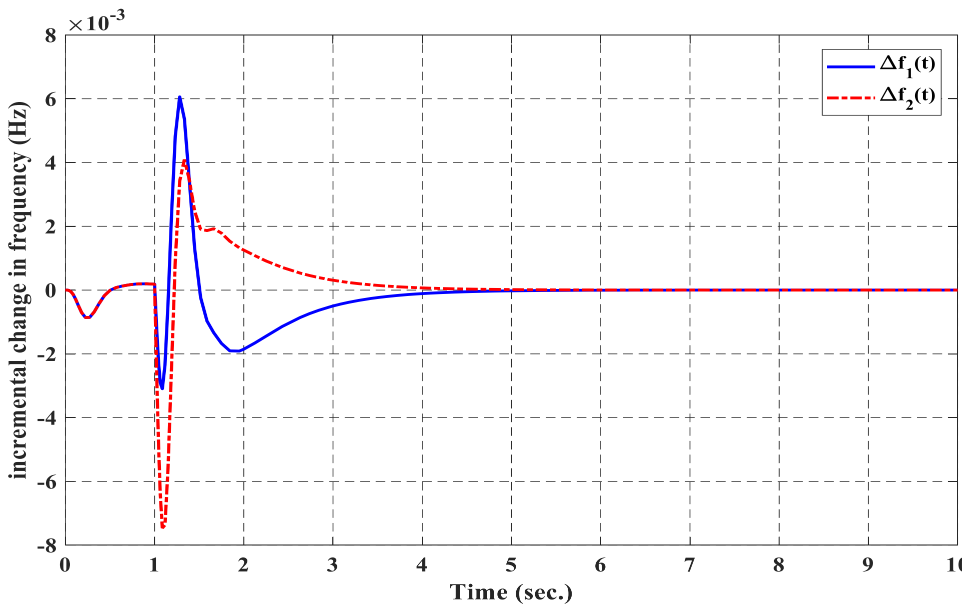

Fig. 4. Frequency deviations [Hz] of the control area 1 and 2 with matched disturbances.

I. Simulation Results

1. Case 1

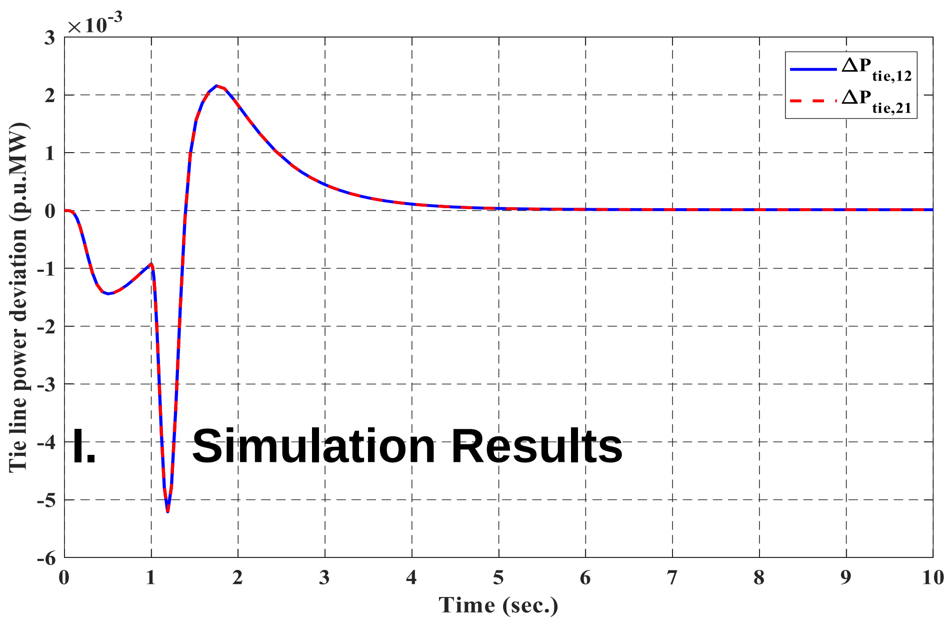

Fig. 5. Tie line power deviation [p.u.MW] with matched disturbances

Remark 1: The newly suggested controller outperforms the prior method as demonstrated in [15-16] in terms of robustness and quick reaction to load disturbance. In specifics, the load disturbance is evident, and the system is quickly brought back to steady state with reduced overshoots

Case 2: Once more, the suggested controller is tested using random load changes. Fig. 5 depicts random load disturbances that are delivered to the system together with parameter nominal values that are within 20% of the mean to further test the proposed controller's resilience. While Fig. 8 displays the tie-line power flow signal, Fig. 7 displays the proposed controller response to deviations in frequency of the first and second area.

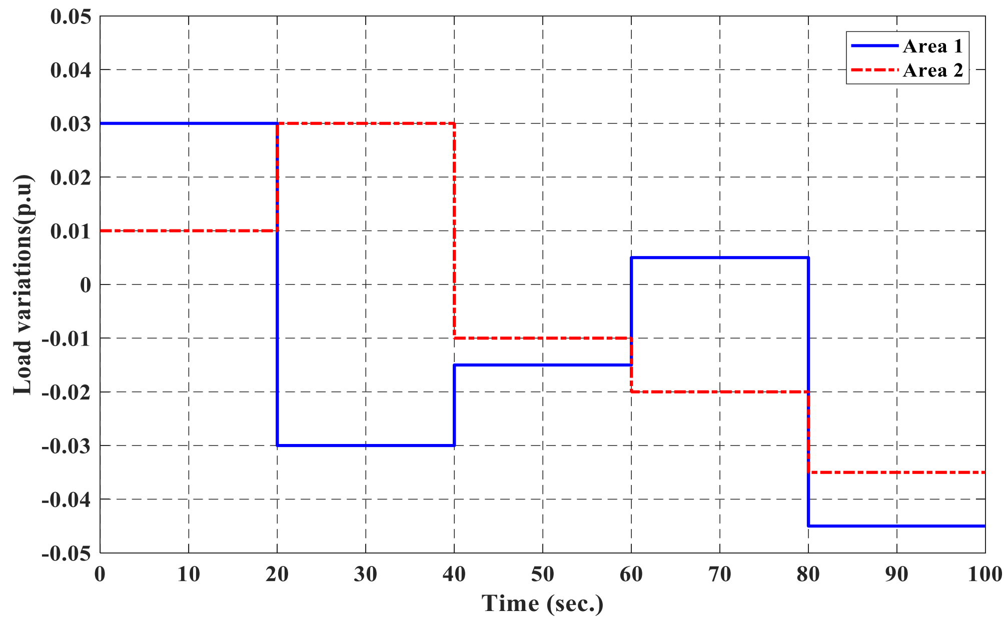

Fig. 6. Variation load [p.u] of the area 1 and 2 of the power system

Case 2:

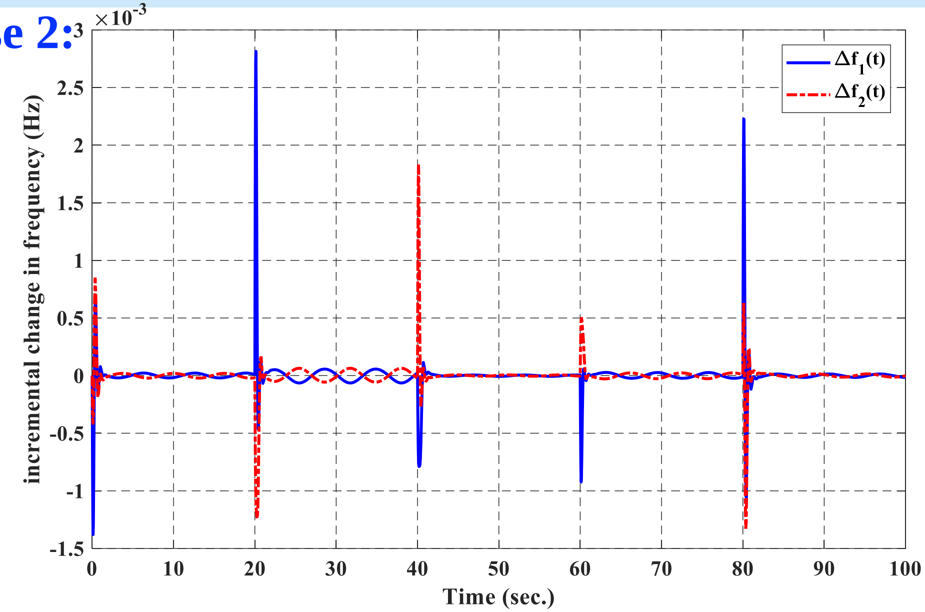

Fig. 7. Frequency deviations [Hz] of the control area 1 and 2 with matched disturbances.

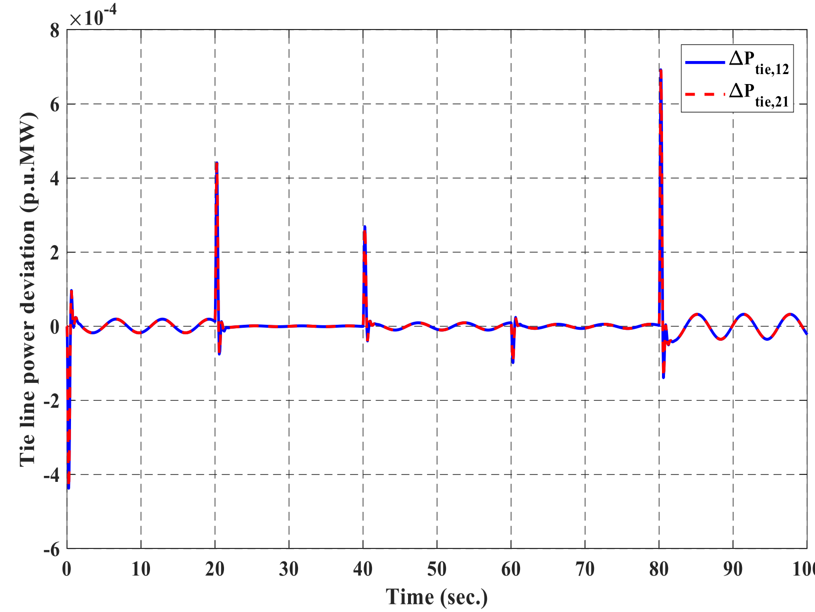

Fig. 8. Tie line power deviation [p.u.MW] with matched disturbances.

Remark 2. Actuators utilized in power systems are severely harmed by this chattering issue in SMC. The suggested controller provides the right signal and uses energy to account for frequency dampening for the governor-based primary control. For the governor's droop speed control to properly open the valve and provide the turbine with the necessary steam to boost mechanical inertia power to meet the changing load or demand. Therefore, when compared to the suggested approach presented in [15-16], the setting time and overshoot are better.

V. Conclusion

The SOSMC method is described and suggested as a way to construct the controller for resolving and balancing the active power of an interconnected multi-area power system (MMIPS) at the conclusion of this study. The recommended method not only guarantees the stability of power networks but also significantly reduces the chattering issue in power systems. To assure shorter transient frequency response, lower high overshoot, and solve the priority issue of active power balance, a second order SMC based on an integral sliding surface is given. By contrasting it with the prior control approach, the performance of an MMIPS is demonstrated in the removal of the chattering issue. Again, to the best of our knowledge, the proposed SMC based on the FLC scheme obtained great benefits, such as the benefits of SMC's robustness and utility, and chattering elimination of FLC in practical applications

2023 INTERNATIONAL CONFERENCE ON SYSTEM SCIENCE AND ENGINEERING

July 27-28, 2023 - Ho Chi Minh City, Vietnam

HYBRID EVENT

Email: tranthanhphong.st@tdtu.edu.vn;huynhvanvan@tdtu.edu.vn

Hindawi
Complexity
Volume 2021, Article ID 5564184, 19 pages
https://doi.org/10.1155/2021/5564184

Research Article

Adaptive Integral Second-Order Sliding Mode Control Design for Load Frequency Control of Large-Scale Power System with Communication Delays

Anh-Tuan Tran [1], Bui Le Ngoc Minh [2,3], Phong Thanh Tran [1], Van Van Huynh [1], Van-Duc Phan [4], Viet-Thanh Pham [1], and Tam Minh Nguyen [2]

[1] *Modeling Evolutionary Algorithms Simulation and Artificial Intelligence, Faculty of Electrical & Electronics Engineering, Ton Duc Thang University, Ho Chi Minh City, Vietnam*
[2] *Faculty of Electrical and Electronics Engineering, Ho Chi Minh City University of Technology and Education, Ho Chi Minh City, Vietnam*
[3] *Faculty of Industrial Engineering, Tien Giang University, Mỹ Tho, Tien Giang Province 840000, Vietnam*
[4] *Faculty of Automobile Technology, Van Lang University, Ho Chi Minh City, Vietnam*

Correspondence should be addressed to Van Van Huynh; huynhvanvan@tdtu.edu.vn

Received 7 January 2021; Revised 12 February 2021; Accepted 10 March 2021; Published 22 March 2021

Academic Editor: Rui Wang

Nowadays, the power systems are getting more and more complicated because of the delays introduced by the communication networks. The existence of the delays usually leads to the degradation and/or instability of power system performance. On account of this point, the traditional load frequency control (LFC) approach for power system sketches a destabilizing impact and an unacceptable system performance. Therefore, this paper proposes a new LFC based on adaptive integral second-order sliding mode control (AISOSMC) approach for the large-scale power system with communication delays (LSPSwCD). First, a new linear matrix inequality is derived to ensure the stability of whole power systems using Lyapunov stability theory. Second, an AISOSMC law is designed to ensure the finite time reachability of the system states. To the best of our knowledge, this is the first time the AISOSMC is designed for LFC of the LSPSwCD. In addition, the report of testing results presents that the suggested LFC based on AISOSMC can not only decrease effectively the frequency variation but also make successfully less in mount of power oscillation/fluctuation in tie-line exchange.

1. Introduction

In modern power networks, the frequency stability is one of the significant problems related to the large-scale power system (LSPS) with communication delays. The system has been more and more complicated for LFC due to matched or mismatched uncertainties, load variations, and time-delays [1–4]. Communications time-delay is necessary in the LSPS; it cannot ignore and remove in the practical LSPS. So, the time-delay must consider in the area control error (ACE) signal. Normally, the time-delay can appear in the state variables or in the input channel of LSPS. The input control signal is transported to the power plants through communication networks with delay time. The state delay-time is the essential reason to effect on delaying the basic elements of communication or transportation in the LSPS. The deviation of tie-line exchange power and frequency are combined and known as an ACE to confirm the control frequency aim for the LSPS. The balance in both the tie-line and frequency exchange power is assured when an ACE is controlled and limited. In the LSPS model, the time-delay of ACE from regulation station to control area of the system is important [4–6]. Moreover, the time-delay is known as time lag in the power system model. That is, a big challenge to design the control algorithm to deal with the time-delay in the LSPS. In ACE control signal, the time lag may occur and lead to oscillation and instability in the LSPS [6–9]. Therefore, it is absolutely necessary to consider and explore the LFC for the LSPSwCD. The main objectives of LFC for each control area are continuing to keep the nominal value of the system frequency in range of the standard value and to act in accordance with the scheduled active power interchange with neighboring control areas.

In general, the previous LFC scheme such as PID control has been used to maintain tie-line power and frequency at schedule value which is one of the simplest controllers [10–13]. A suitable design of PID controller which is constructed on the direct synthesis method in frequency domain is given in [10]. In [11], a fractional-order PID control approach is built for the single-area LFC model using the Kharitonov's theorem to eliminate steady state error. Robust PID controller-based stability boundary locus and Kharitonov's theorem were used for LFC of the LSPS [12]. In [13], an ant lion algorithm is combined with PID to optimize the LFC loop parameters for improving the frequency regulation. The above approaches are suitable for application to design LFC of power network with nominal parameter and no uncertainty. However, the practical power network is always influenced or touched by an external factor of the uncertainties such as different load disturbances, which effect on the stability of power network. In order to overcome drawbacks and resolve the LFC problem effectively, advanced control techniques are developed for LFC design consisting of neural network and fuzzy control [14–16]. In [14], the LFC scheme for the LSPS was established and constructed on the adaptive fuzzy control method. A novel fuzzy PID control strategy with the fractional-order integrator and filtered derivative action was suggested to resolve automatic generation control for the power network [15]. In [16], the optimized operation of LFC is proposed for the LSPS with hybrid energy storage system.

On the other hand, as a powerful robust control strategy, SMC has been successfully applied to a wide variety of practical systems [17–19]. The terminal SMC is designed for LFC with the renewable power networks [20]. In [21], the adaptive double integral SMC is proposed for LFC of the LSPS where the time-delay is not considered. The goal of Sarkar was to design an adaptive integral higher order SMC for LFC problems to guarantee the frequency variation [22]. In [23], this article indicated nonlinear SMC with parametric uncertainties for LFC utilization in the LSPS to vary the system damping characteristics under uncertainties and step load disturbances. The approach given in [24] developed the strategy of SMC by model order-reduction of the LFC approach of the microhydropower system. A new full order SMC scheme in the paper [25] is utilized to eliminate and avoid the singularity of derivative of terms with fractional power elements. A novel adaptive SMC method has been used and developed for the LFC of the LSPS [26]. The proportional and integral switching surface was established for LFC of LSPS where the chattering problem is existed due to first-order SMC used [27]. The SMC-based LFC of above approaches can reduce the tie-line power and frequency deviations to ensure the stability of power network. However, the performance of LSPS using control scheme given in [20–27] is achieved without considering the time-delay in the power grids. In addition, the existence of the delays usually leads to the degradation and/or instability of power network performance. In order to solve this problem, the control scheme given in [28–30] is proposed to regulate the frequency deviation of the LSPS in the presence of communication delays and sudden load change. In [31], the LFC of the LSPS with nonlinear perturbations and time-varying delays are proposed using SMC. In [32], the sliding mode LFC is designed for the LSPS with time-delay and load disturbance. The sliding mode LFC strategy is suggested for the LSPS with time-delay and significant wind power penetration [33]. However, these SMC approaches are developed based on first-order time derivative [31–33]. In addition, the first-order SMC provides low accuracies due to chattering phenomenon in the control input. Therefore, in this paper, the second-order SMC is proposed to solve this problem. Moreover, an adaptive control method is adopted to estimate the unknown upper bound of aggregated uncertainties. To the best of our knowledge, the adaptive integral second-order sliding mode control (AISOSMC) scheme has not been developed for LFC problem in the LSPSwCD so far. The major contributions of this paper are displayed as follows:

- The novel theory based on AISOSMC approach is offered for the LSPSwCD
- The continuous control law is developed to deal with the influence of time-delay related to ACE on the LFC problem of the LSPSwCD
- A state feedback controller containing both present and delayed state information is designed to improve tolerable delay margin of the LSPSwCD
- A new LMI is established for proving the stability of whole PSPS based on Lyapunov stability theory
- The proposed LFC based on AISOSMC can not only decrease effectively the frequency variation but also make successfully less in mount of power oscillation/fluctuation in tie-line exchange

2. Mathematical Model of a Large-Scale Power System with Communication Delays (LSPSwCD)

In this part, we model the LSPSwCD. Figure 1 is the block diagram of the i^{th} area of the LSPS with communication delay [28–30]. The model of the i^{th} area system is composed of a governor, a nonreheat turbine, and a generator. The output of the generator is the frequency error. The tie-line power error is linearly proportional to the integration of frequency error. The linear combination of frequency error and the tie-line power error is the area control error (ACE). In addition, the time-delay of ACE signal is considered in the power network.

Nevertheless, when the load variation with minor change occurs during its conventional process, then the

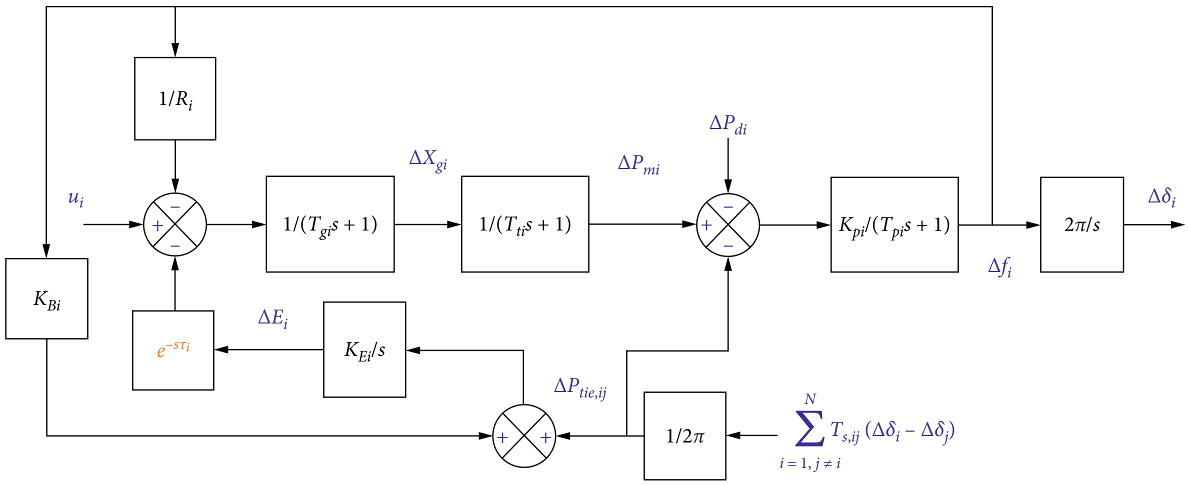

FIGURE 1: The structure of i^{th} area of the LSPSwCD.

mathematical model of power network can be linearized near the stable operating point. Therefore, the dynamic equations of the above i^{th} area system are expressed as follows:

$$\begin{aligned}
\Delta\dot{f}_i(t) &= -\frac{1}{T_{pi}}\Delta f_i(t)+\frac{K_{Pi}}{T_{pi}}\Delta P_{mi}(t)-\frac{K_{Pi}}{T_{pi}}\Delta P_{di}(t)-\frac{K_{Pi}}{2\pi T_{pi}}\sum_{i=1,j\neq i}^{N}T_{s,ij}\left[\Delta\delta_i(t)-\Delta\delta_j(t)\right],\\
\Delta\dot{P}_{mi}(t) &= -\frac{1}{T_{ti}}\Delta P_{mi}(t)+\frac{1}{T_{ti}}\Delta X_{gi}(t),\\
\Delta\dot{X}_{gi}(t) &= -\frac{1}{T_{gi}R_i}\Delta f_i(t)-\frac{1}{T_{gi}}\Delta X_{gi}(t)-\frac{1}{T_{gi}}\Delta E_i(t-\tau_i)+\frac{1}{T_{gi}}u_i(t),\\
\Delta\dot{E}_i(t) &= K_{Bi}K_{Ei}\Delta f_i(t)+\frac{K_{Ei}}{2\pi}\sum_{i=1,j\neq i}^{N}T_{s,ij}\left[\Delta\delta_i(t)-\Delta\delta_j(t)\right],\\
\Delta\dot{\delta}_i(t) &= 2\pi\Delta f_i(t),
\end{aligned} \tag{1}$$

with $i=1$ to N and N is denoted as the number of areas, where $\Delta f_i(t)$ and $\Delta f_j(t)$ are the frequency variation of the i^{th} area and the j^{th} area, $\Delta P_{mi}(t)$ is the variation in governor output command, $\Delta X_{gi}(t)$ is the governor valve position of each area, $\Delta\delta_i(t)$ and $\Delta\delta_j(t)$ are the changes of rotor angle deviations of the i^{th} area and the j^{th} area, $\Delta P_{di}(t)$ is the incremental change in local load of each area, $T_{s,ij}$ is the tie-line power coefficient between the i^{th} area and the j^{th} area, T_{gi} is the time constant of governor, T_{ti} is the turbine time constant, and T_{pi} is the time constant in power network, respectively. K_{pi}, R_i, K_{Ei}, and K_{Bi} are power network gain, droop coefficient of individual area, speed regulation coefficient, and frequency bias factor. $\Delta E_i(t-\tau_i)$ is the area control error with the time-delay and $u_i(t)$ is the control input.

In state-space form, the system state variables are used as

$$z_i(t)=\left[\Delta f_i(t)\ \ \Delta P_{mi}(t)\ \ \Delta X_{gi}(t)\ \ \Delta E_i(t)\ \ \Delta\delta_i(t)\right]^T. \tag{2}$$

So, the LSPSwCD described by Figure 1 can be written and expressed in state-space representation as follows:

$$\begin{aligned}
\dot{z}_i(t) &= A_iz_i(t)+D_iz_i(t-\tau_i)+B_iu_i(t)\\
&\quad+\sum_{j=1;j\neq i}^{N}H_{ij}z_j(t)+F_i\Delta P_{di}(t),
\end{aligned} \tag{3}$$

where $i=1,2,\ldots,N$ and N *is* denoted as the number of areas.

The state-space matrix $A_i, B_i, D_i, F_i, H_{ij}$ in mathematical model is given as follows:

$$A_i = \begin{bmatrix} \frac{-1}{T_{Pi}} & \frac{K_{Pi}}{T_{Pi}} & 0 & 0 & -\frac{K_{Pi}}{2\pi T_{Pi}} \sum_{i=1, j\neq i}^{N} T_{s,ij} \\ 0 & -\frac{1}{T_{Ti}} & \frac{1}{T_{Ti}} & 0 & 0 \\ -\frac{1}{R_i T_{Gi}} & 0 & -\frac{1}{T_{Gi}} & 0 & 0 \\ K_{Bi}K_{Ei} & 0 & 0 & 0 & \frac{K_{Ei}}{2\pi} \sum_{i=1, j\neq i}^{N} T_{s,ij} \\ 2\pi & 0 & 0 & 0 & 0 \end{bmatrix},$$

$$D_i = \begin{bmatrix} 0 & 0 & 0 & 0 & 0 \\ 0 & 0 & 0 & 0 & 0 \\ 0 & 0 & 0 & -\frac{1}{T_{Gi}} & 0 \\ 0 & 0 & 0 & 0 & 0 \\ 0 & 0 & 0 & 0 & 0 \end{bmatrix},$$

$$H_{ij} = \begin{bmatrix} 0 & 0 & 0 & 0 & -\frac{K_{Pi}}{2\pi T_{Pi}} \sum_{i=1, j\neq i}^{N} T_{s,ij} \\ 0 & 0 & 0 & 0 & 0 \\ 0 & 0 & 0 & 0 & 0 \\ 0 & 0 & 0 & 0 & \frac{K_{Ei}}{2\pi} \sum_{i=1, j\neq i}^{N} T_{s,ij} \\ 0 & 0 & 0 & 0 & 0 \end{bmatrix}, \quad (4)$$

$$B_i = \begin{bmatrix} 0 \\ 0 \\ \frac{1}{T_{Gi}} \\ 0 \\ 0 \end{bmatrix};$$

$$F_i = \begin{bmatrix} -\frac{K_{Pi}}{T_{Pi}} \\ 0 \\ 0 \\ 0 \\ 0 \end{bmatrix}.$$

In applied LSPSwCD, the operating point fluctuates continually induced by the fluctuating resource and load disturbance. In addition, by considering CDs element, the dynamic model of LSPSwCD with the uncertainties and parameter variations in equation (3) are further redefined as

$$\begin{aligned}\dot{z}_i(t) &= [A_i + \Delta A_i(z_i,t)]z_i(t) + [D_i + \Delta D_i(z_i,t-\tau_i)]z_i(t-\tau_i) + B_i[u_i(t) + \xi_i(z_i,t)] \\ &\quad + \sum_{j=1;j\neq i}^{N}\left[H_{ij} + \Delta H_{ij}(z_j,t)\right]z_j(t) + F_i\Delta P_{di}(t) \\ &= A_i z_i(t) + D_i z_i(t-\tau_i) + B_i u_i(t) + \sum_{j=1;j\neq i}^{N} H_{ij}z_j(t) + w_i(z_i,t),\end{aligned} \tag{5}$$

where $A_i, D_i, B_i,$ and H_{ij} are the system matrices with nominal value, $\Delta A_i(z_i,t)$, $\Delta H_{ij}(z_j,t)$, and $\Delta D_i(z_i,t-\tau_i)$ are the parameter uncertainties, and $B_i\xi_i(z_i,t)$ is the disturbance input signal. The lumped uncertainty $w_i(z_i,t)$ is defined as follows:

$$\begin{aligned}w_i(z_i,t) &= \Delta A_i(z_i,t)z_i(t) + \Delta D_i(z_i,t-\tau_i)z_i(t-\tau_i) \\ &\quad + B_i\xi_i(z_i,t) + \sum_{i=1;j\neq i}^{N}\Delta H_{ij}z_j(t) + F_i\Delta P_{di}(t).\end{aligned} \tag{6}$$

Assumption 1. The lumped uncertainties $w_i(z_i,t)$ and the differential of $\dot{w}_i(z_i,t)$ are bounded, i.e., there exist known scalars γ_i and ∂_i such that $\|w_i(z_i,t)\| \leq \gamma_i$ and $\|\dot{w}_i(z_i,t)\| \leq \partial_i$, where $\|.\|$ is the matrix norm.

Assumption 2. The time-delay state vector must satisfy the condition $\|z_i(t-\tau_i)\| \leq z_{i\max}$, $z_{i\max} = \max\|z_{i\max}\|$, where $\|.\|$ is the matrix norm.

In order to prove the system stability, we recall some lemmas.

Lemma 1 (see [34]). *Let* $\mathbf{X}$ *and* $\mathbf{Y}$ *be actual matrices with appropriate dimension, then, for any scalar* $\mu > 0$, *the sequent matrix inequality obtains*

$$\mathbf{X}^{\mathbf{T}}\mathbf{Y} + \mathbf{Y}^{\mathbf{T}}\mathbf{X} \leq \mu\mathbf{X}^{\mathbf{T}}\mathbf{X} + \mu^{-1}\mathbf{Y}^{\mathbf{T}}\mathbf{Y}. \tag{7}$$

Lemma 2 (see [35]). *ie following matrix inequality*

$$\begin{bmatrix} P(z) & \Gamma(z) \\ \Gamma^T(z) & Q(z)\end{bmatrix} > 0, \tag{8}$$

where $P(z) = P^T(z)$, $Q(z) = Q^T(z)$, $\Gamma(z)$ *depends affinely on* z, *is equivalent to* $Q(z) > 0$ *and* $P(z) - \Gamma(z)Q^{-1}(z)\Gamma^T(z) > 0$.

Lemma 3 (see [35]). *Assume that* $x \in R^n$, $y \in R^n$, $\mathbf{N} \in R^{n\times n}$, *and* $\mathbf{N}$ *is the positive definite matrix. Then, the inequality*

$$x^T\mathbf{N}y + y^T\mathbf{N}x \leq \frac{1}{\varepsilon}x^T\mathbf{N}x + \varepsilon y^T\mathbf{N}y, \tag{9}$$

holds for all $\varepsilon > 0$.

3. Adaptive Integral Second-Order Sliding Mode Control (AISOSMC) Design for LFC of Large-Scale Power System with Communication Delays (LSPSwCD)

In this section, the AISOSMC method is developed for LFC of the LSPSwCD under mismatched parameter uncertainties and load disturbances. To solve this problem, we work step by step to design and implement the new controller approach. Firstly, the integral sliding surface (ISS) is represented for LSPSwCD to assure that the whole system is asymptotically stable. Secondly, the decentralized adaptive integral second-order sliding mode control law (DAISOSMCL) is designed to force the system trajectories to the sliding manifold and keep it there for after.

3.1. Stability Analysis of a LSPSwCD in Sliding Mode Dynamics

In detail, we first begin to propose and build an ISS for a LSPS:

$$\sigma_i[z_i(t)] = E_i z_i(t) - \int_0^t E_i(A_i - B_iT_i)z_i(\tau)\mathrm{d}\tau, \tag{10}$$

where E_i is the constant matrix and T_i is the design matrix, matrix E_i is designed to guarantee that matrix E_iB_i is nonsingular and matrix T_i is chosen via pole assignment such that the eigenvalues of matrix $(A_i - B_iT_i)$ are always less than zero.

If we recognize and differentiate $\sigma_i[z_i(t)]$ with respect to time combined with (3), then

$$\dot{\sigma}_i[z_i(t)] = E_i\left[A_iz_i(t) + D_iz_i(t-\tau_i) + B_iu_i(t) + \sum_{j=1;j\neq i}^{N}H_{ij}z_j(t) + w_i(z_i,t)\right] - E_i(A_i - B_iT_i)z_i(t). \tag{11}$$

So, the setting $\sigma_i[z_i(t)] = \dot{\sigma}_i[z_i(t)] = 0$; the equivalent control is rewritten by

$$\begin{aligned} u_i^{\mathrm{eq}}(t) = &-(E_iB_i)^{-1}\left[E_iA_iz_i(t) + E_iD_iz_i(t-\tau_i) + \sum_{j=1;j\neq i}^{N} E_iH_{ij}z_j(t) + E_iw_i(z_i,t)\right] \\ &-[E_i(A_i - B_iT_i)z_i(t)]. \end{aligned} \tag{12}$$

Substituting $u_i(t)$ with $u_i^{\mathrm{eq}}(t)$ into the LSPSwCD yields the sliding motion:

$$\begin{aligned} \dot{z}_i(t) = &(A_i - B_iT_i)z_i(t) + \left[I - B_i(E_iB_i)^{-1}E_i\right]D_iz_i(t-\tau_i) + \sum_{j=1;j\neq i}^{N}\left[I - B_i(E_iB_i)^{-1}E_i\right]H_{ij}z_j(t) \\ &+\left[I - B_i(E_iB_i)^{-1}E_i\right]w_i(z_i,t). \end{aligned} \tag{13}$$

The introduction of the following theorem makes a condition that the AISOSMC dynamic equation (11) is asymptotically stable.

Theorem 1. *The sliding motion (13) is asymptotically stable if and only if there includes symmetric positive definite matrix Q_i, P_i, $i = 1, 2, \ldots, N$, and positive scalars q, φ_i. and β_j such that the following LMIs hold:*

$$\begin{bmatrix} \Omega_i + \sum\limits_{\substack{j=1 \\ j\neq i}}^{N} \beta_j^{-1}H_{ji}^TH_{ji} & 0 & D_i^T\left[I - B_i(E_iB_i)^{-1}E_i\right]^T & Q_i\left[I - B_i(E_iB_i)^{-1}E_i\right] \\ 0 & -P_i & 0 & 0 \\ \left[I - B_i(E_iB_i)^{-1}E_i\right]D_i & 0 & -qQ_i^{-1} & 0 \\ \left[I - B_i(E_iB_i)^{-1}E_i\right]^TQ_i & 0 & 0 & -\varphi_i^{-1} \end{bmatrix} < 0, \tag{14}$$

where $\Omega_i = (A_i - B_iT_i)^TQ_i + Q_i(A_i - B_iT_i) + Q_i + P_i$.

Proof. To study and analyze stability of the sliding motion (13), we use the Lyapunov function as follows:

$$V = \sum_{i=1}^{N}\left[z_i^T(t)Q_iz_i(t) + \int_{t-\tau_i}^{t} z_i^T(s)P_iz_i(s)\mathrm{d}s\right], \tag{15}$$

where $Q_i, P_i > 0$ satisfies (14). Then, taking the time derivative of (15) and using equation (13), we obtain

$$\begin{aligned} \dot{V} = \sum_{i=1}^{N}\Big\{&\left[z_i^T(t)\left[(A_i - B_iT_i)^TQ_i + Q_i(A_i - B_iT_i)\right]z_i(t)\right. \\ &+ z_i^T(t-\tau_i)D_i^T\left[I - B_i(E_iB_i)^{-1}E_i\right]^TQ_iz_i(t) + z_i^T(t)Q_i\left[I - B_i(E_iB_i)^{-1}E_i\right]D_iz_i(t-\tau_i) \\ &+ \sum_{j=1;j\neq i}^{N} z_j^T(t)H_{ij}^T\left[I - B_i(E_iB_i)^{-1}E_i\right]^TQ_iz_i(t) + \sum_{j=1;j\neq i}^{N} z_i^T(t)Q_i\left[I - B_i(E_iB_i)^{-1}E_i\right]H_{ij}z_j(t) \\ &\left.+ w_i^T(z_i,t)\left[I - B_i(E_iB_i)^{-1}E_i\right]^TQ_iz_i(t) + z_i^T(t)Q_i\left[I - B_i(E_iB_i)^{-1}E_i\right]w_i(z_i,t)\right] \\ &+ z_i^T(t)P_iz_i(t) - z_i^T(t-\tau_i)P_iz_i(t-\tau_i)\Big\}. \end{aligned} \tag{16}$$

To apply Lemma 1 in equation (16), we obtain

$$
\begin{aligned}
\dot{V} \leq \sum_{i=1}^{N} \Big\{ & z_i^T(t)\left[\left(A_i - B_i T_i\right)^T Q_i + Q_i\left(A_i - B_i T_i\right)\right] z_i(t) \\
& + z_i^T(t-\tau_i) D_i^t \left[I - B_i\left(E_i B_i\right)^{-1} E_i\right]^T Q_i z_i(t) + z_i^T(t) Q_i \left[I - B_i\left(E_i B_i\right)^{-1} E_i\right] D_i z_i(t-\tau_i) \\
& + \sum_{j=1; j\neq i}^{N} z_i^T(t) \beta_i^{-1} Q_i \left[I - B_i\left(E_i B_i\right)^{-1} E_i\right]\left[I - B_i\left(E_i B_i\right)^{-1} E_i\right]^T Q_i z_i(t) \\
& + \sum_{j=1; j\neq i}^{N} z_j^T(t) \beta_i H_{ij}^T H_{ij} z_j(t) + z_i^T(t) P_i z_i(t) - z_i^T(t-\tau_i) P_i z_i(t-\tau_i) \\
& + \chi_i^{-1} z_i^T(t) Q_i \left[I - B_i\left(E_i B_i\right)^{-1} E_i\right]\left[I - B_i\left(E_i B_i\right)^{-1} E_i\right]^T Q_i z_i(t) + \chi_i w_i^T(z_i, t) w_i(z_i, t) \Big\}.
\end{aligned} \tag{17}
$$

Using Lemma 3 and equation (17), we get

$$
\begin{aligned}
\dot{V} \leq \sum_{i=1}^{N} \Big\{ & z_i^T(t)\left[\left(A_i - B_i T_i\right)^T Q_i + Q_i\left(A_i - B_i T_i\right)\right] z_i(t) \\
& + z_i^T(t-\tau_i) D_i^T \left[I - B_i\left(E_i B_i\right)^{-1} E_i\right]^T Q_i \left[I - B_i\left(E_i B_i\right)^{-1} E_i\right] D_i z_i(t-\tau_i) + z_i^T(t) Q_i z_i(t) \\
& + \sum_{j=1; j\neq i}^{N} z_i^T(t) \beta_i^{-1} Q_i \left[I - B_i\left(E_i B_i\right)^{-1} E_i\right]\left[I - B_i\left(E_i B_i\right)^{-1} E_i\right]^T Q_i z_i(t) \\
& + \sum_{j=1; j\neq i}^{N} z_j^T(t) \beta_i H_{ij}^T H_{ij} z_j(t) + z_i^T(t) P_i z_i(t) - z_i^T(t-\tau_i) P_i z_i(t-\tau_i) \\
& + \chi_i^{-1} z_i^T(t) Q_i \left[I - B_i\left(E_i B_i\right)^{-1} E_i\right]\left[I - B_i\left(E_i B_i\right)^{-1} E_i\right]^T Q_i z_i(t) + \chi_i w_i^T(z_i, t) w_i(z_i, t) \Big\}.
\end{aligned} \tag{18}
$$

Since $\sum_{i=1}^{N} \sum_{j=1, j\neq i}^{N} z_j^T(t) \beta_i^{-1} H_{ij}^T H_{ij} z_j(t) = \sum_{i=1}^{N} \sum_{j=1, j\neq i}^{N} z_i^T(t) \beta_j^{-1} H_{ji}^T H_{ji} z_i(t)$, we achieve that

$$
\begin{aligned}
\dot{V} \leq \sum_{i=1}^{N} \Big\{ & z_i^T(t)\Big[\left(A_i - B_i T_i\right)^T Q_i + Q_i\left(A_i - B_i T_i\right) + Q_i \\
& + \varphi_i Q_i \left[I - B_i\left(E_i B_i\right)^{-1} E_i\right]\left[I - B_i\left(E_i B_i\right)^{-1} E_i\right]^T Q_i \Big] z_i(t) \\
& + \sum_{j=1; j\neq i}^{N} z_i^T(t) \beta_j H_{ji}^T H_{ji} z_i(t) + \chi_i w_i^T(z_i, t) w_i(z_i, t) \\
& + z_i^T(t-\tau_i) D_i^T \left[I - B_i\left(E_i B_i\right)^{-1} E_i\right]^T Q_i \left[I - B_i\left(E_i B_i\right)^{-1} E_i\right] D_i z_i(t-\tau_i) \\
& + z_i^T(t) P_i z_i(t) - z_i^T(t-\tau_i) P_i z_i(t-\tau_i) \Big\},
\end{aligned} \tag{19}
$$

where $\varphi_i = \chi_i^{-1} + (N-1)\beta_i^{-1}$.

The matrix $D_i^T[I - B_i(E_iB_i)^{-1}E_i]^T Q_i[I - B_i(E_iB_i)^{-1}E_i]D_i$ is the semipositive definite. Since the $z_i(t)$ for $i = 1, 2, \ldots, N$ are independent of each other. Then, from equation (32) of paper [36], the following is true:

$$V(z_1(t-\tau_1), z_2(t-\tau_2), z_3(t-\tau_3), \ldots, z_N(t-\tau_N)) \le qV(z_1(t), z_2(t), z_3(t), \ldots, z_N(t)), \tag{20}$$

for $q > 1$ is equivalent to

$$\begin{aligned}&\sum_{i=1}^{N}\left\{z_i^T(t-\tau_i)D_i^T\left[I - B_i(E_iB_i)^{-1}E_i\right]^T Q_i\left[I - B_i(E_iB_i)^{-1}E_i\right]D_i z_i(t-\tau_i)\right\}\\ &\le q\sum_{i=1}^{N}\left\{z_i^T(t)D_i^T\left[I - B_i(E_iB_i)^{-1}E_i\right]^T Q_i\left[I - B_i(E_iB_i)^{-1}E_i\right]D_i z_i(t)\right\}.\end{aligned} \tag{21}$$

Then, we can get the following equation:

$$\begin{aligned}\dot{V} \le \sum_{i=1}^{N}\Big\{&z_i^T(t)\Big[(A_i - B_iT_i)^T Q_i + Q_i(A_i - B_iT_i) + Q_i + P_i\\ &+ \varphi_i Q_i\left[I - B_i(E_iB_i)^{-1}E_i\right]\left[I - B_i(E_iB_i)^{-1}E_i\right]^T Q_i\\ &+ qD_i^T\left[I - B_i(E_iB_i)^{-1}E_i\right]^T Q_i\left[I - B_i(E_iB_i)^{-1}E_i\right]D_i\Big]z_i(t)\\ &+ \sum_{j=1;j\ne i}^{N} z_i^T(t)\beta_j H_{ji}^T H_{ji} z_i(t) - z_i^T(t-\tau_i)P_i z_i(t-\tau_i)\\ &+ \chi_i w_i^T(z_i, t)w_i(z_i, t)\Big\}.\end{aligned} \tag{22}$$

Based on Assumption 1, the following equation can be achieved:

$$\begin{aligned}\dot{V} \le \sum_{i=1}^{N}\Big\{&z_i^T(t)\Big[(A_i - B_iT_i)^T Q_i + Q_i(A_i - B_iT_i) + Q_i + P_i\\ &+ \varphi_i Q_i\left[I - B_i(E_iB_i)^{-1}E_i\right]\left[I - B_i(E_iB_i)^{-1}E_i\right]^T Q_i\\ &+ qD_i^T\left[I - B_i(E_iB_i)^{-1}E_i\right]^T Q_i\left[I - B_i(E_iB_i)^{-1}E_i\right]D_i\Big]z_i(t)\\ &+ \sum_{j=1;j\ne i}^{N} z_i^T(t)\beta_j H_{ji}^T H_{ji} z_i(t) - z_i^T(t-\tau_i)P_i z_i(t-\tau_i) + \iota_i\Big\},\end{aligned} \tag{23}$$

where $\iota_i = \chi_i\gamma_i^2$.

Define the augmented vector

$$\begin{aligned}\Psi_i(t) &= \left[\, z_i^T(t) \;\; z_i^T(t-\tau_i)\,\right]^T,\\ \dot{V} &\le \Psi_i^T(t)\Theta_i\Psi_i(t) + \iota_i.\end{aligned} \tag{24}$$

From Lemma 2 and LMI (14), we get

$$\Theta_i = -\begin{bmatrix}\Xi_i & 0\\ 0 & -P_i\end{bmatrix} > 0, \tag{25}$$

where

$$\begin{aligned}\Xi_i = {}&(A_i - B_iT_i)^T Q_i + Q_i(A_i - B_iT_i) + Q_i + P_i + \varphi_i Q_i\left[I - B_i(E_iB_i)^{-1}E_i\right]\left[I - B_i(E_iB_i)^{-1}E_i\right]^T Q_i\\ &+ qD_i^T\left[I - B_i(E_iB_i)^{-1}E_i\right]^T Q_i\left[I - B_i(E_iB_i)^{-1}E_i\right]D_i + \sum_{j=1,j\ne i}^{N}\beta_j^{-1}H_{ji}^T H_{ji}.\end{aligned} \tag{26}$$

According to equations (23) and (25), we obtain

$$\dot{V} \leq \sum_{i=1}^{N}\left[-\lambda_{\min}(\Theta_i)\left\|\Psi_i(t)\right\|^2 + \iota_i\right], \tag{27}$$

where the constant value ι_i and the eigenvalue $\lambda_{\min}(\Theta_i) > 0$. Therefore, $\dot{V} < 0$ is achieved with $\|\Psi_i(t)\| > \sqrt{(\iota_i/\lambda_{\min}(\Theta_i))}$. Hence, the sliding motion of system (13) is asymptotically stable. □

Remark 1. The adaptive integral second-order sliding mode control design is composed of the hitting phase and the sliding phase. The proposed controller is used to force the system state trajectories to sliding phase and keep the system state trajectories on it thereafter. If the disturbance and uncertainty satisfy the matching condition $\text{rank}[B_i, w_i(z_i, t)] = \text{rank}[B_i]$, the system in the sliding mode is invariant to disturbance and uncertainty. The stability of system under matched condition is easier than mismatched condition. The proposed controller can compensate for disturbance and uncertainty directly under matched condition. Therefore, the stability of the system in the sliding mode under mismatched condition $\text{rank}[B_i, w_i(z_i, t)] \neq \text{rank}[B_i]$ has been considered and proved using LMI technique based on Lyapunov stability theory.

3.2. First-Order SMC Design

In order to guarantee the reachability of state variables to the ISS (10), the decentralized first-order integral SMC law is designed as follows [18]:

$$\begin{aligned} u_i^{\text{FOSMC}}(t) = -(E_iB_i)^{-1}\Bigg\{&\|E_i\|\|B_i\|\|T_i\|\|z_i(t)\| + \|E_i\|\|D_i\|\|z_i(t-\tau_i)\| \\ &+ \sum_{j=1;j\neq i}^{N}\|E_j\|\|H_{ji}\|\|z_i(t)\| + \|E_i\|\overline{\gamma}_i + \tilde{\varepsilon}_i\text{sat}\{\sigma_i[z_i(t)]\}\Bigg\}, \end{aligned} \tag{28}$$

where $\tilde{\varepsilon}_i > 0$ and

$$\text{sat}\{\sigma_i[z_i(t)]\} = \begin{cases} 1, & \sigma_i[z_i(t)] > 1, \\ \sigma_i[z_i(t)], & \text{When } -1 \leq \sigma_i[z_i(t)] \leq 1, \\ -1, & \sigma_i[z_i(t)] < -1. \end{cases} \tag{29}$$

Remark 2. The first-order SMC can be used to study LFC of power system under matched uncertainties. However, the parametric uncertainties not usually satisfy the matched condition in real power network. Consequently, some main constraints are necessary to design the first-order SMC to compensate the uncertainties, which can guarantee the convergence in nominal frequency and the system stability but the system trajectories cannot reach to origin point. Therefore, the second-order ISS has been used as the following part to force the system trajectory to equivalent point and to make better the transient performance.

3.3. Decentralized Adaptive Integral Second-Order Sliding Mode Control Law (DAISOSMCL) Design

In this step, the DAISOSMCL is developed for the LSPSwCD to reduce the frequency deviation. The main purpose of the proposed control scheme is to effect on the second-order derivative of the sliding variables $\sigma_i[z_i(t)]$. By using the discontinuous control signal $\dot{u}_i(t)$, it is simple to make $\sigma_i[z_i(t)]$ and $\dot{\sigma}_i[z_i(t)]$ converge to zero. So, the input control signal $u_i(t)$ of LSPSwCD can get by integrating the discontinuous signal $\dot{u}_i(t)$ to make continuous signal $u_i(t)$. Therefore, the DAISOSMCL approach removes some undesired frequency oscillations in the control signal of LSPSwCD.

We define and establish the sliding manifold (SMd) $G_i[z_i(t)]$ as

$$G_i[z_i(t)] = \dot{\sigma}_i[z_i(t)] + \varepsilon_i\sigma[z_i(t)], \tag{30}$$

$$\dot{G}_i[z_i(t)] = \ddot{\sigma}_i[z_i(t)] + \varepsilon_i\dot{\sigma}_i[z_i(t)], \tag{31}$$

where $\varepsilon_i > 0$ is a positive constant, according to equation (30); the equation (31) can be redefined as

$$\begin{aligned} \dot{G}_i[z_i(t)] = E_i&\left[A_i\dot{z}_i(t) + D_i\dot{z}_i(t-\tau_i) + B_i\dot{u}_i(t) + \sum_{j=1;j\neq i}^{N}H_{ij}\dot{z}_j(t) + \dot{w}_i(z_i,t)\right] \\ &- E_i(A_i - B_iT_i)\dot{z}_i(t) + \varepsilon_i\dot{\sigma}_i[z_i(t)]. \end{aligned} \tag{32}$$

Based on the definition of sliding surface and SMd, the continuous DAISOSMCL for LFC of a LSPSwCD is given as follows:

$$\dot{u}_i(t) = \dot{u}_i^{\mathrm{SOSMC}}(t) + \dot{u}_i^{\mathrm{adt}}(t), \tag{33}$$

where

$$\begin{aligned}\dot{u}_i^{\mathrm{SOSMC}}(t) = -\left(E_iB_i\right)^{-1}\Bigg[&\left\|E_i\right\|\left\|B_i\right\|\left\|T_i\right\|\left\|\dot{z}_i(t)\right\| + \left\|E_i\right\|\left\|D_i\right\|\left\|\dot{z}\left(t-\tau_i\right)\right\| + \sum_{j=1;j\neq i}^{N}\left\|E_j\right\|\left\|H_{ji}\right\|\left\|\dot{z}_i(t)\right\| \\ &+ \varepsilon_i\left\|\dot{\sigma}_i\left[z_i(t)\right]\right\| + \left\|E_i\right\|\partial_i + \overline{\varepsilon}_i\Bigg]\frac{G_i\left[z_i(t)\right]}{\left\|G_i\left[z_i(t)\right]\right\|}, \\ \dot{u}_i^{\mathrm{adt}}(t) = -\left(E_iB_i\right)^{-1}I\Bigg[&\widehat{\partial}_i(t)\left\|E_i\right\| + \overline{p}_i\frac{\partial_i^2}{4}\Bigg], \quad i = 1, 2, \ldots, N,\end{aligned} \tag{34}$$

where

$$\dot{\widehat{\partial}}_i(t) = p_i\left(-\overline{p}_i\widehat{\partial}_i(t) + \left\|E_i\right\|\right), \quad i = 1, 2, \ldots, N, \tag{35}$$

in which p_i and $\overline{p}_i$ are the positive constants.

Then, we have the main result which is presented as follows.

Theorem 2. *Consider the closed loop of the power systems with the DAISOSMCL (33). Then, every solution trajectory of system state is directed towards the SMd $G_i[z_i(t)]$, and once the trajectory hits the SMd $G_i[z_i(t)]$, it remains on the sliding manifold thereafter.*

Proof. The Lyapunov function is introduced as follows:

$$\overline{V}(t) = \sum_{i=1}^{N}\left\{\left\|G_i\left[z_i(t)\right]\right\| + \frac{0.5}{p_i}\widetilde{\partial}_i^{\,2}\right\}, \tag{36}$$

where $\widetilde{\partial}_i(t) = \partial_i - \widehat{\partial}_i(t)$.

So, taking the derivative of $\overline{V}(t)$, we have

$$\begin{aligned}\dot{\overline{V}} &= \sum_{i=1}^{N}\left[\frac{G_i^T\left[z_i(t)\right]}{\left\|G_i\left[z_i(t)\right]\right\|}\dot{G}_i\left[z_i(t)\right] - \widetilde{\partial}_i(t)\frac{\dot{\widehat{\partial}}_i(t)}{p_i}\right] \\ &= \sum_{i=1}^{N}\frac{G_i^T\left[z_i(t)\right]}{\left\|G_i\left[z_i(t)\right]\right\|}\Bigg\{E_i\Bigg[A_i\dot{z}_i(t) + D_i\dot{z}\left(t-\tau_i\right) + B_i\dot{u}_i(t) + \sum_{\substack{j=1\\ j\neq i}}^{N}H_{ij}\dot{z}_j(t) + \dot{w}_i\left(z_i,t\right)\Bigg] \\ &\quad - E_i\left(A_i - B_iT_i\right)\dot{z}_i(t) + \varepsilon_i\dot{\sigma}_i\left[z_i(t)\right]\Bigg\} - \sum_{i=1}^{N}\widetilde{\partial}_i(t)\frac{\dot{\widehat{\partial}}_i(t)}{p_i}.\end{aligned} \tag{37}$$

According to equation (37) and property $\|AB\| \leq \|A\|\|B\|$, we have

$$\begin{aligned}
\dot{V} &= \sum_{i=1}^{N}\left\{E_i\left[A_i\dot{z}_i(t) + D_i\dot{z}(t-\tau_i) + B_i\dot{u}_i(t) + \sum_{\substack{j=1\\ j\neq i}}^{N} H_{ij}\dot{z}_j(t) + \dot{w}_i(z_i,t)\right]\right\} \\
&\quad + \sum_{i=1}^{N}\frac{G_i^T[z_i(t)]}{\|G_i[z_i(t)]\|}E_iB_i\dot{u}_i(t) - \sum_{i=1}^{N}\widetilde{\partial}_i(t)\frac{\dot{\widehat{\partial}}_i(t)}{p_i} \\
&\leq \sum_{i=1}^{N}\left\{\|E_i\|\|B_i\|\|T_i\|\|\dot{z}_i(t)\| + \|E_i\|\|D_i\|\|\dot{z}_i(t-\tau_i)\| + \delta_i\|\dot{\sigma}_i[z_i(t)]\|\right. \\
&\quad \left. + \sum_{\substack{j=1\\ j\neq i}}^{N}\|E_i\|\left\|H_{ij}\right\|\|\dot{z}_i(t)\| + \|E_i\|\|\dot{w}_i(z_i,t)\|\right\} + \sum_{i=1}^{N}\frac{G_i^T[z_i(t)]}{\|G_i[z_i(t)]\|}E_iB_i\dot{u}_i(t) - \sum_{i=1}^{N}\widetilde{\partial}_i(t)\frac{\dot{\widehat{\partial}}_i(t)}{p_i}.
\end{aligned} \tag{38}$$

Using Assumption 1, we achieve

$$\begin{aligned}
\dot{V} &\leq \sum_{i=1}^{N}\left\{\|E_i\|\|B_i\|\|T_i\|\|\dot{z}_i(t)\| + \|E_i\|\|D_i\|\|\dot{z}_i(t-\tau_i)\| + \|E_i\|\partial_i\right. \\
&\quad \left. + \sum_{\substack{j=1\\ j\neq i}}^{N}\left\|E_j\right\|\left\|H_{ji}\right\|\|\dot{z}_i(t)\| + \varepsilon_i\|\dot{\sigma}_i[z_i(t)]\|\right\} \\
&\quad + \sum_{i=1}^{N}\frac{G_i^T[z_i(t)]}{\|G_i[z_i(t)]\|}E_iB_i\dot{u}_i(t) - \sum_{i=1}^{N}\widetilde{\partial}_i(t)\frac{\dot{\widehat{\partial}}_i(t)}{p_i}.
\end{aligned} \tag{39}$$

Using the DAISOSMCL (33) yields

$$\begin{aligned}
\dot{V} &\leq \sum_{i=1}^{N}\left[-\overline{\varepsilon}_i - \widehat{\partial}_i(t)\|E_i\| - \overline{p}_i\frac{\partial_i^2}{4} + \|E_i\|\partial_i\right] - \sum_{i=1}^{N}\left[\partial_i\|E_i\|\right] - \sum_{i=1}^{N}\left[\overline{p}_i\widehat{\partial}_i^2(t) - \overline{p}_i\partial_i\widehat{\partial}_i(t) - \widehat{\partial}_i(t)\|E_i\|\right] \\
&= \sum_{i=1}^{N}\left(-\overline{\varepsilon}_i - \overline{p}_i\frac{\partial_i^2}{4}\right) - \sum_{i=1}^{N}\left[\overline{p}_i\widehat{\partial}_i^2(t) - \overline{p}_i\partial_i\widehat{\partial}_i(t)\right] \\
&= \sum_{i=1}^{N}\left[\left(-\overline{\varepsilon}_i - \overline{p}_i\frac{\partial_i^2}{4}\right) - \sum_{i=1}^{N}\left[\overline{p}_i\left(\widehat{\partial}_I(t) - \partial_i\right)^2 - \overline{p}_i\frac{\partial_i^2}{4}\right]\right. \\
&= \sum_{i=1}^{N}-\overline{\varepsilon}_i - \sum_{i=1}^{N}\left[\overline{p}_i\left(\widehat{\partial}_I(t) - \partial_i\right)^2\right].
\end{aligned} \tag{40}$$

The above inequality implies that the system trajectories of the LSPSwCD (3) reach the SMd $G_i[z_i(t)]$ and keep it for later. □

Remark 3. The SMC is capable to reach the bounded system stability and is able to maintain within a range to converge zero, and then the power system is notably stable. Equation

(10) indicates that the integral term $\int_0^t E_i(A_i - B_iT_i)z_i(\tau)d\tau$ is only reflected in the proposed DAISOSMCL (33). Therefore, the control law (33) is to improve the performance of steady state error in comparison with the traditional integral SMC.

4. Results and Discussion

Based on the interconnected time-delay power network, the four cases are offered to prove the strength of the suggested AISOSMC approach under the required conditions such as the different load disturbances and the parameter variations. A LSPSwCD is analyzed to explain the robustness and effectiveness of the suggested AISOSMC approach. The parameters of LSPSwCD were given in [22] as shown Table 1.

Case 1. The presented LFC based on AISOSMC is used to compare with the traditional LFC approach under the same condition in [22]. The proposed LFC based on AISOSMC has been examined with different step load disturbance effect on the thermal power plant with nominal parameter conditions. We have considered the system parameters of matched uncertainties. In this case, the load disturbances are $\Delta P_{d1} = 0.02, \Delta P_{d2} = 0.015$, and $\Delta P_{d3} = 0.01$ (p.u.MW) at $t_1 = 0$ in three areas of the LSPS. The frequency deviations of $\Delta f_1, \Delta f_2$, and Δf_3 for the LSPS with delay-time as $\tau_i = 0.1$ s ($i = 1, 2, 3$) are displayed in Figures 2–4 which are the tie-line power deviation and control input signal for three-area power networks. It is easy to realize that the transient responses achieved in the proposed LFC based on AISOSMC is faster in the settling time, but it has less magnitude of overshoot percentage with the proposed recent controller in [22].

Remark 4. Due to Figures 2 to 4, the testing simulation results in this part are appointed in Table 2. In particular, the report of results can show in an effective comparison while the time-delay communication is considered for the large-scale power network. Therefore, the system performance of the suggested AISOSMC is well balanced, and frequency variation is zero after 1s.

Case 2. As the same matched parameter uncertainty of the three areas is used in [22], the cosine function around the nominal operation point is used to verify the usefulness and robustness of the suggested controller to load disturbance. The step load disturbances in LSPSwCD are chosen as $\Delta P_{d1} = 0.01$ p.u.MW at $t_1 = 0$ s and $\Delta P_{d2} = 0.015$ p.u.MW at $t_2 = 0$ and $\Delta P_{d3} = 0.02$ p.u.MW at $t_3 = 0$.

$$\Delta A_1 = \begin{bmatrix} 0 & 0 & 0 & 0 & 0 \\ 0 & 0 & 0 & 0 & 0 \\ -2.26\cos(t) & 2\cos(t) & -2.604\cos(t) & 3\cos(t) & 0 \\ 0 & 0 & 0 & 0 & 0 \\ 0 & 0 & 0 & 0 & 0 \end{bmatrix}$$

and the matched uncertainty among subsystems are assumed the same as [22] and $\Delta A_1 = \Delta A_2 = \Delta A_3$.

TABLE 1: The parameters of three-area power system.

Areas	T_{Pi}	K_{Pi}	T_{Ti}	T_{Gi}	R_i	K_{Ei}	K_{Bi}	K_{ij}
1	20	120.0	0.30	0.080	2.4	10.0	0.41	0.550
2	25	112.5	0.33	0.072	2.7	9.0	0.37	0.650
3	20	115.0	0.35	0.070	2.5	7.1	0.40	0.545

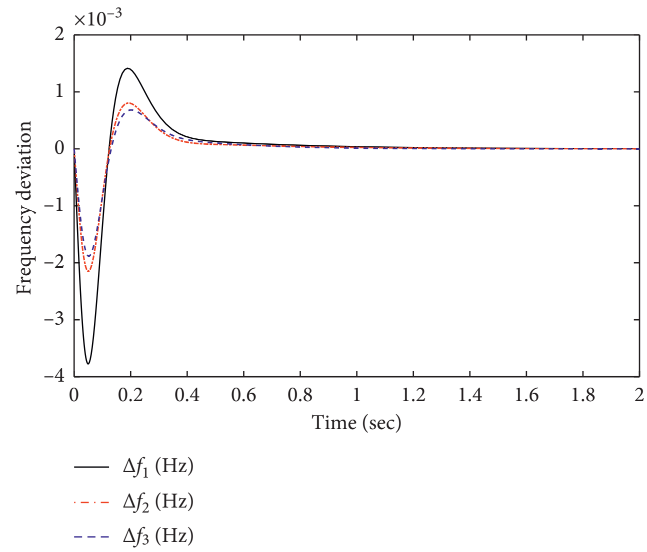

FIGURE 2: Frequency variation of the system.

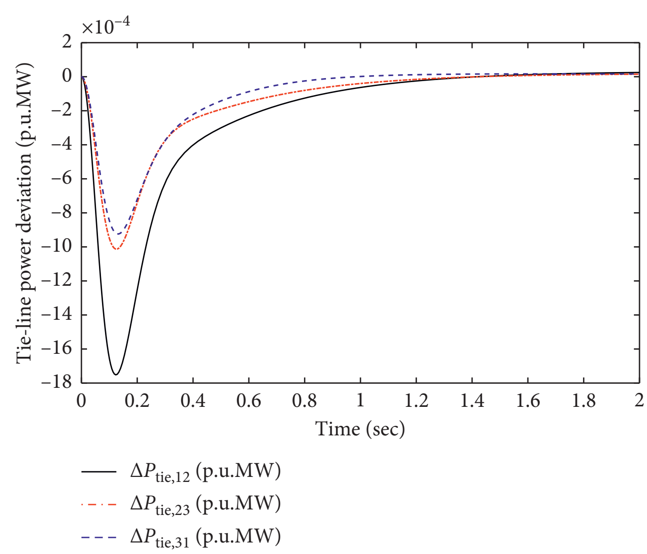

FIGURE 3: Tie-line variation of the system.

Figure 5 indicates that the proposed LFC based on AISOSMC to three areas with CDs, $\tau_i = 0.1$; the frequency deviation reaching to zero is about 2 s much smaller than the comparative LFC used in [22] within 10 s. Figure 6 plots the control signal of the system under matched uncertainty. The tie-line power variations of three areas with LFC based on

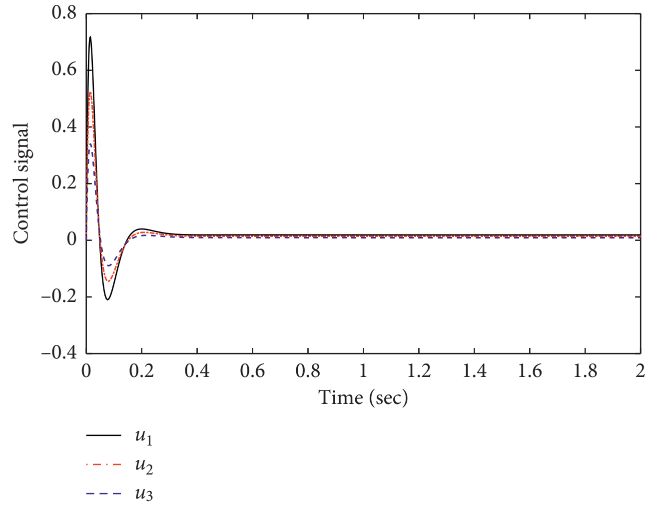

Figure 4: Control signal of the system.

Table 2: Comparison between the proposed AISOSMC method with the previous method in [22].

Kinds of controller	The AISOSMC approach		Previous load frequency controller in [22]	
Parameters	T_s (s)	Max. $O.\ S$ (pu)	T_s (s)	Max. $O.\ S$ (pu)
Δf_1	1	-3.8×10^{-3}	2	-3.8×10^{-3}
Δf_2	1	-2.1×10^{-3}	2	-2.1×10^{-3}
Δf_3	1	-1.9×10^{-3}	2	-2.0×10^{-3}

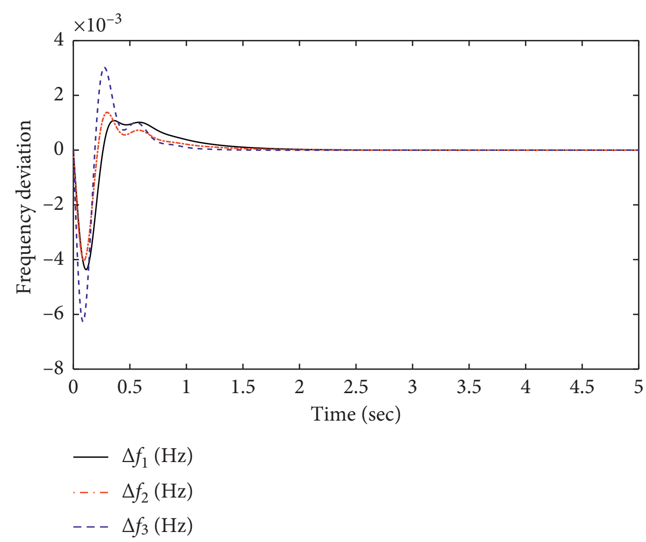

Figure 5: Frequency deviation of the system under matched uncertainty.

AISOSMC always are kept with maximum value as 4.7×10^{-3} p.u.MW in Figure 7.

Remark 5. In this configuration, the influents of time-delay signals are considered to compare with the simulation result in [22], the DAISOSMCL based on the offered switching surface can not only make better in the response speed but also upgrade the transient performance to decrease the overshoot percentage. So, the designed control method is powerful and strong enough to regulate and control the matched parameter uncertainties of multiarea interconnected time-delay grids.

Case 3. In this case, the load disturbances are$\Delta P_{d1} = 0.01$ p.u.MW at $t_1 = 0$ s, $\Delta P_{d2} = 0.02$ p.u.MW at $t_2 = 0$, and $\Delta P_{d3} = 0.03$ p.u.MW at $t_3 = 0$ in area 1, area 2, and area 3,

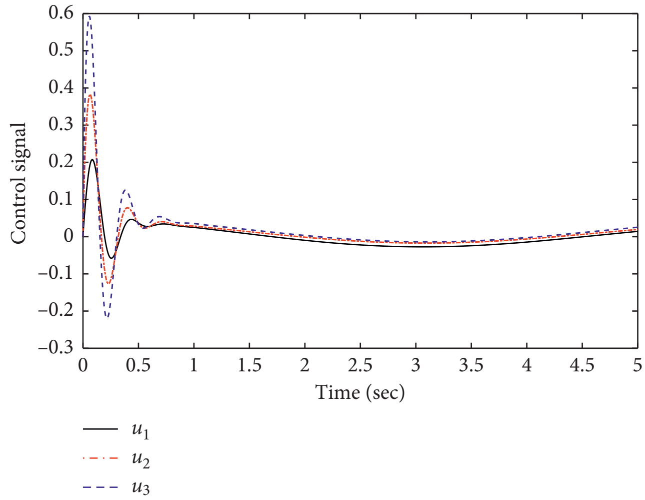

FIGURE 6: Control signal of the system under matched uncertainty.

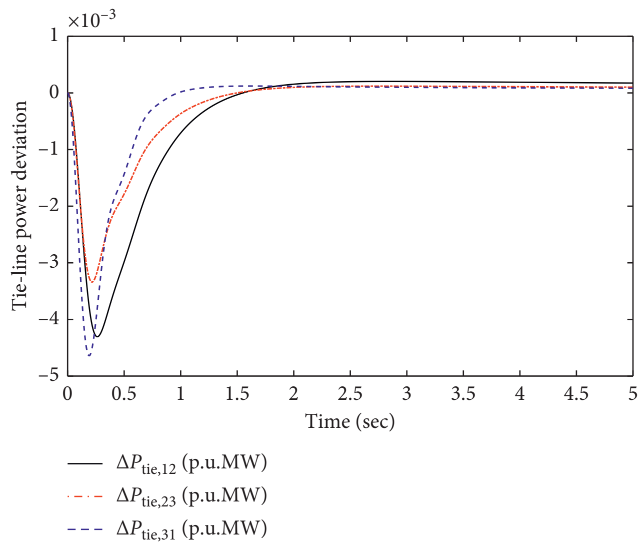

FIGURE 7: Tie-line deviation of the system under matched uncertainty.

respectively. We discuss about the impact of mismatch parameter uncertainty in the state matrix and values of the time-delay as $\tau_i = 0.2\,\text{s}$ $(i = 1, 2, 3)$ for all the subsystems of LSPSwCD which are designed as follows:

$$\Delta A_1 = \begin{bmatrix} 0 & \Delta f_1 & 0 & 0 & 0 \\ \sin(t) & 0 & 0 & 0 & 0 \\ 0 & 0 & \cos(t) & \cos(t) & 0 \\ 0 & 0 & 0 & 0 & \cos(t) \\ \cos(t) & 0 & 0 & 0 & 0 \end{bmatrix}, \qquad (41)$$

$$\Delta A_2 = \Delta A_3 = \Delta A_1.$$

The mismatch interconnected between subsystems is designed as follows:

$$\Delta H_{12} = \begin{bmatrix} 0 & 0 & 0 & 0 & 0.178\cos(t) \\ 0 & 0 & 0 & 0 & 0 \\ 0 & 0 & 0 & 0 & 0 \\ 0 & 0 & 0 & 0 & -0.296\sin(t) \\ 0 & 0 & 0 & 0 & 0 \end{bmatrix}, \qquad (42)$$

$$\Delta H_{12} = \Delta H_{23} = \Delta H_{31}.$$

The frequency variation in LSPSwCD is displayed in Figure 8, the control input signal is presented in Figure 9, and tie-line power variation is displayed in Figure 10. We observe the system performance, the transient response makes achievement by the proposed control scheme which reduces the amplitude of over/undershoot percentage. It is

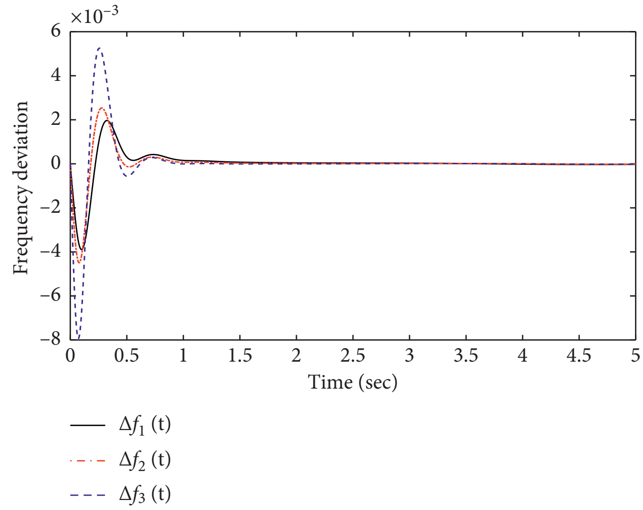

Figure 8: Frequency deviation of the system under mismatched uncertainty.

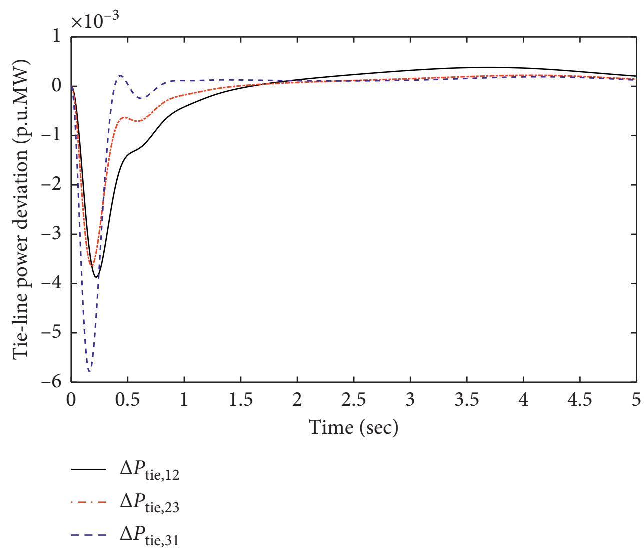

Figure 9: Tie-line deviation of the system under mismatched uncertainty.

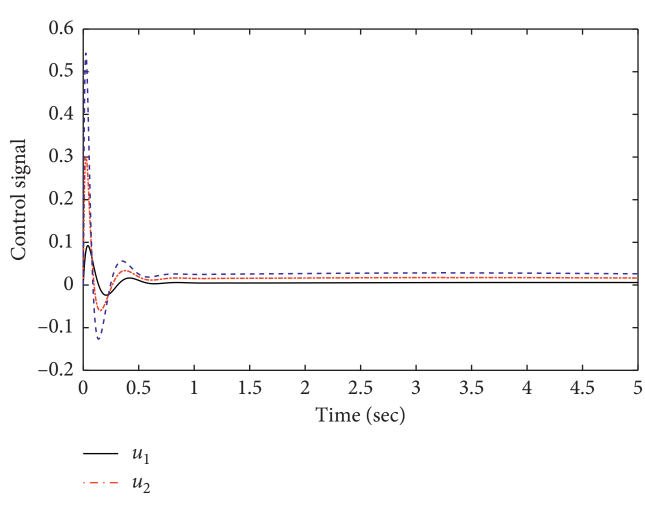

Figure 10: Control signal of the system under mismatched uncertainty.

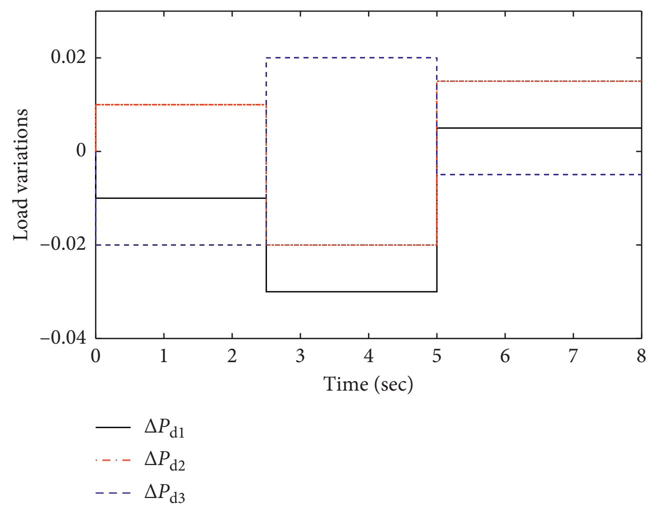

Figure 11: Load variations of three-area power network.

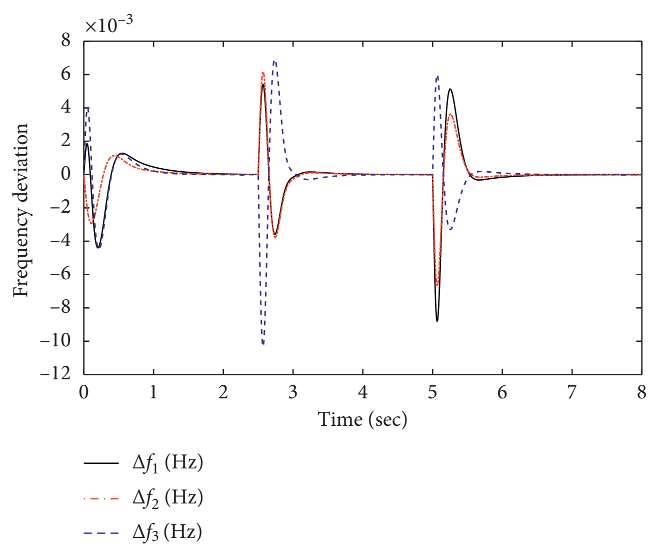

Figure 12: Frequency variation of the system under load variations and mismatched uncertainty.

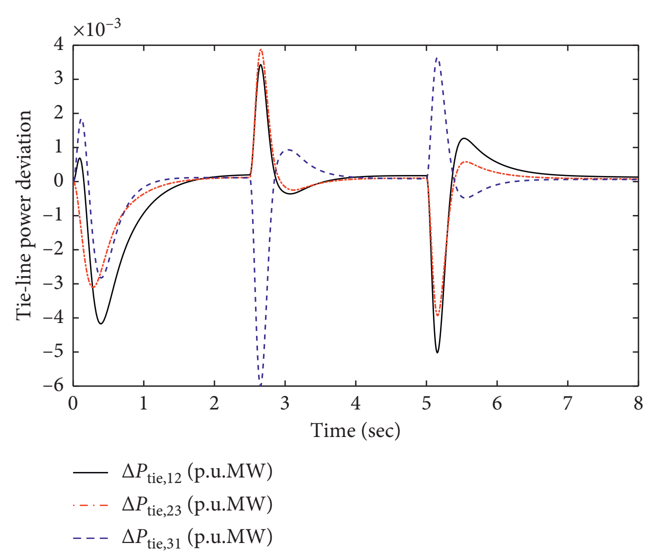

Figure 13: Tie-line power variation of the system under load variations and mismatched uncertainty.

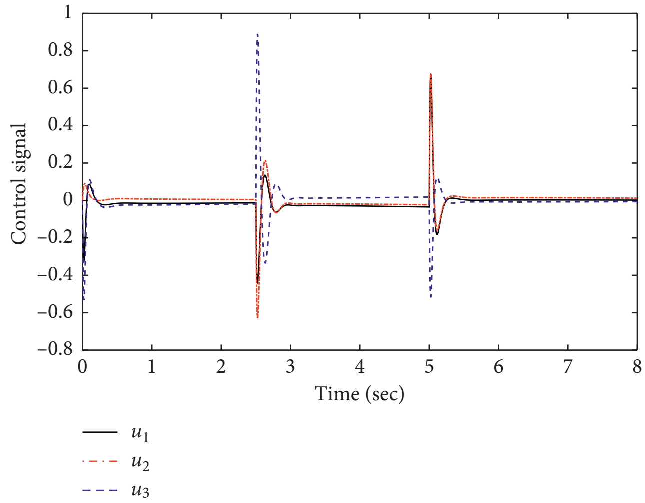

Figure 14: Control signal of the system under load variations and mismatched uncertainty.

to be clear that the input control signal is to converge quickly and drive the tie-line power variation and frequency variation to zero. Therefore, the suggested controller carried out with better design, both in terms of reducing the over/undershoots and minimizing the settling time in comparison to [21, 22].

Remark 6. In this case, though considering to the influence of the mismatched uncertainty of LSPSwCD, the performance of proposed controller still is kept powerful and stable. Therefore, the proposed ISOSMC is proved to be suitable for LSPSwCD. The approach given in [21, 22] cannot be applied for the LSPSwCD of this case.

Case 4. In this case, the nominal parameters of LSPSwCD are in Table 1 and the same parameters with previous cases. However, in the practical power system, the parameters of LSPSwCD are always varied due to different operation conditions. Therefore, the parameters of LSPSwCD are selected to vary by ±20% synchronously from their normal values. The delay time is 0.2 s and load variation is as shown in Figure 11. The tie-line power and frequency deviation decay quickly as observed in Figures 12 and 13. The control signal has been presented in Figure 14. It is to be clear that the proposed control scheme is able to handle with the time-delay and random load disturbances. It is proved that the proposed DAISOSMCL has the good quality and achievement to reject disturbance with small control signal.

Remark 7. In this approach, the structure of LSPSwCD is more general than the approach given in [28–33]. Also, the system responses in terms of convergence of frequency variation and power exchange error are improved by using the proposed DAISOSMCL. Therefore, the proposed design controller is suitable for LFC of LSPSwCD.

5. Conclusions

In this paper, the LFC based on decentralized adaptive integral second-order sliding mode control (DAISOSMC) has been developed for the large-scale power system with communication delays (LSPSwCD), load variations, and parameter uncertainties. It is shown that the proposed DAISOSMCL ensures the finite time reachability of the system states and moreover the dynamics of LSPSwCD in the sliding mode is asymptotically stable under certain conditions. To the best of our knowledge, this is the first time the DAISOSMC approach is designed for LFC of the LSPSwCD. The report of simulation results indicates that the proposed DAISOSMC approach can adequately make less the deviation of the tie-line power and frequency variation of LSPSwCD. The suggested control scheme is therefore proved to be more effective for the LSPSwCD implementation.

Data Availability

Data used to support the findings of this study are included within the article.

Conflicts of Interest

The authors declare no conflicts of interest.

Acknowledgments

This research was funded by the Foundation for Science and Technology Development of Ton Duc Thang University (FOSTECT), website: http://fostect.tdtu.edu.vn, under Grant FOSTECT.2017.BR.05.

References

[1] D. Guha, P. K. Roy, and S. Banerjee, “Load frequency control of interconnected power system using grey wolf

optimization," *Swarm and Evolutionary Computation*, vol. 27, pp. 97–115, 2016.

[2] M. Ma, C. Zhang, X. Liu, and H. Chen, "Distributed model predictive load frequency control of the multi-area power system after deregulation," *IEEE Transactions on Industrial Electronics*, vol. 27, pp. 5129–5139, 2016.

[3] K. Liao and Y. Xu, "A robust load frequency control scheme for power systems based on second-order sliding mode and extended disturbance observer," *IEEE Transactions on Industrial Informatics*, vol. 14, no. 7, pp. 3076–3086, 2017.

[4] K. P. S. Parmar, S. Majhi, and D. P. Kothari, "LFC of an interconnected power system with multi-source power generation in deregulated power environment," *International Journal of Electrical Power & Energy Systems*, vol. 57, pp. 277–286, 2014.

[5] V. Çelik, M. T. Özdemir, and K. Y. Lee, "Effects of fractional-order PI controller on delay margin in single-area delayed load frequency control systems," *Journal of Modern Power Systems and Clean Energy*, vol. 7, no. 2, pp. 380–389, 2019.

[6] R. Dey, S. Ghosh, G. Ray, and A. Rakshit, "H∞ load frequency control of interconnected power systems with communication delays," *International Journal of Electrical Power & Energy Systems*, vol. 42, no. 1, pp. 672–684, 2012.

[7] Y. Cui, G. Shi, L. Xu, X. Zhang, and X. Li, "Decentralized *H*∞ load frequency control for multi-area power systems with communication uncertainties," *In Advanced Computational Methods in Energy, Power, Electric Vehicles, and Their Integration*, vol. 4, pp. 429–438, 2017.

[8] H. Zhang, J. Liu, and S. Xu, "H-infinity load frequency control of networked power systems via an event-triggered scheme," *IEEE Transactions on Industrial Electronics*, vol. 67, no. 8, pp. 7104–7113, 2019.

[9] S. Prasad, S. Purwar, and N. Kishor, "H -infinity based non-linear sliding mode controller for frequency regulation in interconnected power systems with constant and time-varying delays," *IET Generation, Transmission & Distribution*, vol. 10, no. 11, pp. 2771–2784, 2016.

[10] M. N. Anwar and S. Pan, "A new PID load frequency controller design method in frequency domain through direct synthesis approach," *International Journal of Electrical Power & Energy Systems*, vol. 67, pp. 560–569, 2015.

[11] S. Sondhi and Y. V. Hote, "Fractional order PID controller for load frequency control," *Energy Conversion and Management*, vol. 85, pp. 343–353, 2014.

[12] S. Saxena and Y. V. Hote, "Decentralized PID load frequency control for perturbed multi-area power systems," *International Journal of Electrical Power & Energy Systems*, vol. 81, pp. 405–415, 2016.

[13] N. Kouba, M. Menaa, K. Tehrani, and M. Boudour, "Optimal tuning for load frequency control using ant lion algorithm in multi-area interconnected power system," *Intelligent Automation & Soft Computing*, vol. 25, no. 2, pp. 279–294, 2019.

[14] H. A. Yousef, K. AL-Kharusi, M. H. Albadi, and N. Hosseinzadeh, "Load frequency control of a multi-area power system: an adaptive fuzzy logic approach," *IEEE Transactions on Power Systems*, vol. 29, no. 4, pp. 1822–1830, 2014.

[15] M. Gheisarnejad and M. H. Khooban, "Design an optimal fuzzy fractional proportional integral derivative controller with derivative filter for load frequency control in power systems," *Transactions of the Institute of Measurement and Control*, vol. 41, no. 9, pp. 2563–2581, 2019.

[16] D. Xu, J. Liu, X. Yan, and W. Yan, "A novel adaptive neural network constrained control for multi-area interconnected power system with hybrid energy storage," *IEEE Transactions on Industrial Electronics*, vol. 65, no. 8, pp. 6625–6634, 2017.

[17] Z. Sun, F. Xing, S. Che, B. Hu, and D. Sun, "Designing and optimization of fuzzy sliding mode controller for nonlinear systems," *Computers, Materials & Continua*, vol. 61, no. 1, pp. 119–128, 2019.

[18] Q. Zhu and Z. Yang, "Intelligent power compensation system based on adaptive sliding mode control using soft computing and automation," *Computer Systems Science and Engineering*, vol. 34, no. 4, pp. 179–189, 2019.

[19] K. Khayati, "Multivariable adaptive sliding-mode observer-based control for mechanical systems," *Canadian Journal of Electrical and Computer Engineering*, vol. 38, no. 3, pp. 253–265, 2015.

[20] D. Qian and G. Fan, "Neural-network-based terminal sliding mode control for frequency stabilization of renewable power systems," *IEEE/CAA Journal of Automatica Sinica*, vol. 5, no. 3, pp. 706–717, 2018.

[21] B. Le Ngoc Minh, V. V. Huynh, T. M. Nguyen, and Y. W. Tsai, "Decentralized adaptive double integral sliding mode controller for multi-area power systems," *Mathematical Problems in Engineering*, vol. 2018, Article ID 2672436, 11 pages, 2018.

[22] M. K. Sarkar, A. Dev, P. Asthana, and D. Narzary, "Chattering free robust adaptive integral higher order sliding mode control for load frequency problems in multi-area power systems," *IET Control Theory & Applications*, vol. 12, no. 9, pp. 1216–1227, 2018.

[23] S. Prasad, S. Purwar, and N. Kishor, "Non-linear sliding mode load frequency control in multi-area power system," *Control Engineering Practice*, vol. 61, pp. 81–92, 2017.

[24] D. Qian, S. Tong, and X. Liu, "Load frequency control for micro hydro power plants by sliding mode and model order reduction," *Automatika*, vol. 56, no. 3, pp. 318–330, 2015.

[25] J. Guo, "Application of full order sliding mode control based on different areas power system with load frequency control," *ISA Transactions*, vol. 92, pp. 23–34, 2019.

[26] J. Guo, "Application of a novel adaptive sliding mode control method to the load frequency control," *European Journal of Control*, vol. 12, pp. 3050–3071, 2020.

[27] Y. Mi, Y. Fu, C. Wang, and P. Wang, "Decentralized sliding mode load frequency control for multi-area power systems," *IEEE Transactions on Power Systems*, vol. 28, no. 4, pp. 4301–4309, 2013.

[28] S. K. Pradhan and D. K. Das, "H∞ Load frequency control design based on delay discretization approach for interconnected power systems with time delay," *Journal of Modern Power Systems and Clean Energy*, vol. 2, pp. 1–10, 2020.

[29] C. Fu and W. Tan, "Decentralized load frequency control for power systems with communication delays via active disturbance rejection," *IET Generation, Transmission & Distribution*, vol. 12, no. 6, pp. 1397–1403, 2017.

[30] C. Fu, C. Wang, L. Y. Wang, and D. Shi, "An alternative method for mitigating impacts of communication delay on load frequency control," *International Journal of Electrical Power & Energy Systems*, vol. 119, Article ID 105924, 2020.

[31] A. E. Onyeka, Y. Xing-Gang, Z. Mao, B. Jiang, and Q. Zhang, "Robust decentralized load frequency control for interconnected time delay power systems using sliding mode techniques," *IET Control Theory and Applications*, vol. 14, no. 3, pp. 470–480, 2019.

[32] Y. Sun, Y. Wang, Z. Wei, G. Sun, and X. Wu, "Robust H∞ load frequency control of multi-area power system with time delay: a sliding mode control approach," *IEEE/CAA Journal of Automatica Sinica*, vol. 5, no. 2, pp. 610–617, 2017.

[33] Y. Mi, X. Hao, Y. Liu et al., "Sliding mode load frequency control for multi-area time-delay power system with wind power integration," *IET Generation, Transmission & Distribution, Transmission & Distribution*, vol. 11, no. 18, pp. 4644–4653, 2017.

[34] S. Boyd, E. L. Ghaoui, E. Feron, and V. Balakrishna, "Linear matrix inequalities in system and control theory," *Society for Industrial and Applied Mathematics*, vol. 15, 1994.

[35] V. V. Huynh, Y.-W. Tsai, and P. V. Duc, "Adaptive output feedback sliding mode control for complex interconnected time-delay systems," *Mathematical Problems in Engineering*, vol. 2015, Article ID 239584, 15 pages, 2015.

[36] X.-G. Yan, S. K. Spurgeon, and C. Edwards, "Global decentralised static output feedback sliding-mode control for interconnected time-delay systems," *IET Control Theory & Applications*, vol. 6, no. 2, pp. 192–202, 2012.

TELKOMNIKA Telecommunication, Computing, Electronics and Control
Vol. 19, No. 3, June 2021, pp. 1001~1009
ISSN: 1693-6930, accredited First Grade by Kemenristekdikti, Decree No: 21/E/KPT/2018
DOI: 10.12928/TELKOMNIKA.v19i3.18777

Extended state observer based load frequency controller for three area interconnected power system

Van Van Huynh[1], Phong Thanh Tran[2], Tuan Anh Tran[3], Dao Huy Tuan[4], Van-Duc Phan[5]
[1,2,3,4]Faculty of Electrical and Electronics Engineering, Ton Duc Thang University, Ho Chi Minh City, Vietnam
[5]Faculty of Automobile Technology, Van Lang University, Ho Chi Minh City, Vietnam

Article Info

Article history:

Received Jun 15, 2020
Revised Nov 23, 2020
Accepted Dec 5, 2020

Keywords:

Area control error
Full-order state observer design
Load frequency control
Multi-area power system
Tie-line area in power system

ABSTRACT

In this paper, we develop a new extended state variable observer based load frequency controller (LFC) scheme for three-area interconnected power systems. The extended state observerbased load frequency controllers are developed which utilize disturbance estimation techniques. The propose control approach assures that the fluctuating things of the load frequencies reaches to a safer range and the load frequencies can also be made at a very minimal not to have an effect on power quality and power flow in multi-area interconnected power system. The results of the simulations using MATLAB/SIMULINK done did not only address that the proposed newly control method works effectively but also change powerfully the parameter variations of the interconnected areas of the power system. Especially, it works very well to limit disturbances impact on interconnected areas in the system. Therefore, the performance of interconnected power system under different multi-conditions is simulated with the new control method to demonstrate the feasibility of the system.

Corresponding Author:

Dao Huy Tuan
Faculty of Electrical and Electronics Engineering
Ton Duc Thang University,
19 Nguyen Huu Tho Street, Tan Phong Ward, District 7, Ho Chi Minh City, Vietnam
Email: daohuytuan@tdtu.edu.vn

1. INTRODUCTION

In multi-area interconnected power system, stability of frequency is a very signify indicator of power quality as the loads of the tie-line multiple areas keep increasing and changing progressively. Meanwhile, load disturbances can occur suddenly which can cause deviations in tie-line power area exchange and nominal frequencies instability [1, 2]. Load frequency control for years now has been one of the basic robust control mechanisms in larger scale power electric systems with interconnected area and the main criteria of the load frequency control is to keep and maintain the system frequency uniform at its nominal value during and when there is load change. A large power electric system can be divided and separated into several load frequency area control that is interconnected by tie-lines and it relates to operational procedures to be followed in the event of major faults or of tie-line power. Generally, the main goal and duty of load frequency control is simply to adjust the frequencies of the separated areas and to simultaneously modulate power flowing across the tie-lines according with the agreement of an inter area power system. Moreover, load frequency control normalizes frequency, maintains dynamics, and makes quality assurance of the power supply, requires the use of load frequency controller (LFC) scheme in [3-6].

Load frequency control is also greatly significant in power electric system operational for delivering reliable and efficient power without poor quality. Therefore, a novel control technique needs to be developed in other to achieve LFC aims, thereby, maintaining and sustaining reliability of the electrical power system in multi-areas. In order to solve above problems, researchers and control engineers have proposed wide range of methods of state-of-the-art load frequency controllers to be applied in multi-area interconnected power system [7-15]. That is, the method of adaptive control proposed to take care parameter variation in [7-9]. But it cannot lead strongly to a general solution to the problem faced by LFC in power system. Many kinds of control technique such as proportional integral (PI) or proportional integral derivative (PID) controller for LFC were used. In the prescribed environment, some factors like uncertainties make it difficult to apply the above-mentioned LFC techniques in practice, which implies [10-12] to introduce some internal model control to design PID type LFC controllers. In [10] proposed fuzzy Proportional Integral controllers for LFC of power electric systems. While the different methods show that it is possible to enhance the performance of LFC in specified environments. The PID controller proposed in [11] combined with new structure shown to be robustly and to enhance the damping of the power electric system tracing with a small significant step changes in load. The strategy of tuning is based solely on the maximum peak resonance of the system specifications in [12]. However, most conventional PID controllers with gains fixed was designed under nominal system operating conditions, the selected mode of its gains is usually always on trial and error with no analytically methods of determining its parameters optimally which sometimes fails to give out the best and accurate control schemes and performance over a wider range of system operating conditions and exhibits, thereby, a poor dynamic response and performance during operations. Some of the control methods need to apply the full-state of the control area as feedback input while some will lead to higher-order controllers, these factors were too complex to be understood and comprehended by control and electrical engineers in [13, 14].

Among various control techniques mentioned, the optimal control with state feedback technique is one of the best options. Also, a robust decentralized linear controller was applied in [15-19]. Another control technique to look at is the “sliding mode control (SMC)”. Sliding mode control techniques is another better way and approach to solve LFC problem. SMC has ofcoursed been applied for LFC in power electric system in [19-25] to achieve fast response and robustly performance in the power network, this method is a nonlinear control strategy with a famous rule. It is also insensitive perhaps to changes of the plant parameters and as well improves system transient control performance. The above approaches are achieved under assumption that all system state variables are to be measurable and readily available for feedback. In fact, not all system state variables are measurable for feedbacks, and then we need to estimate the state variables that are not unmeasurable. Estimating unmeasurable state variables is often called observation in [21-25]. This scheme can adapt the unknown upper bounds of matched nonlinearity and disturbance. It gets not only the system state trajectories accomplishment but also satisfies in parameters of the system state errors. The work illustrated above, achieve a significant result related to LFC’s of interconnected power systems applying various control techniques.

However, there are some limitations of the above approaches. Firstly, the disturbances are not truncated from the output points in steady state. Secondly, the controller gains are not set to be extremely high to attenuate disturbances of unknown boundaries. Thirdly, the controller is designed in accordance to the nominal transfer function of the plant when a no-load disturbance is considered. In order to solve the above limitations, in the paper we develop newly extended state observer-based LFC scheme for three-area interconnected power electric system. The main contributions of the paper are as following:

- Extended state observer is first design to estimate the unmeasurable system state variables and also the load uncertainties.
- The extended state observer-based load frequency controllers are developed which utilize disturbance estimation techniques. Thus, the controller gains are not set to be extremely high to attenuate disturbances of unknown boundaries, which is very useful in load frequency controller design.
- The simulation results indicate that the proposed newly method improves the system dynamic response which provides a system control to adapt and meet up the LFC requirement.

The other parts of the proposed paper are structured in the following. A mathematical dynamics model of three-area power electric system is presented in section 2. The following proposed extended observer controller is showed in section 3. The results of the various simulations of three-area power system applying the proposed newly based control approaches are described in section 4. Lastly, conclusions are discussed in section 5.

2. THE MATHEMATICAL MODEL OF THREE-AREA INTERCONNECTED POWER SYSTEM MODEL

At first, we analyze LFC of power system of multi-areas. Figure 1 illustrates three-area interconnected systems [16] as desmostrated. The sole mission in the research work is simply to examine the various tie-line areas in power systems in other to control the frequencies of the following multi-area and to regulate simultaneously power flowing throught the tie-lines according to an inter-area operating agreement. In three-area networks, each control area is indicated by a turbine, generator, and governor system. The tie-line power in the interconnected three-area must be considered to generate the increment power stability equation of each power system area, since there is power flow in each area through the tie line.

From [3, 4], the tie line power increment that is out of area is:

$$\Delta P_{tie_i(p.u)} = 2\pi \sum_{\substack{j\in N \\ j\neq i}} T_{ij}\left(\int \Delta f_i \, dt - \int \Delta f_j \, dt\right) \tag{1}$$

To achieve balance between interconnected control areas, the frequency deviation and tie-line power fluctuation are detected in other to determine the area control error (ACE) of each control area. The ACE can be expressed for each control area as a linearity combination of tie-line power flunctuation and frequency deviation.

$$ACE_i = \Delta P_{tie_i} + K_{B_i}\Delta f_i \tag{2}$$

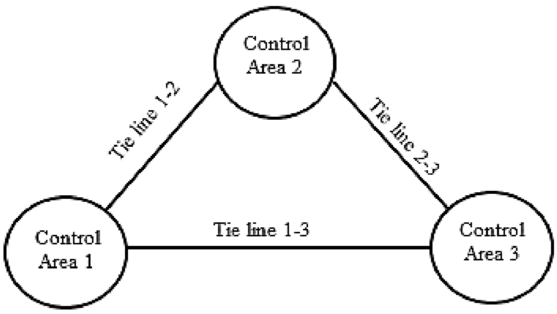

Figure 1. A simplified sketch of 3-area interconnected power system

A power network is stable if and only if $ACE_i = 0$. In other words: Δf_iandΔP_{tie_i}tend towards zero over a short time frame. In practice, a typical interconnected generation system is nonlinearity and also dynamics; application of the linearity model is allowable in the LFC power problems that is, in modern's power system, small changes in load is always anticipated under normal operations in [18, 26-28].

$$\Delta \dot{f}_1(t) = -\frac{1}{T_{P_1}}\Delta f_1(t) + \frac{K_{P_1}}{T_{P_1}}\Delta P_{m1}(t) - \frac{k_{ps1}}{T_{ps1}}\Delta P_{tie1}(t) - \frac{k_{ps1}}{T_{ps1}}\Delta P_{tie3}(t) - \frac{k_{ps1}}{T_{ps1}}\Delta P_{d_1} \tag{3}$$

$$\Delta \dot{P}_{m1}(t) = -\frac{1}{T_{T_1}}\Delta P_{m1}(t) + \frac{1}{T_{T_1}}\Delta P_{v1}(t) \tag{4}$$

$$\Delta \dot{P}_{v1}(t) = -\frac{1}{R_1 T_{G_1}}\Delta f_1(t) - \frac{1}{T_{G_1}}\Delta P_{v1}(t) + \frac{1}{T_{G_1}}u_1 \tag{5}$$

$$\Delta \dot{E}_1(t) = B_1\Delta f_1(t) + \Delta P_{tie1}(t) + \Delta P_{tie3}(t) \tag{6}$$

$$\Delta \dot{P}_{tie1}(t) = 2\pi T_{12}\Delta f_1(t) - 2\pi T_{12}\Delta f_2(t) + 2\pi T_{13}\Delta f_1(t) - 2\pi T_{13}\Delta f_3(t) \tag{7}$$

$$\Delta \dot{f}_2(t) = -\frac{1}{T_{P_2}}\Delta f_2(t) + \frac{K_{P_2}}{T_{P_2}}\Delta P_{m2}(t) - \frac{k_{ps2}}{T_{ps2}}\Delta P_{tie1}(t) - \frac{k_{ps1}}{T_{ps1}}\Delta P_{tie2}(t) - \frac{k_{ps1}}{T_{ps1}}\Delta P_{d_2} \tag{8}$$

$$\Delta \dot{P}_{m2}(t) = -\frac{1}{T_{T_2}}\Delta P_{m2}(t) + \frac{1}{T_{T_2}}\Delta P_{v2}(t) \tag{9}$$

$$\Delta \dot{P}_{v2}(t) = -\frac{1}{R_2 T_{G_2}}\Delta f_2(t) - \frac{1}{T_{G_2}}\Delta P_{v2}(t) + \frac{1}{T_{G_2}}u_2 \tag{10}$$

$$\Delta\dot{E}_2(t) = B_2\Delta f_2(t) + \Delta P_{tie1}(t) + \Delta P_{tie2}(t) \quad (11)$$

$$\Delta\dot{P}_{tie2}(t) = 2\pi T_{12}\Delta f_2(t) - 2\pi T_{12}\Delta f_1(t) + 2\pi T_{23}\Delta f_2(t) - 2\pi T_{23}\Delta f_3(t) \quad (12)$$

$$\Delta\dot{f}_3(t) = -\frac{1}{T_{P_3}}\Delta f_3(t) + \frac{k_{P3}}{T_{P_3}}\Delta P_{m3}(t) - \frac{k_{ps3}}{T_{ps3}}\Delta P_{tie2}(t) - \frac{k_{ps3}}{T_{ps3}}\Delta P_{tie3}(t) - \frac{k_{ps3}}{T_{ps3}}\Delta P_{d_3} \quad (13)$$

$$\Delta\dot{P}_{m3}(t) = -\frac{1}{T_{T_3}}\Delta P_{m3}(t) + \frac{1}{T_{T_3}}\Delta P_{v3}(t) \quad (14)$$

$$\Delta\dot{P}_{v3}(t) = -\frac{1}{R_3 T_{G_3}}\Delta f_3(t) - \frac{1}{T_{G_3}}\Delta P_{v3}(t) + \frac{1}{T_{G_3}}u_3 \quad (15)$$

$$\Delta\dot{E}_3(t) = B_3\Delta f_3(t) + \Delta P_{tie2}(t) + \Delta P_{tie3}(t) \quad (16)$$

$$\Delta\dot{P}_{tie3}(t) = 2\pi T_{23}\Delta f_3(t) - 2\pi T_{23}\Delta f_2(t) + 2\pi T_{13}\Delta f_3(t) - 2\pi T_{13}\Delta f_1(t) \quad (17)$$

The matrix form shows in the dynamic equations from (3) to (17), the there-area interconnected power system described by Figure 2 which can be written and expressed in state-space representation below:

$$\dot{x}(t) = \tilde{A}x(t) + \tilde{B}u(t) + \tilde{F}\Delta P(t) \quad (18)$$

where $x(t) \in R^n$ is the state vector, $u(t) \in R^m$ is the control vector, and $\tilde{A}, \tilde{B}, \tilde{F}$is constant matrix equivalent ith of each area. ($\tilde{A} \in R^{n\times n}$, $\tilde{B} \in R^{n\times m}$, $F \in R^{n\times k}$).

$$\tilde{B} = \begin{bmatrix} 0 & 0 & \frac{1}{T_{G1}} & 0 & 0 & 0 & 0 & 0 & 0 & 0 & 0 & 0 & 0 & 0 & 0 \\ 0 & 0 & 0 & 0 & 0 & 0 & 0 & \frac{1}{T_{G2}} & 0 & 0 & 0 & 0 & 0 & 0 & 0 \\ 0 & 0 & 0 & 0 & 0 & 0 & 0 & 0 & 0 & 0 & 0 & 0 & \frac{1}{T_{G3}} & 0 & 0 \end{bmatrix}^T$$

$$\tilde{F} = \begin{bmatrix} -\frac{K_{p1}}{T_{P1}} & 0 & 0 & 0 & 0 & 0 & 0 & 0 & 0 & 0 & 0 & 0 & 0 & 0 & 0 \\ 0 & 0 & 0 & 0 & 0 & -\frac{K_{P2}}{T_{P2}} & 0 & 0 & 0 & 0 & 0 & 0 & 0 & 0 & 0 \\ 0 & 0 & 0 & 0 & 0 & 0 & 0 & 0 & 0 & 0 & -\frac{K_{P3}}{T_{P3}} & 0 & 0 & 0 & 0 \end{bmatrix}^T$$

$$\tilde{A} = \begin{bmatrix} -\frac{1}{T_{ps1}} & \frac{k_{ps1}}{T_{ps1}} & 0 & 0 & -\frac{k_{ps1}}{T_{ps1}} & 0 & 0 & 0 & 0 & 0 & 0 & 0 & 0 & 0 & -\frac{k_{ps1}}{T_{ps1}} \\ 0 & -\frac{1}{T_{T1}} & \frac{1}{T_{T1}} & 0 & 0 & 0 & 0 & 0 & 0 & 0 & 0 & 0 & 0 & 0 & 0 \\ -\frac{1}{R_1T_{G1}} & 0 & -\frac{1}{T_{G1}} & \frac{1}{T_{G1}} & 0 & 0 & 0 & 0 & 0 & 0 & 0 & 0 & 0 & 0 & 0 \\ B_1 & 0 & 0 & 0 & 1 & 0 & 0 & 0 & 0 & 0 & 0 & 0 & 0 & 0 & 1 \\ 2\pi(T_{12}+T_{13}) & 0 & 0 & 0 & 0 & -2\pi T_{12} & 0 & 0 & 0 & 0 & -2\pi T_{13} & 0 & 0 & 0 & 0 \\ 0 & 0 & 0 & 0 & \frac{k_{ps2}}{T_{ps2}} & -\frac{1}{T_{ps2}} & \frac{k_{ps2}}{T_{ps2}} & 0 & 0 & -\frac{k_{ps2}}{T_{ps2}} & 0 & 0 & 0 & 0 & 0 \\ 0 & 0 & 0 & 0 & 0 & 0 & -\frac{1}{T_{T2}} & \frac{1}{T_{T2}} & 0 & 0 & 0 & 0 & 0 & 0 & 0 \\ 0 & 0 & 0 & 0 & 0 & -\frac{1}{R_2T_{G2}} & 0 & -\frac{1}{T_{G2}} & \frac{1}{T_{G2}} & 0 & 0 & 0 & 0 & 0 & 0 \\ 0 & 0 & 0 & 0 & 1 & B_2 & 0 & 0 & 0 & 1 & 0 & 0 & 0 & 0 & 0 \\ -2\pi T_{21} & 0 & 0 & 0 & 0 & 2\pi(T_{21}+T_{23}) & 0 & 0 & 0 & 0 & -2\pi T_{23} & 0 & 0 & 0 & 0 \\ 0 & 0 & 0 & 0 & 0 & 0 & 0 & 0 & 0 & -\frac{k_{ps3}}{T_{ps3}} & -\frac{1}{T_{ps3}} & \frac{k_{ps3}}{T_{ps3}} & 0 & 0 & \frac{k_{ps3}}{T_{ps3}} \\ 0 & 0 & 0 & 0 & 0 & 0 & 0 & 0 & 0 & 0 & 0 & -\frac{1}{T_{T3}} & \frac{1}{T_{T3}} & 0 & 0 \\ 0 & 0 & 0 & 0 & 0 & 0 & 0 & 0 & 0 & 0 & -\frac{1}{R_3T_{G3}} & 0 & -\frac{1}{T_{G3}} & \frac{1}{T_{G3}} & 0 \\ 0 & 0 & 0 & 0 & 0 & 0 & 0 & 0 & 0 & 1 & B_3 & 0 & 0 & 0 & 1 \\ -2\pi T_{13} & 0 & 0 & 0 & 0 & -2\pi T_{23} & 0 & 0 & 0 & 0 & 2\pi(T_{31}+T_{32}) & 0 & 0 & 0 & 0 \end{bmatrix}$$

$$\dot{x}(t) = [\Delta f_1(t) \quad \Delta P_{m1}(t) \quad \Delta P_{v1}(t) \quad \Delta E_1(t) \quad \Delta P_{tie1}(t) \quad \Delta f_2(t) \quad \Delta P_{m2}(t) \quad \Delta P_{v2}(t) \quad \Delta E_2(t) \quad \Delta P_{tie2}(t) \quad \Delta f_3(t) \quad \Delta P_{m3}(t) \quad \Delta P_{v3}(t) \quad \Delta E_3(t) \quad \Delta P_{tie3}(t)]^T$$

Because it is tedious to determine the values of the system exact parameters of $\tilde{A}, \tilde{B}, \tilde{F}$due to nonlinearity and dynamics of a power electric system, the dynamic model (18) is revised to the nominal parameters and parameter variations separations in the following:

$$\dot{x}(t) = [A + \Delta A(x,t)]x(t) + [B + \Delta B(x,t)]u(t) + \tilde{F}\Delta P_D(t) \quad = Ax(t) + Bu(t) + f(x,t) \quad y(t) = Cx(t) \tag{19}$$

where A, B is the exact values of $\tilde{A}, \tilde{B}$; the unknown matrices $\Delta A(x,t)$ and $\Delta B(x,t)$ denotes by their time-variant system of parametric variations; and $f(x,t)$ is called the lumped uncertainties and we can also denote by (20).

$$f(x,t) = \Delta A(x,t)x(t) + \Delta B(x,t)u(t) + \tilde{F}\Delta P_D(t) \tag{20}$$

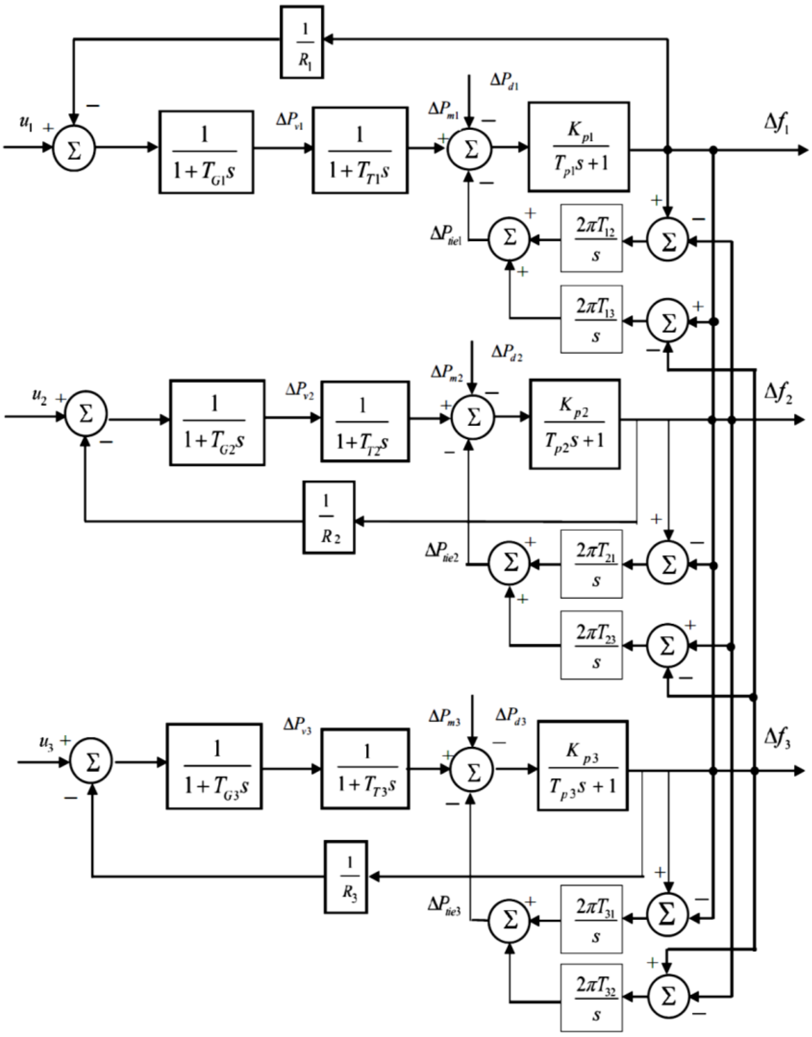

Figure 2. Block diagram of 3-area LFC system

3. PROPOSED EXTENDED OBSERVER-BASED LOAD FREQUENCY CONTROLLER

The proposed newly control technique that is, states observer performs the functions by estimating the state variables of the systems typically the output and control variables. State observers can be designed and applied only when the observability required condition is satisfied. First, we extend lumped uncertainty as an additional state variable to design and initiate an extended observer-based load frequency controller in the system as (21).

$$x_{n+1}(t) = f(x,t) \tag{21}$$

Then, the three-area power system in (19) can be written as:

$$\dot{\bar{x}}(t) = \bar{A}\bar{x}(t) + \bar{B}u(t) + Eh(t)\bar{y}(t) = \bar{C}\bar{x}(t) \quad (22)$$

$$h(t) = \frac{df(x,t)}{dt} \quad (23)$$

where: $\bar{x}(t) = \begin{bmatrix} x(t) \\ x_{n+1}(t) \end{bmatrix}$; $\bar{A} = \begin{bmatrix} A_{n\times n} & I_{n\times n} \\ 0_{n\times n} & 0_{n\times n} \end{bmatrix}$; $\bar{B} = \begin{bmatrix} B_{n\times m} \\ 0_{n\times m} \end{bmatrix}$; $E = \begin{bmatrix} 0_{n\times n} \\ I_{n\times n} \end{bmatrix}$; $\bar{C} = [C_{r\times n}, \quad 0_{r\times n}]$.

With regards to the state observers discussed, we will apply the notation $\hat{\bar{x}}$ to indicate the vector observed state. The vector $\hat{\bar{x}}$ of the observed state is used and applied in the state feedback to initiate the desired and required control vector. If we call the state$\bar{x}$is approximated to state, $\widehat{\bar{x}}$ the dynamical model:

$$\dot{\hat{\bar{x}}}(t) = \bar{A}\hat{\bar{x}}(t) + \bar{B}u(t) + L(\bar{y}(t) - \hat{\bar{y}}(t))\dot{\hat{\bar{y}}}(t) = \bar{C}\hat{\bar{x}}(t) \quad (24)$$

The states observed have u and $\bar{y}$ as the input and output signal. The gain L of state observer is chosen so that the eigenvalue of $\bar{A} - L\bar{C}$lie in the desired locations in the left-half s-plane. The control input is chosen as;

$$u(t) = -K\hat{\bar{x}} = [\widetilde{K} \quad \widehat{K}]\hat{\bar{x}} \quad (25)$$

where, $\widetilde{K}$is the feedback control gain to be chosen so that the eigenvalues of $A - B\widetilde{K}$lie in specific locations in the left-half s-plane and the lumped uncertainty compensation gain $\widetilde{K}$is designed:

$$\widehat{K} = [C(A - B\widetilde{K})^{-1}B]^{-1}C(A - B\widetilde{K})^{-1}F \quad (26)$$

Combine (22) and (24), the estimation error of state observers $e(t) = \bar{x}(t) - \hat{\bar{x}}(t)$ can be revised by:

$$\dot{e}(t) = \bar{A}e(t) - L(\bar{y}(t) - \hat{\bar{y}}(t)) + Eh(t) = (\bar{A} - L\bar{C})e(t) + Eh(t) \quad (27)$$

Denote $Eh(t)$ by $u(t)$ and using final-value theorem, we have:

$$\lim_{t\to\infty} e(t) = \lim_{t\to\infty}(s(sI - (\bar{A} - L\bar{C}))^{-1}U(s) = \lim_{t\to\infty}(sI - (\bar{A} - L\bar{C}))^{-1} \times \lim_{s\to\infty} sU(s) = \lim_{s\to\infty}(sI - (\bar{A} - L\bar{C}))^{-1} \times \lim_{t\to\infty} u(t) \quad (28)$$

Sine$\lim_{s\to\infty}(sI - (\bar{A} - L\bar{C}))^{-1}$is bounded and $\lim_{t\to\infty} u(t) = 0$. Therefore, estimation error of state observers is: $e(t) = \bar{x}(t) - \hat{\bar{x}}(t)$ is asymptotically stable.

Remark 1: If the system states are not measurable, then the estimation of the lumped uncertainty and the parameters of system states can be applying in the design control. Therefore, the composite control law will be designed as in (21).

Remark 2: It is noted that the lumped uncertainty cannot be attenuated completely and totally from the state equation no matter what controller was designed. In this approach, one of the most recent achievable objectives is simply to truncate the disturbances at the output point in steady state by the application of the composite control law. Therefore, the limitations recorded by other control strategies in this paper [21-25] has been solved.

4. SIMULATION RESULTS

In the case to evaluate the newly extended state observer approach, two simulations by using the MATLAB/SIMULINK software are given as following:

Simulation 1: The parameters of the three-area interconnected power system were seen as given in [16, 17].

Case 1. For the simulation at this instance in case 1, the parameters with there nominal values of the 3-area power network are applied. At this point, we assume zero disturbances occuring on the given system, i.e., $f(x,t) = 0$. Therefore, the frequency flunctuation or deviations of the 3-area interconnected power network according to the instance of case 1 whereby, applying the newly extended state observer controller are displayed in the results of simulation in Figure 3 to Figure 4. In Figure 3, the frequency deviation approaches to zero mark at exactly 1.5s. Consequently, Figure 4 shows tie line power deviation getting to zero mark with the designed extended state observer controller. By comparing the simulation results from the newly extended observer controller with results given shown in [16, 17], the newly extended state observer controller was able to assure fast response to the system and also capable of truncate smaller overshoots.

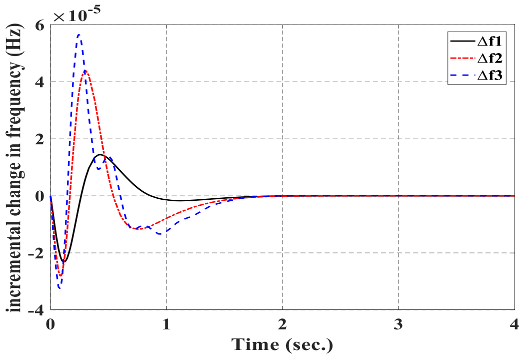

Figure 3. Frequency deviations (Hz) of the three-area without disturbances

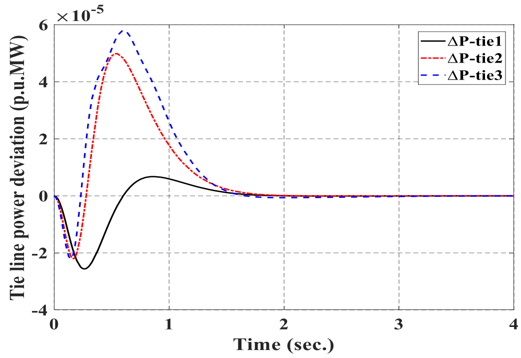

Figure 4. Tie line power deviation for power system without disturbances

Case 2: Designing a controller with the aim and capacity to perform excellent within an uncertainty environment of power networks are always the main goal of several electrical and control engineers. In this case, the proposed extended state observer controller was applied under uncertainties with matched parameters and load disturbance in other to examine the network performance under matched parameter uncertainties and load disturbances. The load disturbance; $\Delta P_{d_1}(t) = 0.02$ pu, $\Delta P_{d_2}(t) = 0.015$ pu, and $\Delta P_{d_3}(t) = 0.01$ pu were presume to take place at area 1, area 2, and area 3 accordingly. The responses in the closed-loop for everyone of the control area applying the extended state observer controller and the controller given in [16, 17] are shown in Figure 5 and Figure 6.

Figure 5, Figure 6 and Table 1 show clearly that the responses of the system are not only great to deal with overshoot-problems, but also ensures quick and fast settling period as matched-to the recent approach in [16, 17]. In the same condition, it is seen that frequency deviation converged to zero in about 1.6s with the newly proposed extended state observer that is, satisfied requiment of LFC problems.

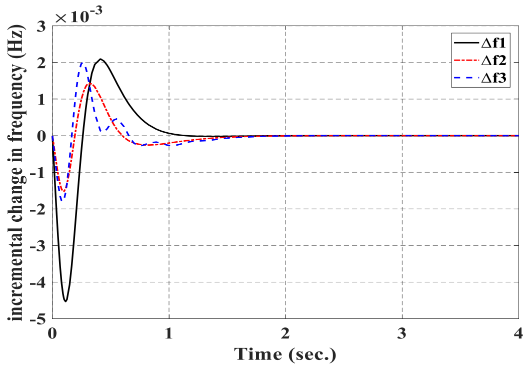

Figure 5. Frequency deviations (Hz) of the three-area under matched uncertainties and load disturbances

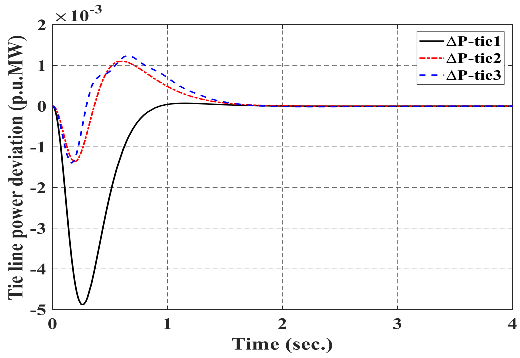

Figure 6. Tie line power deviation under matched uncertainties and load disturbances

Table 1. Setting time - T_s and Max.O.S (maximun- over-shoot-calculation) of ELFC and DLFC

Kinds of controller	Extended state observer-based load frequency controller (ELFC)		Decentralized load frequency controller (DLFC) [16]	
Parameters	T_s *(s)*	*Max.O. S (pu)*	T_s *(s)*	*Max.O. S (pu)*
Δf_1	1.5	2.1×10^{-3}	7.5	3.7×10^{-3}
Δf_2	2.0	1.45×10^{-3}	7.5	3.8×10^{-3}
Δf_3	1.8	2.0×10^{-3}	7.5	4.0×10^{-3}

Simulation 2: The practical power system with load disturbance is considered in this example. The conditions and parameters using in this simulation are the same with the recent research in [18]. Figure 7 and Figure 8 show that the proposed extended state observer control scheme has faster response and lesser signicant overshoot in comparing the previous control in [18].

Remark 3: By matching-up the results of the simulation for the two simulations above, the newly extended state observer-based load frequency controllers displayed robustness and fast response to distortions and disturbance occurring on the system correlated with variant of the matched uncertainties and load disturbances used for simulations.

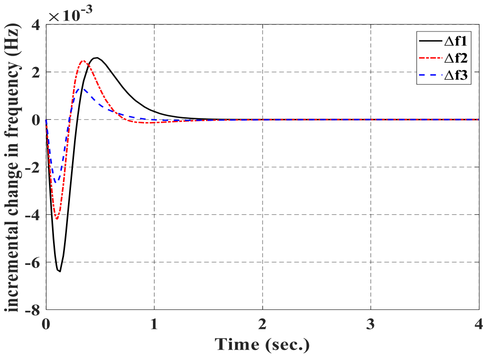

Figure 7. Frequency deviations of the three-area under matched uncertainties and load disturbances

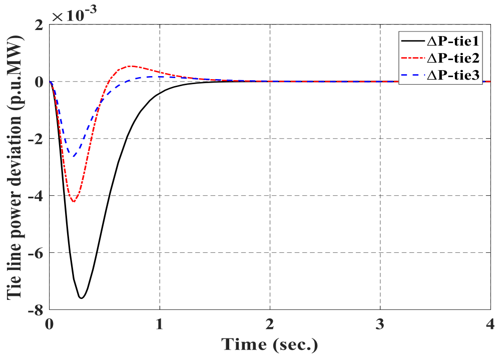

Figure 8. Tie line power deviation under matched uncertainties and load disturbances

5. CONCLUSION

In this paper, the newly extended state observer for LFC for an interconnected system is performed. In real environment, some various state variables are not measurable in load frequency control system for instance area control error or combination of area control errors. To resolve this unmeasurable state variables problem, the extended state observer is proposed for estimating the unmeasurable state variables. The extended state observer-based load frequency controllers utilize disturbance estimation techniques; thus, the controller gains are not set to be extremely high to attenuate disturbances of unknown boundaries, which is very useful in load frequency controller design. Therefore, it can be concluded that the application of the proposed extended state observer for load frequency controls of interconnected power system can operate effectively in practical sight. By using MATLAB/SIMULINK, the simulation results above present that the newly method improves the dynamics responses of the system and provide designs for new LFC's system that satisfies the LFC requirements. In the future work, we tend to design extended state observer for robust LFC's in multi-area power systems combined with renewable energy systems.

ACKNOWLEDGMENT

This research is funded by Foundation for Science and Technology Development of Ton Duc Thang University (FOSTECT), website: http://fostect.tdtu.edu.vn, under Grant FOSTECT.2017.BR.05

REFERENCES

[1] Fu C., & Tan W., "Decentralised Load Frequency Control for Power Systems with Communication Delays via Active Disturbance Rejection," *IET Generation, Transmission & Distribution*, vol. 12, no. 6, pp. 1751-8687, 2018.
[2] Zhang Y., & Yang T., "Decentralized Switching Control Strategy for Load Frequency Control in Multi-Area Power Systems with Time Delay and Packet Losse," *IEEE Access*, vol. 8, pp. 15838-15850, Jan 2020.
[3] Devendra K. Chaturvedi, "Techniques and its Applications in Electrical Engineering" *Springer*, 2008.
[4] Vijay Vittal, James D. McCalley, Paul M. Anderson, A. A. Fouad P., "Power System Control and Stability," *Wiley 3rd Edition.*, October 2019.
[5] Guha D., Roy P. K., & Banerjee S., "Load Frequency Control of Interconnected Power System Using Grey Wolf Optimization," *Swarm and Evolutionary Computation*, vol. 27, pp. 97-115, Apr 2016.
[6] Yousef H. A., AL-Kharusi K., Albadi M. H., & Hosseinzadeh N., "Load Frequency Control of a Multi-Area Power System: An Adaptive Fuzzy Logic Approach," *IEEE Transactions on Power Systems*," vol. 29, no. 4, pp.1822-1830, Jan 2014.
[7] Zeng G. Q., Xie X. Q., & Chen M. R., "An Adaptive Model Predictive Load Frequency Control Method for Multi-Area Interconnected Power Systems with Photovoltaic Generations," *Electrical Power and Energy System*, vol. 10, no. 11, pp. 1-23, Nov 2017.
[8] Beni Rehiara A., Yorino N., Sasaki Y., & Zoka Y., "An Adaptive Load Frequency Control Based on Least Square Method," *Advances in Modelling and Control of Wind and Hydrogenerators*, vol. 49, pp. 220, 2020.

[9] Dong L. L, Zhang Y., Gao Z. Q., "A Robust Decentralized Load Frequency Controller for Interconnected Power Systems," *ISA Transactions*, vol. 51, no. 3, pp. 410-419, May 2012.
[10] Gheisarnejad M., & Khooban, M. H., "Design an Optimal Fuzzy Fractional Proportional Integral Derivative Controller with Derivative Filter for Load Frequency Control in Power Systems," *Transactions of the Institute of Measurement and Control*, vol. 41, no. 9, pp. 1-19, Jan 2019.
[11] Anwar M. N., and Pan S., "A New PID Load Frequency Controller Design Method in Frequency Domain Through Direct Synthesis Approach," *Electric Power and Energy Systems*, vol. 67, pp. 560-569, May 2015.
[12] Sonkar P., & Rahi O. P., "Tuning of Modified PID Load Frequency Controller for Interconnected System with Wind Power Plant via IMC Tuning Method," 2017 *4th IEEE Uttar Pradesh Section International Conference on Electrical*, *Computer and Electronics*, Jan 2018.
[13] K. Liao and Y. Xu, "A Robust Load Frequency Control Scheme for Power Systems Based on Second-Order Sliding Mode and Extended Disturbance Observer," *IEEE Transactions on Industrial Informatics*, vol. 14, no. 7, pp. 3076-3086, July 2018.
[14] Zheng Y., Liu J., Liu X., Fang D., & Wu L., "Adaptive Second-Order Sliding Mode Control Design for a Class of Nonlinear Systems with Unknown Input," *Mathematical Problems in Engineering*, vol. 2015, no. 1, pp.1-7, 2015.
[15] Y. Sun, Y. Wang, Z. Wei and X. Wu, "Robust H∞ Load Frequency Control of Multi-Area Power System with Time Delay: A Sliding Mode Control Approach," *IEEE/CAA Journal of Automatica Sinica*, vol. 5, no. 2, pp. 610-617, 2018.
[16] Yang M., Yang F., Chengshan W., and Peng W., "Decentralized Sliding Mode Load Frequency Control for Multi-Area Power Systems," *IEEE Transactions on Power System*, vol. 28, no. 4, pp. 4301-4309, Aug 2013.
[17] Muthana T. Alrifai, Mohamed F. Hassan, Mohamed Zribi., "Decentralized Load Frequency Controller for A Multi-Area Interconnected Power System," *Electrical Power and Energy Systems*, vol. 33, no. 2, pp.198-209, 2011.
[18] Yang Mi *et al.*, "The Sliding Mode Load Frequency Control for Hybrid Power System Based on Disturbance Observer," *Electrical Power and Energy Systems*, vol. 74, pp. 446-452, Jan 2016.
[19] D. Qian, and G. Fan, "Neural-Network-Based Terminal Sliding Mode Control for Frequency Stabilization of Renewable Power Systems," *IEEE/CAA Journal of Automatica Sinica*, vol. 5, no. 3, pp. 706-717, Apr 2018.
[20] S. Trip *et al.*, "Passivity-Based Design of Sliding Modes for Optimal Load Frequency Control," *IEEE Transactions on Control Systems Technology*, vol. 27, no. 5, pp.1893-1906, 2019.
[21] Li H. Y., Shi P., Yao D. Y., Wu L. G., "Observer-Based Adaptive Sliding Mode Control of Nonlinear Markovian Jump Systems," *Automatica*, vol. 64, pp.133-142, Mar 2016.
[22] Khayati K., "Multivariable Adaptive Sliding-Mode Observer-Based Control for Mechanical Systems," *Canadian Journal of Electrical and Computer Engineering*, vol. 38, no. 3, pp.253-265, Nov 2015.
[23] Wang B., Shi P., Karimi H. R., & Lim C. C, "Observer-Based Sliding Mode Control for Stabilization of a Dynamic System with Delayed Output Feedback,"*Mathematical Problems in Engineering*, vol. 3, pp. 1-6, Sep 2013.
[24] Ouassaid M., Maaroufi M., & Cherkaoui M, "Observer-Based Nonlinear Control of Power System Using Sliding Mode Control Strategy," *Electric Power Systems Research*, vol. 84, no. 1, pp. 135-143, Jan 2012.
[25] Yang B., Yu T., Shu H., Yao W., & Jiang L., "Sliding-Mode Perturbation Observer-Based Sliding-Mode Control Design for Stability Enhancement of Multi-Machine Power Systems," *Transactions of the Institute of Measurement and Control*, vol. 41, no. 15, pp. 1418-1434, Jul 2018.
[26] Prasad S., Purwar S., & Kishor N., "Non-Linear Sliding Mode Load Frequency Control in Multi-Area Power System," *Control Engineering Practice*, vol. 61, pp. 81-92, Dec 2017.
[27] Dianwei Q., Shiwen T., Xiangjie L., "Load Frequency Control for Micro Hydro Power Plants by Sliding Mode and Model Order Reduction," *Automatika*, vol. 56, no. 3, pp. 318-330, Jan 2017.
[28] Dianwei Q., Shiwen T., Hong L., Xiangjie L., "Load Frequency Control by Neural-Network-Based Integral Sliding Mode for Nonlinear Power Systems with Wind Turbines," *Neurocomputing*, vol. 173, pp. 875-885, Jan 2016.

electronics

Article

Highly Robust Observer Sliding Mode Based Frequency Control for Multi Area Power Systems with Renewable Power Plants

Van Van Huynh [1], Bui Le Ngoc Minh [2,3], Emmanuel Nduka Amaefule [1,*], Anh-Tuan Tran [1] and Phong Thanh Tran [1]

1 Faculty of Electrical & Electronics Engineering, Ton Duc Thang University, Ho Chi Minh City 700000, Vietnam; huynhvanvan@tdtu.edu.vn (V.V.H.); trananhtuan.st@tdtu.edu.vn (A.-T.T.); tranthanhphong.st@tdtu.edu.vn (P.T.T.)
2 Faculty of Electrical and Electronics Engineering, Ho Chi Minh City University of Technology and Education, Ho Chi Minh City 700000, Vietnam; 1726002@student.hcmute.edu.vn
3 Faculty of Industrial Engineering, Tien Giang University, Tien Giang Province 840000, Vietnam
* Correspondence: ndukaamaefuleemmanuel.st@tdtu.edu.vn

Abstract: This paper centers on the design of highly robust observer sliding mode (HROSM)-based load frequency and tie-power control to compensate for primary frequency control of multi-area interconnected power systems integrated with renewable power generation. At first, the power system with external disturbance is model in the state space form. Then the state observer is used to estimate the system states which are difficult or expensive to measure. Secondly, the sliding mode control (SMC) is designed with a new single phase sliding surface (SPSS). In addition, the whole system asymptotic stability is proven with Lyapunov stability theory based on the linear matrix inequality (LMI) technique. The new SPSS without reaching time guarantees rapid convergence of high transient frequency, tie-power change as well as reduces chattering without loss of accuracies. Therefore, the superiority of modern state-of-the-art SMC-based frequency controllers relies on good practical application. The experimental simulation results on large interconnected power systems show good performance and high robustness against external disturbances when compared with some modern state of art controllers in terms of overshoots and settling time.

Keywords: load frequency control; renewable plants; sliding mode control

Citation: Huynh, V.V.; Minh, B.L.N.; Amaefule, E.N.; Tran, A.-T.; Tran, P.T. Highly Robust Observer Sliding Mode Based Frequency Control for Multi Area Power Systems with Renewable Power Plants. *Electronics* **2021**, *10*, 274. https://doi.org/10.3390/electronics10030274

Academic Editor: Davide Astolfi
Received: 15 December 2020
Accepted: 21 January 2021
Published: 24 January 2021

1. Introduction

High level penetration of renewable generation systems into interconnected multi-area generation systems will make power sectors more economical and reliable to deliver power to end users. Since each area consists of increase numbers of generating sets, renewable power sets can be used as reservation for peak load demand. However, external disturbances such as intermittent generation associated with renewable sources and continuous load demand on one area can cause a high spike of frequency and tie-power flow in the multi-area [1]. Thus, frequency spike can damage power system equipment; can cause wear and tear of steam actuator valve, affects primary frequency control, etc. To solve this issue, load frequency control (LFC) is applied. LFC is one vital aspect of automatic generation control. Its duty is to compensate for primary control to ensure frequency and tie line flow at scheduled value [1]. Its design application in power systems follows two approaches, i.e., centralized and decentralized. The decentralized approach is commonly used since each local area is controlled on its own without interfering with neighboring areas. Furthermore, different techniques have been designed for LFC studies in various power systems. In the literature, early existing LFC methods were proportional-integral (PI) and proportional-integral-derivative (PID). These traditional schemes benefit in simple structures and performed well under parameters' nominal operating points. However, they are degraded at variable points [2–4]. The degradation of PI and PID were solved with the development of intelligent control such as artificial neural network (ANN) and fuzzy logic given in [5–8]. Moreover, with the use of fuzzy logic, determining the accurate fuzzy set for tuning traditional control method is challenging. Optimal control techniques were applied with fuzzy logic to improve fuzzy set decision [9]. So far, both PI and intelligent control were combined to improve traditional LFC method [10–15]. Meanwhile, PI tuning has further improved with new algorithms given in [16–18]. Nevertheless, the major problem with interconnected power systems integrated with renewable power sets is that they result in a higher increase of the system order, the number of tuning control parameters, uncertainties in the system states and large external disturbances. When the power system is modeled, the external disturbance most especially cannot be avoided. Therefore, the requirement of the LFC must be robust against external disturbance in reality. Thus, sliding mode control (SMC) is used nowadays due to it robust against disturbance [19]. However, SMC based LFC is not new to control engineers. Various SMC-based LFC for power systems are briefly discussed. SMC was designed to control frequency, tie-power and area control errors for three area power system consisting of non-reheat, reheat and hydro-plant distributed in the areas [19]. Discrete-time SMC based LFC was constructed for controlling areas in power system with full state feedback [20]. A nonlinear SMC was proposed for mismatch power system with wind farms [21]. Furthermore, optimal LFC based SMC was designed for nonlinear power system [22]. Adaptive SMC based LFC for power systems are discussed in [23–26]. However, the SMC controllers discussed in the literature were designed with all power system states assumed to be measured. In practical power system, it is difficult to measure all system states [27]. To solve this problem, the SMC based observer technique is employed [28,29]. It estimates system states and filters higher frequency harmonics [30]. In addition, it provides cost effective design of LFC for power systems. SMC combined with an observer has been applied for LFC studies in power systems [31,32]. A robust higher observer SMC via nonlinear super twisting LFC was recently designed for multi-area power system with good performance and robustness of SMC which lies on the control switching law and sliding surface [31]. The switching laws ensure all system states deviations are driven to the sliding surface and remain therein. In studies, the robustness of an integral sliding surface combined with an observer was designed for the LFC of a power system which guarantees frequency deviation in the nominal value. However, these above SMCs combined with observer need time for the trajectories to reach the sliding surface, which may decrease the system performance [33]. In addition, a more robust controller without reaching time ensures system state trajectories starts from its surface at the initial time moment [33]. Therefore, the single phase sliding surface (SPSS) choice emerges to design sliding mode control. Thus, this motivates my interest to design an SMC via SPSS based on an observer for LFCs of a large power network. The novelties of this article are stated below:

- ❖ The new SMC via SPSS does not need reaching time as compared to [31,32] which can guarantee better system performance.
- ❖ The new SPSS and controller are designed to depend only on the observer which is useful for real power application where the system states variables are difficult or expensive to measure.
- ❖ The whole system stabilization is theoretically proven using Lyapunov stability theory based new linear matrix inequality (LMI) technique.
- ❖ Experimental simulation results depict the better performance in terms settling time and overshoot in comparison with recently results.

2. State Space Power System Model

In this part, we model the considered large interconnected power system and also the wind farms. Before proceeding, we briefly describe the power system which consists of three area interconnected electricity systems with non-reheat turbines shown in Figure 1. Areas 1 and 3 are integrated with wind power. Each block represents power generation components with their dynamics and subsystem parameters.

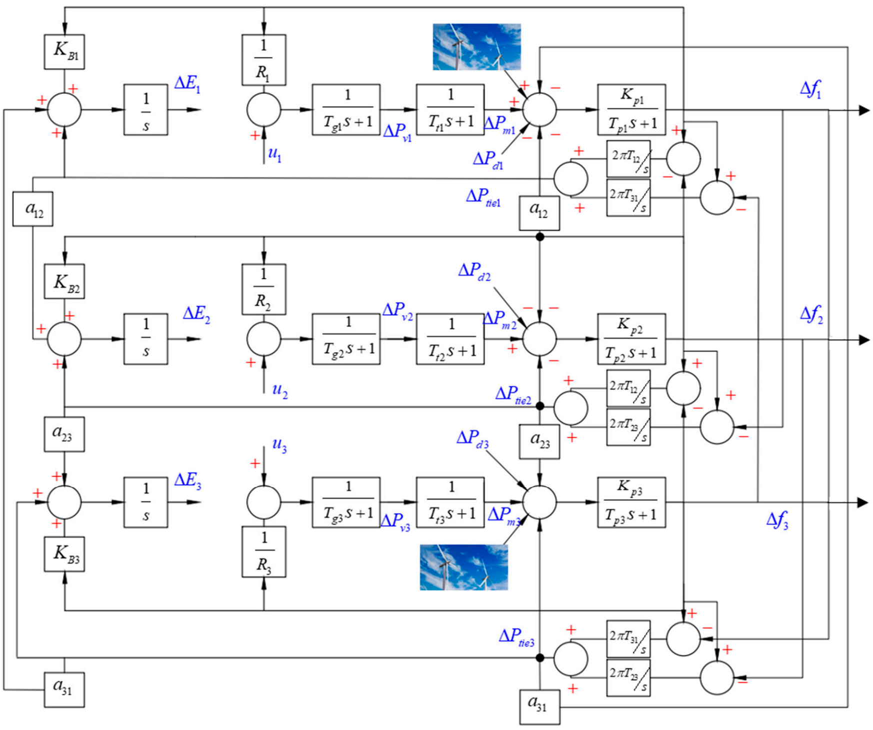

Figure 1. Block diagram of 3-area LFC (load frequency control) system with renewables.

To derive the system states model, we begin from Area 1 to Area 3 in the following equation.

The frequency deviation of Areas 1, 2 and 3 is

$$\Delta \dot{f}_1(t) = -\frac{1}{T_{p1}}\Delta f_1(t) + \frac{K_{p1}}{T_{p1}}\Delta P_{m1}(t) - \frac{K_{p1}}{T_{p1}}\Delta P_{tie1}(t) - a_{31}\frac{K_{p1}}{T_{p1}}\Delta P_{tie3}(t) - \frac{K_{p1}}{T_{p1}}\Delta P_{d_1} - \frac{K_{p1}}{T_{p1}}\Delta P_{\mathrm{W}_1} \tag{1}$$

$$\Delta \dot{f}_2(t) = -\frac{1}{T_{p2}}\Delta f_2(t) + \frac{K_{p2}}{T_{p2}}\Delta P_{m2}(t) - a_{12}\frac{K_{p2}}{T_{p2}}\Delta P_{tie1}(t) - \frac{K_{p2}}{T_{p2}}\Delta P_{tie2}(t) - \frac{K_{p2}}{T_{p2}}\Delta P_{d_2} \tag{2}$$

$$\Delta \dot{f}_3(t) = -\frac{1}{T_{p3}}\Delta f_3(t) + \frac{K_{p3}}{T_{p3}}\Delta P_{m3}(t) - a_{23}\frac{K_{p3}}{T_{p3}}\Delta P_{tie2}(t) - \frac{K_{p3}}{T_{p3}}\Delta P_{tie3}(t) - \frac{K_{p3}}{T_{p3}}\Delta P_{d_3} - \frac{K_{p3}}{T_{p3}}\Delta P_{\mathrm{W}_3} \tag{3}$$

The mechanics power deviation of the 3-area power system are

$$\Delta \dot{P}_{m1}(t) = -\frac{1}{T_{t1}}\Delta P_{m1}(t) + \frac{1}{T_{t1}}\Delta P_{v1}(t) \tag{4}$$

$$\Delta \dot{P}_{m2}(t) = -\frac{1}{T_{t2}}\Delta P_{m2}(t) + \frac{1}{T_{t2}}\Delta P_{v2}(t) \tag{5}$$

$$\Delta \dot{P}_{m3}(t) = -\frac{1}{T_{t3}}\Delta P_{m3}(t) + \frac{1}{T_{t3}}\Delta P_{v3}(t) \tag{6}$$

The valve position deviation of the 3-area power system are given as

$$\Delta \dot{P}_{v1}(t) = -\frac{1}{R_1 T_{g1}}\Delta f_1(t) - \frac{1}{T_{g1}}\Delta P_{v1}(t) + \frac{1}{T_{g1}}u_1 \tag{7}$$

$$\Delta \dot{P}_{v2}(t) = -\frac{1}{R_2 T_{g2}}\Delta f_2(t) - \frac{1}{T_{g2}}\Delta P_{v2}(t) + \frac{1}{T_{g2}}u_2 \tag{8}$$

$$\Delta \dot{P}_{v3}(t) = -\frac{1}{R_3 T_{g3}}\Delta f_3(t) - \frac{1}{T_{g3}}\Delta P_{v3}(t) + \frac{1}{T_{g3}}u_3 \tag{9}$$

The area control error of Areas 1, 2 and 3 are as follows

$$\Delta\dot{E}_1(t) = K_{B1}\Delta f_1(t) + \Delta P_{tie1}(t) + a_{31}\Delta P_{tie3}(t) \tag{10}$$

$$\Delta\dot{E}_2(t) = K_{B2}\Delta f_2(t) + a_{12}\Delta P_{tie1}(t) + \Delta P_{tie2}(t) \tag{11}$$

$$\Delta\dot{E}_3(t) = K_{B3}\Delta f_3(t) + a_{23}\Delta P_{tie2}(t) + \Delta P_{tie3}(t) \tag{12}$$

The tie-line power deviation between the second area of Areas 1, 2 and 3 are presented as

$$\Delta\dot{P}_{tie1}(t) = 2\pi(T_{12} + T_{31})\Delta f_1(t) - 2\pi T_{12}\Delta f_2(t) - 2\pi T_{31}\Delta f_3(t) \tag{13}$$

$$\Delta\dot{P}_{tie2}(t) = 2\pi(T_{12} + T_{23})\Delta f_2(t) - 2\pi T_{12}\Delta f_1(t) - 2\pi T_{23}\Delta f_3(t) \tag{14}$$

$$\Delta\dot{P}_{tie3}(t) = 2\pi(T_{31} + T_{23})\Delta f_3(t) - 2\pi T_{31}\Delta f_1(t) - 2\pi T_{23}\Delta f_2(t) \tag{15}$$

where Δf_1, $\Delta f_2(t)$ and $\Delta f_3(t)$ are frequency errors in area 1, 2 and 3, $\Delta E_1(t)$, $\Delta E_2(t)$ and $\Delta E_3(t)$ are the control area errors, and $\Delta P_{tie1}(t)$, $\Delta P_{tie2}(t)$ and $\Delta P_{tie3}(t)$ are total changes in tie-power. Equations (1)–(15) represent the dynamic characteristics of the power system with wind turbines. Therefore, the power system model is written in the state space form below

$$\begin{aligned} \dot{x}(t) &= Ax(t) + Bu(t) + F\Delta P(t) \\ y(t) &= Cx(t) \end{aligned} \tag{16}$$

where $x(t)$ is the system states variable $x(t) \in R^n$, $u(t)$ is the control vector matrix $u(t) \in R^m$ and $\Delta P(t)$ is the disturbance vector matrix. The detail of the above variables are as follows: $x(t) = [x_1(t) \;\; x_2(t) \;\; x_3(t)]^T$ in which $x_1(t) = [\Delta f_1(t) \;\; \Delta P_{m1}(t) \;\; \Delta P_{v1}(t) \;\; \Delta E_1(t) \;\; \Delta P_{tie1}(t)]$; $x_2(t) = [\Delta f_2(t) \;\; \Delta P_{m2}(t) \;\; \Delta P_{v2}(t) \;\; \Delta E_2(t) \;\; \Delta P_{tie2}(t)]$; $x_3(t) = [\Delta f_3(t) \;\; \Delta P_{m3}(t) \;\; \Delta P_{v3}(t) \;\; \Delta E_3(t) \;\; \Delta P_{tie3}(t)]$; $u(t) = [u_1 u_2 u_3]^T$; $\Delta P(t) = [\Delta P_{d1}\Delta P_{d2}\Delta P_{d3}\Delta P_{W1}\Delta P_{W3}]^T$ and $y(t)$ is denoted the system output vector and A, B, F are the system matrices with $A \in R^{n\times n}$, $B \in R^{n\times m}$, $F \in R^{n\times k}$

$$A = \begin{bmatrix}
-\frac{1}{T_{p1}} & \frac{K_{p1}}{T_{p1}} & 0 & 0 & -\frac{K_{p1}}{T_{p1}} & 0 & 0 & 0 & 0 & 0 & 0 & 0 & 0 & 0 & -a_{31}\frac{K_{p1}}{T_{p1}} \\
0 & -\frac{1}{T_{t1}} & \frac{1}{T_{t1}} & 0 & 0 & 0 & 0 & 0 & 0 & 0 & 0 & 0 & 0 & 0 & 0 \\
-\frac{1}{R_1 T_{g1}} & 0 & -\frac{1}{T_{g1}} & \frac{1}{T_{g1}} & 0 & 0 & 0 & 0 & 0 & 0 & 0 & 0 & 0 & 0 & 0 \\
K_{B1} & 0 & 0 & 0 & 1 & 0 & 0 & 0 & 0 & 0 & 0 & 0 & 0 & 0 & a_{31} \\
2\pi(T_{12}+T_{31}) & 0 & 0 & 0 & 0 & -2\pi T_{12} & 0 & 0 & 0 & 0 & -2\pi T_{31} & 0 & 0 & 0 & 0 \\
0 & 0 & 0 & 0 & -a_{12}\frac{K_{p2}}{T_{p2}} & -\frac{1}{T_{p2}} & \frac{K_{p2}}{T_{p2}} & 0 & 0 & -\frac{K_{p2}}{T_{p2}} & 0 & 0 & 0 & 0 & 0 \\
0 & 0 & 0 & 0 & 0 & 0 & -\frac{1}{T_{t2}} & \frac{1}{T_{t2}} & 0 & 0 & 0 & 0 & 0 & 0 & 0 \\
0 & 0 & 0 & 0 & 0 & -\frac{1}{R_2 T_{g2}} & 0 & -\frac{1}{T_{g2}} & \frac{1}{T_{g2}} & 0 & 0 & 0 & 0 & 0 & 0 \\
0 & 0 & 0 & 0 & a_{12} & K_{B2} & 0 & 0 & 0 & 1 & 0 & 0 & 0 & 0 & 0 \\
-2\pi T_{12} & 0 & 0 & 0 & 0 & 2\pi(T_{12}+T_{23}) & 0 & 0 & 0 & 0 & -2\pi T_{23} & 0 & 0 & 0 & 0 \\
0 & 0 & 0 & 0 & 0 & 0 & 0 & 0 & 0 & -a_{23}\frac{K_{p3}}{T_{p3}} & -\frac{1}{T_{p3}} & \frac{K_{p3}}{T_{p3}} & 0 & 0 & -\frac{K_{p3}}{T_{p3}} \\
0 & 0 & 0 & 0 & 0 & 0 & 0 & 0 & 0 & 0 & 0 & -\frac{1}{T_{t3}} & \frac{1}{T_{t3}} & 0 & 0 \\
0 & 0 & 0 & 0 & 0 & 0 & 0 & 0 & 0 & 0 & -\frac{1}{R_3 T_{g3}} & 0 & -\frac{1}{T_{g3}} & \frac{1}{T_{g3}} & 0 \\
0 & 0 & 0 & 0 & 0 & 0 & 0 & 0 & 0 & a_{23} & K_{B3} & 0 & 0 & 0 & 1 \\
-2\pi T_{31} & 0 & 0 & 0 & 0 & -2\pi T_{23} & 0 & 0 & 0 & 0 & 2\pi(T_{31}+T_{23}) & 0 & 0 & 0 & 0
\end{bmatrix};$$

$$B = \begin{bmatrix}
0 & 0 & \frac{1}{T_{g1}} & 0 & 0 & 0 & 0 & 0 & 0 & 0 & 0 & 0 & 0 & 0 & 0 \\
0 & 0 & 0 & 0 & 0 & 0 & 0 & \frac{1}{T_{g2}} & 0 & 0 & 0 & 0 & 0 & 0 & 0 \\
0 & 0 & 0 & 0 & 0 & 0 & 0 & 0 & 0 & 0 & 0 & 0 & \frac{1}{T_{g3}} & 0 & 0
\end{bmatrix}^T;$$

$$F = \begin{bmatrix}
-\frac{K_{p1}}{T_{P1}} & 0 & 0 & 0 & 0 & 0 & 0 & 0 & 0 & 0 & 0 & 0 & 0 & 0 & 0 \\
0 & 0 & 0 & 0 & 0 & -\frac{K_{P2}}{T_{P2}} & 0 & 0 & 0 & 0 & 0 & 0 & 0 & 0 & 0 \\
0 & 0 & 0 & 0 & 0 & 0 & 0 & 0 & 0 & 0 & 0 & -\frac{K_{P3}}{T_{P3}} & 0 & 0 & 0 \\
\frac{K_{p1}}{T_{P1}} & 0 & 0 & 0 & 0 & 0 & 0 & 0 & 0 & 0 & 0 & 0 & 0 & 0 & 0 \\
0 & 0 & 0 & 0 & 0 & 0 & 0 & 0 & 0 & 0 & 0 & \frac{K_{P3}}{T_{P3}} & 0 & 0 & 0
\end{bmatrix}^T.$$

T_{gi}, T_{ti} and T_{pi} are governor, turbine and subsystem time constant in seconds. K_{pi}, R_i, and K_{Bi} are power system gain (Hz/p.u. MW), speed regulation coefficient (Hz/p.u. MW), and frequency bias factor (p.u. MW/Hz), respectively. T_{ij} is the synchronized coefficient. If there is no power exchange between each area $T_{ij} = 0$. Furthermore, the wind output power is expressed below

$$P_\omega = \frac{1}{2}\rho\alpha V_\omega{}^3 C_P(\lambda, \beta) \tag{17}$$

where ρ is the air density, α is the cross section of rotor, λ is the tip speed ratio, β is the pitch angle, and $C_P(\lambda, \beta)$ is the power coefficient and V_ω is the wind speed. Variation of wind speed can cause external disturbance to the interconnected power system. To proceed, we make some assumptions that will be beneficial in this work. The assumptions are as follows.

Assumption 1. *If the A, B pair are controllable by $u(t)$ then A, C are observable [21].*

Assumption 2. *The load disturbance $\Delta P(t)$ is unknown and bounded, i.e., there exists a known scalar κ such that $\|\Delta P(t)\| \leq \kappa$, where $\|.\|$ is the norm.*

3. Observer Design

To achieve a better LFC in power systems, all parameters values related to LFC are assumed to be measured probably by sensors. This will create a high cost. Therefore, to design a cost effective controller, an observer approach is introduced. The observer estimates system state variables to overcome the use of sensors. By applying the state observer, the estimator of the system state in Equation (16) is written as follows

$$\begin{aligned} \dot{\hat{x}}(t) &= A\hat{x}(t) + Bu(t) + L(y - \hat{y}) \\ \hat{y}(t) &= C\hat{x}(t) \end{aligned} \tag{18}$$

where $\hat{x}(t) \in \Re^n$ is the estimate of $x(t)$, $\hat{y}(t) \in \Re^p$ is the output of the observer, $L \in \Re^{nxp}$ is the gain of the observer. The observer takes a discontinuous signal in $u(t)$ and $y(t)$ as the input and $\hat{y}(t)$ as output signal. The observer gain Γ is chosen such that the eigenvalue of $A^T - C^T\Gamma$ lie in the desire location in the hyper plane. The observer gains matrix L for the original system, therefore, can be determined by using the relation L and Γ^T give as

$$L = \Gamma^T \tag{19}$$

4. SMC via Single Phase Surface Design

In this section, we design the SMC based single phase switching surface for large power systems and prove the system dynamics stabilization. To begin, a single phase switching surface is first designed and discussed below.

4.1. New Single Phase Sliding Surface

To design an SM controller, the choice for switching techniques and sliding surface are very important. The switching scheme is used to move the system states and maintain convergence at a designated sliding surface [21]. Hence, a new single phase sliding surface is constructed. The robustness at reaching stage without reaching time is guaranteed by the single phase switching surface given below.

$$\sigma[\hat{x}(t)] = S\hat{x}(t) - \int_0^t S(A - BK)\hat{x}(\tau)d\tau - S\hat{x}(0)e^{-\beta t} \tag{20}$$

where $\sigma[\hat{x}(t)]$ denotes the single phase sliding surface. We take into account the SMC law that variables must reach the surface and remain therein that is, $\sigma[\hat{x}(t)]\dot{\sigma}[\hat{x}(t)] < 0$ which denotes reachability of the system states trajectories, $\dot{\sigma}[\hat{x}(t)] = \sigma[\hat{x}(t)] = 0$. At the beginning time t = 0, the SPSS in Equation (20) is equal zero $\sigma[\hat{x}(t)] = 0$ which shows the system remain on the single phase sliding surface for all time. In Equation (20), K is the design matrix gain. The matrix S is chosen carefully to ensure SB is invertible. Therefore, if we take the time derivative of Equation (20), we have

$$\dot{\sigma}[\hat{x}(t)] = S\dot{\hat{x}}(t) - S(A - BK)\hat{x}(t)S\beta\hat{x}(0)e^{-\beta t} \tag{21}$$

Substituting $\dot{\hat{x}}(t)$ into Equation (21) gives us

$$\begin{aligned}\dot{\sigma}[\hat{x}(t)] &= S[A\hat{x}(t) + Bu(t) + L(y - \hat{y})] - S(A - BK)\hat{x}(t) + S\beta\hat{x}(0)e^{-\beta t} \\ &= SA\hat{x}(t) + SBu(t) + SL(y - \hat{y}) - S(A - BK)\hat{x}(t) + S\beta\hat{x}(0)e^{-\beta t} \\ &= SA\hat{x}(t) + SBu(t) + SL(y - \hat{y}) - SA\hat{x}(t) + SBK\hat{x}(t) + S\beta\hat{x}(0)e^{-\beta t} \\ &= SBu(t) + SL(y - \hat{y}) + SBK\hat{x}(t) + S\beta\hat{x}(0)e^{-\beta t}\end{aligned} \tag{22}$$

Therefore, if $\dot{\sigma}[\hat{x}(t)] = 0$ then, the corresponding equivalent controller $u_{eq}(t)$ can be determine as

$$u_{eq}(t) = -(SB)^{-1}\left[SBK\hat{x}(t) + SL(y - \hat{y}) + S\beta\hat{x}(0)e^{-\beta t}\right] \tag{23}$$

However, to satisfy the reaching condition of system state trajectories, the design controller becomes

$$u(t) = u_{eq}(t) - (SB)^{-1}\delta sgn(\sigma[\hat{x}(t)]) \tag{24}$$

where $u(t)$ is the designed controller for the power system. In practice, this new controller maintains nominal frequency at agreed value, i.e., 50 Hz/60 Hz and tie-power exchange between the multi-areas. The new controller is designed to depend only on the state observer written as

$$u(t) = -(SB)^{-1}\{SBK\hat{x}(t) + SL(y - \hat{y}) + S\beta\hat{x}(0)e^{-\beta t} + \delta sgn(\sigma[\hat{x}(t)])\} \tag{25}$$

Next, we determine the system dynamic equation in the single phase sliding surface, we start by making $u(t) = u_{eq}(t)$ and substitute into (16) in the following

$$\dot{x}(t) = Ax(t) - BK\hat{x}(t) - B(SB)^{-1}SL(y - \hat{y}) - B(SB)^{-1}S\beta\hat{x}(0)e^{-\beta t} + F\Delta P(t) \tag{26}$$

where $y(t)$ is the real output which is given as $y(t) = Cx(t)$ and $\hat{y}(t)$ is the estimated output from the observer given as $\hat{y}(t) = C\hat{x}(t)$. Therefore, the Equation (26) can be achieved.

$$\begin{aligned}\dot{x}(t) = {} & Ax(t) - BKx(t) + BKx(t) - BK\hat{x}(t) - B(SB)^{-1}SLC[x(t) - \hat{x}(t)] \\ & -B(SB)^{-1}S\beta\hat{x}(0)e^{-\beta t} + F\Delta P(t)\end{aligned} \tag{27}$$

By simplifying (27), the equation is written in the following

$$\dot{x}(t) = (A - BK)x(t) + \left[BK - B(SB)^{-1}SLC\right]\mathfrak{A}(t) + F\Delta P(t) - B(SB)^{-1}S\beta\hat{x}(0)e^{-\beta t} \tag{28}$$

where $\mathfrak{A}(t)$ represents the error between the real system state and observer state given below

$$\mathfrak{A}(t) = x(t) - \hat{x}(t) \tag{29}$$

If we take the time derivative of Equation (29) and using Equations (16) and (18), we have

$$\dot{\mathfrak{A}}(t) = (A - LC)\mathfrak{A}(t) + F\Delta \mathrm{P}(t) \tag{30}$$

Combining (28) and (30), therefore, the dynamic equation in the SPSS becomes

$$\begin{bmatrix} \dot{x}(t) \\ \dot{\mathfrak{A}}(t) \end{bmatrix} = \begin{bmatrix} (A - BK) & \left[BK - B(SB)^{-1}SLC\right] \\ 0 & (A - LC) \end{bmatrix}\begin{bmatrix} x(t) \\ \mathfrak{A}(t) \end{bmatrix} + \begin{bmatrix} I & \Pi \\ I & 0 \end{bmatrix}\begin{bmatrix} F\Delta P(t) \\ e^{-\beta t} \end{bmatrix}. \tag{31}$$

where

$$\Pi = -B(SB)^{-1}S\beta\hat{x}(0)$$

Equation (31) represents the dynamic equation in the SPSS. It is designed in such a way that both $x(t)$ and $\mathfrak{A}(t)$ deviation begins at the surface at initial time moment. Meanwhile, $(BK - B(SB)^{-1}SLC)$ reflects the fact that system is constrained to remain on the defined single phase sliding surface at $\sigma[\hat{x}(t)] = 0$.

4.2. Theoretical Prove of System Dynamic Stabilization

It is very important to prove the stabilization of the whole system. In studies, Lyapunov stability theory is used theoretically to investigate differential systems. Some lemmas are also adopted and LMI theorem stated to support the stabilization proves which are given.

Lemma 1 ([34]). *If X and Y are real matrix of suitable dimension then, for any scalar $\mu > 0$, the following matrix inequality holds*

$$X^TY + Y^TX \leq \mu X^TX + \mu^{-1}Y^TY$$

Lemma 2 ([34]). *For a given inequality*

$$\begin{bmatrix} Q(x) & S(x) \\ S(x)^T & R(x) \end{bmatrix} < 0 \tag{32}$$

where $Q(x) = Q(x)^T$ and $R(x) = R(x)^T$ such that $S(x)$ depend affinity on x, therefore, $R(x) < 0$ and $Q(x) - S(x)R(x)^{-1}S(x)^T < 0$.

Theorem 1. *The system (31) is asymptotically stable, if there exist symmetric positive definite matrices $R > 0$ and $P > 0$ and positive scalars μ, γ and π such that the below LMI holds*

$$\begin{bmatrix} R(A-BK) + (A-BK)^TR & R\left[BK - B(SB)^{-1}SLC\right] & 0 & RIF & R\Pi \\ \left[BK - B(SB)^{-1}SLC\right]^TR & P(A-LC) + (A-LC)^TP & PIF & 0 & 0 \\ 0 & F^TI^TP & -\pi^{-1}I & 0 & 0 \\ F^TI^TR & 0 & 0 & \mu^{-1} & 0 \\ \Pi^TR & 0 & 0 & 0 & \gamma^{-1} \end{bmatrix} < 0 \tag{33}$$

To prove the stability of the system (31), the Lyapunov function $V(x(t), \mathfrak{A}(t))$ is selected as

$$V(x(t), \mathfrak{A}(t)) = \begin{bmatrix} x(t) \\ \mathfrak{A}(t) \end{bmatrix}^T \begin{bmatrix} R & 0 \\ 0 & P \end{bmatrix} \begin{bmatrix} x(t) \\ \mathfrak{A}(t) \end{bmatrix} \tag{34}$$

When we take the time derivative of (34), we have

$$\dot{V}(x(t), \mathfrak{A}(t)) = \begin{bmatrix} x(t) \\ \mathfrak{A}(t) \end{bmatrix}^T \begin{bmatrix} R & 0 \\ 0 & P \end{bmatrix} \begin{bmatrix} \dot{x}(t) \\ \dot{\mathfrak{A}}(t) \end{bmatrix} + \begin{bmatrix} \dot{x}(t) \\ \dot{\mathfrak{A}}(t) \end{bmatrix}^T \begin{bmatrix} R & 0 \\ 0 & P \end{bmatrix} \begin{bmatrix} x(t) \\ \mathfrak{A}(t) \end{bmatrix} \tag{35}$$

Substitute $\dot{x}(t)$ and $\dot{\mathfrak{A}}(t)$ into (35), $\dot{V}(x(t), \mathfrak{A}(t))$ becomes

$$\begin{aligned} \dot{V}(x(t), \mathfrak{A}(t)) = {} & \begin{bmatrix} x(t) \\ \mathfrak{A}(t) \end{bmatrix}^T \begin{bmatrix} R & 0 \\ 0 & P \end{bmatrix} \left[\begin{bmatrix} (A-BK) & \left[BK - B(SB)^{-1}SLC\right] \\ 0 & (A-LC) \end{bmatrix} \begin{bmatrix} x(t) \\ \mathfrak{A}(t) \end{bmatrix} + \begin{bmatrix} I & \Pi \\ I & 0 \end{bmatrix} \begin{bmatrix} F\Delta P(t) \\ e^{-\beta t} \end{bmatrix} \right] \\ & + \left[\begin{bmatrix} (A-BK) & \left[BK - B(SB)^{-1}SLC\right] \\ 0 & (A-LC) \end{bmatrix} \begin{bmatrix} x(t) \\ \mathfrak{A}(t) \end{bmatrix} + \begin{bmatrix} I & \Pi \\ I & 0 \end{bmatrix} \begin{bmatrix} F\Delta P(t) \\ e^{-\beta t} \end{bmatrix} \right]^T \begin{bmatrix} R & 0 \\ 0 & P \end{bmatrix} \begin{bmatrix} x(t) \\ \mathfrak{A}(t) \end{bmatrix} \end{aligned} \tag{36}$$

By simplifying (36) further, we have

$$\dot{V}(x(t),\mathfrak{A}(t)) = \begin{bmatrix} x(t) \\ \mathfrak{A}(t) \end{bmatrix}^T \begin{bmatrix} R(A-BK) & R\left[BK-B\,(SB)^{-1}\,SLC\right] \\ 0 & P(A-LC) \end{bmatrix} \begin{bmatrix} x(t) \\ \mathfrak{A}(t) \end{bmatrix} + \begin{bmatrix} x(t) \\ \mathfrak{A}(t) \end{bmatrix}^T \begin{bmatrix} RI & R\Pi \\ PI & 0 \end{bmatrix} \begin{bmatrix} F\Delta P(t) \\ e^{-\beta t} \end{bmatrix}$$
$$+ \begin{bmatrix} x(t) \\ \mathfrak{A}(t) \end{bmatrix}^T \begin{bmatrix} (A-BK)^T\,R & 0 \\ \left[BK-B\,(SB)^{-1}\,SLC\right]^T R & (A-LC)^T\,P \end{bmatrix} \begin{bmatrix} x(t) \\ \mathfrak{A}(t) \end{bmatrix} + \begin{bmatrix} F\Delta P(t) \\ e^{-\beta t} \end{bmatrix}^T \begin{bmatrix} I^T R & I^T P \\ \Pi^T R & 0 \end{bmatrix} \begin{bmatrix} x(t) \\ \mathfrak{A}(t) \end{bmatrix}$$
$$= \begin{bmatrix} x(t) \\ \mathfrak{A}(t) \end{bmatrix}^T \begin{bmatrix} R(A-BK) + (A-BK)^T\,R & R\left[BK-B\,(SB)^{-1}SLC\right] \\ \left[BK-B\,(SB)^{-1}SLC\right]^T R & P(A-LC)+(A-LC)^T\,P \end{bmatrix} \begin{bmatrix} x(t) \\ \mathfrak{A}(t) \end{bmatrix} +$$
$$x(t)^T\,RIF\Delta P(t) + x(t)^T\,R\Pi\,e^{-\beta t} + \Delta P(t)^T\,F^T\,I^T\,Rx(t) + \Delta P(t)^T\,F^T\,I^T\,P\mathfrak{A}(t) + \mathfrak{A}(t)^T\,PIF\Delta P(t) + \left(e^{-\beta t}\right)^T\,\Pi^T\,Rx(t) \tag{37}$$

By applying Lemma 1 into (37), we therefore re-write Equation (37) in the following form

$$\dot{V}(x(t),\mathfrak{A}(t)) \le \begin{bmatrix} x(t) \\ \mathfrak{A}(t) \end{bmatrix}^T \begin{bmatrix} R(A-BK) + (A-BK)^T R & R\left[BK-B(SB)^{-1}SLC\right] \\ \left[BK-B(SB)^{-1}SLC\right]^T R & \mathrm{P}(A-LC)+(A-LC)^T P \end{bmatrix} \begin{bmatrix} x(t) \\ \mathfrak{A}(t) \end{bmatrix}$$
$$+\mu x(t)^T RIFF^T I^T Rx(t) + (\mu^{-1}+\pi^{-1})\Delta P(t)^T \Delta P(t) + \gamma x(t)^T R\Pi\Pi^T Rx(t)$$
$$+\gamma^{-1}\,(e^{-\beta t})^T e^{-\beta t} + \pi\mathfrak{A}(t)^T PIFF^T I^T P\mathfrak{A}(t) \tag{38}$$

Equation (38) is further simplified to give

$$\dot{V}(x(t),\mathfrak{A}(t)) \le \begin{bmatrix} x(t) \\ \mathfrak{A}(t) \end{bmatrix}^T \begin{bmatrix} R(A-BK) + (A-BK)^T R + \mu RIFF^T I^T R + \gamma R\Pi\Pi^T R & R\left[BK-B(SB)^{-1}SLC\right] \\ \left[BK-B(SB)^{-1}SLC\right]^T R & P(A-LC)+(A-LC)^T P + \pi PIFF^T I^T P \end{bmatrix} \begin{bmatrix} x(t) \\ \mathfrak{A}(t) \end{bmatrix}$$
$$+\varphi\Delta P(t)^T \Delta P(t) + \gamma^{-1}(e^{-\beta t})^T e^{-\beta t}$$
$$= \begin{bmatrix} x(t) \\ \mathfrak{A}(t) \end{bmatrix}^T \begin{bmatrix} R(A-BK) + (A-BK)^T R + \mu RIFF^T I^T R + \gamma R\Pi\Pi^T R & R\left[BK-B(SB)^{-1}SLC\right] \\ \left[BK-B(SB)^{-1}SLC\right]^T R & P(A-LC)+(A-LC)^T P + \pi PIFF^T I^T P \end{bmatrix} \begin{bmatrix} x(t) \\ \mathfrak{A}(t) \end{bmatrix}$$
$$+\varphi\|\Delta P(t)\|^2 + \gamma^{-1}(e^{-\beta t})^T e^{-\beta t}$$
$$\le \begin{bmatrix} x(t) \\ \mathfrak{A}(t) \end{bmatrix}^T \begin{bmatrix} R(A-BK) + (A-BK)^T R + \mu RIFF^T I^T R + \gamma R\Pi\Pi^T R & R\left[BK-B(SB)^{-1}SLC\right] \\ \left[BK-B(SB)^{-1}SLC\right]^T R & P(A-LC)+(A-LC)^T P + \pi PIFF^T I^T P \end{bmatrix} \begin{bmatrix} x(t) \\ \mathfrak{A}(t) \end{bmatrix}$$
$$+\varphi\kappa^2 + \gamma^{-1}(e^{-\beta t})^T e^{-\beta t} \tag{39}$$

where $\varphi = \mu^{-1} + \pi^{-1}$. By applying Lemma 2, the LMI (33) can be rewritten as

$$\begin{bmatrix} R(A-BK) + (A-BK)^T R + \mu RIFF^T I^T R + \gamma R\Pi\Pi^T R & R\left[BK-B(SB)^{-1}SLC\right] \\ \left[BK-B(SB)^{-1}SLC\right]^T R & P(A-LC)+(A-LC)^T P + \pi PIFF^T I^T P \end{bmatrix} < 0 \tag{40}$$

The term $\gamma^{-1}(e^{-\beta t})^T e^{-\beta t}$ in Equation (39) will approach zero when the time approaches infinity. Therefore $\dot{V}(x(t),\mathfrak{A}(t)) \le 0$ is achieved by using Equations (39) and (40). If $\dot{V}(x(t),\mathfrak{A}(t)) \le 0$ shows that the LMI given in (33) holds, therefore, it further explains that the system (16) is asymptotically stable.

Furthermore, we theoretically prove the reachability of the system states to the SPSS. We assumed that $\hat{x}(t) > 0$ little above the equilibrium part at the surface, then the Lyapunov function is selected

$$V[\hat{x}(t)] = \frac{1}{2}\,\sigma[\hat{x}(t)]^T \sigma[\hat{x}(t)] \tag{41}$$

If we take the time derivative of (41), we have

$$\dot{V}[\hat{x}(t)] = \sigma[\hat{x}(t)]^T \dot{\sigma}[\hat{x}(t)] \tag{42}$$

Substituting Equation (22) into Equation (42) then it becomes

$$\dot{V}[\hat{x}(t)] = \sigma[\hat{x}(t)]^T\{S[A\hat{x}(t)+Bu(t)+L(y-\hat{y})] - S(A-BK)\hat{x}(t) + S\beta\hat{x}(0)e^{-\beta t}\} \tag{43}$$

Using the controller (24), then

$$\dot{V}[\hat{x}(t)] = -\delta\|\sigma[\hat{x}(t)]\| \tag{44}$$

Therefore, Equation (44) indicates that $\dot{V}[\hat{x}(t)] < 0$ which proves the reachability of the system states to the SPSS. Next, the flowchart of the proposed control algorithm of highly robust observer sliding mode can be implemented as Figure 2.

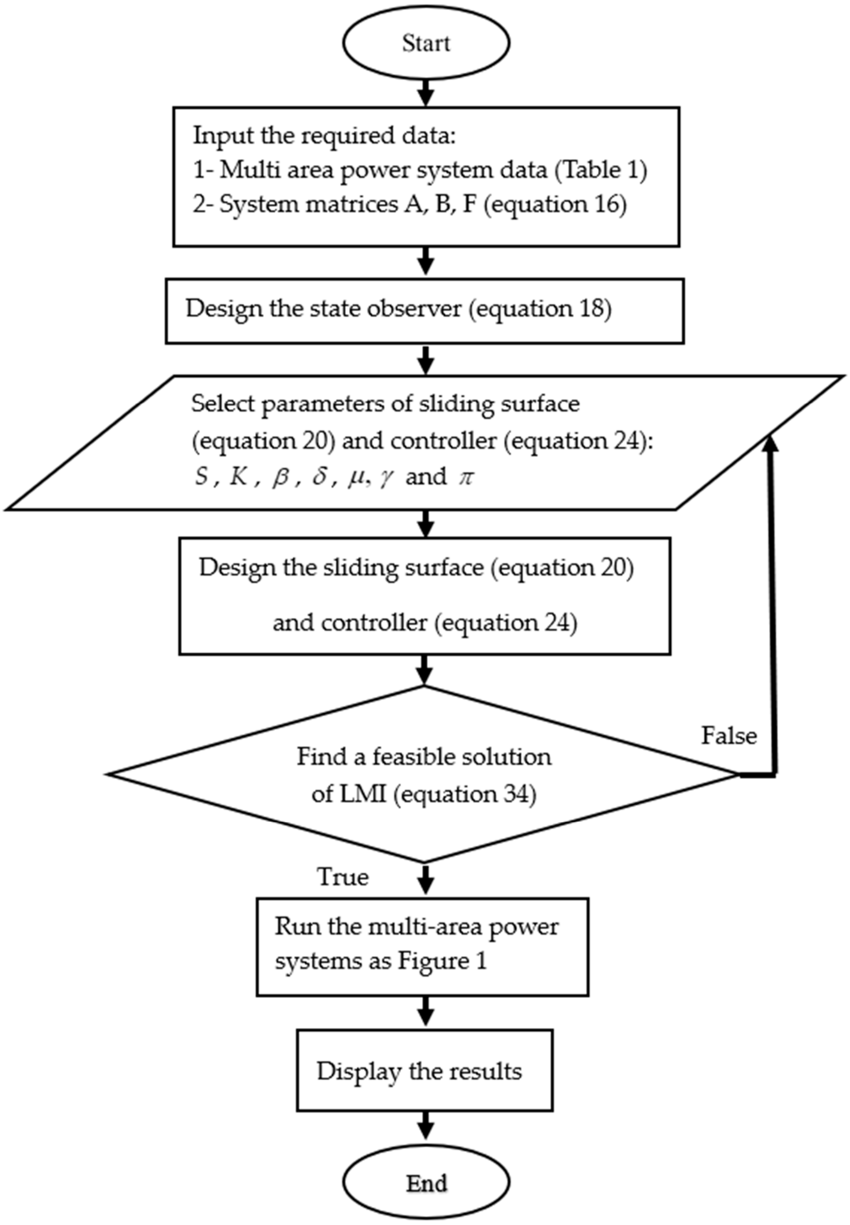

Figure 2. The flowchart of the proposed highly robust observer sliding mode based load frequency control.

Remark 1. *The stability of the LFC in power system using LMI technique can be seen in [35]. However, the above approach needs to find four positive matrices in the LMI equations. Thus, the proposed approach only needs to find two positive matrices in LMI equations making it easier to find a feasible solution.*

5. Simulation Results and Discussions

In this part, two simulations are done and the results are discussed and compared with other recent results.

5.1. Simulation 1

Parameters of the subsystem are obtained for simulation as given in [31] shown in Table 1.

Table 1. Power system parameters.

Parameters	T_{Pi}	K_{Pi}	T_{Ti}	T_{Gi}	R_i
Area 1	20	120	0.3	0.08	2.4
Area 2	25	112.5	0.33	0.072	2.7
Area 3	20	115	0.35	0.07	2.5

The system matrices are calculated as

$$A = \begin{bmatrix} -0.05 & 6 & 0 & 0 & -6 & 0 & 0 & 0 & 0 & 0 & 0 & 0 & 0 & 0 & -6 \\ 0 & -3.3 & 3.3 & 0 & 0 & 0 & 0 & 0 & 0 & 0 & 0 & 0 & 0 & 0 & 0 \\ -5.2 & 0 & -12.5 & 12.5 & 0 & 0 & 0 & 0 & 0 & 0 & 0 & 0 & 0 & 0 & 0 \\ 0.42 & 0 & 0 & 0 & 1 & 0 & 0 & 0 & 0 & 0 & 0 & 0 & 0 & 0 & 1 \\ 6.28 & 0 & 0 & 0 & 0 & -3.45 & 0 & 0 & 0 & 0 & -3.42 & 0 & 0 & 0 & 0 \\ 0 & 0 & 0 & 0 & 4.5 & -0.04 & 4.5 & 0 & 0 & -4.5 & 0 & 0 & 0 & 0 & 0 \\ 0 & 0 & 0 & 0 & 0 & 0 & -3.03 & 3.03 & 0 & 0 & 0 & 0 & 0 & 0 & 0 \\ 0 & 0 & 0 & 0 & 0 & -5.14 & 0 & -13.8 & 13.8 & 0 & 0 & 0 & 0 & 0 & 0 \\ 0 & 0 & 0 & 1 & 0.42 & 0 & 0 & 0 & 1 & 0 & 0 & 0 & 0 & 0 & 0 \\ -3.4 & 0 & 0 & 0 & 0 & 6.28 & 0 & 0 & 0 & 0 & -4.08 & 0 & 0 & 0 & 0 \\ 0 & 0 & 0 & 0 & 0 & 0 & 0 & 0 & 0 & -5.75 & -0.05 & 5.75 & 0 & 0 & 5.75 \\ 0 & 0 & 0 & 0 & 0 & 0 & 0 & 0 & 0 & 0 & 0 & -2.85 & 2.85 & 0 & 0 \\ 0 & 0 & 0 & 0 & 0 & 0 & 0 & 0 & 0 & 0 & -5.71 & 0 & -14.28 & 14.28 & 0 \\ 0 & 0 & 0 & 0 & 0 & 0 & 0 & 0 & 0 & 1 & 0.42 & 0 & 0 & 0 & 1 \\ -3.42 & 0 & 0 & 0 & 0 & -4.08 & 0 & 0 & 0 & 0 & 6.28 & 0 & 0 & 0 & 0 \end{bmatrix}$$

The design parameters in the propose control are chosen to be $\beta = 0.015$, $\mu = 1.3$,

$$\gamma = 2.2, \vartheta = 2.2,$$

$$S = \begin{bmatrix} 0 & 0 & 12.5 & 0 & 0 & 0 & 0 & 0 & 0 & 0 & 0 & 0 & 0 & 0 & 0 \\ 0 & 0 & 0 & 0 & 0 & 0 & 0 & 13.89 & 0 & 0 & 0 & 0 & 0 & 0 & 0 \\ 0 & 0 & 0 & 0 & 0 & 0 & 0 & 0 & 0 & 0 & 0 & 0 & 14.28 & 0 & 0 \end{bmatrix}$$

and

$$K = \begin{bmatrix} 172.5 & 58.8 & 5.3 & -401.9 & -592.8 & 5.7 & -0.8 & -0.07 & -427.6 & -731.7 & -10.4 & -1.4 & -0.04 & -1028 & -768 \\ 15.9 & 0.6 & -0.04 & -1498.8 & -1093.1 & 222.1 & 59.1 & 4.7 & -922.2 & -1125.2 & 13.1 & 2.6 & 0.11 & -979 & -1229 \\ -9.6 & -2.46 & -0.1 & -839 & -942.06 & 12.1 & 4.7 & 0.3 & -1127.5 & -1015.7 & 196.7 & 59.6 & 4.45 & -740 & -790 \end{bmatrix}$$

By solving LMI (33), we have

$$R = \begin{bmatrix} 0.001 & 0 & 0 & 0.009 & 0 & 0 & 0 & 0 & 0.002 & 0 & 0 & 0 & 0 & -0.004 & 0 \\ 0 & 0 & 0 & 0 & 0 & 0 & 0 & 0 & 0 & 0 & 0 & 0 & 0 & 0 & 0 \\ 0 & 0 & 0 & 0 & 0 & 0 & 0 & 0 & 0 & 0 & 0 & 0 & 0 & 0 & 0 \\ 0.009 & 0 & 0 & 8.612 & 3.4 & -0.21 & -0.01 & 0 & -6.53 & 3.6 & -0.078 & -0.008 & 0 & 5.9 & 3.68 \\ 0 & 0 & 0 & 3.40 & 2.12 & -0.1 & -0.02 & 0 & 2.87 & 2.14 & -0.06 & -0.013 & 0 & 2.5 & 2.18 \\ -0.001 & 0 & 0 & -0.21 & -0.1 & 0.03 & 0.002 & 0 & -0.13 & -0.1 & 0 & 0 & 0 & -0.13 & -0.11 \\ 0 & 0 & 0 & -0.014 & -0.02 & 0 & 0.001 & 0 & 0 & -0.02 & 0 & 0 & 0 & -0.008 & -0.02 \\ 0 & 0 & 0 & -0.001 & 0 & 0 & 0 & 0 & 0 & 0 & 0 & 0 & 0 & 0 & 0 \\ 0.002 & 0 & 0 & 6.53 & 2.87 & -0.13 & -0.008 & 0 & 6.07 & 3.04 & -0.11 & -0.01 & 0 & 5.029 & 3.04 \\ 0 & 0 & 0 & 3.61 & 2.14 & -0.1 & -0.015 & 0 & 3.04 & 2.19 & -0.06 & -0.01 & 0 & 2.655 & 2.2 \\ 0 & 0 & 0 & -0.078 & -0.06 & 0 & 0 & 0 & -0.11 & -0.07 & 0.016 & 0.001 & 0 & -0.08 & -0.05 \\ 0 & 0 & 0 & -0.007 & -0.01 & 0 & 0 & 0 & -0.01 & -0.01 & 0.001 & 0.001 & 0 & -0.007 & -0.01 \\ 0 & 0 & 0 & 0 & 0 & 0 & 0 & 0 & 0 & 0 & 0 & 0 & 0 & 0 & 0 \\ -0.003 & 0 & 0 & 5.91 & 2.5 & -0.13 & -0.008 & 0 & 5.03 & 2.65 & -0.08 & -0.007 & 0 & 4.49 & 2.6 \\ 0 & 0 & 0 & 3.68 & 2.18 & -0.11 & -0.018 & 0 & 3.05 & 2.2 & -0.06 & -0.01 & 0 & 2.67 & 2.2 \end{bmatrix} > 0$$

and

$$P = \begin{bmatrix} 0 & 0 & 0 & 0 & -0.01 & 0 & 0 & 0 & 0 & 0 & 0 & 0 & 0 & -0.01 & 0 \\ 0 & 15864 & 0 & 0.01 & 0 & 0 & 0 & 0 & -0.01 & 0 & 0 & 0.001 & 0 & 0 & 0 \\ 0 & 0 & 13564 & 0 & 0 & 0 & 0 & 0 & 0 & 0 & 0 & 0 & 0 & 0 & 0 \\ 0 & 0.01 & 0 & 11847 & -0.03 & -0.35 & 0.3 & 0 & 0.12 & -0.02 & -0.1 & -0.02 & 0 & -0.05 & -0.11 \\ -0.01 & 0 & 0 & -0.03 & 10516 & -0.22 & 0 & 0 & -0.36 & -0.3 & -0.1 & 0.02 & 0 & -0.21 & -0.2 \\ 0 & 0 & 0 & -0.35 & -0.22 & 0.06 & 0.01 & 0 & -0.13 & -0.16 & 0 & 0 & 0 & -0.1 & -0.13 \\ 0 & 0 & 0 & 0.028 & 0 & 0.011 & 8586 & 0 & -0.03 & -0.01 & 0 & 0.002 & 0 & 0 & 0 \\ 0 & 0 & 0 & 0.002 & 0 & 0 & 0 & 7865 & 0 & 0 & 0 & 0 & 0 & 0 & 0 \\ 0 & -0.01 & 0 & 0.12 & -0.36 & -0.13 & -0.02 & 0 & 7255 & -0.41 & -0.14 & 0.04 & 0 & -0.26 & -0.2 \\ 0 & 0 & 0 & -0.02 & -0.3 & -0.15 & -0.01 & 0 & -0.4 & 6733 & -0.12 & 0.02 & 0 & -0.2 & -0.18 \\ 0 & 0 & 0 & -0.12 & -0.14 & 0 & 0 & 0 & -0.14 & -0.12 & 0.03 & 0.006 & 0 & -0.07 & -0.07 \\ 0 & 0 & 0 & -0.02 & 0.02 & 0 & 0 & 0 & 0.03 & 0.02 & 0 & 5886 & 0 & 0.01 & 0 \\ 0 & 0 & 0 & 0 & 0 & 0 & 0 & 0 & 0 & 0 & 0 & 0 & 5538 & 0 & 0 \\ -0.01 & 0 & 0 & -0.05 & -0.21 & -0.11 & 0 & 0 & -0.26 & -0.2 & -0.07 & 0.01 & 0 & 5228 & -0.13 \\ 0 & 0 & 0 & -0.11 & -0.19 & -0.13 & 0 & 0 & -0.2 & -0.18 & -0.07 & 0.009 & 0 & -0.13 & 4952 \end{bmatrix} > 0$$

Therefore, the LMI (33) is feasible.

5.1.1. Case 1

To examine the power system under the new algorithm, we apply step load changes with values of 0.01 p.u, 0.015 p.u and 0.02 p.u for Area 1, 2, and 3 together with wind speed variation in Figure 3. The respective results for incremental change in frequency and tie-flow distortion for the three areas are displayed in Figures 4 and 5.

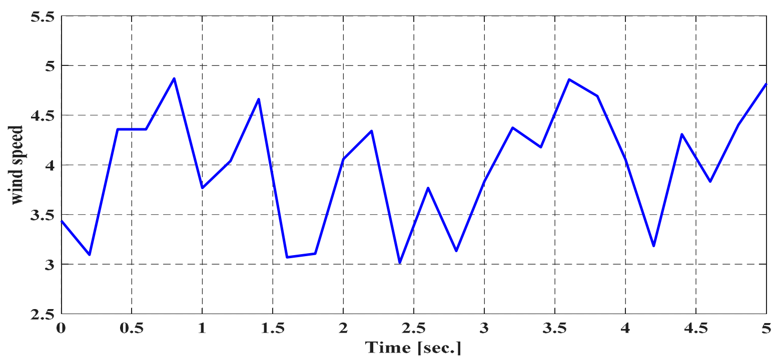

Figure 3. Wind speed (m/s).

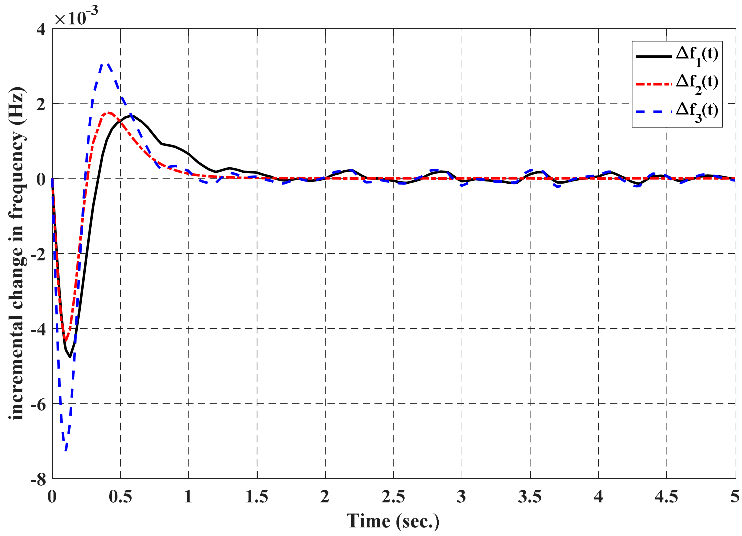

Figure 4. Frequency spikes against step load disturbance and wind speed variation.

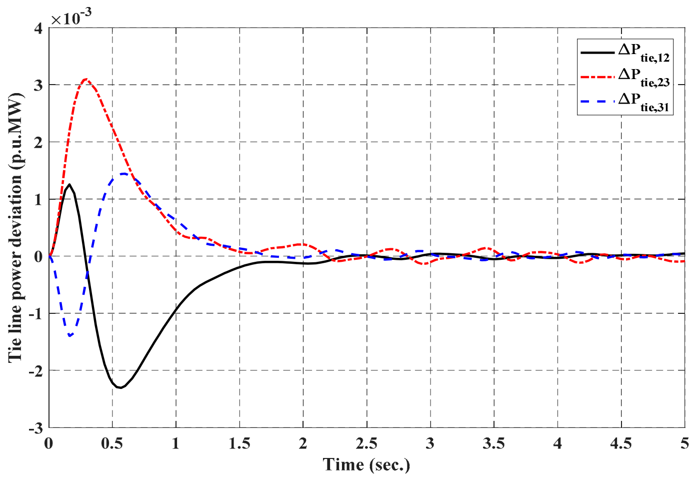

Figure 5. Tie-line power deviation.

Both frequencies and tie-power flows spike at the initial point. At 2 s, the spikes are restored to zero point with lesser overshoots as compared to [31]. Table 2 gives a comparison result of both controllers. The single phase sliding surface without reaching time is used to cut-off the smaller overshoots.

Table 2. Setting time T_s and Maximum Overshoot (M.O.S).

	Proposed HROSM via Single Phase Sliding Surface		The Approach Given in [31]	
Frequency Errors	**Settling Time T_s [s]**	**Max.O. S [pu]**	**Settling Time T_s [s]**	**Max.O. S [pu]**
Δf_1	1.5	0.003	2	0.005
Δf_2	1.5	0.0019	2	0.003
Δf_3	1.5	0.0019	2	0.003

HROSM: highly robust observer sliding mode.

Remark 2. *The power system response is seen better in terms of overshoots and settling time when compared with [31].*

5.1.2. Case 2

In reality, there is always continuous load demand from industries, households, etc., therefore, we assumed random load variations at every 5 s intervals as shown in Figure 6. We simulate again and the incremental frequency and tie-flow fluctuation for the three areas are shown in Figures 7 and 8, accordingly. At this time, the new controller proves to be robust and converge the errors to zero at every interval without loss of control accuracies. The power system response is seen to be much better. This is to say the new controller provides good correction signal to adjust the reference load in the speed changer motor (non-reheat systems).

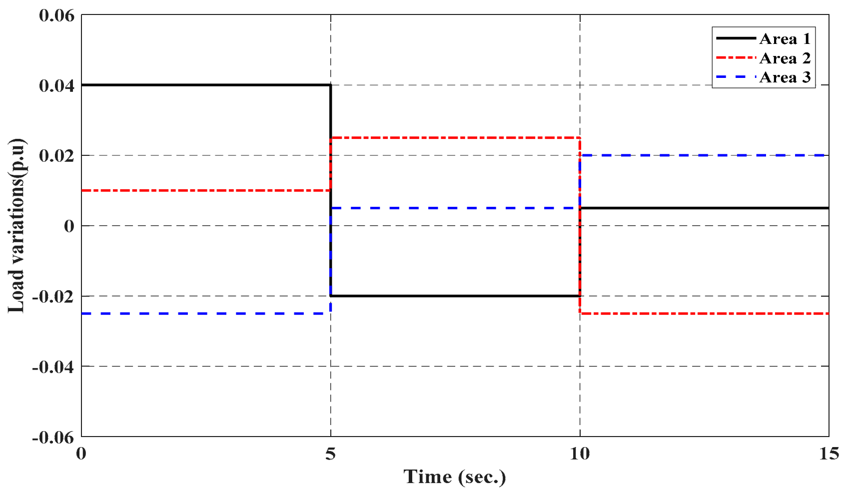

Figure 6. Load variations of three areas.

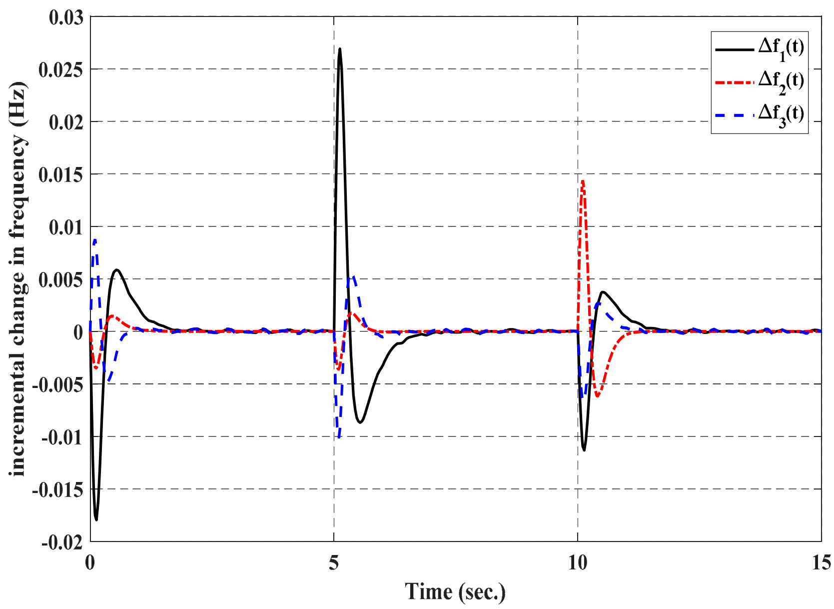

Figure 7. Frequency spikes against load variations.

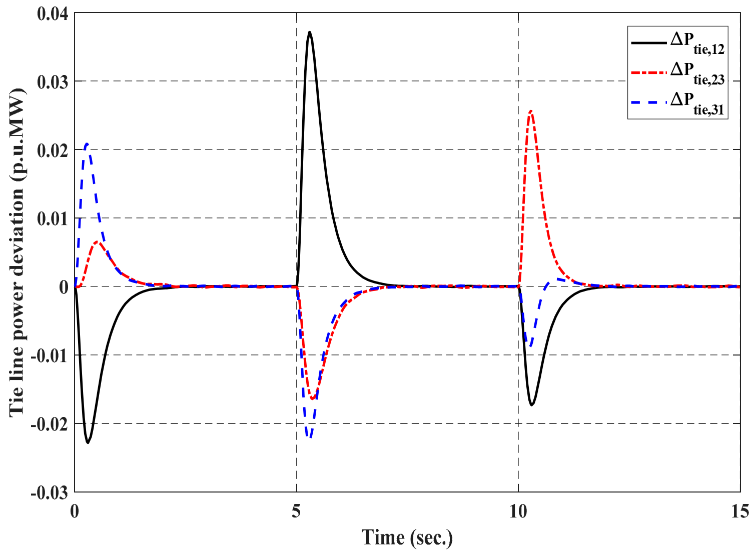

Figure 8. Tie-line power deviation.

Remark 3. *The new controller robustness is validated against random load change and variable wind speed. It also proves to be applicable in real power system in terms of the smaller overshoots seen which do not have any significant effect as to cause wear and tear of the actuator valve.*

5.2. Simulation 2

In this section, we simulate the performance of HROSM control design in a New England (IEEE 39 bus system) with parameters and the performance indices calculation shown in Table 3 as given in [36]. This system consists of 10 machines. The one-line diagram of the test system with its tie-line is displayed in Figure 9. Areas 1 and 2 have three generators, and there are four generators in Area 3; all generators are synchronized and operating in parallel running in a non-deregulated environment. The generators are equipped with governors. The total generated power and loads connected in Areas 1, 2 and 3 are 265.5, 233, 125 and 842 MW, respectively [36].

Table 3. Parameters of the New England IEEE 39 bus power system.

Generations (bus No.)	M (Moment of Inertia of the Generator)	D (Generator's Damping Rations)	T_g (Governor Time Constant)	T_T (Turbine-Generator Time Constant)	Linearization Parameter of the Governor Characteristic		
					K_t	e_T	r
G1 (39)	3.0	4.0	0.25	0.2	250	39.4	19
G2 (31)	2.5	4.0	0.25	0.2	250	39.4	19
G3 (32)	4.0	6.0	0.25	0.2	250	39.4	19
G4 (33)	2.0	3.5	0.25	0.2	250	39.4	19
G5 (34)	3.5	3.0	0.25	0.2	250	39.4	19
G6 (35)	3.0	7.5	0.25	0.2	250	39.4	19
G7 (36)	2.5	4.0	0.25	0.2	250	39.4	19
G8 (37)	2.0	6.5	0.25	0.2	250	39.4	19
G9 (38)	6.0	5.0	0.25	0.2	250	39.4	19
G10 (30)	4.0	5.0	0.25	0.2	250	39.4	19

The New England system is simulated with the designed HROSM against variable load changes as shown in Figure 3. Figure 10 displayed the results of the frequency error of Area 3, while Figure 11 shows the tie-power exchange error results. In the results, it is seen that the new controller performance is good by damping the frequency and tie-power flow changes without loss of control and chattering free. The New England system response is better in terms of lesser settling time and overshoots which also cannot have any significant effect (i.e., wear and tear) on the governor steam actuator valve.

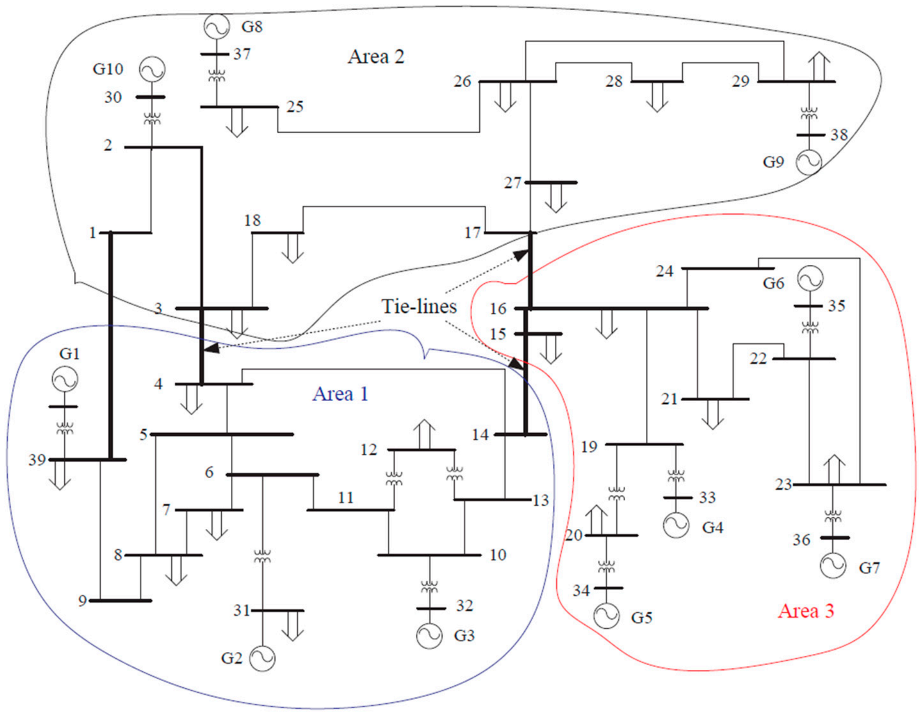

Figure 9. The New England IEEE 39 bus power system.

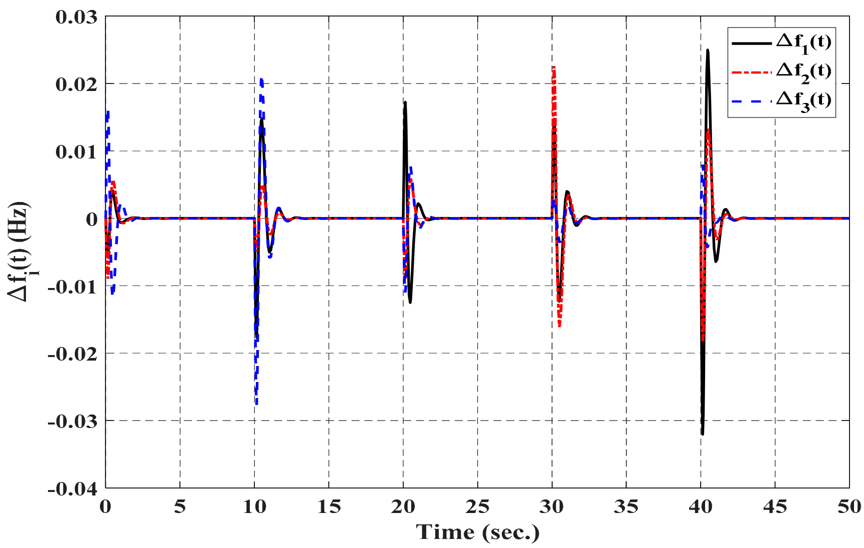

Figure 10. Frequency deviation of three areas.

Remark 4. *It is seen that the new SPSS and the controller without reaching time keep frequency and tie-power flow at desired values in the New England 39 bus system with better response in overshoots and settling time. Therefore, this is the evidence that the new SPSS and controller without reaching time is good application for LFC of large power system.*

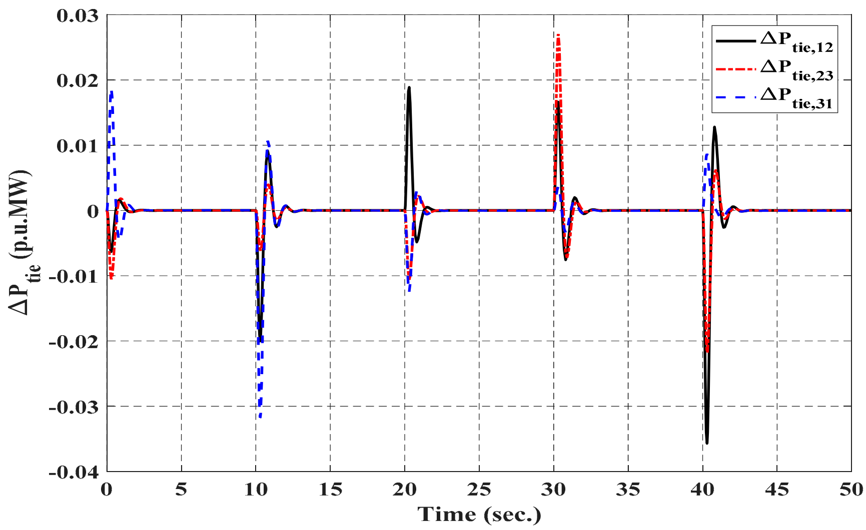

Figure 11. Tie-line power deviation.

6. Conclusions

In this paper, LFC problems in multi-area power integrated with renewable power plants is solved with proposed design of highly robust observer sliding mode via single phase switching. The proposed controller is designed to act only on the observer information and a single phase sliding is selected for SMC such that all estimated states trajectories begin at the surface at an initial time moment which makes it highly robust for applications. System stability is proved via the Lyapunov theory based on a new LMI scheme. Experimental simulation results show the new controller performed better when compared with recent SMC in terms of the rapid control of frequency and tie-flow spikes, and achieved chattering free without any weak control accuracies against external disturbances acting on the large multi-area power system. In addition, the proposed sliding surface and new controller, which depend on only the observer state estimation, are useful in applications for real power systems where all system state variables are difficult or expensive to measure.

Author Contributions: Conceptualization V.V.H., E.N.A.; Methodology P.T.T., A.-T.T., E.N.A.; Software A.-T.T., E.N.A.; Validation B.L.N.M., P.T.T.; Writing—original draft preparation E.N.A.; Writing—review and editing V.V.H.; Supervision B.L.N.M. All authors have read and agreed to the published version of the manuscript.

Funding: This research is funded by Foundation for Science and Technology Development of Ton Duc Thang University (FOSTECT), website: http://fostect.tdtu.edu.vn, under Grant FOSTECT.2017.BR.05.

Data Availability Statement: All data used is reported in the paper.

Conflicts of Interest: The authors declare no conflict of interest.

References

1. Pandey, S.K.; Mohanty, S.R.; Kishor, N. A literature survey on load–frequency control for conventional and distribution generation power systems. *Renew. Sustain. Energy Rev.* **2013**, *25*, 318–334. [CrossRef]
2. Thirunavukarasu, R.; Chidambaram, I. PI2 controller based coordinated control with Redox flow battery and unified power flow controller for improved restoration indices in a deregulated power system. *Ain Shams Eng. J.* **2016**, *7*, 1011–1027. [CrossRef]
3. Farahani, M.; Ganjefar, S.; Alizadeh, M. PID controller adjustment using chaotic optimization algorithm for multi-area load frequency control. *IET Control. Theory Appl.* **2012**, *6*, 1984–1992. [CrossRef]
4. Saxena, S.; Hote, Y.V. Decentralized PID load frequency control for perturbed multi-area power systems. *Int. J. Electr. Power Energy Syst.* **2016**, *81*, 405–415. [CrossRef]
5. Yousef, H. Adaptive fuzzy logic load frequency control of multi-area power system. *Int. J. Electr. Power Energy Syst.* **2015**, *68*, 384–395. [CrossRef]
6. Chaturvedil, D.K.; Satsangi, P.S.; Kalra, P.K. Load frequency control: A generalized neural network approach. *Electr. Power Energy Syst.* **1999**, *21*, 405–415. [CrossRef]

7. Indulkar, C.S.; Raj, B. Application of fuzzy controller to automatic generation control. *Electr. Mach. Power Syst.* **1995**, *23*, 209–220. [CrossRef]
8. Ghoshal, S.P. Multi area frequency and tie line power flow control with fuzzy logic based integral gain scheduling. *J. Inst. Eng.* **2003**, *84*, 135–141.
9. Sinha, S.K.; Patel, R.N.; Prasad, R. Application of GA and PSO tuned fuzzy controller for AGC of three area thermal-thermal-hydro power system. *Int. J. Comput. Theory Eng.* **2010**, *2*, 238–244. [CrossRef]
10. Juang, C.-F.; Lu, C.-F. Load-frequency control by hybrid evolutionary fuzzy PI controller. *IEE Proc. Gener. Transm. Distrib.* **2006**, *153*, 196–204. [CrossRef]
11. Arya, Y.; Kumar, N. BFOA-scaled fractional order fuzzy PID controller applied to AGC of multi-area multi-source electric power generating sys-tems. *Swarm Evol. Comput.* **2017**, *32*, 202–218. [CrossRef]
12. Fathy, A.; Kassem, A.M.; Abdelaziz, A.Y. Optimal design of fuzzy PID controller for deregulated LFC of multi-area power system via mine blast algorithm. *Neural Comput. Appl.* **2018**, *32*, 4531–4551. [CrossRef]
13. Haroun, A.G.; Li, Y. A novel optimized hybrid fuzzy logic intelligent PID controller for an interconnected multi-area power system with physical constraints and boiler dynamics. *ISA Trans.* **2017**, *71*, 364–379. [CrossRef] [PubMed]
14. Kouba, N.E.Y.; Menaa, M.; Hasni, M.; Boudour, M. Load frequency control in multi-area power system based on Fuzzy Logic-PID Controller. In Proceedings of the 2015 IEEE International Conference on Smart Energy Grid Engineering (SEGE), Oshawa, ON, Canada, 17–19 August 2015; pp. 1–6.
15. Sahu, R.K.; Panda, S.; Yegireddy, N.K. A novel hybrid DEPS optimized fuzzy PI/PID controller for load frequency control of multi-area intercon-nected power systems. *J. Process. Control.* **2014**, *24*, 1596–1608. [CrossRef]
16. Jagatheesan, K.; Anand, B.; Samanta, S.; Dey, N.; Ashour, A.S.; Balas, V.E. Design of a proportional-integral-derivative controller for an automatic generation control of multi-area power thermal systems using firefly algorithm. *IEEE/CAA J. Autom. Sin.* **2017**, *6*, 503–5151. [CrossRef]
17. Mohapatra, T.K.; Sahu, B.K. Design and implementation of SSA based fractional order PID controller for automatic generation control of a multi-area, multi-source interconnected power system. In Proceedings of the Technologies for Smart-City Energy Security and Power (ICSESP), Bhubaneswar, India, 28–30 March 2018; pp. 1–6.
18. Raju, M.; Saikia, L.C.; Sinha, N. Automatic generation control of a multi-area system using ant lion optimizer algorithm based PID plus second order derivative controller. *Int. J. Electr. Power Energy Syst.* **2016**, *80*, 52–63. [CrossRef]
19. Jianping, G. Sliding Mode Based Load Frequency Control for an Interconnected Power System with Nonlinearities. Ph.D. Thesis, Cleveland State University, Cleveland, OH, USA, 2015.
20. Vrdoljak, K.; Perić, N.; Petrović, I. Sliding mode based load-frequency control in power systems. *Electr. Power Syst. Res.* **2010**, *80*, 514–527. [CrossRef]
21. Prasad, S.; Purwar, S.; Kishor, N. Non-linear sliding mode control for frequency regulation with variable-speed wind turbine systems. *Int. J. Electr. Power Energy Syst.* **2019**, *107*, 19–33. [CrossRef]
22. Trip, S.; Cucuzzella, M.; De Persis, C.; van der Schaft, A.; Ferrara, A. Passivity-based design of sliding modes for optimal load frequency control. *IEEE Trans. Control. Syst. Technol.* **2018**, *27*, 1893–1906. [CrossRef]
23. Huynh, V.V.; Tsai, Y.-W.; Duc, P.V. Adaptive output feedback sliding mode control for complex interconnected time-delay systems. *Math. Probl. Eng.* **2015**, 1–15. [CrossRef]
24. Lee, S.-W.; Chun, K.-H. Adaptive sliding mode control for PMSG wind turbine systems. *Energies* **2019**, *12*, 595. [CrossRef]
25. Lv, X.; Sun, Y.; Wang, Y.; Dinavahi, V. Adaptive event-triggered load frequency control of multi-area power systems under networked environ-ment via sliding mode control. *IEEE Access* **2020**, *8*, 86585–86594. [CrossRef]
26. Le Ngoc Minh, B.; Van Huynh, V.; Nguyen, T.M.; Tsai, Y.W. Decentralized adaptive double integral sliding mode controller for multi-area power systems. *Math. Probl. Eng.* **2018**, *2018*, 1–11. [CrossRef]
27. Guo, J. Application of full order sliding mode control based on different areas power system with load frequency control. *ISA Trans.* **2019**, *92*, 23–34. [CrossRef] [PubMed]
28. Sarkar, M.K.; Dev, A.; Asthana, P.; Narzary, D. Chattering free robust adaptive integral higher order sliding mode control for load frequency problems in multi-area power systems. *IET Control. Theory Appl.* **2018**, *12*, 1216–1227. [CrossRef]
29. Dev, A.; Sarkar, M.K.; Asthana, P.; Narzary, D. Event-triggered adaptive integral higher-order sliding mode control for load frequency problems in multi-area power systems. *Iran. J. Sci. Technol. Trans. Electr. Eng.* **2019**, *43*, 137–152. [CrossRef]
30. Hu, R.; Deng, H.; Zhang, Y. Novel dynamic-sliding-mode-manifold-based continuous fractional-order nonsingular terminal sliding mode control for a class of second-order nonlinear systems. *IEEE Access* **2020**, *8*, 19820–19829. [CrossRef]
31. Dev, A.; Sarkar, M.K. Robust higher order observer based non-linear super twisting load frequency control for multi area power systems via sliding mode. *Int. J. Control. Autom. Syst.* **2019**, *17*, 1814–1825. [CrossRef]
32. Prasad, S.; Purwar, S.; Kishor, N. Load frequency regulation using observer based non-linear sliding mode control. *Int. J. Electr. Power Energy Syst.* **2019**, *104*, 178–193. [CrossRef]
33. Tsai, Y.W.; Van, H.V. Adaptive Output Feedback Control for Mismatched Uncertain Systems: Single Phase Sliding Mode Approach. In Proceedings of the International Symposium on Computer, Consumer and Control, Taichung, Taiwan, 10–12 June 2014; pp. 990–993.
34. Boyd, S.; El Ghaoui, L.; Feron, E.; Balakrishnan, V. *Linear Matrix Inequalities in System and Control Theory*; Society for Industrial and Applied Mathematics (SIAM): Philadelphia, PA, USA, 1994.

35. Manikandan, S.; Kokil, P. Stability analysis of load frequency control system with constant communication delays. *IFAC Papersonline* **2020**, *53*, 338–343. [CrossRef]
36. Liao, K.; Xu, Y. A robust load frequency control scheme for power systems based on second-order sliding mode and extended disturbance observer. *IEEE Trans. Ind. Inform.* **2017**, *14*, 3076–3086. [CrossRef]

energies

Article

Load Frequency Regulator in Interconnected Power System Using Second-Order Sliding Mode Control Combined with State Estimator

Anh-Tuan Tran [1], Bui Le Ngoc Minh [2,3], Van Van Huynh [1,*], Phong Thanh Tran [1], Emmanuel Nduka Amaefule [1], Van-Duc Phan [4] and Tam Minh Nguyen [2]

1 Modeling Evolutionary Algorithms Simulation and Artificial Intelligence, Faculty of Electrical & Electronics Engineering, Ton Duc Thang University, Ho Chi Minh City 700000, Vietnam; trananhtuan.st@tdtu.edu.vn (A.-T.T.); tranthanhphong.st@tdtu.edu.vn (P.T.T.); ndukaamaefuleemmanuel.st@tdtu.edu.vn (E.N.A.)
2 Faculty of Electrical and Electronics Engineering, Ho Chi Minh City University of Technology and Education, Ho Chi Minh City 700000, Vietnam; 1726002@student.hcmute.edu.vn (B.L.N.M.); tamnm@hcmute.edu.vn (T.M.N.)
3 Faculty of Industrial Engineering, Tien Giang University, My Tho City 840000, Vietnam
4 Faculty of Automobile Technology, Van Lang University, Ho Chi Minh City 700000, Vietnam; duc.pv@vlu.edu.vn
* Correspondence: huynhvanvan@tdtu.edu.vn

Abstract: In multi-area interconnected power systems (MAIPS), the measurement of all system states is difficult due to the lack of a sensor or the fact that it is expensive to measure. In order to solve this limitation, a new load frequency controller based on the second-order sliding mode is designed for MAIPS where the estimated state variable is used fully in the sliding surface and controller. Firstly, a model of MAIPS integrated with disturbance is introduced. Secondly, an observer has been designed and used to estimate the unmeasured variables with disturbance. Thirdly, a new second-order sliding mode control (SOSMC) law is used to reduce the chattering in the system dynamics where slide surface and sliding mode controller are designed based on system states observer. The stability of the whole system is guaranteed via the Lyapunov theory. Even though state variables are not measured, the experimental simulation results show that the frequency remains in the nominal range under load disturbances, matched and mismatched uncertainties of the MAIPS. A comparison to other controllers illustrates the superiority of the highlighted controller designed in this paper.

Keywords: load frequency control; multi area power system; sliding mode control

Citation: Tran, A.-T.; Minh, B.L.N.; Huynh, V.V.; Tran, P.T.; Amaefule, E.N.; Phan, V.-D.; Nguyen, T.M. Load Frequency Regulator in Interconnected Power System Using Second-Order Sliding Mode Control Combined with State Estimator. *Energies* **2021**, *14*, 863. https://doi.org/10.3390/en14040863

Academic Editor: Muhammad Aziz
Received: 15 January 2021
Accepted: 4 February 2021
Published: 7 February 2021

1. Introduction

In modern multi-area power systems (MAPS), where the power plants are geographically distributed, maintaining the tie-power flow and frequency are the central aspects of the MAPS. At sudden change in the net load, frequency and tie-schedule power deviate from nominal. Therefore, it is essential to preserve the quality of the generated power in the power plant through designing a load frequency control (LFC) [1–6]. The general function of the LFC is to maintain the balance between the new net-load demand and the generated power by regulating the tie-line and frequency power flow in MAPS.

In general, power plants are connected together via tie-lines. Maintaining scheduled power flows between interconnected large systems is very crucial. Moreover, keeping the frequencies of each area in a nominal range where the plant model exhibits the following drawbacks: random load change, and mismatched uncertainties. These made the LFC design more complex [7]. Thus, two approaches are used for LFC in the interconnected power network: a centralized and decentralized LFC scheme where the second scheme is preferable as the controller feed-in by the regional information [8–10].

There are a lot of control methods that have been designed for LFC, and the significant research papers were proposed for LFC as summarized in [11]. Proportional integral (PI) is the first control method studied in the field of LFC, where the mismatched parameters were neglected. It follows that the PI tuned once for specific operating conditions, hence the PI controller failed under variable operating points [12]. In recent years, some advanced control methods have also been developed. Some intelligent control schemes such as particle swarm optimization, fuzzy logic, artificial neural network and genetic algorithm have been proposed for LFC in MAPS [13–17]. In addition, the optimal control scheme with Proportional integral derivative (PID), particularly the particle swarm optimization (PSO) algorithm, was implemented for tuning PID-based LFC [18]. However, the above-proposed controllers consider the mismatched uncertainty of the power systems [19].

Robust control scheme such as variable structure control (VSC) is used to control power frequency. VSC is robust against various power system problems. VSC for LFC for MAPS is presented in [20]. Among the VSC control methods, sliding mode control (SMC) has been greatly used by control engineers. The SMC method is discussed in [21]. The SMC control strategy provides robust performance and fast response. Discrete and continuous time SMC for LFC are examined for power systems [22,23], respectively. A decentralized SMC with an integral sliding surface is studied and presented in [24]. In the literature, the SMC discussed acts on a first-order time derivative. The first-order SMC combination with state observer is provided for LFC in MAPS which is suffered from chattering phenomenon [25]. The second-order sliding mode control (SOSMC) has been proposed to handle this problem [26]. The system state variables were assumed to be measured [20–26]. In contrast, some state variables of the real power system are difficult to measure. The direct measurements with sensors in some cases are difficult or expensive for the measurement. In order to solve the above problem, the state observer has been widely explored for industrial application such as the Luenberger observer [27], unscented Kalman filter [28] and extended observer [29] where the system performance is also affected by matched uncertainty. The state estimator for LFC of MAPS is employed and presented in [29]. With the aim of improving the system performance, first-order SMC based on an observer has been used to observe the load disturbance of the power network given in [30,31]. Also, SOSMC combined with a state estimator has been used to observe the disturbance of the MAPS to improve the system performance with making it free of chattering [32,33]. These controllers above were designed to observe the load change and keep the frequency at nominal if all the system state variables are measured. However, this cannot guarantee for the practical application of these above controllers where some state variables of MAPS are not measurable or difficult to measure. Therefore, this motivates the design of LFC based on a new SMC where the state observer is used fully in the sliding surface and a decentralized second-order sliding mode controller (SOSMCr) is used to solve the above the problems. The major contributions of the paper are as below:

- The integral sliding surface (ISS) and the decentralized controller are designed based on the estimated system state variables (SSV) so that we do not need to measure the power SSV to achieve LFC. Therefore, the limitation of measuring the power system state variables to achieve LFC in [32,33] has been solved.
- A new LMI technique is proposed to ensure the stability of MAPS via the Lyapunov theory.
- SOSMC combined with state estimator is designed to improve the system performance due to a decrease in chattering in the control input.
- The simulation results indicate the proposed approach has a better performance in terms of settling time and under/overshoots. Thus, this provides evidence of the new controller application for large MAPS.

2. Model of Two-Area Power System (TAPS) in State Space Form

In this section, we introduce the linear dynamic equations for TAPS. A representative diagram of a decentralized LFC for the system is presented in Figure 1. Both areas have their proposed local controller which will be designed in the following sections. The interconnected power line and frequency are kept constant by the proposed local controller. In general, the frequency regulator scheme consists of two feedback loops, mainly the primary LFC loop (inner loop) and secondary LFC loop (outer loop). The inner loop consists of governor droop speed. The outer loop consists of the proposed controller.

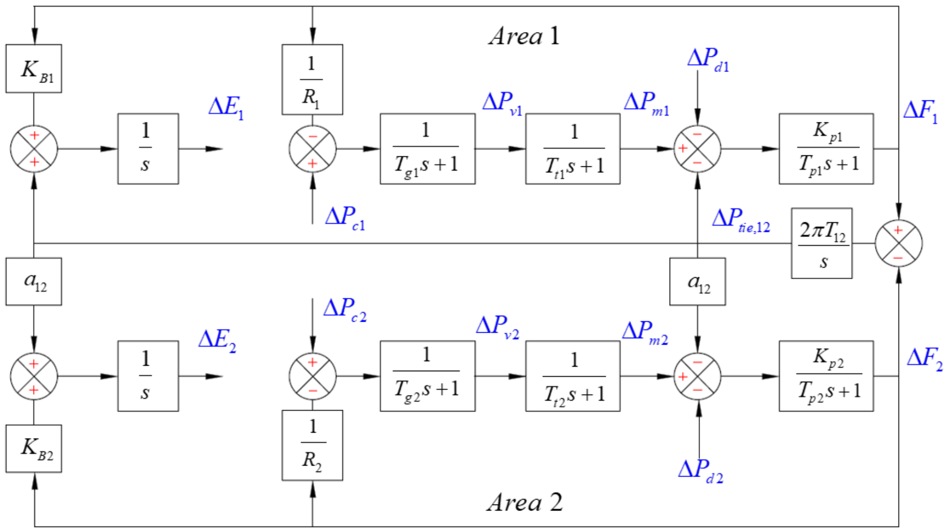

Figure 1. Schematics of TAPS interconnection.

The SSV denoted in Figure 1 describes the dynamics of the TAPS.
Using the above system model, the following differential equations are obtained

$$\Delta \dot{f}_1 = -\frac{1}{T_{p1}}\Delta f_1 + \frac{K_{p1}}{T_{p1}}\Delta P_{m1} - \frac{K_{p1}}{T_{p1}}\Delta P_{tie1,2} - \frac{K_{p1}}{T_{p1}}\Delta P_{d1} \tag{1}$$

$$\Delta \dot{P}_{m1} = -\frac{1}{T_{t1}}\Delta P_{m1} + \frac{1}{T_{t1}}\Delta P_{v1} \tag{2}$$

$$\Delta \dot{P}_{v1} = -\frac{1}{R_1 T_{g1}}\Delta f_1 - \frac{1}{T_{g1}}\Delta P_{v1} + \frac{1}{T_{g1}}\Delta P_{c1} \tag{3}$$

$$\Delta \dot{f}_2 = -\frac{1}{T_{p2}}\Delta f_2 + \frac{K_{p2}}{T_{p2}}\Delta P_{m2} - \frac{a_{12}K_{p2}}{T_{p2}}\Delta P_{tie1,2} - \frac{K_{p2}}{T_{p2}}\Delta P_{d2} \tag{4}$$

$$\Delta \dot{P}_{m2} = -\frac{1}{T_{t2}}\Delta P_{m2} + \frac{1}{T_{t2}}\Delta P_{v2} \tag{5}$$

$$\Delta \dot{P}_{v2} = -\frac{1}{R_2 T_{g2}}\Delta f_2 - \frac{1}{T_{g2}}\Delta P_{v2} + \frac{1}{T_{g2}}\Delta P_{c2} \tag{6}$$

$$\Delta P_{tie1,2} = 2\pi T_{12}\Delta f_1 - 2\pi T_{12}\Delta f_2 \tag{7}$$

$$\Delta \dot{E}_1 = K_{B1}\Delta f_1 + \Delta P_{tie1,2} \tag{8}$$

$$\Delta \dot{E}_2 = K_{B2}\Delta f_2 + a_{12}\Delta P_{tie1,2} \tag{9}$$

where Δf_1 and Δf_2 are the frequency deviations of the first and second areas, ΔP_{m1} and ΔP_{m2} are the generator mechanical output deviations of the first and second areas, ΔP_{v1} and ΔP_{v2} are the valve position deviations of first and second areas, ΔE_1 and ΔE_2 are the area control errors of first and second areas, $\Delta P_{tie1,2}$ is the tie-line active power deviation between the first and second areas. K_{p1} and K_{p2} are operations of the system power of the first and second areas, T_{p1} and T_{p2} are time constants of the power system of the first and second areas, T_{t1} and T_{t2} are turbine time constants of the first and second areas, T_{g1} and

T_{g2} are governor time constants of steam of the first and second areas, R_1 and R_2 are speed drops of the first and second areas, K_{B1} and K_{B2} are frequency bias factors of the first and second areas, T_{12} is the tie-line reactance and synchronizing coefficient between the first and second areas, and a_{12} is the control area capacity ratio.

The system dynamic Equations (1)–(9) are defined in the state space form

$$\begin{aligned} \dot{x}(t) &= Ax(t) + Bu(t) + Fw(t) \\ y(t) &= Cx(t) \end{aligned} \tag{10}$$

where

$$B = \begin{bmatrix} 0 & 0 & \frac{1}{T_{g1}} & 0 & 0 & 0 & 0 & 0 & 0 \\ 0 & 0 & 0 & 0 & 0 & \frac{1}{T_{g2}} & 0 & 0 & 0 \end{bmatrix}^T; \quad F = \begin{bmatrix} -\frac{K_{p1}}{T_{p1}} & 0 & 0 & 0 & 0 & 0 & 0 & 0 & 0 \\ 0 & 0 & 0 & -\frac{K_{p2}}{T_{p2}} & 0 & 0 & 0 & 0 & 0 \end{bmatrix}^T$$

$$A = \begin{bmatrix} -\frac{1}{T_{p1}} & \frac{K_{p1}}{T_{p1}} & 0 & 0 & 0 & 0 & -\frac{K_{p1}}{T_{p1}} & 0 & 0 \\ 0 & -\frac{1}{T_{t1}} & \frac{1}{T_{t1}} & 0 & 0 & 0 & 0 & 0 & 0 \\ -\frac{1}{R_1 T_{g1}} & 0 & -\frac{1}{T_{g1}} & 0 & 0 & 0 & 0 & 0 & 0 \\ 0 & 0 & 0 & -\frac{1}{T_{p2}} & \frac{K_{p2}}{T_{p2}} & 0 & -\frac{a_{12}K_{p2}}{T_{p2}} & 0 & 0 \\ 0 & 0 & 0 & 0 & -\frac{1}{T_{t2}} & \frac{1}{T_{t2}} & 0 & 0 & 0 \\ 0 & 0 & 0 & -\frac{1}{R_2 T_{g2}} & 0 & -\frac{1}{T_{g2}} & 0 & 0 & 0 \\ 2\pi T_{12} & 0 & 0 & -2\pi T_{12} & 0 & 0 & 0 & 0 & 0 \\ B_1 & 0 & 0 & 0 & 0 & 0 & 1 & 0 & 0 \\ 0 & 0 & 0 & B_2 & 0 & 0 & a_{12} & 0 & 0 \end{bmatrix}$$

System variable: $x(t) = [\Delta f_1 \;\; \Delta P_{m1} \;\; \Delta P_{v1} \;\; \Delta f_2 \;\; \Delta P_{m2} \;\; \Delta P_{v2} \;\; \Delta P_{tie,12} \;\; \Delta E_1 \;\; \Delta E_2]^T$
Control input: $u(t) = \begin{bmatrix} \Delta P_{c1} & \Delta P_{c2} \end{bmatrix}^T$
Disturbance: $w(t) = \begin{bmatrix} \Delta P_{d1} & \Delta P_{d2} \end{bmatrix}^T$
The basic assumptions are derived for the progress of this work.

Assumption 1. *The pair matrices (A, B) are controllable and the pair matrices (A, C) are observable.*

Assumption 2. *The disturbance in Equation (10) is bounded and defined by $\|w(t)\| \leq \varsigma$, where $\|.\|$ is the norm.*

In addition, some Lemma are adopted for the progress of the paper.

Lemma 1 ([34])**.** *Let $\mathbf{X}$ and $\mathbf{Y}$ be a real matrix of suitable dimension then, for any scalar $\mu > 0$, the below matrix inequality holds:*

$$\mathbf{X}^T\mathbf{Y} + \mathbf{Y}^T\mathbf{X} \leq \mu\mathbf{X}^T\mathbf{X} + \mu^{-1}\mathbf{Y}^T\mathbf{Y}. \tag{11}$$

Lemma 2 ([34])**.** *The following matrix inequality*

$$\begin{bmatrix} R(z) & I(z) \\ I(z)^T & P(z) \end{bmatrix} > 0 \tag{12}$$

where $R(z) = R(z)^T$, $P(z) = P(z)^T$ and $I(z)$ depend affinity on z, is equivalent to $P(z) > 0$

$$R(z) - I(z)P(z)^{-1}I(z)^T > 0. \tag{13}$$

3. New Second Order-Sliding Mode Control Based Observer Design

3.1. Design of Observer

In control system engineering, it is costly or hard (or sometimes impossible) to measure all system variables; the direct observation of the physical state of the system cannot be done in some cases. Analyzing the indirect effect between the measured input and output signal is considered. Observing and estimating the unmeasured states by measuring enough state variables has been used to overcome this limitation. Due to the estimations, inaccurate results would be inevitable. The state observer is a subsystem that computes the internal state of a given system which cares for unmeasured state variables, by knowing the input and output of the real power system. We use a state space form of the systems open loop to design the observer, and it is written as follows:

$$\begin{aligned} \dot{z}(t) &= Az(t) + Bu(t) + L[y(t) - \hat{y}(t)] \\ \hat{y}(t) &= Cz(t) \end{aligned} \tag{14}$$

The states observed take two inputs from measuring the real power system, which is $u(t)$ and $y(t)$, the estimated state $\hat{y}(t)$ is the output signal coming from the observer. To make the system stable, we chose proper feedback gain K via the pole assignment method which makes the eigenvalues of $A^T - C^T K$ lie in the predefined locations in the negative hyperplane. The observer gain L for the system can be calculated by using the following relationship: $L = K^T$.

3.2. Integral Sliding Surface (ISS) with State Observer

In this subsection, the design of the proposed controller includes two steps. Firstly, the design of ISS which the states of the system in the ISS can asymptotically converge to zero. Secondly, a robust SOSMCr is designed for the system states which always converged to the predefined sliding surface.

We begin by proposing an ISS for the power system

$$\sigma[z(t)] = Gz(t) - \int_0^t G(A - BK)z(\tau)d\tau \tag{15}$$

where G is the constant matrix and K is the design matrix. G is calculated to ensure that matrix GB is invertible. $K \in R^{m \times n}$ satisfies the inequality in Equation (16)

$$\mathrm{Re}[\lambda_{\max}(A - BK)] < 0 \tag{16}$$

Taking time derivative of Equation (15) and combined with Equation (14), then

$$\dot{\sigma}[z(t)] = G\{Az(t) + Bu(t) + L[y(t) - \hat{y}(t)]\} - G(A - BK)z(t) \tag{17}$$

Setting $\dot{\sigma}[z(t)] = \sigma[z(t)] = 0$, we can see that the equivalent control is presented as

$$u^{eq}(t) = -(GB)^{-1}[GAz(t) + GL[y(t) - \hat{y}(t)] - G(A - BK)z(t)] \tag{18}$$

Substituting Equation (18) into the MAPS in Equation (10) yields

$$\begin{aligned} \dot{x}(t) &= Ax(t) + Bu(t) + Fw(t) \\ &= Ax(t) - BKz(t) - B(GB)^{-1}GL[y(t) - \hat{y}(t)] + Fw(t) \\ &= (A - BK)x(t) + (BK - B(GB)^{-1}GLC)d(t) + Fw(t) \end{aligned} \tag{19}$$

where $d(t)$ is the difference of the estimated and real SSV. Then the time derivative of $d(t)$ is as below

$$\dot{d}(t) = \dot{x}(t) - \dot{z}(t) = (A - LC)d(t) + Fw(t) \tag{20}$$

The sliding motion equation can be rewritten as the equation below:

$$\begin{bmatrix} \dot{x}(t) \\ \dot{d}(t) \end{bmatrix} = \begin{bmatrix} A-BK & (BK - B(GB)^{-1}GLC) \\ 0 & A-LC \end{bmatrix} \begin{bmatrix} x(t) \\ d(t) \end{bmatrix} + \begin{bmatrix} Fw(t) \\ Fw(t) \end{bmatrix} \tag{21}$$

Equation (21) is the power system in the ISS where an eigenvalue of $(A - BK)$ is used to drive the estimated SSV to the hyperplane. The stability of MAPS can be stated as follows.

Theorem 1. *The dynamic system as described in Equation (21) is asymptotically stable, if there exist two positive definite matrices R, P and positive scalars μ, γ such that the following LMIs hold*

$$\begin{bmatrix} R(A-BK)+(A-BK)^T R & R(BK-B(GB)^{-1}GLC) & F^T R & 0 \\ (BK-B(GB)^{-1}GLC)^T R & P(A-LC)+(A-LC)^T P & 0 & F^T P \\ RF & 0 & -\mu^{-1} & 0 \\ 0 & PF & 0 & -\gamma^{-1} \end{bmatrix} < 0. \tag{22}$$

To demonstrate the stability of the system dynamic, the Lyapunov function is selected as follows:

$$V[x(t), d(t)] = \begin{bmatrix} x(t) \\ d(t) \end{bmatrix}^T \begin{bmatrix} R & 0 \\ 0 & P \end{bmatrix} \begin{bmatrix} x(t) \\ d(t) \end{bmatrix} \tag{23}$$

The derivative of $V[x(t), d(t)]$ is given by

$$\dot{V}[x(t), d(t)] = \begin{bmatrix} x(t) \\ d(t) \end{bmatrix}^T \begin{bmatrix} R & 0 \\ 0 & P \end{bmatrix} \begin{bmatrix} \dot{x}(t) \\ \dot{d}(t) \end{bmatrix} + \begin{bmatrix} \dot{x}(t) \\ \dot{d}(t) \end{bmatrix}^T \begin{bmatrix} R & 0 \\ 0 & P \end{bmatrix} \begin{bmatrix} x(t) \\ d(t) \end{bmatrix} \tag{24}$$

According to Equations (19) and (24), we have

$$\begin{aligned}
&\dot{V}[x(t), d(t)] = \begin{bmatrix} x(t) \\ d(t) \end{bmatrix}^T \begin{bmatrix} R & 0 \\ 0 & P \end{bmatrix} \left\{ \begin{bmatrix} A-BK & (BK-B(GB)^{-1}GLC) \\ 0 & A-LC \end{bmatrix} \begin{bmatrix} x(t) \\ d(t) \end{bmatrix} + \begin{bmatrix} Fw(t) \\ Fw(t) \end{bmatrix} \right\} \\
&+ \left[\begin{bmatrix} A-BK & (BK-B(GB)^{-1}GLC) \\ 0 & A-LC \end{bmatrix} \begin{bmatrix} x(t) \\ d(t) \end{bmatrix} + \begin{bmatrix} Fw(t) \\ Fw(t) \end{bmatrix} \right]^T \begin{bmatrix} R & 0 \\ 0 & P \end{bmatrix} \begin{bmatrix} x(t) \\ d(t) \end{bmatrix} \\
&= \begin{bmatrix} x(t) \\ d(t) \end{bmatrix}^T \begin{bmatrix} R(A-BK) & R(BK-B(GB)^{-1}GLC) \\ 0 & P(A-LC) \end{bmatrix} \begin{bmatrix} x(t) \\ d(t) \end{bmatrix} + \begin{bmatrix} x(t) \\ d(t) \end{bmatrix}^T \begin{bmatrix} R & 0 \\ 0 & P \end{bmatrix} \begin{bmatrix} Fw(t) \\ Fw(t) \end{bmatrix} \\
&+ \begin{bmatrix} x(t) \\ d(t) \end{bmatrix}^T \begin{bmatrix} (A-BK)^T R & 0 \\ (BK-B(GB)^{-1}GLC)^T R & (A-LC)^T P \end{bmatrix} \begin{bmatrix} x(t) \\ d(t) \end{bmatrix} + \begin{bmatrix} Fw(t) \\ Fw(t) \end{bmatrix}^T \begin{bmatrix} R & 0 \\ 0 & P \end{bmatrix} \begin{bmatrix} x(t) \\ d(t) \end{bmatrix} \\
&= \begin{bmatrix} x(t) \\ d(t) \end{bmatrix}^T \begin{bmatrix} R(A-BK)+(A-BK)^T R & R(BK-B(GB)^{-1}GLC) \\ (BK-B(GB)^{-1}GLC)^T R & P(A-LC)+(A-LC)^T P \end{bmatrix} \begin{bmatrix} x(t) \\ d(t) \end{bmatrix} \\
&+ x^T(t)RFw(t) + w^T(t)F^T Rx(t) + d^T(t)PFw(t) + w^T(t)F^T Pd(t)
\end{aligned} \tag{25}$$

Applying Lemma 1 to Equation (25), we obtain

$$\begin{aligned}
&\dot{V}[x(t), d(t)] \leq \begin{bmatrix} x(t) \\ d(t) \end{bmatrix}^T \begin{bmatrix} R(A-BK)+(A-BK)^T R & R(BK-B(GB)^{-1}GLC) \\ (BK-B(GB)^{-1}GLC)^T R & P(A-LC)+(A-LC)^T P \end{bmatrix} \begin{bmatrix} x(t) \\ d(t) \end{bmatrix} \\
&+ \mu x^T(t)RFF^T Rx(t) + \mu^{-1} w^T(t)w(t) + \gamma d^T(t)PFF^T Pd(t) + \gamma^{-1} w^T(t)w(t) \\
&\leq \begin{bmatrix} x(t) \\ d(t) \end{bmatrix}^T \begin{bmatrix} R(A-BK)+(A-BK)^T R + \mu RFF^T R & R(BK-B(GB)^{-1}GLC) \\ (BK-B(GB)^{-1}GLC)^T R & P(A-LC)+(A-LC)^T P + \gamma PFF^T P \end{bmatrix} \begin{bmatrix} x(t) \\ d(t) \end{bmatrix} \\
&+ \lambda \varsigma^2
\end{aligned} \tag{26}$$

where $\lambda = \gamma^{-1} + \mu^{-1}$.

Simplifying Equation (26), we get

$$\dot{V}[x(t), d(t)] \leq \begin{bmatrix} x(t) \\ d(t) \end{bmatrix}^T \Phi \begin{bmatrix} x(t) \\ d(t) \end{bmatrix} + \lambda\varsigma^2 \tag{27}$$

In addition, by using Lemma 2 to Equation (22), the LMI (22) is equivalent to the below equation

$$\Phi = -\begin{bmatrix} R(A-BK) + (A-BK)^T R + \mu RFF^T R & R(BK - B(GB)^{-1}GLC) \\ (BK - B(GB)^{-1}GLC)^T R & P(A-LC) + (A-LC)^T P + \gamma PFF^T P \end{bmatrix} > 0 \tag{28}$$

From Equations (27) and (28), it can be obtained

$$\dot{V} \leq -\lambda_{\min}(\Phi) \| \begin{bmatrix} x(t) \\ d(t) \end{bmatrix} \|^2 + \partial \tag{29}$$

where the constant value is $\partial = \lambda\varsigma^2$ and the eigenvalue is $\lambda_{\min}(\Phi) > 0$.Therefore, $\dot{V}[x(t), d(t)] < 0$ is achieved with $\| \begin{bmatrix} x(t) \\ d(t) \end{bmatrix} \| > \sqrt{\frac{\partial}{\lambda_{\min}(\Phi)}}$. Hence, the sliding motion (21) is asymptotically stable.

3.3. Design of Second-Order Sliding Mode Controller Based on State Estimator

In the previous step, we designed the new ISS based on a state observer and proved the whole system is asymptotically stable. In this step, the SOSMC is designed. The concept behind the SOSMC is to take the advantage of the second-order time derivative of the sliding variable $\sigma[z(t)]$ rather than first derivative.

We consider the following sliding manifold $M[z(t)]$

$$M[z(t)] = \dot{\sigma}[z(t)] + \varepsilon\sigma[z(t)] \tag{30}$$

and

$$\dot{M}[z(t)] = \ddot{\sigma}[z(t)] + \varepsilon\dot{\sigma}[z(t)] \tag{31}$$

where $\varepsilon > 0$ is a positive constant. Using the above Equations (17) and (31) yield

$$\begin{aligned} \dot{M}[z(t)] &= G\Big\{A\dot{z}(t) + B\dot{u}(t) + L[\dot{y}(t) - \dot{\hat{y}}(t)]\Big\} - G(A-BK)\dot{z}(t) + \varepsilon\dot{\sigma}[z(t)] \\ &= GB\dot{u}(t) + GL[\dot{y}(t) - \dot{\hat{y}}(t)] + GBK\dot{z}(t) + \varepsilon\dot{\sigma}[z(t)] \end{aligned} \tag{32}$$

As sliding surface and sliding manifold are defined above, the continuous decentralized SOSMC scheme which only depends on the state observer for LFC of the MAPS can be designed as follows

$$\dot{u}(t) = -(GB)^{-1}\Big\{GL[\dot{y}(t) - \dot{\hat{y}}(t)] + GBK\dot{z}(t) + \varepsilon\dot{\sigma}[z(t)] + \delta sat(M[z(t)])\Big\} \tag{33}$$

where

$$sat(M[z(t)]) = \begin{cases} -1 & if \quad M[z(t)] < -1 \\ M[z(t)] & if \quad -1 < M[z(t)] < 1 \\ 1 & if \quad M[z(t)] > 1 \end{cases}$$

To prove reachability of the estimated SSV to the sliding manifold, the following theorem is given as

Theorem 2. *The reachability of the estimated SSV is guaranteed, if the trajectory of the estimated SSV is directed towards the sliding manifold $M[z(t)] = 0$ and once the trajectory hits the sliding manifold $M[z(t)] = 0$ it remains on the sliding manifold thereafter.*

The Lyapunov function is described as

$$\overline{V}(t) = \frac{1}{2}M^2[z(t)] \tag{34}$$

Taking the derivative of $\overline{V}(t)$ yields

$$\begin{aligned}\dot{\overline{V}}(t) &= \tfrac{1}{2}\Big\{\dot{M}[z(t)] \times M^T[z(t)] + M[z(t)] \times \dot{M}^T[z(t)]\Big\} \\ &= M^T[z(t)]\Big\{GA\dot{z}(t) + GB\dot{u}(t) + GL[\dot{y}(t) - \dot{\hat{y}}(t)] - G(A - BK)\dot{z}(t) + \varepsilon\dot{\sigma}[z(t)]\Big\}\end{aligned} \tag{35}$$

According to Assumption 1 we achieve

$$\dot{\overline{V}}(t) = M^T[z(t)]\Big\{GBK\dot{z}(t) + GL[\dot{y}(t) - \dot{\hat{y}}(t)] + \varepsilon\dot{\sigma}[z(t)]\Big\} + M^T[z(t)]GB\dot{u}(t) \le 0 \tag{36}$$

Using the control law (33), we have

$$\begin{aligned}\dot{\overline{V}} &\le M^T[z(t)]\Big\{GBK\dot{z}(t) + GL[\dot{y}(t) - \dot{\hat{y}}(t)] + \varepsilon\dot{\sigma}[z(t)]\Big\} \\ &\quad - M^T[z(t)]GB[(GB)^{-1}\Big\{GL[\dot{y}(t) - \dot{\hat{y}}(t)] + GBK\dot{\hat{x}}(t) + \varepsilon\dot{\sigma}[z(t)] + \delta sat(M[z(t)])\Big\}] \\ &\le -\delta M^T[z(t)]sat(M[z(t)]) \\ &\le -\delta\|M[z(t)]\|^2\end{aligned} \tag{37}$$

Therefore, $\dot{\overline{V}}$ is less than zero which shows that the reachability of the estimated SSV to the ISS is guaranteed.

4. Results and Discussions

4.1. Simulation 1: Two-Area Power System (TAPS)

In the first simulation, a numerical simulation for three cases was conducted to examine the feasibility of the proposed designed SOSMC. Subsystem parameters are used to simulate the model as written in Table 1. The three cases can be summarized as follows:

Case 1: Step load disturbance under a nominal condition.
Case 2: Step load disturbance under mismatched uncertainty.
Case 3: Random load disturbance under mismatched uncertainty.

And their results are compared with ref [31].

Table 1. Nominal parameters of TAPS.

Areas	T_p	K_p	K_B	R	T_g	T_t	K_E	T_{12}
1	8	0.67	81.5	0.05	0.4	0.17	0.5	3.77
2	10	1.00	41.5		0.1	0.30		

Case 1: Step load disturbance with nominal conditions

First, we simulated the response of the TAPS with SOSMC by introducing a step load change of magnitude $\Delta P_{d1} = 0.02\,(p.u\,MV)$ in area 1 and $\Delta P_{d2} = 0.045\,(p.u\,MV)$ in area 2. The frequency divergence in area one (solid line) and area two (dashed line) are illustrated in Figure 2. The tie-line variation is illustrated in Figure 3. The control input signal for area one and two are given in Figure 4.

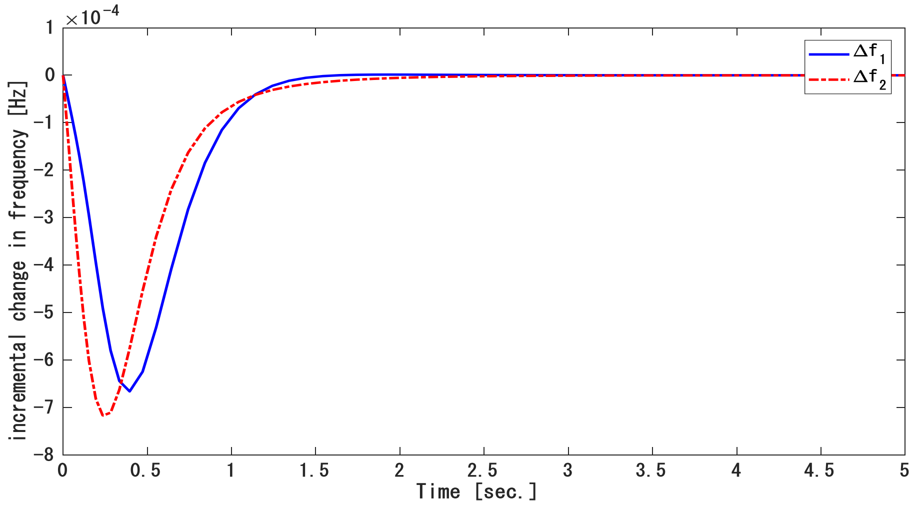

Figure 2. The frequency variation.

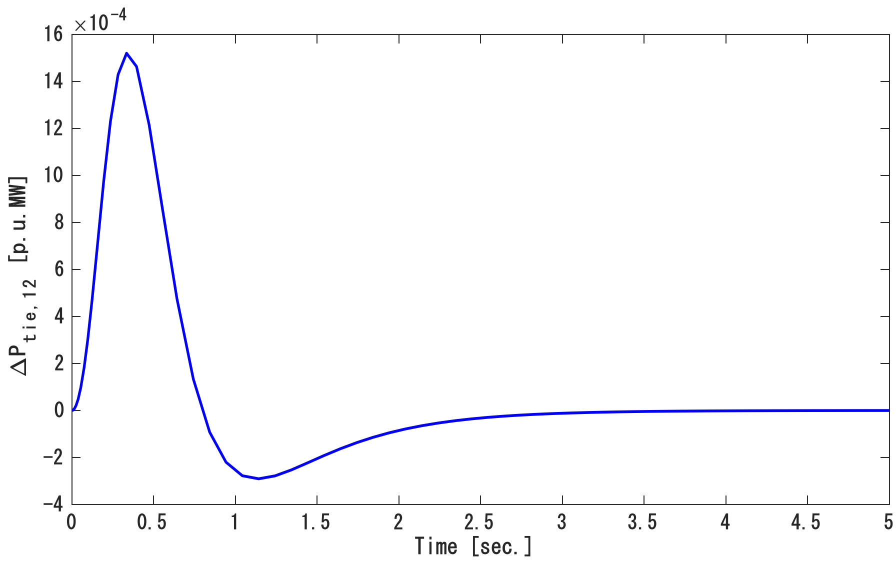

Figure 3. The tie-line power deviations.

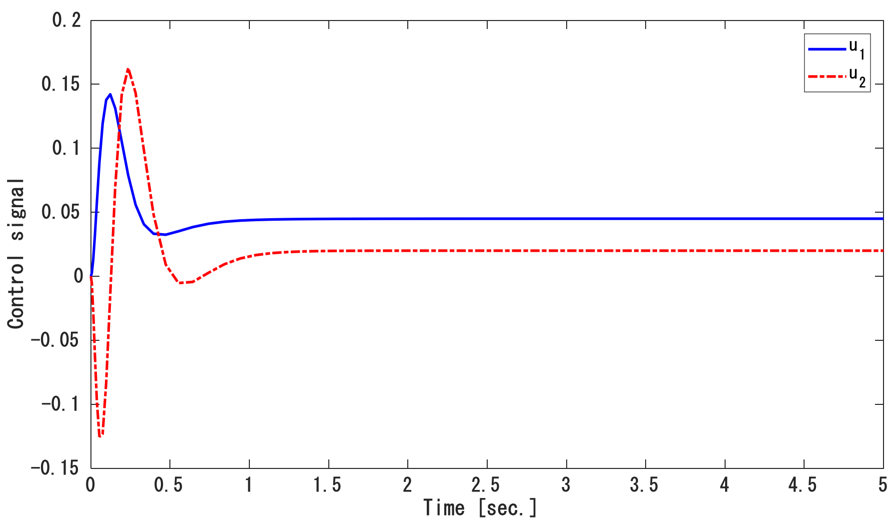

Figure 4. Control signal.

Frequency and tie-line deviate away from the initial point under the step load. The overshoots seen are damped by the propose controller at a fast response time of 2.5 s. This is achieved by the designed controller gain matrix K in the integral surface. A lack of chattering with control accuracy is also seen in the results, which are due to the SOSMC technique employed. In Figure 4, the small overshoot showed lesser energy used by the designed controller.

Remark 1. *Even though we used the information of the system state variables from the observer rather than from the sensor, the frequency deviation and the tie-line power fluctuation are kept in a safer range and the system response is better about under/overshoot and settling time.*

Case 2. Step load disturbance under the mismatched uncertainty.

The proposed SMC scheme was carried out in the presence of the mismatched condition, and the nonlinear term was linearized to make the model of the system consistent in Figure 1, which consists of deleting some higher order terms, where some error will occur between the real system and the simulation model. The step load disturbances were chosen in the same way as case 1. Furthermore, un-modeled dynamics can degrade the stability of the MAPS. To show the robustness of the new controller, a $\pm$ 20% of the nominal value was applied to the system parameters and the un-model dynamic was considered and represented by the cosine function [31]:

$$\Delta A = \begin{bmatrix} 0 & 0 & 0 & 0 & 0 & 0 & 0 & 0 & 0 \\ 0 & 0 & 0 & 0 & 0 & 0 & 0 & 0 & 0 \\ 40\cos(t) & 0 & 1.6\cos(t) & 0 & 0 & 0 & 0 & 1.6\cos(t) & 0 \\ 0 & 0 & 0 & 0 & 0 & 0 & 0 & 0 & 0 \\ 0 & 0 & 0 & 0 & 0 & 0 & 0 & 0 & 0 \\ 0 & 0 & 0 & 0.46\cos(t) & 0 & 6\cos(t) & 0 & 0 & 6\cos(t) \\ 0 & 0 & 0 & 0 & 0 & 0 & 0 & 0 & 0 \\ 0 & 0 & 0 & 0 & 0 & 0 & 0 & 0 & 0 \\ 0 & 0 & 0 & 0 & 0 & 0 & 0 & 0 & 0 \end{bmatrix} \quad (38)$$

The deviation in the frequency of the first and second areas is displayed in Figure 5, and the tie-line power fluctuation is displayed in Figure 6. Figure 7 gives the input of the controller u_1 and u_2. Once again, at normal operation, the dynamic changes are at zero marks. With the matched condition in the state matrix as shown in [31], both dynamic change values fluctuated, respectively. At 3 s the dynamic spikes were brought to a safe range. The response of the MAPS in terms of the maximum overshoots and settling time are in comparison with [31]. The values of both are written in Table 2.

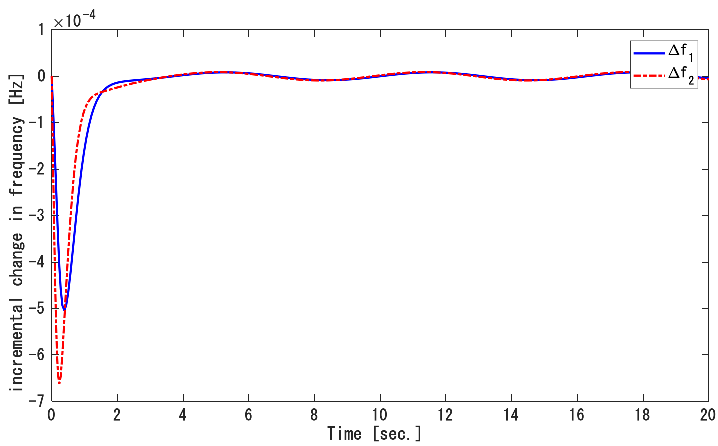

Figure 5. The frequency deviations.

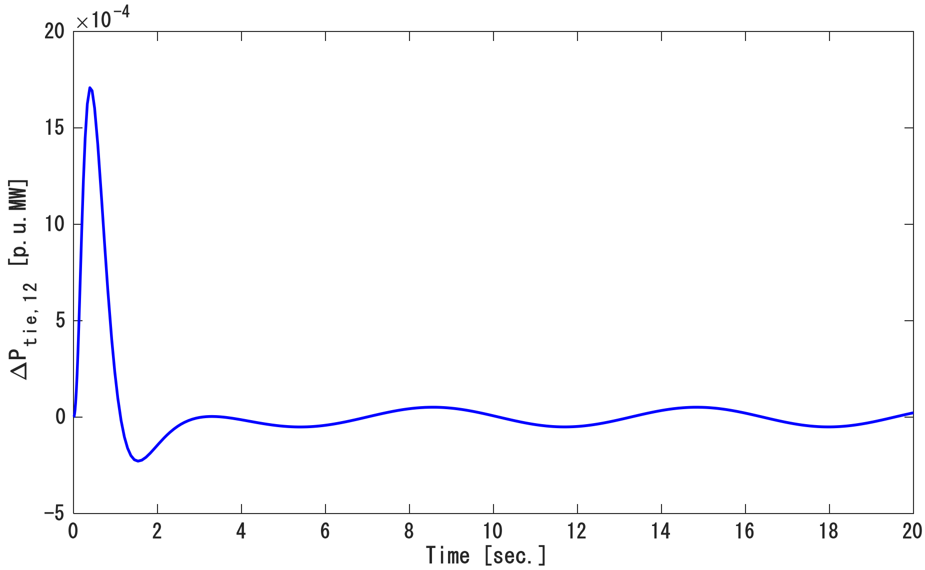

Figure 6. Tie line power deviation.

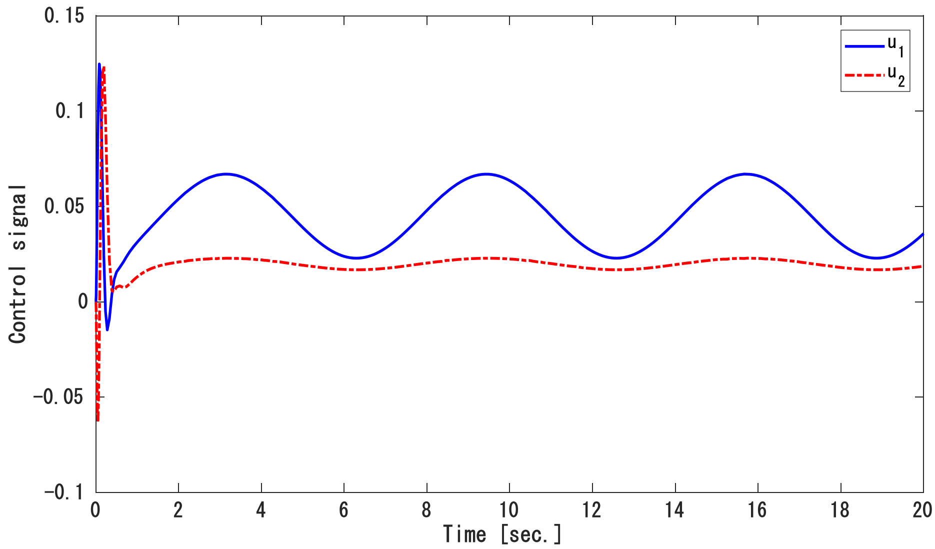

Figure 7. Control signal.

Table 2. Setting time and maximum overshoot calculation of SOSMC and observer based SMC [31].

Kind of the Controller	Proposed Method SOSMC		Observer Based SMC [31]	
Parameters	$T_s(t)$	*Max.O. S (pu)*	$T_s(t)$	*Max.O. S (pu)*
Δf_1	3	-5.0×10^{-4}	7	-5.0×10^{-4}
Δf_2	3	-6.5×10^{-4}	7	-8.0×10^{-4}

Remark 2. *Under the mismatched condition, the proposed controller has good performance in terms of fast response time to bring the dynamic to the zero mark, lesser overshoots seen, and chattering free control without loss of accuracies when compared with [31].*

Case 3. Random load disturbance under mismatched uncertainty

To validate the robustness of the suggested controller, a random load at 10 s intervals was applied to the power plants. We considered a random load variations pattern given in

Figure 8, while the mismatched uncertainty was still kept the same as with case 2. Figure 9 shows the frequency divergence. The tie-line power variation is displayed in Figure 10 and the control signals in both areas are displayed in Figure 11.

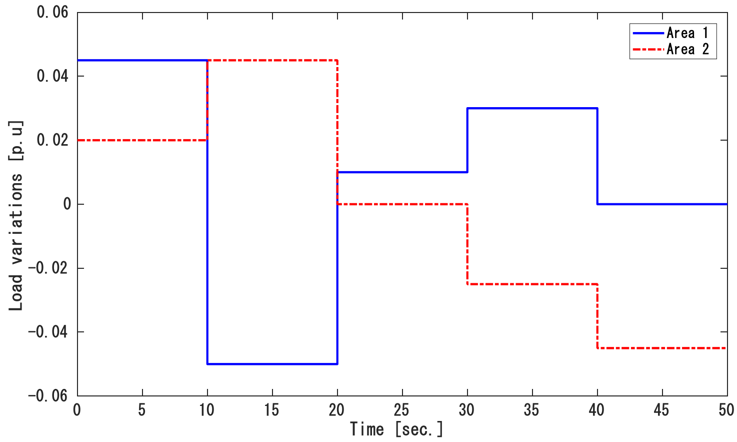

Figure 8. Random load variation.

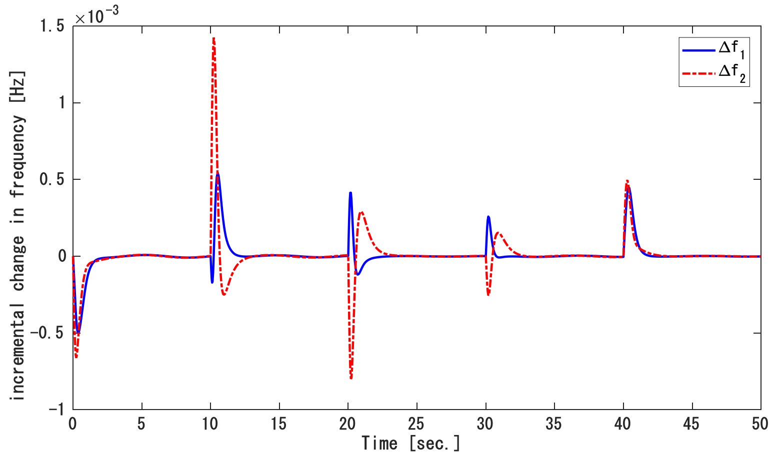

Figure 9. The frequency variation.

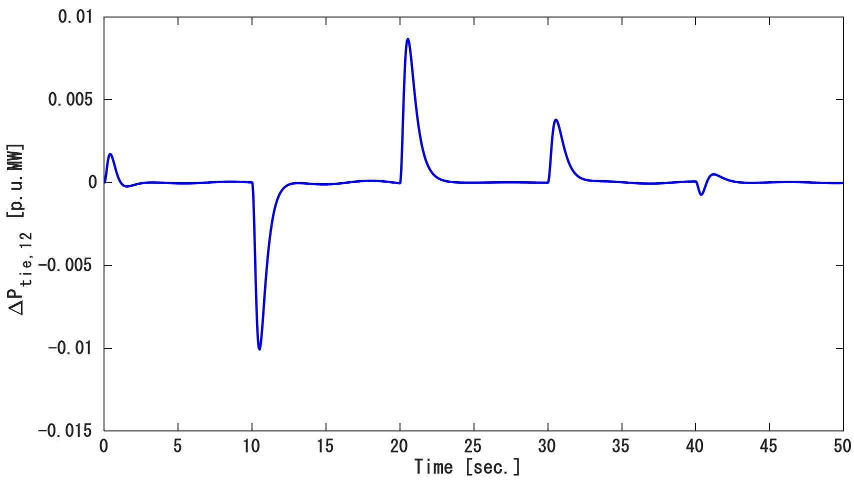

Figure 10. Tie-line power variation.

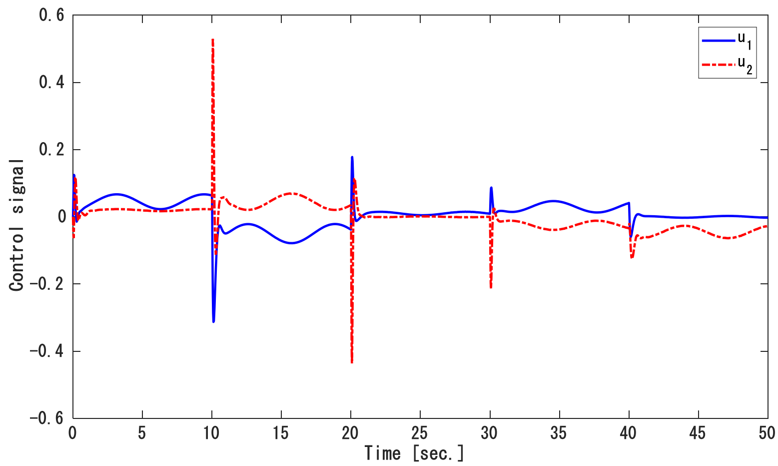

Figure 11. Control signal.

Thus, the tie-line power deviation and frequency deviation converge to zero by using the sliding surface and the controller based on the state estimator. The response of the power system is better in terms of overshoot even when the system state variables are not measured. Therefore, the new controller can be applied in large power systems.

Remark 3. *Even at random load variation and mismatched uncertainties, the ISS and the controller based on the state observer performed well by keeping the tie-line power and frequency at a safer point at every interval. The response of the power system is better with minimal overshoot which have no effect on damage to the actuator valve.*

4.2. Simulation 2: England 10 Generation 39 Bus Power System

To extend the proposed controller based on state observer performance, we simulated it in a New England 39 bus system as Figure 12 and system parameters are from [33]. It comprised of three area power systems with 10 generators and 39 bus nodes. All generators were synchronized and connected in parallel.

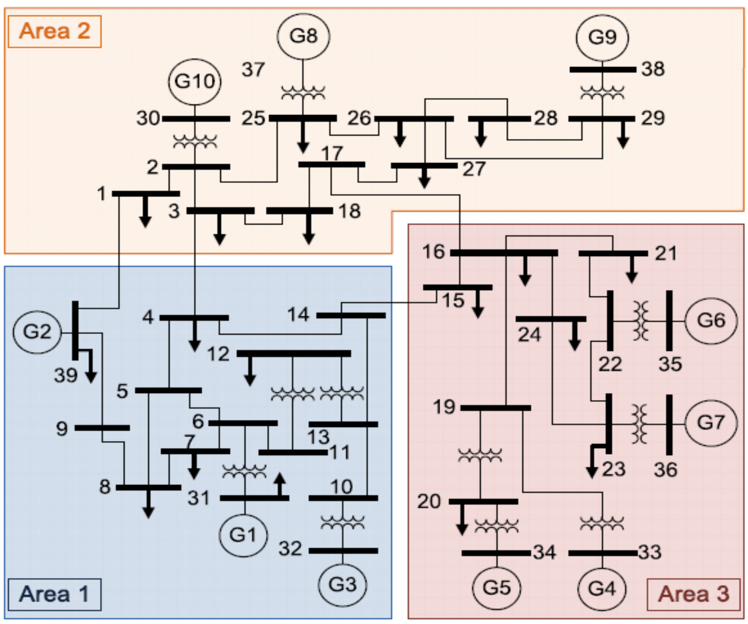

Figure 12. New England test system.

Because load demands in a real power system keep changing, we applied random load variation in each area as shown in Figure 13. Figures 14–16 show the frequency variation of area 1, 2, and 3, respectively, and the tie-line power deviation is displayed in Figure 17. The tie-line power flow and frequency fluctuation rapidly converged to zero even though the system state variables were not measured. Therefore, this approach is better to maintain frequency and tie-line power at a safe range in a large power network where SSV are difficult to measure.

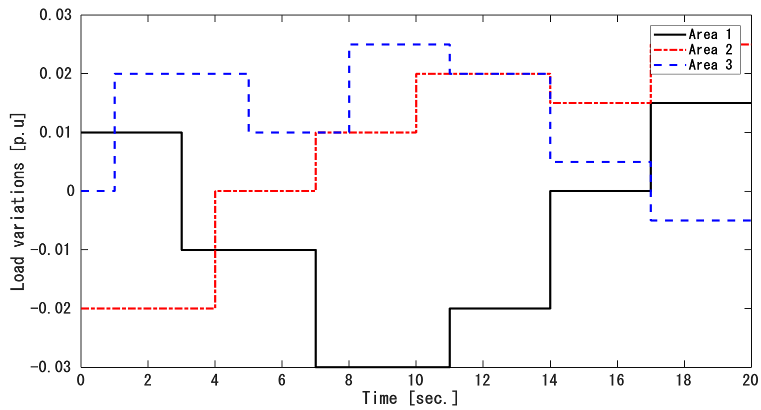

Figure 13. Random load variation.

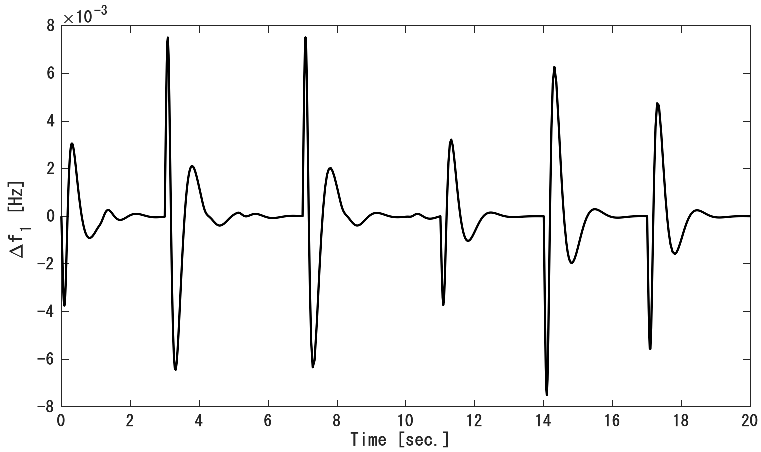

Figure 14. The frequency variation of 1st area.

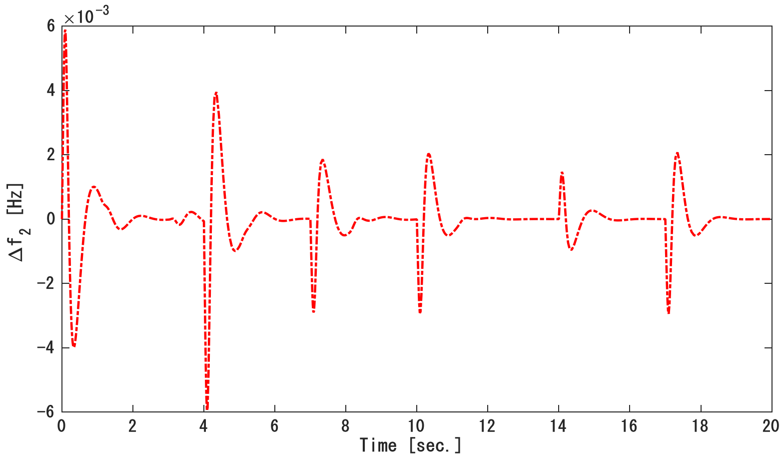

Figure 15. The frequency variation of 2nd area.

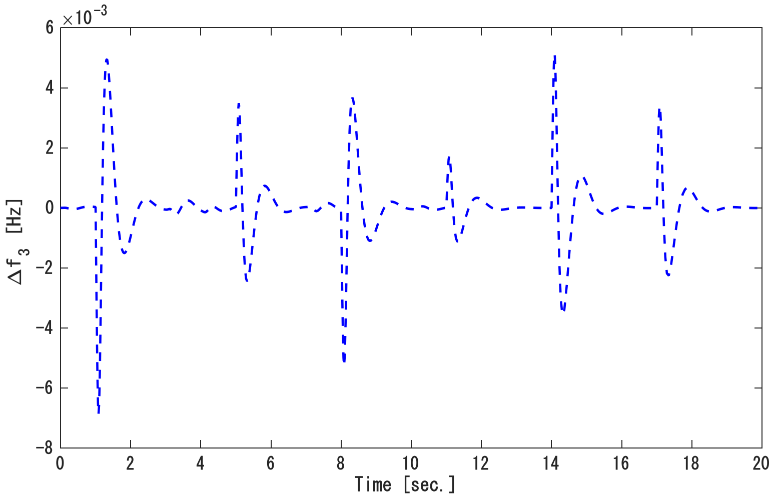

Figure 16. The frequency deviation of 3rd area.

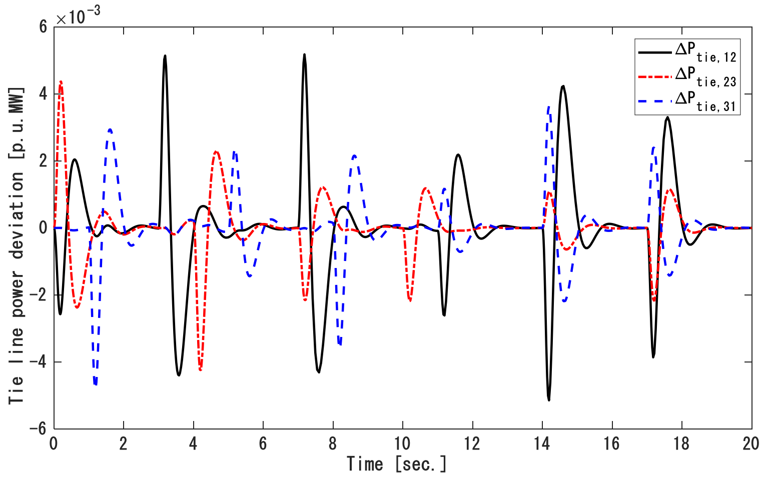

Figure 17. Tie-line variation of 3 areas.

Remark 4. *In this approach, the suggested controller based on observer is tested with a real power network and the results indicate that the suggested method is powerful for the control of a large power network under load variations depending on time, with fast settling time and small overshoot.*

Remark 5. *In general, the proposed method achieved better control performance in terms of keeping tie-line power and frequency at the accepted point for the power system where SSVs are difficult to measure. The proposed scheme is extremely powerful, and not only reduces chattering but also guarantees the robustness of the MAPS.*

5. Conclusions

The system state variables are difficult or expensive to measure for load frequency control (LFC) of a multi area power system. In this paper, a new method based on SMC combined with an observer has been proposed to estimate the system state variables for LFC. The estimated state observer is used fully in the sliding surface and continuous second order sliding mode controller, which reduces the chattering problem and improves the system performance. In addition, the new linear matrix inequality technique is derived to prove the stability of the whole system which includes estimated state variables and the real state variables. Experimental simulation results show that the frequency deviation and the tie-line power flow are observed with reduced settling time and magnitude of overshoot in comparison with existing methods in the literature. Furthermore, the second order sliding mode-based observer has been successfully applied for an IEEE 39 bus multi area power system with the load variations, with matched and mismatched uncertainties. Therefore, it can be concluded that the proposed scheme is not only robust in the presence of matched and mismatched uncertainties but also can be successfully applied to a real power system.

Author Contributions: Conceptualization, A.-T.T. and V.V.H.; methodology, A.-T.T. and V.V.H.; software, A.-T.T. and P.T.T.; validation, A.-T.T. and V.V.H.; resources, A.-T.T.; writing—original draft preparation, E.N.A. and P.T.T.; writing—review and editing, V.-D.P., A.-T.T. and V.V.H.; visualization, T.M.N. and A.-T.T.; supervision, T.M.N., B.L.N.M. and V.V.H. All authors have read and agreed to the published version of the manuscript.

Funding: This research was funded by Science and Technology Development of Ton Duc Thang University (FOSTECT), website: http://fostect.tdtu.edu.vn, under Grant FOSTECT.2017.BR.05.

Institutional Review Board Statement: Not applicable.

Informed Consent Statement: Not applicable.

Data Availability Statement: All data used is reported in the paper.

Conflicts of Interest: The authors declare no conflict of interest.

References

1. Parmar, K.P.S.; Majhi, S.; Kothari, D.P. Load frequency control of a realistic power system with multi-source power generation. *Int. J. Electr. Power Energy Syst.* **2012**, *42*, 426–433. [CrossRef]
2. Liu, X.; Nong, H.; Xi, K.; Yao, X. Robust Distributed Model Predictive Load Frequency Control of Interconnected Power System. *Math. Probl. Eng.* **2013**, *15*, 10–20. [CrossRef]
3. Vittal, V.; Mc Calley, J.D.; Anderson, P.M.; Fouad, A.A. *Power System Control and Stability*, 3rd ed.; Electric Power Systems: Richardson, TX, USA, 2019; pp. 19–400.
4. Tan, W.; Hao, Y.; Li, D. Load frequency control in deregulated environments via active disturbance rejection. *Int. J. Electr. Power Energy Syst.* **2015**, *66*, 166–177. [CrossRef]
5. Pandey, S.K.; Mohanty, S.R.; Kishor, N. A literature survey on load–frequency control for conventional and distribution generation power systems. *Renew. Sustain. Energy Rev.* **2013**, *25*, 318–334. [CrossRef]
6. Tan, W.; Zhou, H.; Fu, C. Linear active disturbance rejection control for load frequency control of power systems. *Control Theory Appl.* **2013**, *30*, 1607–1615.
7. Lu, X.; Yu, X.; Lai, J.; Guerrero, J.M.; Zhou, H. Distributed Secondary Voltage and Frequency Control for Islanded Microgrids with Uncertain Communication Links. *IEEE Trans. Ind. Inform.* **2017**, *13*, 448–460. [CrossRef]
8. Lim, K.Y.; Wang, Y.; Zhou, R. Robust decentralised load-frequency control of multi-area power systems. *IEEE Proc.-Gener. Transm. Distrib.* **1996**, *143*, 377–386. [CrossRef]
9. Dong, L.; Zhang, Y.; Gao, Z. A robust decentralized load frequency controller for interconnected power systems. *ISA Trans.* **2012**, *51*, 410–419. [CrossRef]
10. Alrifai, M.; Hassan, M.; Zribi, M. Decentralized load frequency controller for a multi-area interconnected power system. *Int. J. Electr. Power Energy Syst.* **2011**, *33*, 198–209. [CrossRef]
11. Pappachen, A.; Fathima, A.P. Critical research areas on load frequency control issues in a deregulated power system: A state-of-the-art-of-review. *Renew. Sustain. Energy Rev.* **2017**, *72*, 163–177. [CrossRef]
12. Sharma, J.; Hote, Y.V.; Prasad, R. Robust PID Load Frequency Controller Design with Specific Gain and Phase Margin for Multi-area Power Systems. *IFAC Pap.* **2018**, *51*, 627–632. [CrossRef]
13. Aditya. Design of Load Frequency Controllers Using Genetic Algorithm for Two Area Interconnected Hydro Power System. *Electr. Power Compon. Syst.* **2010**, *31*, 81–94. [CrossRef]
14. Ramachandran, R.; Madasamy, B.; Veerasamy, V.; Saravanan, L. Load frequency control of a dynamic interconnected power system using generalized Hopfield neural network based self-adaptive PID controller. *IET Gener. Transm. Distrib.* **2018**, *12*, 5713–5722. [CrossRef]
15. Bevrani, H.; Daneshmand, P.R. Fuzzy logic-based load-frequency control concerning high penetration of wind turbines. *IEEE Syst. J.* **2012**, *6*, 173–180. [CrossRef]
16. Yousef, H.A.; AL-Kharusi, K.; Albadi, M.H.; Hossetinzadeh, N. Load frequency control of a multi-area power system: An adaptive fuzzy logic approach. *IEEE Trans. Power Syst.* **2014**, *29*, 1822–1830. [CrossRef]
17. Sinha, S.; Patel, R.; Prasad, R. Application of GA and PSO Tuned Fuzzy Controller for AGC of Three Area Thermal-Thermal-Hydro Power System. *Int. J. Comput. Theory Eng.* **2010**, *2*, 238–244. [CrossRef]
18. Daneshfar, F.; Bevrani, H. Multiobjective design of load frequency control using genetic algorithms. *Int. J. Electr. Power Energy Syst.* **2012**, *42*, 257–263. [CrossRef]

19. Rahman, M.M.; Chowdhury, A.H.; Hossain, M.A. Improved load frequency control using a fast acting active disturbance rejection controller. *Energies* **2017**, *10*, 1718. [CrossRef]
20. Vijaya Chandrakala, K.R.M.; Balamurugan, S.; Sankaranarayanan, K. Variable structure fuzzy gain scheduling based load frequency controller for multi area hydro thermal system. *Int. J. Electr. Power Energy Syst.* **2013**, *53*, 375–381. [CrossRef]
21. Yang, B.; Yu, T.; Shu, H.; Yao, W.; Jiang, L. Sliding-mode perturbation observer-based sliding-mode control design for stability enhancement of multi-machine power systems. *Trans. Inst. Meas. Control* **2018**, *41*, 1418–1434. [CrossRef]
22. Pradhan, S.K.; Das, D.K. H∞ Load Frequency Control Design Based on Delay Discretization Approach for Interconnected Power Systems with Time Delay. *J. Mod. Power Syst. Clean Energy* 2020. [CrossRef]
23. Sun, Y.; Wang, Y.; Wei, Z.; Sun, G.; Wu, X. Robust H∞ Load Frequency Control of Multi-Area Power System with Time Delay: A Sliding Mode Control Approach. *IEEE/Caa J. Autom. Sin.* **2018**, *5*, 610–617. [CrossRef]
24. Mi, Y.; Fu, Y.; Wang, C.; Wang, P. Decentralized Sliding Mode Load Frequency Control for Multi-Area Power Systems. *IEEE Trans. Power Syst.* **2013**, *28*, 4301–4309. [CrossRef]
25. Huynh, V.V.; Minh, B.L.N.; Amaefule, E.N.; Tran, A.-T.; Tran, P.T. Highly Robust Observer Sliding Mode Based Frequency Control for Multi Area Power Systems with Renewable Power Plants. *Electronics* **2021**, *10*, 274. [CrossRef]
26. Huynh, V.V.; Tran, P.T.; Minh, B.L.N.; Tran, A.-T.; Tuan, D.H.; Nguyen, T.M.; Vu, P.T. New Second-Order Sliding Mode Control Design for Load Frequency Control of a Power System. *Energies* **2020**, *13*, 6509. [CrossRef]
27. Wei, Z.; Dong, G.; Zhang, X.; Pou, J.; Quan, Z.; He, H. Noise-Immune Model Identification and State-of-Charge Estimation for Lithium-Ion Battery Using Bilinear Parameterization. *IEEE Trans. Ind. Electron.* **2020**, *68*, 312–323. [CrossRef]
28. Wei, Z.; He, H.; Pou, J.; Tsui, K.L.; Quan, Z.; Li, Y. Signal-Disturbance Interfacing Elimination for Unbiased Model Parameter Identification of Lithium-Ion Battery. *IEEE Trans. Ind. Inform.* 2020. [CrossRef]
29. Chen, C.; Zhang, K.; Yuan, K.; Wang, W. Extended partial states observer based load frequency control scheme design for multi-area power system considering wind energy integration. *IFAC Pap.* **2017**, *50*, 4388–4393. [CrossRef]
30. Mi, Y.; Fu, Y.; Li, D.; Wang, C.; Loh, P.C.; Wang, P. The sliding mode load frequency control for hybrid power system based on disturbance observer. *Int. J. Electr. Power Energy Syst.* **2016**, *74*, 446–452. [CrossRef]
31. Prasad, S.; Purwar, S.; Kishor, N. Load frequency regulation using observer based non-linear sliding mode control. *Int. J. Electr. Power Energy Syst.* **2019**, *104*, 178–193. [CrossRef]
32. Dev, A.; Sarkar, M.K. Robust higher order observer based non-linear super twisting load frequency control for multi area power systems via sliding mode. *Int. J. Control Autom. Syst.* **2019**, *17*, 1814–1825. [CrossRef]
33. Liao, K.; Xu, Y. A robust load frequency control scheme for power systems based on second-order sliding mode and extended disturbance observer. *IEEE Trans. Ind. Inform.* **2017**, *14*, 3076–3086. [CrossRef]
34. Tsai, Y.W.; Huynh, V.V. A multitask sliding mode control for mismatched uncertain large-scale systems. *Int. J. Control* **2015**, *88*, 1911–1923. [CrossRef]

applied sciences

Article

Load Frequency Control for Multi-Area Power Plants with Integrated Wind Resources

Van Van Huynh [1], Bui Le Ngoc Minh [2,3], Emmanuel Nduka Amaefule [1], Anh-Tuan Tran [1], Phong Thanh Tran [1], Van-Duc Phan [4,*], Viet-Thanh Pham [1] and Tam Minh Nguyen [2]

[1] Modeling Evolutionary Algorithms Simulation and Artificial Intelligence, Faculty of Electrical & Electronics Engineering, Ton Duc Thang University, Ho Chi Minh City 700000, Vietnam; huynhvanvan@tdtu.edu.vn (V.V.H.); ndukaamaefuleemmanuel.st@tdtu.edu.vn (E.N.A.); trananhtuan.st@tdtu.edu.vn (A.-T.T.); tranthanhphong.st@tdtu.edu.vn (P.T.T.); phamvietthanh@tdtu.edu.vn (V.-T.P.)

[2] Faculty of Electrical and Electronics Engineering, Ho Chi Minh City University of Technology and Education, Ho Chi Minh City 700000, Vietnam; 1726002@student.hcmute.edu.vn (B.L.N.M.); tamnm@hcmute.edu.vn (T.M.N.)

[3] Faculty of Industrial Engineering, Tien Giang University, My Tho City 840000, Vietnam

[4] Faculty of Automobile Technology, Van Lang University, Ho Chi Minh City 700000, Vietnam

* Correspondence: duc.pv@vlu.edu.vn

Abstract: To provide a more practical method of controlling the frequency and tie-line power flow of a multi-area interconnected power system (MAIPS), a state observer based on sliding mode control (SOboSMC) acting under a second-order time derivative is proposed. The proposed design is used to study load frequency control against load disturbance, matched and mismatched uncertainty and parameter measurement difficulties of power systems that exist in the modern power plant, such as multi-area systems integrated with wind plants. Firstly, the state observer is designed to optimally estimate system state variables. The estimated states are applied to construct the model of the MAIPS. Secondly, a SOboSMC is designed with an integral switching surface acting on the second-order time derivative to forcefully drive the dynamic errors to zero and eliminate chattering, which can occur in the first-order approach to sliding mode control. In addition, the stability of the total power system is demonstrated with the Lyapunov stability theory based on a new linear matrix inequality (LMI) technique. To extend the validation of the proposed design control for practical purposes, it was tested in a New England system with 39 bus power against random load disturbances. The simulation results confirm the superiority of the proposed SOboSMC over other recent controllers with respect to overshoot and settling time.

Keywords: renewables plants; state observer; sliding mode control; load frequency control

Citation: Huynh, V.V.; Minh, B.L.N.; Amaefule, E.N.; Tran, A.-T.; Tran, P.T.; Phan, V.-D.; Pham, V.-T.; Nguyen, T.M. Load Frequency Control for Multi-Area Power Plants with Integrated Wind Resources. *Appl. Sci.* **2021**, *11*, 3051. https://doi.org/10.3390/app11073051

Academic Editors: Luigi Fortuna and Salvina Gagliano

Received: 9 February 2021
Accepted: 26 March 2021
Published: 29 March 2021

1. Introduction

Recently, more electrical power can be generated from wind turbines due to improvements in technology. Many power companies are investing in wind farms to supply electricity to their end0users. Moreover, remote geographical locations that are outside of grid services have been fed by wind farms. Efforts are on-going to integrate wind turbines with the existing MAIPS in order to increase grid services. However, wind farms integrated with the existing power network raise some concerns due to frequency deviations. These concerns are intermittent problems associated with the wind energy source, which involve maximum power point tracking, synchronization problems, uncertainty, difficulty in system parameter measurements (since the dynamic behaviors are different from conventional power plants), etc. These are additional to the existing disturbances, such as nonlinearity, random and step-load disturbances, matched and mismatched uncertainty, etc., which are found in conventional MAIPSs. Thus, these factors give rise to large frequency errors and affect the power quality. The load frequency control (LFC) scheme has been utilized to take care of the frequency deviation and to ensure the quality of the power supply. Moreover, the concerns, characteristics and behaviors of MAIPSs, as mentioned above, are vital issues in LFC design [1]. Classical, intelligent and optimal control techniques have been applied to LFC of MAIPSs in the past and are discussed in [2–17]. A major problem with the interconnection of the power systems is increasingly related to the system and system parameter uncertainties. Therefore, the control approaches outlined in [2–17] exhibit some limitations, as discussed in [18]. Thus, a robust LFC technique for MAIPS was proposed in [18].

The sliding mode control (SMC) scheme is one of the robust control approaches proposed in order to solve the above problem. It was selected because of its robustness against load disturbances and parameter variations. The SMC scheme was designed for the LFC of MAIPSs in various operating conditions, which are presented in [19,20]. Recently, the adaptive technique combined with sliding mode control has been developed to study the LFC of MAIPSs [21]. Adaptive event-triggered SMC was used to investigate the LFC of an MAIPS under a deregulated environment [22]. More recently, double-integral SMC was applied for the decentralized adaptive LFC of an MAIPS, presented in [23]. However, these above SMC approaches act under the first-order time derivative. In further studies, the first-order SMC may suffer from the chattering phenomenon, which can cause inaccuracies in LFC due to the discontinuous control signal in the SMC controller, which causes harmonics and affects the system performance and the power quality. Therefore, second-order SMC is used to eliminate the above chattering problem. Second-order SMC was applied for the LFC of an MAIPS to solve the chattering problem and discussed in [24]. An adaptive SMC combined with the higher-order SMC for the LFC of an MAIPS was invented to improve the elimination of chattering, as presented in [25–27]. However, in a real MAIPS, the LFC design is better when load disturbances are not required to be measured. To solve this difficulty, the use of a disturbance observer has been applied for the LFC of MAIPSs [28]. In addition, the disturbance observer combination with SMC for the LFC of MAIPSs was also discussed in [29–31]. Recently, a state observer was used to estimate the non-measurement system state variables for designing the LFC of MAIPSs [32]. A non-linear SMC based on a generalized observer was developed to regulate frequency in a large power system [33,34]. However, there are some limitations of the above approaches for the LFC of the MAIPS. First, the system state variables need to be measured for the feedback of the load frequency controller [23–31]. Second, the controller suffers from the chattering problem inherent in the first-order SMC [32–34]. Therefore, this article focuses on a more realistic LFC design for an MAIPS integrated with a wind plant. Thus, the estimated system state variables (SSVs) from the observer are used in the sliding surface, along with a decentralized second-order SMC, so that the SSVs are not required to be measured. The novelties of the paper are discussed below.

- The sliding surface and the decentralized continuous load frequency controller are designed to be fully dependent on the SSVs estimated by the observer; thus, the limitation of using state variables for the feedback of the control (discussed in [23–31]) has been solved.
- The MAIPS state variables and the estimated MAIPS state variables are asymptotically stable with the new linear matrix inequality (LMI) method.
- A sliding mode acting under the second-order time derivative is developed to improve the system performance by eliminating the problem of chattering, in contrast with the approaches given in [32–34].
- The simulation results show that the MAIPS performance is better in terms of overshoot and settling time in comparison with some recent approaches. Therefore, the proposed method is useful for the LFC of real MAIPSs.

2. Multi-Area Interconnected Power System (MAIPS) Model in the State Space Form for Load Frequency Control

For the purpose of LFC, we first derive an MAIPS model. A power network with three areas is contemplated. Thus, areas 1 and 3 are integrated with a wind plant, whereas area 2 consists of a non-reheat turbine alone, as shown in Figure 1. In general, if *i*th area is considered, then the system is re-sketched as shown in Figure 2.

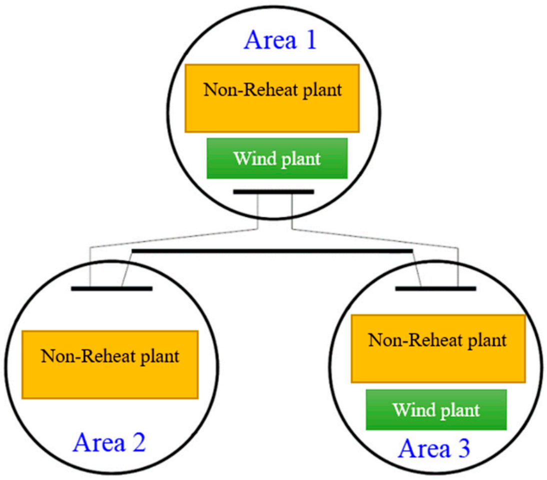

Figure 1. A simplified sketch of a three-area integrated wind plant system.

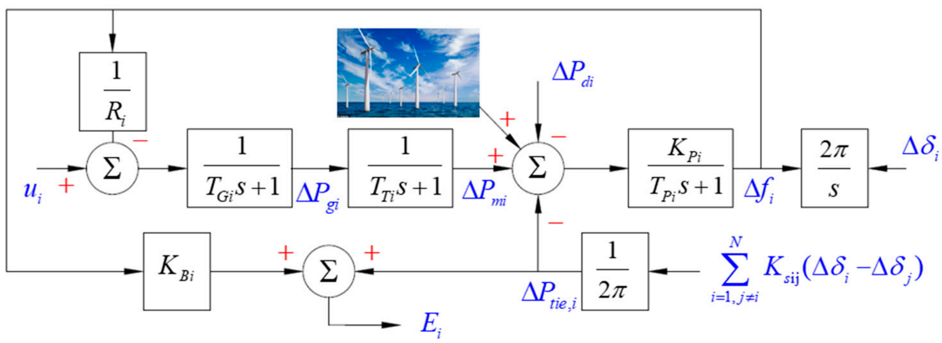

Figure 2. Schematic block diagram sketch for *i*th area network, including a wind farm.

For simplicity, we have modeled the conventional and wind power networks separately. As we know, the conventional power system considered consists of a speed changer motor, governor, non-reheat turbine and generation. We model each component of the conventional MAIPS in the *i*th area, as displayed in Figure 2, in same way as [24,31]. Frequency change is made to be the output of the generator so that LFC can be achieved. Next, we determine the dynamic relations, which consist of a speed changer motor, a governor, a non-reheat turbine and a generator of the *i*th area model, as expressed by:

$$\Delta\dot{f}_i(t) = \frac{K_{pi}}{T_{Pi}}\Delta P_{mi}(t) - \frac{K_{pi}}{T_{Pi}}\Delta P_{di}(t) + \frac{K_{pi}}{T_{Pi}}\Delta P_{Wi}(t) - \frac{1}{T_{Pi}}\Delta f_i(t) - \frac{K_{Pi}}{2\pi T_{Pi}}\sum_{i=1,j\neq i}^{N} K_{ij}\{\Delta\delta_i(t) - \Delta\delta_j(t)\} \tag{1}$$

$$\Delta\dot{P}_{mi}(t) = \frac{1}{T_{Ti}}\Delta P_{gi}(t) - \frac{1}{T_{Ti}}\Delta P_{mi}(t) \tag{2}$$

$$\Delta\dot{P}_{gi}(t) = -\frac{1}{R_i T_{Gi}}\Delta f_i(t) - \frac{1}{T_{Gi}}\Delta P_{gi}(t) + \frac{1}{T_{Gi}}u_i(t) \tag{3}$$

$$\Delta\dot{E}_i(t) = K_{Ei}K_{Bi}\Delta f_i(t) + \frac{K_{Ei}}{2\pi}\sum_{i=1,j\neq i}^{N} K_{ij}\{\Delta\delta_i(t) - \Delta\delta_j(t)\} \tag{4}$$

$$\Delta\dot{\delta}_i(t) = 2\pi\,\Delta f_i(t) \tag{5}$$

where $\Delta f_i(t)$ is the individual area frequency deviation, $\Delta P_{mi}(t)$ is the mechanical power deviation of each area, $\Delta P_{gi}(t)$ is each area turbine valve position deviation, $\Delta P_{di}(t)$ is each unit load deviation, R_i is the individual area droop coefficient and K_{ij} is the synchronization coefficient. $\Delta P_{\mathrm{W}i}(t)$ is the wind disturbance, $\Delta\delta_i(t)$ and $\Delta\delta_j(t)$ are small change in power angle, K_{Bi} and K_{Ei} are the frequency response coefficient. T_{Pi}, T_{Gi} and T_{Ti} are the subsystem parameters. $\Delta\dot{E}_i(t)$ is denoted as the area control error. The system state space form of ith area is shown as follows.

$$\begin{aligned} \dot{x}_i(t) &= A_i x_i(t) + B_i u_i(t) + \sum_{\substack{j=1 \\ j\neq i}}^{N} H_{ij} x_j(t) + F_i \Delta P_{di}(t) \\ y_i(t) &= C_i x_i(t) \end{aligned} \tag{6}$$

The system matrices A_i, B_i, F_i, H_{ij} in the state space model are given below:

$$A_i = \begin{bmatrix} \frac{-1}{T_{Pi}} & \frac{K_{Pi}}{T_{Pi}} & 0 & 0 & -\frac{K_{Pi}}{2\pi T_{Pi}}\sum\limits_{i=1, j\neq i}^{N} \mathrm{K_{ij}} \\ 0 & -\frac{1}{T_{Ti}} & \frac{1}{T_{Ti}} & 0 & 0 \\ -\frac{1}{R_i T_{Gi}} & 0 & -\frac{1}{T_{Gi}} & 0 & 0 \\ K_{Bi}K_{Ei} & 0 & 0 & 0 & \frac{K_{Ei}}{2\pi}\sum\limits_{i=1, j\neq i}^{N} \mathrm{K_{ij}} \\ 2\pi & 0 & 0 & 0 & 0 \end{bmatrix}, H_{ij} = \begin{bmatrix} 0 & 0 & 0 & 0 & -\frac{K_{Pi}}{2\pi T_{Pi}}\sum\limits_{i=1, j\neq i}^{N} \mathrm{K_{ij}} \\ 0 & 0 & 0 & 0 & 0 \\ 0 & 0 & 0 & 0 & 0 \\ 0 & 0 & 0 & 0 & \frac{K_{Ei}}{2\pi}\sum\limits_{i=1, j\neq i}^{N} \mathrm{K_{ij}} \\ 0 & 0 & 0 & 0 & 0 \end{bmatrix}$$

$$, B_i = \begin{bmatrix} 0 \\ 0 \\ \frac{1}{T_{Gi}} \\ 0 \\ 0 \end{bmatrix} \text{and } F_i = \begin{bmatrix} -\frac{1}{2H_i} & \frac{1}{2H_i} \\ 0 & 0 \\ 0 & 0 \\ 0 & 0 \\ 0 & 0 \end{bmatrix}$$

$x_i(t) = \begin{bmatrix} \Delta f_i(t) & \Delta P_{mi}(t) & \Delta P_{gi}(t) & E_i(t) & \Delta\delta_i(t) \end{bmatrix}^T$ represent the state variables in the state space model. $u_i(t) \in R^m$ is the control input. $\Delta P_{di}(t)$ is the load uncertainty.

The model of the wind farm in the ith area is further discussed in the next section.

3. Wind Plant Model

A typical variable speed wind turbine generator system (VS-WTGS) is evaluated. For the VS-WTGSs, the wind power generates mechanical torque via the turbine generator shaft; thus, electrical torque is produced. The mechanical system acceleration, deceleration or constant speed depend on the change in mechanical and electrical torque. Thus, the net power output is related to the mechanical power.

Building the dynamic equations of the wind plant is based on the relationship of mechanical output power and wind velocity. The output power is therefore given as [35]

$$P_m = C_p(\lambda, \beta)\frac{1}{2}\rho A V^3{}_{wind} \tag{7}$$

where P_m is the turbine mechanical output (W), C_p is the turbine performance coefficient, λ is the tip speed ratio, β is the pitch angle of the blade (deg), ρ is the air density (kg/m^3), A is the turbine swept area (m^2) and V_{wind} is the wind speed (m/s).

- The tip speed ratio (λ)

$$\lambda = \frac{\omega_r R_r}{V_w} \tag{8}$$

where R_r and ω_r are radius and spin speed of the wind plant, respectively.

– Performance coefficient (C_p) of the turbine is given by.

$$C_p(\lambda, \beta) = c_1\left(\frac{c_2}{\lambda_i} - c_3\beta - c_4\right)e^{\frac{-c_5}{\lambda_i}} + c_6\lambda \tag{9}$$

with

$$\frac{1}{\lambda_i} = \frac{1}{\lambda + 0.08\beta} - \frac{0.035}{\beta^3 + 1} \tag{10}$$

where the coefficients c_1 to c_6 are dependent on the wind plant.

Finally, we can present the equation of the wind plant via a per-unit (p.u) system, as given below.

$$P_{m\_pu} = k_p \times C_{p\_pu} \times V^3_{\text{wind\_pu}} \tag{11}$$

P_{m_pu} is the mechanical power in per unit, $k_p \leq 1$ is the amplified power factor, C_{p_pu} is the power factor and $V_{\text{wind\_pu}}$ is the wind speed.

To design the new LFC for the MAIPS, we derive the following basic assumption. A lemma is also adopted to accompany the progress of the work.

Assumption 1. *Load uncertainty $\Delta P_{di}(t)$ and the differential of $\Delta P_{di}(t)$ is bounded such that $\|\Delta P_{di}(t)\| \leq \tau_i$ and $\|\Delta\dot{P}_{di}(t)\| \leq \overline{\tau}_i$, where γ_i and $\overline{\gamma}_i$ are known scalars and $\|.\|$ is a matrix norm.*

Assumption 2. *The eigenvalues of the matrix $A_i - T_iC_i$ can be chosen arbitrarily by appropriate choice of the observer gain T_i when the pair $[A_i, C_i]$ is observable.*

Lemma 1 [24]. *Let $\mathbf{X}$ and $\mathbf{Y}$ be a real matrix of suitable dimension then, for any scalar $\mu > 0$, the below matrix inequality holds:*

$$\mathbf{X}^T\mathbf{Y} + \mathbf{Y}^T\mathbf{X} \leq \mu\mathbf{X}^T\mathbf{X} + \mu^{-1}\mathbf{Y}^T\mathbf{Y}. \tag{12}$$

4. State Observer Based on Sliding Mode Control Strategies

4.1. Multi-Area Power System State Observer Design

This part, we considered the fact that the power network state variables are difficult to measure. Therefore, the state observer technique is applied. The original internal state of (6) is then estimated by the state observer using the experience of the output and input; therefore, the observer is designed as follows.

$$\begin{aligned} \dot{z}_i(t) &= A_iz_i(t) + B_iu_i(t) + \sum_{\substack{j=1 \\ j \neq i}}^{N} H_{ij}z_j(t) + T_i(y_i(t) - n_i(t)) \\ n_i(t) &= C_iz_i \end{aligned} \tag{13}$$

where z_i is the estate of x_i and T_i is a matrix gain, which is selected to ensure that the continuous-time dynamics error converges to zero faster. $y_i(t)$ is the output signal of the power system and $n_i(t)$ is the state observer output, respectively.

4.2. Stability Analysis of Whole System in Sliding Mode Dynamic

The new SMC is designed with a better sliding surface for sliding variables to rapidly reach the surface and remain thereon. The sliding surface is therefore given below

$$\sigma_i[z_i(t)] = L_iz_i(t) - \int_0^t L_i(A_i - B_iJ_i)z_i(\tau)d\tau \tag{14}$$

where L_i is a constant matrix and J_i is the design matrix. Matrix L_i is selected to guarantee that the matrix L_iB_i is invertible. The design matrix $J_i \in R^{m_i \times n_i}$ is given, satisfying the non-linearity condition

$$\text{Re}[\lambda_{\max}(A_i - B_iJ_i)] < 0 \tag{15}$$

For the continuous system observability rule, the estimation error defined by $e_i(t) = x_i(t) - z_i(t)$ must satisfy the below equation

$$\dot{e}_i = (A_i - T_iC_i)e_i + \sum_{\substack{j=1 \\ j\neq i}}^{N} H_{ij}e_j + F_i\Delta P_{di}(t) \tag{16}$$

If we take the derivative of (13) with respect to time, we therefore obtain

$$\begin{aligned}\dot{\sigma}_i[z_i(t)] = L_i[A_iz_i(t) \quad &+ B_iu_i(t) + \sum_{\substack{j=1 \\ j\neq i}}^{N} H_{ij}z_j(t) + T_i(y_i - n_i)] \\ &- L_i(A_i - B_iJ_i)z_i(t)\end{aligned} \tag{17}$$

Setting $\dot{\sigma}(t) = \sigma(t) = 0$, we can see that the equivalent control signal is as below

$$\begin{aligned} u_i^{eq}(t) &= -(L_iB_i)^{-1}[L_iA_iz_i(t) + \sum_{\substack{j=1 \\ j\neq i}}^{N} L_iH_{ij}z_j(t) + L_iT_i(y_i - n_i)] - L_i(A_i - B_iJ_i)z_i(t)] \\ &= -(L_iB_i)^{-1}[L_iB_iJ_iz_i(t) + L_iT_i(y_i - n_i) + \sum_{\substack{j=1 \\ j\neq i}}^{N} L_iH_{ij}z_j(t)] \end{aligned} \tag{18}$$

Substituting $u(t)$ into (6) yields the sliding motion:

$$\begin{aligned} \dot{x}_i(t) &= A_ix_i(t) - B_iJ_iz_i(t) - B_i(L_iB_i)^{-1}L_iT_i(y_i - n_i) \\ &- \sum_{\substack{j=1 \\ j\neq i}}^{N} B_i(L_iB_i)^{-1}L_iH_{ij}z_j(t) + \sum_{\substack{j=1 \\ j\neq i}}^{N} H_{ij}x_j(t) + F_i\Delta P_{di}(t) \\ &= (A_i - B_iJ_i)x_i(t) + (B_iJ_i - B_i(L_iB_i)^{-1}L_iT_iC_i)e_i(t) \\ &+ \sum_{\substack{j=1 \\ j\neq i}}^{N} \left[H_{ij} - B_i(L_iB_i)^{-1}L_iH_{ij}\right]x_j(t) + \sum_{\substack{j=1 \\ j\neq i}}^{N} B_i(L_iB_i)^{-1}L_iH_{ij}e_j(t) + F_i\Delta P_{di}(t) \end{aligned} \tag{19}$$

Combining system (6) and error system (18), the closed-loop system is written as

$$\begin{bmatrix} \dot{x}_i \\ \dot{e}_i \end{bmatrix} = \begin{bmatrix} A_i - B_iJ_i & \Phi_i \\ 0 & A_i - T_iC_i \end{bmatrix} \begin{bmatrix} x_i \\ e_i \end{bmatrix} + \sum_{\substack{j=1 \\ j\neq i}}^{N} \begin{bmatrix} H_{ij} - \Lambda_iH_{ij} & \Lambda_iH_{ij} \\ 0 & H_{ij} \end{bmatrix} \begin{bmatrix} x_j \\ e_j \end{bmatrix} + \begin{bmatrix} F_i\Delta P_{di}(t) \\ F_i\Delta P_{di}(t) \end{bmatrix} \tag{20}$$

where $\Phi_i = B_iJ_i - B_i(L_iB_i)^{-1}L_iT_iC_i$ and $\Lambda_i = B_i(L_iB_i)^{-1}L_i$.

Equation (19) provides the condition that the MAIPS in the sliding surface is stable if the sliding motion (19) is stable and the observability condition holds following assumption 2. Therefore, the sliding motion (19) is also made Hurwitz, so the observer error $e(t) \to 0$ when $t \to \infty$. To prove the above condition, we postulate a theorem as follows.

Theorem 1. *The sliding motion (19) is asymptotically stable, if there exist symmetric positive definite matrices P_i , Q_i , $i = 1, 2, \ldots N$ and positive scalars λ_i , ρ_i , $\hat{\gamma}_i$ and $\overline{\gamma}_i$ so that the below linear matrix inequality is feasible*

$$\begin{bmatrix} \mathrm{X}_i + \sum\limits_{\substack{j=1\\ j\neq i}}^{N} \left[\overline{\lambda}_j (H_{ji} - \Lambda_j H_{ji})^T (H_{ji} - \Lambda_j H_{ji})\right] & P_i\Phi_i & P_i & P_iF_i & 0 & 0 \\ \Phi_i^T P_i & \overline{\mathrm{X}}_i + \sum\limits_{\substack{j=1\\ j\neq i}}^{N} \left[\widetilde{\lambda}_j^{-1} H_{ji}^T H_{ji}\right] + \sum\limits_{\substack{j=1\\ j\neq i}}^{N} \left[\hat{\lambda}_j (\Lambda_j H_{ji})^T \Lambda_j H_{ji}\right] & 0 & 0 & Q_i & F_i^T Q_i \\ P_i & 0 & -\lambda_i^{-1} & 0 & 0 & 0 \\ F_i^T P_i & 0 & 0 & -\hat{\gamma}_i^{-1} & 0 & 0 \\ 0 & Q_i & 0 & 0 & -\rho_i^{-1} & 0 \\ 0 & F_i^T Q_i & 0 & 0 & 0 & -\nu_i^{-1} \end{bmatrix} < 0 \quad (21)$$

where $\mathrm{X}_i = P_i(A_i - B_iJ_i) + (A_i - B_iJ_i)^T P_i$ *and* $\overline{\mathrm{X}}_i = Q_i(A_i - T_iC_i) + (A_i - T_iC_i)^T Q_i$.

Proof. In the analysis of the stability of the sliding motion (19), we choose the below Lyapunov function

$$V = \sum_{i=1}^{N} \begin{bmatrix} x_i \\ e_i \end{bmatrix}^T \begin{bmatrix} P_i & 0 \\ 0 & Q_i \end{bmatrix} \begin{bmatrix} x_i \\ e_i \end{bmatrix} \quad (22)$$

where $P_i > 0$ and $Q_i > 0$ satisfy (20) for $i = 1, 2, \ldots N$. By getting the time derivative along the system state trajectory of MAIPS, we have

$$\begin{aligned} \dot{V} &= \sum_{i=1}^{N} \begin{bmatrix} \dot{x}_i \\ \dot{e}_i \end{bmatrix}^T \begin{bmatrix} P_i & 0 \\ 0 & Q_i \end{bmatrix} \begin{bmatrix} x_i \\ e_i \end{bmatrix} + \sum_{i=1}^{N} \begin{bmatrix} x_i \\ e_i \end{bmatrix}^T \begin{bmatrix} P_i & 0 \\ 0 & Q_i \end{bmatrix} \begin{bmatrix} \dot{x}_i \\ \dot{e}_i \end{bmatrix} \\ &= \sum_{i=1}^{N} \Bigg\{ \begin{bmatrix} x_i \\ e_i \end{bmatrix}^T \begin{bmatrix} (A_i - B_iJ_i)^T P_i & 0 \\ \Phi_i^T P_i & (A_i - T_iC_i)^T Q_i \end{bmatrix} \begin{bmatrix} x_i \\ e_i \end{bmatrix} + \sum_{\substack{j=1\\ j\neq i}}^{N} \begin{bmatrix} x_j \\ e_j \end{bmatrix}^T \begin{bmatrix} (H_{ij} - \Lambda_i H_{ij})^T P_i & 0 \\ (\Lambda_i H_{ij})^T P_i & H_{ij}^T Q_i \end{bmatrix} \begin{bmatrix} x_i \\ e_i \end{bmatrix} \\ &+ \left[(F_i\Delta P_{di})^T P_i \ (F_i\Delta P_{di})^T Q_i\right] \begin{bmatrix} x_i \\ e_i \end{bmatrix} \Bigg\} + \sum_{i=1}^{N} \Bigg\{ \begin{bmatrix} x_i \\ e_i \end{bmatrix}^T \begin{bmatrix} P_i(A_i - B_iJ_i) & P_i\Phi_i \\ 0 & Q_i(A_i - T_iC_i) \end{bmatrix} \begin{bmatrix} x_i \\ e_i \end{bmatrix} \\ &+ \sum_{\substack{j=1\\ j\neq i}}^{N} \begin{bmatrix} x_i \\ e_i \end{bmatrix}^T \begin{bmatrix} P_i(H_{ij} - \Lambda_i H_{ij}) & P_i\Lambda_i H_{ij} \\ 0 & Q_i H_{ij} \end{bmatrix} \begin{bmatrix} x_j \\ e_j \end{bmatrix} + \begin{bmatrix} x_i \\ e_i \end{bmatrix}^T \begin{bmatrix} P_iF_i\Delta P_{di} \\ Q_iF_i\Delta P_{di} \end{bmatrix} \Bigg\} \\ &= \sum_{i=1}^{N} \Bigg\{ \begin{bmatrix} x_i \\ e_i \end{bmatrix}^T \begin{bmatrix} P_i(A_i - B_iJ_i) + (A_i - B_iJ_i)^T P_i & P_i\Phi_i \\ \Phi_i^T P_i & Q_i(A_i - T_iC_i) + (A_i - T_iC_i)^T Q_i \end{bmatrix} \begin{bmatrix} x_i \\ e_i \end{bmatrix} \\ &+ \sum_{i=1}^{N} \sum_{\substack{j=1\\ j\neq i}}^{N} \left[x_j^T (H_{ij} - \Lambda_i H_{ij})^T P_i x_i + x_i^T P_i (H_{ij} - \Lambda_i H_{ij}) x_j + e_j^T (\Lambda_i H_{ij})^T P_i x_i + x_i^T P_i \Lambda_i H_{ij} e_j\right] \\ &+ \sum_{i=1}^{N} \sum_{\substack{j=1\\ j\neq i}}^{N} (e_i^T Q_i H_{ij} e_j + e_j^T H_{ij}^T Q_i e_i) \\ &+ \sum_{i=1}^{N} \left[e_i^T Q_i F_i \Delta P_{di} + x_i^T P_i F_i \Delta P_{di} + (F_i\Delta P_{di})^T P_i x_i + (F_i\Delta P_{di})^T Q_i e_i\right] \end{aligned} \quad (23)$$

Applying Lemma 1 to Equation (22), we have

$$\begin{aligned}
\dot{V} &\leq \sum_{i=1}^{N}\left\{\begin{bmatrix} x_i \\ e_i \end{bmatrix}^T \begin{bmatrix} P_i(A_i - B_iJ_i) + (A_i - B_iJ_i)^T P_i & P_i\Phi_i \\ \Phi_i^T P_i & Q_i(A_i - T_iC_i) + (A_i - T_iC_i)^T Q_i \end{bmatrix}\begin{bmatrix} x_i \\ e_i \end{bmatrix}\right. \\
&+ \sum_{i=1}^{N} \sum_{\substack{j=1 \\ j \neq i}}^{N} \left[\overline{\lambda}_i x_j^T (H_{ij} - \Lambda_i H_{ij})^T (H_{ij} - \Lambda_i H_{ij}) x_j + \overline{\lambda}_i^{-1} x_i^T P_i P_i x_i + \hat{\lambda}_i e_j^T (\Lambda_i H_{ij})^T \Lambda_i H_{ij} e_j + \hat{\lambda}_i^{-1} x_i^T P_i P_i x_i\right] \\
&+ \sum_{i=1}^{N} \sum_{\substack{j=1 \\ j \neq i}}^{N} (\widetilde{\lambda}_i e_i^T Q_i Q_i e_i + \widetilde{\lambda}_i^{-1} e_j^T H_{ij}^T H_{ij} e_j) \\
&+ \sum_{i=1}^{N}\left[\nu_i e_i^T Q_i F_i F_i^T Q_i e_i + \nu_i^{-1} \Delta P_{di}^T \Delta P_{di} + \widetilde{\gamma}_i x_i^T P_i F_i F_i^T P_i x_i + \widetilde{\gamma}_i^{-1} \Delta P_{di}^T \Delta P_{dii}\right]
\end{aligned} \tag{24}$$

Since $\sum_{i=1}^{N} \sum_{\substack{j=1 \\ j \neq i}}^{N} \overline{\lambda}_i x_j^T (H_{ij} - \Lambda_i H_{ij})^T (H_{ij} - \Lambda_i H_{ij}) x_j = \sum_{i=1}^{N} \sum_{\substack{j=1 \\ j \neq i}}^{N} \overline{\lambda}_j x_i^T (H_{ji} - \Lambda_j H_{ji})^T (H_{ji} - \Lambda_j H_{ji}) x_i$ $\sum_{i=1}^{N} \sum_{\substack{j=1 \\ j \neq i}}^{N} \hat{\lambda}_i e_j^T (\Lambda_i H_{ii})^T \Lambda_i H_{ij} e_j = \sum_{i=1}^{N} \sum_{\substack{j=1 \\ j \neq i}}^{N} \hat{\lambda}_j e_i^T (\Lambda_j H_{ji})^T \Lambda_j H_{ji} e_i$ and $\sum_{i=1}^{N} \sum_{\substack{j=1 \\ j \neq i}}^{N} \widetilde{\lambda}_i^{-1} e_j^T H_{ij}^T H_{ij} e_j = \sum_{i=1}^{N} \sum_{\substack{j=1 \\ j \neq i}}^{N} \widetilde{\lambda}_j^{-1} e_i^T H_{ji}^T H_{ji} e_i$, we achieve

$$\begin{aligned}
\dot{V} &\leq \sum_{i=1}^{N}\left\{\begin{bmatrix} x_i \\ e_i \end{bmatrix}^T \begin{bmatrix} P_i(A_i - B_iJ_i) + (A_i - B_iJ_i)^T P_i & P_i\Phi_i \\ \Phi_i^T P_i & Q_i(A_i - T_iC_i) + (A_i - T_iC_i)^T Q_i \end{bmatrix}\begin{bmatrix} x_i \\ e_i \end{bmatrix}\right. \\
&+ \sum_{i=1}^{N} \sum_{\substack{j=1 \\ j \neq i}}^{N} \left[\overline{\lambda}_j x_i^T (H_{ji} - \Lambda_j H_{ji})^T (H_{ji} - \Lambda_j H_{ji}) x_i + \overline{\lambda}_i^{-1} x_i^T P_i P_i x_i + \hat{\lambda}_j e_i^T (\Lambda_j H_{ji})^T \Lambda_j H_{ji} e_i + \hat{\lambda}_i^{-1} x_i^T P_i P_i x_i\right] \\
&+ \sum_{i=1}^{N} \sum_{\substack{j=1 \\ j \neq i}}^{N} (\widetilde{\lambda}_i e_i^T Q_i Q_i e_i + \widetilde{\lambda}_j^{-1} e_i^T H_{ji}^T H_{ji} e_i) \\
&+ \sum_{i=1}^{N}\left[\nu_i e_i^T Q_i F_i F_i^T Q_i e_i + \nu_i^{-1} \Delta P_{di}^T \Delta P_{di} + \widetilde{\gamma}_i x_i^T P_i F_i F_i^T P_i x_i + \widetilde{\gamma}_i^{-1} \Delta P_{di}^T \Delta P_{dii}\right] \\
&= \sum_{i=1}^{N}\left\{\begin{bmatrix} x_i \\ e_i \end{bmatrix}^T \begin{bmatrix} \mathrm{X}_i + \lambda_i P_i P_i + \widetilde{\gamma}_i P_i F_i F_i^T P_i + \sum_{\substack{j=1 \\ j \neq i}}^{N} [\overline{\lambda}_j (H_{ji} - \Lambda_j H_{ji})^T (H_{ji} - \Lambda_j H_{ji})] & P_i\Phi_i \\ \Phi_i^T P_i & \overline{\mathrm{X}}_i + \rho_i Q_i Q_i + \nu_i Q_i F_i F_i^T Q_i + \sum_{\substack{j=1 \\ j \neq i}}^{N} \left[\widetilde{\lambda}_j^{-1} H_{ji}^T H_{ji}\right] + \sum_{\substack{j=1 \\ j \neq i}}^{N} [\hat{\lambda}_j (\Lambda_j H_{ji})^T \Lambda_j H_{ji}] \end{bmatrix}\begin{bmatrix} x_i \\ e_i \end{bmatrix}\right\} \\
&+ \sum_{i=1}^{N} [(\nu_i^{-1} + \widetilde{\gamma}_i^{-1}) \Delta P_{di}^T \Delta P_{di}]
\end{aligned} \tag{25}$$

where $\lambda_i = (N-1)(\overline{\lambda}_i^{-1} + \hat{\lambda}_i^{-1})$, $\rho_i = \widetilde{\lambda}_i (N-1)$, $\mathrm{X}_i = P_i(A_i - B_iJ_i) + (A_i - B_iJ_i)^T P_i$ and $\overline{\mathrm{X}}_i = Q_i(A_i - T_iC_i) + (A_i - T_iC_i)^T Q_i$.

In addition, using the Schur complement, the LMI (20) is equivalent to the below inequality

$$\Omega_i = -\begin{bmatrix} X_i + \lambda_i P_i P_i + \widetilde{\gamma}_i P_i F_i F_i^T P_i + \sum\limits_{\substack{j=1 \\ j \neq i}}^{N} [\nu_j (H_{ji} - \Lambda_j H_{ji})^T (H_{ji} - \Lambda_j H_{ji})] & P_i \Phi_i \\ \Phi_i^T P_i & \overline{X}_i + \rho_i Q_i Q_i + \nu_i Q_i F_i F_i^T Q_i + \sum\limits_{\substack{j=1 \\ j \neq i}}^{N} \left[\widetilde{\lambda}_j^{-1} H_{ji}^T H_{ji}\right] + \sum\limits_{\substack{j=1 \\ j \neq i}}^{N} [\hat{\lambda}_j (\Lambda_j H_{ji})^T \Lambda_j H_{ji}] \end{bmatrix} > 0 \tag{26}$$

According to Equations (24) and (25), we obtain

$$\dot{V} \leq \sum_{i=1}^{N} (-\lambda_{\min}(\Omega_i) \|\hat{x}_i(t)\|^2 + \mu_i) \tag{27}$$

where the constant value $\mu_i = \sum\limits_{i=1}^{N} \left[(\nu_i^{-1} + \widetilde{\gamma}_i^{-1})\tau_i^2\right]$ and the eigenvalue $\lambda_{\min}(\Omega_i) > 0$. Therefore, $\dot{V} < 0$ is achieved with $\|\hat{x}_i(t)\| > \sqrt{\frac{\mu_i}{\lambda_{\min}(\Omega_i)}}$. Hence, the sliding motion (19) is asymptotically stable. □

4.3. Decentralized State Estimator Feedback Integral Sliding Mode Control (DSEFISMC) Design

Previously, we designed the integral surface and proved the power system asymptotically stability in the sliding motion. Next, a continuous second-order DSEFISMC law is developed to reduce the chattering inherent in the first-order design. We start by defining the second-order sliding manifold $S_i[z_i(t)]$ such that the estimated system state trajectories are forcefully driven to zero asymptotically, which is given as

$$S_i[z_i(t)] = \dot{\sigma}_i[z_i(t)] + \varepsilon_i \sigma_i[z_i(t)] \tag{28}$$

and

$$\dot{S}_i[z_i(t)] = \ddot{\sigma}_i[z_i(t)] + \varepsilon_i \dot{\sigma}_i[z_i(t)] \tag{29}$$

where $\varepsilon_i > 0$ is a positive constant. Using Equation (16) yields

$$\begin{aligned} \dot{S}_i[z_i(t)] = L_i[A_i \dot{z}_i(t) + B_i \dot{u}_i(t) + \sum_{\substack{j=1 \\ j \neq i}}^{N} H_{ij} \dot{z}_j(t) + T_i(\dot{y}_i(t) - \dot{n}_i(t))] \\ -L_i(A_i - B_i J_i)\dot{z}_i(t) + \varepsilon_i \dot{\sigma}_i[z_i(t)] \end{aligned} \tag{30}$$

Based on the definition of the sliding surface and sliding manifold, the continuous DSEFISMC law for the MAIPS is known as follows

$$\begin{aligned} \dot{u}_i(t) = -(L_i B_i)^{-1}\{L_i B_i J_i \dot{z}_i(t) + \varepsilon_i \dot{\sigma}_i[z_i(t)] + \sum_{\substack{j=1 \\ j \neq i}}^{N} L_j H_{ji} \dot{z}_i(t) \\ + L_i T_i(\dot{y}_i(t) - \dot{n}_i(t)) - \delta_i sat(S_i[z_i(t)])\} \end{aligned} \tag{31}$$

We propound a theorem to demonstrate the reachability of the estimated system state trajectories to the manifold in the following.

Theorem 2. *Consider Equation (6) with the continuous DSEFISMC law (30). Then, system state trajectory is directed towards the sliding manifold $S_i[z_i(t)]$ and once the trajectory hits the sliding manifold $S_i[z_i(t)]$ it remains on the sliding manifold thereafter.*

Proof. A Lyapunov function is therefore, obtained:

$$\overline{V}(t) = \sum_{i=1}^{N} \|S_i[z_i(t)]\| \tag{32}$$

Now using the time derivative of $\overline{V}(t)$ yields

$$\begin{aligned}
\dot{\overline{V}} &= \sum_{i=1}^{N} \frac{S_i^T[z_i(t)]}{\|S_i[z_i(t)]\|} \dot{S}_i[z_i(t)] \\
&= \sum_{i=1}^{N} \frac{S_i^T[z_i(t)]}{\|S_i[z_i(t)]\|} \{L_i[A_i\dot{z}_i(t) + B_i\dot{u}_i(t) + \sum_{\substack{j=1 \\ j \neq i}}^{N} H_{ij}\dot{z}_j(t) + T_i(\dot{y}_i(t) - \dot{n}_i(t))] \\
&\quad -L_i(A_i - B_iJ_i)\dot{z}_i(t) + \varepsilon_i\dot{\sigma}_i[z_i(t)]\} \\
&= \sum_{i=1}^{N} \frac{S_i^T[z_i(t)]}{\|S_i[z_i(t)]\|} \{L_iB_iJ_i\dot{z}_i(t) + \varepsilon_i\dot{\sigma}_i[z_i(t)] + \sum_{\substack{j=1 \\ j \neq i}}^{N} L_iH_{ij}\dot{z}_i(t) + L_iT_i(\dot{y}_i(t) - \dot{n}_i(t))\} \\
&\quad + \sum_{i=1}^{N} \frac{S_i^T[z_i(t)]}{\|S_i[z_i(t)]\|} L_iB_i\dot{u}_i(t)
\end{aligned} \tag{33}$$

Using the DSEFISMC law (30), Equation (32) yields

$$\dot{\overline{V}} \leq -\sum_{i=1}^{N} \delta_i \tag{34}$$

The above Equation implies that the system state trajectories reach the sliding manifold $S_i[z_i(t)]$ and stay on it thereafter. □

5. Result Discussions

In this segment, we simulate the performance of the MAIPS with the proposed state observer based on sliding mode control (SOboSMC) and the results are compared and discussed with the load frequency double integral sliding mode controller given in [23] and the sliding mode controller in combination with the extended state observer in [34].

5.1. Simulation 1

In this simulation, the test was carried out in three cases and the parameters of the power network considered were the same as those in [23]. The one-line diagram of the MAIPS integrated with the wind plant is shown in Figure 3.

Case 1. In this case, the initial values of the MAIPS are assumed to be nominal values at time zero. The load disturbances of the areas 1, 2 and 3 are given as $\Delta P_{d_1} = 0.01\ p.u.\ MW$, $\Delta P_{d_2} = 0.015\ p.u.\ MW$, $\Delta P_{d_3} = 0.02\ p.u.\ MW$ at 1 s and the wind variations are neglected.

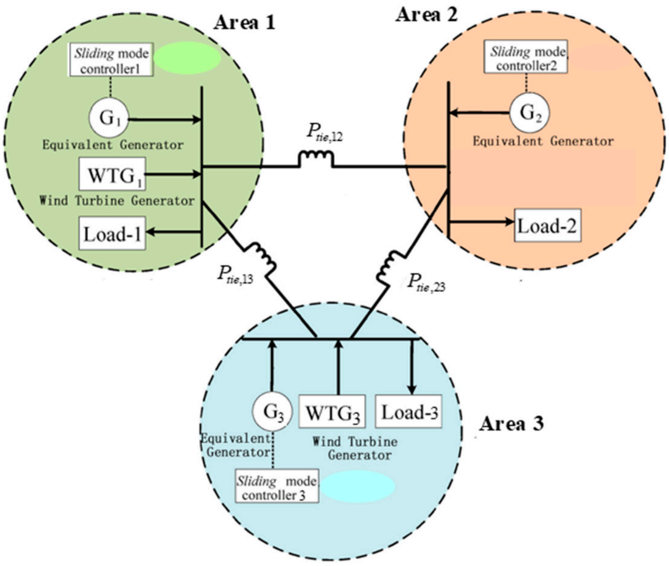

Figure 3. Diagram of a three-area power system integrated with a wind plant.

The incremental frequency is displayed in Figure 4 and the tie-line power deviation is shown in Figure 5, whereas the control signal is given in Figure 6.

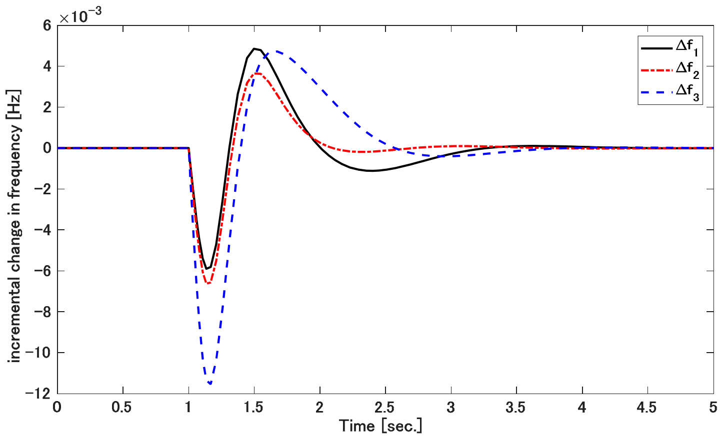

Figure 4. Frequency deviation of three-area power system.

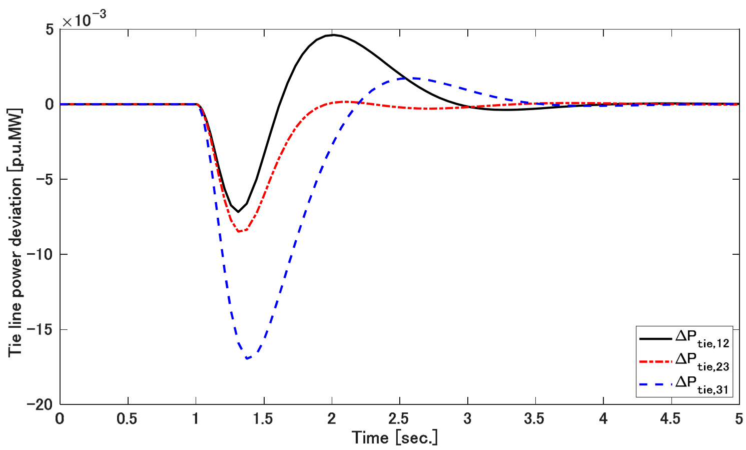

Figure 5. Tie-line power of three-area power system.

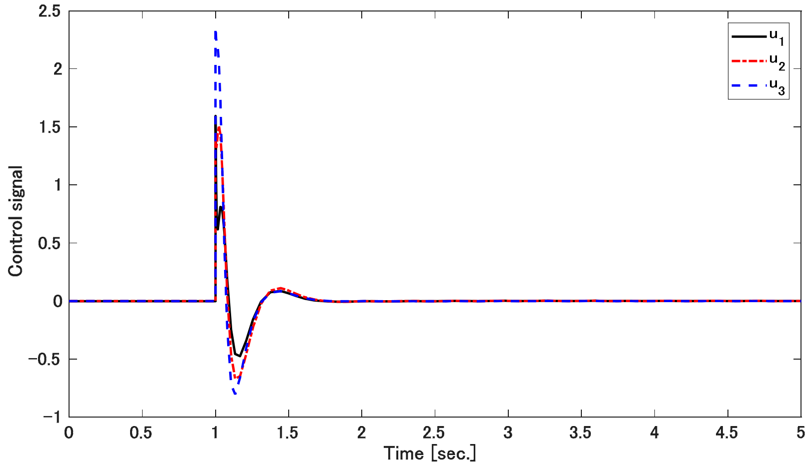

Figure 6. Control signal of three-area power system.

Remark 1. *Under the assumed initial conditions of the MAIPS, the proposed SOboSMC acted quickly to converge the frequency error to zero at 3 s, with a maximum overshoot of 0.005 Hz as compared to the 6-s settling time and maximum overshoot of 0.08 Hz seen in [23]. This validates that the MAIPS performance is better when using the proposed SOboSMC.*

Case 2. This simulation was done with the MAIPS with and without wind turbines. The load disturbances of the areas 1, 2 and 3 were assumed to be the same as those in case 1 and [23]. The parametric uncertainty is considered in the form of matched uncertainty ΔA_i, which is expressed as

$$\Delta A_1 = \begin{bmatrix} 0 & 0 & 0 & 0 & 0 \\ 0 & 0 & 0 & 0 & 0 \\ -2.26\cos(t) & 2\cos(t) & -2.604\cos(t) & 3\cos(t) & 0 \\ 0 & 0 & 0 & 0 & 0 \\ 0 & 0 & 0 & 0 & 0 \end{bmatrix} \text{where } \Delta A_1 = \Delta A_2 = \Delta A_3.$$

The wind variation is shown in Figure 7. The frequency error with and without the wind plant can be seen in Figures 8 and 9, whereas the tie-line power error with and without the wind farm are shown in Figures 10 and 11. For the MAIPS without wind farms, the response of the power network is better, pertaining to overshoot and settling time, and is also chattering-free in comparison with the design presented in [23]. Once more, the frequency transient is kept within the operational safety range, which is ±0.2 Hz for the safety of the power system frequency [36]. Therefore, the proposed approach shows good control performance for the LFC of an MAIPS with load disturbances, parameter uncertainties and wind variations, without the loss of control accuracy.

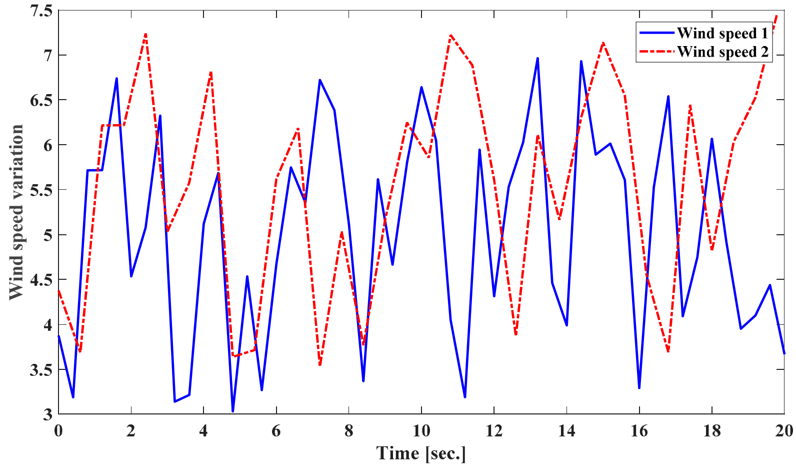

Figure 7. Wind speed variation.

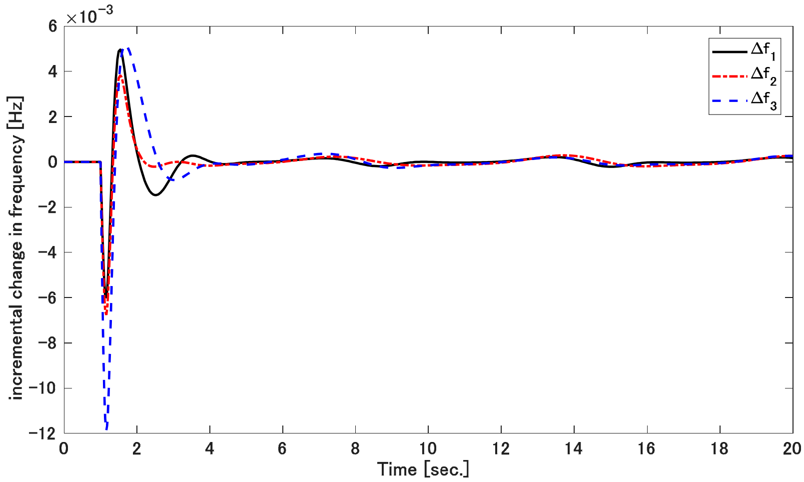

Figure 8. Frequency deviation of three-area power system without a wind plant.

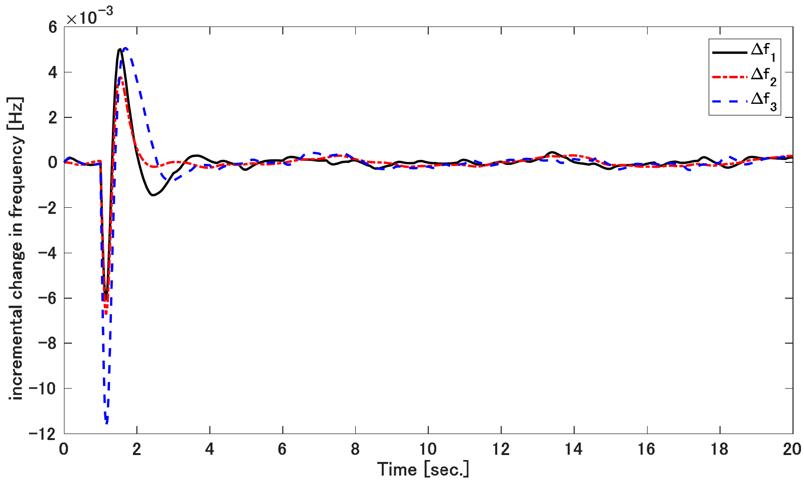

Figure 9. Frequency deviation of three-area power system with a wind plant.

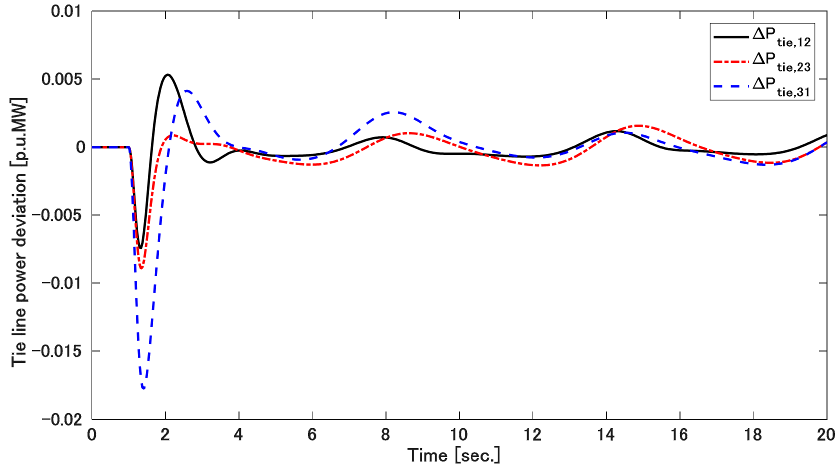

Figure 10. Tie-line power deviation of three-area power system without a wind plant.

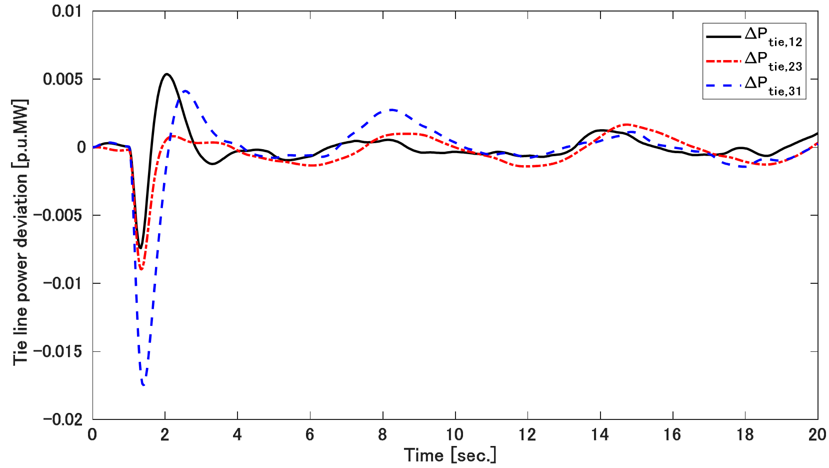

Figure 11. Tie-line power deviation of three-area power system with a wind plant.

Remark 2. *The LFC for the MAIPS with load disturbance and matched uncertainty can be seen in [23]. However, the above approach cannot be applied to an MAIPS with a wind turbine; therefore, this new approach is a better choice to handle the LFC in the MAIPS integrated with renewable plants.*

Case 3. The load change and the wind variation were the same as those in case 2. The parametric uncertainty was in the form of mismatched uncertainty in the system matrix and in the interconnected matrix [23].

$$\Delta A_1 = \begin{bmatrix} 0 & \Delta f_1 & 0 & 0 & 0 \\ \sin(t) & 0 & 0 & 0 & 0 \\ 0 & 0 & \cos(t) & \cos(t) & 0 \\ 0 & 0 & 0 & 0 & \cos(t) \\ \cos(t) & 0 & 0 & 0 & 0 \end{bmatrix} \text{ and } \Delta H_{12} = \begin{bmatrix} 0 & 0 & 0 & 0 & 0.178\cos(t) \\ 0 & 0 & 0 & 0 & 0 \\ 0 & 0 & 0 & 0 & 0 \\ 0 & 0 & 0 & 0 & -0.296\sin(t) \\ 0 & 0 & 0 & 0 & 0 \end{bmatrix}$$

We also assumed that $\Delta H_2 = \Delta H_3 = \Delta H_1$ and $\Delta A_2 = \Delta A_3 = \Delta A_1$.

Figures 12–15 represent the frequency and tie-line power error of the MAIPS with and without a wind turbine under the mismatched uncertainties, coupled with load disturbance. The results indicate that the new approach is highly robust against power system uncertainties and wind variation in comparison with [23].

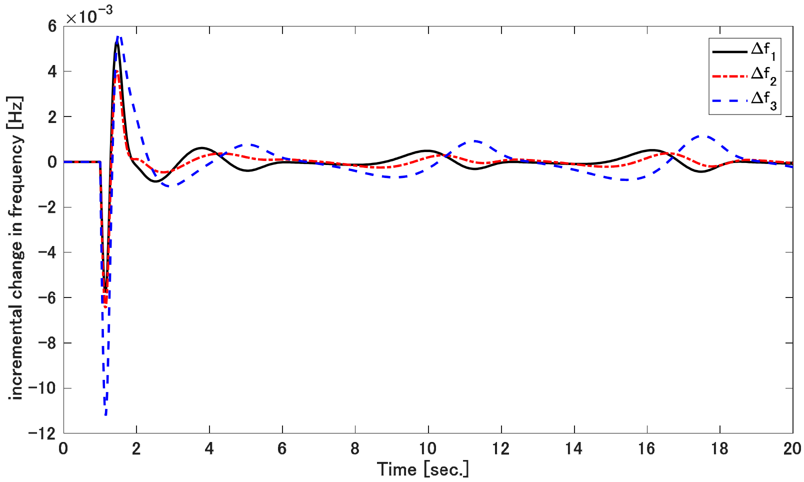

Figure 12. Frequency deviation of three-area power system without a wind plant.

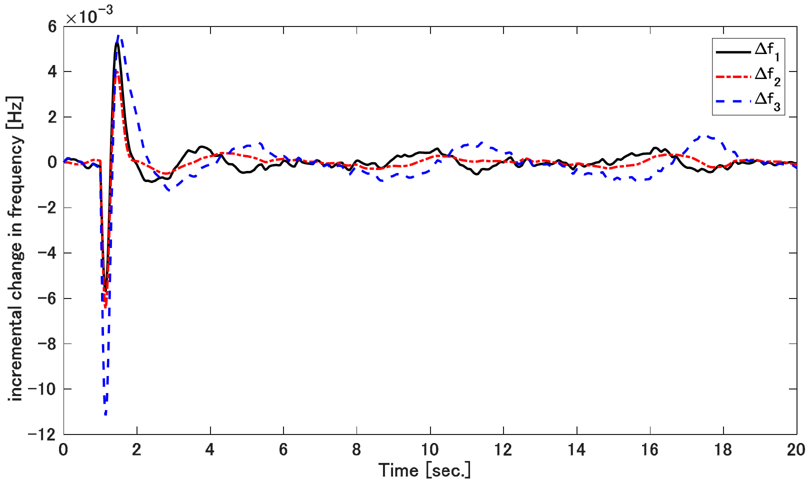

Figure 13. Frequency deviation of three-area power system with a wind plant.

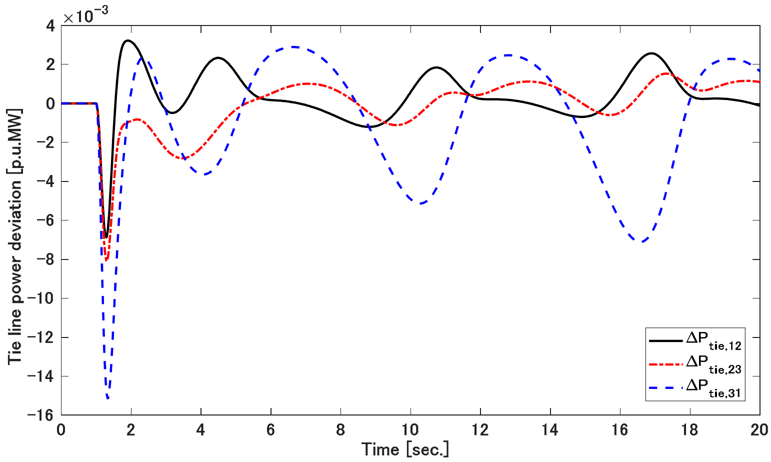

Figure 14. Tie-line power deviation of three-area power system without a wind plant.

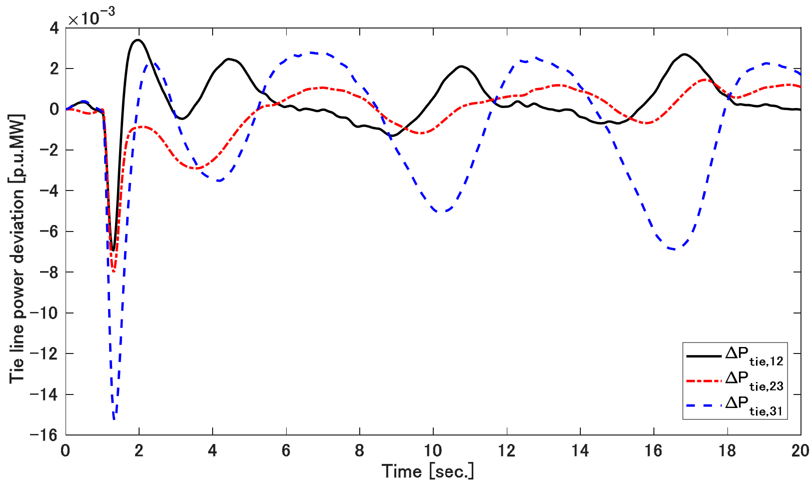

Figure 15. Tie-line power deviation of three-area power system with a wind plant.

Remark 3. *Even with load disturbances, wind variation and matched and mismatched parametric uncertainties, the results from Table 1 show that the proposed SOboSMC preserves the frequency of the MAIPS, which is better in terms of overshoot and settling time in comparison with [23]. Thus, the new controller is proven to be a preferred choice to cope with a power system with the above conditions. Unlike the approach given in [23], the system state variables are not required to be measured, so the proposed SOboSMC is much easier to apply to a large power network. The proposed SOboSMC is also intended to be applied to imperfect systems, which are mentioned in [37].*

Table 1. Setting time and maximum overshoot of the proposed state observer based on sliding mode control (SOboSMC) and double-integral SMC [23].

Kind of Controller	Proposed SOboSMC		Double Integral SMC [23]	
Parameters	$T_s(t)$	*Max.O. S (pu)*	$T_s(t)$	*Max.O. S (pu)*
Δf_1	3	-5.8×10^{-3}	7	-0.06
Δf_2	3	-6.5×10^{-3}	7	-0.07
Δf_3	3	-11.5×10^{-3}	7	-0.07

5.2. Simulation 2

In other to test the proposed SOBoSMC for the real MAIPS, a New England 39 bus power system (PS) was used. The configuration and parameters of the power system in this simulation were taken from [34].

In addition, the importance of integrating renewable energy with MAIPSs has been discussed in [32]. Therefore, we considered integrating wind energy with area 1 at bus 5 and area 3 at bus 21 of the New England 39 bus PS. A single line diagram of the New England 39 bus PS integrated with a wind plant is shown in Figure 16. The proposed SOBoSMC was tested for the LFC of the New England PS with and without wind plants. The wind variation was assumed as shown in Figure 17 and the load disturbance was applied for the MAIPS as shown in Figure 18. On the other hand, the SMC combined with the disturbance observer was used to increase the damping ratio for the LFC of the New England PS under random loads, as given in [34]. However, the stability of the frequency and tie-line power of the PS were attained without wind variation and the controller was required to measure all the system state variables. IN addition, an observer-based SMC used for the LFC of a New England PS was also seen in [32]. However, that controller suffered from chattering problems due to the first-order SMC used and the stability of the New England device was also achieved while neglecting wind disturbance. Therefore, there are doubts about the above approaches' applications in the LFC of a real PS integrated with renewable energies.

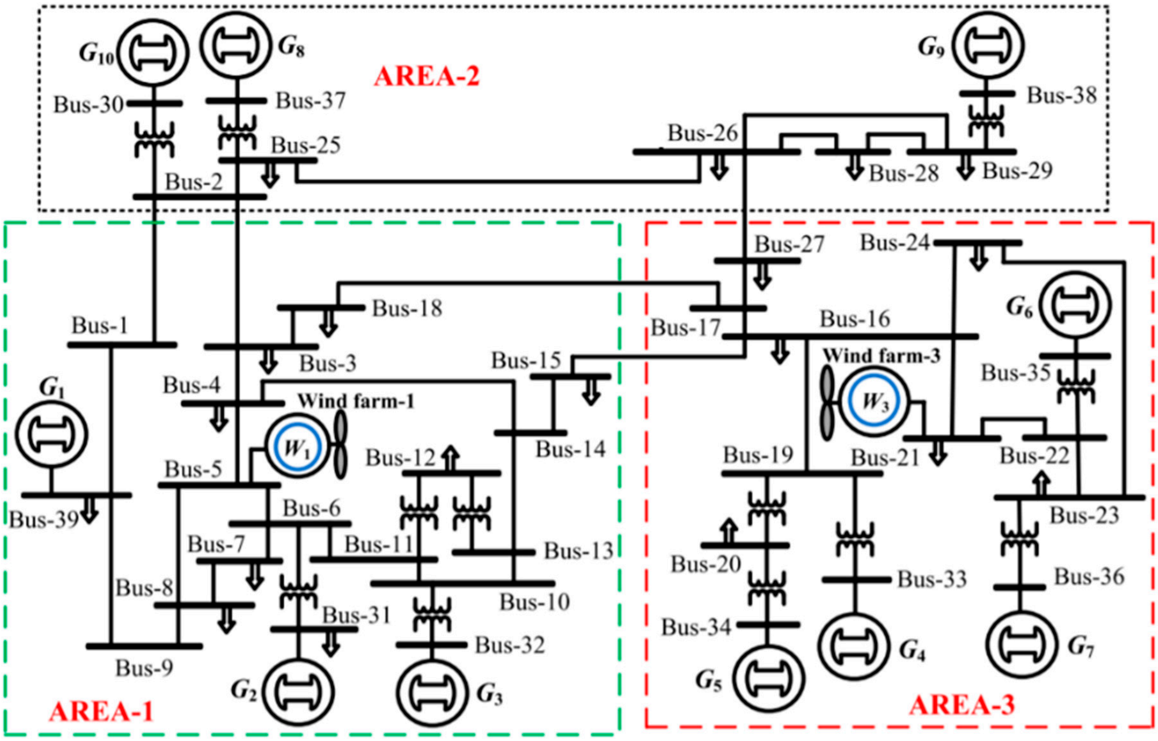

Figure 16. Diagram of IEEE 39-bus integrated with wind plant.

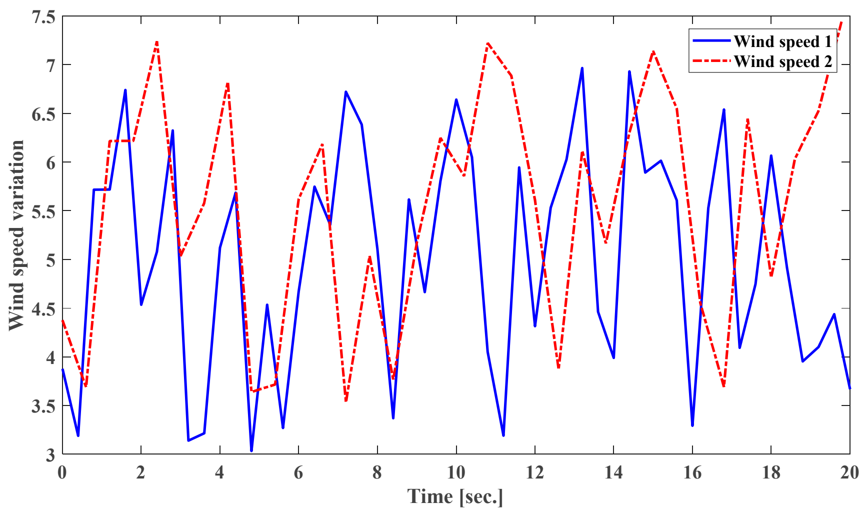

Figure 17. Wind speed variation.

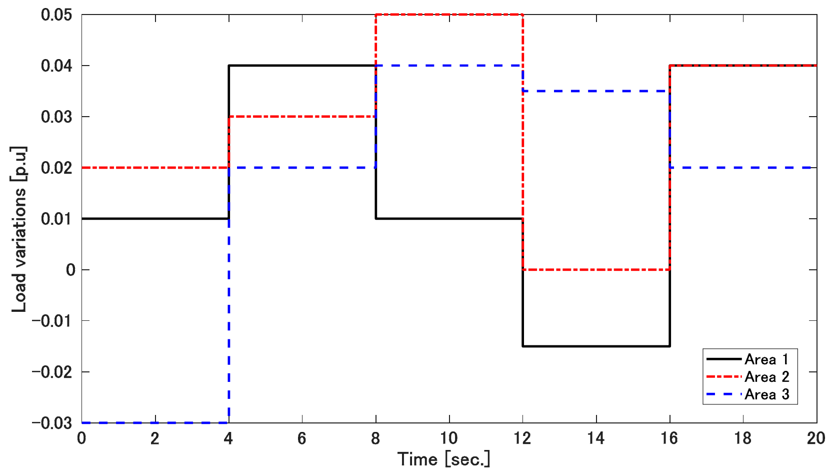

Figure 18. Load variations.

Therefore, the New England PS was simulated with and without wind plants to test the proposed continuous decentralized second-order SMC based observer. Figures 19 and 20 illustrate the results of the frequency error and the tie-line power error of the New England PS without wind. With the use of system states estimated by the observer, the frequency maximum overshoot and settling time were comparatively lower than the results presented in [34]. This is evidence that the new approach has a higher damping ratio than the scheme in [34]. In addition, the proposed approach solved the chattering phenomenon inherent in the first-order SMC presented in [32]. On the other hand, Figures 21 and 22 display the results of the frequency deviation and tie-power error of the New England PS with wind turbines. As seen in Figures 21 and 22, the MAIPS was also stable with good performance.

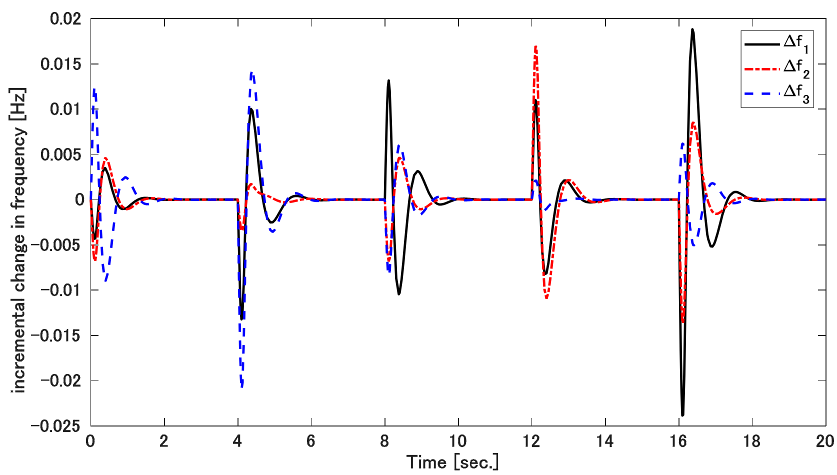

Figure 19. Frequency deviation without wind plant.

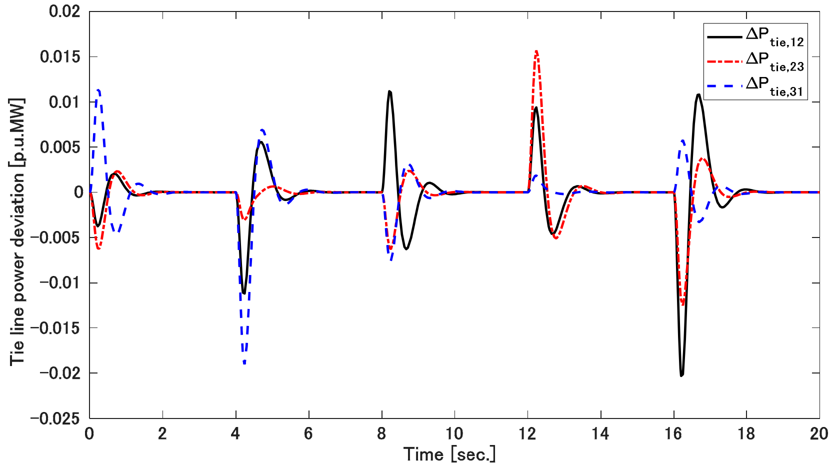

Figure 20. Tie-line power deviation without wind plant.

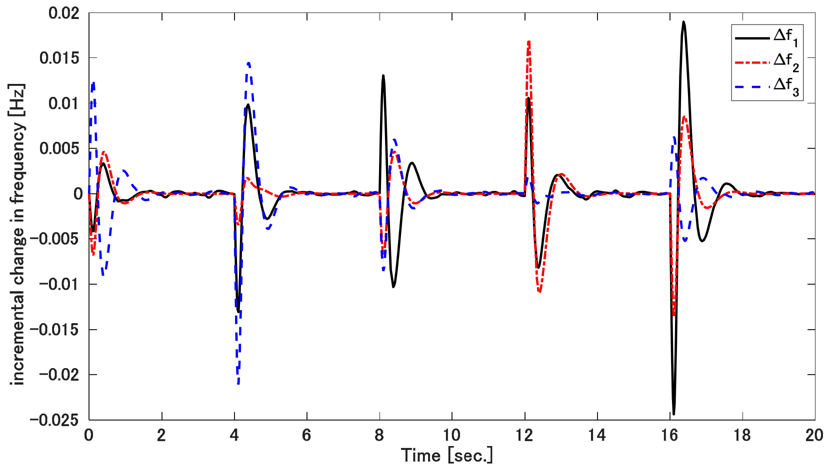

Figure 21. Frequency deviation with wind plant.

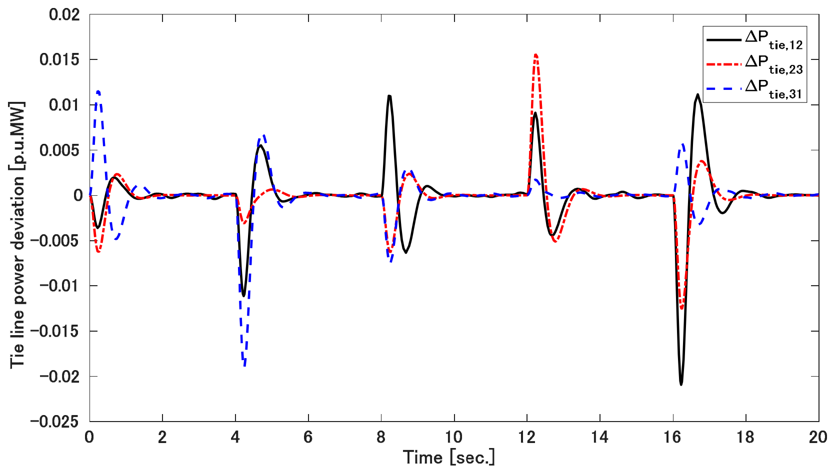

Figure 22. Tie-line power deviation with wind plant.

Remark 4. *An SMC based on the observer used for the LFC of the New England PS can be seen in [34]. However, there are two limitations of the above approach. The first is that the system state variables need to be measured in order to provide feedback for the controller. The second is that the* *control suffers from the chattering problem inherent in the first-order SMC. In this approach, the state observer is used in the sliding surface and second-order sliding mode controller. Therefore, the two above limitations have been solved.*

6. Conclusions

The need for the MAIPS integrated with wind plants is increasing day by day because of the need for efficient power generation. However, the wind variation problem associated with wind turbines can make MAIPS frequency unstable. Therefore, the LFC is important in order to regulate frequency and provide better power quality to consumers. In order to solve the above problem, a new LFC for an MAIPS integrated with wind plants using a state observer based on sliding mode, acting under a second-order time derivative, has been developed. The continuous decentralized sliding mode controller guarantees the control signal accuracy so that the performance of the MAIPS and the power quality are improved. In addition, the stability of the entire power network was demonstrated by means of the Lyapunov method based on the new LMI technique. The simulation results show that the frequency error and the tie-line power error rapidly converge to zero, with better settling time and overshoot when compared to existing designs. Furthermore, the proposed controller can handle with the wind variation because the results show less impact on the power system frequency and tie-line power deviation. In order to verify this new approach with a real MAIPS, a New England PS with and without a wind plant was used and the results showed an improvement in the system performance with respect to maximum overshoot and settling time. Thus, the proposed approach is a better choice for the LFC of a real MAIPS with a wind plant.

Author Contributions: Conceptualization V.V.H., E.N.A. and T.M.N.; methodology P.T.T., A.-T.T., E.N.A., and V.-T.P.; software A.-T.T. and E.N.A.; validation B.L.N.M., P.T.T. and V.-T.P.; writing—original draft preparation E.N.A., A.-T.T. and P.T.T.; writing—review and editing V.V.H., V.-T.P., T.M.N., B.L.N.M. and V.-D.P.; supervision B.L.N.M., T.M.N., V.V.H. and V.-D.P. All authors have read and agreed to the published version of the manuscript.

Funding: This research was funded by the Foundation for Science and Technology Development of Ton Duc Thang University (FOSTECT), website: http://fostect.tdtu.edu.vn, under Grant FOSTECT.2017.BR.05.

Institutional Review Board Statement: Not applicable.

Informed Consent Statement: Not applicable.

Data Availability Statement: The data presented in this study are available on reasonable request from the corresponding author.

Conflicts of Interest: The authors declare no conflict of interest.

References

1. Hsu, K.C. Decentralized variable structure model-following adaptive control for interconnected systems with series nonlinearities. *Int. J. Syst. Sci.* **1998**, *29*, 365–372. [CrossRef]
2. Bevrani, H.; Mitani, Y.; Tsuji, K. Robust decentralized load-frequency control using an iterative linear matrix inequalities algorithm. *IEE Proc. Gener. Trans. Distrib.* **2004**, *151*, 347–354. [CrossRef]
3. Thirunavukarasu, R.; Chidambaram, I.A. PI2 controller based coordinated control with redox flow battery and unified power flow controller for improved restoration indices in a deregulated power system. *Ain Shams Eng. J.* **2016**, *7*, 1011–1102. [CrossRef]
4. Farahani, M.; Ganjefar, S.; Alizadeh, M. PID controller adjustment using chaotic optimization algorithm for multi-area load frequency control. *IET Control Theory Appl.* **2012**, *6*, 1984–1992. [CrossRef]
5. Saxena, S.; Hote, Y.V. Decentralized PID load frequency control for perturbed multi-area power systems. *Int. J. Electr. Power Energy Syst.* **2016**, *81*, 405–415. [CrossRef]
6. Alrifai, M.T.; Hassan, M.F.; Zribi, M. Decentralized load frequency controller for a multi-area interconnected power system. *Int. J. Electr. Power Energy Syst.* **2011**, *33*, 198–209. [CrossRef]
7. Zhao, C.; Topcu, U.; Low, S.H. Optimal load control via frequency measurement and neighborhood area communication. *IEEE Trans. Power Syst.* **2013**, *28*, 3576–3587. [CrossRef]

8. Abdennour, A. Adaptive optimal gain scheduling for the load frequency control problem. *Electr. Power Compon. Syst.* **2002**, *30*, 45–56. [CrossRef]
9. Daneshfar, F.; Bevrani, H. Load-frequency control: A GA based multi-agent reinforcement learning. *IET Gener. Trans. Distrib.* **2010**, *4*, 13–26. [CrossRef]
10. Saxena, S.; Hote, Y.V. Load frequency control in power systems via internal model control scheme and model-order reduction. *IEEE Trans. Power Syst.* **2013**, *28*, 2749–2757. [CrossRef]
11. Ersdal, A.M.; Imsland, L.; Uhlen, K. Model predictive load-frequency control. *IEEE Trans. Power Syst.* **2016**, *31*, 777–785. [CrossRef]
12. Chang-Chien, L.R.; Wu, Y.S.; Cheng, J.S. Online estimation of system parameters for artificial intelligence applications to load frequency control. *IET Gener. Trans. Distrib.* **2010**, *5*, 895–902. [CrossRef]
13. Yousef, H. Adaptive fuzzy logic load frequency control of multi-area power system. *Int. J. Electr. Power Energy Syst.* **2015**, *68*, 384–395. [CrossRef]
14. Liu, F.; Li, Y.; Cao, Y.; She, J.; Wu, M. A two-layer active disturbance rejection controller design for load frequency control of interconnected power system. *IEEE Trans. Power Syst.* **2016**, *31*, 3320–3321. [CrossRef]
15. Liu, Y.; Lan, Q.; Qian, C.; Qian, W.; Chu, H. Universal finite time observer design and adaptive frequency regulation of hydraulic turbine systems. *IET Control Theory Appl.* **2016**, *10*, 363–370. [CrossRef]
16. Chen, H.; Sun, N. Nonlinear control of under-actuated systems subject to both actuated and unactuated state constraints with experimental verification. *IEEE Trans. Ind. Electr.* **2019**, *67*, 7702–7714. [CrossRef]
17. Sun, Y.; Qiang, H.; Mei, X.; Teng, Y. Modified repetitive learning control with unidirectional control input for uncertain nonlinear systems. *Neural Comput. Appl.* **2018**, *30*, 2003–2012. [CrossRef]
18. Bevrani, H. *Robust Power System Frequency Control*; Springer: New York, NY, USA, 2009.
19. Mi, Y.; Fu, Y.; Wang, C.; Wang, P. Decentralized sliding mode load frequency control for multi-area power systems. *IEEE Trans. Power Syst.* **2013**, *28*, 4301–4309. [CrossRef]
20. Onyeka, A.E.; Xing-Gang, Y.; Mao, Z.; Jiang, B.; Zhang, Q. Robust decentralized load frequency control for interconnected time delay power systems using sliding mode techniques. *IET Control Theory Appl.* **2019**, *14*, 470–480. [CrossRef]
21. Guo, J. Application of a novel adaptive sliding mode control method to the load frequency control. *Eur. J. Control* **2020**, *57*, 172–178.
22. Lv, X.; Sun, Y.; Wang, Y.; Dinavahi, V. Adaptive event-triggered load frequency control of multi-area power systems under networked environment via sliding mode control. *IEEE Access* **2020**, *8*, 86585–86594. [CrossRef]
23. Le Ngnoc Minh, B.; Huynh, V.V.; Nguyen, T.M.; Tsai, Y.W. Decentralized adaptive double integral sliding mode controller for multi-area power systems. *Math. Probl. Eng.* **2018**, *2018*, 1–11. [CrossRef]
24. Huynh, V.V.; Tran, P.T.; Minh, B.L.N.; Tran, A.T.; Tuan, D.H.; Nguyen, T.M.; Vu, P.T. New second-order sliding mode control design for load frequency control of a power system. *Energies* **2020**, *13*, 6509. [CrossRef]
25. Kalla, U.K.; Singh, B.; Murthy, S.S.; Jain, C.; Kant, K. Adaptive sliding mode control of standalone single-phase microgrid using hydro, wind, and solar PV array-based generation. *IEEE Trans. Smart Grid* **2017**, *9*, 6806–6814. [CrossRef]
26. Dev, A.; Sarkar, M.K.; Asthana, P.; Narzary, D. Event-Triggered adaptive integral higher-order sliding mode control for load frequency problems in multi-area power systems. *Iran. J. Sci. Technol. Trans. Electr. Eng.* **2019**, *43*, 137–152. [CrossRef]
27. Sarkar, M.K.; Dev, A.; Asthana, P.; Narzary, D. Chattering free robust adaptive integral higher order sliding mode control for load frequency problems in multi-area power systems. *IET Control Theory Appl.* **2018**, *12*, 1216–1227. [CrossRef]
28. Rosyiana, F.I.; Kim, J.S.; Song, H. High-gain disturbance observer-based robust load frequency control of power systems with multiple areas. *Energies* **2017**, *10*, 595.
29. Mi, Y.; Fu, Y.; Li, D.; Wang, C.; Loh, P.C.; Wang, P. The sliding mode load frequency control for hybrid power system based on disturbance observer. *Int. J. Electr. Power Energy Syst.* **2016**, *74*, 446–452. [CrossRef]
30. Wang, C.; Mi, Y.; Fu, Y.; Wang, P. Frequency control of an isolated micro-grid using double sliding mode controllers and disturbance observer. *IEEE Trans. Smart Grid* **2016**, *9*, 923–930. [CrossRef]
31. Liao, K.; Xu, Y. A robust load frequency control scheme for power systems based on second-order sliding mode and extended disturbance observer. *IEEE Trans. Ind. Inf.* **2017**, *14*, 3076–3086. [CrossRef]
32. Huynh, V.V.; Minh, B.L.N.; Amaefule, E.N.; Tran, A.T.; Tran, P.T. Highly robust observer sliding mode based frequency control for multi area power systems with renewable power plants. *Electronics* **2021**, *10*, 274. [CrossRef]
33. Tummala, A.S.; Inapakurthi, R.; Ramanarao, P.V. Observer based sliding mode frequency control for multi-machine power systems with high renewable energy. *J. Mod. Power Syst. Clean Energy* **2018**, *6*, 473–474. [CrossRef]
34. Prasad, S.; Purwar, S.; Kishor, N. Load frequency regulation using observer based non-linear sliding mode control. *Int. J. Electr. Power Energy Syst.* **2019**, *104*, 178–193. [CrossRef]
35. Liu, X.; Wang, P.; Loh, P.C. A hybrid AC/DC microgrid and its coordination control. *IEEE Trans. Smart Grid* **2011**, *2*, 278–286.
36. Obaid, Z.A.; Cipcigan, L.M.; Abrahim, L.; Muhssin, M.T. Frequency control of future power systems: Reviewing and evaluating challenges and new control methods. *J. Mod. Power Syst. Clean Energy* **2019**, *7*, 9–25. [CrossRef]
37. Bucolo, M.; Buscarino, A.; Famoso CFortuna, L.; Frasca, M. Control of imperfect dynamical systems. *Nonlinear Dyn.* **2019**, *98*, 2989–2999. [CrossRef]

VOLUME: 5 | ISSUE: 1 | 2021 | June

Load Frequency Control for Power System using Generalized Extended State Observer

Anh-Tuan TRAN[1], *Phong Thanh TRAN*[1], *Van Van HUYNH*[1,*]

[1]Faculty of Electrical & Electronics Engineering, Ton Duc Thang University, Ho Chi Minh City, Viet Nam

*Corresponding Author: Van Van HUYNH (Email: huynhvanvan@tdtu.edu.vn)
(Received: 25-Oct-2020; accepted: 13-Jan-2021; published: 31-Mar-2021)
DOI: http://dx.doi.org/10.25073/jaec.202151.307

Abstract. *This study investigates load frequency control based generalized extended state observer (GESO) for interconnected power system subject to multi-kind of the power plant. First, the mathematical model of the interconnected power system is proposed based on the dynamic model of thermal power plant with reheat turbine and hydro power plant. Second, the GESO is designed to estimate the system states and disturbances. In addition, the problem of unmeasurable of system states in the interconnected power network due to lack of sensor has been solved by using the proposed load frequency control based GESO. The numerical experiments are carried out by using MATLAB/ SIMULINK simulation. The simulation results point out that the proposed control approach has capacity to handle the uncertainties and disturbances in the interconnected power system with better transient performances in comparison with the existing control approach. The relevant dynamic models have already been used for the simulation of the physical constraints of governor dead band (GDB) and generation rate constraint (GRC) effect in the power plants. It is evident that the robustness of the suggested controller in terms of stability and effectiveness of the system.*

Keywords

Interconnected power system, load frequency control, generalized extended state observer.

1. Introduction

In large power systems, load frequency control (LFC) is one of the essential operation problems in electrical power under load and resource variation. Consequently, any changes in frequency not only impact truthfully on the operation of power networks and power system reliability but also lead to an uncertain condition for interconnected power networks. The primary goals of a power network LFC are to keep and maintain the frequency deviation and tie line power exchanges with neighbor control areas at the planned value according to a schedule [1–6].

In a power system, it is not easy to regulate the frequency in power exchange/interchange through tie-lines. Many academic researchers represented the LFC approach of typical power system utilizing different control methods in both traditional and developed techniques that have been applied to resolve the LFC problems of interconnected power networks [7–22].

To resolve problems of frequency deviation occurred by various matched or mismatched uncertainties, adaptive control is one of modern control schemes for complex power system included in various load and power control areas [7–10]. LFC control approach for interconnected power networks is introduced to establish in the direct-indirect adaptive fuzzy control strategy [7] which extends and builds up the parameter algorithms and the appropriate adaptive control law. An adaptive model predictive LFC approach in [8] for multi-area power network is used with photovoltaic generation by regrading some nonlinear features. An adaptive LFC controller is suggested [9] by making use of the least square strategy with an internal model control design in structure. In [10], the hypothesis of the suggested adaptive way is constructed by the on-line tuning method of the gain of an integral controller which is applied in the electrosearch optimization. However, the adaptive control schemes above were presented to be complex in control algorithms to deal with the variations of power network parameters subjected to the LFC approaches.

The conventional PID controllers of constant parameters and fixed system structure were investigated to solve the LFC problem for normal operating condition [11–13]. However, the characteristic of power networks is nonlinear system. Therefore, some traditional PID control methods may not have ability to improve the better performance for other operating conditions and to make the best of optimizing the PID parameters and to develop stability performance in power network with the parameter uncertainties and load disturbances.

In the different way of doing the research, sliding mode control (SMC) is not only another way to resolve LFC difficult problems but also a nonlinear control approach to be well known for improving the system performance. In detail, the SMC approach is very sensitive to validate of plant parameters as well as improve effectively in system transient performance. In recent times, there are many the SMC frequency approaches implemented to work out the problems of power networks with parameter uncertainties or load variations [14–17]. The LFC controller is suggested and developed for the interconnected power system to upgrade the system performance using the decentralized SMC [14]. However, the matched and unmatched uncertainties in power networks are not always suitable and satisfied in all of conditions. A novel adaptive SMC approach [15] is designed to the LFC in terms of the parametric derivation the external disturbances. However, there are some existing limitations such as the computation of dynamic model and control design is complex, the state cannot be observed, the response performance and waveform need to improve. In [16], the proposed SMC is applied in the basic control method with the adaptive dynamic programming approach is utilized to improve the extra control signal and to modify the frequency scheme. However, parameter uncertainties due to variable operation point was not considered and the transient performance were not very good as compared previous research. [17] is distributed sliding mode control scheme for optimal LFC to adopt a nonlinear model of a multi-area power system, including dynamic of voltage and dynamics of second order turbine-governor. However, the suggested strategy is complicated and difficult for practical implementation. The parameter uncertainties of power generation were not discussed.

From above control researches such as adaptive control, PID control and SMC control, the results are achieved under assumption that all state variables of power system can to be measurable and willingly available for system feedback. In practical application, not all state variables are measurable for system feedbacks, and then we must compute and estimate the state variables that cannot measure in the system. The proposed approach of estimating state variables is often used in observation [18–22], [26-29]. These schemes can modify and improve the unknown upper bounds of matched and mismatch uncertainties. It not only obtains the system state trajectories accomplishment but also satisfies in parameters of the system state errors. The achievement of results is correlated to LFC's of power networks in various control techniques [18-22], [26-29]. However, there are still some limitations of the above approaches such as the disturbances are not truncated from the output points in steady state and the gains of controller are not set to be really high to reduce disturbances of unknown boundaries and even, the parameter uncertainties or load variations of power system are not considered in some proposed controllers. The GESO scheme based on the non-linear SMC controller are combined to investigate the frequency variation problem and to estimate the disturbance in interconnected power network [30]. However, the performance of power system is not always satisfied under required conditions in the settling time, transient frequency variations considering GDB and GRC effect. In detail, GRC is normally considered by adding a limiter and a hysteresis pattern to the governor-turbine system model. It is essential to take into consideration the practical constraints and natural conditions such as physical constraint of generation rate constraint (GRC). The GRC has negative affect on the power network performance due to its nonlinearity nature. The GRC denotes practical constraint on the ratio of the variation in the generating power due to physical drawbacks. Governor dead band (GDB) is principle for power network frequency control in the presence of disturbances. GDB has a definite outline as the total magnitude of a continued speed change that there is no resulting variation in valve position. An observer-based control scheme is offered for LFC scheme against cyberattack uncertainties [31]. However, to test the effective response of the proposed controller of power networks, the GDB and GRC effect are not considered in the power plant.

The process of being mentally stimulated to do the control approaches is to eliminate and improve perturbations by feedback control instead of feedforward compensation control which uses the disturbance estimations to cancel out the affections in real time manner. The suggested control approach is one way of approaches for estimating and compensating the system disturbances. This scheme proves the powerful and robustness to again matched uncertainties. The contributions of the proposed GESO in this paper are as follows:

- GESO is designed to estimate the unmeasurable system state variables and the load uncertainties in the complex power system. The proposed scheme of making power system is not only secure or stable but also useful to solve the satisfactory performance with uncertainties.

- The generalized extended observer approach improves the system dynamic response to fast response in setting time and to reduce over or undershoots in power network with the dynamic model of thermal power plant with reheat turbine and hydro power plant.

- The simulation result with various cases indicates the effectively and robustness of generalized extended controller by considering parametric uncertainties in power networks.

- The report of simulation results is used to compare with the cases of considering and without considering the GDB and GRC nonlinearity effects on power network.

The paper is outlined as follows: section II shows the mathematical model of power network. The generalized extended state observer for multi-area power systems is designed in section III. Section IV represents stability analysis of power system and control scheme design of power system, the following session by simulation results in section V.

2. Mathematical model of power system

The dynamic models of power systems are generally nonlinear. The block chart of power system is presented in Fig. 1, Fig. 2 and Fig. 3. The power system includes two types of the plant as thermal power plant with reheat turbine and hydro power plant with mechanical hydraulic governor connected through tie-line power.

2.1. The thermal power plant with reheat turbine model

A thermal power plant is an electric power station to convert heat energy to electric power. Reheat turbine is a part of thermal power plants in power network in Fig. 2.

The frequency dynamic behavior of area i^{th} details in this section which can use in the fol-

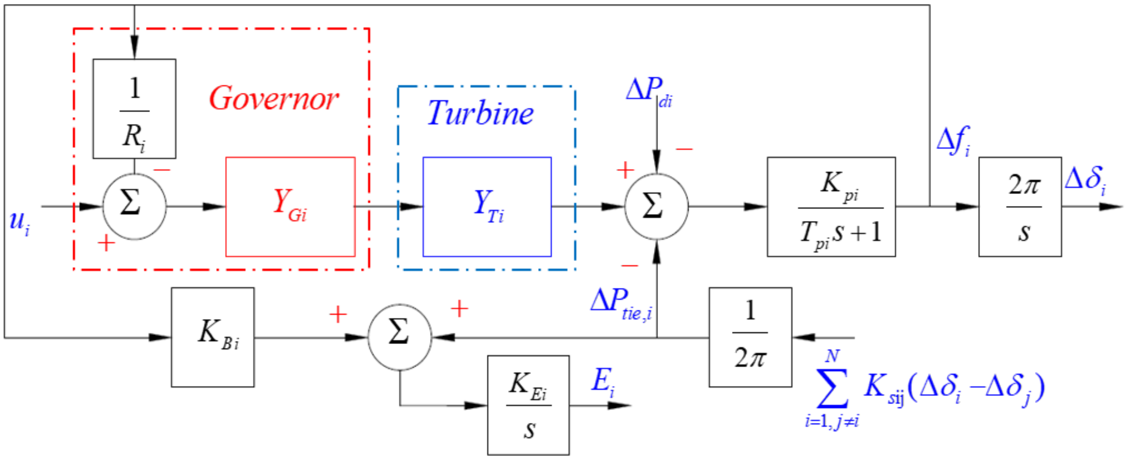

Fig. 1: The block chart of complex power network.

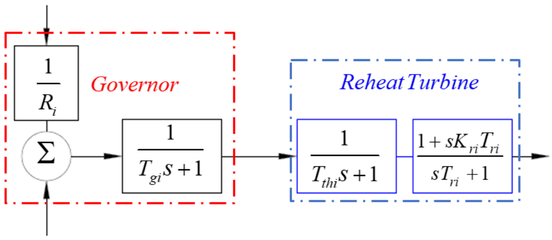

Fig. 2: The block chart of i^{th} area with reheat turbine.

lowing differential equations:

$$\Delta\dot{f}_i(t) = -\frac{1}{T_{pi}}\Delta f_i(t) + \frac{K_{Pi}}{T_{pi}}\Delta P_{mi}(t) - \frac{K_{Pi}}{2\pi T_{Pi}}\sum_{i=1,j\neq i}^{N} K_{sij}[\Delta\delta_i(t) - \Delta\delta_j(t)] - \frac{K_{Pi}}{T_{pi}}\Delta P_{di}(t) \quad (1)$$

$$\Delta\dot{P}_{mi}(t) = (\frac{1}{T_{ri}} - \frac{K_{ri}}{T_{thi}})\Delta P_{thi}(t) + \frac{K_{ri}}{T_{thi}}\Delta P_{vi}(t) - \frac{1}{T_{ri}}\Delta P_{mi}(t) \quad (2)$$

$$\Delta\dot{P}_{thi}(t) = \frac{1}{T_{thi}}\Delta P_{vi}(t) - \frac{1}{T_{thi}}\Delta P_{thi}(t) \quad (3)$$

$$\Delta\dot{P}_{vi}(t) = -\frac{1}{T_{gi}R_i}\Delta f_i(t) - \frac{1}{T_{gi}}\Delta P_{vi}(t) + \frac{1}{T_{gi}}u_i(t) \quad (4)$$

$$\Delta\dot{E}_i(t) = K_{Bi}K_{Ei}\Delta f_i(t) + \frac{K_{Ei}}{2\pi}K_{sij}[\Delta\delta_i(t) - \Delta\delta_j(t)] \quad (5)$$

$$\Delta\dot{\delta}_i(t) = 2\pi\,\Delta f_i(t) \quad (6)$$

The variables of interconnected power system are the frequency deviation, power output, governor valve position, integral control and rotor angle variation as following as bellow:

$$x_i(t) = \begin{bmatrix} \Delta f_i(t) \\ \Delta P_{mi}(t) \\ \Delta P_{thi}(t) \\ \Delta P_{vi}(t) \\ \Delta E_i(t) \\ \Delta\delta_i(t) \end{bmatrix}$$

where $i = 1, 2, .., N$ and N is the area numbers.

The interconnected power network with thermal power plant described by Fig. 1 and Fig. 2, which can be written and expressed in state-space representation below:

$$\dot{x}_i(t) = A_i x_i(t) + B_i u_i(t) + \sum_{i=1,i\neq j}^{N} H_{ij}x_j + \Gamma_i\Omega_i(t)$$
$$y_i(t) = C_i x_i(t) \quad (7)$$

The definition of following matrices is as given in the following:

$$A_i = \begin{bmatrix} -\frac{1}{T_{pi}} & \frac{K_{Pi}}{T_{pi}} & 0 & 0 & 0 & -\frac{K_{Pi}}{2\pi T_{Pi}}K_{ij} \\ 0 & -\frac{1}{T_{ri}} & (\frac{1}{T_{ri}} - \frac{K_{ri}}{T_{thi}}) & \frac{K_{ri}}{T_{thi}} & 0 & 0 \\ 0 & -\frac{1}{T_{thi}} & \frac{1}{T_{thi}} & 0 & 0 & 0 \\ -\frac{1}{T_{gi}R_i} & 0 & 0 & -\frac{1}{T_{gi}} & 0 & 0 \\ K_{Bi} & 0 & 0 & 0 & 0 & \frac{K_{Ei}}{2\pi}K_{sij} \\ 2\pi & 0 & 0 & 0 & 0 & 0 \end{bmatrix}$$

$$H_{ij} = \begin{bmatrix} 0 & 0 & 0 & 0 & 0 & -\frac{K_{Pi}}{2\pi T_{Pi}}K_{ij} \\ 0 & 0 & 0 & 0 & 0 & 0 \\ 0 & 0 & 0 & 0 & 0 & 0 \\ 0 & 0 & 0 & 0 & 0 & 0 \\ 0 & 0 & 0 & 0 & 0 & \frac{K_{Ei}}{2\pi}K_{sij} \\ 0 & 0 & 0 & 0 & 0 & 0 \end{bmatrix}$$

$$B_i = \begin{bmatrix} 0 & 0 & 0 & \frac{1}{T_{gi}} & 0 & 0 \end{bmatrix}^T$$

$$\Gamma_i = \begin{bmatrix} -\frac{K_{Pi}}{T_{pi}} & 0 & 0 & 0 & 0 & 0 \end{bmatrix}^T$$

where $x_i(t) \in R^{n_i}$ is state vector of the i^{th} area, $x_j(t) \in R^{n_i}$ is state vector of the j^{th} area, $u_i(t) \in R^{m_i}$ is the control vector, $\Omega_i(t) \in R^{m}$is the vector of the load disturbance, $y_i(t)$ is the output signal of the i^{th} area, A_i is the variable matrix of the power system of the i^{th} area, $B_i$is the output matrix of the i^{th} area, H_{ij} is the power flow between two-area, C_i is the output matrix of the i^{th} area, Γ_i is the disturbance matrix of the i^{th} area, $\Delta\dot{f}_i(t)$ is the frequency deviation of the i^{th} area, $\Delta P_{mi}(t)$ is the mechanics power variation of the turbine of the i^{th} area and $\Delta\dot{\delta}_i(t)$ is the rotor angle deviation of the i^{th} area.

2.2. The hydro power plant with hydro turbine

The hydroelectric power plant is the most common type of power system in Fig. 3. The function of a hydraulic turbine is to convert the energy of the flowing water into mechanical energy and this mechanical energy is converted from hydro-electric generator to electricity.

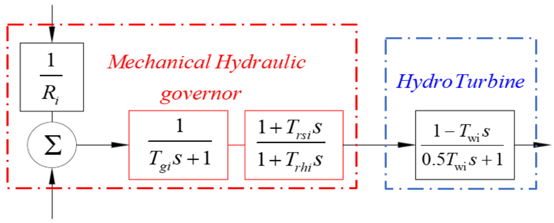

Fig. 3: The block chart of i^{th} area with hydro turbine.

$$\begin{aligned}\Delta\dot{f}_i(t) = &-\frac{1}{T_{pi}}\Delta f_i(t) + \frac{K_{pi}}{T_{pi}}\Delta P_{mi}(t) \\ &- \frac{K_{pi}}{T_{pi}}\Delta P_{di}(t) \\ &- \frac{K_{Pi}}{2\pi T_{Pi}}K_{sij}[\Delta\delta_i(t) - \Delta\delta_j(t)]\end{aligned} \quad (8)$$

$$\begin{aligned}\Delta P_{mi}(t) = &\frac{2T_{rsi}}{T_{rhi}T_{gi}R_i}\Delta f_i(t) \\ &+ (\frac{2}{T_{wi}} + \frac{2}{T_{rhi}})\Delta P_{vi}(t) \\ &- \frac{2}{T_{wi}}\Delta P_{mi}(t) - \frac{2}{T_{wi}}\Delta P_{mi}(t) \\ &+ (\frac{2T_{rsi}}{T_{rhi}T_{gi}} - \frac{2}{T_{rhi}})\Delta P_{gi}(t) \\ &- \frac{2T_{rsi}}{T_{rhi}T_{gi}}u_i(t)\end{aligned} \quad (9)$$

$$\begin{aligned}\Delta P_{vi}(t) = &\frac{-T_{rsi}}{T_{rhi}T_{gi}R_i}\Delta f_i(t) + \frac{-1}{T_{rhi}}\Delta P_{vi}(t) \\ &+ (\frac{1}{T_{rhi}} - \frac{T_{rsi}}{T_{rhi}T_{gi}})\Delta P_{gi}(t) \\ &+ \frac{T_{rsi}}{T_{rhi}T_{gi}}u_i(t)\end{aligned} \quad (10)$$

$$\Delta \dot{P}_{gi}(t) = -\frac{1}{T_{gi}R_i}\Delta f_i(t) - \frac{1}{T_{gi}}\Delta P_{gi}(t) + \frac{1}{T_{gi}}u_i(t) \quad (11)$$

$$\Delta \dot{\delta}_i(t) = 2\pi\, \Delta f_i(t) \quad (12)$$

The variables of interconnected power system are the frequency deviation, power output, governor valve position, integral control and rotor angle variation as following as bellow:

$$x_i(t) = \begin{bmatrix} \Delta f_i(t) \\ \Delta P_{mi}(t) \\ \Delta P_{vi}(t) \\ \Delta P_{gi}(t) \\ \Delta E_i(t) \\ \Delta \delta_i(t) \end{bmatrix}$$

where $i = 1, 2, .., N$ and N is the area numbers.

The interconnected power system with hydro power plant described by Fig. 1 and Fig. 3, which can be written and expressed in state-space representation below:

$$\begin{aligned} \dot{x}_i(t) &= A_i x_i(t) + B_i u_i(t) \\ &\quad + \sum_{i=1, i\neq j}^{N} H_{ij}x_j + \Gamma_i \Omega_i(t) \\ y_i(t) &= C_i x_i(t) \end{aligned} \quad (13)$$

The definition of following matrices is as given in:

$$B_i = \begin{bmatrix} 0 & -\frac{2T_{rsi}}{T_{rhi}T_{gi}} & \frac{T_{rsi}}{T_{rhi}T_{gi}} & \frac{1}{T_{gi}} & 0 & 0 \end{bmatrix}^T$$

$$\Gamma_i = \begin{bmatrix} -\frac{K_{Pi}}{T_{pi}} & 0 & 0 & 0 & 0 & 0 \end{bmatrix}^T$$

$$H_{ij} = \begin{bmatrix} 0 & 0 & 0 & 0 & 0 & -\frac{K_{Pi}}{2\pi T_{Pi}}K_{sij} \\ 0 & 0 & 0 & 0 & 0 & 0 \\ 0 & 0 & 0 & 0 & 0 & 0 \\ 0 & 0 & 0 & 0 & 0 & 0 \\ 0 & 0 & 0 & 0 & 0 & \frac{K_{Ei}}{2\pi}K_{sij} \\ 0 & 0 & 0 & 0 & 0 & 0 \end{bmatrix}$$

3. Generalized extended state observer design

In practical application, not all state variables are measurable for system feedbacks, and then we must compute and estimate the state variables that cannot measure for the parametric uncertainties in power system. Therefore, states observer performs the function by estimating the state variables of the systems typically the output and control variable. State observers can be designed and applied only when the observability of required condition is satisfied. The GESO is recommended for using in this system because it is more sensitive with changes in parameters of load disturbance variations. To estimate state variables in the power system included both variables and load disturbances, GESO is defined as following bellow:

$$[x_i]_{n_i+1}(t) = \Omega_i(t) \quad (14)$$

and

$$\gamma_i(t) = \frac{\Omega_i(t)}{dt} \quad (15)$$

Then, the system in equation can be presented below:

$$\begin{aligned} \dot{\bar{x}}_i(t) &= \bar{A}_i \bar{x}_i(t) + \bar{B}_i u_i(t) \\ &\quad + \sum_{i=1, i\neq j}^{N} \bar{H}_{ij}x_j + F_i \gamma_i(t) \\ \bar{y}_i(t) &= \bar{C}_i \bar{x}_i(t) \end{aligned} \quad (16)$$

where

$$\bar{x}_i(t) = \begin{bmatrix} [x_i]_{n_i \times 1} \\ [(x_i)_{n_i+1}]_{n\_i \times 1} \end{bmatrix}_{(n_i+n_i)\times 1}$$

$$A_i = \begin{bmatrix} -\frac{1}{T_{pi}} & \frac{K_{pi}}{T_{pi}} & 0 & 0 & 0 & -\frac{K_{Pi}}{2\pi T_{Pi}}K_{sij} \\ \frac{2T_{rsi}}{T_{rhi}T_{gi}R_i} & -\frac{2}{T_{wi}} & (\frac{2}{T_{wi}} + \frac{2}{T_{rhi}}) & (\frac{2T_{rsi}}{T_{rhi}T_{gi}} - \frac{2}{T_{rhi}}) & 0 & 0 \\ \frac{-T_{rsi}}{T_{rhi}T_{gi}R_i} & 0 & \frac{-1}{T_{rhi}} & (\frac{1}{T_{rhi}} - \frac{T_{rsi}}{T_{rhi}T_{gi}}) & 0 & 0 \\ -\frac{1}{T_{gi}R_i} & 0 & 0 & -\frac{1}{T_{gi}} & 0 & 0 \\ K_{Bi} & 0 & 0 & 0 & 0 & \frac{K_{Ei}}{2\pi}K_{sij} \\ 2\pi & 0 & 0 & 0 & 0 & 0 \end{bmatrix}$$

$$\bar{A}_i = \begin{bmatrix} [A_i]_{n_i\times n_i} & I_{n_i\times n_i} \\ 0_{n_i\times n_i} & 0_{n_i\times n_i} \end{bmatrix}_{(n_i+n_i)\times(n_i+n_i)}$$

$$\bar{H}_{ij} = \begin{bmatrix} [H_{ij}]_{n_i\times n_i} & 0_{n_i\times n_i} \\ 0_{n_i\times n_i} & 0_{n_i\times n_i} \end{bmatrix}_{(n_i+n_i)\times(n_i+n_i)}$$

$$\bar{B}_i = \begin{bmatrix} [B_i]_{n_i\times p_i} \\ 0_{n_i\times p_i} \end{bmatrix}_{(n_i+n_i)\times p_i}$$

$$F_i = \begin{bmatrix} 0_{n_i\times r_i} \\ I_{n_i\times r_i} \end{bmatrix}_{(n_i+n_i)\times r_i}$$

$$\bar{C}_i = \begin{bmatrix} [C_i]_{m_i\times n_i} \\ 0_{m_i\times n_i} \end{bmatrix}_{m_i\times(n_i+n_i)}$$

Assumption 1: (A_i, B_i) is controllable and $(\bar{A}_i, \bar{C}_i)$ is observable.

With regards to the state observers discussed, we will apply the notation $\hat{\bar{x}}_i$ to indicate the vector observer state. The vector $\hat{\bar{x}}_i$ of the observed state is used and applied in the state feedback to initiate the desired and required control vector.

If we call the state $\bar{x}_i$ is approximated to state$\hat{\bar{x}}_i$,the dynamical model in (17):

$$\begin{aligned}\dot{\hat{\bar{x}}}_i(t) &= \bar{A}_i\hat{\bar{x}}_i(t) + \bar{B}_i u_i(t) \\ &\quad + \sum_{i=1, i\neq j}^{N} \bar{H}_{ij}\hat{\bar{x}}_j + L_i(\bar{y}_i(t) - \hat{\bar{y}}_i(t)) \\ \dot{\hat{\bar{y}}}_i(t) &= \bar{C}_i\hat{\bar{x}}_i(t) \end{aligned} \tag{17}$$

where, $\dot{\hat{\bar{y}}}_i(t)$ is the estimator state of the output variables and matrix L_i is the observer gain, which can be designed through to place any desired eigenvalues in the left half s-plane of $(\bar{A}_i - L_i\bar{C}_i)$.

The control input is chosen as following as (18):

$$u_i(t) = K_{xi}x_i(t) + K_{di}\hat{\Omega}_i(t) \tag{18}$$

or

$$u_i(t) = K_{xi}\hat{x}_i(t) + K\_{di}\hat{\Omega}_i(t) \tag{19}$$

where $\hat{\Omega}_i(t) = [\hat{x}_i]_{n_i+1}$

From Eqs. (18) and (19), we can rewrite:

$$u_i(t) = K_i\hat{\bar{x}}_i(t) = [K_{xi} \quad K_{di}]\hat{\bar{x}}_i(t) \tag{20}$$

where, K_{xi} is the feedback control gain to be chosen so that the eigenvalues of $(A_i - B_iK_{xi})$lie in specific locations in the left-half s-plane and the lumped uncertainty compensation gain$K_{di}$is designed:

$$\begin{aligned} &K_{di} \\ &= [C_i(A_i - B_iK_{xi})^{-1}B_i]^{-1}C_i(A_i - B_iK_{xi})^{-1}\Gamma_i \end{aligned} \tag{21}$$

To solve the disturbance compensation gain: The disturbance compensation gain in (21) is no longer available since $C_i(A_i - B_iK_{xi})^{-1}B_i$ is probably non-invertible or even not a square matrix. In a case in point, it can be proved that an alternative but more typical condition.

$$\begin{aligned} &[C_i(A_i - B_iK_{xi})^{-1}B_i]^{-1}K_{di} \\ &= C_i(A_i - B_iK_{xi})^{-1}\Gamma_i \end{aligned} \tag{22}$$

It must be gratified to assure the viability of the proposed control scheme. The gain K_{di} can be resolved from (22) if the following rank condition holds:

$$\begin{aligned} &rank[C_i(A_i - B_iK_{xi})^{-1}B_i]^{-1} \\ &= rank[C_i(A_i - B_iK_{xi})^{-1}B_i]^{-1}, \\ &\qquad [C_i(A_i - B_iK_{xi})^{-1}\Gamma_i] \end{aligned} \tag{23}$$

The simple configuration of the suggested GESO is presented in Fig. 4. It shows the uncertainties which can be designed and eliminated from the output channel in steady state by this control law.

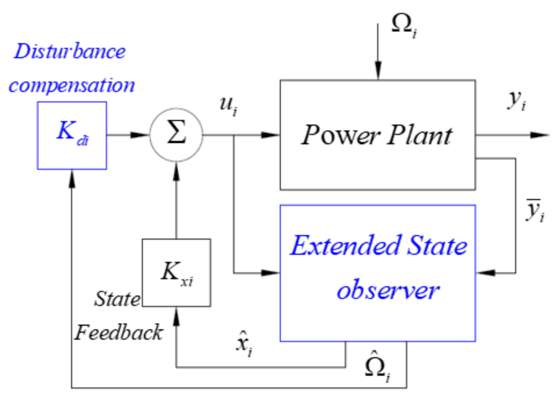

Fig. 4: The configuration of the proposed GESO [23-25], [30-31].

4. Stability of power system

The stability analysis of the multi-area power system as represented in Fig. 1 is performed in this part. The suggested control approach goals at the fundamental boundedness of all the power system signals.

Assumption 2: The lumped disturbances have to the satisfaction of the following conditions.

They get constant value in steady state of system, i.e.; $\lim_{t\to\infty}\Omega_i(t) = \zeta_i$ and $\lim_{t\to\infty}\gamma_i(t) = \lim_{t\to\infty}\dot{\Omega}_i(t) = 0$.

The state and disturbance estimation errors are defined as:

$$e_{xi}(t) = \hat{x}_i(t) - x_i(t) \tag{24}$$

and

$$e_{di}(t) = \hat{\Omega}_i(t) - \Omega_i(t) \tag{25}$$

where: $\hat{\Omega}_i(t) = [\hat{x}_i]_{n_i+1}$ is presented the estimation of the system uncertainties.

Combine (16) and the estimation error of state observers $e_i(t) = \bar{x}_i(t) - \hat{\bar{x}}_i(t)$ can be revised by:

$$\begin{aligned}\dot{e}_i(t) &= \bar{A}_i e_i(t) - L_i(\bar{y}_i(t) - \hat{\bar{y}}_i(t)) + F_i\gamma_i(t)\\ &= (\bar{A}_i - L_i\bar{C}_i)e_i(t) + F_i\gamma_i(t)\end{aligned} \tag{26}$$

Denote $F_i\gamma_i(t)$ by $u_i(t)$ and use final-value theorem, we can be obtained:

$$\begin{aligned}&\lim_{t\to\infty} e_i(t)\\ &= \lim_{t\to\infty} s(sI - (\bar{A}_i - L_i\bar{C}_i))^{-1}U_i(s)\\ &= \lim_{t\to\infty} (sI - (\bar{A}_i - L_i\bar{C}_i))^{-1} \lim_{s\to\infty} sU_i(s)\\ &= \lim_{s\to\infty} (sI - (\bar{A}_i - L_i\bar{C}_i))^{-1} \lim_{t\to\infty} u_i(t)\end{aligned} \tag{27}$$

Since $\lim_{s\to\infty}(sI - (\bar{A}_i - L_i\bar{C}_i))^{-1}$ is bounded and $\lim_{t\to\infty} u_i(t) = 0$

So, the estimation error of state observers is: $e_i(t) = \bar{x}_i(t) - \hat{\bar{x}}_i(t)$ is asymptotically stable.

Remark 1: By applying the control design to the estimation of the lumped uncertainty and the parameters of system states if the system states are not measurable. So, the proposed control law will be designed as in [23-25].

Remark 2: It is recognized that the lumped uncertainty cannot be reduced completely and totally from the state equation no matter what controller was designed. In this strategy, one of the most recent achievable aims is simply to truncate the disturbances at the output point in steady state by applying of the proposed control law. Therefore, the limitations by other control approaches in the previous papers [18-22] have been resolved.

5. Simulations and results

To test the efficiency and robustness of the proposed control strategy, the various cases in two simulations are implemented to prove the performance of GESO controller in estimating of states and avoiding the effect of matched uncertainties with external disturbance. It also reduces effect of the governor dead band (GDB) and generation rate constraint (GRC) in the power plants. These parameters of power network are presented in Table 1. The simulation results are utilized to compare with previous proposed control scheme in [5–6], [15] using MATLAB/SIMULINK.

Tab. 1: The parameters of interconnected multi-area power system [5–6], [15].

No.	Parameters	Value
1	T_{gi}	0.08
2	T_{thi}	0.3
3	K_{ri}	0.5
4	T_{ri}	10
5	T_{rsi}	5
6	T_{rhi}	28.75
7	T_{Wi}	0.3
8	R_i	2.4
9	T_{pi}	20
10	K_{pi}	120
11	K_{bi}	0.425
12	a_{ij}	-1
13	$2\pi K_{sij}$	0.215

We can issue the estimating value to find the real value. The observer gain is designed depend on the pole ρ with the eigenvalue $\bar{A}_i - L_i\bar{C}_i$ of lied in the desired locations in the left-half s-plane.

Simulation 1:

Case 1. In this case, we apply proposed controller for interconnected power network with only thermal power plant in both stations in Fig. 1 and Fig. 2.

To combine between system matrix of thermal power plant and parameter values in Table 1, the matrix values of the power network are calculated as:

$$A_1 = \begin{bmatrix} -0.05 & 6 & 0 & 0 & 0 & -0.0327 \\ 0 & -0.1 & -15667 & 1,6667 & 0 & 0 \\ 0 & -3.3333 & 3.3333 & 0 & 0 & 0 \\ -5.2083 & 0 & 0 & -12.5 & 0 & 0 \\ 0.425 & 0 & 0 & 0 & 0 & 0.0054 \\ 6.2832 & 0 & 0 & 0 & 0 & 0 \end{bmatrix}$$

$$B_1 = \begin{bmatrix} 0 & 0 & 0 & 12.5 & 0 & 0 \end{bmatrix}^T$$

$$\Gamma_1 = \begin{bmatrix} -6 & 0 & 0 & 0 & 0 & 0 \end{bmatrix}^T$$

Feedback control gain in this case can be designed as:

$$K_{x1} = \begin{bmatrix} -0.0417 & 0.0003 & -0.0781 & 0 & -6.0115 & 0.3879 \end{bmatrix} \times 10^6$$

$$K_{d1} = [-210.4250]$$

And the tie line power between both control areas is chosen as:

$$H_{12} = \begin{bmatrix} 0 & 0 & 0 & 0 & 0 & 0.0327 \\ 0 & 0 & 0 & 0 & 0 & 0 \\ 0 & 0 & 0 & 0 & 0 & 0 \\ 0 & 0 & 0 & 0 & 0 & -0.0054 \\ 0 & 0 & 0 & 0 & 0 & 0 \\ 0 & 0 & 0 & 0 & 0 & 0 \end{bmatrix}$$

where:

$A_1 = A_2$, $B_1 = B_2$, $\Gamma_1 = \Gamma_2$, $K_{x1} = K_{x2}$ and $K_{d2} = K_{d2}$

We simulate and illustrate the response of the two-area power system with nominal parameters in Table 1 and the extended observer is tested by applying the load disturbance of $\Delta P_{d1} = 0.01$ (p.u, MW) at $t = 1$ s and at $\Delta P_{d2} = 0.015$ (p.u, MW) $t = 1$ s. The simulation results of the two-area multi-area power network for case 1 that the proposed GESO are presented in Fig. 5 to Fig. 8. It is simply to observe in Fig. 5 that the frequency variation converges to zero in about 2 s. Fig. 6 and Fig. 8 indicate the mechanical power deviation and control signal deviation of two control areas. Fig. 7 presents that the tie-line power deviations reach to zero with the designed controller. In comparison between the results achieved by using proposed control method with previous research in [5–6], [15], the results of using the proposed controller are to reduce the setting time and overshoots of both in power networks. So, it is proved that the proposed controller is powerful and effective.

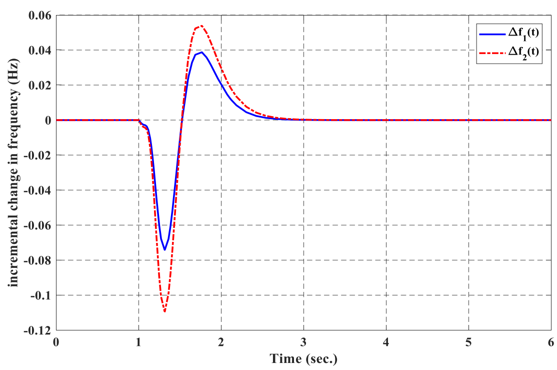

Fig. 5: Frequency deviation of two control areas.

Case 2. In the second case, the performance of proposed GESO scheme is in the presence of nonlinear term such as matched uncertainties to constate the model of the system in Fig. 1 and Fig. 3.

To combine between system matrix of hydro power plant and parameter values in Table 1, the matrix values of the power system are calculated as:

$$A_1 = \begin{bmatrix} -0.05 & 6 & 0 & 0 & 0 & -0.0327 \\ 0.4831 & -6.6667 & 6.7362 & 1.0899 & 0 & 0 \\ -0.1697 & 0 & -0.0348 & -3.2986 & 0 & 0 \\ -1.3889 & 0 & 0 & -3.3333 & 0 & 0 \\ 0.4250 & 0 & 0 & 0 & 0 & 0.0054 \\ 6.2832 & 0 & 0 & 0 & 0 & 0 \end{bmatrix}$$

$$B_1 = \begin{bmatrix} 0 & -1.1594 & 0.5797 & 3.3333 & 0 & 0 \end{bmatrix}^T$$

$$\Gamma_1 = \begin{bmatrix} -6 & 0 & 0 & 0 & 0 & 0 \end{bmatrix}^T$$

Feedback control gain in this case can be designed as:

$$K_{x1} = \begin{bmatrix} -0.0084 & -0.0012 & 0.0043 & -0.0011 & -6.8195 & 0.4481 \end{bmatrix} \times 10^6$$

$$K_{d1} = [-210.4250]$$

And the tie-line power between both control areas are chosen as:

$$H_{12} = \begin{bmatrix} 0 & 0 & 0 & 0 & 0 & 0.0327 \\ 0 & 0 & 0 & 0 & 0 & 0 \\ 0 & 0 & 0 & 0 & 0 & 0 \\ 0 & 0 & 0 & 0 & 0 & -0.0054 \\ 0 & 0 & 0 & 0 & 0 & 0 \\ 0 & 0 & 0 & 0 & 0 & 0 \end{bmatrix}$$

where:

$A_1 = A_2$, $B_1 = B_2$,$\Gamma_1 = \Gamma_2$, $K_{x1} = K_{x2}$ and $K_{d2} = K_{d2}$.

We change the hydro power plant with hydraulic governor instead of thermal power plant and the step load disturbances are kept the same with first case. The deviations in frequency of first and second power area are shown in Fig. 9. Fig. 10 shows mechanical power deviation of two control areas. Fig. 11 and Fig. 12 display in order the tie-line power deviation and control signal deviation. In each control area, the closed loop responses applying the GESO controller are simply to observe from Fig. 9 to Fig. 12 that the response performance is better in terms of settling time about 1s and under/overshoots, in comparison to the recent others proposed in [5–6], [15].

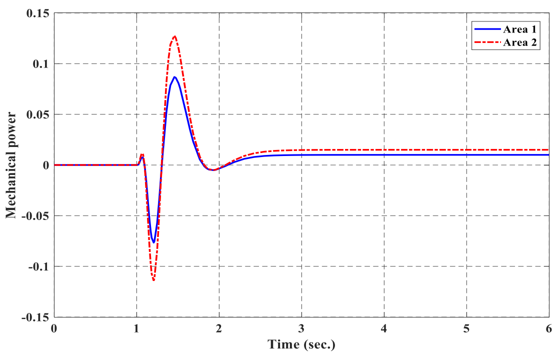

Fig. 6: Mechanical power deviation.

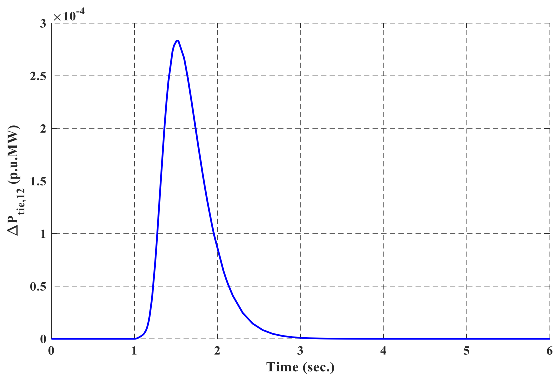

Fig. 7: The tie-line power deviation.

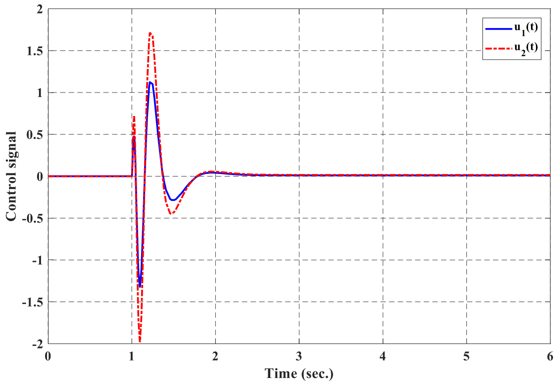

Fig. 8: Control signal deviation of two control areas.

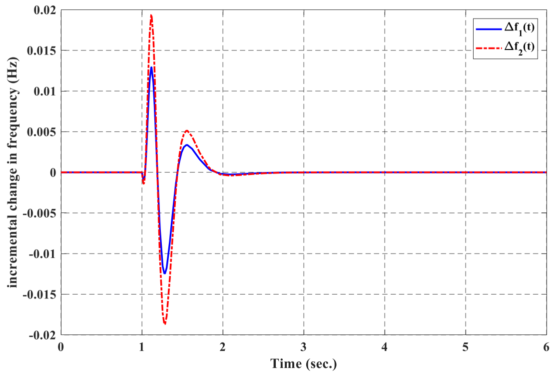

Fig. 9: Frequency deviation of two control areas.

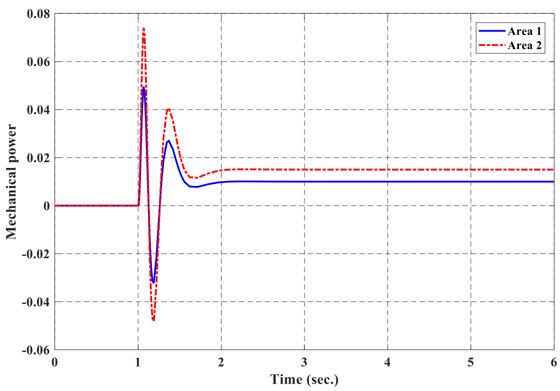

Fig. 10: Mechanical power deviation.

Remark 3: From the reporting of simulation in case 1 and case 2, the proposed approach is one of main objectives to finalize the matched disturbances and achieve shorter setting time and smaller transient deviation in terms of load disturbances for interconnected power system by

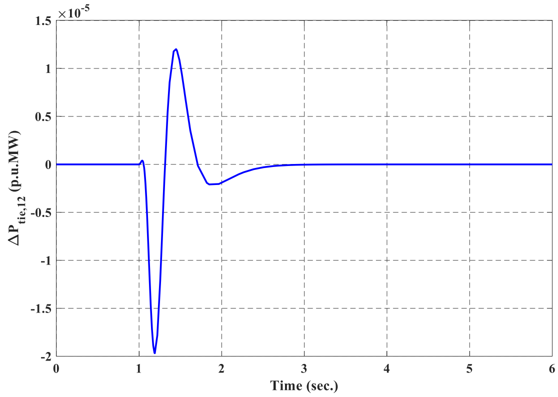

Fig. 11: The tie-line power deviation.

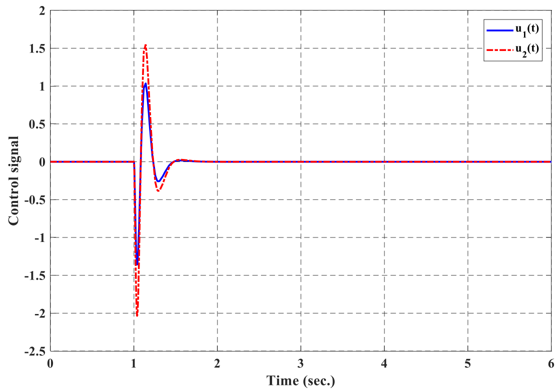

Fig. 12: Control signal deviation.

applying of the proposed GESO law. So, some limitations of other schemes in recent papers [5–6] and [15] have been resolved.

Case 3. Now, the suggested GESO control approach is used to examine by comparing with traditional LFC [5–6], [15] at random load variations. In this specific case, we consider the power system which includes two kinds of the plant as thermal power plant with reheat turbine and hydro power plant with mechanical hydraulic governor. The parameter values of the complex power system are calculated given as:

In the first area:

$$A_1 = \begin{bmatrix} -0.05 & 6 & 0 & 0 & 0 & -0.0327 \\ 0 & -0.1 & -15667 & 1,6667 & 0 & 0 \\ 0 & -3.3333 & 3.3333 & 0 & 0 & 0 \\ -5.2083 & 0 & 0 & -12.5 & 0 & 0 \\ 0.425 & 0 & 0 & 0 & 0 & 0.0054 \\ 6.2832 & 0 & 0 & 0 & 0 & 0 \end{bmatrix}$$

$$B_1 = \begin{bmatrix} 0 & 0 & 0 & 12.5 & 0 & 0 \end{bmatrix}^T$$

$$\Gamma_1 = \begin{bmatrix} -6 & 0 & 0 & 0 & 0 & 0 \end{bmatrix}^T$$

The feedback control gain can be designed:

$$K_{x1} = \begin{bmatrix} -0.0417 & 0.0003 & -0.0781 & 0 & -6.0115 & 0.3879 \end{bmatrix} \times 10^6$$

$$K_{d1} = [-210.4250]$$

And the second area:

$$A_2 = \begin{bmatrix} -0.05 & 6 & 0 & 0 & 0 & -0.0327 \\ 0.4831 & -6.6667 & 6.7362 & 1.0899 & 0 & 0 \\ -0.1697 & 0 & -0.0348 & -3.2986 & 0 & 0 \\ -1.3889 & 0 & 0 & -3.3333 & 0 & 0 \\ 0.4250 & 0 & 0 & 0 & 0 & 0.0054 \\ 6.2832 & 0 & 0 & 0 & 0 & 0 \end{bmatrix}$$

$$B_2 = \begin{bmatrix} 0 & -1.1594 & 0.5797 & 3.3333 & 0 & 0 \end{bmatrix}^T$$

$$\Gamma_2 = \begin{bmatrix} -6 & 0 & 0 & 0 & 0 & 0 \end{bmatrix}^T$$

The feedback control gain can be designed:

$$K_{x2} = \begin{bmatrix} -0.0084 & -0.0012 & 0.0043 & -0.0011 & -6.8195 & 0.4481 \end{bmatrix} \times 10^6$$

$$K_{d2} = [-210.4250]$$

And the tie-line power between two-area are chosen as:

$$H_{12} = \begin{bmatrix} 0 & 0 & 0 & 0 & 0 & 0.0327 \\ 0 & 0 & 0 & 0 & 0 & 0 \\ 0 & 0 & 0 & 0 & 0 & 0 \\ 0 & 0 & 0 & 0 & 0 & -0.0054 \\ 0 & 0 & 0 & 0 & 0 & 0 \\ 0 & 0 & 0 & 0 & 0 & 0 \end{bmatrix}$$

The actual random load disturbances are implemented and applied in both control areas of power system as presented in Fig. 13 to Fig. 17. In flowing detail, Fig. 13 shows the load variations of two control areas. The deviation in frequency of both areas is shown in Fig. 14. Fig. 15, Fig. 16 and Fig. 17 plot the frequency deviation, mechanical power deviation and control signal deviation of two control areas. The generalized extended observer controller is still designed to compute and estimate system variables. In comparison between the deviations in frequency from [5–6], [15] and the simulation results of the proposed GESO controller, the significant improvement is to reduce the magnitude of oscillation as well as minimize under or overshoots and settling time in the response performance.

Remark 4: To observe of 3 cases of simulation results above, the proposed GESO ap-

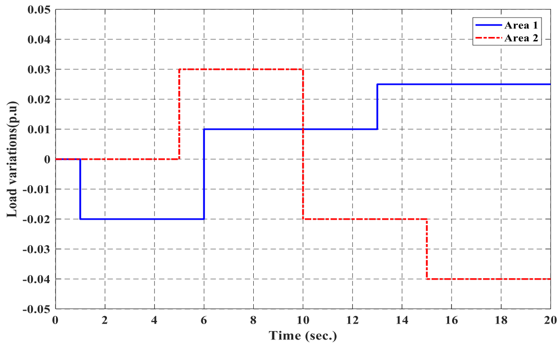

Fig. 13: Load variations of two control areas.

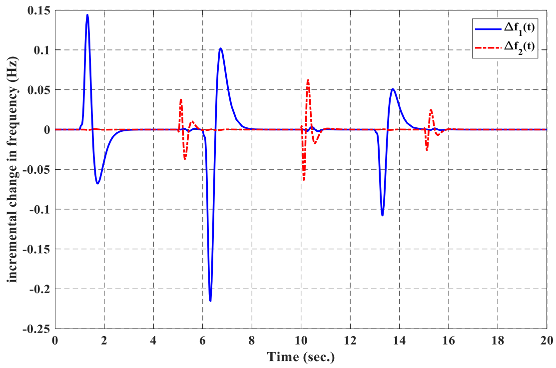

Fig. 14: Frequency deviation of two control areas.

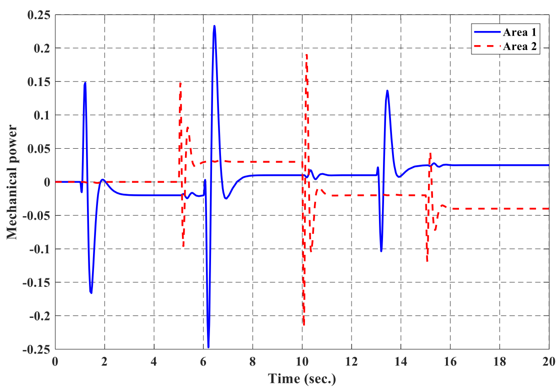

Fig. 15: Mechanical power deviation.

proach achieves affectively the response performance under conditions such as the matched uncertainties and random load variations appearing in complex power networks. The suggested control scheme is applied and developed to eliminate load disturbances and to restore the nominal point of system performance, and to reduce the influence of external disturbances.

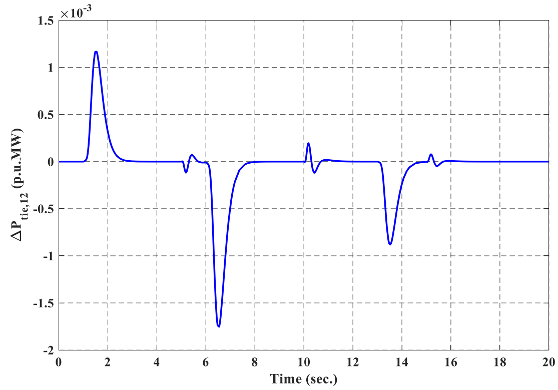

Fig. 16: The tie-line power deviation.

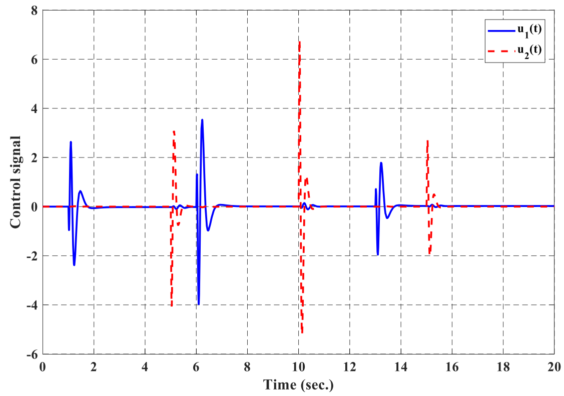

Fig. 17: Control signal deviation of two control areas.

Case 4. In this part, the frequency variation, tie-line power and control input signal are presented from Fig. 18 to Fig. 20 at different step load disturbances $\Delta P_{d1} = 0.1$ (p.u.MW) at $t = 0$ s in the first-area, $\Delta P_{d2} = 0.05$ (p.u.MW) at $t = 0$ s in the second-area. The non-reheat turbine is applied to both areas and system parameters are used the same with the one given in [28].

Delve into data analysis, the goal of any load frequency controllers is to return frequency value to the safe point. It is to be clear that we observe in Fig. 18 and Fig. 19, the proposed GESO controller obtains the normal range in frequency about 1 s at both areas and decreases tie-line power variation to zero about 3 s, respectively. The proposed GESO controller also reduces and minimizes overshoot and settling time as compared with recent studies in [5-6], [15] and with observer controller in [28].

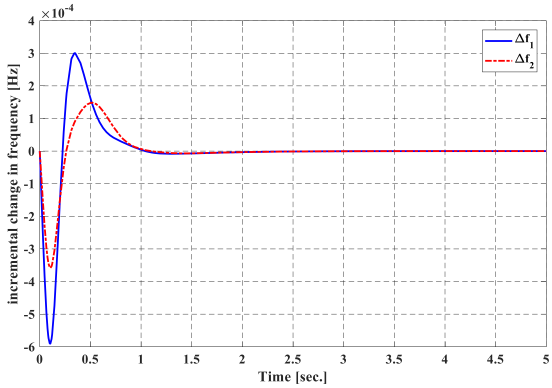

Fig. 18: Frequency deviation of two control areas.

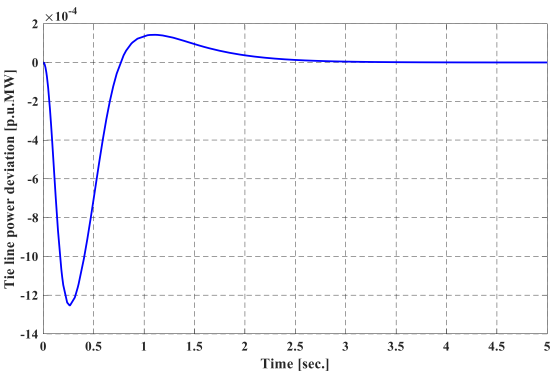

Fig. 19: The tie-line power variation.

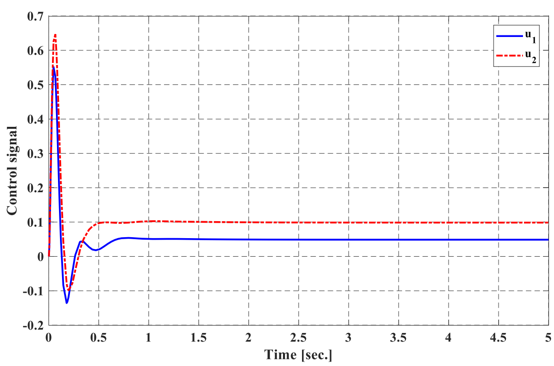

Fig. 20: Control signal.

Remark 5. It is to be noted that the suggested GESO approach has ability to estimate and compensate exactly under the matched uncertainty. In particular, the proposed control scheme makes better the system damping characteristic.

Simulation 2. In the last case, we consider the dynamic models utilized for simulation of physical constraints of GDB and GRC in the thermal power plant with reheat turbine and the hydro power plant with mechanical hydraulic governor in Fig. 21.

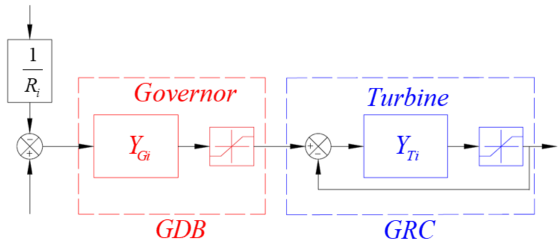

Fig. 21: Nonlinear model with GDB and GRC [32].

We test the proposed controller with the step load disturbance of $\Delta P_{d1} = 0.01$ (p.u MW) at $t = 1$ s and $\Delta P_{d2} = 0.03$ (p.u MW) at $t = 1$ s. Fig. 22, Fig. 23 and Fig. 24 represent the frequency variation, tie-line power variation and mechanical power variation in each control area. The control signal of both control area illustrates in Fig. 25. As it is clear, with the proposed GESO controllers, the transient oscillations are determined a longer time with larger amplitude than in the cases of without considering the GRC and GDB in case 1, case 2, case 3 in simulation 1. The proposed control strategy has also discovered satisfactory even in presence of GRC, GDB and step load disturbances in comparison with [30]. The overshoot percentage and settling time are synchronously significantly decreased in the transient performance of the suggested GESO controller.

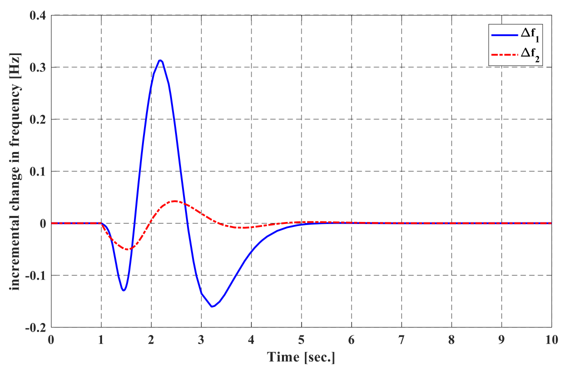

Fig. 22: Frequency variation of two control areas.

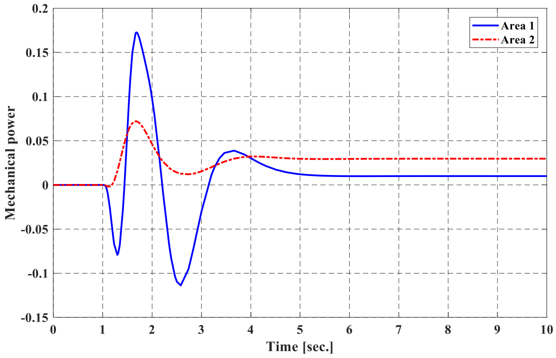

Fig. 23: Mechanical power deviation.

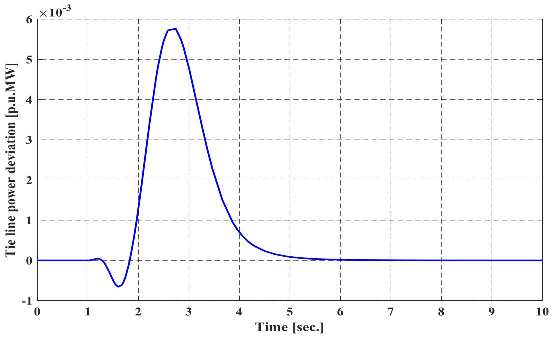

Fig. 24: The tie-line power deviation.

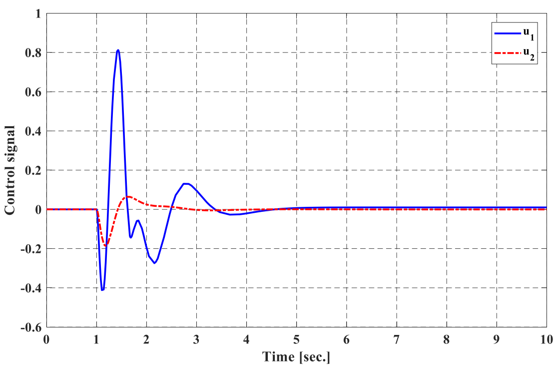

Fig. 25: Control signal.

Remark 6: The GRC and GDB impact significantly to feedback signal of the interconnected power network. To show the robustness of the proposed GESO, the simulation results are used to compare with the case of considering in [30] or without considering the GDB and GRC nonlinearity effects in [31]. The proposed controller clearly indicates that transient performance has adapted with required condition such as the setting time and under/overshoot in comparison with previous research. Thus, the small deviations in frequency with the proposed GESO have less effect on the plant reserve capacity and power market.

6. Conclusions

To solve the problem of unmeasurable of system states in interconnected power system due to lack of sensor, the load frequency control based generalized extended state observer is proposed in this paper. The generalized extended state observer is used to estimate the unmeasurable of system states and load disturbances. The proposed scheme of making the interconnected power system is not only secure and stable but also useful to solve the satisfactory performance with system parameter uncertainties. The simulation results point out that the LFC based GESO approach improves the system dynamic response to fast response in setting time and to reduce over or undershoots in power network with the dynamic model of thermal power plant with reheat turbine and hydro power plant. Moreover, the report of simulation results is used to compare with the cases of considering and without considering the GDB and GRC nonlinearity effects on power network. It is evident that the robustness of the suggested controller in terms of stability and effectiveness of system.

Acknowledgements

This research was funded by Science and Technology Development of Ton Duc Thang University (FOSTECT), website: http://fostect.tdtu.edu.vn, under Grant FOSTECT.2017.BR.05

References

[1] Chaturvedi, D.K. (2008). Techniques and its Applications in Electrical Engineering Springer.

[2] Vittal, V., Mc Calley, J.D., Anderson, P.M., & Fouad, A.A. (2019). Wiley 3rd Edition, Power System Control and Stability.

[3] Fu, C., & Tan, W. (2018). Decentralized Load Frequency Control for Power Systems with Communication Delays via Active Disturbance Rejection. *IET Generation, Transmission & Distribution, 12*(6), 1751-8687.

[4] Bernard, M.Z., Mohamed, T.H., Qudaih, Y.S., & Mitani, Y. (2014). Decentralized load frequency control in an interconnected power system using Coefficient Diagram Method. *International Journal of Electrical Power & Energy Systems, 63*(5), 65–172.

[5] Parmar, K.P.S., Majhi, S., & Kothari, D.P. (2012). Load frequency control of a realistic power system with multi-source power generation. *International Journal of Electrical Power & Energy Systems, 42*(1), 426–433.

[6] Parmar, K.P.S., Majhi, S., & Kothari, D.P. (2014). LFC of an interconnected power system with multi-source power generation in deregulated power environment. *International Journal of Electrical Power & Energy Systems, 57*(2), 277–286.

[7] Yousef, H.A., AL-Kharusi, K., Albadi, M.H., & Hosseinzadeh, N. (2014). Load Frequency Control of a Multi-Area Power System. *An Adaptive Fuzzy Logic Approach, IEEE Transactions on Power Systems, 29*(4), 1822-1830.

[8] Zeng, G.-Q., Xie, X.-Q., & Chen, M.-R., (2017). An Adaptive Model Predictive Load Frequency Control Method for Multi-Area Interconnected Power Systems with Photovoltaic Generations. *Electrical Power and Energy System, 10*(11), 1840.

[9] Rehiara, B.A., Yorino, N., Sasaki, Y., & Zoka, Y. (2020). An Adaptive Load Frequency Control Based on Least Square Method. *Advances in Modelling and Control of Wind and Hydrogenators, 49*(3), 220.

[10] Dahab, Y.A., Abubakr, H., & Mohamed, T.H. (2020). Adaptive Load Frequency Control of Power Systems using Electro-Search Optimization Supported by the Balloon Effect. *IEEE Access*, 7408–7422.

[11] Anwar, M.N.& Pan, S., (2015). A New PID Load Frequency Controller Design Method in Frequency Domain Through Direct Synthesis Approach. *Electric Power and Energy Systems, 67*(4), 560-569.

[12] Kouba, N., Menaa, M., Hasni, M., et al. (2015). Load frequency control in multiarea power system based on fuzzy logic-PID controller. *IEEE Int. Conf. on Smart Energy Grid Engineering SEGE, Oshawa, Canada, 15*(1), 1–6.

[13] Farahani, M., Ganjefar, S., Alizadeh, M. (2012). PID controller adjustment using chaotic optimization algorithm for multi-area load frequency control. *IET Control Theory Appl., 6*(2), 1984–1992.

[14] Yang, M., Yang, F., Chengshan, W., & Peng, W. (2013). Decentralized Sliding Mode Load Frequency Control for Multi-Area Power Systems. *IEEE Transactions on Power System, 28*(4), 4301-4309.

[15] Guo, J. (2020). Application of A Novel Adaptive Sliding Mode Control Method to the Load Frequency Control. *European Journal of Control, 5*(2), 3580-3601.

[16] Mu, C., Tang, Y., & He, H., (2017). Improved Sliding Mode Design for Load Frequency Control of Power System Integrated an Adaptive Learning Strategy. *IEEE Transactions on Industrial Electronics, 64*(8), 6742–6751.

[17] Trip, S., Cucuzzella, M., De Persis, C., van der Schaft, A., & Ferrara, A. (2019). Passivity-Based Design of Sliding Modes for Optimal Load Frequency Control. *IEEE Transactions on Control Systems Technology, 27*(5), 1893-1906.

[18] Li, H.Y., Shi, P., Yao, D.Y., & Wu, L.G. (2016). Observer-Based Adaptive Sliding Mode Control of Nonlinear Markovian

Jump Systems. *Automatica, 64*(1), 133-142.

[19] Khayati, K., (2015). Multivariable Adaptive Sliding-Mode Observer-Based Control for Mechanical Systems. *Canadian Journal of Electrical and Computer Engineering, 38*(3), 253-265.

[20] Wang, B., Shi, P., Karimi, H.R., & Lim, C.C. (2013). Observer-Based Sliding Mode Control for Stabilization of a Dynamic System with Delayed Output Feedback. *Mathematical Problems in Engineering, 3*(1), 1-6.

[21] Yang, B., Yu, T., Shu, H., Yao, W., & Jiang, L. (2018). Sliding-Mode Perturbation Observer-Based Sliding-Mode Control Design for Stability Enhancement of Multi-Machine Power Systems. *Transactions of the Institute of Measurement and Control, 41*(5), 1418-1434.

[22] Mi, Y., Fu, Y., Li, D., Wang, C., Loh, P.C., & Wang, P. (2016). The Sliding Mode Load Frequency Control For Hybrid Power System Based on Disturbance Observer. *International Journal of Electrical Power & Energy Systems, 74* (1), 446-452.

[23] Pawar, S.N., Chile, R.H., & Patre, B.M. (2017). Design of Generalized Extended State Observer based Control for Nonlinear Systems with Matched and Mismatched Uncertainties. *Indian Control Conference (ICC)*, 4-6.

[24] Yao, J., Jiao, Z., & Ma, D. (2014). Adaptive Robust Control of DC Motors with Extended State Observer. *IEEE Transactions on Industrial Electronics, 61*(7), 3630–3637.

[25] Wang, S., Ren, X., Na, J., & Zeng, T. (2017) Extended-State-Observer-Based Funnel Control for Nonlinear Servomechanisms with Prescribed Tracking Performance. *IEEE Transactions on Automation Science and Engineering, 14*(1), 98–108.

[26] Hossain, M., & Peng, C. (2020). Load Frequency Control for multiarea power systems under DoS attacks. *Information Sciences, 243*(1), 437-453.

[27] Haes, A., Hamedani, H., Mohamad, G., Hatziargyriou, E., & Nikos, D. (2019). A Decentralized Functional Observer based Optimal LFC Considering Unknown Inputs, Uncertainties and Cyber-Attacks. *IEEE Transactions on Power Systems, 34*(6), 4408–4417.

[28] Chen, C., Zhang, K., Yuan, K., & Wang, W. (2017). Extended Partial States Observer Based Load Frequency Control Scheme Design for Multi-area Power System Considering Wind Energy Integration. *IFAC-Papers On-Line, 50*(1), 4388–4393.

[29] Rinaldi, G., Cucuzzella, M., & Ferrara, A. (2017). Third order sliding mode observer-based approach for distributed optimal load frequency control. *IEEE Control Systems Letters, 1*(2), 215–220.

[30] Prasad, S., Purwar, S., & Kishor, N. (2019). Load frequency regulation using observer based non-linear sliding mode control. *International Journal of Electrical Power & Energy Systems, 108*(1), 178–193.

[31] Prasad, S. (2020). Counteractive control against cyber-attack uncertainties on frequency regulation in the power system: IET Cyber-Physical Systems. *Theory & Applications Research, 5*(4), 394–408.

[32] Bevrani, H. (2014). Robust Power System Frequency Control, Power Electronics and Power Systems, Springer.

About Authors

Anh-Tuan TRAN received B.Eng. degree in electrical engineering, Ton Duc Thang University (TDTU), Ho Chi Minh City, Vietnam. Currently, he is M.Eng. student in Electrical Engineering, TDTU, HCMC, Vietnam. His research topics included load frequency control and automatic voltage regulator to power systems with sliding mode control and optimal control.

Phong Thanh TRAN received the B.Eng. degree in physics and electronics with a major in automation and control at Ho Chi Minh University of Science, Ho Chi Minh, Vietnam, in 2010, and the M.Eng. degree in electrical engineering with a major in automation and control at International University, Ho Chi Minh National University, in 2015. His current research activities include power systems, siding mode control, dynamic system and load frequency control.

Van Van HUYNH has completed the Ph.D degree in automation and control from Da-Yeh University, Taiwan. He is currently a Lecturer in the Faculty of Electrical and Electronics Engineering, Ton Duc Thang University, Ho Chi Minh City, Vietnam. He has published totally 10 journal papers and more than 11 international conference papers. His current research interests are in sliding mode control, variable structure control, and power system control.